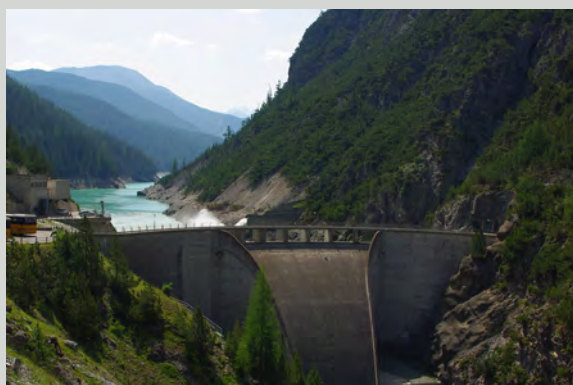


SCCER-SoE Science Report



2018

Supported by:



Schweizerische Eidgenossenschaft
Confédération suisse
Confederazione Svizzera
Confederaziun svizra
Swiss Confederation

Innosuisse – Swiss Innovation Agency

Imprint

Editor

Swiss Competence Center for Energy Research – Supply of Electricity (SCCER-SoE)

Address

SCCER-SoE
Gianfranco Guidati & Ueli Wieland
c/o ETH Zurich
Sonneggstrasse 5
8092 Zurich

Website

www.sccer-soe.ch

Copyright Cover Pictures

Hydropower (left): ETH Zurich
Geo-energy (right): ETH Zurich

Date of Issue

28 September 2018

Content

Editorial.....	1
Work Package 1: Geo-energies	2
Task 1.1	6
Task 1.2	32
Task 1.3	42
Task 1.4	50
Work Package 2: Hydropower.....	52
Task 2.1	56
Task 2.2	68
Task 2.3	86
Task 2.4	92
Work Package 3: Innovation Agenda	96
Task 3.1	98
Task 3.2	112
Work Package 4: Future Supply of Electricity	120
Task 4.1	122
Task 4.2	140
Task 4.3	146
Task 4.4	156
Work Package 5: Pilot & Demonstration Projects	160
WP 5 Projects.....	162

Editorial

The Swiss Competence Center for Energy Research – Supply of Electricity (SCCER-SoE) has been established in 2013 to ensure that the academic community works closely with industry to provide the required research advancement, develop innovative technologies and robust solutions, and ultimately ensure the future provision of electricity and energy to the Swiss country and the transition to a competitive carbon-free economy.

The specific targets are geo-energies and hydropower, the two resources identified by the Energy Strategy 2050 to provide a substantial band-electricity contribution to enable the exit from nuclear power, with the target of up to 7 % electricity production from deep geothermal energy and a 10 % increase of hydropower production.

The SCCER-SoE initiated in 2017 its second implementation phase. More than 200 scientists, engineers, researchers, doctoral and master students and professors are now associated to the SCCER-SoE, working together in inter-disciplinary projects to realize the identified innovation roadmap. Among these, over 90 doctoral students are now carrying out their research in the SCCER-SoE, providing a substantial component of the future capacity building of Switzerland.

The SCCER-SoE Annual Conference 2018, held on 13 and 14 September at the HSLU in Lucerne, aimed at providing a comprehensive overview of the R&D conducted by the SCCER-SoE and its associated projects, and to confront the scientific agenda with the needs and views of stakeholders from industry, public institutions, federal offices and policy makers.

Nearly 140 posters were presented and discussed at the conference, covering all aspects of the scientific portfolio of the SCCER-SoE. These posters are collected in this volume and presented according to the work packages and tasks to which they are associated.

These are exciting times for energy research in Switzerland. The Energy Law 2016 has been confirmed by the public referendum, providing the basis for the implementation of the Energy Strategy 2050. The SCCER-SoE will continue with the development of integrative solutions, testing and installation of innovative technologies, technology assessment and scenario modelling.

In the second phase, we expanded the overall R&D portfolio, with a wider perimeter for geo-energies, adding new targets on usage of hydrothermal resources for direct heating and heat storage; a refocusing of the hydropower area with four tasks and five key overarching targets; a clearer innovation agenda, now including innovative technologies and computational energy innovation; a more integrated approach to the future supply of electricity, with an expanded scope of the risk assessment activities and of the evaluation of global electricity resources and technologies, new resources and a closer integration with the SCCER CREST on the socio-economic-political drivers of electricity supply, and two new SCCER Joint Activities, on Scenario and Modeling and on Socio-political conditions of the extension of hydropower and geothermal energy. Finally, we expanded the focus on pilot and demonstration projects, conducted with industry partners, to validate the technologies and proposed solutions; seven pilot and demonstration projects are now pursued, covering the whole portfolio of technologies and energy sources of the SCCER-SoE.

The Annual Conference 2018 shows a vibrant and integrated scientific community, and the scientific level of the presentations proves that we are on the good way to complete the implementation of the geo-energy and hydropower R&D roadmaps.

We look forward to the future progress of our program!

Domenico Giardini
Head of the SCCER-SoE

Work Package 1: Geo-energies

Geo-science can contribute in various ways to reach the objectives of the Energy Strategy 2050. The first option is to generate baseload electricity, which helps to compensate the future lack of nuclear generation. Alternatively, the extraction and/or seasonal storage of thermal energy can help to reduce emissions from the heating sector, having also a positive impact on the electricity sector. Last but not least, the geological storage of CO₂ can enable near-emission-free fossil power generation or the production of hydrogen for the transport and industrial sector. All three options are being tackled within the SCCER-SoE, especially in a series of demonstration projects.

To enable geothermal electricity generation, solutions must be found for two fundamental and coupled problems:

- a. How do we create an efficient heat exchanger in the hot underground that can produce energy for decades while
- b. at the same time keeping the nuisance and risk posed by induced earthquakes to acceptable levels?

Since petrothermal P&D projects continue to be postponed due to appeals and the effects of an unfavorable market environment, we directed a large effort towards accelerating stimulation process understanding and validation via underground lab experiments. After successfully completing test campaigns in the Grimsel lab we will soon perform experiments at a much larger scale in the new Bedretto Underground Laboratory for Geosciences (BULG).

Our activity on seasonal thermal energy storage and direct heat production is also progressing well. In close collaboration with industrial partners in the Geneva and Bern area, we work on this novel technology to reduce CO₂ emissions from the domestic heating sector, which will also give us direct access to perform research in wells that are drilled for the project.

Drilling has also started in the third area: ELEGANCY, a SFOE funded P&D project, embedded in a larger European framework, has the mission to provide clean hydrogen for heat and mobility based on steam-methane-reforming. CO₂ storage is an essential part of this concept. Underground experiments at the Mt Terri Lab study the potential CO₂ migration through a fault in the caprock and the effects of fault activation. This is complemented by lab experiments on rock samples, modelling of injection and CO₂ migration and the identification of suitable regions in the Swiss sedimentary basin.

Highlights 2018

Deep Underground Laboratory Experiment at Grimsel Test Site completed

The In-situ Stimulation and Circulation (ISC) Experiment has been successfully completed at the end of 2017, with a circulation phase following the hydraulic stimulation campaigns in February and May 2017. The key goal was to generate high-quality data on interacting physical processes during stimulation, in order to provide the basis for a more rigorous understanding and engineering of the stimulation process. It is widely believed that this experiment has by far been the most detailed, best instrumented, and most comprehensive of its kind to date. Experimental highlights are (a) permeability was successfully stimulated by orders of magnitude in all structures, (b) final transmissivity for all stimulated structures is nearly the same, while (c) seismicity during stimulation is strongly varying between experiments. These results are promising for new stimulation and operation techniques, such as multi-stage stimulation. Further innovation potential is demonstrated by a new technique for remote fluid pressure propagation monitoring using seismic wave velocities.

New round of Deep Underground Lab experiments underway

A number of experiments are combined to advance soft, multi-stage hydraulic stimulation techniques in the BULG Lab. The experimental program is a logical continuation of the work in Grimsel, and a pathway towards industrial electricity generation. The BULG Lab is currently being constructed in the Bedretto tunnel (TI). Experiments are planned to start early 2019.

Geneva heat storage and utilization project enters the exploration phase

The prospection phase of Geneva's "Geothermie 2020" program is fully running with wells (production and storage) being drilled at progressively increasing depths (1500-2500 m). The encouraging preliminary results obtained and those ones, which will be obtained with future drilling campaigns, will provide the opportunity to test and validate the effectiveness of exploration concepts and models developed within WP1 as well as proof the feasibility of direct heat production and subsurface storage potential in sedimentary basins at relatively shallow depths.

Geological sequestration of CO₂

Geomechanical challenges related to CO₂ sequestration are investigated at the Laboratory for Soil Mechanics of the EPFL. The performed work consists in both experimental and numerical activities. Recent advances include the establishment of a systematic testing procedure at the laboratory scale for the assessment of the sealing capacity of shale caprock to CO₂ injection; the study carried out in this framework will be linked with the aforementioned ELEGANCY project. Moreover, the development of a semi-analytical seismicity model to evaluate the risk of large-magnitude seismicity induced by the fluid injection is under development.

Overall progress

Our portfolio of individual projects and clusters of projects continues to make significant progress with many "smaller" highlights. UNIL made significant advances on the characterization of fractures with geophysical data (hydrophone VSP data, borehole methods, seismic attenuation of sonic log data). The studies performed at the Center for Hydrology and Geothermics of UNINE focused on the stability of deep deviated wells and the determination of the in-situ stress from 3D displacement data during fault reactivation experiment. The Geo-energy Laboratory at the EPFL is providing significant contribution in the field of fracture propagation with the development of an open-source simulator (PyFrac) and a polyaxial rig to simulate hydraulic stimulation at the lab scale; theoretical work is also carried out to evaluate the effect of dilatancy on the nucleation of dynamic rupture. The Institute of Geochemistry and Petrology of the ETHZ is developing a simulation tool to perform THMC analyses; in particular, numerical simulations have been done to model flow paths in micro and macro fractures. At the Institute of Geological Sciences at UNIBE the characterization of the Muschelkalk reservoir underlying the Swiss Plateau has been completed. UNIBE and the Institute of Earth Sciences at UNIL have completed the evaluation of data collected at the Grimsel Pass drill hole in order to characterize the natural fault-hosted geothermal activity at that site. Temperatures depth below the drill site have been found to be much higher than expected at the outset of the project, thereby raising the exploration potential for orogenic geothermal systems in the crystalline Alps. Finally, a collaboration between ETHZ and Swisstopo has led to a novel geodata-infrastructure, including a new initiative to update the Swiss heat flow map.

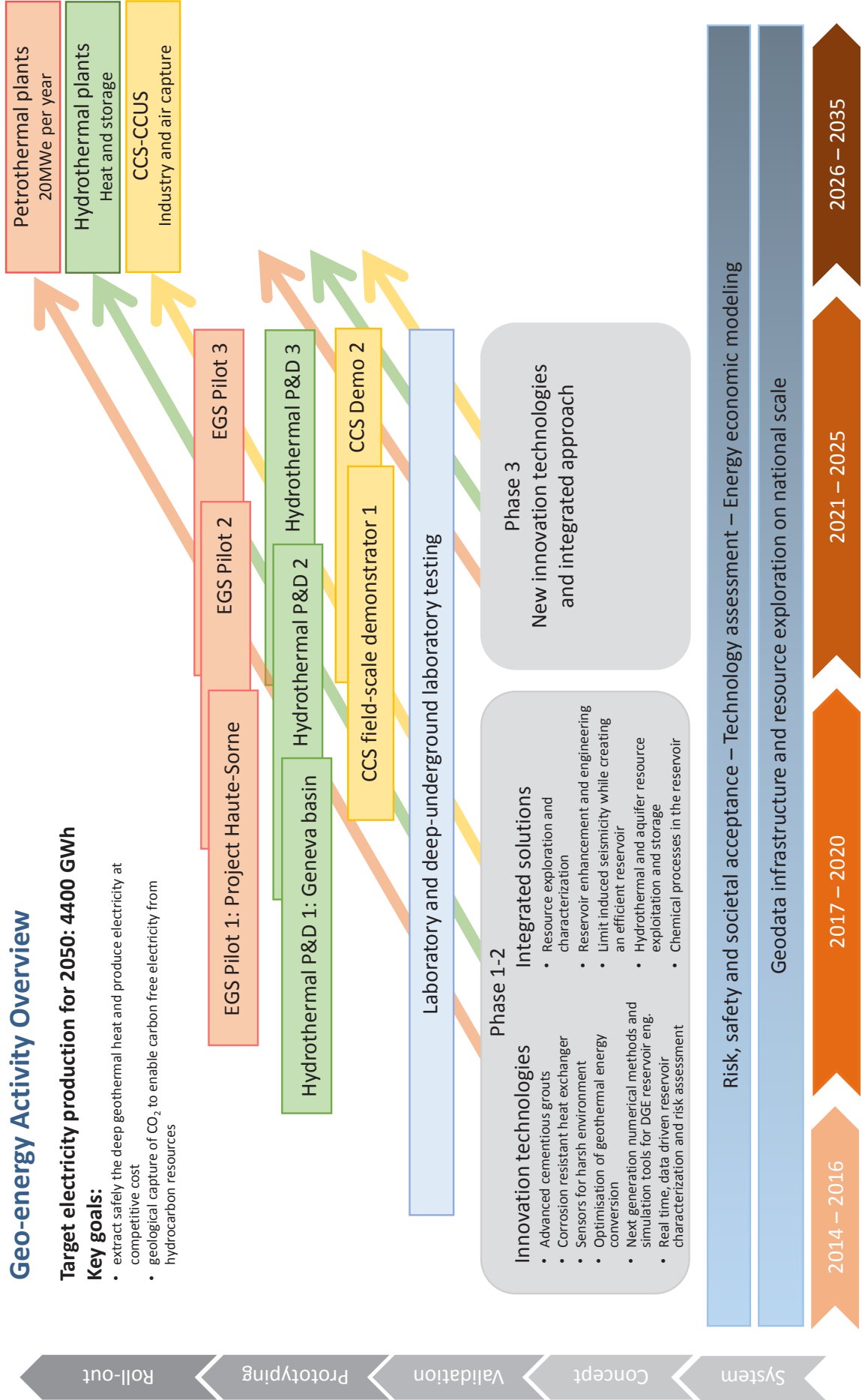
Geo-energy Activity Overview

Target electricity production for 2050: 4400 GWh

Key goals:

- extract safely the deep geothermal heat and produce electricity at competitive cost
- geological capture of CO₂ to enable carbon free electricity from hydrocarbon resources

Energy funding programme
Swiss Competence Centers for Energy Research



Task 1.1

Title

Resource exploration and characterization

Projects (presented on the following pages)

Searching for microseismicity in the Great Geneva basin and surrounding regions

Verónica Antunes, Thomas Planès, Riccardo Minetto, Aurore Carrier, François Martin, Michel Meyer, Matteo Lupi

Mechanical response of Opalinus Clay during CO₂ injection

Alberto Minardi, Lyesse Laloui

Computerized tomography imaging of fracture aperture distribution and fluid flow within sheared fractures

Quinn C. Wenning, Claudio Madonna, Ronny Pini, Takeshi Kurotori, Claudio Petrini, Sayed Alireza Hosseinzadeh Hejazi

Effects of thermal stresses on rocks physical properties: Insights for monitoring at the field scale

Lucas Pimienta, Marie Violay

Seismic activity caused by drilling in supercritical conditions in the Larderello geothermal field

Riccardo Minetto, Domenico Montanari, Thomas Planès, Marco Bonini, Chiara del Ventisette, Matteo Lupi

Estimation of fracture normal compliance from full-waveform sonic log data

Nicolás D. Barbosa, Eva Caspari, J. Germán Rubino, Andrew Greenwood, Ludovic Baron, and Klaus Holliger

Ambient seismic noise tomography of the Geneva basin

Thomas Planès, Anne Obermann, Veronica Antunes, Aurore Carrier, Matteo Lupi

Data acquisition and numerical modeling for a thermally induced breakout experiment

Arnaud Rüegg, Reza Sohrabi, Benoît Valley

Penetration depth of meteoric water and maximum temperatures in orogenic geothermal systems

Larryn W. Diamond, Christoph Wanner, H. Niklaus Waber

How can the borehole three-dimensional displacement data help improving in situ stress estimation across a fault reactivated by fluid injections?

Maria Kakurina, Yves Guglielmi, Christophe Nussbaum and Benoît Valley

Estimating fracture apertures and related parameters using tube-wave data

Jürg Hunziker, Andrew Greenwood, Shohei Minato, Eva Caspari and Klaus Holliger

Characterization of the fracture network in the damage zone of a shear fault with geophysical borehole methods

Eva Caspari, Andrew Greenwood, Ludovic Baron, Daniel Egli, Enea Toschini and Klaus Holliger

Attenuation and velocity anisotropy of stochastic fracture networks

Eva Caspari, Jürg Hunziker, Marco Favino, German Rubino, Klaus Holliger

Seismic attenuation and P-wave modulus dispersion in poroelastic media with fractures of variable aperture distributions

Simon Lissa, Nicolas Barbosa, German Rubino and Beatriz Quintal

GEOTHEST - Building an INTERREG project France-Switzerland on innovation in geophysical exploration for geothermal development in sedimentary basin.

Guillaume Mauri, Jean-Luc Got, Matteo Lupi, Emmanuel Trouver , Andrew Stephen Miller

Reactive transport models of the orogenic hydrothermal system at Grimsel Pass, Switzerland

Peter Alt-Epping, Laryyn W. Diamond, Christoph Wanner

Compilation of data relevant for geothermal exploration – a first step towards a Geothermal Play Fairway Analysis of the Rhône Valley

DB van den Heuvel, S Mock, D Egli, LW Diamond, M Herwegh

In-situ characterization of fluid flow In an EGS analog reservoir

Bernard Brixel, Maria Klepikova, Mohammadreza Jalali, Clément Roques, Clément, Simon Loew

Salt Tracer Flow Path Reconstruction Using Ground Penetrating Radar

Peter-Lasse Giertzuch, Joseph Doetsch, Mohammadreza Jalali, Alexis Shakas, Hannes Krietsch, Bernard Brixel, Cédric Schmelzbach, Hansruedi Maurer

Comparison between DNA nanotracer and solute tracer tests in a fractured crystalline rock – GTS case study

Anniina Kittilä, Mohammedreza Jalali, Keith Frederick Evans, Xian-Zhao Kong, Martin O. Saar

GECOS: Geothermal Energy Chance Of Success

Luca Guglielmetti, Andrea Moscariello, Cédric Schmelzbach, Hansruedi Maurer, Carole Nawratil de Bono, Michel Meyer, Francois Martin, David Dupuy, PierVittorio Radogna

Exploring the interface between shallow and deep geothermal systems: the Tertiary Molasse.

Andrea Moscariello, Nicolas Clerc, Loic Pierdona, Antoine De Haller

Processing and Analysis of Gravity data across the Geneva Basin in a Geothermal Perspective

Luca Guglielmetti, Andrea Moscariello

Searching for microseismicity in the Great Geneva basin and surrounding regions

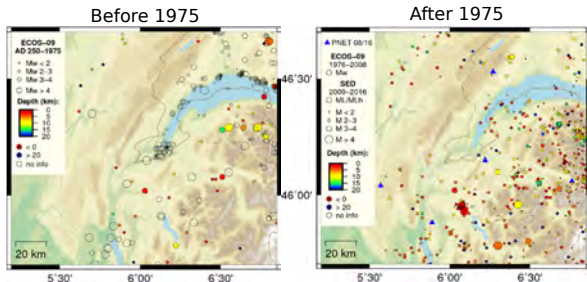
Verónica Antunes¹, Thomas Planès¹, Riccardo Minetto¹, Aurore Carrier¹, François Martin², Michel Meyer², Matteo Lupi¹

1) Department of Earth Sciences, University of Geneva, Switzerland (veronica.antunes@unige.ch); 2) Services Industriels de Genève - SIG, Switzerland

INTRODUCTION

Switzerland is promoting the development of renewable energetic resources. In particular, the Canton of Geneva and the Industrial Services of Geneva (SIG) are investigating the geothermal energy potential of the Greater Geneva Basin, Western Switzerland. Before exploration starts it is crucial to study the local seismicity and its relationship with local tectonic structures. Additionally, it is important to monitor the seismic activity that may occur during geothermal exploitation.

Background seismicity



SED (Swiss Seismological Service) catalogues for the Greater Geneva Basin and surrounding area from AD 250 to August 2016 [1].

Historical Seismicity

> Several earthquakes documented in Geneva

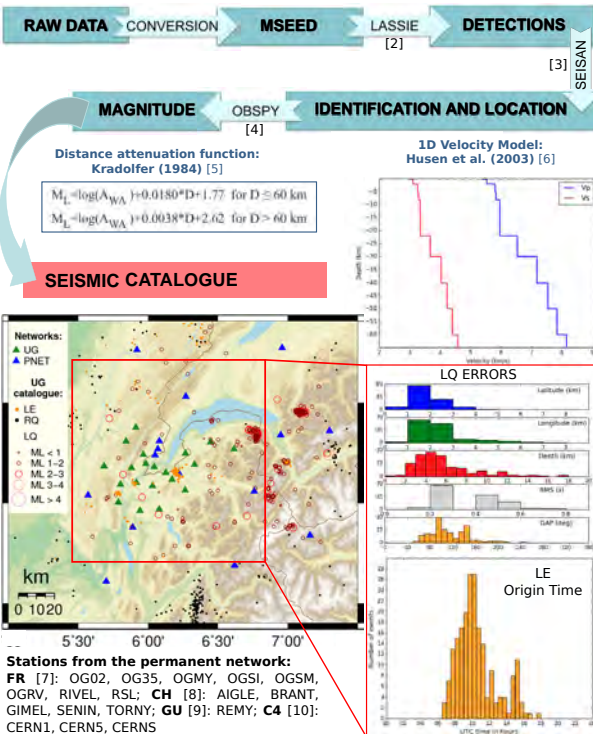
Instrumental Seismicity

> Sparse and disperse seismic activity

Number of Stations ?

We installed 20 broadband stations (UG)

WORKFLOW

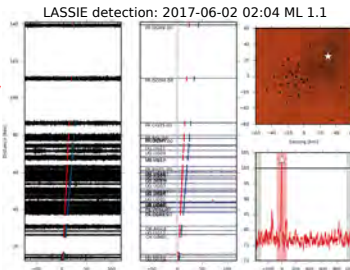


Stations from the permanent network:
FR [7]: OG02, OG35, OGM5, OGS1, OGSM, OGRV, RIVEL, RSL; CH [8]: AIGLE, BRANT, GIMEL, SENIN, TORNY; GU [9]: REMY; C4 [10]: CERN1, CERN5, CERN5

SEISMICITY

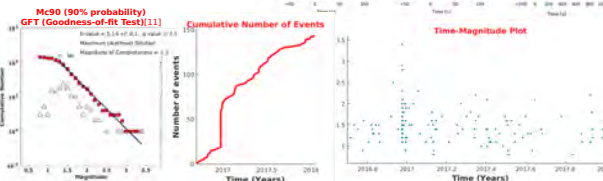
17 months

- LASSIE - 1734 detections:**
- 362 Local earthquakes (LQ)
 - **143 in the area of study**
 - 218 Quarry blasts (LE)
 - 853 Regional (RQ)
 - 218 Distant (DQ)
 - 83 False detections (F)

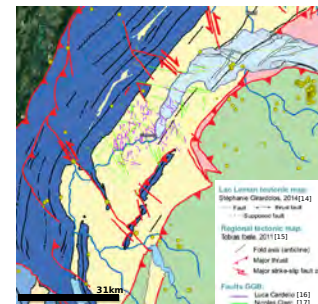


1 month (June):

- 104 real events
- STA/LTA - 2097 detections
- LASSIE - 124 detections



Mc determined using GISMO [12]; we think the Mc value is being overestimated due to the low seismic rate in the area; Evolution of events through time, SEDA [13]: the seismic sequence that occurred in December 2016 is evident.



01/09/2016 - 31/01/2018

- 143 LQ UG catalogue
- 44 LQ Swiss catalogue
- 14 LQ French catalogue

Seismogenic areas:

- Vuache fault
- Lake Leman
- NE of the basin (Pre-Alpine front)
- Arve fault
- Isolated events indicating disperse seismicity

Seismic rate:
17months/143 events
1year/~100 events

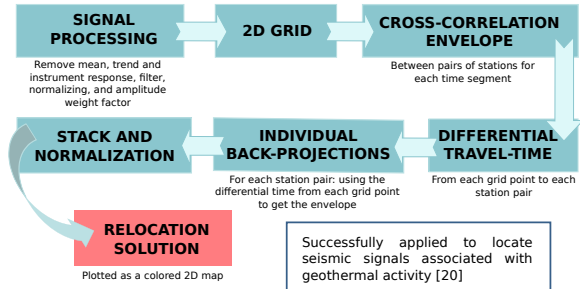
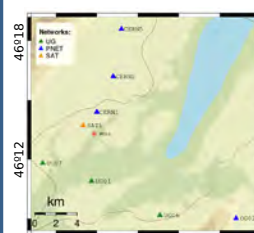
UG catalogue and Tectonic Map of the region

MONITORING

One extra station deployed near the Satigny well

01/01/2018 - 03/05/2018
0 events

We developed a tool capable to locate unconventional events. The method is based on the **back-projection of the cross-correlation envelope** [18] [19] of signals between **pairs of stations**.



Successfully applied to locate seismic signals associated with geothermal activity [20]

REFERENCES:

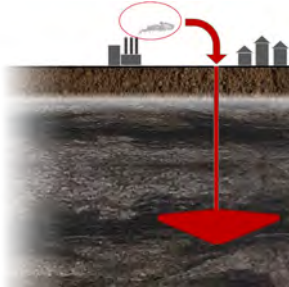
- [1] Foh, D. et al. (2011) DOI: SED/RISK/R001/20110417; [2] Heimann S. et al. (in prep.); [3] Havskov and Ottemoller (1999) <http://seisan.info>; [4] Beyreuther M. (2010) DOI: 10.17788/RESIFR; [5] Kradolfer, U. (1984). Diploma thesis. ETH Zurich; [6] Husen S., et al. (2003) DOI: 10.1029/2002JB001778; [7] RESIF (1995) DOI: 10.15778/RESIFR; [8] SED (1983) DOI: 10.23668/ednetwork/19; [9] University of Geneva (1967) DOI: 10.7914/SVUGU; [10] CERN Seismic Network, C4 (2017); [11] Wiemer, S. et al. (2000) DOI: 10.1785/0119990114; [12] Thompson G and Reyes C. (2017) <http://geoscience-community-codes.github.io/GISMO>; [13] A. M. Lombardi (2017) DOI: 10.1038/nrep44171; [14] Girardos S. et al. (2014). 19^e congrès international de séismotectonique; [15] Beke T. (2011) PhD thesis; [16] Cardello, L., et al. EGU 2017 poster presentation; [17] Clerc N., et al., Proceedings World Geothermal Congress 2015; [18] Shapiro et al. (2006) DOI:10.1029/2006GL027010; [19] Balmer et al. (2013) DOI: 10.1093/gji/ggt112; [20] Minuetto et al., EGU 2018, Oral presentation.

Mechanical response of Opalinus Clay during CO₂ injection

Alberto Minardi and Lyesse Laloui
 École Polytechnique Fédérale de Lausanne - EPFL

Introduction and motivations

Research of the chair “Gaz Naturel” – Petrosvibri at the EPFL contributes to SCCER-SoE WP1: “DGE and CO₂ sequestration”. WP1 research focuses on problems for future realization of CO₂ storage in Switzerland. The deployment of this technology might play a key role in the future for the decarbonization of fossil energy sources.



The sound characterization of reservoirs and caprocks in Switzerland and the assessment of their potential for CO₂ sequestration is therefore fundamental. In order to grant a safe injection of CO₂ into reservoir formations, the overlaying shaly caprock must perform efficiently.

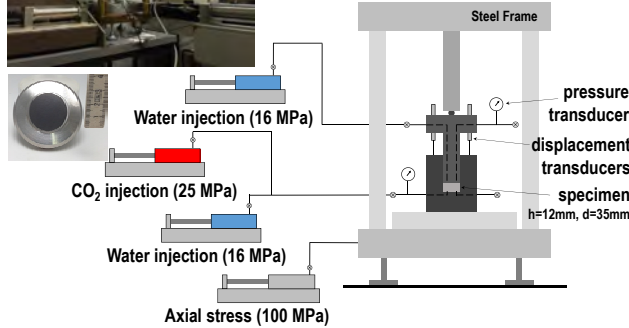
Objectives:

The research activities deal with the assessment of the hydro-mechanical behavior of the Opalinus Clay shale for a safe geological sequestration of carbon dioxide and the identification of the relevant processes related to CO₂ interactions. In particular the presented study focuses on the experimental evaluation of the sealing capacity of the Opalinus Clay shale during CO₂ injection tests for a better quantification of the capillary entry-pressure of the material.

Experimental set-up

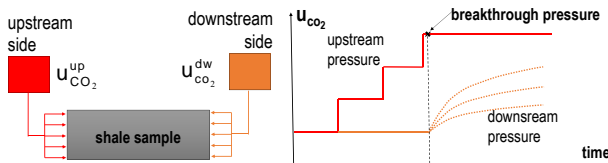


High pressure oedometer cell
 > oedometer conditions (no lateral strain)
 > water and CO₂ injection under constant stress
 > axial LVDTs to monitor displacements



Testing layout and material

- > CO₂ is injected at the upstream side (bottom of the sample) in steps
- > a constant volume reservoir is connected at downstream side
- > CO₂ pressure variations are monitored at the downstream side
- > Shaly Opalinus Clay from Mont Terri URL is tested

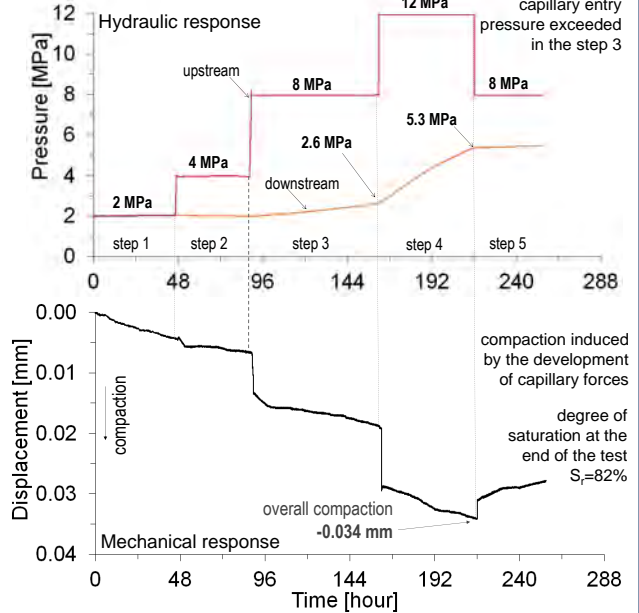


Experimental protocol

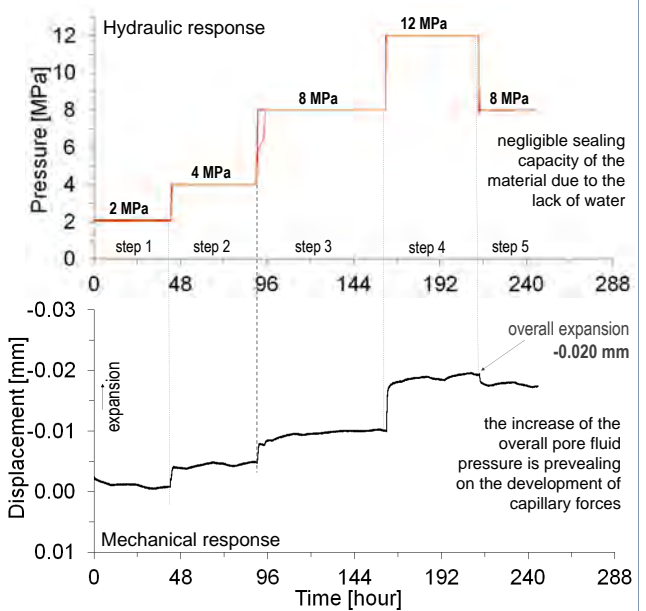
- 1) Samples resaturation with water at constant volume
- 2) Assessment of the hydraulic conductivity (steady state method)
- 3) Consolidation to a target effective stress ($\sigma_a=24$ MPa, $u_w=2$ MPa)
- 4) Initial CO₂ injection at 2 MPa both upstream and downstream side
- 5) CO₂ injection pressure increased at upstream in steps (4, 8, 12 MPa)
- 6) CO₂ injection pressure decreased at upstream side to 8 MPa
- 7) Sample desaturation with free air exposure
- 8) CO₂ injection performed with the same steps of the stages 5 and 6

Experimental results

CO₂ injection in water saturated sample



CO₂ injection in unsaturated sample ($S_r=37\%$)



Summary

- > experimental methodology to evaluate sealing capacity of shale
- > intact Opalinus Clay: capillary entry pressure 2 - 6 MPa
- > mechanical response dependent on water saturation
- > compaction exhibited during injection in saturated sample

The financial support of Swisstopo is acknowledged

- Favero V, Laloui L. (2018) Impact of CO₂ injection on the hydro-mechanical behaviour of a clay-rich caprock. International Journal of Greenhouse Gas Control. 30(71):133-41.
- Makhnenko RY, Vilarrasa V, Mylnikov D, Laloui L. (2017) Hydromechanical aspects of CO₂ breakthrough into clay-rich caprock. Energy Procedia. 1(114):3219-28.

Computerized tomography imaging of fracture aperture distribution and fluid flow within sheared fractures

Quinn Wenning¹, Claudio Madonna¹, Takeshi Kurotori², Claudio Petrini¹, Sayed A. Hosseinzadeh Hejazi², and Ronny Pini²

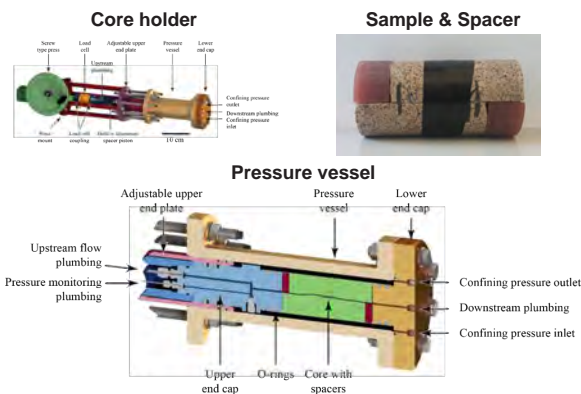
¹Department of Earth Sciences, ETH Zurich, ²Department of Chemical Engineering Imperial College London

1. Introduction

- Knowledge of fracture (aperture) distribution is paramount for sound description of fluid transport in low-permeability rocks.
- In the context of geothermal energy development, quantifying the transport properties of fractures is needed to quantify the rate of heat transfer and optimize the engineering design of the operation.
- Core-flooding experiments coupled with non-invasive imaging techniques (e.g., X-Ray Computed Tomography – X-Ray CT) represent a powerful tool for making direct observations of these properties under representative geologic conditions.
- We coupled the CT imaging with a direct shear apparatus to understand the evolution of fracture aperture with displacement on Westerly granite and Carrara marble.

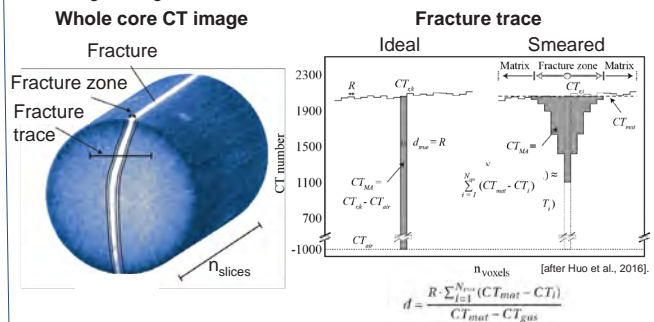
2. Sample preparation and direct shear core-holder

- A single fracture along the Westerly granite and Carrara marble samples was induced via a modified Brazilian test with pointed wedged spacers placed along the top and bottom of the sample.
- Imaging of the fractured sample undergoing direct shear displacement is made possible by a novel X-ray transparent core-holder that was developed and built in-house at ETH Zurich.



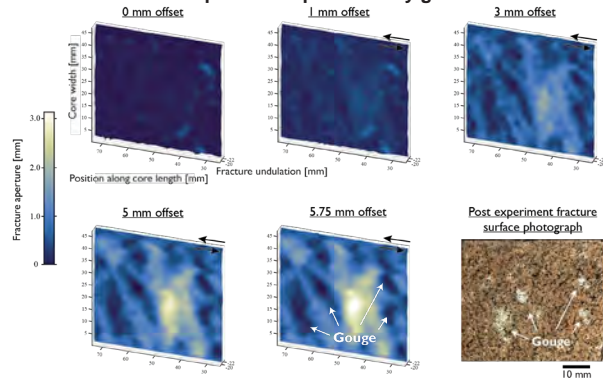
3. Computed tomography methods

- Fracture aperture estimation follows the calibration free missing attenuation method [Huo et al., 2016].
- CT number in the vicinity of a fracture will be reduced due to density deficiency in the gas filled fracture.
- Smearing of the X-ray attenuation due to partial volume effects will cause lower CT numbers adjacent to the fracture.
- Main assumption is that all X-ray attenuation is conserved and that the real CT value of the un-fractured rock can be estimated by neighboring voxels.

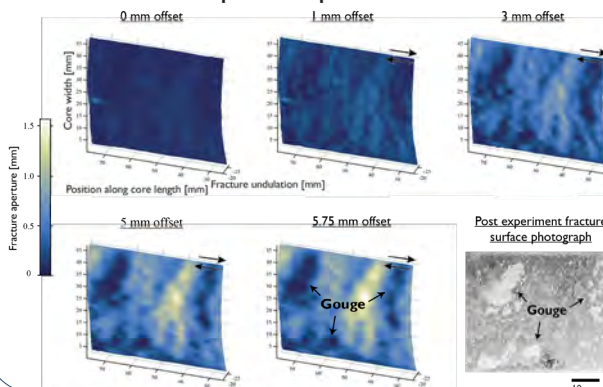


4. Results

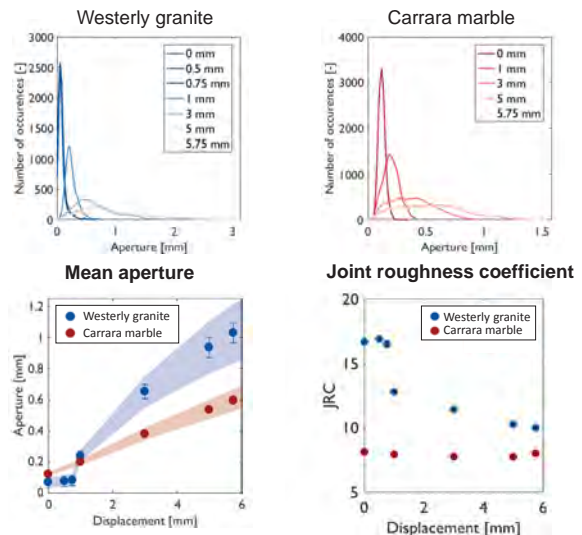
Aperture maps: Westerly granite



Aperture maps: Carrara marble

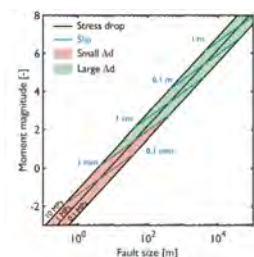


Aperture distribution



5. Conclusions

- We are able to directly image and calculate fracture aperture using CT imaging
- Aperture increases and develops anisotropy with shearing.
- Roughness controls aperture evolution with shearing.
- Minima changes in aperture are expected for (stimulation induced) earthquakes less than ~ 1 M.



Special thanks to: Thomas Mörgele for fabrication of the core-holder, the SASEG Student Grant for partial funding of the core-holder. Reference: Huo et al., 2016. A calibration-free approach for measuring fracture aperture distributions using X-ray computed tomography. Geosphere, v. 12, no. 2.

Effects of thermal stresses on rocks physical properties Insights for monitoring at the field scale

Lucas Pimienta & Marie Violay
Laboratory of Experimental Rock Mechanics, EPFL, Lausanne, Switzerland

Motivation:

Field seismic and electrical resistivity are powerful tools to investigate from the surface geological reservoir rocks at depth.

The two methods are complementary and have been largely used to prospect for oil/gas reservoirs. However, little is still known on the intrinsic dependences of the two properties to the degree of microfracturation (e.g. Pimienta et al., 2017). Moreover, electrical properties have seldom been measured in the high pressure and high temperature range (Violay et al., 2012)

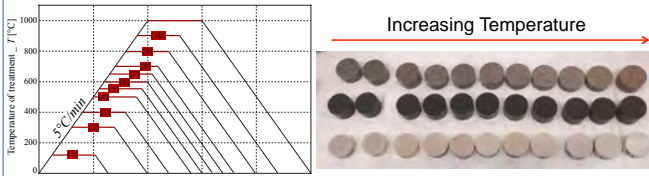
Using thermal treatment at different temperatures, known to induce a variable degree of microfracturation in rocks (e.g. Nasser et al., 2007), the aim of this work is to investigate how the degree of microfracturation affects the physical properties of rocks at both the laboratory and the field scale (e.g. Pimienta et al., 2016).

Project:

- **PROGRESS**: PROspection and PROduction of Geothermal REServoirs
- Understand the links between physical properties in geothermal reservoir rocks.

Samples & Methods:

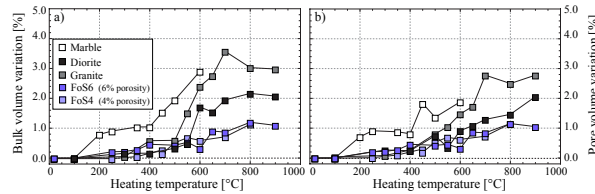
- Approach: Evolution in properties for varying degree of damage
- Thermal treatment in oven for T in the range of [20,1000] °C



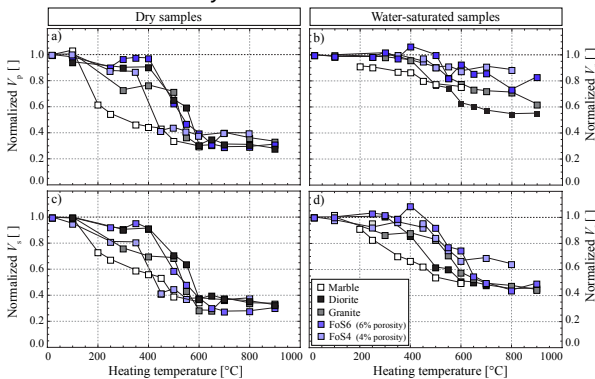
- Rocks samples: (11 for each rock)
 - **Marble** (Carrara) : $\phi = [0.1; 0.3]\%$ // 0% quartz
 - **Diorite** : $\phi = [0.1; 0.3]\%$ // Approx. 30 % quartz
 - **Granite** (Westerly) : $\phi = [0.7; 1.3]\%$ // Approx. 30 % quartz
 - **Sandstones**
 - FoS4 (Fontainebleau): $\phi = [3.8; 4.3]\%$ // 100% quartz
 - FoS6 (Fontainebleau): $\phi = [5.8; 6.3]\%$ // 100% quartz
- Petrophysical characterisation:
 - Pore & Bulk volumes
 - P- & S-wave velocities (frequency of 1 MHz)
 - Electrical impedance (frequency from 0.1 Hz to 100 kHz)

Results

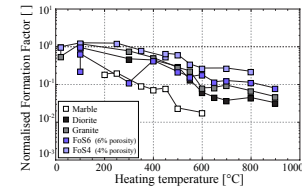
Bulk & Pore volume variations :



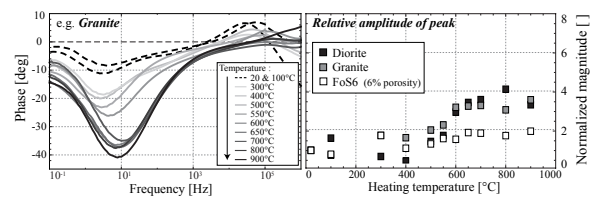
P- and S-wave velocity variations :



Electrical resistivity variations :



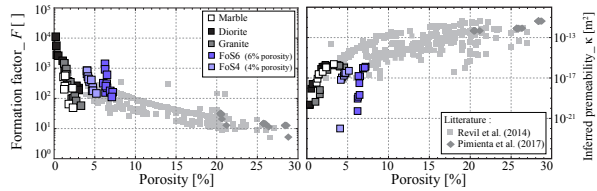
Insights from the electrical impedance measurements :



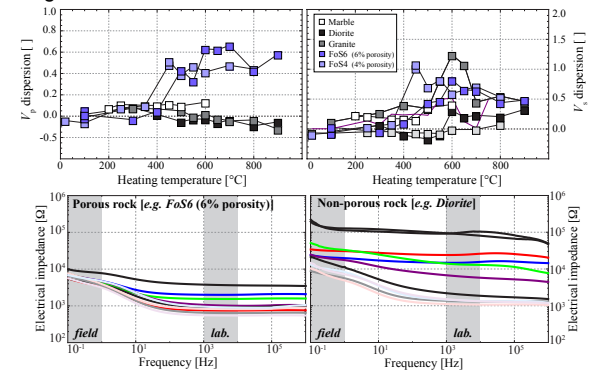
Discussion

Insights on the physics of thermal cracking (lab. scale):

- Dramatic effects of the temperature in rocks, even though temperature rate is kept low
- ⇔ Role of grains anisotropic thermal expansions.
- Variable dependence to the temperature for the different properties, and the different rocks.
- $V_p \Rightarrow$ Crack density \Rightarrow Comparison between transport properties:



Insights for the field scale



- Elastic** ⇔ Strong effects in porous rocks, Little in non-porous ones
- Transport** ⇔ Little effects in porous rocks, Strong in non-porous ones

References

- Nasser, M. H. B., Schubnel, A., & Young, R. P. (2007). Coupled evolutions of fracture toughness and elastic wave velocities at high crack density in thermally treated Westerly granite. *International journal of rock mechanics and mining sciences*, 44(4), 601-616.
- Pimienta L., Sarout, J., Esteban, L., David, C., & Clennell, B. (2017). Pressure-dependent elastic and transport properties of porous and permeable rocks: Microstructural control. *Journal of Geophysical Research*, 122(11), 2169-9356.
- Violay, M., Gibert, B., Azais, P., Pezard, P.A., & Lods, G. (2012). A new cell for electrical conductivity measurement on saturated samples at upper crust conditions. *Transport in porous media*, 91(1), 303-318.
- Pimienta, L., Fortin, J., Borgomano, J.V.M., & Guéguen, Y. (2016). Dispersions & Attenuations in a fully saturated sandstone: Experimental evidence for fluid flows at different scales. *The Leading Edge*, 35(6), 495-501.

Seismic activity caused by drilling in supercritical conditions in the Larderello geothermal field

Riccardo Minetto¹, Domenico Montanari², Thomas Planès³, Marco Bonini², Chiara del Ventisette⁴ and Matteo Lupi³

¹ University of Trieste, Italy. ²National Research Council of Italy, ³University of Geneva, Switzerland, ⁴University of Florence, Italy,

Introduction

Supercritical fluids ($T > 374^{\circ}\text{C}$ and $P > 210$ bar) are an economically attractive resource thanks to their high power-producing potential. One of the most recent attempt to reach supercritical fluids took place in 2017 at the Larderello-Travale geothermal field (LTGF), Italy, with the deepening of the Venelle 2 well. The well did not find supercritical fluids but $T > 500^{\circ}\text{C}$ were measured at 2900 m [1]. To monitor the seismic activity of the ongoing well we deployed 8 seismic stations around the drilling site.

Seismic network

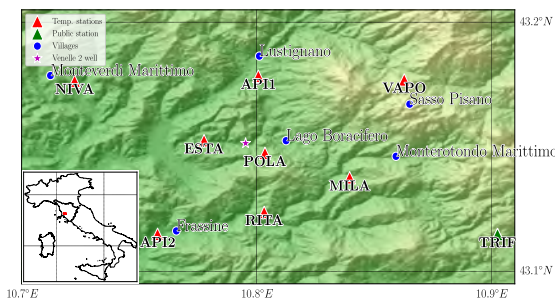


Figure: Map of the study area showing the employed seismic network composed of 9 broadband stations and active from June 2017 to January 2018.

- Acquisition period: 23 June 2017 - 21 January 2018.
- Stations: 8 temporary and 1 permanent (INGV network).
- Instruments: Trillium Compact sensors with period of 20 or 120 s and Data-Cube³ digitizers with sampling frequency of 100 Hz.

Recorded events

On 20 October 2017 the Venelle 2 well experienced a total loss of circulation at 2700 m, with $T > 400^{\circ}\text{C}$ and pressure of 300 bar [1]. Few days after and before such date (between 16-18 October and on 24 October 2017) two swarms were detected.

These events have the following features:

- unclear P and S-waves arrivals;
- low amplitude with values decreasing with increasing distance from the well;
- high similarity, but great variability of the waveforms at different stations;
- almost monochromatic frequency content (7-8 Hz);

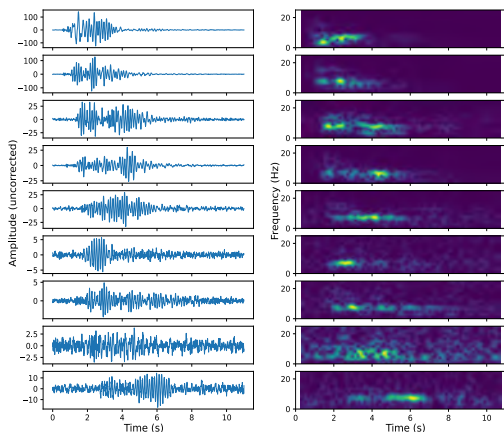


Figure: Seismograms (vertical components) recorded at each station (left) along with the corresponding spectrograms (right).

Temporal evolution

Considering the two swarms, a total of 250 events were distinguished cross-correlating a template and using as threshold a correlation coefficient > 0.8 . In both cases the events occurred in groups with an almost periodic occurrence.

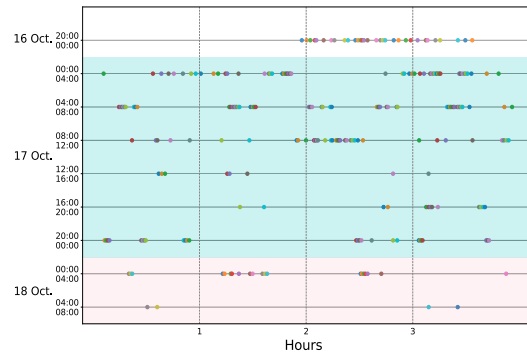


Figure: Temporal evolution of the major swarm recorded from 16 to 18 October 2017. Each dot corresponds to one event (184 in total).

Events location

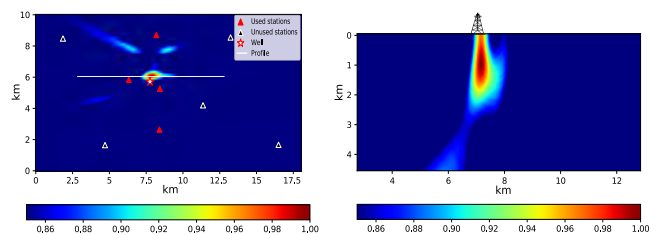


Figure: Swarms location: horizontal slice at 1 km (left) and vertical cross-section (right). The largest values indicate the most likely source location.

The most probable source location has been constrained in the first 2 km below Venelle 2 well. The location was calculated using a method based on cross-correlation [2] supposing a constant velocity of 4 km/s and a straight propagation path.

Discussion and conclusions

- The recorded events have distinctive features reminding LP (low period) events and therefore they may share similar source processes [3], in this case likely related to the presence of geothermal fluids.
- The Venelle 2 well may have played a role in the genesis of the swarms. This theory agrees with the source location of the events, their coincidence with a total loss of circulation and their distinctive characteristics.
- Longer monitoring times may help to understand if the swarms are really related to the well or if they are completely natural expressions in the LTGF.

References

[1] Bertani et al. (2018). The First Results of the DESCRAMBLE Project. 43rd Workshop on Geothermal Reservoir Engineering.
 [2] Ballmer et al. (2013). Ambient seismic noise interferometry in Hawaii reveals long-range observability of volcanic tremor. *Geophysical Journal International*, 194, 512-523.
 [3] Sgatonni et al. (2016). Long-period seismic events with strikingly regular temporal patterns on Katla volcano's south flank (Iceland). *Journal of Volcanology and Geothermal Research*, 324, 28-40.

Contact Information

- Email: minetto.riccardo@gmail.com
- Phone: +39 329 669 8840

Estimation of fracture normal compliance from full-waveform sonic log data

Nicolás D. Barbosa¹, Eva Caspari¹, J. Germán Rubino², Andrew Greenwood¹, Ludovic Baron¹, and Klaus Holliger¹

1- University of Lausanne
 2- CONICET, Centro Atómico Bariloche

Introduction

Fractures can have a predominant influence on the mechanical and hydraulic properties of reservoirs. For this reason, the identification and characterization of fractures is of increasing concern in many domains ranging from the development of hydrocarbon and geothermal reservoirs to the geological storage of CO₂ and nuclear waste. Given that seismic waves propagating through fractured rocks are known to be slowed down and attenuated, seismic methods are valuable for characterizing the hydromechanical behaviour of these environments. In this work, we characterize the mechanical properties of individual fractures from P-wave velocity changes and transmission losses inferred from static full-waveform sonic (FWS) log data.

Experimental background

Static FWS data were acquired at the Grimsel Test Site (GTS) INJ2 borehole using a single transmitter and three receivers at nominal source frequencies of 15 and 25 kHz (Figs. 1 and 2).

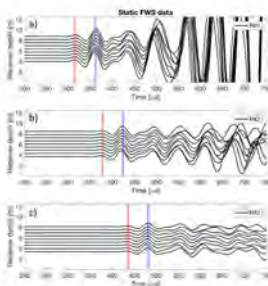


Fig. 1: Sonic log tool with one transmitter (Tx) and three receivers (Rx1, Rx2, Rx3). The offset to the source of the first receiver can be 3 or 6 ft.

Fig. 2: Static FWS data recorded in the upper section of the borehole for receivers (a) Rx1, (b) Rx2, and (c) Rx3. The red and blue vertical lines illustrate the central time of the time windows employed to isolate one and two cycles of the first P-wave arrival, respectively.

Analysis of phase velocity and attenuation from FWS data

Phase velocity: After isolation of the first-arriving P-wave, we determine phase velocities v_p for each interval between receivers (Fig. 3) from the phase difference $\Delta\varphi$ of the corresponding recorded signals

$$v_p(\omega) = \frac{\omega\Delta r}{\Delta\varphi(\omega)} \quad (1)$$

where ω is the angular frequency and Δr the distance between receivers.

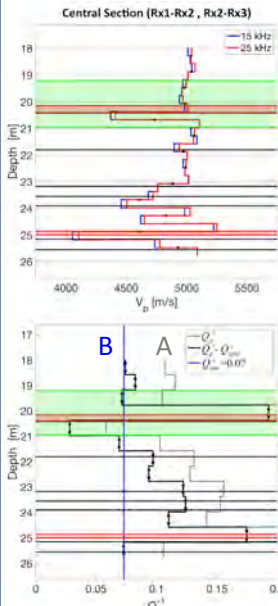


Fig. 3: P-wave velocity for nominal source frequencies of 15 and 25 kHz. The region colored in green corresponds to a shear zone. Horizontal black lines and red layers denote to fractures and dykes, respectively, identified from televiewer images. Notice that fractures can act as planes of mechanical weakness producing significant decreases in the P-wave velocity.

Attenuation: The raw attenuation Q_p^{-1} for a given receiver interval can be computed as

$$Q_p^{-1}(\omega) = \ln \left(\frac{A(\omega, r_i)}{A(\omega, r_{i+1})} \right) \frac{2v_p(\omega)}{\omega\Delta r} \quad (2)$$

where $A(\omega, r_i)$ is the P-wave spectrum at the i th receiver. The attenuation in Eq. 2 can be expressed as

$$Q_p^{-1}(\omega) = Q_{spnd}^{-1}(\omega) + Q_{int}^{-1}(\omega) + Q_{trans}^{-1}(\omega) \quad (3)$$

where $1/Q_{spnd}$, $1/Q_{int}$, and $1/Q_{trans}$ refer to attenuation contributions due to geometrical spreading, intrinsic loss of the host rock, and transmission losses associated with the presence of fractures, respectively.

Fig. 4: Attenuation as a function of depth in the central section of the borehole computed from 25 kHz measurements. Black and grey solid curves correspond to attenuation estimates with and without geometrical spreading correction, respectively. The blue vertical line denotes the mean background intrinsic attenuation ($1/Q_{intr}$ in Eq. 3).

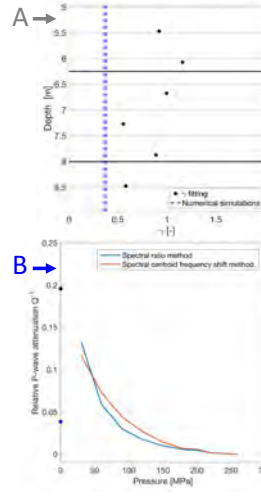


Fig. 5: Geometrical spreading correction. Assuming that, in Eq. 3, the geometrical spreading function defining $1/Q_{spnd}$ can be approximated as $G_r = (1/r)^\gamma$, we use attenuation measurements from different offset configurations (Fig. 1) to estimate the exponent γ . This figure shows γ as a function of depth in the upper section. The blue dashed lines show the range of values of γ estimated from numerical simulations that approximate the borehole environment.

Fig. 6: Background intrinsic attenuation. Relative attenuation estimated from ultrasonic measurements (1 MHz) as functions of applied pressure (data from Wenning et al. (2018)). The reference signal corresponds to that at 260 MPa. Core samples are representative of the host rock of the GTS. Blue and orange curves show the attenuation computed using the spectral ratio and centroid frequency shift methods, respectively. The pressure dependence of Q^{-1} suggest the presence of microcracks. We performed ultrasonic measurements on dry (black dot) and water-saturated (blue dot) samples at ambient conditions, the results of which corroborate this hypothesis.

Effect of individual fractures on the attenuation and phase velocity of sonic waves

The increase of attenuation at the fractures in Fig. 4 is related to transmission losses across them ($1/Q_{trans}$). The P-wave transmission coefficient T of a fracture can be computed as

$$T(\omega) = e^{i(k_p^b - k_p^f)\Delta r} \quad (4)$$

and can be linked to its mechanical compliance Z_N through the linear slip theory

$$Z_N = \frac{2(1-T)}{iT\omega I_b} \quad (5)$$

In Eqs. 4 and 5, k_p^b and k_p^f correspond to the wavenumbers of the background rock and an effective viscoelastic medium representing the fractured section between two receivers, respectively, and I_b is the background impedance.

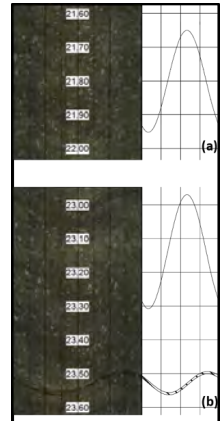
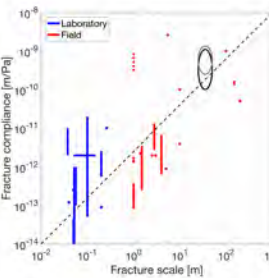


Fig. 7: Televiewer image and its interpretation for the individual fractures in the central section.

Fig. 8: Laboratory (blue) and field (red) fracture compliance values as function of fracture size compiled from the literature. The black and grey ellipses indicate the range of the real components and absolute values of the compliances reported in this work (Eq. 5).

Conclusions

- In this work, we have analyzed the mechanisms contributing to the sonic P-wave attenuation and velocity observed from static FWS log data from a borehole penetrating granodiorite rocks cut by several discrete fractures.
- We have shown that it is possible to compute the P-wave transmission coefficient associated with the presence of a given fracture from the sonic P-wave attenuation due to transmission losses and the corresponding phase velocity between two receivers.
- Our results indicate that the mechanical compliance of the fractures are likely to lie in the range between 1×10^{-10} m/PA and 1×10^{-9} m/PA, which is consistent with the expected values for fractures of the size considered.

Acknowledgements

This work was supported by a grant from the Swiss National Science Foundation and completed within SCCER-SOE with the support of Innosuisse.

Ambient seismic noise tomography of the Geneva basin

Thomas Planès, Anne Obermann, Veronica Antunes, Aurore Carrier, Matteo Lupi

Motivation

- The canton of Geneva is currently strongly promoting the development of geothermal energy [1].
- The lack of exploitation of geothermal energy is in part due to the **lack of knowledge of the subsurface geology**.
- Conventional exploration techniques, such as reflection seismics, present **prohibitive costs** for the geothermal energy sector.
- There is a strong need for **affordable exploration methods** at various depths.
- Unconventional exploration techniques such as deep geoelectrics, gravity, and passive seismics are currently being tested in the Great Geneva Basin (GGB).
- In the present work, we present an application of the passive **Ambient seismic Noise Tomography (ANT)** method in the GGB.
- We aim to retrieve a large scale shear-wave velocity model (V_s) of the basin and to evaluate the potential of the technique for geothermal exploration purposes.

Data and methods

- A temporary seismic network composed of 20 stations was deployed from August 2016 to February 2018 in the GGB (Fig. 1).
- This network aims to: (1) study the local micro-seismicity prior to geothermal-related drilling and injection [2], and (2) perform the ANT shown here.
- The noise correlation technique allows to turn a passive receiver (a seismometer) into a virtual source (Fig. 2) [3].

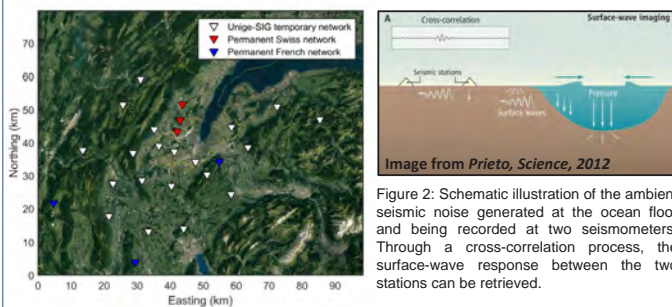


Figure 1: Seismic network used in this study including 20 temporary stations from the University of Geneva (Unige) and the Industrial services of Geneva (SIG), 4 stations from the Swiss permanent network, and 3 stations from the French permanent network.

Figure 2: Schematic illustration of the ambient seismic noise generated at the ocean floor and being recorded at two seismometers. Through a cross-correlation process, the surface-wave response between the two stations can be retrieved.

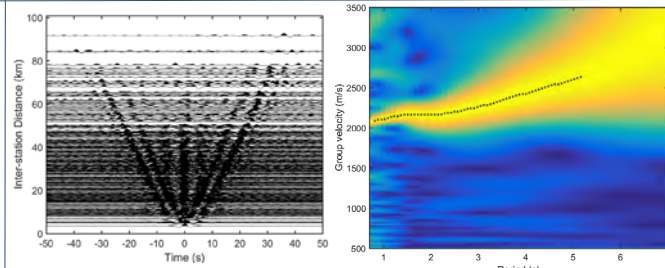


Figure 3: Noise correlation functions ordered by interstation distance showing the retrieval of Rayleigh (surface) waves.

Figure 4: Example of a group-velocity dispersion curve and corresponding picking (dashed line).

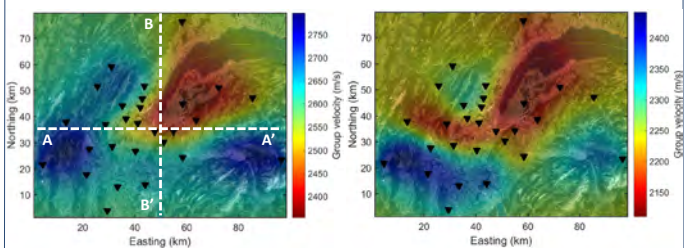


Figure 5: Group velocity maps at periods of 8 s (left) and 4 s (right). A slower velocity (red color) corresponds to softer rocks while a higher velocity (blue color) corresponds to harder rocks. At large periods (eg T=8 s), the velocity pattern is mainly controlled by the basin structure (depth of sediments). At lower periods (eg T=4 s), some observed variations still need to be understood and could be caused by noise-distribution-related biases.

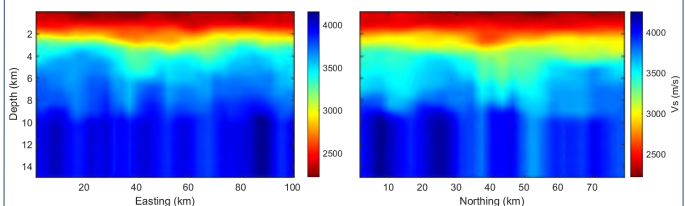


Figure 6: Cross-sections through the retrieved 3D V_s model along profile A-A' (left panel) and along profile B-B' (right panel) marked in Fig. 5. The upper lower-velocity layer in red is related to the geometry of the sedimentary cover.

Discussion and next steps

- Surface wave responses were extracted from ambient seismic noise and allowed to retrieve a large-scale V_s velocity model.
- Eventually, the model will be integrated with other geophysical data to improve our knowledge of the basin.
- Due to the nature of surface waves and to the network “low-density”, the retrieved V_s model is not detailed enough for geothermal exploration purposes.
 - Potential biases induced by a inhomogeneous noise source distribution should be carefully investigated [5].
 - Deploy a dense network and extract body P- (and S-?) waves from ambient noise [6].
 - Take advantage of the upcoming 3D active seismic campaign in Geneva to “ground-truth” and further develop the method.

References

- [1] <http://www.geothermie2020.ch/>
- [2] see the poster of Veronica Antunes
- [3] Campillo and Paul 2003, *Science* **299**:547-549
- [4] Sambridge 2001, *Inverse problems* **17**:3
- [5] Lehujeur 2015, *Geothermal energy* **3**:3
- [6] Nakata 2015, *Journal of Geophysical Research* **120**(2):1159-1173

Results

The ANT comprises the following main steps:

- Cross correlation of the noise traces to retrieve the surface wave responses between stations (Fig. 3).
- Picking the group-velocity dispersion curves (Fig. 4).
- Inversion of 2D group-velocity maps at various frequencies using linear least square inversion (Fig. 5).
- Depth inversion using a guided Monte Carlo approach [4] to retrieve the 3D V_s model (Fig. 6).

**DATA ACQUISITION AND NUMERICAL MODELING
FOR A THERMALLY INDUCED BREAKOUT EXPERIMENT**

Arnaud Rüegg, Reza Sohrabi, Benoît Valley

Centre for Hydrogeology and Geothermics (CHYN), Laboratory of Geothermics and Reservoir Geomechanics, University of Neuchâtel
arnaud.ruegg@unine.ch

Motivation

This research focuses on the thermally induced spalling effect occurring as a result of stress concentration due to excavation in a medium under in-situ stress, combined with thermal expansion of the surrounding material. The Thermally Induced Breakout Experiment (TIBEX) performed at the Grimsel Test Site (GTS) aims to induce borehole failure in a controlled manner, using a borehole heater device by generating thermo-elastic stresses. This methodology mimics breakouts formation in deep wells that form when the rock is recovering its initial temperature after being cooled during the drilling process. The estimation of the needed hoop stress for inducing failure is a key parameter of this study.

Methods

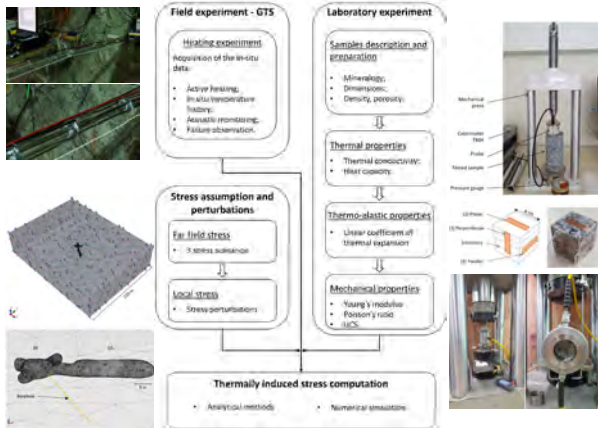


Figure 1: Workflow of the study: Field experiment at the GTS; Stress assumption and perturbations; Laboratory experiment; Thermally induced stress computation.

Theory

Thermo-elastic stress $S_{\Delta T}$ is an important component to assess stress condition and failure at the wall of deep geothermal wells. Thermo-elastic stresses can be approximated by using an analytical solution from Stephens and Voigt [1]:

$$S_{\Delta T} = \frac{\alpha_0 E \Delta T}{1 - \nu} \quad \text{Eq. 1}$$

Superposing it to the stress concentration arising at wellbore wall ($r = a$) using the Kirsch equation allows deriving the total hoop stress at the borehole wall:

$$\sigma_{\theta\theta} = \sigma_H + \sigma_h - 2(\sigma_H - \sigma_h) \cos 2\theta + \Delta P + S_{\Delta T} \quad \text{Eq. 2}$$

Depending on the authors, spalling effect is expected for a stress magnitude at the borehole wall ($\sigma_{\theta\theta}$) between 0.6 to 1 Uniaxial Compressive Strength (UCS) of the rock, although there is no general consensus on the actual wellbore wall strength.

Analytical computation of thermally induced stress

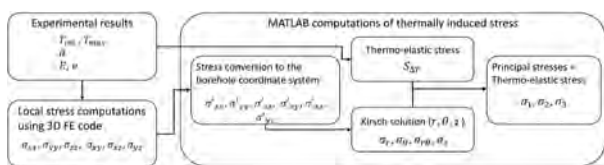


Figure 2: Method for analytical computation of thermally induced stress.

Results

Analytical Computation of Thermally Induced Stress

Stress along the borehole is computed using the analytical solution of Stephens and Voigt [1] and the complete form of the Kirsch solution, for three far-field stress scenarios (Figure 3).

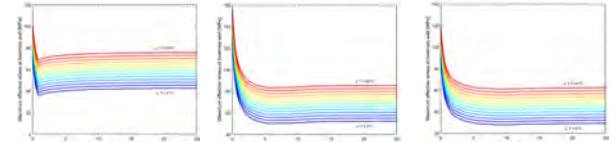


Figure 3: Analytical solution for thermally induced stress.

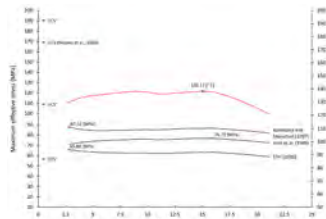


Figure 4: Maximum effective principal stress considering three stress scenarios ([2], [3], [4]), and compared to measured and estimated UCS.

Using the temperature history from the in-situ TIBEX experiment, we computed the maximum effective principal stress acting on the borehole wall (Figure 4).

Numerical simulation of thermo-elastic stresses

Using COMSOL Multiphysics 5.3, we simulated thermo-elastic stress in the surrounding rock of the 15 m depth borehole section (Figure 5).

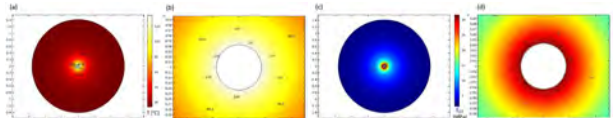


Figure 5: Numerical simulation of: (a), (b) temperature repartition; (c), (d) thermo-elastic stress

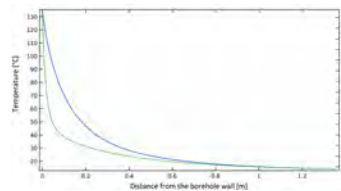


Figure 6: Numerical simulation of thermo-elastic stress (green curve) and temperature (blue curve) around the investigated borehole.

The simulation of the temperature and the induced thermo-elastic stress distribution in the surrounding rock is presented on Figure 6.

Conclusion

The experimental setup and the method used in this study proved their efficiency for heating a borehole of a ΔT of 120° C and reliably computing the induced thermo-elastic stress. The maximum effective principal stress at the borehole wall was estimated in a range between 60 and 80% of the UCS. However, no spalling was observed. This provides some constraints on the minimum wellbore wall strength. Future studies will be performed in higher stress conditions to generate failure.

References

[1] Stephens, G. & Voigt, B. (1982). Hydraulic fracturing theory for conditions of thermal stress. International Journal of Rock Mechanics and Mining Sciences & Geomechanics Abstracts, 19(6), 279-284.
[2] Konietzky, H. & Marschall, P. (1997). Excavation Disturbed Zone around tunnels in fractured rocks-example from Grimsel Test Site, page 235-240, Rotterdam, Balkema.
[3] Pahl, A., Heusermann, S., Bräuer, V. & Glögger W. (1989). Grimsel test site: Rock Stress investigations. Technical Report TR 88-39E, Nagra, Baden.
[4] Ziegler, M., Loew, S. & Amann, F. (2016). Near-surface rock stress orientations in alpine topography derived from exfoliation fracture surface markings and 3D numerical modelling. International Journal of Rock Mechanics and Mining Sciences, 85, 129–151. doi:10.1016/j.ijrmm.2016.03.009.

Penetration depth of meteoric water and maximum temperatures in orogenic geothermal systems

Larryn W. Diamond, Christoph Wanner, H. Niklaus Waber
Rock–Water Interaction, Institute of Geological Sciences, University of Bern

Motivation

Orogenic belts without active igneous activity are recognized as plays for geothermal energy. In these systems, meteoric water circulation is typically expressed by thermal springs discharging at temperatures up to 70 °C from deep-reaching faults. The hydraulic gradients that drive circulation arise from the conjunction of high orographic precipitation, mountainous topography and permeable faults that link topographic highs with valley floors via the hot bedrock. Since the bedrock geotherm is the only source of heat for the circulating water, its maximum depth of penetration defines the maximum temperature attainable by surface springs and their upflow zones, thereby setting limits on their potential for geothermal energy exploitation. In the framework of the SCCER-SoE Task 1.1 we have performed geochemical modeling on chemically and isotopically well-characterized thermal waters currently discharging from the orogenic geothermal system at Grimsel Pass (Switzerland) to unravel the maximum penetration depth of meteoric water in such systems.

The Grimsel Pass geothermal system

- Discharge of warm springs with $T \leq 28$ °C into a gas tunnel beneath Grimsel Pass
- The springs occur where the tunnel intersects the WSW–ENE-striking Grimsel Breccia Fault (GBF), a major regional strike-slip shear zone
- Stable water-isotope analyses reveal a meteoric fluid origin
- Hydrothermal activity is also manifested by 3 million year old hydrothermal breccias formed ~2 km below the paleosurface
- Fluid inclusions in quartz and adularia indicate breccia formation at 165 °C (Hofmann et al., 2004)

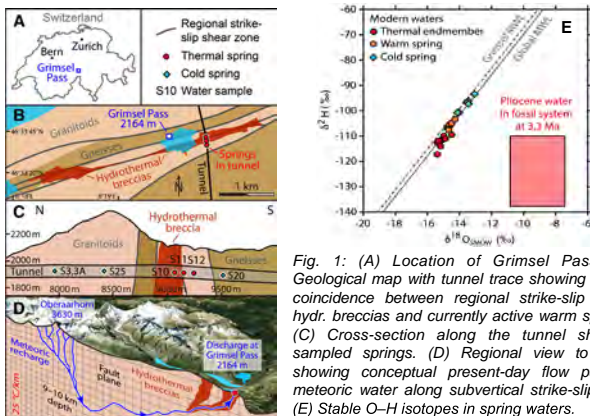


Fig. 1: (A) Location of Grimsel Pass. (B) Geological map with tunnel trace showing spatial coincidence between regional strike-slip faults, hydr. breccias and currently active warm springs. (C) Cross-section along the tunnel showing sampled springs. (D) Regional view to NNW showing conceptual present-day flow path of meteoric water along subvertical strike-slip fault. (E) Stable O–H isotopes in spring waters.

Approach

- Chemical and isotopic analyses of cold and warm springs
- Correction for admixture of modern surface water using ^3H , Na and Cl
- Numerical simulation (1D) of chemical evolution of thermal water as it rises and cools from its maximum penetration depth
- Assumption of chemical equilibrium between thermal water and granitic host rock at the lower model boundary (quartz + albite + muscovite + microcline)
- Dissolution reactions during upflow suppressed at T defined by Na/K ratio ($= \text{min-}T_{\text{eq}}$)
- Precipitation reactions during upflow suppressed at T defined by silica geothermometer ($T_{\text{qtz}}=174$ °C), as this matches reconstructed SiO_2 conc. in warm springs
- Iterative determination of deep fluid temperature ($\text{min-}T_{\text{eq}}$) by comparing simulated with observed geothermal endmember composition at tunnel level

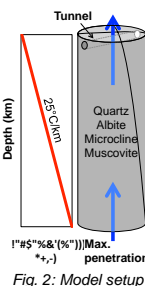


Fig. 2: Model setup

Reconstruction of the geothermal endmember water

- All warm springs show a detectable ^3H activity, despite the inferred residence time of 30 ka (Waber et al., 2017)
- Further, they show a strong linear correlation between Na and Cl
 - Represents a mixture of an old geothermal water with a modern cold water (Waber et al., 2017)
- Cold water fractions were reconstructed using coupled binary mixing models for Na, Cl and ^3H , while assuming that the thermal water is ^3H free (minimisation of uncertainty)
- Indicates cold water fractions of 50–70% in the various spring samples
 - Allows the composition of the geothermal endmember water to be determined at the tunnel level

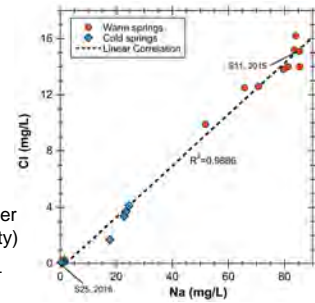


Fig. 3: Linear relationship between Na- and Cl-concentrations observed in warm and cold springs.

Results of geochemical modeling (TOUGHREACT V3)

- The Na/K ratio of the thermal water at depth is controlled by the following temperature-dependent equilibrium:
 $\text{Albite} + \text{K}^+ = \text{Microcline} + \text{Na}^+$
- Precipitation of small amounts of microcline and muscovite during upflow does not significantly change the Na/K ratio
- Setting $\text{min-}T_{\text{eq}}$ to 214 °C explains the observed composition of the geothermal endmember water at the tunnel level
- As chemical equilibrium likely prevails along the hottest and deepest section of the flow path, the max. temperature is very probably 230–250 °C
- The local 25 °C/km geotherm is the only heat source. Attainment of 230–250 °C therefore requires a penetration depth of at least 9–10 km
- The Grimsel Pass system is unusually favorable for application of the Na–K solute geothermometer (cf. Giggenbach, 1998)
 - Similar penetration depths are possible at other orogenic geothermal systems worldwide

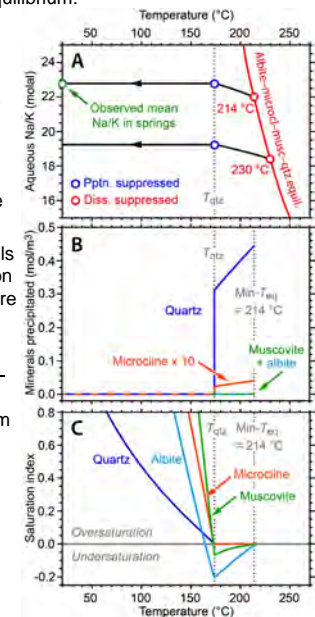


Fig. 4: Numerical simulation of the chemical evolution of the thermal water upon upflow and cooling. (A) The observed Na/K ratio of the thermal endmember water at its discharge site is reproduced if the minimum temperature of equilibrium between the water and its wall rock ($\text{min-}T_{\text{eq}}$) is set at 214 °C. (B) Amounts of minerals precipitated in a nominal 40 year period of upflow in mol per m^3 of porous rock. (C) Saturation indices normalized to the amount of Si in each mineral.

Conclusions

- This study provides robust evidence that in the Grimsel Pass geothermal system, meteoric water has penetrated at least 9–10 km deep into the continental crust to attain 230–250 °C.
- Far more enthalpy may be accessible for exploitation around the upflow zones of orogenic geothermal systems than previously thought.!

References

Giggenbach, W.F. 1998. *Geochimica et Cosmochimica Acta* 52. 2749-2765. Hofmann, B. A. et al. 2004: *Schweizerische Mineralogische und Petrographische Mitteilungen* 84, 271-302. Waber, H.N. et al. 2017. *Procedia Earth and Planetary Science* 17. 774-777.

How can the borehole three-dimensional displacement data help improving in situ stress estimation across a fault reactivated by fluid injections?

Maria Kakurina¹, Yves Guglielmi², Christophe Nussbaum³ and Benoit Valley¹

(1)University of Neuchâtel, CHYN, Neuchâtel, Switzerland, (2) Lawrence Berkeley National Laboratory, Berkeley, CA, United States, (3)Swisstopo, Wabern, Switzerland

Introduction

Standard in-situ stress measurement methods using fluid injection in deep boreholes are based on the analyses of pressure, flowrate and post-injection fracture mapping. Here we apply a new methodology to improve the estimation of the in-situ stress by adding the record of three-dimensional (3D) displacement in the pressured interval measured continuously during the injection. The direct measurement of displacements corresponding to slip on reactivated faults appear as a critical information to obtain the orientations and relative magnitudes of the principal stress components. Here we investigate and compare the data from two fault reactivation experiments conducted in carbonate rocks at the Rustrel Low Noise Underground Laboratory (LSBB URL), France, and in shale rocks at the Mont Terri Underground Laboratory, Switzerland. Both experiments consisted of fluid injections into the fault damages zone to reactivate the fault planes and trigger the slip, which will be used for solving the stress inverse problem.

Experimental and geological settings

The experiments protocol followed the step-rate injection method for fracture in-situ properties (SIMFIP) developed by Guglielmi et al. (2013). In comparison to standard double packer probes, the SIMFIP probe allows measuring the 3D displacement in the injection chamber together with the fluid pressure and flowrate. In both underground laboratories we performed pressure step-rate tests to activate a fault at different depths and different geological intervals (Figure 2). The experimental zone in carbonates includes the fractured damage zone of a natural fault. The experiment in Mont Terri has been conducted by injecting fluids in the upper, middle and lower parts of the main tectonic structure of the Opalinus Clay, called the Main Fault.

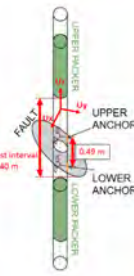


Figure 1. SIMFIP probe setup

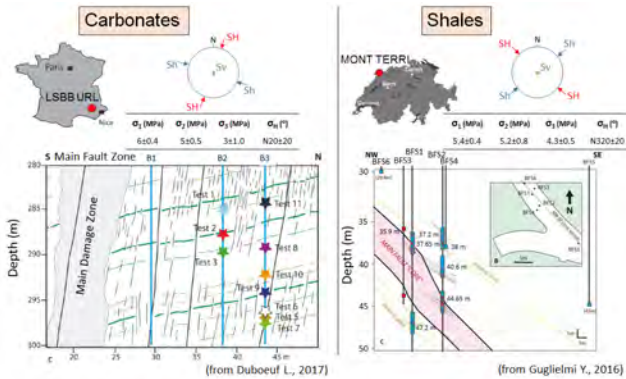


Figure 2. The experimental sites: left column – Rustrel LSBB URL, b) right column – Mont Terri URL. For each of the sites, there is an experimental location, far-field stress orientations and magnitudes, and cross sections showing the different testing intervals and simplified geology. Stars represent the 10 injection intervals.

Results

The maximum pressure in test 8 is 5.2 MPa, and in test 37.2 - 6.2 MPa (Figure 3a). There is a linear flowrate-vs-pressure increase until 4.8 MPa in test 8 and 5.6 MPa in test 37.2 followed by a non-linear variation (Figure 3b). This pressure corresponds to the point when there is a significant increase in flowrate associated with a large displacement variation independently from pressure – Fault Opening Pressure (FOP). Below the FOP, the displacement linearly varies with pressure and correspond to the borehole expansion as well as to the poro-elastic response of the fracture. Above the FOP, the displacement shows independent non-linear response to pressure and a residual displacement is observed at the end of the test. We pick the displacement vectors when the pressure is “constant” in the interval. There are eight vectors in test 8 (carbonates) and seven vectors in test 37.2m (shales). The direction of the displacement vectors is given in Figure 4. The displacement vectors 1 to 4 in carbonates are aligned with the elastic response of the chamber that was observed below the FOP and orientated WNW.

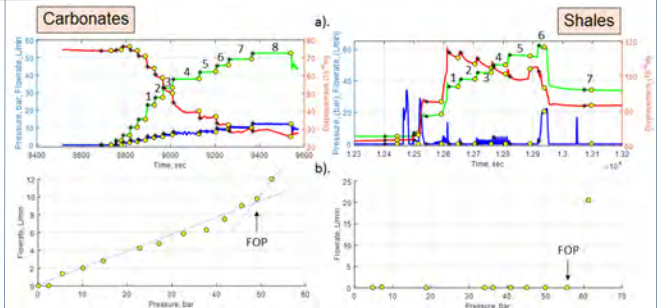


Figure 3. Protocol of the high-pressure step-rate test monitored during Test 8 in carbonates (left column) and Test 37.2 in shales (right column). (a) – Pressure (green), Flowrate (blue), Displacements (red) versus Time. Black asterisk and yellow circle are picked at each constant pressure step and correspond to the beginning and the end of the investigated (displacement) vector. (b) - Injected flowrate versus pressure (points correspond to the end on investigated vector).

At 4.8 MPa the displacement vector 7 shows a N310° dip direction and a 70° dip angle which are significantly different from the elastic response of the chamber. It is observed in Figure 4 that the vector 7 aligns with the fracture N135-72°. It is interpreted as pure shear slip on that reactivated plane. The vectors 1 to 4 are located close to the pole of the fracture, interpreted as it is initial borehole opening. Vectors 5 and 6 correspond to the change between two directions and the vector 8 to the dilation of the activated plane. The displacements in test 37.2 m show more complex reorientations than in test 8. The displacement vectors mainly show almost normal opening of the bedding planes with a slight strike component. This is in a good accordance with the not-so-favorable orientation of the planes towards stress.

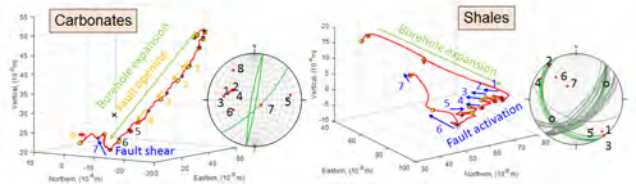


Figure 4. Orientations of the 3D displacement for carbonates (left) and for shales (right). Red asterisks correspond to the orientations of the displacement vector from the 3D plot. Black circles correspond to the potential fault slip under the far-field stress state. Green planes correspond to the planes located in the interval of the deformation unit of the SIMFIP probe.

Conclusions

In this study, we develop a protocol of how to estimate the in-site stress using the 3D displacement data obtained from the fault reactivation experiments. First, it was observed that the data obtained from shales is more complex. This may be caused by the difference in permeability and plasticity between carbonates and shales. However, it clearly appears that the activated fractures identified from the displacement measurements of both shales and carbonates match reasonably well with the stress tensors. Indeed, the fractures which are most favorably oriented towards the far-field stress are the ones which are identified from the analysis of the displacement vectors. Moreover, these vectors are useful in identifying the FOP, which can be consistent with the normal stress on the activated fracture. These data are then to be used to solve the reverse stress problem to estimate the in-situ stress. However, more work is required to estimate the range of the in-site stresses for all the tests, especially on the unicity of the solution using both the critical pressure values and the displacement vectors to estimate both the minimum and the maximum horizontal stress.

References

Duboeuf, L., De Barros, L., Cappa, F., Guglielmi, Y., Deschamps, A., & Seguy, S. (2017). Aseismic motions drive a sparse seismicity during fluid injections into a fractured zone in a carbonate reservoir. *Journal of Geophysical Research: Solid Earth*.
Guglielmi, Y. (2016). Mont Terri Project. Technical note 2015-60. Phase 21. In-situ clay faults slip hydromechanical characterization (FS experiment), Mont Terri underground rock laboratory.
Guglielmi, Y., Cappa, F., Lançon, H., Janowczyk, J. B., Rutqvist, J., Tsang, C. F., & Wang, J. S. Y. (2013). ISRM suggested method for step-rate injection method for fracture in-situ properties (SIMFIP): Using a 3-components borehole deformation sensor. In *The ISRM Suggested Methods for Rock Characterization, Testing and Monitoring: 2007-2014* (pp. 179-186). Springer International Publishing.

Estimating fracture apertures and related parameters using tube-wave data

Jürg Hunziker, Andrew Greenwood, Shohei Minato, Eva Caspari and Klaus Holliger

Introduction

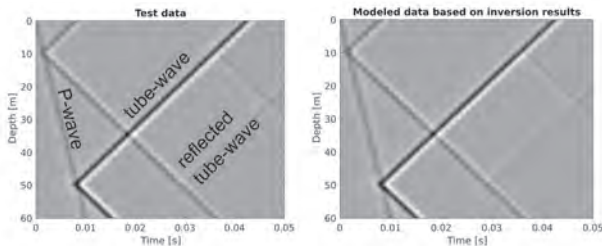
Fractures are only detected by televiewers if their aperture is above a resolution-dependent threshold. Furthermore, the inferred aperture is only representative within the immediate vicinity of the borehole. Tube-waves are interface waves, which are created at fractures and propagate along the borehole wall. Here, we use tube-waves to estimate the effective hydraulic fracture aperture, which is an average aperture related to the fluid content within the fracture. Furthermore, we also estimate the fracture compliance and the formation moduli.

Method

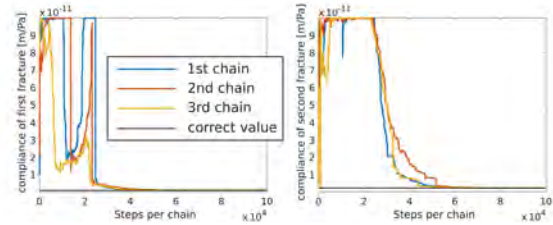
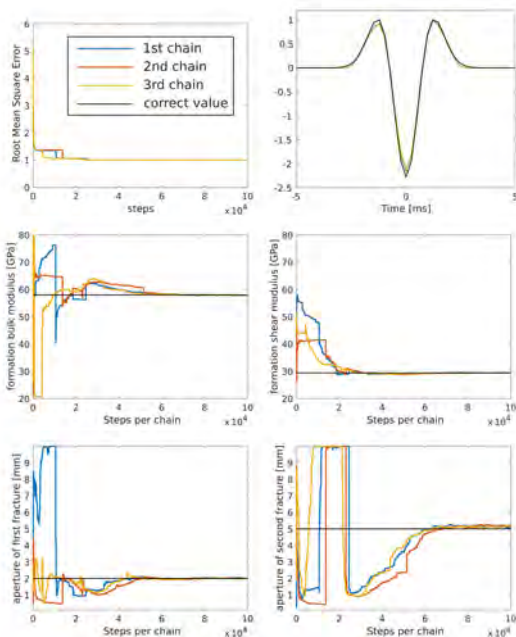
Full-waveform vertical seismic profiling (VSP) data serves as input for our stochastic inversion algorithm to infer the fracture parameters, the formation moduli, the standard deviation of the data error and the shape of the source-wavelet. As a forward solver we use the semi-analytical model derived by Minato and Ghose (2017). To sample the posterior distribution we use the DREAM(ZS) algorithm (ter Braak and Vrugt, 2008; Laloy and Vrugt, 2012), which is an efficient Markov chain Monte Carlo algorithm using differential evolution and parallel interacting chains to achieve faster convergence.

Results: Synthetic data with Gaussian noise

The test data were contaminated with Gaussian random noise. The depth of the fractures (10 and 50 m) and their inclination (10 and 45°) are assumed to be known from televiewer data. The receiver spacing is 0.1 m.

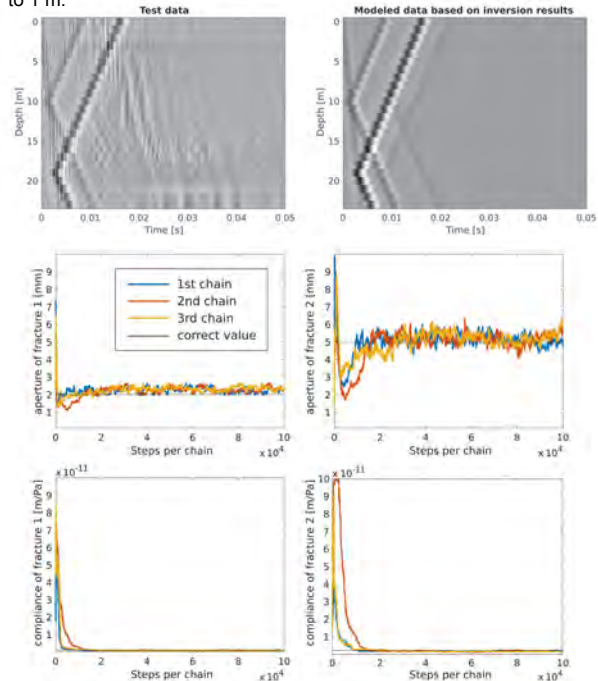


Results of the Markov chain Monte Carlo inversion. The weighted root mean square error and six unknowns estimated by the inversion are shown as functions of forward simulation steps. The estimates of the wavelet shown are samples taken from the end of the Markov chains.



Results: Synthetic data with real noise

The synthetic test data were contaminated with real noise measured at the Grimsel Test Site in Switzerland. The fractures are located at 10 and 19 m depth. The receiver spacing has been increased from 0.1 m to 1 m.



Conclusions

- The proposed tube-wave inversion approach allows to reliably estimate the fracture aperture, fracture compliance and the formation moduli.
- If the source wavelet is estimated incorrectly, the estimates of the remaining parameters are biased.

Outlook

- More reliable estimation of the source wavelet.
- Apply the algorithm on real data from the Grimsel Test Site in Switzerland.
- Longer Markov chains will allow to compute marginal posterior distributions of the unknowns.

References

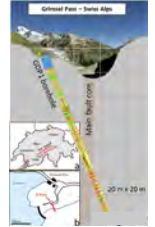
• Laloy, E., & Vrugt, J. A., 2012: High-dimensional posterior exploration of hydrologic models using multiple-try DREAM(ZS) and high-performance computing, *Water Resources Research*, 48, WO1526.
 • Minato, S. & Ghose, R., 2017: Low-frequency guided waves in a fluid-filled borehole: Simultaneous effects of generation and scattering due to multiple fractures, *Journal of Applied Physics*, 121, 104902.
 • ter Braak, C. J. F., & Vrugt, J. A., 2008: Differential evolution Markov Chain with snooker updater and fewer chains, *Statistics and Computing*, 18, 435–446.

Characterization of the fracture network in the damage zone of a shear fault with geophysical borehole methods

Eva Caspari¹, Ludovic Baron¹, Andrew Greenwood¹, Enea Toschini¹, Daniel Egl² and Klaus Holliger¹
¹University of Lausanne and ²University of Bern

Introduction

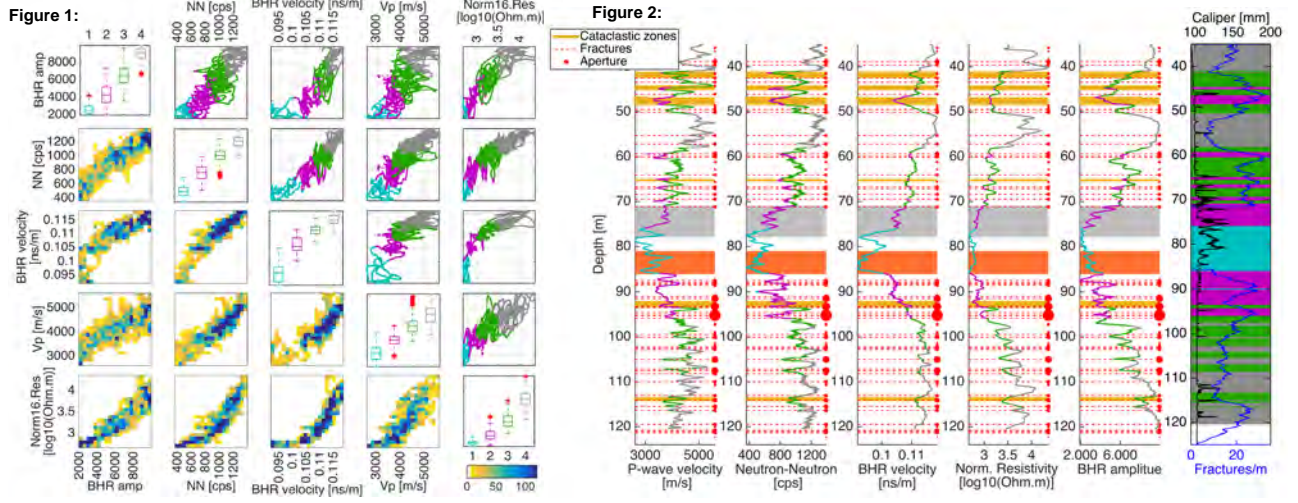
Hydrothermally active shear zones in crystalline rocks are considered potential analogs for petrothermal reservoirs. The shear zone of interest in this study is the Grimsel breccia fault (GBF), a major WSW-ENE striking sub-vertical ductile shear zone in the Southwestern Aar Granite. The GBF has been exhumed from 3-4 km depth, is brittlely overprinted and exhibits fossil and active hydrothermal activity. A shallow borehole was drilled in 2015, which acutely intersects the main fault core and is situated in its damage zone. The focus is the characterization of the fracture network in the damage zone from geophysical borehole data. We employ geophysical logs to analyse fine-scale petrophysical variations, borehole radar (BHR) to image the fracture network and self-potential and fluid resistivity logs to examine the hydraulic system. To verify the observations we utilize the structural characterization of Egl et al. (2018).



Petrophysical properties: Cluster analysis

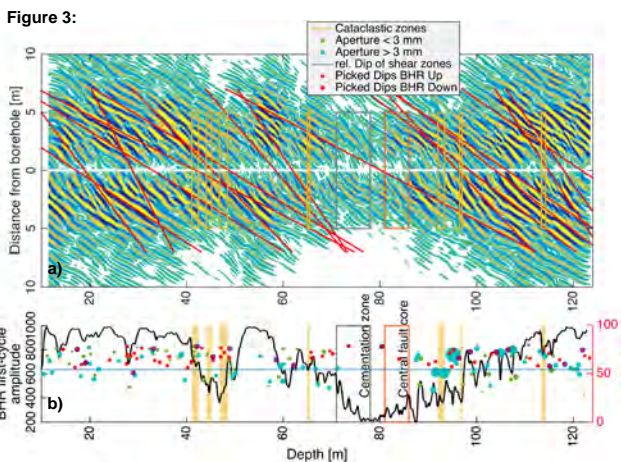
A simple cluster analysis of some of the well logs (Figure 1) and a comparison (Figure 2) to the deformation data from the optical televiewer (OTV) shows that the response of the well logs and thus the variations in petrophysical properties are predominantly driven by the brittle deformation. As a result, the petrophysical properties can be categorized by four groups with varying intensity of brittle deformation.

- Cluster groups:
1. Main fault core
 2. Intensely fractured/Cataclastic
 3. Highly fractured/ Large aperture fractures
 4. Moderately fractured



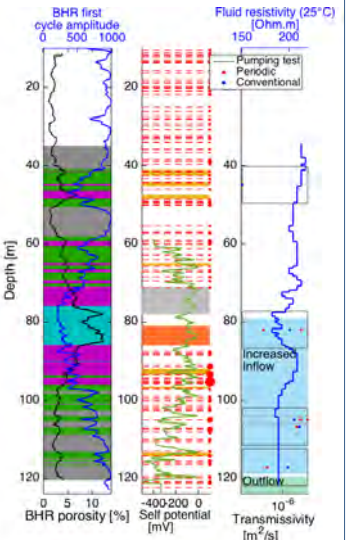
Fracture network: BHR and OTV

The migrated BHR image reveals a network of intersecting reflectors in the damage zone surrounding the main fault core (Figure 3a). A comparison of selected picked reflector dips with fractures dips from the OTV show a good agreement (Figure 3b) and thus, allows to link the reflections to fluid-filled fractures and cataclastic zones. The reflectors can be tracked a few meters into the formation in zones with low signal attenuation, which are indicated by the BHR first-cycle amplitude.



Hydraulic characteristics

The fracture network and cataclastic zones are the main flow pathways of the system. The self-potential data (Figure 4) contains an abundance of anomalies with varying magnitude, which can be linked to fractures and are likely to be of electrokinetic origin. As such they are indicative of zones of in- and out-flow into the borehole. Further, the fluid resistivity shows a distinctive layering. This may suggest the inflow of water from different sources and a compartmentalized system. The latter is supported by findings of Cheng et al. (2018) from pumping test. Their estimates of transmissivity are shown in Figure 4.



References

Cheng, Y. and J. Renner (2018), Exploratory use of periodic pumping tests for hydraulic characterization of faults. *Geophysical Journal International* 212(1), 543-565.
 Egl, D., Baumann, R., Küng, S., Berger, A., Baron, L. and M. Herwegh (2018), Structural characteristics, bulk porosity and evolution of an exhumed long-lived hydrothermal reservoir. *Tectonophysics* in submission



Attenuation and velocity anisotropy of stochastic fracture networks

Eva Caspari¹, Jürg Hunziker¹, Marco Favino², J. Germán Rubino³ and Klaus Holliger¹
¹University of Lausanne, ²Università della Svizzera italiana and ³CONICET, Centro Atómico Bariloche - CNEA, Argentina

Summary

Fracture networks tend to have preferential orientations, which in turn translate into anisotropy of the seismic velocity and attenuation. An attenuation mechanism of interest is fluid pressure diffusion due to its potential sensitivity to fracture network characteristics. There are two manifestations of the mechanism: fracture-to-background wave induced fluid flow (FB-WIFF) and fracture-to-fracture wave induced flow (FF-WIFF). In this study, we use a quasi-static poroelastic numerical upscaling procedure (Rubino et al. 2016, Favino et al. 2018) to model the aforementioned mechanism for anisotropic stochastic fracture networks with varying length distributions and fracture densities. The aim is to systematically analyse the dependence of the resulting attenuation and velocity anisotropy with regard to these network characteristics. Here we present preliminary results.

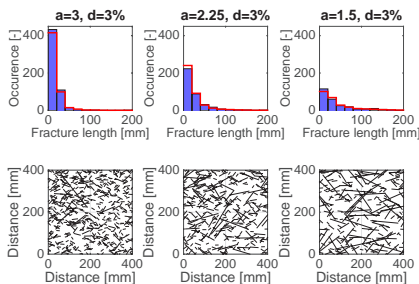
References

M. Favino, J. Hunziker, E. Caspari, B. Quintal, K. Holliger, R. Krause (2018), Fully-automated adaptive mesh refinement for the simulation of fluid pressure diffusion in strongly heterogeneous media, *submitted to Journal of Computational Physics*.

J. G. Rubino, E. Caspari, T. M. Müller, M. Milani, N. D. Barbosa, K. Holliger (2016), Numerical upscaling in 2-D heterogeneous poroelastic rocks: Anisotropic attenuation and dispersion of seismic waves, *Journal of Geophysical Research: Solid Earth*, 121, 6698-6721.

Anisotropic fracture networks

The fracture dip is limited to angles between 30° and 150°, where 0° denotes a vertical fracture and 90° a horizontal one. The characteristic exponent a defines the steepness of the distribution and d is the area covered by fractures.



Network parameters	
Exponent a	1.5 - 3
Length [mm]	10, 200
Fracture area d [%]	1.5 - 3.25
Aperture [mm]	0.5
Simulations per set	25

Velocity and attenuation as function of angle and frequency ($a = 1.5$)

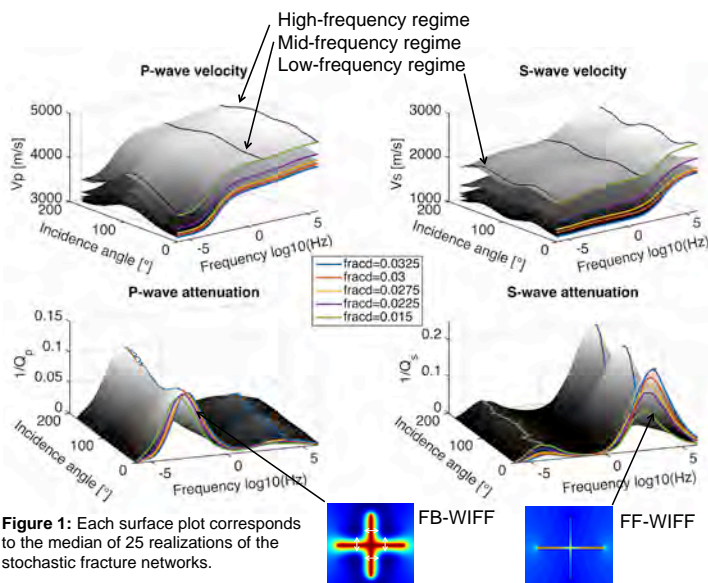


Figure 1: Each surface plot corresponds to the median of 25 realizations of the stochastic fracture networks.

Attenuation anisotropy

For P-waves, the attenuation anisotropy rotates by 45° between FF-WIFF and FB-WIFF. This is not the case for S-waves. In general, the attenuation increases with fracture area d and the exponent a . An exception is FF-WIFF for S-waves.

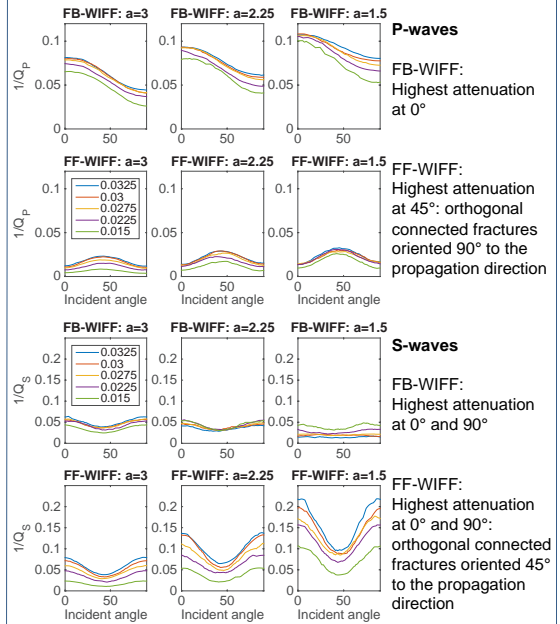


Figure 2: Variation of attenuation with incidence angle at the peak frequencies of FB-WIFF and FF-WIFF.

Velocity anisotropy

Overall, the velocity anisotropy is larger for P- than S-waves. For P-waves, the anisotropy is highest in the low-frequency regime and, in general, decreases with a decrease in the exponent a . Contrarily, for S-waves, the anisotropy tends to be higher in the high-frequency regime and increases with a decrease in the exponent a .

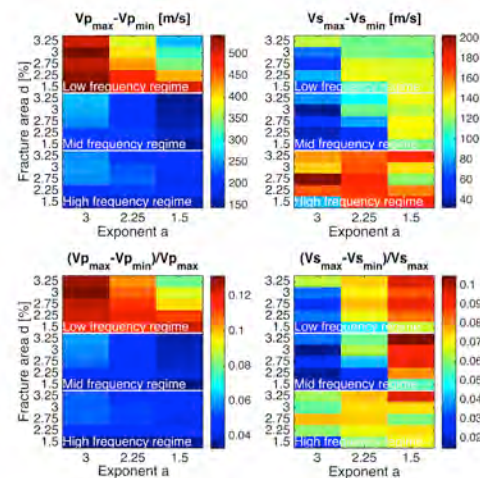


Figure 3: Maximum absolute and relative angle-dependent velocity change for three characteristic frequency regimes.

Seismic attenuation and P-wave modulus dispersion in poroelastic media with fractures of variable aperture distributions

Simón Lissa¹, Nicolás D. Barbosa¹, J. Germán Rubino², & Beatriz Quintal¹

¹ Institute of Earth Sciences, University of Lausanne, Switzerland.
² CONICET, Centro Atómico Bariloche - Comisión Nacional de Energía Atómica, Argentina.

Introduction

Fractures in rocks occur in a wide range of scales and their identification and characterisation are important for several areas such as oil and gas exploration and extraction, production of geothermal energy, nuclear waste disposal, civil engineering works, among others. Given that seismic waves properties are significantly affected by the presence of fractures, seismic methods are a valuable tool for characterising them. In particular, when a fluid-saturated fractured rock is compressed by a propagating wave, a pressure gradient is generated due to the compressibility contrast between the fracture and the embedding background. Consequently, energy dissipation occurs during the corresponding fluid pressure equilibration process. This mechanism can be an important cause of seismic wave attenuation and stiffness modulus dispersion. In this work we numerically quantify the effects of contact areas on seismic wave attenuation and P-wave modulus dispersion using 3D models containing a horizontal fracture.

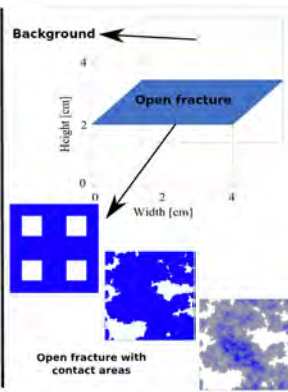


Methodology

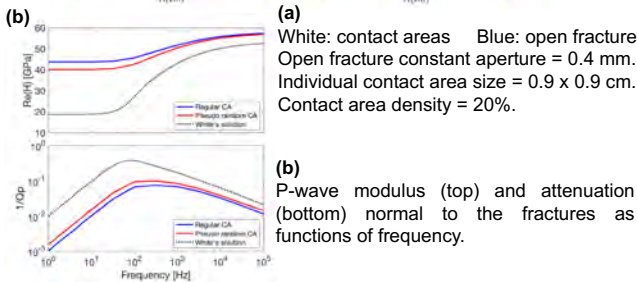
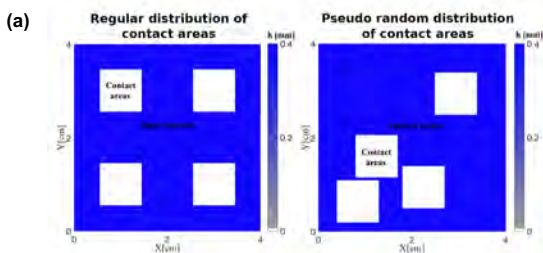
- Biot's (1941) equations in the $u-p$ formulation.
- Solved using finite element method.
- Relaxation test normal to the fracture (undrained conditions).
- Water saturated.

Material properties:

	Background (oil contact area)	Open fracture
Grain bulk modulus (GPa)	$K_1=37$	$K_2=37$
Grain density (g/cm^3)	$\rho_1=2.65$	$\rho_2=2.65$
Porosity	$\phi_1=0.1$	$\phi_2=0.9$
Permeability (mD)	$k_{10}=2.37$	$k_{20}=10^6$
Dry rock bulk modulus (GPa)	$K_{10}=26$	$K_{20}=0.02$
Dry rock shear modulus (GPa)	$\mu_{10}=80$	$\mu_{20}=0.01$
Fluid bulk modulus (GPa)	$K_f=2.23$	$K_f=2.23$
Fluid density (g/cm^3)	$\rho_f=1.00$	$\rho_f=1.00$
Fluid viscosity (P)	$\eta_1=0.01$	$\eta_2=0.01$



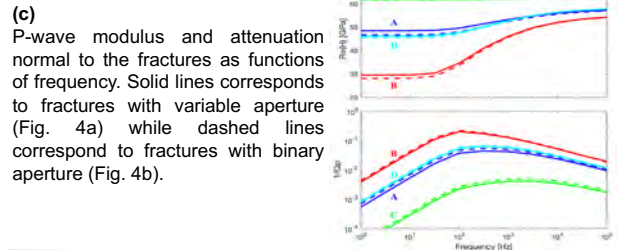
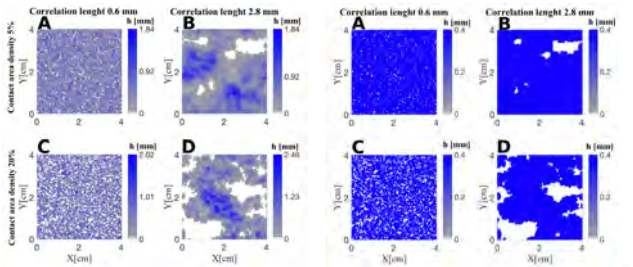
Effects of contact areas



Regular distribution → - Attenuation
 - Fracture excess compliance
 Pseudo random distribution → + Attenuation
 + Fracture excess compliance

Realistic aperture distributions

- (a) Fracture models with variable aperture. All models have a mean aperture of 0.4 mm.
- (b) Fracture models with binary aperture distribution. The aperture in the open fracture zone is set to the mean aperture.



Comparison between realistic and simplified fracture models

P-wave modulus and attenuation normal to the fractures as functions of frequency. Solid lines correspond to models with variable aperture distributions (Fig. 4a). Dashed lines correspond to models with open fracture zones with constant aperture and without contact areas but using equivalent fracture bulk and shear modulus (which effectively incorporate the effect of contact areas) and equivalent porosity and aperture.

Conclusions

1. For a given contact area density, fractures with correlated distributions of contact areas exhibit higher P-wave modulus dispersion and seismic attenuation. Although the effects of distribution of contact areas is maximal at the low frequency limit, these distributions also play an important role in the effective compliance of the rock at the high frequency limit.
2. The seismic response of a fracture with realistic aperture distributions can be approximated by a thin layer with constant thickness, provided that appropriate equivalent poroelastic properties are employed.

Acknowledgments

This work has been supported by a grant from the Swiss National Science Foundation.

GEOTHEST - Building an INTERREG project France-Switzerland on innovation in geophysical exploration for geothermal development in sedimentary basins.

Mauri G.(1), Got J-L.(2), Lupi M.(3), Trouver E.(2), Miller S.A.(4)

(1) previously Centre d'hydrogéologie et de Géothermie (CHYN), Université de Neuchâtel (UNINE), Neuchâtel, Switzerland (guillaume.mauri@unine.ch , g.mauri10@bluewin.ch)

(2) Université Savoie Mont-Blanc, Chambéry, France. (Jean-Luc.Got@univ-smb.fr, Emmanuel.Trouve@univ-smb.fr)

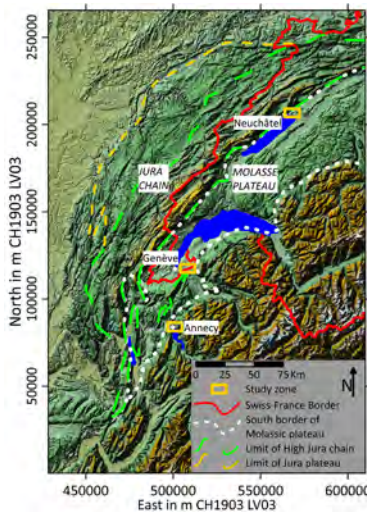
(3) Sciences de la Terre et de l'environnement, Université de Genève, Genève, Switzerland. (Matteo.Lupi@unige.ch)

(4) Centre d'hydrogéologie et de Géothermie (CHYN), Université de Neuchâtel (UNINE), Neuchâtel, Switzerland. (stephen.miller@unine.ch)

Context

In urban and peri-urban regions, such as Switzerland and France, the first stage of a geothermal study relies on active seismic acquisition methods (2D or 3D), which are costly and often logistically complex. Seismic data provide valuable information on contrasts of impedances between geological formations. However, geothermal reservoirs can either extend throughout several geological units or be confined within one lithology. Hence, it is key to first constrain the extent of the geothermal reservoir.

For hydrothermal reservoirs new and innovative electrical methods, such as Deep Electrical Resistivity Tomography (DERT), are cost-effective and logistically easy to handle (from topography surface to 1km depth).



For reservoirs at larger depths (i.e. below 1 km) magnetotelluric methods (MT) are a viable solution. However, in urban areas the electromagnetic noise is often too strong, and MT cannot properly locate the reservoir.

Figure 01: Geographical context of western Switzerland and along the French border. Both Jura mountain range and Molasse plateau are extending from Switzerland to France. The city names locate the study area for GEOTHEST project.

France-Swiss Collaborations

GEOTHEST is an INTERREG project, which is currently in preparation.

It groups two Swiss universities with a French university.

- University of Neuchâtel, Center for Hydrogeology and Geothermics,
- University of Geneva, Earth and environmental Sciences,
- University Savoie Mont Blanc.

It is supported by the:

- Canton of Neuchâtel,
- Industrial Services of Geneva (canton of Geneva)
- Fondation of University Savoie Mont Blanc,
- Communities of Pays de Gex, Genevois, Annecy, Aix-les-Bains, Chambéry.

The Pre-project has been accepted by the INTERREG OFFICE.

Presentation of INTERREG V France-Swiss

INTERREG V France-Swiss is a program of inter-region cooperation founded by the EU and in which Switzerland is a partner.

INTERREG V France-Swiss are bringing together resources, structures from the different region and supporting innovative projects, particularly in the energy field.

Objectives of the Project

The GEOTHEST project aims to develop:

- 1) develop a new methodology for both acquisition and data analyses for MT to overcome electromagnetic distortion from human activity,
- 2) apply DERT surveys to better characterize shallower reservoir,
- 3) build on and improve on existing models to more accurately characterize geothermal reservoirs,
- 4) for the site of Annecy in France, the project also includes a hydrogeological model of the area. Such hydrogeological models for the two sites in Switzerland already exist.

The project will be submitted later this fall and we are searching for industrial partners

Concept

The project implements the innovative method and applies it to investigate geothermal reservoirs at 3 study sites in France and in Switzerland.

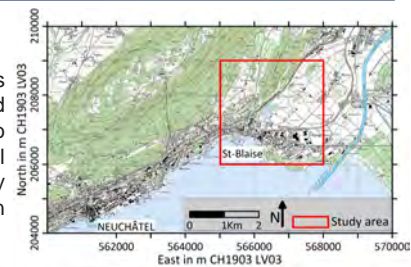


Figure 02: Localisation of the study area near Neuchâtel (CH).

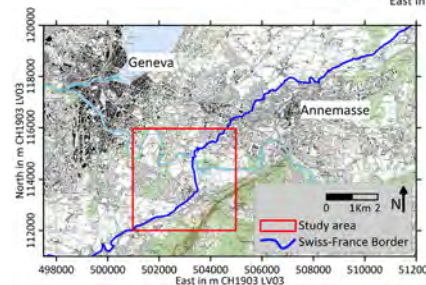
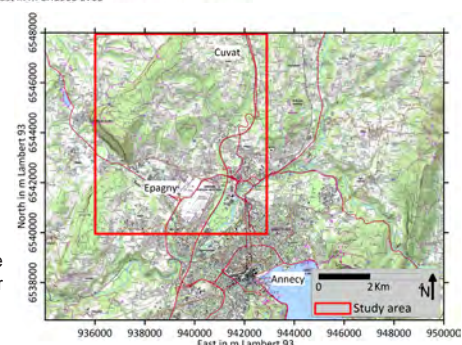


Figure 03: Localisation of the study area in the transborder zone, near Annemasse (France) and Geneva (CH).

Figure 04: Localisation of the study area near Annecy (France).



Acknowledgement

We are thankful to the representative of University Savoie Mont Blanc, University of Neuchâtel, & University of Geneva for their support. We are grateful to Canton of Neuchâtel, Industrial Services of Geneva, Fondation of University Savoie Mont Blanc, Communities of Pays de Gex, Genevois, Annecy, Aix-les-Bains, Chambéry for their support and their financial contribution.

Reactive transport models of the orogenic hydrothermal system at Grimsel Pass, Switzerland

Peter Alt-Epping, Laryn W. Diamond & Christoph Wanner
Rock-Water Interaction, Institute of Geological Sciences, University of Bern

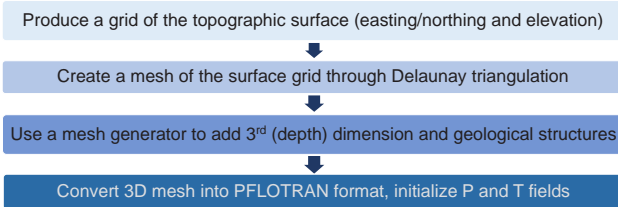
1) Introduction

Thermal waters at temperatures in the range of 17 – 28 °C discharge into a tunnel underneath Grimsel Pass in the Central Alps. The thermal springs are located at an elevation of about 1900 m.a.s.l.. Discharge occurs at low rates (≤ 10 L/min) along the Grimsel Breccia Fault (GBF), which is exposed some 100 m within the tunnel. Geochemical evidence suggests that the water is a mixture of old geothermal water and younger cold water components having residence times of at least 30 ky and about 7 years, respectively. Both components are meteoric in origin (Waber et al., 2017). Reconstruction of the temperature of the geothermal component alone yields a discharge temperature of ~ 50 °C.

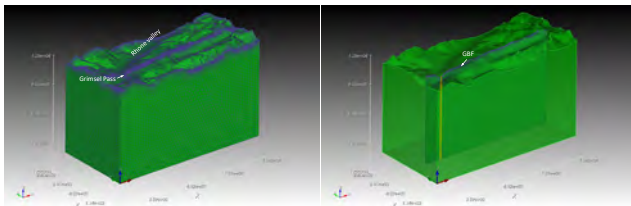
We use the high performance reactive-transport code PFLOTRAN (www.pflotran.org) to model the hydrothermal system in its entirety (i.e. the recharge zone, the reaction zone down to a depth of 10 km and the upflow and discharge zones below Grimsel Pass) and to integrate geological, hydrological, thermal and geochemical observations. We perform simulations that obey the chemical, hydraulic and thermal constraints of the discharging water and the mineralogy of a spatially coincident fossil (3 Ma) upflow zone cemented by quartz and adularia (Hofmann et al., 2004; Belgrano et al., 2016), to explore feasible permeability distributions and flow patterns in the deep fault zone. One of the issues to be resolved is how water recharging the fault system at high altitude can penetrate the rock to a depth of about 10 km and attain the maximum system temperature of about 250 °C as estimated from solute geothermometry.

2) Constructing a regional scale model of the Grimsel system

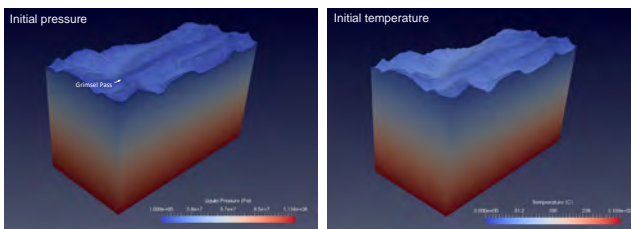
The main driving force for fluid flow in the Grimsel system are gradients in elevation head due to topography of the region. Constructing a 3D model domain that incorporates the regional topography as upper boundary involved the following steps:



3) Numerical model



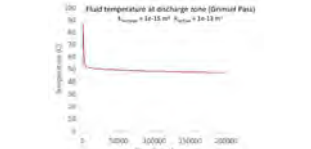
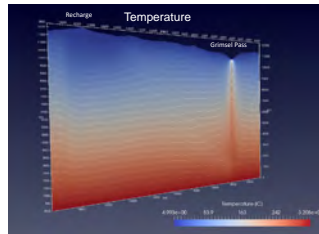
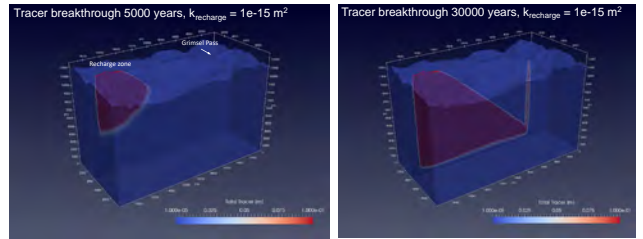
Model dimensions and grid. The GBF (right) is modelled as vertical fault plane extending to a depth of about 10 km. It constitutes a zone of higher permeability. The upflow zone below the Grimsel thermal springs is shown in yellow. It has a permeability of 1×10^{-13} m². The system is heated from below at a constant rate of 0.0705 W/m² consistent with background heat flow values. Quartz is the only reacting mineral in the model.



Initial pressure and temperature fields

4) Model results

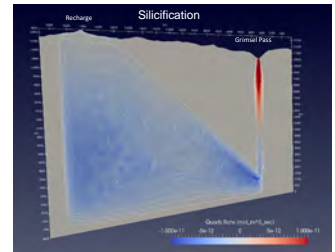
Fluid circulation is driven by meteoric recharge into the GBF at high elevation and focussed discharge of hydrothermal fluid at lower elevation at Grimsel Pass. The permeability contrast between the GBF and the surrounding rock allows the fluid to infiltrate the rock to depths of 10 km (or more). Through water-rock interaction along its pathway the fluid obtains its thermal and chemical fingerprint. The breakthrough of a tracer injected with the infiltrating fluid is used to illustrate the flow pattern and calibrate fluid residence times and fault permeabilities.



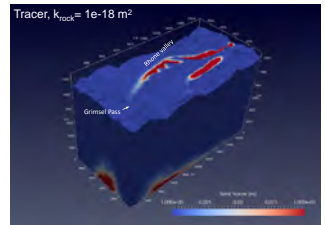
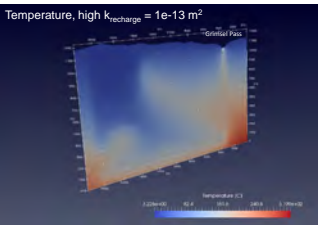
Diffuse recharge of meteoric water leads to a weak depression of isotherms, whereas focussed upflow induces a distinct thermal anomaly.



Breccia with silicified matrix at Grimsel Pass
Belgrano et al. 2016



Silicification is ubiquitous in the GBF at Grimsel Pass within the paleo-upflow zone (left). The model predicts large quantities of quartz to precipitate within the upper part of the upflow zone (i.e. < 6 km depth) where the fluid undergoes cooling (right).



Model variants. A uniform high permeability throughout the recharge zone leads to convective circulation within the zone (left). A high permeability of the rock increases discharge into the surrounding valleys (right).

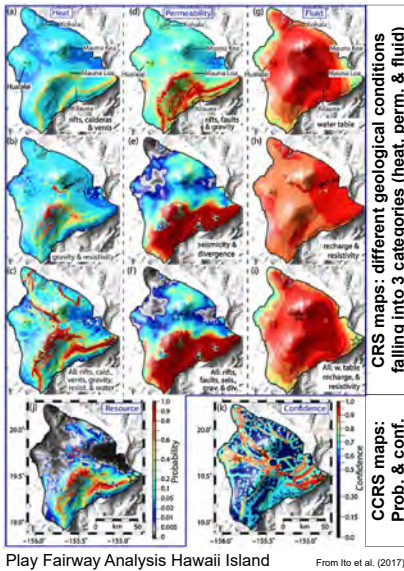
5) Conclusions

We established a workflow from a GIS-based surface grid to a regional-scale 3D PFLOTRAN reactive transport model. Simulations show that fluid recharge to a depth of 10 km requires focussed flow along (one or several) higher permeability pathways.

REFERENCES:
Belgrano, T. M., Hennegh, M. & Berger, A. 2016: Inherited structural controls on fault geometry, architecture and hydrothermal activity: an example from Grimsel Pass, Switzerland, Swiss J Geosci, 109, 345-364.
Hofmann, B. A., Helfer, M., Diamond, L. W., Villa, I., Frei, R. and Eikenberg, J., 2004, Topography-driven hydrothermal breccia mineralization of Pliocene age at Grimsel Pass, Aar massif, Central Swiss Alps; Schweizerische Mineralogische und Petrographische Mitteilungen, v. 84, no. 3, p. 271–302
Waber, H.N., Schneeberger, R., Mäder, U.K., Wanner, C. 2017: Constraints on evolution and residence time of geothermal water in granitic rock at Grimsel (Switzerland), 15th Water-Rock Interaction Symposium, WRI-15, Procedia Earth and Planetary Science 17, 774-777.

Compilation of data relevant for geothermal exploration – a first step towards a Geothermal Play Fairway Analysis of the Rhône Valley

D.B. van den Heuvel, S. Mock, D. Egli, L.W. Diamond, M. Herwegh (Institute of Geological Sciences, University of Bern)



1. What is a Geothermal Play Fairway Analysis (PFA)?

- Tool adapted from hydrocarbon exploration industry: Spatial correlation of data relevant for geothermal systems
- Step by step:
 - ① Compile existing data
 - ② Examine, integrate and interpret data (→ create GIS maps)
 - ③ Construct probability maps for each geologic condition (common risk segment CRS map)
 - ④ Integrate individual maps to a composite common risk segment (CCRS) map
- Favourability map highlighting areas with high chance of exploration success

2. Geothermal activity in the Rhône Valley

Most active geothermal domain in Switzerland

- Many known occurrences of thermal water
- Most not (yet) exploited (few used for district heating)

Why?

- Fluid circulation is gravity driven (up to 10 km depth, i.e. up to 250 °C!)
- Heat source = background geothermal gradient (~25 °C / km)

More thermal water discharge areas expected than the ones currently known

- Obscured by the thick Quaternary sediments (up to 900 m)^[2] and mixing with GW (no surface expression = "blind" system B)
- Perform a geothermal PFA to find such blind systems

3. Geothermal PFA Rhône Valley – data compilation

- Data sources:**
- Online mapping platform of Switzerland
 - Geologic and Tectonic maps of Switzerland
 - Database on Swiss geothermal fluids^[3]
 - Database on geothermal boreholes^[4-7]
 - Evaluation geothermal potential of VS^[8] & VD^[9]
 - Nationwide & regional geophysical surveys^[10-14]
 - Journal articles, BFE reports etc.

Categorise and discuss data available :

Background

- Infrastructure
- Well & spring loc.
- Protected areas

Basics

Geology

- Surface geology
- Thickness of quat. sediments

Seismicity

- Seismic hazard
- Historical earthquakes

GW & river hydrogeol.

- Chemical composition
- Isotopic composition
- Temperatures
- Water level
- Flow rates

- Problems:**
- Well data of thermal baths and NEAT confidential
 - Age of data: Mostly data collected during the 80s and 90s → Reliability of decades old data?
 - Mostly point data at locations with known thermal occurrence; few regional studies or relevant data away from known occurrences

Geophys.	Heat source	Permeability	
	Gravimetry		Tectonic & structural regime/setting
	Geomagnetics		Regional stress field
Fluid	Magnetotellurics	Shear & dilat. strain	
	Chemical composition		Age
	Isotopic composition		Length
Temp.	Direct measurement	Fault geom.	
	Geothermometry		Displacement
	Place names related to thermal water occurrence		Slip & dilat. tendency
		Interfault geometry	

4. How to proceed with the geothermal PFA?

- By the end of 2018:
- Finish creating individual GIS layers for each *topic*
 - Combine the GIS layers of each topic within a subcategory
 - Write a report discussing the data available and its quality
 - Identify areas with a lack of data and the datasets which would benefit most from expanding
 - Suggestion for future sampling campaigns
 - Coordinate the publication of the GIS maps with Swisstopo
- In the long run:
- Extrapolate point data (e.g. by inverse distance weighting (IDW) or kriging) to create a CRS map for each subcategory
 - Combine the CRS maps of the subcategories to two CCRS maps (**heat source** and **permeability**) by a multi-criteria-decision making (MCDM) process
 - Combine these two CCRS maps to an overall favourability map
 - **Permeability** < 50% as a site with little or no permeability could potentially be developed as an EGS system
 - Add layers from the **background** maps such as «protected areas» and «seismicity» to exclude sensitive areas
 - Identify most promising location for a detailed site investigation



In-situ characterization of fluid flow in an EGS-analog reservoir

Brixel B. ¹, Jalali M. ², Klepikova M. ¹, Roques C. ¹, Löw S. ¹

¹ Department of Earth Sciences, ETH Zürich, Switzerland

² Chair of Engineering Geology and Hydrogeology, RWTH Aachen, Germany

Motivation, Goals & Objectives

Better understanding how heterogeneity impacts fluid flow and pore pressure diffusion in geological media *in-situ* is paramount for many disciplines in earth sciences as well as for industries relying on natural resources, including deep geothermal energy (DGE) applications - as is planned as part of the **Swiss Energy Strategy 2050**.

To this end, the goals of our study are to:

- Map out the **3-D permeability structure** of a fault zone (at borehole scale);
- Determine the **connectivity structure** of permeable domains and characterize **diffusion processes** therein;
- Identify the **backbone** of the fracture network amenable to flow, solute and heat transport.

Data used in this study were collected as part of the ISC experiment completed at the Grimsel Test Site, Switzerland (see Figure 1)

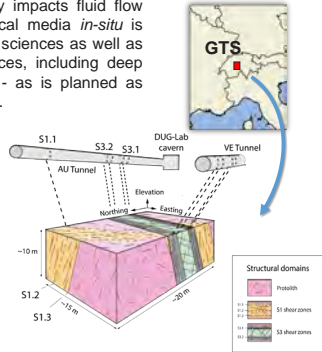


Fig. 1: Site location and geology

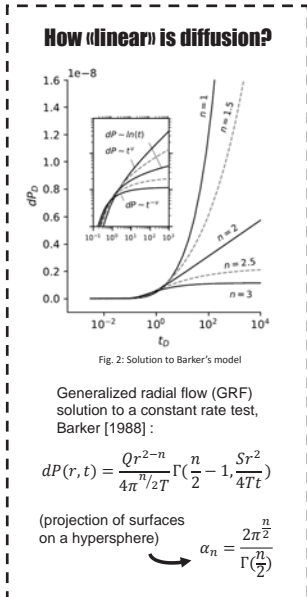


Fig. 2: Solution to Barker's model

Generalized radial flow (GRF) solution to a constant rate test, Barker [1988]:

$$dp(r, t) = \frac{Qr^{2-n}}{4\pi^{n/2} T} \Gamma\left(\frac{n}{2} - 1\right) \frac{S_r^2}{4Tt}$$

(projection of surfaces on a hypersphere) $\alpha_n = \frac{2\pi^{n/2}}{\Gamma(\frac{n}{2})}$

Key Results – Pulse Tests

- The distribution of single-hole Transmissivity estimates appears to be binomial and range as:
 $10^{-10} < T_{SZ} < 10^{-6} \text{ m}^2/\text{s}$
 $10^{-14} < T_{PL} < 10^{-8} \text{ m}^2/\text{s}$

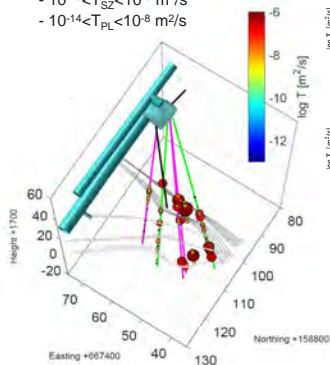


Fig. 4: 3D bubble plot showing single-hole Transmissivity values

Methods & Datasets

Data acquisition was carried out following standard hydrogeological field methods including single and cross-hole packer testing, the purpose of which is to induce a perturbation in the natural head field.

- Pressure pulse tests were used to compute discrete (i.e. local) Transmissivity (T) estimates, using Neuzil's method (Neuzil, 1982). These estimates were then used as a proxy for the permeability (k) structure.
- Constant rate injection tests were conducted over durations of 20 minutes to 2.5 days. Pressure responses were analysed using standard approaches (Cooper and Jacob, 1946) as well as fractional models (Barker, 1988) – see inset on the left.
- Thermal tracer tests were conducted through the injection of hot water and the propagation of thermal anomalies using two loops of distributed fibre-optics temperature sensing systems (FO-DTS).

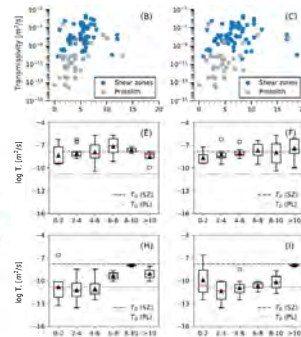


Fig. 3: Scaling of Transmissivity and fracture intensity

- Spatial correlation between high-T clusters and deformation zones (Fig. 4)
- Complex scaling with fracture intensity metrics (Fig. 3)

Key Results – Cross-hole Tests

- Normalized cross-hole pressure responses are distributed into two clusters, generally consistent with known structural domains
- Responses in the S3 shear zone (grey curves) show a strong power-law behaviour (unlike most breakthrough in S1), with a mean fractional dimension of 1.3 – see Fig 5.

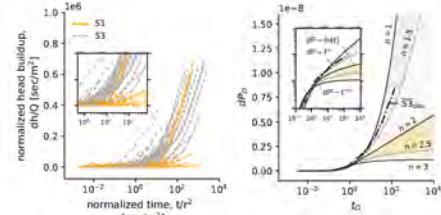


Fig. 5: Cross-hole responses (left) and mean fractional flow model (right) for our study site

- Converging pressure derivatives indicate that the flow dimension increases from $n=1$ to 1.5 as pressure fronts diffuse into the S1 shear zone. We interpret this as the result of the spatial integration of new forms of heterogeneities (Fig. 6).

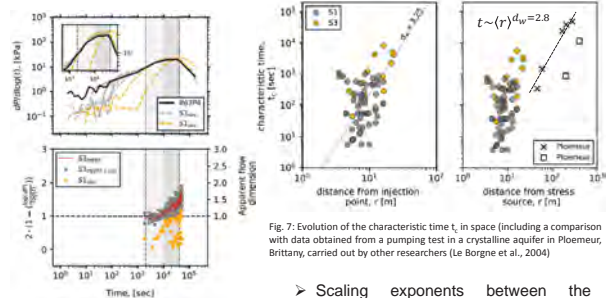


Fig. 7: Evolution of the characteristic time t_c in space (including a comparison with data obtained from a pumping test in a crystalline aquifer in Ploemeur, Brittany, carried out by other researchers (Le Borgne et al., 2004))

Fig. 6: Temporal evolution of the apparent flow dimension

Key Results – Thermal Tracers

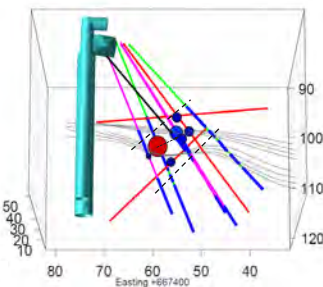


Fig. 8: 3D bubble plot showing the location of thermal breakthroughs

- Scaling exponents between the characteristic time and the Euclidean radial distance from injection are in the order of 3.2 to 3.4, i.e. well above the theoretical value of 2 for normal diffusion, indicating that diffusion is anomalously slow (Fig. 7)

- Based on a 40-day thermal tracer test at 50° C, discrete thermal breakthroughs were observed along every borehole equipped with a FO-DTS system. Thermal anomalies ranged from >1°C to a maximum of 10°C about 4m from the injection point (shown in red on Fig. 8). These field results allow refining the delineation of the backbone of the fracture network and provide insights into the heat carrying capacity of fractures in granite.

Conclusions & Outlook

This study yields significant insights into the hydraulic behaviour of crystalline rocks that have similar properties to the deep reservoirs targeted for the extraction of geothermal energy in Switzerland. Here, we show that

- The permeability structure of crystalline reservoir cross-cut by shear zones is bimodal, with high-Transmissivity zones limited to shear zones
- Steady linear flow regimes develop rapidly in shear zones, even though diffusion appears to be anomalously slow (i.e. slower than expected under normal conditions where $t \sim (r^2)$); Using a model that accounts for anomalous diffusion yields fractal dimensions for the Grimsel Test Site and Ploemeur of 2.11 and 2.24 respectively (Acuna and Yortos, 1995)
- Thermal tracer tests allowed refining the delineation of the principal flow paths and will be used in future studies for the parameterization of DFN models.

References

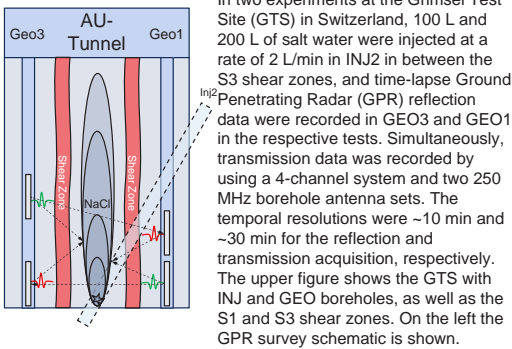
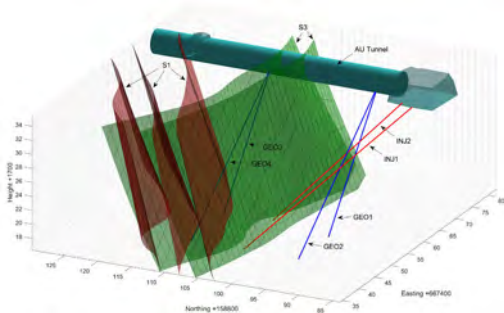
Neuzil, C.E., On conducting the modified "slug" test in tight formations, *Water Resour. Res.*, 18(2), 1982
 Cooper, H.H. and Jacob, C.E., A generalized graphical method for evaluating formation constants and summarizing well field history, *EOS Trans., AGU*, 27(4), 1946
 Barker, J.A., A generalized flow model for hydraulic tests in fractured rock, *Water Resour. Res.*, 24(10), 1796-1804, 1988
 Le Borgne, M. et al., Equivalent mean flow models for fractured aquifers: Insights from a pumping tests scaling interpretation, *Water Resour. Res.*, 40(3), 2004
 Acuna J. A. and Yortos Y.C., Application of fractal geometry to the study of networks of fractures and their pressure transient, *Water Resour. Res.*, 31(3), 1995

Salt Tracer Flow Path Reconstruction Using Ground Penetrating Radar

Peter-Lasse Giertzuch¹, Joseph Doetsch¹, Mohammadreza Jalali¹, Alexis Shakas², Hannes Krietsch¹, Bernard Brixel¹, Cédric Schmelzbach¹, Hansruedi Maurer¹

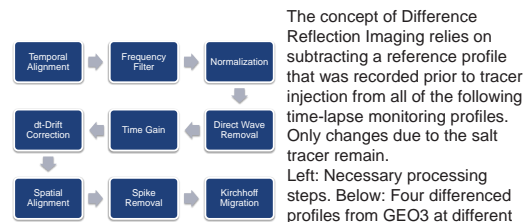
¹Department of Earth Sciences, ETH Zurich, Switzerland, ²Institute of Earth Sciences, University of Lausanne, Lausanne, Switzerland

1 Introduction

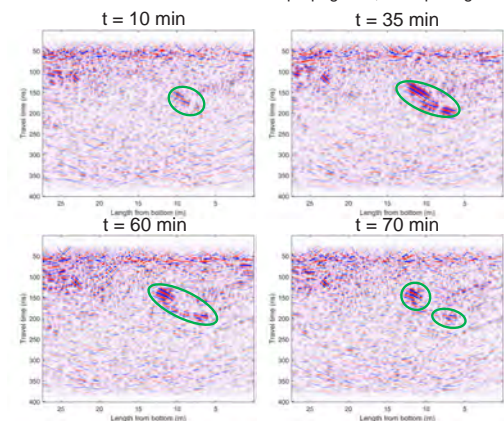


In two experiments at the Grimsel Test Site (GTS) in Switzerland, 100 L and 200 L of salt water were injected at a rate of 2 L/min in INJ2 in between the S3 shear zones, and time-lapse Ground Penetrating Radar (GPR) reflection data were recorded in GEO3 and GEO1 in the respective tests. Simultaneously, transmission data was recorded by using a 4-channel system and two 250 MHz borehole antenna sets. The temporal resolutions were ~10 min and ~30 min for the reflection and transmission acquisition, respectively. The upper figure shows the GTS with INJ and GEO boreholes, as well as the S1 and S3 shear zones. On the left the GPR survey schematic is shown.

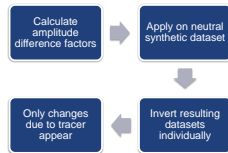
2 Difference Reflection Imaging



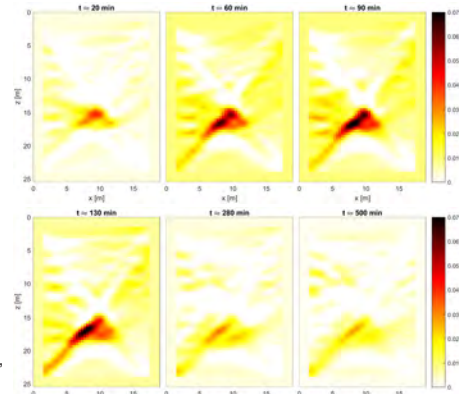
The concept of Difference Reflection Imaging relies on subtracting a reference profile that was recorded prior to tracer injection from all of the following time-lapse monitoring profiles. Only changes due to the salt tracer remain. Left: Necessary processing steps. Below: Four differenced profiles from GEO3 at different times after tracer injection that show tracer injection, propagation, and splitting.



3 Difference Attenuation Tomography

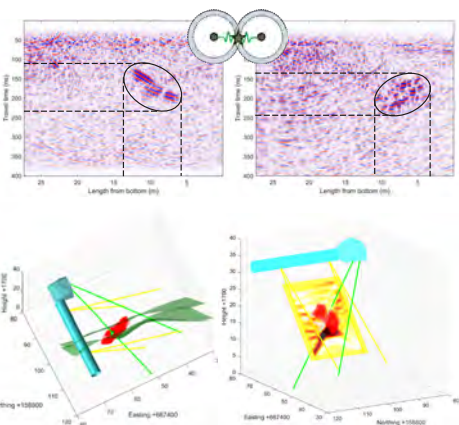


The transmission data is analyzed by a Difference Attenuation Approach. This approach allows to invert for changes due to the tracer only, disregarding all geological information in the GPR data (top). The time-lapse datasets are inverted individually and show clearly the tracer injection, build up and signal decrease in the tomography plane over time.



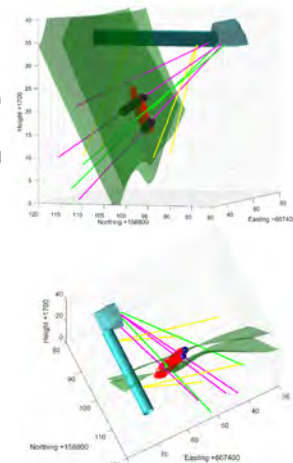
4 3D Flow Path Reconstruction

Single-hole reflection GPR data does not allow for actual localization, as the antennas show a radial symmetry. After migration, a donut shaped form contains the possible reflection locations. The data from the GEO1 and the GEO3 surveys are combined by calculating the intersections of those shapes and thereby allow for a 3D localization of the tracer. Top: The localization scheme by using the tracer locations in GEO1 (right) and GEO3 (left). Bottom left: Result integrated within the GTS model. The green ball marks the injection point, the red dots depict the tracer location. Bottom right: The results of tracer localization and inversion show good agreement.



5 Combination and Verification of Results

The top figure shows that the reconstructed tracer location matches the two grey sampling intervals on the PRP lines (pink). During the test those intervals showed salt tracer breakthroughs that were recorded by STS loggers. The bottom figure shows the main breakthrough events (blue) of a heat tracer survey that was conducted in the same injection interval as the salt tracer survey (see poster by B. Brixel). The thermal data was recorded by optical fibers within the GTS volume. Also these points are well matched by the reconstructed location. The reconstructed tracer flow path shows a tracer propagation within a plane between the two S3 shear zones. In a next step these results will be compared to borehole logs to identify matching fractures that seem to be responsible for the tracer flow and set up a first version of a Discrete Fracture Network, that shall be extended by combining the data with results from the thermal and conventional tracer tests. The tomography results will be further improved by reducing the overexpression of the diagonal ray paths and in the future a Time-Lapse Full Waveform Inversion framework will be developed and applied to this data.



Comparison between DNA nanotracer and solute tracer tests in a fractured crystalline rock – GTS case study

A. Kittilä, M. Jalali, K.F. Evans, X.-Z. Kong, and M.O. Saar
ETH Zurich

Background

The DUG Lab at the Grimsel Test Site hosted an In-Situ Stimulation and Circulation (ISC) experiment (Amann et al. 2018) to investigate the key processes relevant to the development of enhanced geothermal systems (EGS). DNA nanotracer tests were conducted to i) validate and advance the application of the DNA nanotracers in decameter scale fractured rock, and ii) delineate the hydraulic features of the connected fracture volume as part of the pre- and post-stimulation characterization of the ISC experiment.

In this study (Kittilä et al. 2018), temporal moments of the DNA nanotracer breakthrough curves are compared with those of solute dye tracers, followed by the discussion on hydraulic properties of the fracture volume. The data are based on two separate tests, named Test 1 and Test 4. In Test 1, tracers were injected to borehole INJ2, and in Test 4 to borehole INJ1 (Fig. 1).

Methods

Temporal moment (TM) analysis was performed on normalized responses of the system to pulse tracer injections as age distribution functions (Shook and Forsmann 2005):

$$E(t) = \frac{C(t) \rho q_{out}}{M_{inj}}$$

The n th TM was then calculated as:

$$m_n^* = \int_0^\infty t^n E(t) dt,$$

which is a measure of the tracer mass recovery (zeroth TM, M_0), mean residence time (first normalized TM, M_1), and degree of spreading about the center of the mass (second normalized and centralized TM, M_2) (Leube et al. 2012). Furthermore, swept volume (V_p), flow/storage capacities, and the Gini coefficient (G) of the tracer responses (Shook and Forsmann 2005) were calculated.

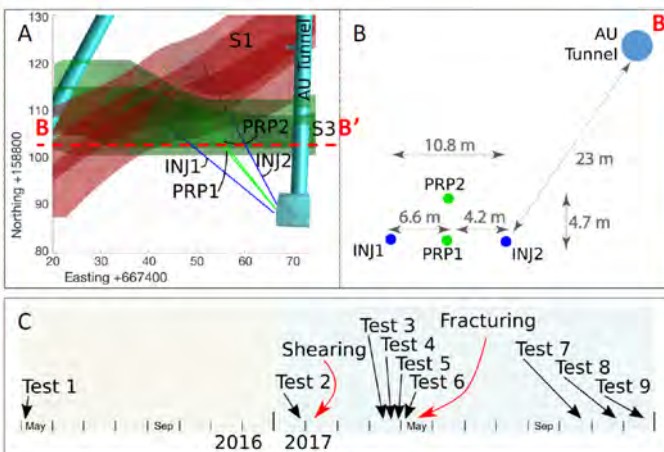


Figure 1. Visualization of two shear zones S1 and S3, the AU Tunnel, and the INJ and PRP boreholes at the DUG Lab (Krietsch et al. 2018) (A), and a sub-vertical cross-section (B-B' dashed line) showing the intersections of the boreholes and the AU Tunnel in the plane of the S3 shear zone (B). The timeline (C) shows when different tracer tests took place, in relation to the stimulation phases.

References

Amann et al. 2018. Solid Earth, 115-137.
Kittilä et al. 2018. In preparation.
Krietsch et al. 2018. In review.
Leube et al. 2012. Water Resources Research 48, W11527.
Shook and Forsmann 2005. INL/EXT-05-00400, 20 p.

Results

Table 1. Results of a temporal moment analysis from DNA nanotracers PT2 and GR-3, and solute dyes uranine (U) and sulfurhodamine B (SB).

Test #	Location	Tracers	Ratio of M0	Ratio of M1	Ratio of M2	V_p (m ³)	G (-)
1	AU Tunnel	PT2/U	0.99	0.71	0.39	0.36/0.50	0.32/0.36
4	INJ2 int4	GR-3/SB	0.03	0.75	0.55	0.0019/0.073	0.29/0.30
	PRP1 int3		0.09	0.41	0.42	0.0010/0.028	0.56/0.43
	PRP2 int2		0.15	0.95	1.94	0.0029/0.020	0.53/0.42
	AU Tunnel		0.10	0.78	1.02	0.060/0.72	0.39/0.33

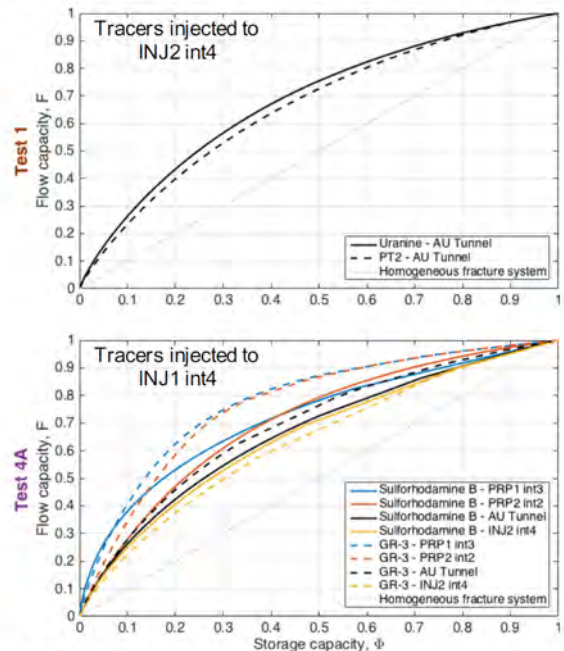


Figure 2. Flow/storage capacity diagrams from Test 1 and Test 4. Line colors indicate measurement location.

Discussion

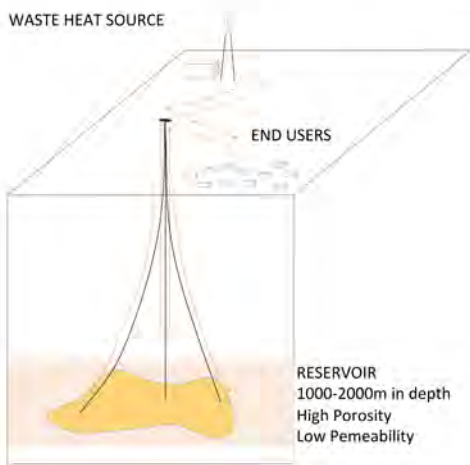
- Tracer-based pre- and post-stimulation characterization of the DUG Lab is comprised of nine different tests (Fig. 1C), two of which (Tests 1 and 4) used DNA nanoparticles with solute dye tracers.
- Before stimulation (Test 1) only the connection between borehole INJ2 and the AU Tunnel could be studied (PRP boreholes did not yet exist).
 - DNA nanotracer and solute had almost identical recoveries, both had relatively large swept volume, and their transport was similarly distributed along that volume (Fig. 2 and Table 1).
- After shearing stimulation (Test 4) several hydraulic connections were studied.
 - DNA nanotracer had smaller mass recoveries and swept volumes from all locations, but no such trend was observed in the degree of spreading and flow distribution along the swept volume.
- The ratios of M1 (mean residence times) are not correlated with travel distance, production rate, or recovered mass.

Geothermal Energy Chance Of Success

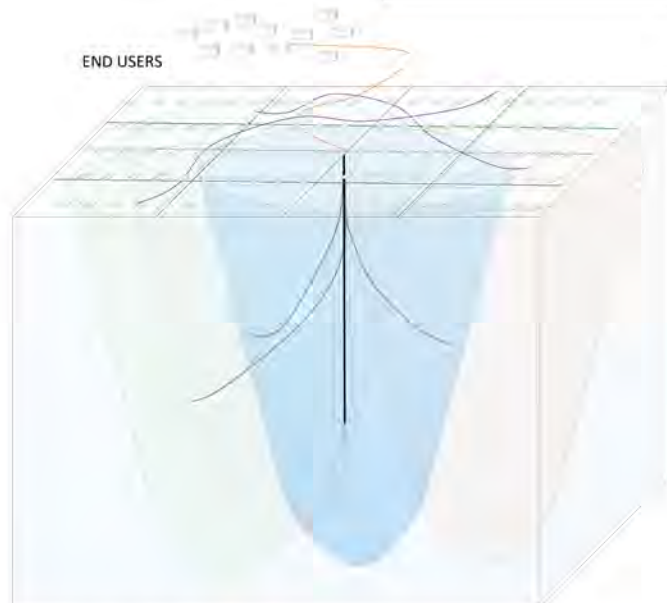
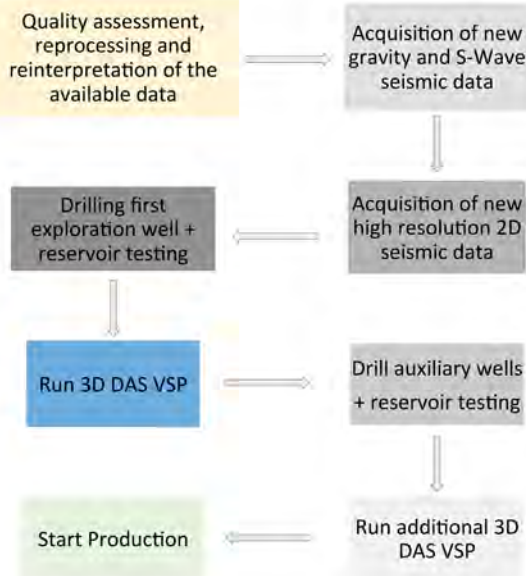
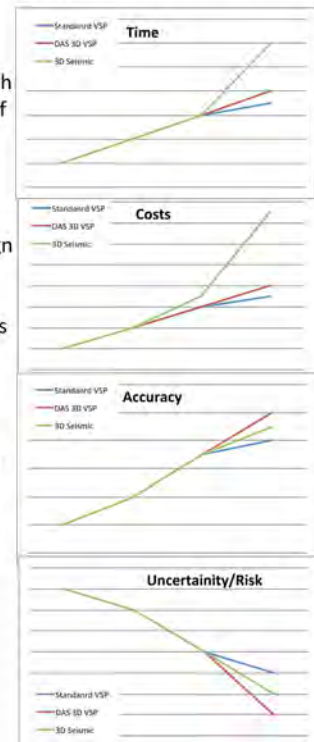
Luca Guglielmetti*, Andrea Moscariello*, Schmelzbach Cédric#, Hansrued Maurer#, Carole Nawratil de Bono^, Michel Meyer^, Francois Martin^, David Dupuy*, PierVittorio Radogna*

*Department of Earth Sciences, University of Geneva – Rue des Maraichers 13, CH-1205 Geneva
 #Institute of Geophysics, Department of Earth Sciences, ETH Zurich - Sonneggstr. 5, CH-8092 Zurich
 ^Services Industriels de Genève – Chemin Chateau-Bloch 2 – CH1219 Le Lignon
 *Geo2X - Rue du centre 6, CH-1377 – Oulens-sous-Echallens

Subsurface exploration for geo-energy resources production is always affected by a degree of uncertainty which reflects into the overall risk of a project
 To reduce the uncertainty and the risk, industrial developers gradually collect more data to increase the accuracy and then locate drilling targets and design the drilling program (i.e. depth, amount, and geometry of the wells)



- Collecting data requires large investments which could likely to hinder the economic feasibility of an innovative projects such as in the case of UTES systems
- When the target volume is rather small (5-10km³) such in the case of UTES, higher imaging resolution is required to properly design multiple wells to optimise the storage and production of waste heat into the subsurface.
- Finding “smart” solutions (e.g. effective and less costly) can therefore help us to achieve the required technical results to support the development of geothermal energy in the Canton of Geneva
- We intend to benefit from the fists exploration wells drileld in Geneva to develop a modular, high resolution and cost-effective geophysical data collection protocol to characterize the potential reservoir for UTES systems



Exploring the interface between shallow and deep geothermal systems: the Tertiary Molasse.

Andrea Moscardello*, Nicolas Clerc[#], Loic Pierdona*, Antoine De Haller*

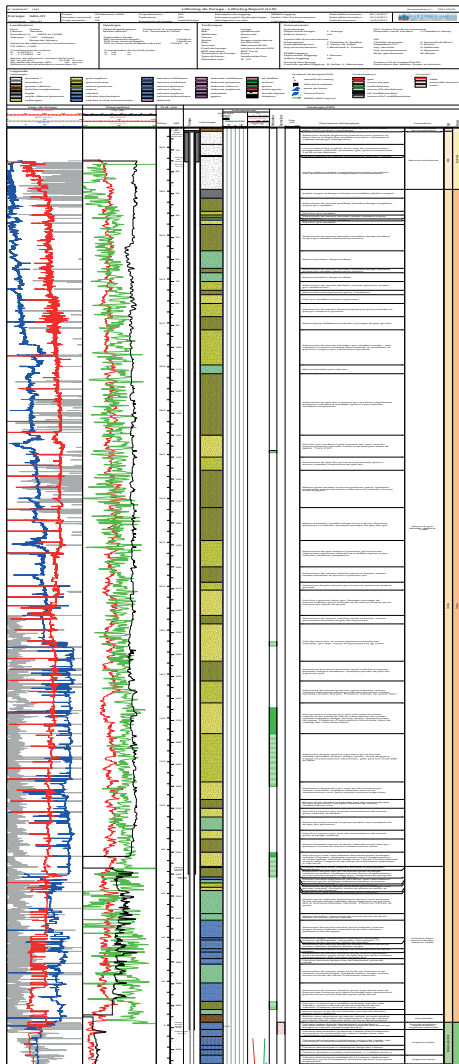
* Department of Earth Sciences, University of Geneva – Rue des Maraichers 13, CH-1205 Geneva
Canton of Geneva, Service de géologie, sols et déchets,



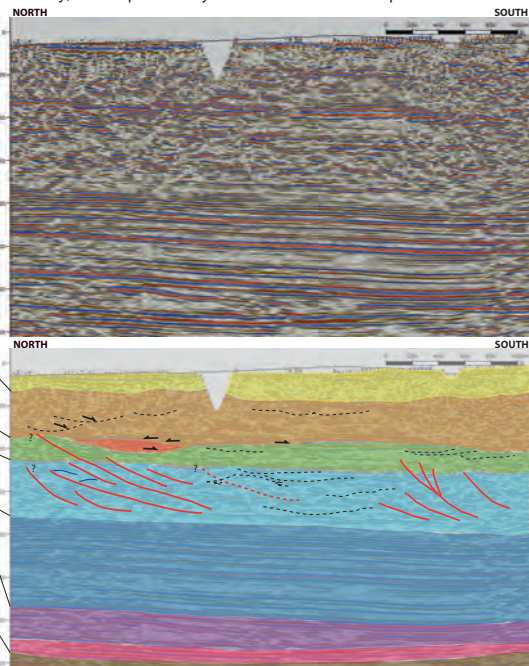
Little is known on the Tertiary Molasse succession accumulated in the Geneva foreland basin despite over the last 60 years a large amount of academic research and geo-energy exploration projects have been carried out in the Greater Geneva Basin. While the general chronostratigraphic framework and the overall sedimentology is generally known, the internal sedimentary architecture, its tectonostratigraphic significance and the reservoir characteristics (i.e. sand body and shale vertical and lateral continuity, etc.) is not yet well described.

The Molasse can play an important role while assessing the potential of deep hydrogeological budget as it could provide both storage and communication paths from the shallow ground water flows, mostly located within Quaternary deposits. and the deep Mesozoic systems, typically charged through pervasive fault systems.

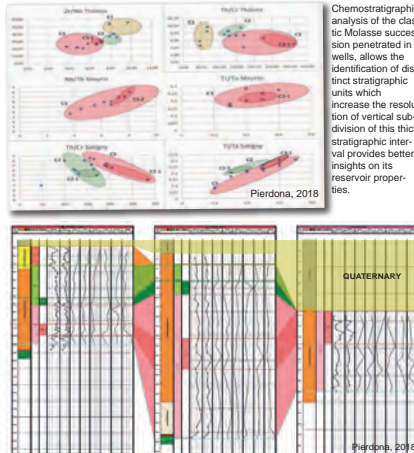
A comprehensive integrated sedimentological, chemostratigraphic and structural study of this interval is under way, whose preliminary results/observations are presented here.



2D seismic line in the western side of the Canton of Geneva where various sedimentological and structural features characterising the interface between the Lower Cretaceous and Tertiary units.



Chemostratigraphy: testing a 'new' correlation tool



Chemostratigraphic analysis of the classic Molasse succession penetrated in 3 wells, allows the identification of distinct stratigraphic units which increase the resolution of vertical subdivision of this thick stratigraphic interval provides better insights on its reservoir properties.

The LK-T interface



Distinct karst and open fracture network are found at the LK-T interface indicating the likely connectivity between the shallow Molasse and the deeper Mesozoic aquifers.





Processing and Analysis of Gravity data across the Geneva Basin in a Geothermal Perspective

Luca Guglielmetti*, Andrea Moscarello*,

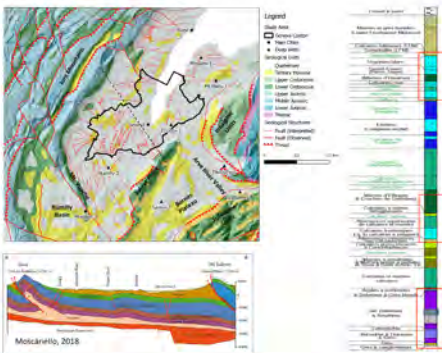
* Department of Earth Sciences, University of Geneva – Rue des Maraichers 13, CH-1205 Geneva

The study aims at understanding how the gravity method can contribute to the characterization of the Geneva Canton subsurface by analysing the gravity anomalies that can be associated with geological structures of geothermal interest.

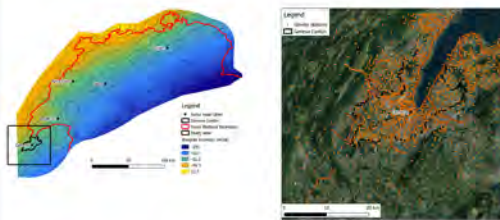
Gravity is part of the solution

It has limitations, but is one of the geophysical methods that can be employed during prospection and monitoring of a geothermal site. Higher benefits from gravity can be achieved if coupled with other exploration techniques routinely employed such as EM methods and 2D/3D seismic. The latter topic is part of the *Innosuisse* GECOS project aimed at reducing the geological risk of geothermal exploration.

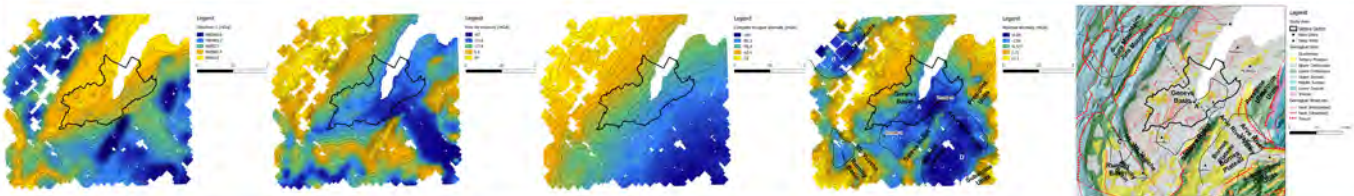
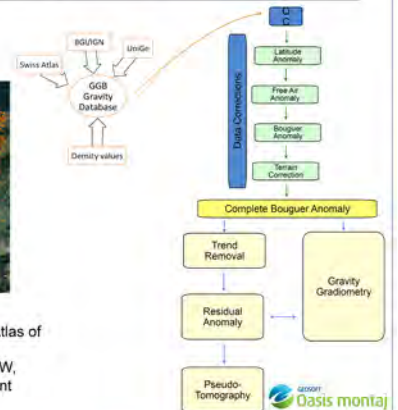
Geological Setting



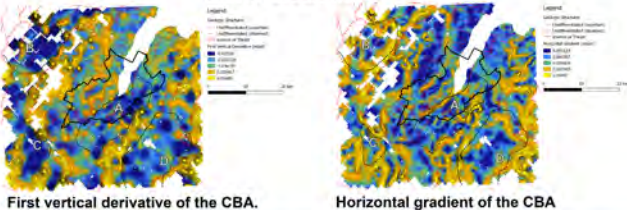
Processing of gravity public data



Bouguer Anomaly of the Swiss Molasse Plateau. Data from the Gravity Atlas of Switzerland. Data used in this study on the left-hand image. Note the rather linear trend NW-SE oriented with lower values towards SW, controlled by the deepening of the lithosphere towards the the Alpine front



Gravity Gradiometry



First vertical derivative of the CBA.

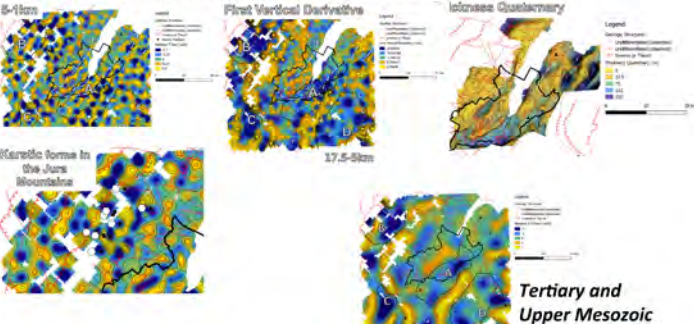
Horizontal gradient of the CBA

Gravity pseudo-tomography: Pseudo-gravity is based on the assumption that at increasing wavelengths correspond increasing depth of the source generating the anomaly. We tested this method by the following strategy:

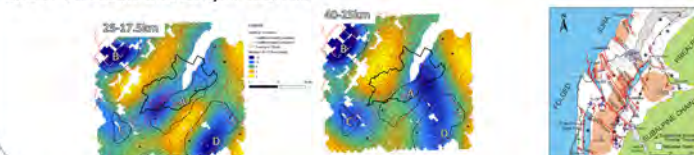
- Keeping the 1km cut-off wavelengths we increased the long wavelengths to 60km
- Keeping the 60km cut-off wavelengths we decreased the short wavelengths to 1km
- We then identified qualitatively those anomalies which show significant features related to the Thickness of the main formations: Quaternary, Tertiary Molasse, Mesozoic, Permo-Carboniferous

This approach is useful to constrain the wavelength bands which can be associated with the main geological features at a certain depth range. We then used the selected wavelengths bands to run 3D forward model and Inversion on an area of geothermal interest in the Geneva Canton

Quaternary and shallow anomaly sources in th Jura Mountains



Lower Mesozoic and Deeper sources



Conclusions

- Gravimetry survey is part of the exploration solution: early, cost & time effective screening of the basin (structural features at shallow to large depths)
- Comprehensive feasibility study carried out in Geneva area allows us to identify the key step processes to obtain significant results for geothermal exploration purposes in the Swiss Plateau subsurface geology.
- High resolution studies can be performed to successfully highlighting possible characteristics of major lineaments.

Task 1.2

Title

Reservoir stimulation and engineering

Projects (presented on the following pages)

Evaporitically-triggered thermo-haline circulation and its influence on geothermal anomalies near unconformities

Julian Mindel

High-resolution temporo-ensembe PIV to resolve pore-scale flow in fractured porous media

Mehrdad Ahkami, Thomas Roesgen, Martin O. Saar, Xiang-Zhao Kong

Fracture process zone in anisotropic rock

Nathan Dutler, Morteza Nejati, Benoît Valley, Florian Amann

On the variability of the seismic response during multiple decameter-scale hydraulic stimulations at the Grimsel Test Site

Linus Villiger, Valentin Gischig, Joseph Doetsch, Hannes Krietsch, Nathan Dutler, Mohammedreza Jalali, Benoit Valley, Florian Amann, Stefan Wiemer

Does a cyclic fracturing process agree with a fluid driven fracture solution?

Nathan Dutler, Benoît Valley, Valentin Gischig, Linus Villiger, Joseph Doetsch, Reza Jalali, Florian Amann

Investigation on Hydraulic Fracturing of Granite

Arabelle de Saussure

Advances in laboratory investigation of fluid-driven fractures

Thomas Blum, Brice Lecampion

Building a geological model for analysis and numerical modelling of hydraulic stimulation experiments

Hannes Krietsch, J. Doetsch, V. Gischig, M.R. Jalali, N. Dutler, F. Amann and S. Loew

Abstract / Background

We hypothesize that downward flow of cooler basin brines may displace and mobilize stagnant, hotter, chemically stratified, and often fracture-hosted brines in sediment-covered basements. Previous conceptual studies postulated fingering as a major hydraulic mechanism allowing for mutually up-/and downward flows of brines from the two reservoirs. We assume this is a potential key factor in establishing geothermal anomalies as well as the formation of basin-hosted ore deposits.

We have thus created the prototype of a hydrothermal simulation tool in which faults and fractures can be explicitly represented within a porous matrix. To understand how geometric complexity of the fractures affects thermo-haline transport, we performed a series of simulations utilizing an accurate equation of state. We designed synthetic geometries to study the propagation of salinity fronts using a simulator based on the CSMP++ library (Paluszny et al., 2007), honoring the governing equations for compressible porous media flow and saline transport (Geiger et al., 2006; Weis et al., 2014).

This work is a further step towards modeling thermo-haline convection within realistic representations of discrete networks of thin fractures, a scenario typically observed in basement rocks of deep geothermal systems and at basement/sediment interfaces and related deposits of U, Pn, Zn, and others.

Conceptual Model

The sequence of events remains debatable in some aspects and could be site-specific. In general, we assume that the heavier and oxidizing/acidic new brine originating from the evaporating sea invades the more permeable basin rock and establishes flow.

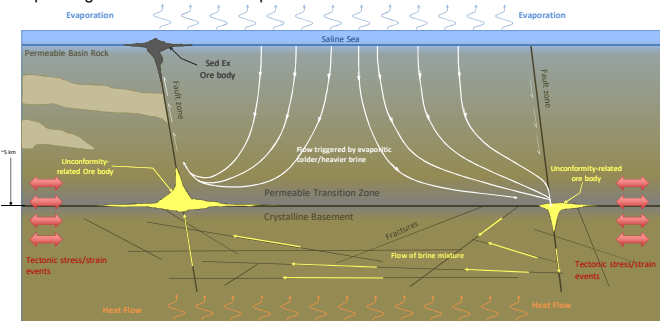


Figure 1: Conceptual model showing at least two main available flow mixing paths created by invading evaporitic brines.

Neglecting any transient effects of tectonics, at least two types of flow paths may form:

1. Invading evaporitic brines mix with and push mineral-rich basin brines upwards via a highly permeable conduit in an "excavating" fashion. Thus, different minerals should form along the flow path at different depths and into what is known as sedimentary exhalative type of deposits.
2. The invading brine, mixed with metal-rich basinal brines, flows into the fractured basement. The new, basinal, and basement brines mix and push out reducing/alkaline basement brines through available exits of the existing basement fracture network.

The permeable transition zone, due to its relatively higher permeability and porosity, acts as a chemical interface for the mixing of brines (i.e. new, basinal, basement) thus contributing to localized redox reactions. Due to temperature, pressure, medium (in terms of pore-space, permeability, and chemistry), and mixing flow conditions, thermal anomalies also very likely to form on and around intersections of fractures and the permeable transition zone.

Governing Equations, Boundary & Initial Conditions

We assume compressible single phase flow in porous media, and thus the continuum governing equations may be written as follows,

$$\begin{aligned}
 \mathbf{v} &= -\frac{k}{\mu} (\nabla p - \rho_f \mathbf{g}) && \text{Darcy} \\
 \frac{\partial(\rho_f \phi)}{\partial t} + \nabla \cdot (\rho_f \mathbf{v}) + q_{pf} &= 0 && \text{Mass} \\
 \frac{\partial(\phi \rho_f h_f)}{\partial t} + \nabla \cdot (\rho_f h_f \mathbf{v}) &= 0 && \text{Energy} \\
 C_p \rho_f \frac{\partial T}{\partial t} - \nabla \cdot (\lambda \nabla T) + q_H &= 0 && \\
 \frac{\partial(\phi \rho_f X)}{\partial t} + \nabla \cdot (\rho_f X \mathbf{v}) + q_{pX} &= 0 && \text{Salinity}
 \end{aligned}$$

Density, enthalpy, and heat capacity are all functions of pressure, temperature, and mass fraction of NaCl. While neglecting salinity diffusion, we also consider the material properties of the porous rock to be isotropic, uniform, and constant. The initial pressure, temperature, and salinity profiles are considered stable, and the mesh we use is static.

We designed synthetic models with a low permeability matrix in the basement, many permeable fractures, and several faults zones. Each one of these regions is assigned independent material properties, including a "thickness" value, to allow dimensional consistency with LDE's.

In all our models, we set up time-invariant Dirichlet conditions for pressure and temperature in the top boundary, and a heat flux boundary condition at the bottom boundary. In contrast, the boundary condition for NaCl mass fraction is initially stable at 5% for the first 10000 years (i.e. simulated time), followed by a time varying period 10000 years. This time-varying period begins at 5% and grows to 25% during the first 1000 years, remains steady for the next 8000, and tapers off back to 5% for the next 1000. The aim is to simulate a period of high evaporation followed by sea replenishment.

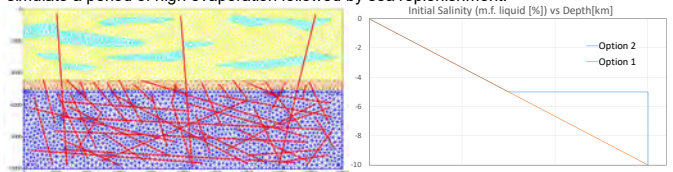


Figure 2: (left) Typical mesh used. (right) Initial conditions assume a stable pressure and temperature profile, while the initial salinity profile varies from 5% at the top to 20% at the bottom.

Results

We set up two separate fluid-tracking tracers: one for the evaporitic brine and the other aimed at the basement brine. With the help of the tracers, as well as temperature conditions, we set up two markers (shown in teal for Marker 1 and orange for Marker 2 in Figures 3 and 4) so that we may approximate and observe the level of mixing.

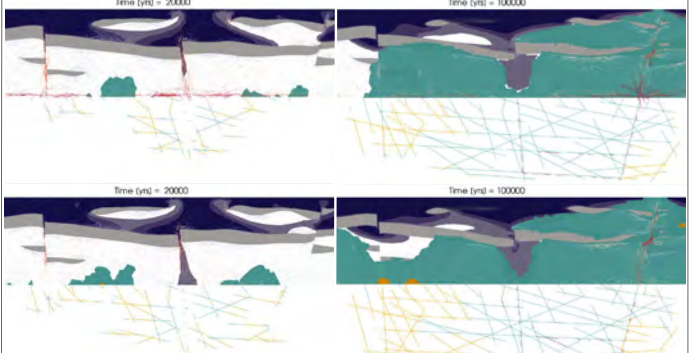


Figure 3: Result snapshots at the end of the evaporation stage (left) and end of simulation (right) with (top row) and without (bottom row) a permeable transition zone. A dark blue tracer is set to track incoming fluid from the top boundary. Through-going basin Obstacle permeability is 10^{-17}

Marker 1 tracks locations in the domain where both the new and basement brine content are above 3% (that is, the total fluid mass fraction of the liquid is 6% basement + new brine, the rest (most of it) is basinal brine) and the temperature is at least 50°C. **Marker 2** follows a similar philosophy, restricting the conditions to 10% (5% of new brine and 5% of basement brine) and the temperature to a typical (at least in the Uranium case) ore forming 130°C. It also restricts its tracking to the permeable transition zone, which is where it is assumed that the likelihood of precipitation is the highest.

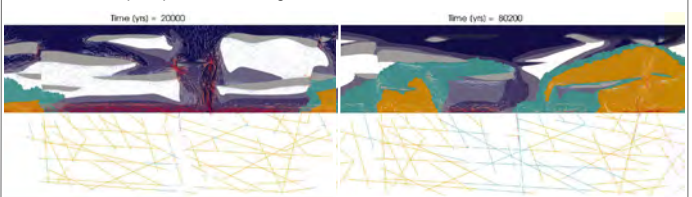


Figure 4: Result snapshots at the end of the evaporation stage (left) and end of simulation (right) with a permeable transition zone and through-going obstacles. Obstacles in sedimentary basin either spread-out in this case. Obstacle permeability is 10^{-17}

The low percentages used in the markers arise from the fact that the only portion of basement brine that is truly mobile is in the fractures, which corresponds to a relatively small amount of the total brine content in the domain, and that the "new" incoming brine is only being fluxed in for a limited time. Most of the mobilized fluid consists of pre-existing basinal brine, which is the richest and metal-bearing one. While the markers do not track actual precipitation because we have not used reactive transport modelling features for this study (i.e. yet!), they indicate where it is very likely that precipitation may happen.

Figure 5 shows a snapshots of a simulation that differs from Figure 3 (top row) only in its initial salinity profile (i.e. using "option 2" from Figure 2). Such a scenario assumes that basement brine salinity is much higher than that of a linear-with-depth profile.

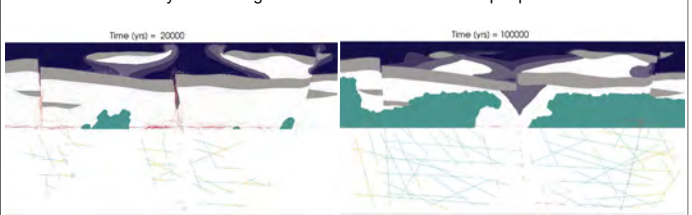


Figure 5: Result snapshots at the end of the evaporation stage (left) and end of simulation (right) with a permeable transition zone and through-going obstacles. Simulation is identical to Figure 3 (top row) with a constant initial salinity m.f. of 0.2 in the basement (see Figure 2 - Initial salinity profile, Option 2).

Conclusions & Outlook

Temperature, pressure, and salinity, together with medium pore-space and permeability create the mixing flow conditions which, as expected, show a particular predilection for the vicinity of unconformities.

We established slightly more-complex-than proof of concept simulations in a bid to understand the onset of geothermal anomalies in particular circumstances/scenarios. Results show promise by pointing out probable locations with the help of markers, which help track pre-selected conditions. They also serve to highlight the importance of initial conditions, sedimentary "obstacle" permeability, and the numerous possible scenarios that would need to be simulated, carrying out a sensitivity analysis, all of which is still needed prior to drafting any strong conclusions.

References

1. Geiger, S. et al.(2006) Transport in Porous Media, 63, 399–434, doi: 10.1007/s11242-005-0108-z
2. Paluszny, A. et al (2007) Geofluids, 7: 186–208.
3. Weis, P. et al. (2014), Geofluids, 14(3): 347–371,doi: 10.1111/gfl.12080

High-resolution temporo-ensemble PIV to resolve pore-scale flow in fractured porous media

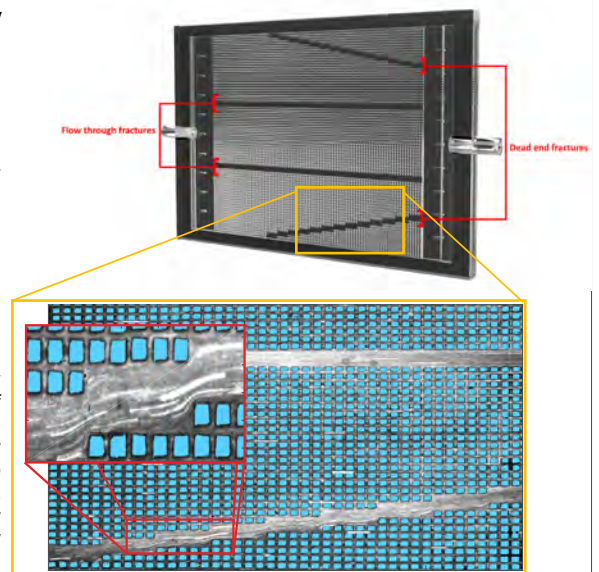
Mehrdad Ahkami, Thomas Roesgen, Martin O. Saar, Xiang-Zhao Kong

Motivation Fractures are conduits that can enable fast advective transfer of (fluid, solute, reactant, particle, etc.) mass and energy. Such fast transfer can significantly affect pore-scale physico-chemical processes which in turn can affect macroscopic mass and energy transport characteristics. Therefore, it is crucial to determine pore-scale transport properties and then upscale these properties to larger scales. However, only a limited number of experimental studies with sufficient spatial resolution over large Representative Elementary Volumes have been conducted to characterize fluid flow and transport features in fractured porous media.

Methodology

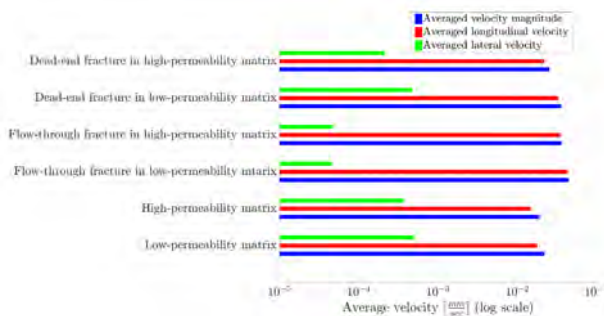
Experimental setup: In this study, 3D-printing technology is employed to manufacture a transparent fractured porous medium to resemble dual-permeability and dual-porosity subsurface formations. Square pillars with a size of 800 μm are 3D-printed to construct fractured porous matrices inside the cell. Parallel to the main flow direction, the cell is divided into two halves: one half being a high-permeability matrix with 300 μm spacing between the pillars and the other half being a low-permeability matrix with 200 μm spacing between the pillars. Moreover, we embed one flow-through fracture and one dead-end fracture within each porous matrix. The permeabilities of two matrices are $\sim 4.0 \times 10^{-9} \text{ m}^2$ and $\sim 7.5 \times 10^{-9} \text{ m}^2$, respectively. Due to an in-line illumination configuration, the seeding particles in the fluid cast shadows on a bright background. We then use Particle Shadow Velocimetry (PSV) method to optically resolve the fluid flow.

Temporo-ensemble PIV: Classical PIV method generally employs a relatively large interrogation window and can thus not resolve pore-scale micro-features of fluid flow. In this study, we introduce a new high-resolution PIV method that we term “temporo-ensemble PIV” that can reduce the size of the interrogation window down to ultimately one single pixel. Such a small interrogation window size enables substantially increased spatial resolutions of velocity vectors per unit area in 2D (or unit volume in 3D), allowing delineations of small, pore-scale flow features that are part of a much larger Field of View (FOV). We apply our new method to visualize a 2D fluid flow in a 3D-printed, fractured porous medium.

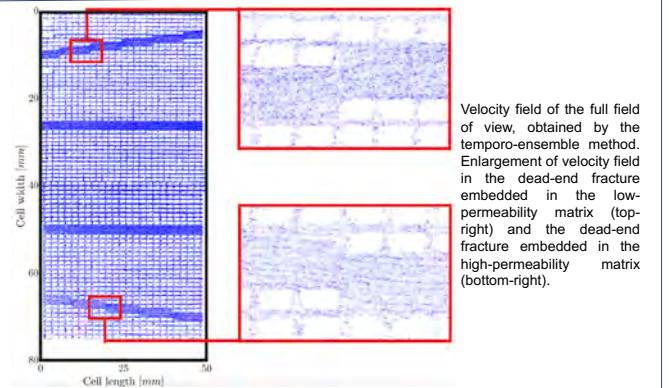


A time-lapse image of particle trajectories, captured during a time interval of 25 sec. The whiteness quantifies the particle density. Blue patches indicate the masks which are applied to exclude regions of impermeable pillars during the PIV calculations.

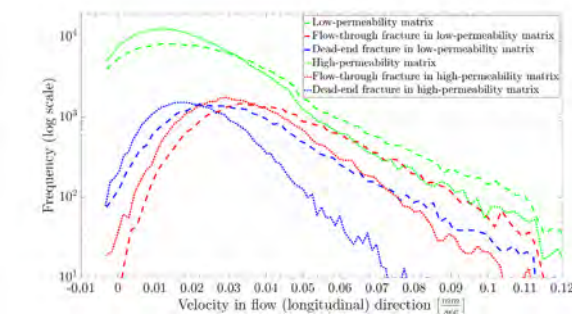
Results



Average Velocity magnitude, average longitudinal velocities, and average lateral velocities of low- and high-permeability matrices as well as embedded dead-end and flow-through fractures.



Velocity field of the full field of view, obtained by the temporo-ensemble method. Enlargement of velocity field in the dead-end fracture embedded in the low-permeability matrix (top-right) and the dead-end fracture embedded in the high-permeability matrix (bottom-right).



Histogram of longitudinal velocities in different regions of the afore-mentioned fractured porous media

Conclusion

- The presented approach can resolve high-resolution 2D velocities in engineered porous media with various levels of heterogeneities.
- Compared to standard PIV methods, our approach preserves high spatial resolutions of velocity vectors, while enabling a large field of view.
- The resulting high-resolution velocity vectors delineate detailed 2D fluid flow structures in various regions of the 3D-printed fractured porous medium. This enables the analysis of various flow interactions, such as those between porous matrices, with different permeabilities and/or porosities, or between fractures and their surrounding porous matrices.
- Our work facilitates experimental investigations of pore-scale physico-chemical processes, with implications for various industrial and scientific fields such as the oil and gas industry, hydrogeology, geothermics, geochemistry.

Fracture process zone in anisotropic rock

Nathan Dutler*, Morteza Nejati**, Benoît Valley*, Florian Amann***
*Centre for Hydrogeology and Geothermics, University of Neuchâtel
** Department of Earth Sciences, ETH Zurich
*** Chair of Engineering Geology and Environmental Management, RWTH Aachen, Germany

1. Motivation

This experimental work aims at assessing the dependency of the **fracture process zone (FPZ)** on the angle between the fracture growth direction and the anisotropy (foliation) for the Grimsel Granodiorite. Samples were collected from cores of the In-situ Stimulation and Circulation project (Amann et al., 2018) and tested using a notched semi-circular bending (NSCB) method. The foliation consist essentially of aligned phyllosilicate minerals.

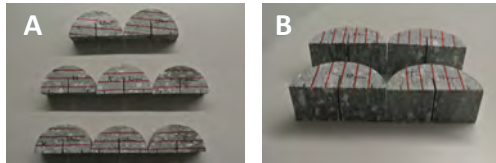
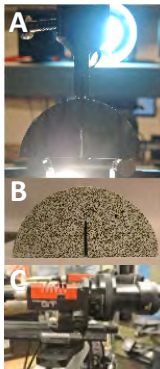


Figure 1: A) and B) presents the two endmembers with the foliation aligned ($\varphi=90^\circ$) and normal ($\varphi=0^\circ$) to the artificial notch.

2. Methods

Three-point-bending tests on notched semi-circular specimens (Kuruppu et al., 2014) were performed. The deformation field of the specimens was monitored using Digital Image Correlation (DIC).



- 15 specimens are tested with 2 different configurations ($0^\circ, 90^\circ$)
- A quasi-static load was applied with controlled displacement rate of 0.1 mm/min
- Specimens are colored in white and afterwards fine sparkled with an air brush (Figure 2B)
- Stereo Digital Image Correlation (DIC) is used to get the strain field with a frequency of 4 Hz during the tests (Cam 1 + 2)

Figure 2: A) Zwick universal testing machine with view on the sample side. B) sparkled specimen for DIC C) The DIC system with two Prosilica GT3400 (red)

3. Localized FPZ at peak load

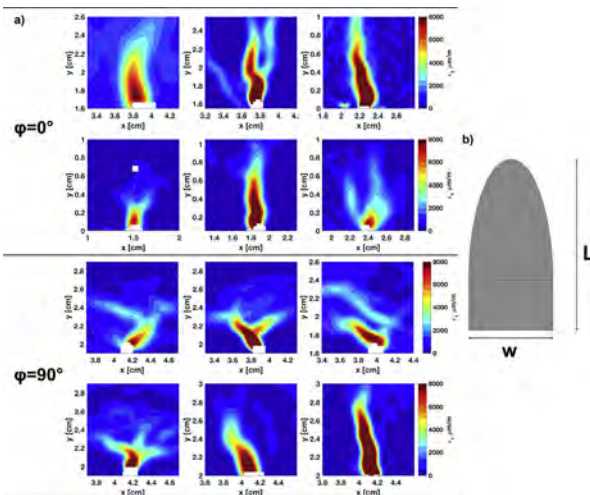
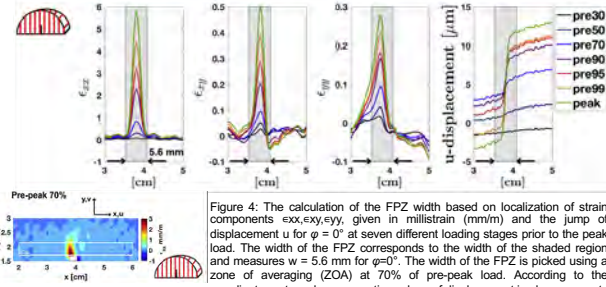


Figure 3: (a) The contours of maximum principal strain showing the FPZ shape at peak load for the configurations $\varphi = 0^\circ, 90^\circ$. (b) The FPZ at the peak load is idealized schematically as a semi-elliptical region with the width of W and the length of L (Dutler et al., 2018).

4. Width of the FPZ and critical strain



It is noteworthy that according to the values of tensile strength and Young's moduli, a **critical tensile strain** of about 270 and 350 micro strains are obtained for the principal directions normal and parallel to the foliation.

φ	σ_t	E	ϵ_c
0°	5.63	21	270
90°	14.69	42	350

From the ϵ_{xx} plot in Fig. 4, it is seen that such values of critical strain are exceeded at a loading stage between 50% and 70% of the peak load. This loading level is in a very good agreement with the general belief that the development of inelastic deformation of quasi-brittle materials start at about 60–70% of the peak load.

5. The size of the FPZ

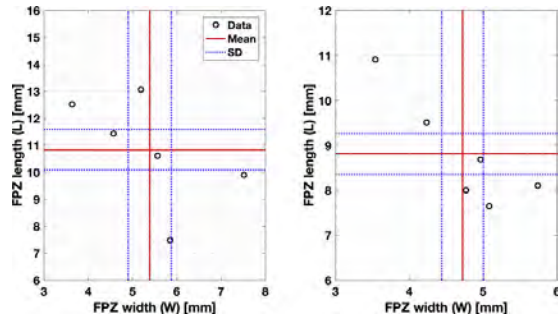


Figure 5: The measured values for the FPZ width (W) and length (L) for two cases of $\varphi = 0^\circ$ and $\varphi = 90^\circ$. The mean values of the six tests are shown by red line, while the blue pointed line show the standard deviation. The results are taken from the fully formed FPZ, i.e. at 70% of pre-peak load for $\varphi = 0^\circ$ and 90% of pre-peak load for $\varphi = 90^\circ$ (Dutler et al., 2018).

- In both configurations $\varphi = 0^\circ$ and $\varphi = 90^\circ$, the average length to width ratio is $L/W \approx 2$.
- The fracture process zone is larger in size when the crack grows along the foliation compared to the case it propagates normal to the foliation. The ratio of the FPZ size in two directions is $L_{\varphi=0^\circ}/L_{\varphi=90^\circ} \approx W_{\varphi=0^\circ}/W_{\varphi=90^\circ} \approx 1.2$. The fracture process zone is anisotropic in terms of size.
- The reason for a bigger FPZ along the foliation may be the preferred direction of micro-crack in such direction. Since the micro-cracks are oriented in the direction of crack growth, their activation and propagation can lead to a wider process zone.
- There is a negative correlation between the length and the width of the FPZ in both configurations. One can explain this trend by considering that the energy dissipated via micro-cracking is a material property, which is constant.

References

F. Amann, V. Gischig, K. Evans, J. Doetsch, R. Jalali, B. Valley, et al., The seismo-hydro-mechanical behavior during deep geothermal reservoir stimulations: open questions tackled in a decameter-scale in situ stimulation experiment, *Solid Earth* 9 (1) (2018) 115–137.
N. Dutler, M. Nejati, F. Amann, B. Valley, and G. Molinari (2018). On the link between fracture toughness, strength and fracture process zone in anisotropic rocks, *EPA*, (in press). <https://doi.org/10.1016/j.epa.2018.08.017>
M.D. Kuruppu, Y. Obara, M.R. Ayatollahi, K.P. Chong, T. Funatsu, ISRM-suggested method for determining the mode I static fracture toughness using semi-circular bend specimen, *Rock Mech Rock Eng* 47 (1) (2014) 267–274.

On the variability of the seismic response during multiple decameter-scale hydraulic stimulations at the Grimsel Test Site

Linus Villiger*, Valentin Gischig**, Joseph Doetsch**, Hannes Krietsch**, Mohammadreza Jalali**, Nathan Dutler***, Benoît Valley***, Florian Amann**, Arnaud Mignan* & Stefan Wiemer*

Motivation

Predicting induced seismic activity or even occurring maximum magnitude events for hydraulic stimulation operations, e.g. used to increase transmissivity in reservoirs for deep geothermal systems (EGS), is an extremely challenging task. However, estimating at least induced large magnitude events is indispensable when it comes to the hazard assessment of possible new EGS sites. The main reason for the difficulty of the task is the limited knowledge of geological conditions as well as the in-situ stress state at depth. When it comes to hydraulic stimulation, one distinguishes between hydraulic fracturing (HF), where an induced fracture is propagated through the rock and hydraulic shearing (HS), where slip is induced on pre-existing fractures or faults. During stimulation, the two end-member mechanisms HF and HS occur in a complex interplay (see also talk by H.Krietsch on Friday, 11:45). The driving force, however, for HS on pre-existing structures are tectonic stresses, which hold a high potential for inducing large magnitude seismic events, if the fracture or fault is well oriented to the stress field.

In order to find strategies to mitigate large magnitude events and to better understand the seismo-hydro-mechanical coupled phenomena involved in hydraulic stimulation we performed six HS and five HF experiments in-situ at a decameter scale. In this contribution we focus on the six HS experiments. All experiments were performed in the framework of the In-situ Stimulation and Circulation (ISC) experiment at the Grimsel Test Site (GTS) (Amann et al., 2018).

Methods

The 6 hydraulic stimulation experiments were performed in a 20 x 20 x 20 m crystalline rock volume, in which the stress state and geology was exceptionally well characterized (Figure 1). The experiments targeted ductile shear zones (referred to as S1) as well as brittle-ductile shear zones (S3). These S3 shear zones contain a highly fractured zone in the East. A standardized injection protocol was used for the six HS experiments. In total 1'000 litres of water was injected in every HS experiment. Aside of the high-resolution deformation- and pressure-monitoring networks, a highly sensitive acoustic emission monitoring network was installed (Figure 2).

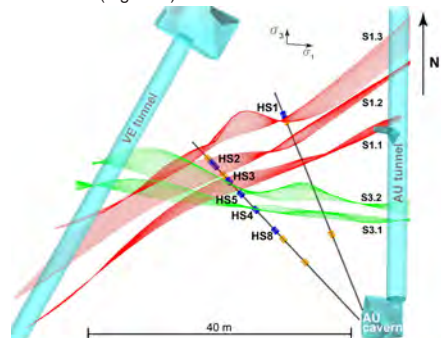


Figure 1: Experimental volume at GTS (top view): Injection boreholes (black lines), HF injection intervals (orange cylinders), HS injection intervals (blue cylinders), the shear zones along with the far field stress state ($\sigma_1 \sim 13.8$ MPa, plunging to the East with $30-40^\circ$, $\sigma_3 \sim 8$ MPa, sub-horizontal North-South, $\sigma_2 \sim 8.5$ MPa, Krietsch et al., 2018)

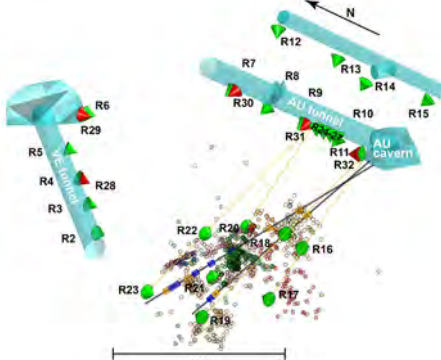
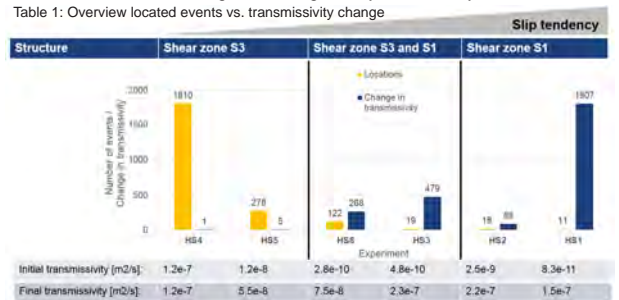


Figure 2: Seismic monitoring network at GTS consisted of 26 acoustic emission (AE) receiver (green cones) and 5 accelerometer (red cones) for calibration purposes along with all located events of the 11 experiments

Results

Table 1 shows an overview of the cumulative number of located events (orange bars) and transmissivity changes (blue bars) of the six HS experiments. The experiments are sorted according to the stimulated structure. Based on the far-field stress state, structures with S1 direction exhibit a larger slip tendency, compared to structures with S3 direction. Note also, that final transmissivities are in the same order of magnitude and generally controlled by S3 structures.



In Figure 3, frequency magnitude distributions (FMD's) along with b- and a₀-values (activation feedback parameter, Mignan et al., 2017) of all HS experiments are shown. The amplitude magnitudes M_A presented are estimated from amplitudes recorded with the uncalibrated AE receiver (Figure 2) and adjusted to absolute magnitudes M_w estimated from AE receiver/accelerometer pairs installed on a tunnel level. M_c for all experiments was estimated at M_A - 2.8.

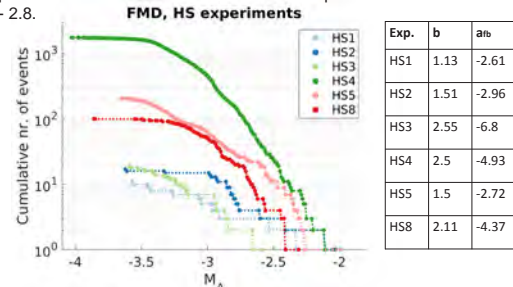


Figure 3: FMD's in addition to b-values and the a₀ for all HS experiments.

Discussion

A highly variable seismic response (number of seismic events, a₀- and b-values) is observed from six 1'000 l water injections into a small 8'000 m³ crystalline rock volume with variable geology following a standardized injection protocol. Furthermore, there is a tendency that an increased seismic response does not necessarily lead to a higher transmissivity increase. But, out of a far-field stress perspective: a higher slip tendency leads to a higher transmissivity increase.

Furthermore, we can observe that the maximum induced magnitude during the stimulation experiments at Grimsel (Figure 4) does not exceed McGarr's (2014) formulation of the upper bound of the seismic moment of an induced seismic event which is proportional to the total volume of injected fluid.

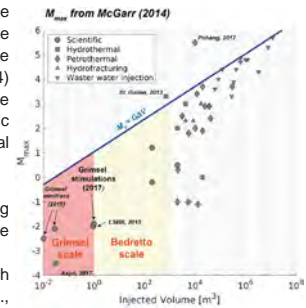


Figure 4: Maximum observed magnitude of induced seismic events of different case studies along with McGarr's (2014) formulation of an upper bound of induced seismic moment.

These outcomes lead to the following questions we would like to tackle in future work:

- What is causing these high variabilities? Is the geology (e.g., increased crack density) the driver for an increased seismic response?
- What can we learn from this scale? Are these findings relevant to the field scale?
- What does this high variability tell us for the predictability of induced seismicity?

References

Amann, F., Gischig, V., Evans, K. F., Doetsch, J., Jalali, M., Valley, B., ... & Giardini, D. (2018). The seismic hydro-mechanical behaviour during deep geothermal reservoir stimulations: open questions tackled in a decameter-scale in-situ stimulation experiment. *Solid Earth*.

Krietsch, H. et al. (2018). Stress measurements for in-situ stimulation experiments in crystalline rock: integration of induced seismicity, stress field and hydraulic methods for reservoirs. *Rock Mech. Fract. Mech. Special Issue: Fracture Mechanics of Rock Mass*, (2018).

McGarr, A. (2014). Maximum magnitude earthquakes induced by fluid injection. *Journal of Geophysical Research: Solid Earth*, 119(2), 1038-1076.

Mignan, A., Broccardi, M., Wiemer, S., & Giardini, D. (2017). Induced seismicity observed from multi-scale systems for accurate decision-making during deep field experiments. *So. Amer. J. Geol.*, doi:10.1007/s12041-017-0250-9

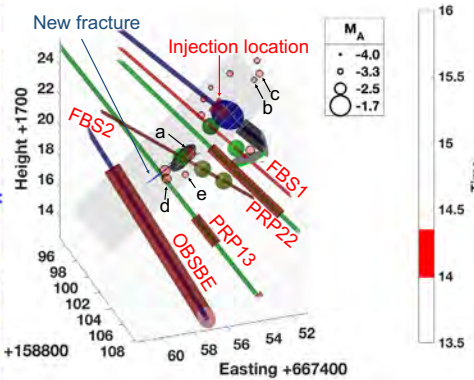
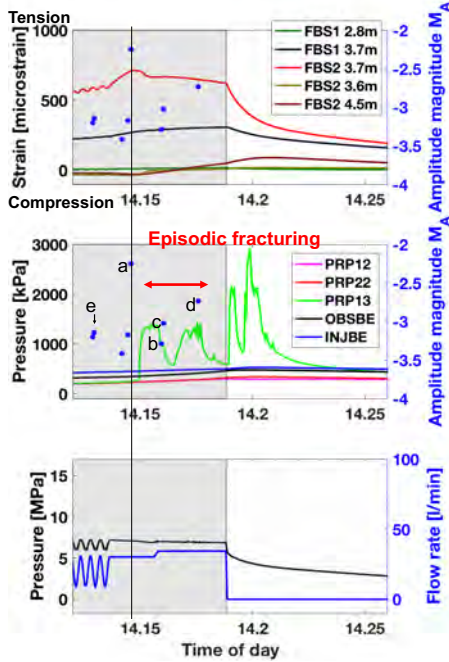
Does a cyclic fracturing process agree with a fluid driven fracture solution?

Nathan Dutler*, Benoît Valley, Valentin Gischig, Linus Villiger, Hannes Krietsch, Joseph Doetsch, Reza Jalali & Florian Amann

ETH zürich

1. Motivation

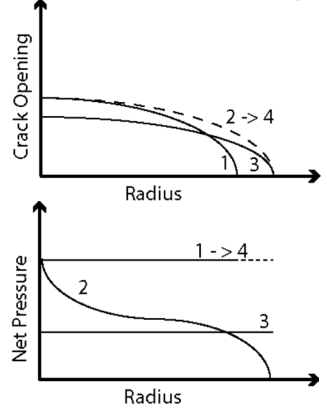
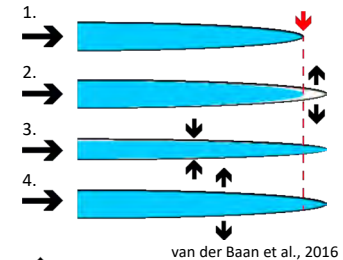
Observation of two stick-split like behaviour in the **pressure response interval PRP13** during the hydraulic fracturing experiment as part of the In-situ Stimulation and Circulation (ISC) project executed in the Grimsel Test Site.



- The FBG sensor in FBS2 at 3.7 m indicates a change in behavior (flattening) at the time the seismic event a) occurs. Shortly afterwards, the interval PRP13 starts to react and at the same time the beforementioned FBG sensor show a slight decrease in tension and stabilizes again.
- The new fracture was observed at a borehole depth of 20 m by the distributed strain system using optical fibers.
- Event b) and c) occur on the other site of the propagating fracture compared to the events a), d) and e)
- Highest increase in pressure is observed during shut-in phase without any located seismic event.
- The located seismic events during the two episodic fracturing cycles indicate an **asymmetric episodic fracturing**.

2. Stick-split mechanism

1. Fluid filled tip building up pressure and increase aperture
2. Tensile failure occurs and pressure drops
3. Fracture closing due to pressure drop brings fluid to the tip
4. Fluid pressure builds up and aperture increase with fluid at the tip

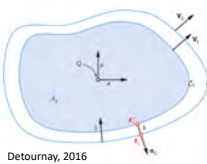


3. Fluid driven fracture solution

The problem can be stated with the following governing equations:

- Elasticity equation
- Lubrication approximation of the non-linear Reynold's equation
- Boundary conditions on both moving fronts:
 - Crack front: $w(x_c, t) = 0, K_I(x_c, t) = K_{Ic}, x_c \in C_c(t)$
 - Fluid front: $p_f(x_f, t) = 0, V_f(x_f) = \frac{q(x_f)}{w(x_f)}, x_f \in C_f(t)$

• A **scaling analysis** revealed that the propagation of a penny-shaped fracture in an impermeable medium is characterised by two time-scales and can be presented by a parametric space OMK with three vertices representing a small-time (O), intermediate-time (M) and large-time (K) self-similar solution (Bunger & Detournay, 2007).

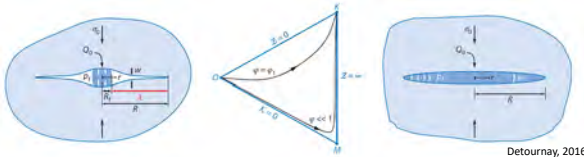


Assuming the fracture radius is $R = 4 \text{ m}$. This leads to a ratio $\frac{\ell_{mk}}{R} \approx 0.3$ which corresponds to a viscosity-dominated case.

If $K_I(x_c, t) < K_{Ic}$ during episodic fracturing, the outer boundary does not move until the $K_I(x_c, t) = K_{Ic}$ is fulfilled. This has a direct influence on the propagation velocity, which decreases when it is averaged over time. We can conclude that the best approximation for the episodic fracturing is a viscosity-dominated case.

Further considerations:

- An asymmetric fracturing behavior, where $K_I(x_c, t) = K_{Ic}$ changes at the fracture boundary needs to be numerically modelled.
- Asymmetric fracturing is often observed, but what is the driving mechanism behind this effect?



• The **energy dissipation mechanism** corresponds either to the viscous fluid flow (M-vertex) or to the creation of new surfaces (K-vertex). The new length scale for the fluid lag is:

$$\ell_{mk} = \frac{K_{Ic}^3}{E^2 \mu^2 v^2} \approx 1.3 \text{ with } E' = \frac{E}{1-\nu^2}, K' = \left(\frac{32}{\pi}\right)^{1/2} K_{Ic}, \mu' = 12\mu$$

using $E = 30 \text{ GPa}, \nu = 0.25, K_{Ic} = 0.8 \text{ MPa}\sqrt{\text{m}}$ and $\mu = 1.2 \cdot 10^{-3} \text{ Pa}\cdot\text{s}, V = 1 \text{ m/s}$

References

- Bunger, A. P., & Detournay, E. (2007). Early-time solution for a radial hydraulic fracture. *Journal of Engineering Mechanics-Asce*, 133(5), 534–540. [https://doi.org/10.1061/\(ASCE\)0733-9399\(2007\)133:5\(534\)](https://doi.org/10.1061/(ASCE)0733-9399(2007)133:5(534))
- Detournay, E. (2016). Mechanics of Hydraulic Fractures. *Annual Review of Fluid Mechanics*, 48(1), 311–339. <https://doi.org/10.1146/annurev-fluid-010814-014736>
- Van der Baan, M., Eaton, D. W., & Preisig, G. (2016). Stick-split mechanism for anthropogenic fluid-induced tensile rock failure. *Geology*, 44(7), 503–506. <https://doi.org/10.1130/G37826.1>

*nathan.dutler@unine.ch

Investigation on Hydraulic Fracturing of Granite

A. de Saussure, L. Laloui¹, H. H. Einstein²

¹Laboratory of Soil Mechanics LMS, Swiss Federal Institute of Technology of Lausanne EPFL, Switzerland
²Earth Resources Laboratory ERL, Massachusetts Institute of Technology MIT, Cambridge, MA, USA

Motivation and Goals

Enhanced Geothermal Systems (EGS) constitute a large renewable source for electricity production. Hydraulic fracturing permits to increase the permeability of the rock in a naturally fractured environment.

- Hydraulic stimulation in deep rock to reactivate existing fractures by injecting pressurized water
- Understand better the mechanisms of hydraulic fracturing for EGS: induce shear failure in Barre Granite

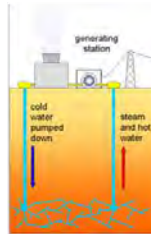


Fig. 1: Enhanced Geothermal System <http://climatereach.blogs.pot.com/>.

Methods

The interaction between hydraulic fractures and pre-existing, non-pressurized flaws is investigated experimentally. The experiments are performed on prismatic specimens of Barre Granite containing two pre-cut flaws under uniaxial or biaxial external load. Fluid is injected in the flaw until failure. Pressure and injected fluid volume are recorded. The crack development is captured with a high-speed camera and a high-resolution camera. Shearing is identified under different flaw geometries and loading conditions.

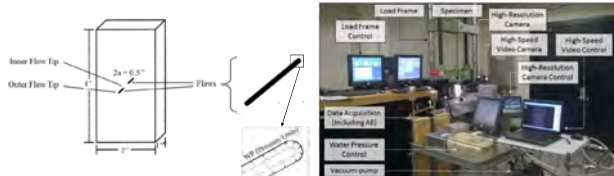


Fig. 2: Schematic of the pre-cut rock specimen with a pressurized flaw (left). Experimental setup for hydraulic fracturing experiments (right).

Analytical investigation on hydrofracturing and hydroshearing

The type of failure (i.e. shear or tensile) is defined by the location of the intersection of the critical Mohr circle with the failure envelope. The evolution of the stress state around a pressurized opening is observed while the external stress and the internal pressure increase. The tangential stress is determined by an analytical solution (Pollard and Fletcher, 2005) and the normal stress corresponds to the internal fluid pressure. The Mohr circles represent the stress state at various locations around the tip of the opening.

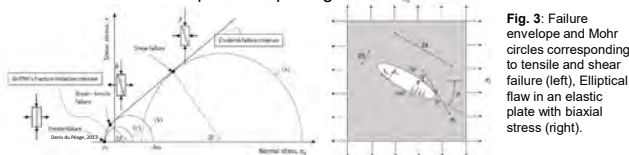


Fig. 3: Failure envelope and Mohr circles corresponding to tensile and shear failure (left). Elliptical flaw in an elastic plate with biaxial stress (right).

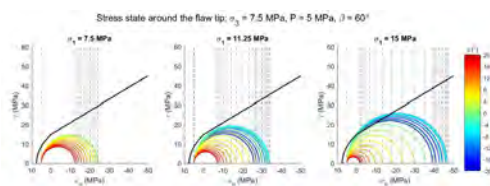


Fig. 4: Effect of an increase of vertical stress on the stress state around the tip of a pressurized flaw leading to shear failure.

Contact: arabelle.desaussure@gmail.com

Types of cracks and grain structure

Different crack types are observed: tensile inter-granular, tensile intra-granular and shear inter-granular cracks. In addition, micro-cracks are observed in the hydroshearing experiments. They are punctual and aligned, linked to the development of a crack, or extended and delimited by grain boundaries.



Fig. 5: Type of cracks and grain boundaries (left). White patching: extended zone (top right) and punctual (bottom right) in hydroshearing experiments.

From hydrofracturing to hydroshearing

Tensile failure is observed in the uniaxial experiments whereas shear failure is observed within the biaxial experiments: dilatancy, en echelon crack patterns and sliding. Hydroshearing occurs with a different test procedure corresponding to an increase of vertical stress and a constant internal pressure leading to the intersection of the Mohr circles with the linear part of the failure envelope (Fig. 4).

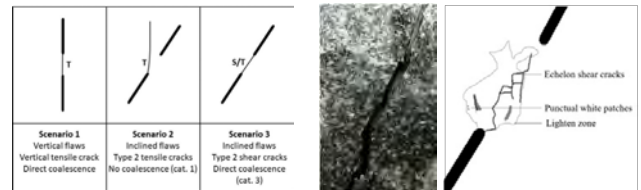


Fig. 6: Crack scenarios with crack types and coalescence categories observed in the uniaxial experiments. Biaxial experiments only show scenario 3.

Fig. 7: Frame (left) and sketch (right) of the crack pattern experiencing scenario 3 in a biaxial experiment showing hydroshearing. En echelon cracks, white patching and dilatancy.

Conclusion

- The experiments have shown that:
 - Visible cracks propagation and crack patterns are highly influenced by the large grains in Barre Granite
 - Micro-cracks develop in the form of white areas in the shear fracture process zone
 - Hydroshearing is observed under a combination of biaxial external stress and hydraulic pressure.

The identification of the conditions leading to either hydrofracturing or hydroshearing will allow to understand better the difference between both mechanisms and its effect on induced seismicity through acoustic emissions measurements

References

[1] Morgan, S. P., Johnson, C. A., & Einstein, H. H. (2013). Cracking processes in Barre granite: fracture process zones and crack coalescence. *International journal of fracture*, 180(2), 177-204.

[2] da Silva, B. G., & Einstein, H. (2018). Physical processes involved in the laboratory hydraulic fracturing of granite: Visual observations and interpretation. *Engineering Fracture Mechanics*, 191, 125-142.

[3] Pollard, D. D. & Fletcher R. C. (2005). *Fundamental of structural geology*. Cambridge University Press.

Advances in laboratory investigation of fluid-driven fractures

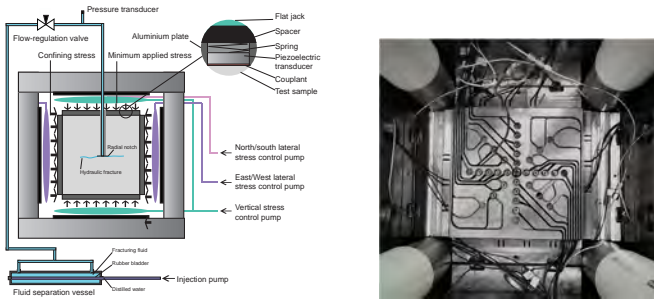
Thomas Blum and Brice Lecampion
Geo-Energy Laboratory, EPFL

1. Introduction

- | | | |
|--|--|---|
| <p>Wide range of applications:</p> <ul style="list-style-type: none"> oil and gas extraction geothermal energy recovery CO2 sequestration | <p>Need for models to:</p> <ul style="list-style-type: none"> efficiently fracture the targeted formation better understand the physics of fluid-driven fracturing get an estimate of fracture size and shape during growth | <p>Scaled laboratory experiments:</p> <ul style="list-style-type: none"> allow to validate theoretical predictions provide datasets under controlled conditions include physical limitations |
|--|--|---|

2. Laboratory setup

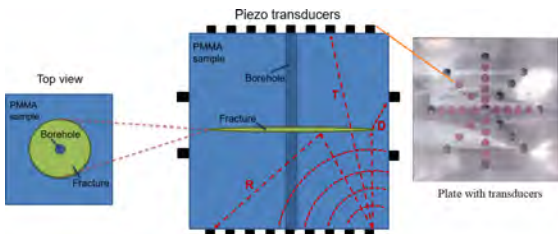
- cubic geologic specimen, 250 x 250 x 250 mm
- reaction frame: confining stresses of up to 25 MPa along each axis
- independently controlled pairs of flat-jacks to apply confining stresses
- high-pressure injection pump: flow rate from 1 μL to 90 mL/s
- notch at the bottom of the wellbore for localized initiation
- experiment duration on the order of minutes to a few hours



Left: schematic of the experimental setup, Right: top-view photo inside the reaction frame, with flat-jacks and platen on the sides of the specimen, and platen with piezo transducers on the top.

3. Acoustic monitoring

- 64 piezoelectric transducer arranged in 32 sources and 32 receivers
- mix of compression and shear in order to use both P- and S-waves
- sequential excitation of all 32 sources every few seconds for snapshots of the acoustic properties during the fracture propagation



Schematic of the transducer layout and different arrival modes.

- R** - reflected signal: fluid content of the fracture
- T** - transmitted signal: fracture thickness
- D** - diffracted signal: position of the fracture tip.

Transmission coefficient through a planar fluid layer of thickness h :

$$T(\omega, h) = \frac{(1 - r_{ff}^2) \exp(i\alpha)}{(1 - r_{ff}^2) \exp(2i\alpha)} \quad (1)$$

where ω the signal frequency; $r_{ff} = \frac{z_r + 1}{z_r - 1}$, $z_r = \frac{\rho_f c_f}{\rho_s c_s}$; ρ_s, ρ_f are the densities of the solid and fracturing fluid, respectively; and c_s, c_f the P-wave velocities of the solid and fracturing fluid, respectively.

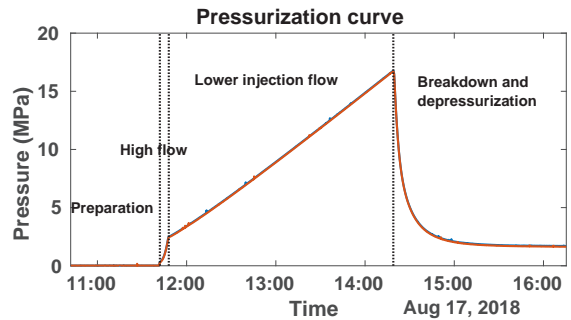
4. Work progress

- Investigations of Carmen slate: highly bedded anisotropic material, relevant for fracture propagation normal to the bedding plane. Currently issues with notching and fracture initiation.
- Fractures in Carrara marble: propagation in fine-grained material, comparison between toughness- and viscosity-dominated regimes of propagation.

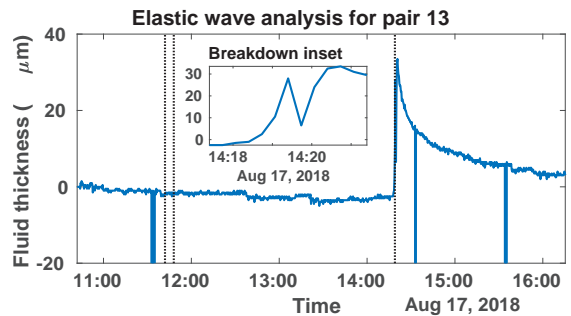


5. Injection in Carrara marble

- No vertical confining stress
- 2 MPa horizontal stresses
- Injection fluid: glycerol, $\eta = 0.6$ Pa.s, flow = 0.02 mL/min



Analysis of transmission measured with one pair of transducers, placed opposite from one another:



6. Conclusions

Extensive analysis of elastic wave data to follow soon for a diverse set of geologic specimens and experimental conditions.

Building a geological model for analysis and numerical modelling of hydraulic stimulation experiments

H. Krietsch¹, J. Doetsch¹, V. Gischig², M.R. Jalali³, N. Dutler⁴, F. Amann³ and S. Loew¹
¹ETH Zurich ²CSD Ingenieure AG Bern ³RWTH Aachen ⁴University of Neuchâtel

Motivation

We build a geological model (Krietsch et al., 2018a) for the in-situ stimulation and circulation experiment (Amann et al., 2018).

The model is used for:

- High resolution of geological visualization
- As a baseline for a DFN
- Hydraulic characterization
- Geophysical characterization
- Analysis and interpretation of experimental data
- Numerical modelling of the experiment

Geological mapping

The test volume is bound by two tunnels and intersected by 15 boreholes. The mapping included mapping of the tunnels using geodetic measurements and panorama images, pictures of the wet and dry cores, and acoustic and optical televiewer borehole logging. Fig. 1 shows a summary of the mapping approach including the interpolation between tunnels and boreholes.

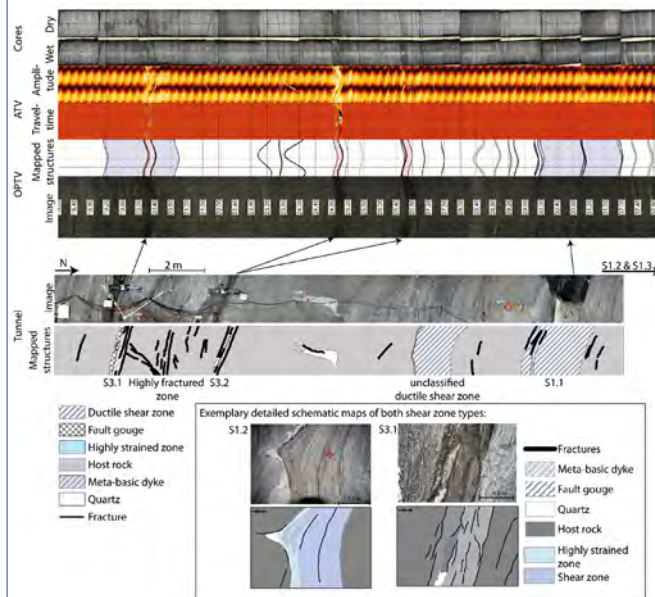


Fig. 1: Summary of geological data, based on which the major shear zones were interpolated. The internal structure of these shear zones (S1 and S3) were mapped in detail. Figure was modified after Krietsch et al., 2018b.

Geological structures

A total of 5 shear zones (3 ductile and 2 brittle-ductile) were mapped. Various brittle fractures (partly open or biotite covered), a pervasive foliation, quartz bands and minor meta-basic dykes were mapped, too (Fig. 2).

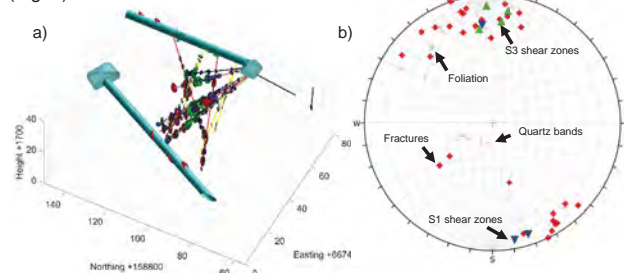


Fig. 2: a) Mapped geological structures inside the test volume, b) orientations of geological structures in a lower hemisphere stereoplots.

Shear zone interpolation steps

- Mapping all shear zones along tunnels and boreholes
- Definition of shear zone sets
- Triangulation between coordinates of each set, neglecting local orientations.
- Third order polynomial interpolation including third order orientations (Fig. 3).

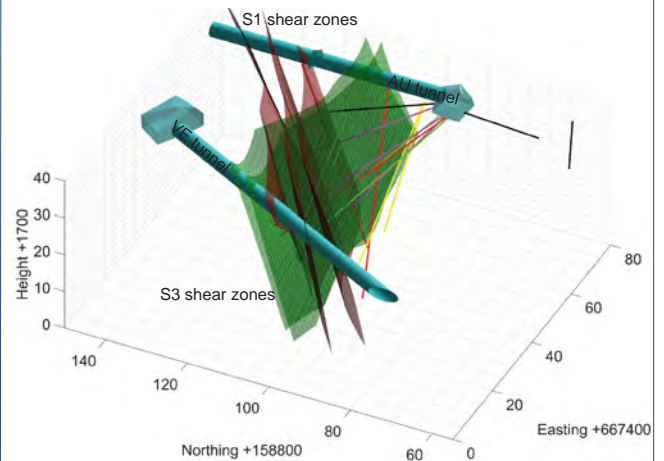


Fig. 3: Interpolated shear zones based on third order polynomial functions.

Technical validation using geophysical methods

Seismic tomography between two tunnels revealed a low velocity zone between two S3 shear zones that correlates with a mapped highly fractured zone (Fig. 4).

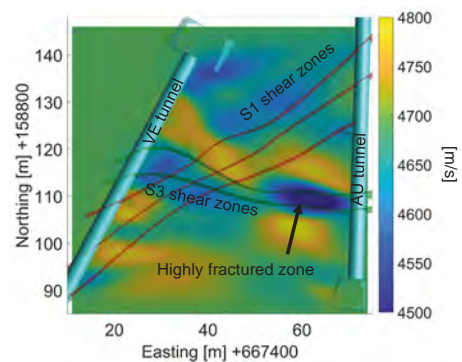


Fig. 4: Seismic tomography with interpolated shear zones.

Summary/Outlook

The geological model represents a high resolution geological baseline visualization of the test volume. It can be used for the construction of a DFN/HydroDFN using e.g., Golder's FracMan, and can be used for setting up a grid for numerical modelling of the stimulation experiment.

References:

Amann et al., 2018 – The seismo-hydro-mechanical behavior during deep geothermal reservoir stimulations: open questions tackled in a decameter-scale in-situ stimulation experiment *Solid Earth*, 9, 115-137
Krietsch et al., 2018a - Comprehensive geological dataset for a fractured crystalline rock volume at the Grimsel Test Site *ETH research collection*
Krietsch et al., 2018b – Comprehensive geological data of a fractured crystalline rock mass analog for hydraulic stimulation experiments *Nature Scientific Data – in review*

Task 1.3

Title

Hydrothermal heat exploitation and storage

Projects (presented on the following pages)

Geoelectrical methods: new insights for geothermal energy prospection and exploration

Aurore Carrier, Matteo Lupi, Carole Nawratil de Bono, Federico Fischanger, Gianfranco Morelli, Julien Gance

Numerical Modelling of the Geneva Basin: from reservoir to geothermal simulations

Marine Collignon, Marion Alcanié, Øystein Klemetsdal, Olav Møyner, Halvard Nilsen, Knut-Andreas Lie, Antonio Rinaldi, Matteo Lupi

Modelling two-phase flow with boiling and gas partitioning

Alina Yapparova, Dmitrii Kulik, George-Dan Miron, Thomas Driesner

Thermo-hydraulic testing of fractured rock mass for heat storage projects

Reza Sohrabi, Benoît Valley

Investigating mineral reactions during high-temperature aquifer thermal energy storage (HT-ATES) in the Swiss Molasse Basin

DB van den Heuvel, C Wanner, U Mäder, LW Diamond

HEATSTORE

Luca Guglielmetti, Andrea Moscariello, Thomas Driesner, Martin Saar, Benoit Valley, Reza Sohrabi, Laryn Diamond, Daniela van den Heuvel, Christoph Wanner, Carole Nawratil de Bono, Michel Meyer, Francois Martin, David Dupuy, PierVittorio Radogna, Energie Wasser Bern

Goelectrical methods : new insights for geothermal energy prospection and exploration

Aurore Carrier, Matteo Lupi, Federico Fischanger, Gianfranco Morelli, Julien Gance

Motivation

- Energetic transition -> developing geothermal energy use
- Previous geological, petrophysical and geophysical studies highlight high geothermal potential of Great Geneva Basin
- To evaluate in situ parameters drillings could be made but are very expensive and do not provide 3D information
- Deep ERT = cheaper alternative

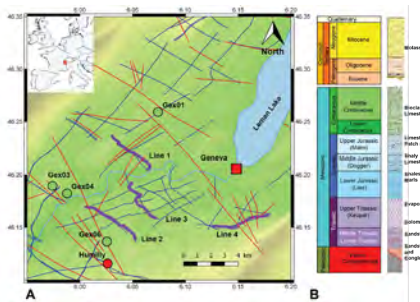
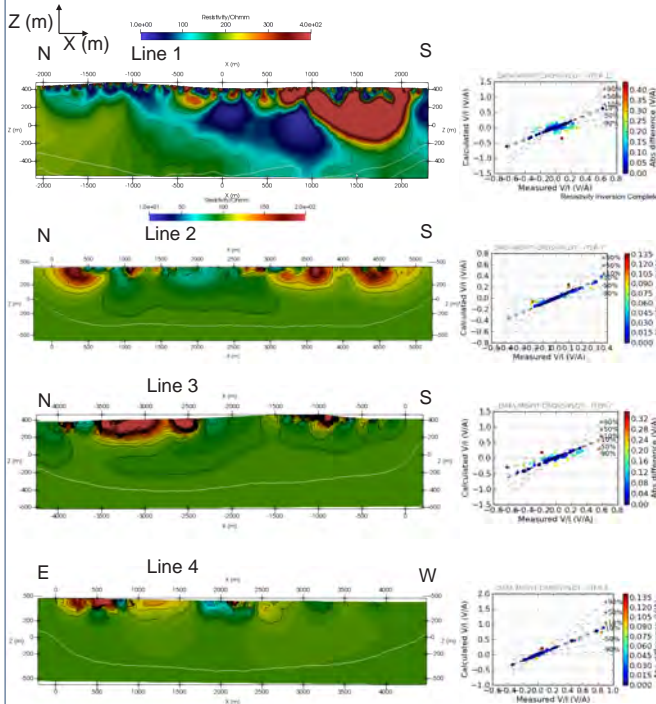


Figure 1: A) Topography of the investigated area and available data. Blue lines : previous active seismic lines, red lines: interpreted faults (GeoMol project), circle points: wells reaching top mesozoic unit, the color corresponds to the lithological unit reached (lithostratigraphic column in panel B). Purple lines: deep ERT profiles performed for this study.

Results

Obtained data are processed and inverted using FullWave Viewer and ERTLab softwares provided by IRIS instruments and GeoStudy Astier.

Figure 3: Resistivity (Ohm.m) profiles obtained for lines 1 to 4 (c.f. location figure 1). Data misfit crossplots are shown on the right of each cross section. Lower coverage areas are below white lines.



- Data are obtained up to 1km depth
- Resistivity values are consistent with local geology and range between 10 to 600 Ohm.m.
- Observed resistivity variations within layers are consistent with previously observed faults

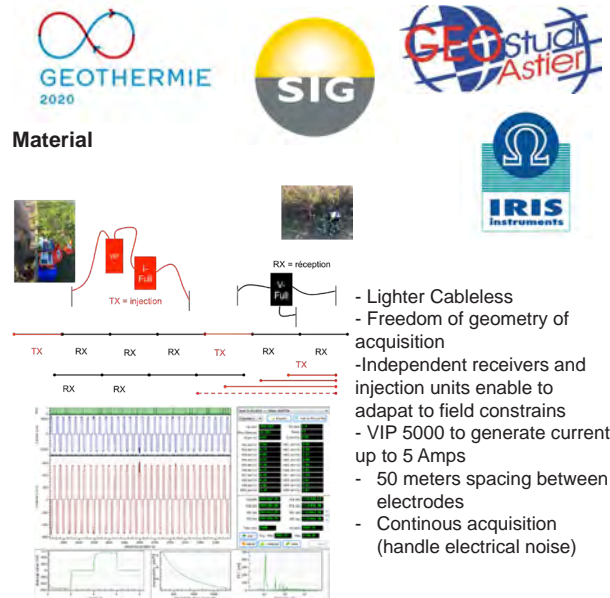


Figure 2: A) Schematic representation of acquisition dispositif for ERT acquisition using FullWavers. Both injection and receivers units record continuously the current. All units are independant and are synchronized in time via GPS data. B) Raw data obtained for one injection (B1-A2 electrodes of injection) at receiver position 1 for the first channel. Signal amplitude on RX1 is the order of 500 mV and chargeability curves can be obtained.

Discussion and Perspectives

- Well data : Molasse 10 to 50 Ohm.m and Cretaceous limestones 100 to 150 Ohm.m, drinkable water 10 to 20 Ohm.m
- Low resistivity body correlated with high porosity/low density rocks
- Improve acquisition geometry** to increase sensitivity would need more time on the field
- 3D** experiment with more receiver units
- Bring key information **for fluid flow modelling**
- Refine inversion** using prior information

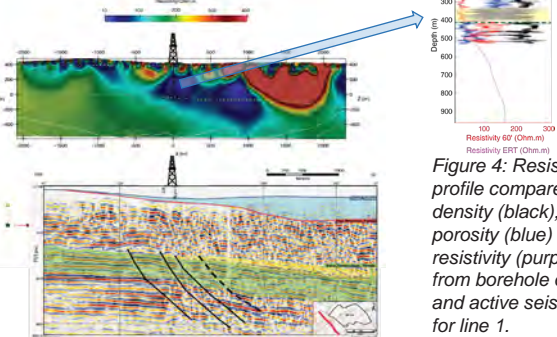


Figure 4: Resistivity profile compares to density (black), porosity (blue) and resistivity (purple) from borehole data and active seismics for line 1.

References

Clerc, N., Rusillon, E., Moscardelli, A., Renard, P., Paolacci, S., & Meyer, M. (2015). Detailed structural and reservoir rock typing characterisation of the Greater Geneva Basin, Switzerland, for geothermal resource assessment.
 Chelle-Michou, C., Do Couto, D., Moscardelli, A., Renard, P., Rusillon, E., 630 2017. Geothermal state of the deep western alpine molasse basin, franceswitzerland. Geothermics.
www.geomol.ch, www.geothermie2020.ch
 Sommaruga, A., Eichenberger, U., Marillier, F., 2012. Seismic Atlas of the Swiss Molasse Basin. Technical Report. Federal office of Topography, swisstopo.
 Morelli, G., Fischanger, F., Gualerzi, D., Occhi, M., Ranieri G., Santarato G., 2010. 3D Cross-hole Electrical Resistivity Tomography to Control the Injection of Expanding Resins: A Case History in Venice (Italy). *Proceedings of 16th European Meeting of Environmental Engineering Geophysics (Near Surface Geophysics)*, Zurich (CH), September 6-8, 2010.

Numerical modelling of the Geneva Basin: From reservoir to geothermal simulations

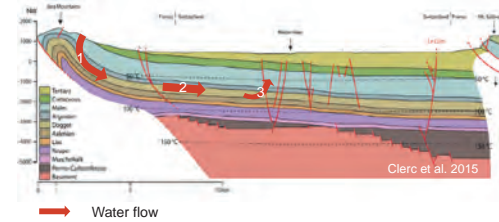
M. Collignon¹, M. Alcanie¹, Ø. Klemetsdal², O. Møyner², H. Nilsen², K.-A. Lie², A. Rinaldi³, M. Lupi¹

1. Department of Earth Sciences, University of Geneva, Rue de Maraichers 13, CH-1205 Genève.
2. Department of Applied Mathematics, SINTEF, Forskningsveien 1, NO-0373 Oslo
3. SED, ETH, Sonneggstrasse 5, Zürich

1. Introduction

The rapid economic development has triggered a constantly rising demand for energy. However, the limited amount of natural resources, as well as the global warming and pollution caused by industrial gas emissions and wastes urge to the development and production of renewable and sustainable energy. In addition to production, energy conservation and storage became equally crucial to make use of excess energy and waste in future times of high energy demand.

Over the last two decades, several geological and geophysical studies were conducted in the Geneva Basin to investigate its geothermal potential for energy production. A large data set is now available, including exploration wells, active seismic, gravity and geoelectrical data. If the production of electricity might be challenging due to the low geothermal gradient, the shallower horizons (within the first 2 km) are now investigated for seasonal heat storage or direct heat production for modern buildings whose heating systems do not require high temperature (> 80°C). However, if a static model of the Geneva Basin has already been proposed based on existing data, no flow modelling model exists. The Geneva Basin is located between two mountain ranges (the Alps and the Jura Mountains) and is drained by the Rhone River which takes its course in the Leman Lake. We here aim at developing a realistic large scale fluid flow model of the Geneva Basin that integrates the influence of the regional geology (i.e. infiltration from the Jura, lake, topography, faults, etc).



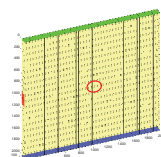
Water flow model
1: Rain infiltration
2: Percolation
3: Resurgence

2. Numerical Model

We are currently developing a Matlab-based geothermal module to investigate the geothermal potential and heat storage strategies in the Geneva Basin. This module is based on MRST (Matlab Reservoir Simulation Toolbox), which is an open source Matlab toolbox, developed by the Department of Applied Mathematics at Sintef, Oslo, Norway (Lie et al., 2016). MRST was initially developed for oil and gas simulations but no thermal equations were implemented in the toolbox. Furthermore, an adequate formulation of the p,T-dependent parameters (i.e. density, viscosity, heat capacity, etc), required to produce realistic models for geothermal applications, is still lacking in MRST.

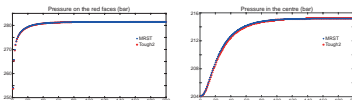
Benchmark

Comparison between MRST and Tough2. Same initial setup and boundary conditions.



Physical domain: 2000x100x2000
Mesh: 20x1x20
Z_{top} = 1000 m
Z_{bot} = 3000 m
P_{top} = P_{hyd}
T_{top} = 293 K

BCs: top: P_{top}, bot: P_{bot} (hydro), face left side: P, 300 bar no flux for T.

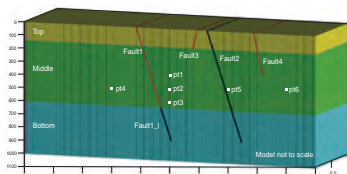


Geothermal module (implemented)
- single phase model (fully saturated)
- two-immiscible phase model
- p, T - dependent density equation for brine (Spivey et al., 2004).

3. "Satigny" type Model

The model of Satigny is loosely based on the preliminary results of the ERT (electric resistivity tomography) done by Carrier et al. (cf. poster). The model dimensions are 5000x1x1000 m (2.5D) with a cell resolution of 10x1x10 m (i.e. 500x1x100 cells). The layers have a dip of ~6°, which is consistent with the regional formation dipping in the Geneva Basin. We considered a model with three layers that represent the quaternary, the molasse and the upper Jurassic.

To mimic the lateral inflow of water from the Jura Mountains, a pressure and associated temperature conditions were applied on the left side of the domain. We considered successively the case where the water is infiltrating in outcropping Jurassic units (simu 1,2) and the case where infiltration takes place in the outcropping molasse (simu 3,4).



We setup for the initial pressure conditions a ca-si-hydrostatic pressure (the density was kept constant to compute the initial pressure) and for the initial temperature conditions a thermal gradient of 32°/km and a surface temperature of 293 K. The infiltrated fluid has either a fixed temperature of 290 K or depth-dependent temperature, with a lower thermal gradient. In the second case we considered that the fluid already warm up since its infiltration in the Jura mountains.

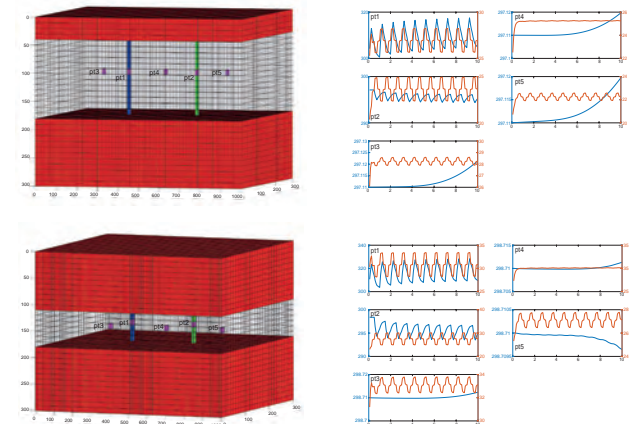
	Simu1	Simu2	Simu3	Simu4
Top	no flux P,T	no flux P,T	no flux P,T	no flux P,T
Bottom	no flux P,T	no flux P,T	no flux P,T	no flux P,T
Left	bottom only, fixed P,T	bottom only, fixed P,T	middle only, fixed P,T	middle only, fixed P,T
Right	fixed P,T	fixed P,T	fixed P,T	fixed P,T
Front	P, Phyd: T: dt	P, Phyd: T: dt	P, Phyd: T: dt	P, Phyd: T: dt
Back (lake)	few cells, fixed P,T	few cells, fixed P,T	few cells, fixed P,T	few cells, fixed P,T
	P: Phyd + 10 bar, T: 290K	P: Phyd + 10 bar, T: 280K	P: Phyd + 10 bar, T: 290K	P: Phyd + 10 bar, T: 290K

	Permeability (mD)	Porosity (%)
Top	0.0035	0.05
Middle	5 (simu 1,2) - 10 (simu 3,4)	0.1
Bottom	5 (simu 3,4) - 10 (simu 1,2)	0.1
Fault1	10	0.1
Fault1_J	0.0001	0.01
Fault2	0.0001	0.01
Fault3	10	0.1
Fault4	10	0.1

4. Heat Storage

For the heat storage simulations, we considered a simple 3D bloc of 1000x300x300 m with a cell resolution of 10x10x10 m and three layers of different thickness. We impose a pressure and temperature conditions on the left and right faces of the model while all other faces have a no flux condition. A ca-si-hydrostatic pressure and a thermal gradient of 32°/km, with a surface temperature of 293K are prescribed as initial conditions. To the left we applied a fixed pressure P = P_{hyd} + 10 bars and a fixed temperature T = dt (initial temperature gradient). To the right we applied a fixed pressure P = P_{hyd} and a fixed temperature T = dt. The aquifer has a permeability of 5 mD and a porosity of 0.1. The top and bottom layers have a permeability of 0.001 mD and a porosity of 0.05.

We considered a cycle of 10 years. From July to September, we inject hot water at a rate of 10⁻⁴ m³s⁻¹ and a temperature of 350K in Well 1 (blue well), while we pump cold water from the reservoir at the same rate in well 2 (green well). October to December is a period of rest, where nothing is injected nor pumped. From January to March, the water is extracted from the reservoir in well 1, while cold water (290 K) is injected in well 2. Finally, April to June is a period of rest. In these two simulations, we investigated the effect of the aquifer thickness on the dissipation of heat in the aquifer. We monitor the temperature and pressure in 6 different points in the reservoir.



5. Further development

Several implementations are still required in the Geothermal Module:

- 2 phase miscible model to account for phase transitions (in high-enthalpy systems) or exsolution of gas in water.
- salt transport to account for convection cells that may develop in the aquifer during heat storage.
- p, T - dependent formulations of the parameters such as density, viscosity, heat capacity.

Additional modules of MRST (some still under development) could be later coupled to the Geothermal Module to build up more realistic but complicated models that take into account the rock-fluid interaction, the dual porosity, or the geochemicals.

References:

Clerc N., Rusillon E., Mascariello A., Renard P., Paolacci S. and Meyer M., 2015. "Detailed Structural and Reservoir Rock Typing Characterization of the Greater Geneva Basin, Switzerland for Geothermal Resource Assessment", World Geothermal Congress 2015.
Lie K.-A., 2016. "An introduction to reservoir simulation using MATLAB: User guide for the Matlab Reservoir Simulation Toolbox (MRST)". SINTEF ICT, <http://www.sintef.no/projectweb/mrst/>.

Acknowledgment:

Marine Collignon and Marion Alcanie are funded by GENERATE, SNF project (PYAPP2_166900), PI Matteo Lupi).



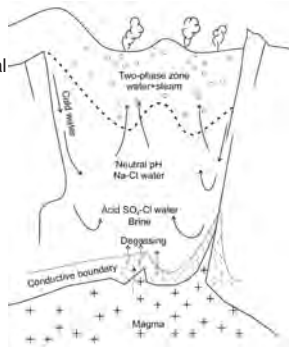
Modelling two-phase flow with boiling and gas partitioning

A. Yapparova (ETH Zurich), D.A. Kulik (PSI), G.D. Miron (PSI), T. Driesner (ETH Zurich)

Motivation: Geothermal systems

Magma-driven, high enthalpy geothermal systems are currently the only type of geothermal reservoirs that is routinely utilized for electrical power generation. The transient evolution of geochemical processes in the subsurface of these systems has remained elusive because direct observation is hampered by the extreme conditions in the boiling reservoir.

Fig. 1. Schematic section of a volcanic geothermal system depicting the origin, interaction, and possible evolution of fluids. (Arnorsson et al., 2007).



Methods

The CSMP++GEM reactive transport code:

- Control volume finite element method (CVFEM) to solve PDEs for two-phase flow and heat transport in terms of pressure, enthalpy and salinity on unstructured grids (Weis et al., 2014).
- Accurate thermodynamic representation of fluid properties – Equation of state for a H₂O-NaCl system (Driesner&Heinrich, 2007; Driesner, 2007).
- Chemical equilibrium calculations using the Gibbs energy minimisation method (GEM), implemented within the GEMS3K code (Kulik et al., 2013).
- Sequential Non-Iterative Approach (SNIA) for transport-chemistry coupling for fast reactive transport calculations (compared to SIA and fully implicit methods).

1D Model Setup

Hot low-salinity vapour at 300°C, 61 bar is injected from the left into the warm 5 wt% NaCl liquid at 200°C, 30 bar. Initial fluid composition is representative of a natural hydrothermal fluid. A boiling/condensation zone develops in the middle part of the model, volatiles partition between the liquid and vapour phases.

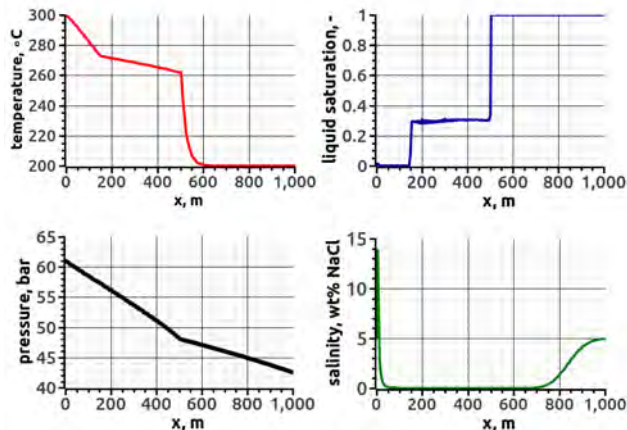


Fig. 2. Temperature, pressure, liquid saturation and aqueous fluid salinity after 300 years of the RTM simulation

Results and Discussion

Volatile species (CO₂, H₂S, CH₄, H₂) preferentially partition into the vapour phase. An increase of CO₂ concentration ahead of the two-phase zone has a major effect on the pH of a boiling solution. The simulation predicts a narrow highly acidic zone that may develop at the border between the vapour-dominated and boiling/condensation zones, due to the specifics of HCl partitioning.

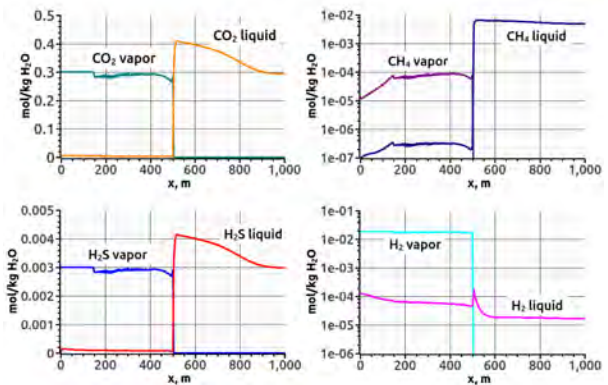


Fig. 3. Molality concentrations of CO₂, H₂S, CH₄ and H₂ in vapour and liquid phases after 300 years of the RTM simulation. Note the logarithmic scale on the right.

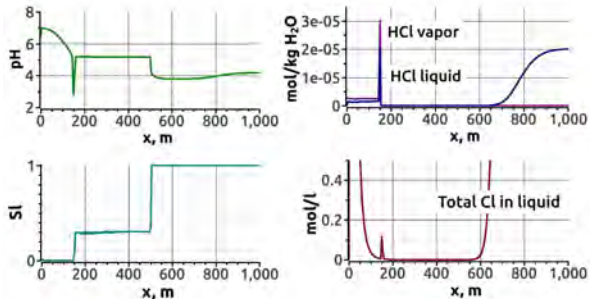


Fig. 4. Solution pH, liquid saturation, molality of HCl in vapour and liquid phases, and total chlorine molarity in liquid after 300 years of the RTM simulation.

Conclusion

The CSMP++GEM reactive transport modelling code represents a powerful tool for studying complex natural systems, having access to state of the art heat flow and chemical models, and allows us to explore the interplay of chemical reactions and two-phase transport in ore forming and high-enthalpy hydrothermal systems.

References

- 1) Arnorsson, S., Stefansson, A., Bjarnason, J.O., Fluid-Fluid interactions in geothermal systems. *Reviews in Mineralogy & Geochemistry* (2007) 65, 259-312.
- 2) Driesner, T., 2007. The system H₂O-NaCl. Part II: Correlations for molar volume, enthalpy, and isobaric heat capacity from 0 to 1000C, 1 to 5000bar, and 0 to 1 XNaCl. *Geochimica et Cosmochimica Acta* 71 (20), 4902–4919.
- 3) Driesner, T., Heinrich, C. A., 2007. The system H₂O NaCl . Part I : Correlation formulae for phase relations in temperature pressure composition space from 0 to 1000C , 0 to 5000 bar , and 0 to 1 XNaCl. *Geochimica et Cosmochimica Acta* 71, 4880–4901.
- 4) Kulik, D. A., Wagner, T., Dmytirenko, S. V., Kosakowski, G., Hingerl, F. F., Chudnenko, K. V., Berner, U. R., 2013. GEM-Selektor geochemical modeling package: Revised algorithm and GEMS3K numerical kernel for coupled simulation codes. *Computational Geosciences* 17 (1), 1–24.
- 5) Weis, P., Driesner, T., Coumou, D., Geiger, S., 2014. Hydrothermal, multi-phase convection of H₂O-NaCl fluids from ambient to magmatic temperatures: A new numerical scheme and benchmarks for code comparison. *Geofluids* 14 (3), 347–371.

Thermo-Hydraulic Testing of Fractured Rock Mass for Heat Storage Projects

Reza Sohrabi & Benoît Valley

Centre for Hydrogeology and Geothermics (CHYN), Laboratory of Geothermics and Reservoir Geomechanics, University of Neuchâtel

reza.sohrabi@unine.ch

Motivation and objectives

Space heating demand is **highly seasonal** while heat production from industrial processes is regular throughout the year. It would be efficient to store excess heat in summer and recover it during the cold season (Figure 1). Medium depth aquifers that are not exploited for drinking water are a **target for heat storage**. It requires however a knowledge of characteristics of the aquifers that cannot be derived from standard well tests. The objectives of this research is to provide **well testing protocols that are adapted for heat storage** projects in fractured aquifers at early project stage, i.e. when a single well is available.

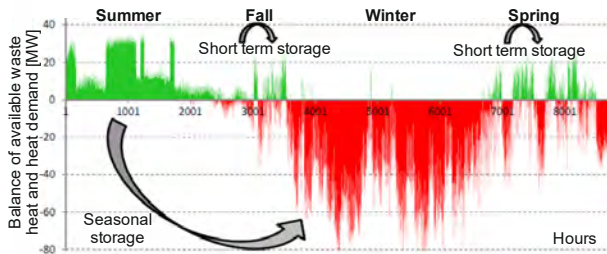


Figure 1: Opportunity for waste heat storage illustrate by heat availability and demand balance in Geneva, after Quiquerez et al. 2015.

Ambient flow

Natural flow occurs in aquifers and it is essential to characterise it for the design of a heat storage system. If ambient flow is too vigorous, the deployment of a heat storage system can even be precluded. In a single well configuration, a **dilution test** can be used to estimate ambient flow. A dilution test consist of mixing a tracer in the well volume and to measure at what rate the tracer is leaving the well, captured by the ambient flow (Figure 2).

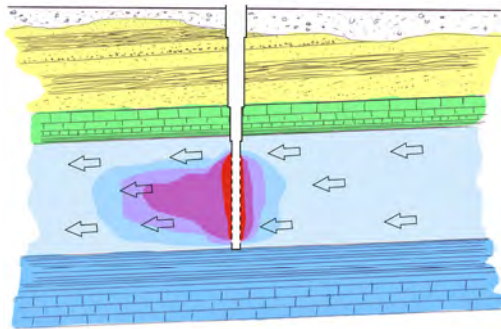


Figure 2: Schematic representation of ambient flow occurring in an aquifer and its impact on heat storage.

Thermo-elastic fracture closure

Hot fluid injection will induce a thermo-mechanical response of the rock that in turn can impact the hydraulic characteristic of the aquifer. For example, **thermo-elastic rock expansion** could induce fracture closure (Figure 4) and thus the transmissivity of the reservoir will decrease. It is required to measure the mechanical conditions in the reservoir (e.g. stress state) in order to assess the impact of such effects on an aquifer thermal storage system.

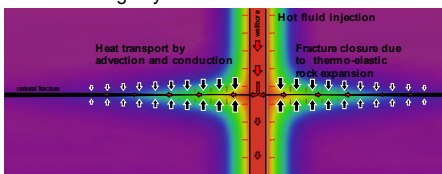


Figure 4: Schematic representation of fracture closure in response to hot water injection.

Approach

The approach in this project is to use numerical simulations and in-situ well tests in order to:

- 1) Define the relevant **key aquifer parameters** that must be determined to provide **reliable heat storage design** in fractured aquifers;
- 2) Propose **well testing approaches** (single well configuration) that can be deployed to estimate these key aquifers parameters;
- 3) Assess the **feasibility of these testing approaches** through numerical simulations and field tests;
- 4) Provide **testing protocols, simplified test design guidelines and application examples** in order to support the acceptance of these testing approaches as an industry standard for heat storage project development in fractured aquifers.

The fundamental assumption of this project is that standard well tests used to determine aquifer transmissivity are not sufficient to generate reliable design parameters for heat storage projects. In the following we present initial ideas concerning the key processes and parameters that need to be determined and possible single well test approaches that could be used to estimate these parameters.

Heat exchanger geometry

The structures in the aquifer will control the **flow geometry** (Figure 3). At same bulk aquifer transmissivity, the flow geometry can differ significantly. This will have a large impact on **heat exchange properties** of the reservoir. **Push-pull tests** of hot water or of tracers mix with variable reactivity with the in-situ rocks can be used to quantify the exchange capacity of a reservoir, which reflect the heat exchanger geometry.

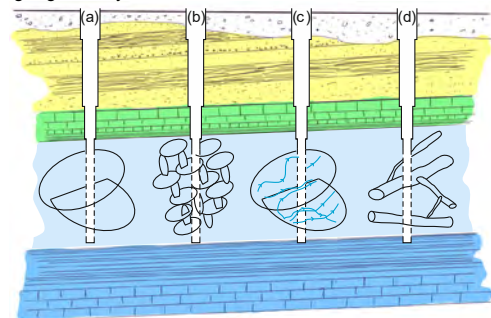
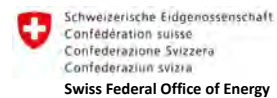


Figure 3: Schematic of various possible heat exchanger geometry. a) dominated by few large features; b) distributed and well connected network of features; c) channelling on planar features and d) conduits formed by karstic processes.

Acknowledgements

These initial ideas will be tested using numerical simulations and in-situ testing in the framework of the European Project Heatstore. It is supported by the Swiss Federal Office of Energy SFOE and is developed in collaboration with Industrial Services of Geneva (SIG).



References

Quiquerez et al. (2015). Réseaux thermiques multi-ressources efficients et renouvelables: Etude de cas de la connexion des réseaux thermiques CADIOM (chaleur fatale) et CADSIG (gaz) à Genève et perspectives d'évolution. SIG, Genève.

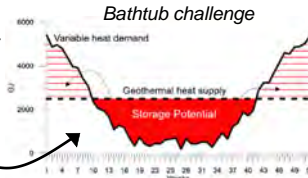
Investigating mineral reactions during high-temperature aquifer thermal energy storage (HT-ATES) in the Swiss Molasse Basin

D.B. van den Heuvel, Ch. Wanner, U. Mäder, P. Alt-Epping & L.W. Diamond (Institute of Geological Sciences, University of Bern)

High-temperature aquifer thermal energy storage (HT-ATES)

What: Storage of excess industrial heat (e.g. from waste incineration) in the subsurface by injecting warm/hot (25 to 90 °C) water into a confined aquifer

Why: Conserve excess heat during summer, then extract hot water during winter for district heating

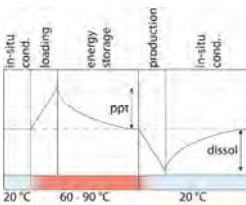


Pilot projects planned in Switzerland

Forsthaus
T = 60 – 90 °C
In porous USM Sandstones
2019 - 2023?

Les Cheneviers
T > 50 °C
In karstified Cretaceous limestone
2018 - 2020

Geochemical challenges during HT-ATES



Dissolution/precipitation reactions in the carbonate system (retrograde solubility)

- Precipitation during loading/storage Clogging?
 - Dissolution during production Does loose sand form?
- ⇒ Can porosity/permeability of the reservoir be maintained?

Dissolution/precipitation of sulphides and silicates (normal solubility)

- Dissolution during loading/storage Release of toxic metals?
- Precipitation during production Scaling in heat exchanger?

Other potential problems

- Corrosion
- Microbial activity: Clogging due to biofilm formation and microbially-induced corrosion (MIC)
- Thermal stratification of aquifer due to density differences

Example HT-ATES Forsthaus: Planned geochemical studies at the Institute of Geological Sciences, UniBe

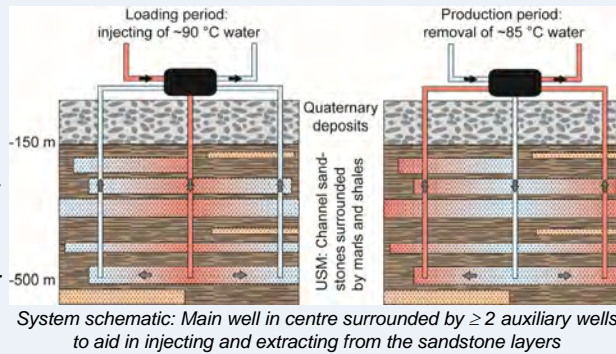
1. Preliminary study

A: Characterisation of **USM sandstones** (composition, porosity, permeability) and comparison with literature data

B: Experimental calibration of **mineral reactions** in contact with synthetic formation water during heating to 60 and 90 °C respectively; partly time-resolved

C: Base-case **reactive transport simulations** using the thermodynamic and kinetic data obtained during the experiments

(preliminary study performed on USM drill cores from a 2017 well drilled at Bern RBS)

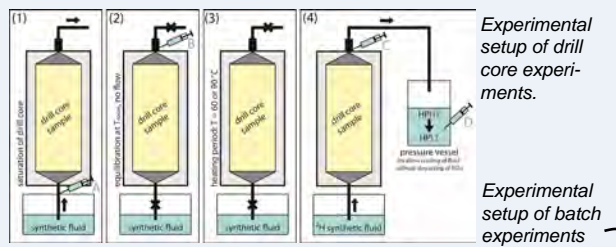


3. Experimental simulation of mineral reactions

A: Identify & quantify **mineral reactions** f(time) under **normal operating conditions (60 and 90 °C)**

B: Assess **mineral reactions** under different chemical conditions (e.g. temperature, pH, pCO₂, salinity, redox conditions)

Two setups: Drill core experiments and batch experiments using powdered or SelfFrag samples



Step by step: Preparation of samples – mounting – saturation with synthetic formation water – equilibration at T_{room} – heating period – cooling period → Samples taken at each step to identify mineral reactions taking place

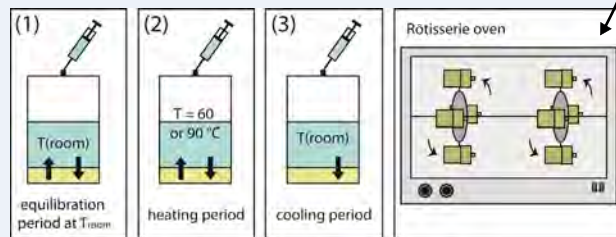
2. Geochemical supervision of drilling and testing at site

A: Characterisation of **USM sandstones** at Forsthaus site (composition, porosity, permeability)

B: Sampling and analysis of **formation water**

C: Characterisation of in-situ **microbial community** in collaboration with GFZ Potsdam

Optionally: Determination of **corrosion rates** of casing and pipes/heat exchanger in collaboration with ETHZ



4. Numerical simulation of Forsthaus system

Expand preliminary simulations with site-specific data:

- Guide testing and system layout (placing of more auxiliary wells)
- Assess long-term behaviour
- Run different scenarios (e.g. reservoir stimulation by injection of CO₂)
- Extrapolate findings to other sites (e.g. Les Cheneviers)



Luca Guglielmetti*, Andrea Moscarello*, Thomas Driesner#, Martin Saar#, Benoit Valley, Reza Sohrabi, Larryn Diamond#, Daniela van den Heuvel, Christoph Wanner#, Carole Nawratil de Bono^, Michel Meyer^, Francois Martin^, David Dupuy^, PierVittorio Radogna^, Energie Wasser Bern^

* Department of Earth Sciences, University of Geneva – Rue des Maraichers 13, CH-1205 Geneva
 # Department of Earth Sciences, ETH Zurich - Sonneggstr. 5, CH-8092 Zurich
 ^ Centre for Hydrogeology and Geothermics, University of Neuchâtel – Rue Emile Argand 11, CH-2000 Neuchâtel
 ^ Rock-Water Interaction Group, Institute of Geological Sciences, University of Bern - Baltzerstrasse 3, CH-3012 Bern
 ^ Services Industriels de Genève – Chemin Chateau-Bloch 2 – CH1219 Le Lignon
 ^ Geo2X - Rue du centre 6, CH-1377 – Oulens-sous-Echallens

Industry uses about 92% of their total energy requirement for generating process heat
 50% of the total energy consumed in Switzerland is needed to supply heat.

Households and services use about 92% of their total energy needs for heating applications

86% of the required heat is generated by the burning of fossil fuel
 Waste heat generated from domestic and industrial processes is continuously discharged into the environment

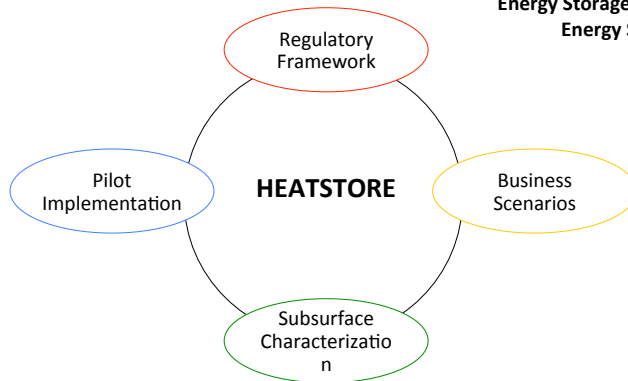


Let's convert waste heat into a resource

In Switzerland hundreds of industrial activities can be suitable for this technology at different scales of application

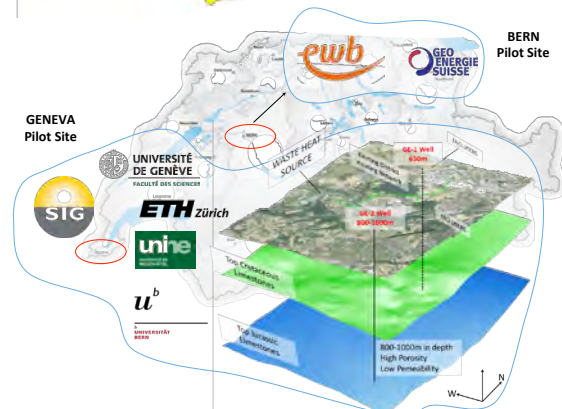
Underground Heat Storage provides several solutions to optimize the whole energy system and reduce the CO₂ footprint by replacing fossil fuels

Energy Storage is one of the most important key elements within the Swiss Federal Energy Strategy in order to meet the CO₂ emission reduction targets.



Objectives:

- De-risk and prove the feasibility of deep (>300m) high-temperature (25-130°C) aquifer thermal energy storage (HT-ATES)
- Characterize the geological, hydrogeological, and hydro-chemical settings
- Develop a toolbox to predict and optimise the subsurface dynamics, performances and economics
- Design and implement pilot demonstration projects
- Monitor the performance
- Determine the current and required stakeholder engagement and adapt the regulatory conditions
- Deliver a fast-track market uptake from demonstration to commercial deployment



Task 1.4

Title

Geo-data infrastructure and analysis

Project (presented on the following page)

GeoTherm: The federal data infrastructure for deep geothermal energy
Lise Boulicault, Ladina Glaus, Christian Minnig, Roland Baumberger

GeoTherm

The federal data infrastructure for deep geothermal energy

L. Boulicault*, L. Glaus**, C. Minnig*, R. Baumberger*

* Federal Office of Topography swisstopo, Swiss Geological Survey, Seftigenstrasse 264, CH-3084 Wabern
 ** SCCER-SoE, ETH Zürich, Sonneggstrasse 5, CH-8092 Zürich

GeoTherm is the federal information system for deep geothermal energy exploration and production. It was launched by the Swiss Federal Office of Energy and swisstopo and support the Energy Strategy 2050.

Challenges for geothermal projects in Switzerland

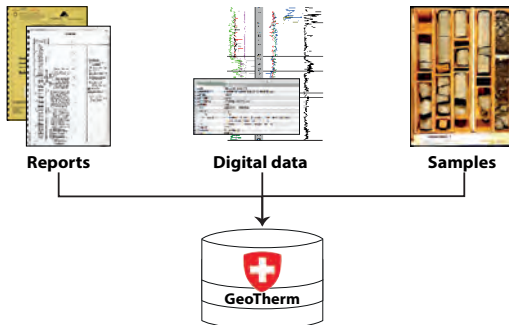
- Overview of the existing and fully accessible geological datasets
- Harmonisation and standardisation of geological data

Advantages of GeoTherm

- All relevant geological data are displayed
- Datasets are structured, harmonised and archived
- Offers free access to non-confidential datasets

Infrastructure

The Swiss Geological Survey collects raw, processed and interpreted geological data that are relevant for developing deep geothermal projects in Switzerland.



Stakeholders and data sources

- Federal Offices
- SCCER-SoE Universities and partners
- 26 Cantons and Liechtenstein
- Private companies (NAGRA, SEAG, Schweizer Salinen, etc.)
- Scientific associations (Geothermie - Schweiz, etc.)

Definition of standards

Publication of 3 data models:
 Data model «Geology» (2017) [1], «Boreholes» (2014) [2] and «Deep wells» (in prep.) [3].

Standards facilitate the collection and the long-term storage of the data.

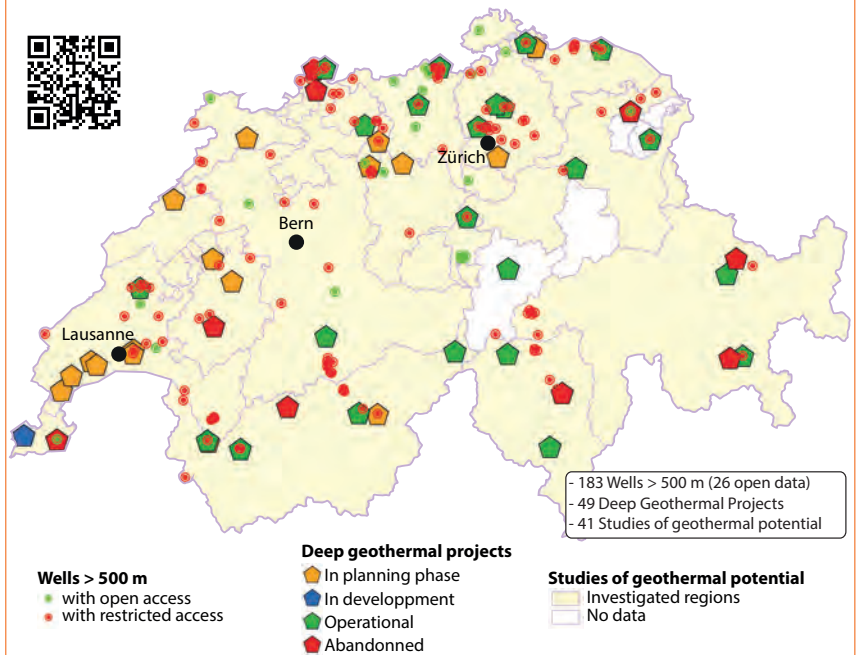
Data harmonisation and quality control (QC)

- Well metadata (location, depth, physical properties, etc.)
- Strata data harmonisation using the lithostratigraphic Lexicon of Switzerland HARMOS [4]

Web-publication

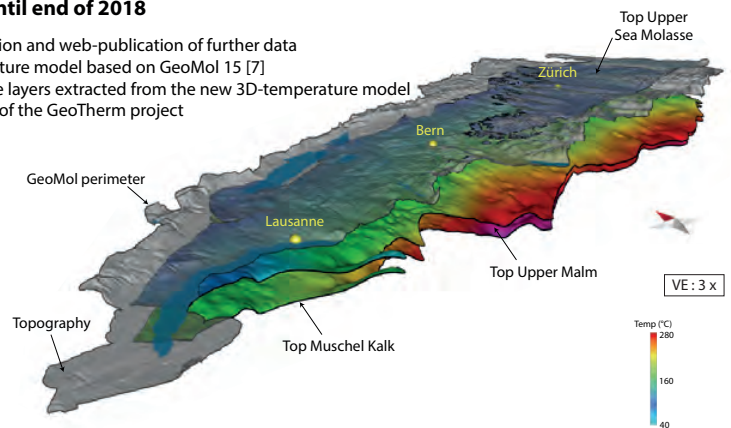
Only the non-confidential data is available on the federal portal (according to agreements with the data owner(s), [5] and [6]).

Results : 3 new layers published on <https://map.geo.admin.ch>



Outlook until end of 2018

- QC, integration and web-publication of further data
- 3D-temperature model based on GeoMol 15 [7]
- Temperature layers extracted from the new 3D-temperature model
- Final report of the GeoTherm project



After 2018

- Continuous data collection, QC, harmonisation and storage
- Iterative process embedded in the ISO-management System of the Swiss Geological Survey.

Take Home Message

GeoTherm Project (2015 - 2018) supports the development of deep geothermal projects by providing visibility of geological data and facilitates data exchanges through a robust data model. Continuous **collaboration** between stakeholders is the key to maintain the basis to achieve the geothermal targets of the Energy Strategy 2050.

[1] Brodhag S. (2017): Datenmodell Geologie. Beschreibung im UML-Format und Objektkatalog. Version 3.0. Bundesamt für Landestopographie swisstopo
 [2] Brodhag S. & Oesterling N. (2014): Datenmodell Bohrdaten. Beschreibung des Kernmodells mit Objektkatalog und UML-Model. Version 2.0, Bundesamt für Landestopographie swisstopo
 [3] Glaus L. & Oesterling N. (unpublished, in prep.): Datenmodell Bohrdaten Modul Tiefbohrungen. Bundesamt für Landestopographie swisstopo
 [4] Strasky S. et al. (2016): Swiss Journal of Geosciences, Vol. 109, issue 2, pp 123-136

[5] Ordonnance sur la géoinformation (Og6o) 510.620, 2008.05.21
 [6] Kettiger, D. (2017): Rechtlicher Rahmen für das Erheben, Nachführen und Verwalten von geologischen Daten. Landesgeologie, No.9, Bundesamt für Landestopographie swisstopo
 [7] GeoMol GST-Viewer : <https://viewer.geomol.ch/>

Work Package 2: Hydropower

According to the Energy Strategy 2050, the mean annual hydropower production has to be increased by 3.16 TWh/a. Considering more stringent environmental regulation that will reduce production by 1.4 TWh/a, the actual target is a plus of 4.56 TWh/a. Such increase is challenging and can be reached only by innovative and sustainable solutions for new large and small hydropower plants and by the extension and optimization of existing schemes. Especially new small hydropower plants require criteria for a careful site selection and strategies to optimize power production within a river network while at the same time minimizing the negative impacts on stream ecology. The effect of climate change will not only impact the availability of water resources in time but also the behavior of the catchment areas by an increased sediment yield and more frequent natural hazards, and thus considerably endanger hydropower production in the near future. The critical period of energy supply in Switzerland is still the winter half year, where 4 TWh had to be imported in average over the past 10 years. Therefore, Switzerland has to increase its storage capacity by new reservoirs where possible and to increase the volumes of existing ones.

Based on feedback from industry and on recent developments in Switzerland and Europe, WP2 focuses on five key objectives. The Highlights 2018 are structured accordingly. Note that a major part of the hydro power related work is reported under WP5, namely the three demonstrators for large hydropower (FLEXSTOR), small hydropower (SMALLFLEX), and the problem of reservoir sedimentation (SEDMIX).

Highlights 2018

Objective 1: To increase flexibility of HP production

Improved hydrological forecasts: The feasibility of hydrological forecasts with a lead time of 1 month has been demonstrated. The quality could be improved with the help of pre-processing. For the new HP plant Gletsch-Oberwald, a runoff forecast system has been implemented to allow short-term operations. This forecast system makes use of a newly developed “now-casting” product by MeteoSwiss (INCA) providing very accurate runoff estimates for the next 3 to 5 hours (based on precipitation radar tracking).

Effects of hydropower on stream temperature: Two projects started in 2018 that aim at assessing effects of hydropower on stream temperature and the resulting ecological impacts. One of these projects will assess the effects of hydropeaking on the spatio-temporal heterogeneity of stream temperature, using a combination of field observations and coupled hydraulic and temperature modelling. The second project will assess the effects of hydropower-induced temperature alterations in streams on trout populations.

Objective 2: To assess the climate change impact on HP production

Assessment of future HP production: Runoff simulations for entire Switzerland have been re-run with the new climate change scenarios CH2018. In addition, simulations on specific catchments are performed using stochastically downscaled climate scenarios, which account for the natural variability of climate and for finer spatial and temporal resolution. Results are further used within the Joint Activity Scenarios & Modelling that aims at generating scenarios for the Swiss energy system 2050.

HPP potential of Switzerland: Accounting for long-term reservoir sedimentation and based on current glacier runoff projections, suitable reservoir sites for new potential HPPs in the Swiss periglacial environment were selected and compared to each other by applying an evaluation matrix. New HPPs at the best-rated seven sites could in theory meet the Swiss Energy Strategy goals for 2035 in terms of an additional annual hydropower production of 1.1 TWh/yr relative to 2016. As a side effect, these HPPs also greatly increase the winter production with a storage energy equivalent of 1.3 TWh.

Objective 3: To assess the risk of extreme natural events and hazards on HP operation

Landslide-induced spatial impulse waves in lakes and reservoirs: Field experiments in a gravel pit in Bülach were prepared and are about to be conducted in September 2018. The basin is 20 m wide 60 m

long and has a water depth of 3 m. Rigid bodies with weights of up to 5 tons will be slid down a 40 m long ramp and impact the water body. The investigation will help to quantify scale effect in hydraulic modelling and give new insights into the process understanding of spatial impulse waves which represent important natural hazards in dam safety assessment.

Objective 4: To enable new projects under uncertainty

Integrated modelling framework for hydrological processes and hydropower systems: The framework allows to simulate the feedbacks between the operation of hydropower systems and the natural hydrological processes leading to streamflow generation and inflow to reservoirs. It can be used to assess how hydropower infrastructure operation responds to different drivers, such as changes of climate, electricity price and demand. The model is currently applied to two hydro-power system configurations representing different typical Alpine hydroclimatic regimes (ice/snow & rain/snow dominated) and hydro-power schemes (storage and pump-storage plants). Both stochastic and robust optimisation model runs are being produced, which focus on three objectives: maximization of production and of revenue, and minimization of environmental impacts under the forcing of climate and price scenarios. The model is suitable to consider additional objectives such as changes in the demand structure and or technical adaptation of the investigated hydropower plant.

Environmental impacts of small-scale hydropower plants: The basin-scale effects of small-scale hydropower plants on biodiversity dynamics were reviewed and published. The review highlighted the importance of assessing cumulative effects of multiple hydropower plants within a catchment in addition to the impacts at the reach scale. Furthermore, a field campaign was conducted for assessing aquatic-terrestrial linkages in streams exploited by small hydropower plants. Eight pairs of sister streams were investigated, with one of the streams in each pair being impacted.

Objective 5: To analyse reservoir sedimentation and enable sustainable use of storage HP

Sediment discharge from glaciers: In recent years, proglacial areas seem to be stabilizing and more sediment originates subglacially. A new physically-based numerical model uses a glacier hydrology model to evolve a subglacial till layer. This allows for the model to capture sediment discharge which is controlled by both sediment transport conditions and sediment availability. When the model is calibrated, it can capture the quantities of sediment discharge, peak events and seasonal evolution of sediment discharge with reasonable quality.

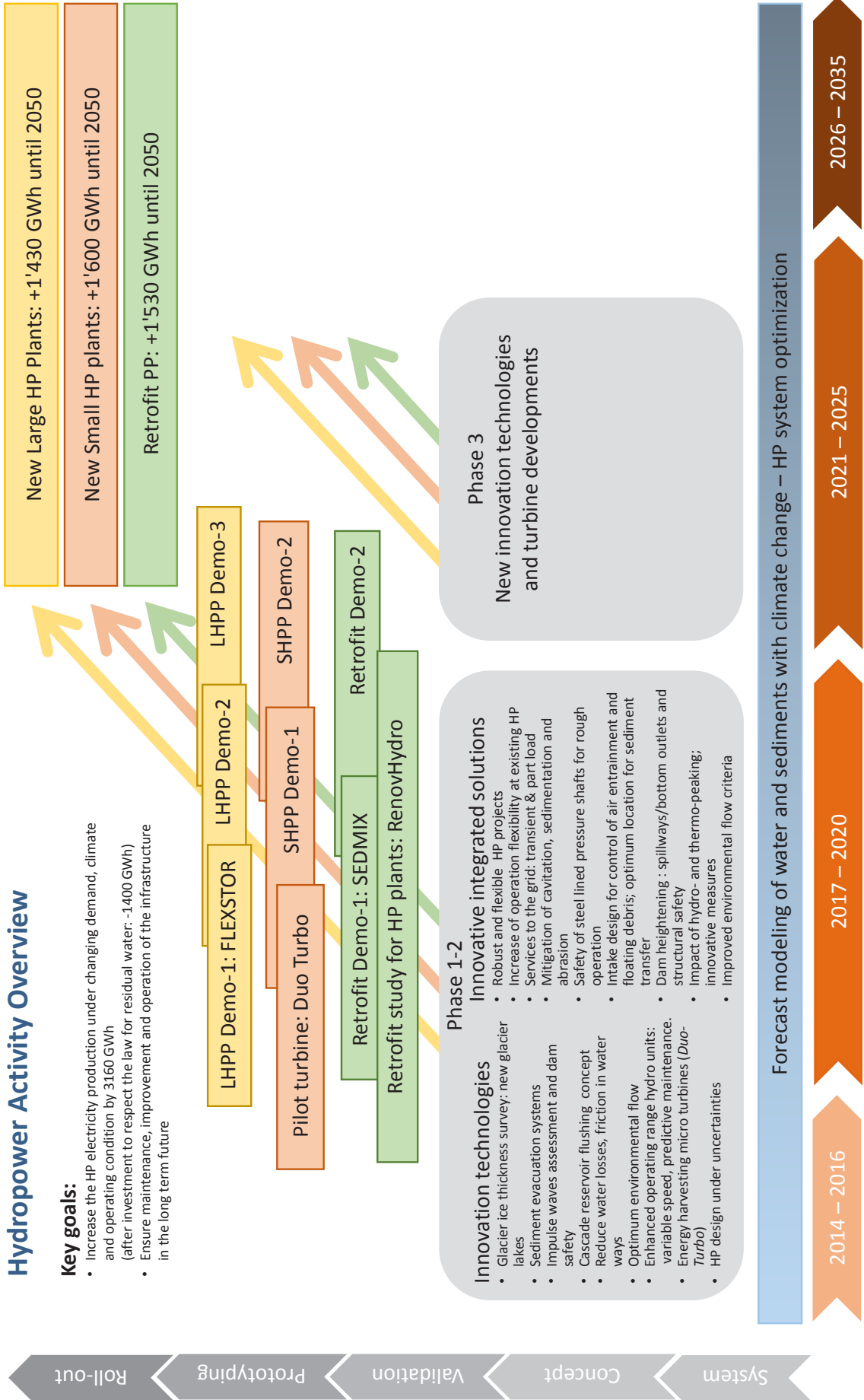
Numerical modelling of long-term reservoir sedimentation: A 1D reservoir sedimentation model was developed with the VAW software BASEMENT, enabling simulations of both the delta formation of coarse sediments and the lake-wide sedimentation from homopycnal flows. The model was used to assess the effects and significance of varying boundary conditions like inflow, SSC, PSD or reservoir operation. It was demonstrated that future reservoir operation and PSD are as important for sedimentation as future runoff evolution.

Desanding facilities: Desanding facilities are key structures for hydropower schemes fed by sediment-laden water from mountain streams to limit the sediment input into the power waterway. Many such facilities do not function properly due to inadequate design often following a classical approach that does not take approach flow and various geometrical boundary conditions into account, thereby resulting in too short desanding basins with low settling efficiencies. The flow and settling processes occurring in desanding facilities and particularly the effect of approach flow conditions such as curvature, Froude number, tranquilizing racks, and transition zone geometry on the trapping efficiency were studied in a hybrid experimental-numerical study. A new design guideline was developed based on systematic numerical simulations to optimize the geometrical design of desanding facilities. The numerical model was carefully validated with flow and sediment data from precedent experimental campaigns at three Swiss desanding facilities using sophisticated measurement instrumentation.

Hydropower Activity Overview

Key goals:

- Increase the HP electricity production under changing demand, climate and operating condition by 3160 GWh (after investment to respect the law for residual water: -1400 GWh)
- Ensure maintenance, improvement and operation of the infrastructure in the long term future



Task 2.1

Title

Morpho-climatic controls

Projects (presented on the following pages)

Multiple-purpose use of reservoirs in high alpine areas under climate change: a national view
Manuela Brunner, Astrid Björnsen Gurung, Massimiliano Zappa, Manfred Stähli

High resolution climate scenarios for snowmelt modelling in small alpine catchments
Michael Schirmer, Nadav Peleg

The role of glacier retreat for Swiss hydropower production
Bettina Schaefli, Pedro Manso, Mauro Fischer, Matthias Huss, Daniel Farinotti

Ice volume and bedrock topography estimation of the Swiss glaciers
Melchior Grab, Andreas Bauder, Lino Schmid, Lasse Rabenstein, Lisbeth Langhammer, Kevin Déléze, Philipp Schaer, Patrick Lathion, Hansruedi Maurer

HEPS4Power - Extended-range Hydrometeorological Ensemble Predictions for Improved Hydropower Operations and Revenues
Samuel Monhart, Philippe Gerber, Frédéric Jordan, Christoph Spirig, Massimiliano Zappa

Sub-seasonal hydrometeorological ensemble predictions in small- and medium size mountainous catchments: Benefits of the NWP approach
Samuel Monhart, Massimiliano Zappa, Christoph Spirig, Christoph Schär, Konrad Bogne

Changes in future river sediment yield: preliminary results from the Guerbe river
Nadav Peleg, Jorge Ramirez

Simulating climate at high spatial and temporal resolutions using the new CH2018 climate scenarios
Nadav Peleg, Paolo Burlando

Online prediction tool for hydropower energy (Opt-HE)
Jordan, Guillaume Artigue, Kevin Cros, Claude-Aline Loetscher, Oriane Etter, Anton Schleiss

Helicopter-borne ground-penetrating radar surveying of temperate Alpine glaciers
Lisbeth Langhammer, Lasse Rabenstein, Lino Schmid, Melchior Grab, Andreas Bauder & Hansruedi Maurer

Multiple-purpose use of reservoirs in high alpine areas under climate change: a national view

Manuela Brunner, Astrid Björnson Gurung, Massimiliano Zappa, Manfred Stähli
 (Swiss Federal Research Institute WSL)

Background

The drought of the past months (summer 2018) rise our awareness for the anticipated impacts of climate change on Alpine water resources associated with an increased probability of local water shortages towards the end of this century. The negative effects of runoff regime shifts triggered by rising temperature, reduced snow pack and glacier cover might be alleviated by the multiple-purpose use of reservoirs for electricity production, irrigation, snow-making, drinking water supply, ecological needs, or flood control. We investigate the potential role of such multiple-purpose reservoirs for alleviating water shortages.

The present study – issued by the Federal Office of the Environment FOEN – aims at providing a country-wide assessment of this potential by comparing the seasonal availability of water in reservoirs to the total demand of water by different users in the adjacent area.

Data and Methods

Water availability (A)

- calculated on a monthly and yearly time resolution, for current and future climate conditions (new scenarios CH2018), using the numerical model PREVAH (Viviroli, D., Zappa, M., et al. 2009)

Reservoirs (B)

- calculated based on available inventories and statistics by the FSO (2017)



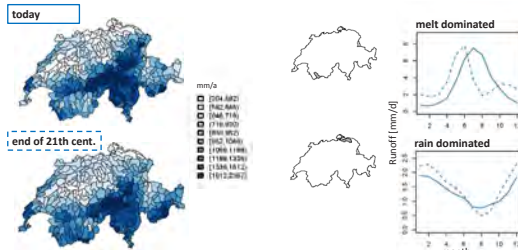
Water demand (C)

- calculated based on methods and data from the NRP 61 and FSO (2017)

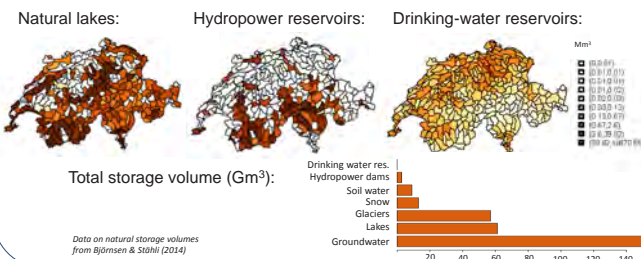


Results

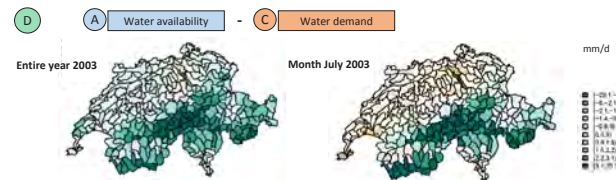
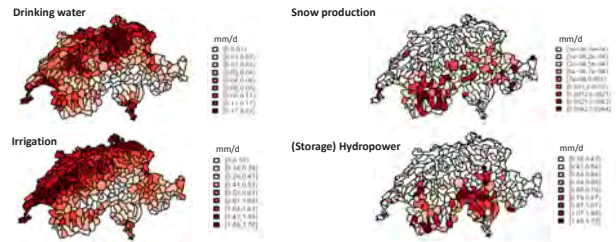
Water availability in Switzerland:



Existing water reservoirs:

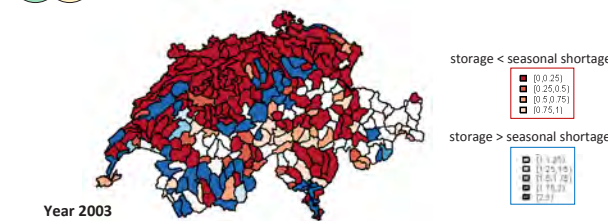


Water demand



Water scarcity: water demand > water availability only consumptive use and ecological flow

Potential of reservoirs for alleviating water shortages



Red sub-areas don't have enough reservoir storage capacities to alleviate water shortages, such as in 2003.

Blue sub-areas have considerable storage compared to estimated seasonal shortage. Here, there is potential to alleviate water shortage in adjacent regions (downstream).

Discussion

A regional comparison of water availability, water reservoirs and water demand – on a monthly time scale – reveals areas with seasonal water shortage and can indicate where (available or future) reservoirs can alleviate seasonal water shortage.

The present results do not consider water transfers between sub-areas.

More specific calculations (including water transfer within and between sub-areas) will be made for Val de Bagnes (VS), Surses (GR) and a region in the Swiss plateau.

Acknowledgement

- Funding from Federal Office of the Environment (FOEN), (Focus area NCCS – CH2018 Hydro)
- Meteorological Data from MeteoSwiss
- Innosuisse (CTI) through SCCER Supply of Electricity (Task 2.1)
- This project is elaborated in close collaboration with HSR Rapperswil

High resolution climate scenarios for snowmelt modelling in small alpine catchments

Michael Schirmer, Nadav Peleg

Motivation

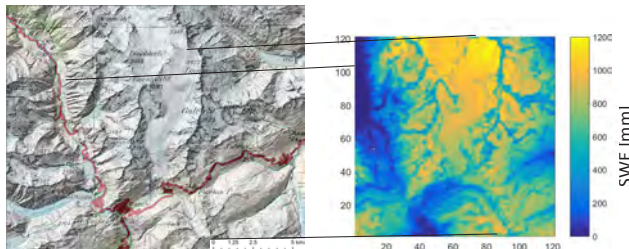
The aim of this project is to support economic risk assessments of long-term investments by small hydropower plant (SHP) operations due to a changing climate. We estimate the impact of climate change on snow water equivalent (SWE) and snowmelt using an innovative combination of novel components: a stochastic 2-dimensional weather generator, and a high-resolution energy balance snow cover model. This allows to include relevant uncertainty sources at a local scale (e.g. natural climate variability).

Methods

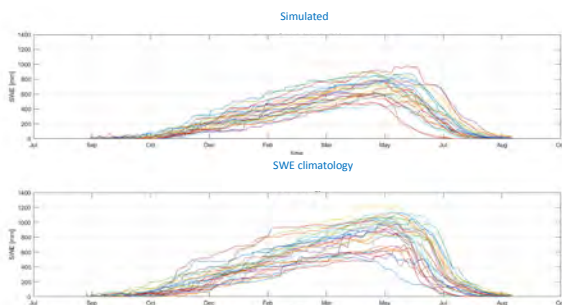
Future climate scenarios are generated based on newest global and regional climate models for the extreme RCP8.5 scenario for the mid and the end of this century. Multiple realisations of future climate periods (30 years) are considered to assess the irreducible impact of natural climate variability. The likelihood of a single winter in a future climate (or of a climate period of 30 years) to be significantly different to our current climate can be assessed.

The model chain in high resolution (100 m x100 m) ensures that relevant processes are considered as for example terrain shading of shortwave radiation, realistic space-time structure of precipitation fields influenced by orographic enhancement, as well as redistribution of snow by wind based on terrain roughness.

Location and spatial model output example

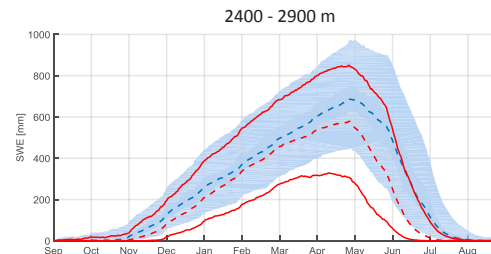


Model results against 'observations'



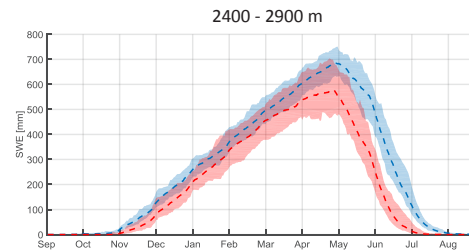
- SWE of 30 years in an elevation band of 2900 to 3400 m
- Dynamics well preserved
- Conservative spread between the years
- Approx. 10% less precipitation (under further investigation)

Natural variability of single years – mid of century



- Simulated SWE (5, 50,95 percentiles)
- Current climate (blue), 900 years
- Future climate (red), 5 climate models (RCP8.5) x 300 years
- The spread between dry and wet years is substantially larger than the effect of climate change.
- This spread evolves mainly from natural variability.
- A relevant change between current and future climate can be observed during melt season, while the amount of SWE is not changing relevantly.
- Changes are more evident in lower elevation bands, however, in the shown band most of SWE is stored.

Variability/Uncertainty of climate period predictions



- Same as above, however, the spread of median values of 30-year blocks are analyzed (5 and 95 percentiles) , i.e.:
- "How uncertain are our predictions of a future climate including natural variability and climate model uncertainty?"
- Overlapping areas can be interpreted as a likelihood of no change in SWE between the current und future climate period.
- Mid of this century there is a substantial likelihood of having as much snow as today during peak winter, although considering the extreme climate scenario RCP8.5. However, a substantial change in average melt out is very likely.
- Both natural climate variability and climate model uncertainty contribute to this range.

Conclusion and Outlook

- Natural climate variability is responsible for single years to be different from another. Also whole climate periods of 30 years may be dryer or wetter.
- We quantified the effect of natural variability and climate model uncertainty. We can conclude that it is quite uncertain that there will be less SWE in a substantially warmer climate (RCP8.5, mid if this century) in the presented elevation range (2400 - 2900 m).
- **For the end of this century RCP8.5 scenarios show a significant change in the amount of SWE for all elevation bands.**
- We want to answer, for which climate scenario and for which elevation ranges the impact of climate change is clearly visible, and how this uncertainty in SWE can be translated to runoff.

The role of glacier retreat for Swiss hydropower production

Bettina Schaeffli¹, Pedro Manso², Mauro Fischer^{3,4}, Matthias Huss^{3,5}, Daniel Farinotti^{5,6}
 1: University of Lausanne, 2: EPFL, 3: University of Fribourg, 4: University of Zurich, 5: ETHZ, 6: WSL

Motivation

- High elevation **hydropower production (HP)** strongly relies on water resources that are influenced by glacier melt
 ⇒ **High sensitivity to climate warming**
- First Swiss-wide quantification for the share of Alpine hydropower production that directly relies on the waters released by glacier mass loss
 ⇒ **HP from depletion of long-term ice storage** that cannot be replenished by precipitation in the coming decades

Data sets

- HYDROGIS database of the Swiss HP infrastructure (Balmer, 2012)
 ⇒ 401 powerhouses grouped into 284 HP schemes, total installed power of 14.5 GW (Fig. 1)
- Swiss hydropower production statistics (Swiss Fed. Office for Energy, 2016),
 ⇒ Aggregated to 6 regions: Ticino, Grisons, Valais, Northern Alps, Jura, Plateau
- Swiss-wide raster data set (500 m x 500 m) of monthly natural streamflows for the period 1981-2000 (Zappa et al., 2012)
- Geodetic glacier mass changes of all glaciers between 1980 & 2010 (Fischer et al., 2015); Swiss Glacier Inventory SGI 2010 (Fischer et al., 2014)
- Simulated past & future glacier runoff (GloGEM, Huss & Hock, 2015)
 ⇒ Model forced with ERA-interim climate re-analysis data for past
 ⇒ Future simulations (2040 – 2060, 2070 – 2090) with 14 Global Circulation Models and three different CO2-emission pathways



Fig. 1: Swiss HP infrastructure according to main catchments and HP type

Methods

- Hydropower production $E(t)$ from a given runoff $Q(t)$ estimated via **electricity coefficient**, γ [kWh m^{-3}] (energy conversion factor):
 (1) $E(t) = \gamma Q(t)$
- Glacier melt HP share estimated as: (2) $\rho = \frac{E_m}{E_q} = \frac{V_m}{V_q}$
m: glacier melt (index)
 q: total runoff (index)
 V: runoff volume, $\text{m}^3 \text{ yr}^{-1}$
 (second equality holds from linearity assumption, eq. 1)
- Estimation of γ_h [kWh m^{-3}] at powerhouse scale * indicates design variables
 (3) $\gamma_h^* = \frac{E_h^*}{Q_h^* \tau_h^*} = \frac{P_h^*}{Q_h^* \tau_h^*}$
 E_h^* [Wh yr⁻¹]: expected annual electricity production
 P_h^* [W]: total available power
 Q_h^* [$\text{m}^3 \text{ s}^{-1}$]: total design discharge through turbines
 τ_h^* [h yr⁻¹]: powerhouse operating hours (estimated)
- Estimation of scheme-scale γ_j & regional γ_r :
 (4) $\hat{\gamma}_j = \frac{\sum_{h \in j} E_h^*}{3600 \sum_{h \in j} Q_h^* \tau_h^*}$ (5) $\hat{\gamma}_r = \frac{\sum_{j \in r} \hat{\gamma}_j E_j^*}{\sum_{j \in r} E_j^*}$

Results

- Very high electricity coefficients for glacier catchments (Fig. 2a), regional relationship of electricity coefficients vs catchment elevation (Fig. 2b)

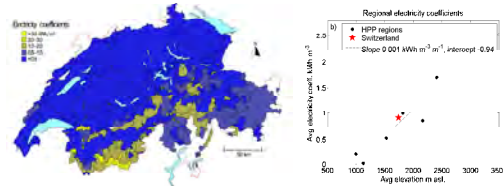


Fig. 2: a) Spatial distribution of scheme-scale electricity coefficients, b) relationship of regional electricity coefficient with average elevation

- Regional estimate of HP from glacier mass loss**
 ⇒ Avg glacier mass loss 1980-2010 (CH): **0.62 m yr^{-1}** (water equivalent)
 ⇒ Avg glacier elevation 2010: 3042 m asl ⇒ average electricity coefficient (trend fig. 2b): **2.11 kWh m^{-3}**
 ⇒ Avg glacier extent 1980-2010: **1072 km^2**
 ⇒ Glacier loss HP: **2.11 $\text{kWh m}^{-3} \times 1072 \text{ km}^2 \times 0.620 \text{ m yr}^{-1} = 1.4 \text{ TWh yr}^{-1}$**
- Catchment-scale estimate of HP from glacier mass loss** (Fig. 3)
 ⇒ CH average 1980-2010: **1.3 TWh yr^{-1}** or **3.8 %** of annual HP, reduction to **0.4 TWh yr^{-1}** by 2070 – 2090 (Fig. 4)

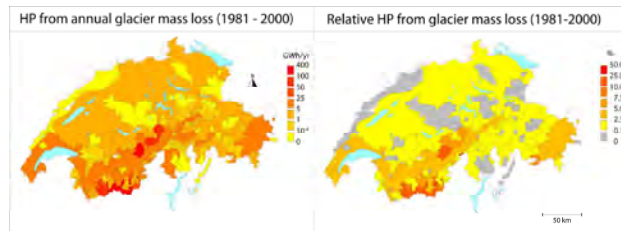


Fig. 3: Left: HP from glacier mass loss in GWh yr^{-1} for the period 1981-2000, right: HP production ratios ρ_g from glacier mass loss for the same period.

- Regional differences in shares and timing of decline (Fig. 4)

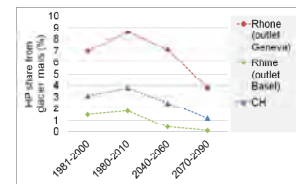


Fig. 4: HP share from glacier mass loss for different periods, for selected large catchments (attention: time scale not linear)

Conclusion

Swiss-wide HP from glacier mass loss since 1980 around **1.4 TWh yr^{-1}**

⇒ Reduction to **0.4 TWh yr^{-1}** by 2070 – 2090

Future reduction of HP from glacier mass loss

⇒ Same order of magnitude as reduction expected from application of water protection act

Reference: Schaeffli, B., Manso, P., Fischer, M., Huss, M., and Farinotti, D.: **The role of glacier retreat for Swiss hydropower production**, Renewable Energy, 132, 615-627, 2019

Other references: Balmer, M.: Nachhaltigkeitsbezogene Typologisierung der schweizerischen Wasserkraftanlagen - GIS-basierte Clusteranalyse und Anwendung in einem Erfahrungskurvenmodell, ETHZ, Zurich, 2012; Fischer, M., Huss, M., Barboux, C., and Hoelzle, M.: The New Swiss glacier inventory SGI2010: relevance of using high-resolution source data in areas dominated by very small glaciers, Arctic, Antarctic, and Alpine Research, 46, 933-945, 2014; Fischer, M., Huss, M., and Hoelzle, M.: Surface elevation and mass changes of all Swiss glaciers 1980-2010, Cryosphere, 9, 525-540, 2015; Huss, M., and Hock, R.: A new model for global glacier change and sea-level rise, Frontiers in Earth Science, 3, 54, 10.3389/feart.2015.00054, 2015; Swiss Federal Office for Energy: Swiss Electricity statistics 2015, Bern, 2016; Zappa, M., Bernhard, L., Fundel, F., and Joerg-Hess, S.: Vorhersage und Szenarien von Schnee- und Wasserressourcen im Alpenraum. Data set available from the lead author., Forum für Wissen, 19-27, 2012.

Ice volume and bedrock topography estimation of the Swiss glaciers

M. Grab^{1,2}, A. Bauder², L. Schmid^{1,2}, L. Rabenstein³, L. Langhammer¹, K. Déléze⁴, P. Schaer⁴, P. Lathion⁴, H.R. Maurer¹

¹Institute for Geophysics, ETH Zurich ²Laboratory of Hydraulics, Hydrology and Glaciology, ETH Zurich ³Drift & Noise Polar Services GmbH, Bremen ⁴Geosat SA, Sion

1. Overview

For overcoming future challenges arising from the ongoing melting of glaciers, an accurate prediction of the future river discharge and the topography of deglaciating regions is needed. A good knowledge of the current ice thickness distribution builds the basis for such predictions.

We developed a helicopter-borne ground penetrating radar (GPR) device and implemented the software for data processing and glaciological modeling. The ice thickness of glaciers is measured with the GPR on a sparse grid. The data is then used as input for glaciological modeling, to calculate continuous ice thickness maps. The goal of the project is to estimate the total ice volume in the Swiss Alps and to deliver information about the glacier bed topography.

2. Current status of the project

Fig. 1 schematically shows the components of the project. The following capabilities build the “pillars” of the project:

- Instrumentation for GPR-surveying (e.g. Langhammer et al., 2017)
- Data processing software (e.g. Grab et al. 2018):
- GIS-based database.

They have been completed in 2017. For more detailed information, we refer to the SCCER-SoE conference contributions from previous years. Based on these “pillars”, we have worked on the “roof” during 2017 and 2018. The main focus was on:

- GPR data acquisition and processing
- Implementation of the GlaTE algorithm

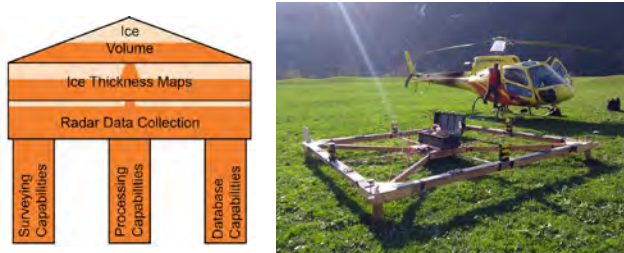


Figure 1: Left: Project sketch. Acquiring of ice thickness data (roof), based on surveying, processing and database capabilities (pillars). Completed sections shaded in dark. Right: The GPR-instrument during a mission in spring 2018.

3. Data acquisition and processing

To date, a total of around 1'000 km of GPR profiles has been recorded on glaciers all over the Swiss Alps. A data example is shown in Fig. 2. It was recorded in Spring 2017 in the tongue area of the Morteratsch glacier. GPR-reflections from the bedrock are marked with arrows. Together with data recorded in earlier years (1999-2015, around 1'400 km), the database now comprises data for most glaciated regions in Switzerland (see Fig. 3):

- 2016-2018: +/- complete data coverage of the corresponding glaciers
- 1999-2016: +/- complete data coverage (blue in Fig. 3) or partial data coverage due only partial surveying or limited data quality (light blue).

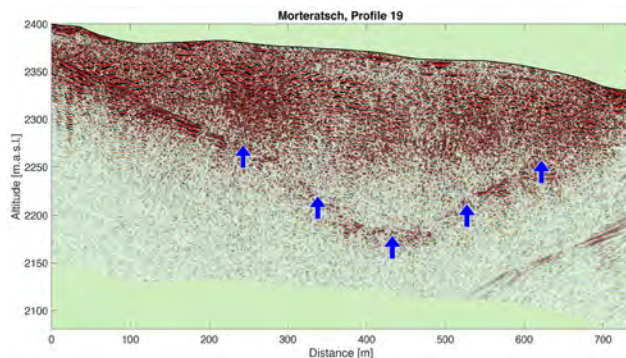


Figure 2: Example profile with processed GPR-data from Morteratsch glacier. Bedrock interpretation indicated by blue arrows.

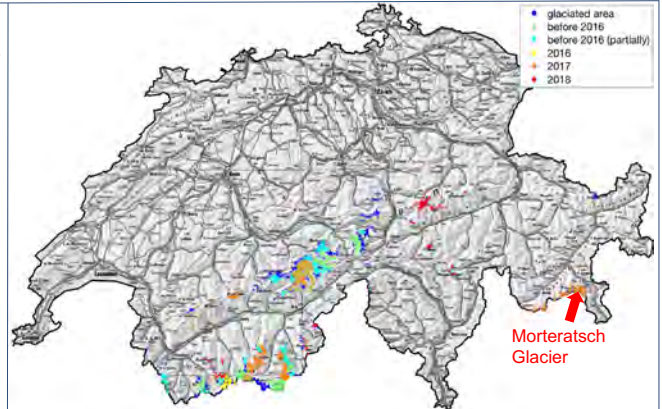


Figure 3: Current (September 2018) status of the data acquisition. Colors indicate the year of the most recent GPR-recording for a specific glacier.

4. Continuous ice thickness maps – the GlaTE algorithm

The GPR data are recorded on a sparse grid across the glaciers. For estimating the ice thickness h_{est} on continuous maps, an interpolation between the GPR profiles is needed. The interpolation procedure should take into account the dynamics of the ice flow and the conservation of mass, given by the ice thickness h_{mod} from glaciological modeling. Simultaneously, it should also adequately account for the ice thickness measured with GPR, h_{GPR} . Therefore, an inversion problem has been formulated for estimating the ice thickness h_{est} while considering a unlimited number of constrains, using the relationship

$$\begin{bmatrix} \lambda_1 \mathbf{G} \\ \lambda_2 \mathbf{L} \\ \lambda_3 \mathbf{B} \\ \lambda_4 \mathbf{S} \end{bmatrix} h_{est} = \begin{bmatrix} \lambda_1 h_{GPR} \\ \lambda_2 \nabla h_{mod} \\ 0 \\ 0 \end{bmatrix}$$

In our case, we implemented four different constrains, each weighted by λ_i in order to account for its specific confidence. The constrains are:

1. ice thickness from GPR measurements, h_{GPR} , obtained at the locations \mathbf{G}
2. gradient of the modelled ice thickness, ∇h_{mod} , at locations \mathbf{L}
3. glacier boundary \mathbf{B} where the ice thickness is zero,
4. smoothness constrain using the smoothness matrix \mathbf{S}

GlaTE Model for Morteratsch

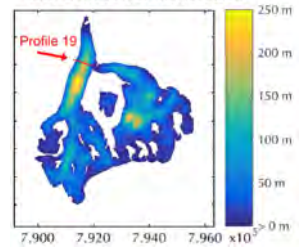


Figure 4: Ice thickness for Morteratsch glacier resulting from GlaTE modeling

A more detailed description is given by L. Langhammer (2018), together with several application examples (e.g. Morteratsch glacier, Fig. 4).

5. Outlook

The data processing of all the recorded GPR-data is accomplished and we are currently completing the interpretation. The resulting bedrock information is used for GlaTE modeling to obtain the ice volume of each glacier and finally to provide the total ice volume in the Swiss Alps. For the near future, some more campaigns are planned to fill the major gabs in the database (blue and light blue parts in Fig. 3).

Acknowledgments: The authors thank BRTECHNIK and C. Bärlocher for constructing the GPR-platform. Financial support was provided by ETH Zurich, the Swiss Geophysical Commission, and SCCER-SoE/Innosuisse.

References:

- Grab, M., et al (2018): "Ice volume estimates of Swiss glaciers using helicopter-borne GPR—an example from the Glacier de la Plaine Morte." In 2018 17th International Conference on Ground Penetrating Radar (GPR), pp. 1-4. IEEE.
- Langhammer, L., et al. (2017), "Groundpenetrating radar antenna orientation effects on temperate mountain glaciers", in Geophysics, vol. 82, no. 3, pp. H15-H24, 2017
- Langhammer, L., PhD Thesis "Helicopter-borne ground-penetrating radar surveying of temperate Alpine glaciers" (in preparation for final submission, successfully defended in August 2018)

HEPS4Power Extended-range Hydrometeorological Ensemble Predictions for Improved Hydropower Operations and Revenues

Samuel Monhart^{1,2,3}, Philippe Gerber⁴, Frédéric Jordan⁴, Christoph Spirig², and Massimiliano Zappa¹

¹Swiss Federal Research Institute, WSL, ²Federal Office of Meteorology and Climatology, MeteoSwiss, ³ETH Zurich, Institute for Atmospheric and Climate Science, ⁴Hydrique Ingénieurs, Lausanne

What is the value of sub-seasonal streamflow forecasts?

In the framework of the NRP70 project HEPS4power, hydrometeorological ensemble predictions for up to one month in advanced are used for the optimization of hydropower system.

In this poster the added value of using sub-seasonal hydrometeorological streamflow predictions is presented.

Problem: Combine the sub-seasonal streamflow prediction with hydropower optimization procedures and assesment their economic value.

Method: Compare the revenues resulting from the optimization with different streamflow forecasts (Climatology, NWP-hydro-chain, Reference)

Goal: Determine the added value of sub-seasonal streamflow predictions for hydropower operations in term of its revenues.

Methods

Meteorological predictions:

- Sub-seasonal ECMWF IFS Cy40r1 predictions (up to 32 days, 50km spatial resolution)
- Operational predictions from April 2014 – March 2015 (51 members)
- Corresponding 5-member reforecasts (1994-2014)

Pre-processing: (See Poster by Monhart et al. for details)

- Leave one year out crosscalibration of the reforecasts using QM
- Gridded observations for precipitation and temperature (2km spatial resolution → downscaling)

Hydrological modelling:

- 2 Hydrological models: **Routing System** and **PREVAH**

Optimization Scenarios:

- **Climatological scenario:**
Optimization with climatological streamflow data
→ lower benchmark scenario
- **Reference Simulation:**
Optimization with streamflow from hydrological model runs with observed meteorological inputs
→ upper hydrological benchmark (best possible scenario given the hydrological model)
- **Perfect scenario:**
Optimization with observed streamflow
→ upper optimization benchmark (best possible scenario given the optimization scheme)

Optimization

Release schedule based on two key factors at each time step

- **Lake level** difference to predefined target level (multiannual optimum)
- **Price** difference to optimum fixed cost (p)

Algorithm steps:

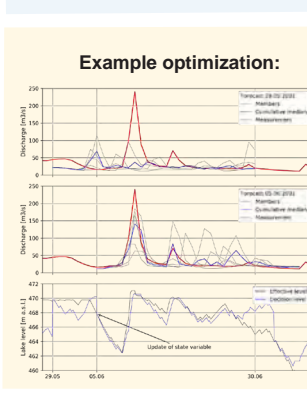
1. Compute the maximal theoretical release time over the optimization lead time
2. Identify the period with highest prices
3. Adapt the prices identified in point 2 using a correction factor ($c(t)$) depending on the current lake level ($h(t)$), the target level (h_{target}) and the level elasticity factor (c_l):
$$c(t) = 1 - c_l \frac{h(t) - h_{target}}{h_{target}}$$
4. Release decision if $p_t \geq p * c(t)$

If the lake level is above close to or above spill level a release is always scheduled.

To run this deterministic optimization scheme, the ensemble members of the prediction is not individually used. Therefore, the cumulative median of the members is determined and used for the optimization scheme. In the cumulative median, the flow peaks are not smoothed out.

Hydrological model performance for the period 1994-2014

	NSE	NSElog	MAE [m³/s]	Bias [m³/s]
Routing System	0.78	0.81	4.37	-0.25
PREVAH	0.81	0.88	3.58	0.55



Different scores to characterizing the performance of the hydrological reference simulations (Nash-Sutcliffe Efficiency (NSE) range from $-\infty$ to 1 with best score $NSE = 1$ and forecast not better than climatology $NSE = 0$; $NSElog = \logarithmic\ NSE$; $MAE = Mean\ Absolute\ Error$, $Bias = Mean\ Error$)

Optimization for two selected forecast dates. The lake level evolution is shown at the bottom. "Effective level" = lake level using the real inflows with the optimized release schedule. "Decision level" = forecasted lake level using the forecasted inflows

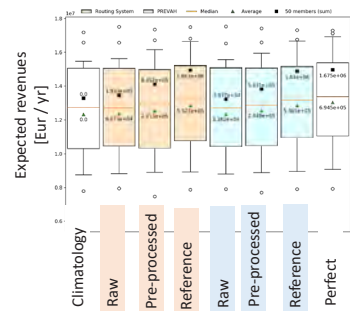
Result

Added value of forecasts up to 4% gain in annual revenues

Importance of pre-processing temperature and precipitation

Gain related to reduction in spill

Optimization using the individual (single) members and considering the median optimized release yields similar results



Scenario	Reforecasts (1994-2014)				Forecasts (2014-2015)			
	Average	%	Maximum	Minimum	Average	%	Maximum	Minimum
Perfect	13 021 460	9.88	17 281 680	6 202 512	14 962 995	12.81	19 480 916	10 446 400
RS-raw	12 548 405	0.49	17 555 530	5 961 600	14 132 910	4.36	18 949 610	9 546 810
RS-Reference	12 859 750	4.32	17 491 540	6 335 936	14 950 280	12.51	19 480 916	10 446 400
PREVAH-raw	12 360 925	0.27	17 523 510	6 101 384	13 248 330	0.30	18 949 610	9 546 810
PREVAH-avg. pro.	12 971 910	1.29	17 409 380	6 078 352	13 850 790	4.09	18 949 610	9 546 810
PREVAH-Reference	12 663 205	4.35	17 303 080	6 535 392	14 897 960	12.12	19 480 916	10 446 400
Climatology	11 327 106	-	17 172 260	6 076 344	13 287 700	-	18 949 610	9 546 810

Scenario	Annual spillings (m³)				Annual spillings (m³)			
	Average	%	Maximum	Minimum	Average	%	Maximum	Minimum
Perfect	5 405 893	-79.8	23 285 800	-	22 973 530	-75.01	37 973 530	-
RS-raw	12 478 477	-4.6	76 758 930	-	81 201 090	-11.67	127 973 530	-
RS-pre. pro.	14 951 113	-44.0	48 374 460	-	59 680 630	-35.08	81 201 090	-
RS-Reference	11 860 118	-35.6	39 943 700	-	27 342 580	-81.14	48 374 460	-
PREVAH-raw	27 179 920	1.8	77 175 340	-	91 143 620	-0.85	127 973 530	-
PREVAH-avg. pro.	17 392 704	-32.7	57 398 390	-	70 045 040	-23.78	91 143 620	-
PREVAH-Reference	8 834 071	-66.5	31 110 160	-	23 202 080	-34.76	48 374 460	-
Climatology	26 700 997	-	73 908 930	-	91 930 830	-	127 973 530	-

Revenues of the different scenarios

Spill in the different scenarios

Conclusion, Discussion and Outlook

- Sub-seasonal ensemble predictions can provide an added value for hydropower operations.
- Positive effects of pre-processing (Bias correction and downscaling)
- Limiting factor: the prices used in this study are observed historical prices. Thus, this added value can be expected if the future price is known. The impact of a price forecast should be considered in further studies.

Outlook:

- Probabilistic optimization instead of deterministic
- Additional post-processing (statistical correction of the hydrological output) could further enhance the performance of the streamflow forecasts and thus increase the value of the forecast.

Sub-seasonal hydrometeorological ensemble predictions in small- and medium size mountainous catchments: Benefits of the NWP approach

Samuel Monhart^{1,2,3}, Massimiliano Zappa¹, Christoph Spirig², Christoph Schär³ and Konrad Bogner¹

Swiss Federal Research Institute, WSL, Federal Office of Meteorology and Climatology, MeteoSwiss, ETH Zurich, Institute for Atmospheric and Climate Science

How well can we forecast streamflows 1 month in advance?

In the framework of the NRP70 project *HEPS4Power* hydrometeorological ensemble predictions for up to one month in advanced are used for the optimization of hydropower system (see separate Poster).

In this poster, the streamflow predictions used to run the optimization scheme are analysed in terms of their performance:

- **Problem:** optimal combination of meteorological and hydrological models
- **Method:** Bias correction and Downscaling of meteorological forecast using Quantile Mapping (QM)
- **Goal:** Characterization of the skill / performance of the resulting streamflow predictions and comparison with a traditional Ensemble Streamflow Prediction (ESP) system

Methods

Meteorological predictions:

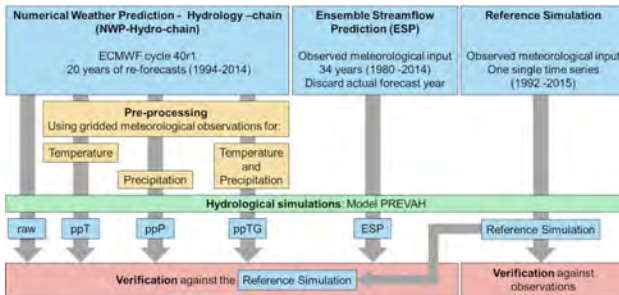
- Sub-seasonal ECMWF IFS Cy40r1 predictions (up to 32 days)
- Operational predictions from April 2014 – March 2015 (51 members)
- Corresponding 5 member reforecasts (1994-2014)

Pre-processing:

- Leave one year out crosscalibration of the reforecasts using QM
- Gridded observations for precipitation and temperature

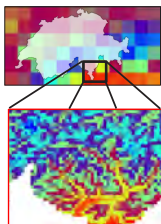
Hydrological modelling:

- Hydrological model PREVAH
- Traditional Ensemble Streamflow Prediction System (ESP)
- Reference Simulation for verification



Downscaling Quantile Mapping (QM)

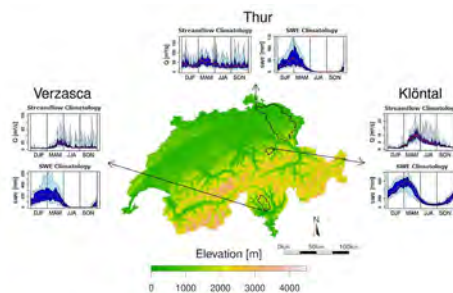
Raw
(20 km spatial resolution)



Downscaled
(2km spatial resolution)

Catchment characteristics

System analysed for 3 catchments with different hydroclimatic conditions

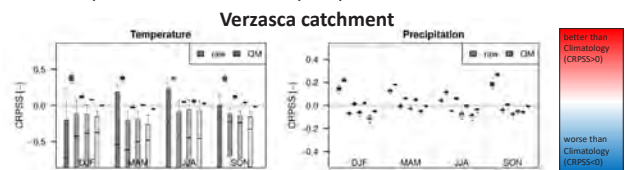


	Verzasca	Klöntal	Thur
Catchment area (km ²)	235	33	2036
altitude range (m)	2864	2883	2000
average elevation	1651	84	770
maximum elevation	490	842	336
dominant hydroclimatic regime	snow	none and glacial	precipitation

Results

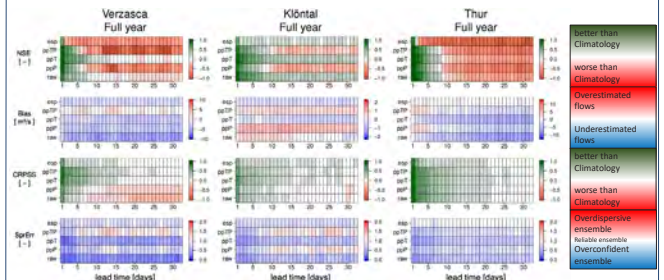
Meteorological forecast performance

- Importance of statistical correction (meteorological post-processing)
- Positive skill in terms of CRPSS up to 3 weeks for weekly mean temperature and 1 week for precipitation



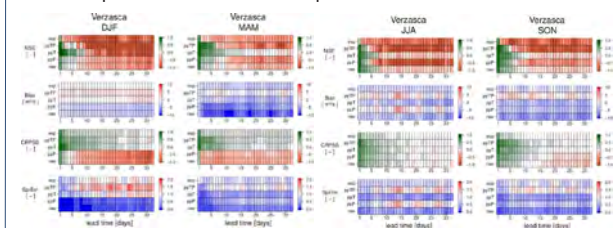
Hydrological forecast performance

- Importance of statistical corrections (hydrological pre-processing)
- NWP-hydro approach outperforms traditional ESP
- Importance of correcting both temperature and precipitation
→precipitation important to correct ensemble spread
- Pre-processing effect on performance is more pronounced in snow-dominated catchments
- Different verification Scores need to be taken into account



Seasonal differences in performance:

- Best performance in MAM and DJF → pronounced effect of pre-processing
- Importance of snow-related processes



Conclusion

- Meteorological forecast performance is limited to 3 weeks for temperature and 1 week for precipitation.
- NWP-hydro chain can provide skilful predictions up to 30 days, depending on catchment characteristics and season.
→non-linear propagation of the meteorological forecast skill to streamflow forecast skill
- Best performance and largest effect of the pre-processing are found in winter (DJF) and spring (MAM)
→Such prediction system have a great potential for different applications where the forecast performance can further translate into forecast value. Such an example is presented in the poster describing the project *HEPS4power* for hydropower optimization (Monhart et al.). Furthermore, forecast of droughts could benefit from such a pre-processing as well (see poster by Zappa et al.).

Changes in future river sediment yield: preliminary results from the Guerbe river

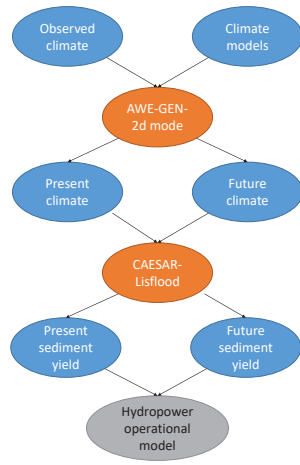
Nadav Peleg, Jorge Ramirez

Motivation

Fine sediments affect the operation of small river hydropower turbine. Climate change may impact the sediment yield along rivers, as changes in rainfall intensity and occurrence are expected. Here, a modeling framework is suggested in order to explore the effect of climate change on the sediment production in rivers. The framework is tested for the Guerbe river as a feasibility study.

Modeling approach

- AWE-GEN-2d model is used to generate multiple gridded rainfall realizations for present and future climates using observed data and data from climate models.
- Climate variables generated by AWE-GEN-2d are used as input into CAESAR-Lisflood model to generate the sediment yield for present and future climates.
- Sediment yield and discharge outputs from CAESAR-Lisflood will be used as inputs into an hydropower operational model (yet to be developed).



AWE-GEN-2d model

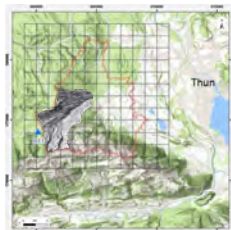
AWE-GEN-2d (Advanced WEather GENERator for 2-Dimensional grid) model is a stochastic weather generator used to downscale climate variables for present and future periods using information from climate models. Further details on the model are given in the poster entitled "Simulating climate at high spatial and temporal resolutions using the new CH2018 climate scenarios" by Peleg and Burlando.

CAESAR-Lisflood model

Caesar-Lisflood is a geomorphological/Landscape Evolution Model that combines the Lisflood-FP 2d-hydrodynamic flow model that conserves mass and partial momentum with the CAESAR geomorphic model to simulate erosion and deposition in river catchments and reaches. The model operates over a wide range in space and time (1km² to 1000km², hours to 1000 years).

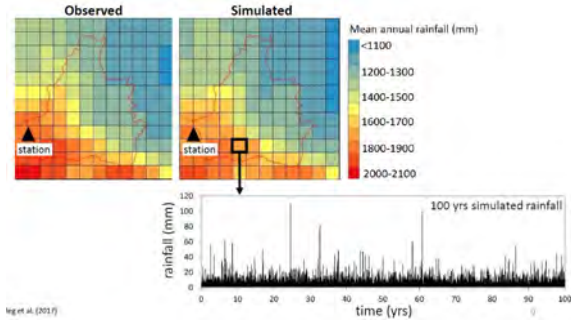
Study site: Guerbe river

Guerbe river is located in the Swiss pre-Alps, with a catchment area of 12 km². Rainfall is simulated over a 12 x 12 grid cell domain (cells of 2 x 2 km²) overlapping the MeteoSwiss (present climate) and CH2018 (future climate) gridded products. The hydrological model is calibrated using observed discharge and simulated rainfall. Sediment yield is estimated at the river's outlet.

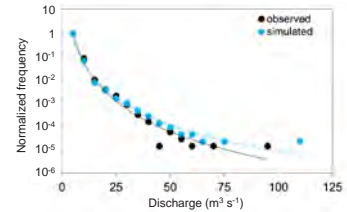


Preliminary results

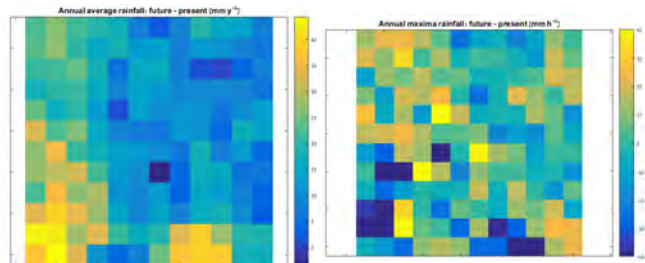
- AWE-GEN-2d model is calibrated for present climate conditions



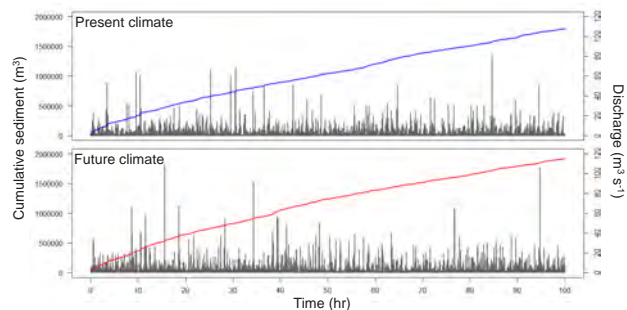
- CAESAR-Lisflood model is calibrated for present climate conditions



- AWE-GEN-2d is re-parameterize to simulate rainfall for future climate conditions (2030-2059, RCP85, multi-model mean)



- Sediment yields are computed using CAESAR-Lisflood



Final remarks

We use the Guerbe river site as a proof of concept, proving that the suggested modeling approach to simulate future sediment yield using both AWE-GEN-2d and CAESAR-Lisflood models work.

Next, a case study with a small hydropower turbine will be chosen, for which an hydropower operational model will be developed.

Simulating climate at high spatial and temporal resolutions using the new CH2018 climate scenarios

Nadav Peleg, Paolo Burlando

Motivation

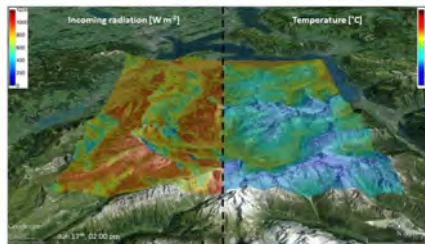
The new CH2018 official future climate scenarios for Switzerland are soon to be released (November 2018). The climate scenarios are based on analysis from Regional Climate Models (RCM) and are given at a daily and 11-km resolutions at best, with a single climate realization for each climate trajectory.

Using the new AWE-GEN-2d model, multiple stochastic realizations representing the future climate at hourly and sub-kilometre scales can be generated. By doing so we: (1) are able to simulate the climate variables needed as input for hydrological/geomorphological models at the local (catchment) scale; and (2) are able to address the uncertainty in climate emerging from the natural (stochastic) variability, which is needed to better constrain the climate impact.

AWE-GEN-2d in a nutshell

AWE-GEN-2d (Advanced WEather GENERator for 2-Dimensional grid) model (Peleg et al., 2017) follows the philosophy of combining physical and stochastic approaches to generate gridded climate variables in a high spatial and temporal resolution. It is relatively fast and parsimonious in terms of computational demand.

An example of the model output (100-m and hourly) is given to the right.



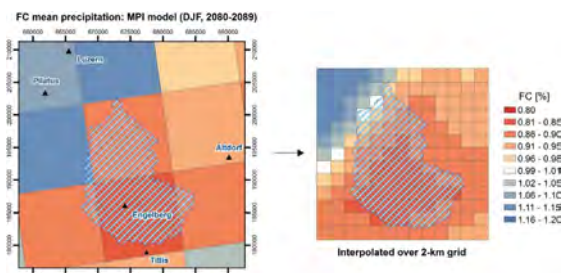
Method to re-parameterize AWE-GEN-2d

The Factors of Change (FC) approach is used for the re-parameterization of AWE-GEN-2d. It was chosen as it allows considering changes in the long-term mean and is accounting for seasonality:

$$S(h)_v^{FUT} = \frac{S(h)_v^{CLM,FUT}}{S(h)_v^{CLM,CON}} S(h)_v^{OBS} \quad (1)$$

$$S(h)_v^{FUT} = S(h)_v^{OBS} + (S(h)_v^{CLM,FUT} - S(h)_v^{CLM,CON}) \quad (2)$$

where S is a statistical property (e.g. mean), h is the time aggregation (daily), the subscript v is the climate variable (precipitation), the superscript FUT and CON denote future and control realization, CLM denotes the climate model, and OBS denotes the observed data. The control realization is the period for which both observed data and climate model simulations are available.

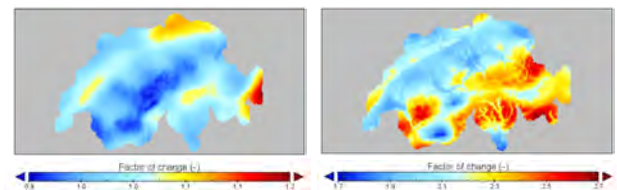


An example of the spatial interpolation of FC from a RCM grid to the AWE-GEN-2d grid is given in the figure above for the Engelberg area.

Calculating FC from the CH2018 database

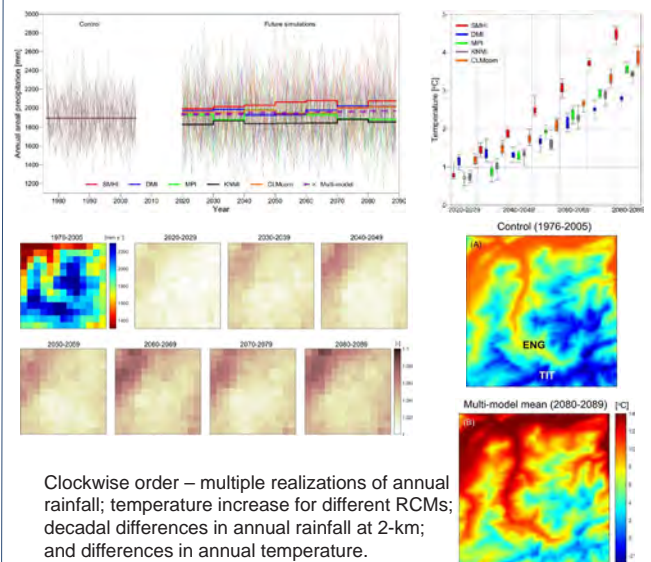
FC were computed for all RCMs in the CH2018 repository (RCP2.6, 4.5 and 8.5) on decadal (for the period of 2020-2099) and seasonal basis for the entire area of Switzerland. The FC are computed for the statistics of mean, standard deviation and occurrence of precipitation, and for mean and standard deviation of near-surface air temperature on a 2-km and daily resolution. Data is available upon request for the SCCER-SoE partners.

Examples for the FC of mean precipitation (left) and temperature (right) obtained from a single RCM (SMHI-RCA-ECEARTH-EUR11) for RCP8.5 and for the decade 2040-2049 are given below.



Case study

The Engelberg region was chosen as a case study to demonstrate AWE-GEN-2d abilities to simulate an ensemble of climate variables (precipitation, cloud cover, temperature, solar radiation, vapor pressure and relative humidity) for the period 2020-2089. Results for precipitation and temperature are presented below.



Clockwise order – multiple realizations of annual rainfall; temperature increase for different RCMs; decadal differences in annual rainfall at 2-km; and differences in annual temperature.

Final remarks

AWE-GEN-2d is already set for the following regions in Switzerland: Engelberg, Maggia, Thur, Kleine Emme, Gletsch, Gurbe and Oberhasli. Calibrating the model for Valais area is next in line.

High-resolution climate data will be available for the partners of SCCER-SoE upon request.

Peleg, N., Molnar, P., Burlando, P., and Fatichi, S. Exploring stochastic climate uncertainty using a gridded hourly weather generator. Paper under review in Journal of Hydrology.

Online prediction tool for hydropower energy (Opt-HE)



Dr F. Jordan, Dr G. Artigue (Hydrique Engineers)
K. Cros, C.-A. Loetscher, O. Etter, Prof. Dr A. Schleiss (LCH-EPFL)
fred.jordan@hydrique.ch



The OPT-HE project

OPT-HE : Optimal Prediction Tool for HydroElectricity

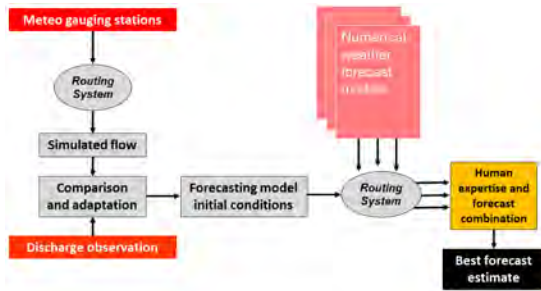
Hydrological prediction is a key factor in the optimization of hydropower production, by limiting the water spillings and increasing the water value. These objectives are perfectly in line with the Energy Strategy 2050, allowing an increase of the total electricity production with no new impact on the environment.

The partners of the project are five hydropower suppliers, MeteoSwiss and Hydrique Engineers.

The research is realized by Hydrique Engineers, the Laboratory of Hydraulic Constructions (EPFL) and the Institute for Climate and Atmosphere (ETHZ).

Structure of the project

The existing forecasting system at Hydrique Engineers is based on rainfall-runoff simulation, combining the assimilation of discharge gauging stations and human expertise. All these single processes are to be optimized within this project. Four workpackages are completed: general methodology, weather forecast, hydrological processes, operation.



Outcomes

For this project, various tests have been realized, focusing on the specific characteristics of the catchment areas. As the existing system already had a satisfying performance, it was difficult to highlight improvements in the different methods showing a high performance. Out of the 18 different methods tested within the simulation and operation processes, 5 methods have been directly implemented. 3 additional methods, with less impact, have also been applied in the operational forecasting system at Hydrique.

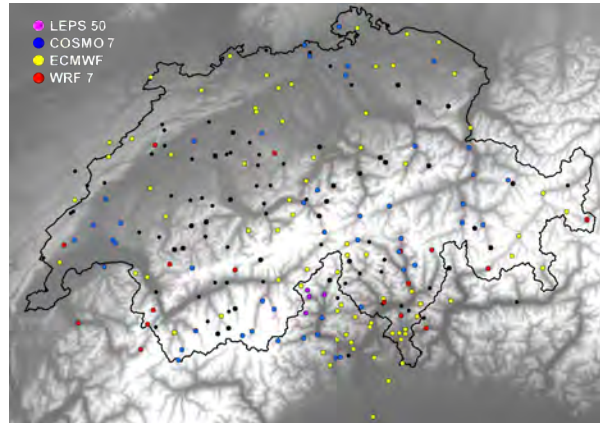
Type of catchment area	Glacier	Prealpine	Jura-region	Added value
Temperature forecast bias	In operation			Very good
Analysis of the sources of forecast error		In operation	In operation	Very good
Influence of new precipitation stations			Rejected	Poor
Glacier model post-processing with spline correction	In operation			Very good
Discharge assimilation in automatic correction	In operation	In operation	In operation	Very good
Uncertainty quantification and forecast	In operation	In operation	In operation	Very good
Combined glacier model with simulation and machine learning	In operation			Good
Assimilation of CombiPrecip data		Rejected	Rejected	Poor
Precipitation forecast quality assessment		In operation	In operation	Good
Pre-processing of stochastic weather forecast (COSMO-E)	In operation	In operation	In operation	Good
Seasonal forecasting	Rejected	In operation		Good
Precipitation forecast bias		Rejected	Rejected	Poor
Assimilation of COSMO-1 high-resolution forecast		In operation	In operation	Good
Use of COSMO-E instead of sensitivity method for the uncertainty prediction	Rejected	Rejected	Rejected	Poor
Short-term precipitation forecast by combination of observation and numerical weather forecast	Rejected	Rejected	Rejected	Poor
Post-processing of runoff forecasts using previous runs	Rejected	Rejected		Poor
Validation tests of the combined new methods	In operation	In operation	In operation	Very good
Inflow forecast by neural networks	Rejected	Rejected	Rejected	Poor
Influence of vegetation cover interception	Rejected	Rejected	Rejected	Poor

Intercomparison of meteorological models

Weather models are the main inputs for hydrological forecast. Mainly precipitation and temperature forecast is of highest importance. In order to better choose the models during particular situations, it is crucial of knowing the real performance of the precipitation forecast.

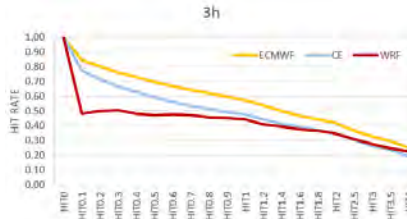
A systematic performance analysis was realized over:

- 231 weather stations
- 5 different weather models
- 3 precipitation durations, 3 lead times (D, D1, D2). HIT* and FAR* rates for 20 intensity classes



Best model for the HIT rate over 24 hours for a 24 mm threshold, D1 * the HIT rate indicate the success rate of a forecast. 1 is the best value (all observed events were predicted).

the FAR rate indicates the number of false alarms given by the model. 0 is the best value (no false alarm was produced by the model)



Comparison of HIT rates for 3 weather models and a 3 hours duration. Aggregation of all 231 weather stations.

Similar analysis but for FAR indicator. ECMWF produce the best results, in average, compared to cosmo-e and WRF.

Indicator	JURA	PLATEAU	PREALPES	VALAIS	TESSIN	GRISONS
D HIT 3h	CE	ECMWF	CE / WRF	ECMWF	CE / WRF	CE / WRF
D HIT 24h	ALL	ECMWF	ALL	ECMWF	ALL	WRF
D FAR 3h	CE	ECMWF / WRF	CE / ECMWF	ECMWF	CE	ALL
D FAR 24h	CE	ECMWF / WRF	ECMWF	ECMWF	CE	ECMWF
D1 HIT 3h	CE / WRF	ECMWF / WRF	WRF	WRF	ALL	ALL
D1 HIT 24h	CE / WRF	CE / WRF	CE / WRF	CE / WRF	ECMWF	
D1 FAR 3h	CE	CE / ECMWF	ECMWF	ECMWF	CE	ALL
D1 FAR 24h	ECMWF	ECMWF	ECMWF / WRF	ECMWF	CE	
D2 HIT 3h	ECMWF / WRF	ECMWF / WRF	WRF	ALL	ECMWF	CE / ECMWF
D2 HIT 24h	ECMWF	ECMWF	WRF	ECMWF	ECMWF	WRF
D2 FAR 3h	CE	CE / ECMWF	CE	ECMWF	CE / ECMWF	ECMWF
D2 FAR 24h	CE	ECMWF	ECMWF	ECMWF	ECMWF	ECMWF

Regional summary of the "best model" for precipitation forecasting, according to the systematic analysis and result ponderation between HIT and FAR performance.

Helicopter-borne ground-penetrating radar surveying of temperate Alpine glaciers

Lisbeth Langhammer¹, Lasse Rabenstein², Lino Schmid^{1,3}, Melchior Grab^{1,3}, Andreas Bauder³ & Hansruedi Maurer¹

¹Institute for Geophysics, ETH Zurich ²Drift & Noise Polar Services GmbH, Bremen ³Laboratory of Hydraulics, Hydrology and Glaciology, ETH Zurich

For understanding the past, present and future change of glaciers, it is fundamentally important to gain knowledge about surface and subsurface glacier structures. Ground-penetrating radar (GPR) is an excellent method to investigate the thickness of glaciers. It was demonstrated in a PhD study (Lisbeth Langhammer, 2018), how traditional GPR methods can be advanced to survey Alpine glaciers more efficiently, and how the recorded data can be exploited to derive three-dimensional ice thickness maps. In the following, the three main thesis chapters are presented.

1. Ground-penetrating radar antenna orientation effects on temperate mountain glaciers

Extensive helicopter-borne and ground-based GPR investigations on the Glacier d'Otemma, Switzerland, demonstrated that the detectability of the ice-bedrock interface varies substantially with dipole orientation (Fig. 1). Dipole alignments parallel to the glacier flow generated considerably stronger and more coherent bedrock reflections than a perpendicular dipole setup. To help explain these findings, a 3D numerical modeling was performed using the open source software gprMax. The simulations indicated that the changes of the bedrock reflection amplitude are primarily governed by the bedrock topography. Scattering and intrinsic attenuation may also influence the amplitudes of the bedrock reflections, but these effects seem to be much less pronounced.

To increase the GPR bedrock reflection quality, antennas should be orientated parallel to the glacier flow direction on glaciers confined to a valley (Fig. 2). Since the directional dependence is a first-order effect, it is advisable to perform multi-component surveys, when the general shape of the bedrock topography is unknown.

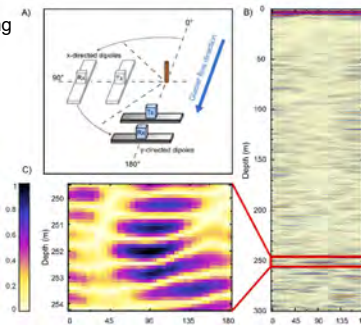


Figure 1: Ground-based rotation experiment. Antennas were rotated for 180° in 5° steps, starting with y-directed dipoles at 0° position. Bedrock reflection is at ~250m.

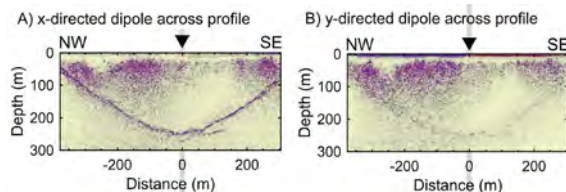


Figure 2: Comparison of ground-based pulseEKKO PRO 25-MHz Profiles

2. Glacier bed surveying with helicopter-borne dual-polarization ground-penetrating radar

Traditionally, helicopter-borne GPR systems are operated with a single pair of bistatic dipole antennas. It is demonstrated numerically that the directivity of the radiation pattern of single airborne dipoles (Fig. 3) does not correspond to an ideal full-space solution, if the antennas are employed at typical flight heights. These directionality effects can degrade the quality of the subsurface images significantly, when the GPR antennas are orientated unfavourably. Since an adjustment of the antenna orientation is impractical during flight, a novel dual-polarization helicopter-borne GPR system has been developed, consisting of two orthogonal pairs of commercial antennas in broadside configuration.

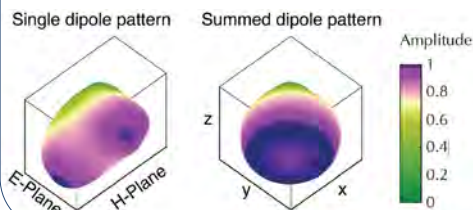


Figure 3: Single and summed interpolated 3D amplitude radiation pattern of an infinitesimal dipole placed 20 m above a half space interface (air - ice).

To overcome the image quality deficits of the individual channels, a pseudo-scalar approach was applied in which the data of both polarizations are combined. Results of helicopter-borne GPR surveys reveal more coherent bedrock reflections in the summed data compared to single dipole pair profiles (Fig. 4). Generally, the dual-polarization setup is more suitable than single antenna systems, because it is more versatile and less prone to directional effects caused by the placement of the dipole antennas in relation to undulating subsurface reflectors.

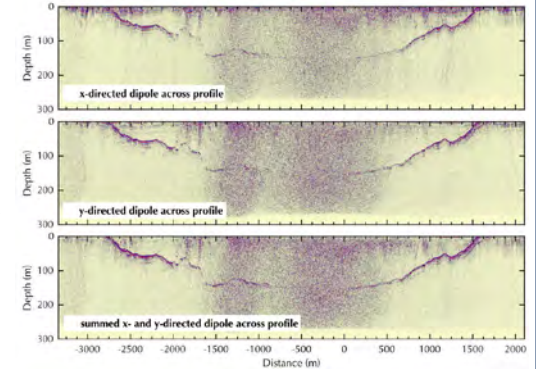


Figure 4: Profile from Plaine Morte Glacier with x-, y- and summed x- and y-directed dipoles.

3. Glacier thickness estimations and optimized survey design based on joint inversions of data and modeling constraints

The GlaTE inversion algorithm was developed to adequately invert for the 3-D ice thickness, based on physical modeling and observable data constraints. As an input, GPR-based bedrock reflection measurements are used to constrain the absolute thickness while the gradients of a mass conservation glaciological model are integrated to force the overall distribution. To account for parameter and data uncertainties, the constraints are formulated such that they can be merged into a single set of equations and the thickness derived with the unconstrained glacier model is adjusted. The ice thickness e.g. of Morteratsch glacier is calculated successfully and improved in comparison to traditional mass conservation methods (Fig. 5). The GlaTE inversion is afterwards used to perform sequential optimized survey design for GPR campaigns in high mountain environments. It was found that for narrow valley-shaped glaciers, longitudinal profiles are generally sufficient, while wider saddle and convergence zone should be surveyed with additional across GPR profiles.

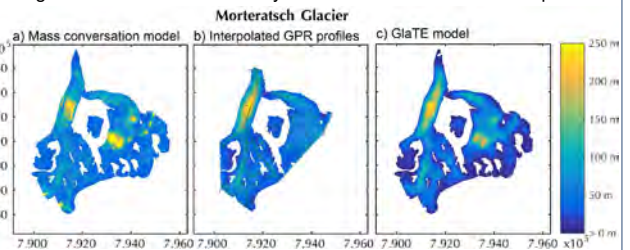


Figure 5: Comparison of glacier thickness estimations for the Morteratsch Glacier

Conclusion

The presented investigations and achieved results in this study substantially impact the field of ground-penetrating radar research on Alpine glaciers. With the novel helicopter-borne GPR acquisition unit, the optimized survey planning, advanced processing routines and the ice thickness estimation inversion, a complete set of tools has been developed to assess the glacier mass in the Swiss Alps and in other high-mountain regions.

Acknowledgments: This work was financed by ETH Zürich, the Swiss Geophysical Commission, and SCCER-SoE. The authors thank Geosat and BRTechnik for their collaboration and Christoph Bärlocher for his support.

Reference: Langhammer, L., PhD Thesis "Helicopter-borne ground-penetrating radar surveying of temperate Alpine glaciers" (in preparation for final submission, successfully defended in August 2018)

Task 2.2

Title

Infrastructure adaption

Projects (presented on the following pages)

Gestion de sédiments dans les retenues suisses : expériences vécues et défis à relever
Samuel Vorlet, Pedro Manso

Hydro-abrasion at hydraulic structures and steep bedrock rivers
Dila Demiral, Ismail Albayrak, Robert Boes

Storage hydropower potential from dam heightening in Switzerland
Andrin Leimgruber, David Felix, Michelle Müller-Hagmann, Robert Boes

Storage hydropower potential from dam heightening in the cantons of FR, NW, OW, UR, VD and VS
Jule Claire Holland, Samuel Wolf, Hannes Zimmermann, David Felix, Michelle Müller-Hagmann, Robert Boes

Storage hydropower potential from dam heightening in the cantons of BE, TI and SZ
Cecilia Parravicini, Damiano Vicari, Raphael Werlen, David Felix, Michelle Müller-Hagmann, Robert Boes

Storage hydropower potential from dam heightening in the cantons of GL, GR and SG
Marco Baumann, Alain Emmenegger, Andrin Kasper, David Felix, Michelle Müller-Hagmann, Robert Boes

Nucleation of laboratory earthquakes: Implications for EGS induced seismicity
Mateo Acosta, Francois Passelègue, Alexandre Schubnel, Benoit Gibert, Marie Violay

Blocking probability at spillway inlets under driftwood impact
Paloma Furlan, Michael Pfister, Jorge Matos, Anton J. Schleiss

Spatial Impulse Wave Generation and Propagation
Eva Sauter, Frederic Evers, Helge Fuchs, Robert Boes

Impulse waves: run-up behavior and overtopping at dam structures
Fabian, Küttel, Frederic Evers, David Vetsch, Robert Boes

Wave generation by submarine mass failures
Nina Landolt, Frederic Evers, Helge Fuchs, Robert Boes

Influence of tunnel slope on air demand and flow conditions in bottom outlets
Alexander Williams, Benjamin Hohermuth, Lukas Schmocker, Robert Boes

Numerical Simulations of Two-Phase Flow in Bottom Outlets
Matthias Bürgler, Benjamin Hohermuth, David Vetsch, Robert Boes

Les principaux vecteurs d'adaptation d'installations hydroélectriques de montagne en Suisse
Vincent Gaertner, Sabine Chamoun, Pedro Manso

Valorisation des mesures de mitigation des éclusées en systèmes complexes : quelle échelle spatiale privilégier ?

Mathieu Barnoud, Sabine Chamoun, Pedro Manso

Gestion de sédiments dans les retenues suisses : expériences vécues et défis à relever

Samuel L. Vorlet*, Pedro Manso

Platform of Hydraulic Construction (PL-LCH), Ecole Polytechnique Fédérale de Lausanne (EPFL), Switzerland
 *Corresponding author: samuel.vorlet@epfl.ch



Contexte de l'étude

La sédimentation est un des problèmes actuels principaux dans les réservoirs en Suisse. Dans un contexte de transition énergétique et de vieillissement des infrastructures, la gestion des sédiments dans les retenues représente un défi majeur pour les exploitants, qui doivent trouver des solutions innovantes pour assurer le rétablissement du transfert des sédiments à travers les réservoirs, tout en limitant les pertes d'eau, en respectant les contraintes égales et les contraintes liées à la production hydroélectrique. Cette étude vise à illustrer le problème que représente la sédimentation en Suisse ainsi que sa gestion par les divers exploitants. L'objectif est d'obtenir des informations pour catégoriser les retenues sujettes à des problèmes liés aux sédiments.



Figure 1: Déposition de sédiments; Giétroz du Fond, 2018

Méthodes

Une étude a été réalisée auprès de divers exploitants de barrages en Suisse par rapport à la gestion sédimentaire et aux principaux problèmes liés aux sédiments auxquels ils sont confrontés. Un questionnaire a été élaboré au sein du groupe de travail « Purgés et Vidanges de Retenues » du Comité Suisse des Barrages (CSB), qui a ensuite été transmis aux exploitants. Au total, 34 participants ont pris part à l'enquête qui regroupe les résultats concernant 69 retenues en Suisse et permet de mettre en évidence les expériences vécues et les principaux défis à relever au niveau national. Les résultats permettent également de mettre en avant l'importance de la gestion des sédiments pour les retenues en Suisse.



Figure 2: Localisation des retenues ayant participé à l'enquête en Suisse.

Résultats

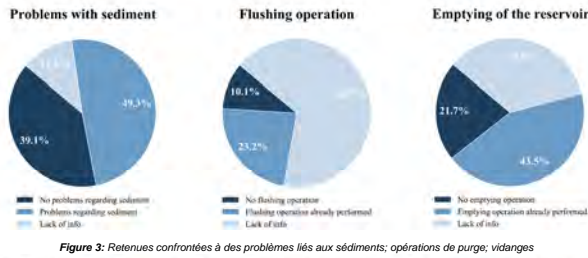


Figure 3: Retenues confrontées à des problèmes liés aux sédiments; opérations de purge, vidanges

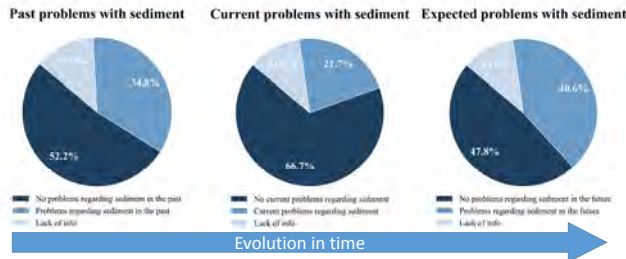


Figure 4: Retenues confrontées à des problèmes liés aux sédiments: évolution temporelle

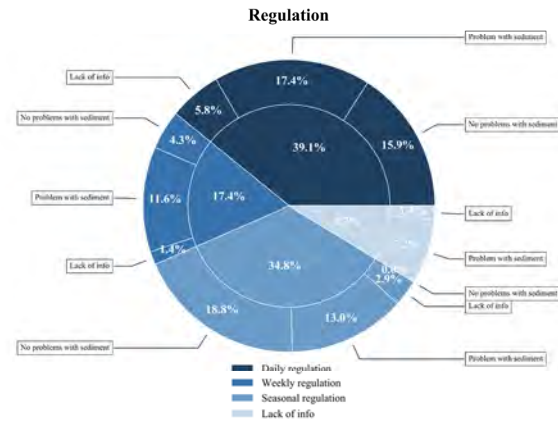


Figure 5: Régulation des réservoirs et problèmes liés aux sédiments

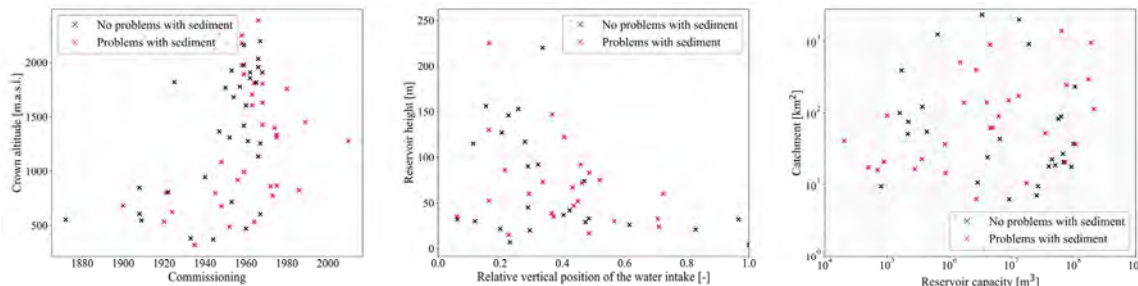


Figure 6: Classification des réservoirs en fonction de: l'année de mise en service et l'altitude de la couronne, de la hauteur relative de la prise d'eau et de la hauteur du barrage, de la capacité du réservoir et de la taille du bassin versant; en noir: pas de problèmes avec les sédiments, en rouge: problèmes avec les sédiments

Conclusions

Les résultats de l'enquête concernant 69 retenues en Suisse montrent que la gestion des sédiments en Suisse représente un défi majeur. A terme, une majorité de retenues sera sujette à des problèmes liés à la sédimentation. De plus, on observe que peu importe l'année de mise en service, l'altitude, la position relative de la prise d'eau, la hauteur du barrage, la capacité du réservoir ou la taille du bassin versant, toutes les retenues peuvent faire face à des problèmes liés aux sédiments. L'expérience vécue des exploitants doit permettre de mettre en place une uniformisation des mesures concernant la gestion des sédiments dans les retenues en Suisse. Par la suite, il sera nécessaire d'intégrer un plan de gestion des sédiments dans les directives sécuritaires et environnementales des barrages, afin de gérer au mieux les problèmes liés à la sédimentation dans les décennies à venir.

Remerciements

Cette enquête a été réalisée dans le cadre du groupe de travail «Purgés et Vidanges de Retenues» du Comité Suisse des Barrages (CSB). Les remerciements sont adressés à tous les membres du groupe de travail (P. Manso, A. Baumer, N. Bretz, D. Ehrbar, G. Federer, M. Müller, M. Nitsche, A. Ricciardi, T. Rüesch, J. Stamm, T. Ziegler) ainsi qu'à tous les exploitants ayant répondu aux questionnaires.

Hydro-abrasion at hydraulic structures and steep bedrock rivers

*Dila Demiral, Ismail Albayrak, Robert Boes
 ETH Zurich, Switzerland*

Motivation and objectives

Sediment transport from glacier basins, rivers and waterways, and reservoir sedimentation worldwide have strongly increased under the strong impact of climate change. As a consequence, high transport rates of bed load particles combined with high flow velocities cause severe abrasion such as (I) hydro-abrasion at hydraulic structures, such as Sediment Bypass Tunnels (SBTs) and Sediment Flushing Channels (SFCs) (Fig 1), and (II) bedrock incision in high-gradient mountain streams (Fig 2). Despite the large number of studies mainly in alluvial channels, only few exist for steep bedrock rivers and non-movable bed open channels. However, their applicability is still in question for highly supercritical flow due to the lack of information on the physical processes of turbulent flow characteristics, bed load particle motion, and abrasion and their interrelations. The proposed project aims at filling the research gaps by a systematic laboratory investigation.



Fig 1. Hydro-abrasion at Palagnedra SBT (Photo: VAW, ETH)



Fig 2. Bedrock incision at Ukak River, Alaska, US

The main objectives of this study are to: (1) investigate the mean and turbulent flow characteristics in supercritical narrow open channel flows (i.e. channel width to water depth, $b/h < 3-5$) over fixed and abraded-fixed beds, (2) investigate single and multi-particle motions over fixed and abraded-fixed beds, (3) determine the hydro-abrasion depth and pattern for a range of polyurethane foams and erodible mortars, (4) develop a mechanistic hydro-abrasion model to forecast hydro-abrasion at both laboratory and prototype scales.

Experimental setup and research tasks

The experiments of the present study are conducted in a $b = 20$ cm wide, $h = 50$ cm deep and $l = 13.50$ m long laboratory flume (Fig 3). The flume bottom is concrete lined and the bed slope is $S_0 = 0.01$.



Fig 3. Experimental flume (Photo: VAW, ETH)

To meet the objectives, the project is divided into four tasks, namely Task A, B, C and D.

In Task A, velocity measurements were conducted using a 2D Laser Doppler Anemometer (LDA) to determine the cross-sectional mean flow velocities and turbulence intensities, bed and Reynolds shear stresses on different flow conditions (i.e. $b/h_0 = 1, 1.33$ and 2 ; and $F=2, 3$ and 4).

In Task B, high speed video recordings of particles are made to determine the particle transport mode, trajectory, velocity, and impact energy under various hydraulics conditions for a range of particle differing in size, shape and hardness.

In Task C, the goal is to systematically investigate the effects of the sediment size, hardness, and transport rate on hydro-abrasion of different types of bed lining materials (foam and erodible mortar) under various hydraulic conditions.

Task D focuses on the development of an abrasion prediction model based on the data from Tasks A, B and C.

First results

Figure 4 shows the contour lines of mean streamwise (U) and vertical (W) velocities normalized by the max. streamwise velocity, U_{max} together with the sketches of the secondary current cells for $b/h_0 = 2$ and $F = 2, 3$ and 4 . From the streamwise and vertical velocity distributions, a pair of surface and a pair of corner vortices called 'secondary currents' were identified at each side of the flume, resulting in a 3D flow pattern. The streamwise velocities are symmetrical and the maximum flow velocity occurs below the surface around $z/h = 0.5-0.6$, which is so-called 'velocity dip phenomenon' (Fig 4 a-c). Additionally, vertical contour plots show a quasi-symmetrical flow pattern with strong downward flows below the water surface at the flume center ($y/h = 0$). The results show that the secondary currents are not affected by the Froude number. These currents not only affect the mean flow characteristics but also cause a redistribution of bed and Reynolds shear stresses, which plays an important role in sediment transport, and hence the hydro-abrasion mechanism.

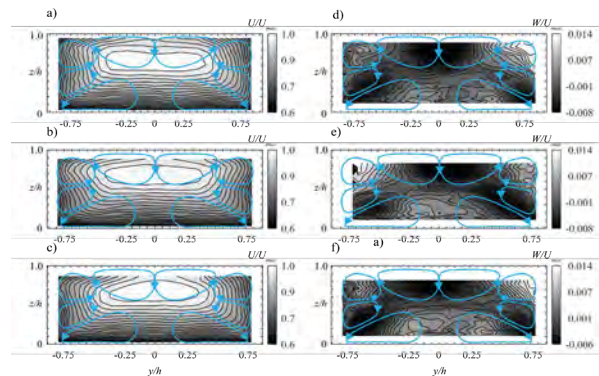


Fig 4. Contour plots of streamwise and vertical flow velocities for $h_0 = 10$ cm and $F = 2$ (a-d), 3 (b-e) and 4 (c-f).

Outlook

The measurements and data analysis in Task A were completed. The experiments in Task B are on-going. Task C will be conducted in autumn 2018 while Task D will be done in 2019. The outputs of this project will contribute to design and sustainable use of hydraulic structures i.e. SBTs, SFCs and modelling of bedrock incision in steep rivers and landscape evolution exposed to heavy sediment loads.



Storage hydropower potential from dam heightening in Switzerland

Andrin Leimgruber, David Felix, Michelle Müller-Hagmann, Robert Boes – VAW ETH Zürich

Introduction

In winter, the domestic electricity production in Switzerland has not been sufficient to cover the demand since more than 10 years. With the planned shutdown of the nuclear power plants according to the Swiss Energy Strategy 2050, the need for imports of electric energy in winter will increase. Existing storage hydropower plants (HPPs) could provide more electric energy in winter if their headwater storages (reservoirs) would be enlarged by dam heightening (Schleiss 2012). This study aimed firstly at estimating the potentially achievable additional storage volumes in Switzerland and the corresponding amount of electricity production which could be shifted from summer to winter. Secondly, a case study at the Griessee was conducted to investigate examples of site-specific aspects.

Part I: Potential study of dam heightening in Switzerland

Methods

Dam heightening options by 5%, 10% and 20% of the existing dam heights were roughly analyzed for the 38 largest HPP reservoirs in Switzerland. The options were assessed based on multiple criteria including technical, ecological, economical and social aspects. The future additional reservoir area, the dam and the HPP system were considered.

The additional storage volumes and the corresponding energy production which can be additionally transferred from summer to winter were estimated for two scenarios. In Scenario 1 the most promising heightening options were identified (16 dams). In scenario 2, also further heightening options with a smaller probability of realization were considered (totally 29 dams).

Results

The electricity production which could be additionally transferred from summer to winter is estimated as **1.7** and **2.8 TWh** per year for Scenario 1 and 2, respectively. The contributions of the reservoirs are shown in Figure 1. In both scenarios, the achievable potential depends significantly on the feasibility of specific heightening projects at single large reservoirs (e.g. Lac des Dix impounded by the Grande Dixence dam, Emosson, Grimsel and Oberaar).

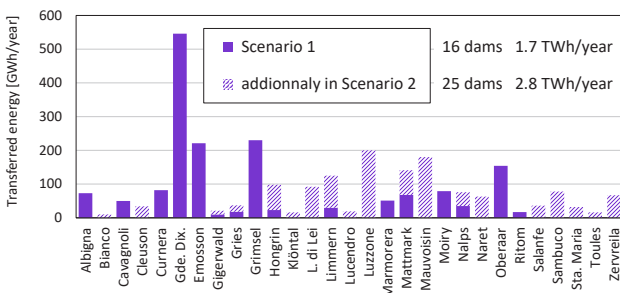


Fig. 1: Annual electricity which could be additionally transferred from summer to winter after dam heightenings

Conclusion

Dam heightening with the corresponding adaptation of HPP operation has the potential to considerably reduce the need for electricity imports in winter, which are presently about 3 TWh/year and could increase up to 10 TWh/year (Piot 2014).

It is recommended to study dam heightening options as well as the required adaptation of HPPs and neighbouring infrastructures in more detail. Moreover it is recommended to review the energy policy to set additional incentives for more winter electricity production if a high degree of domestic production is aimed at in the future.

Part II: Dam heightening at Griessee (Case study)

Existing HPP

The Griessee is located in the canton of Valais close to the Nufenen pass. The full supply level of this reservoir with a storage capacity of 18.4 Mio. m³ is 2386.5 m a.s.l. The arch gravity dam was built in 1966 and is 60 m high (Fig. 2). The water of the Griessee is turbined first in Altstafel and then in several HPP stages of the Maggia cascade. The elevation difference down to the Lago Maggiore (193 m a.s.l.) is almost 2200 m. About 5 kWh are generated from each m³ of water.



Fig. 2: Arch gravity dam Gries

Dam heightening alternatives

Five heightening alternatives by 5%, 10% and 20% of the existing dam height were investigated considering two structural options (Table 1). From an energy-policy point of view and to increase the operational flexibility, Alternative 3 was preferred in this study despite the relatively high specific costs.

Alternative	Heightening [m]	Storage capacity [Mio m ³]	Structural option for reinforcement	Production shifted to winter [GWh]	Add. specific costs [CHF/kWh]
1.1	3	20.8	Crown	11.4	0.012
1.2	3	20.8	Downstream face	11.4	0.12
2.1	6	22.2	Crown	18.1	0.016
2.2	6	22.2	Downstream face	18.1	0.12
3	12	26.2	Downstream face	37.3	0.09

Because the inflows are not sufficient to fill the enlarged reservoir every year, a new compensation basin is proposed, from which additional water can be pumped up to the Griessee (Fig. 3). Figure 4 shows the cross section of the dam at the location of the spillway.



Fig. 3: Map of the hydropower scheme

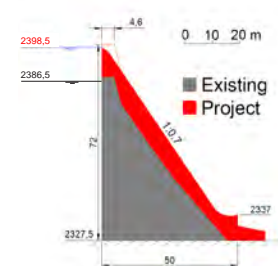


Fig. 4: Cross section of the dam

Conclusion

It is recommended to further investigate the option of heightening the Gries dam because the impact on the additional reservoir area is relatively low and the specific energy is high. However, due to the rather small storage volume, the additional winter energy production is relatively low compared to that of major Swiss HPP reservoirs.

References

Schleiss, A. (2012): Talsperrenenerhöhungen in der Schweiz: Energiewirtschaftliche Bedeutung und Randbedingungen, *Wasser Energie Luft* 104 (3), 199-203.
Piot, M. (2014): Bedeutung der Speicher- und Pumpspeicherkraftwerke für die Energiestrategie 2050 der Schweiz, *Wasser Energie Luft* 106 (4), 259-265.

Storage hydropower potential from dam heightening in the cantons of FR, NW, OW, UR, VD and VS

Jule C. Holland, Samuel Wolf, Hannes Zimmermann, David Felix, Michelle Müller-Hagmann, Robert Boes – VAW ETH Zürich

Introduction

Since 2003, the Swiss demand for electric energy in the winter semester (about 31 TWh) has exceeded the domestic production by 3 TWh on average (BFE 2016). With the planned phase-out from nuclear energy the needs for imports could increase to up to 10 TWh (Piot 2014). The storage hydropower plants (HPPs) are important for the electricity supply, particularly in winter. This contribution can be increased if reservoirs (storage lakes) are enlarged by dam heightening. The present study comprises two parts: Firstly, an analysis of the energy potential of dam heightening at the existing HPP reservoirs in the Swiss cantons of Fribourg, Nidwalden, Obwalden, Uri, Vaud and Valais. These HPPs provide nowadays 49% of the Swiss electricity in winter. Secondly, heightening options for the Sera arch dam (Fig. 1), located in the Zwischbergen valley in the canton Valais, were investigated as a case study in collaboration with Alpiq Group SA.



Fig. 1: Aerial view of the Sera reservoir (left) and downstream view on Sera arch dam

Part I: Energy potential study

Various options to heighten the dams in the mentioned cantons by 5, 10 or 20 percent were assessed based on multiple criteria. These considered the additional areas occupied by the extended reservoirs, the dams with their appurtenant structures and the HPP systems. In Scenario 1 the most promising options were considered, in Scenario 2 also options with a lower probability of realization.

Results

It was estimated that the **active storage volumes** of the reservoirs in the considered cantons could be increased by **180 or 440 Mio. m³** in Scenario 1 or 2, respectively. This corresponds to 12 to 28% of the existing active storage. With enlarged reservoirs, **0.5 to 1.5 TWh of electricity production** could be additionally shifted from summer to winter (Fig. 2). The electricity production in winter would hence increase by 7 to 20% in the considered cantons. These results strongly depend on single large reservoirs (e.g. heightening of the Grande Dixence dam by 10% makes up 520 GWh in Scenario 2).

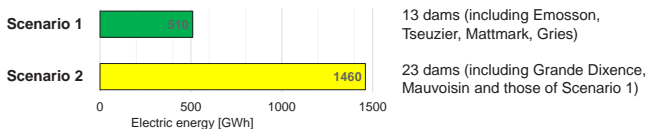


Fig. 2: Potential transfer of electricity production from summer to winter with enlarged reservoirs due to dam heightening in the cantons of FR, NW, OW, UR, VD and VS

Conclusions and Outlook

Heightening of existing dams with the corresponding HPP adaptations has the potential to contribute significantly to a higher electricity production in winter. Moreover, larger storage volumes increase the operational flexibility of HPPs which is also important to reach the goals of the *Energy Strategy 2050*. It is recommended to study dam heightening options in more detail and to introduce additional incentives to foster the increase of storage capacities of HPPs.

References

BFE (2016): Schweizerische Elektrizitätsstatistik, Bundesamt f. Energie.
Piot, M. (2014): Bedeutung der Speicher- und Pumpspeicherkraftwerke für die Energiestrategie 2050 der Schweiz, *Wasser Energie Luft* 106 (4), 259-265.

Part II: Heightening of Sera dam (case study)

Various options to heighten the Sera arch dam and its full supply level by 3 or 6 m were investigated, also based on previous studies. Preference was given to the option of 6 m, keeping the unregulated spillway.

Results

Previous studies and structural analysis by means of the Trial Load Method showed that the existing arch dam can be heightened from 19.5 to 26.4 m without any reinforcement on its downstream face (Fig. 3). It is proposed to increase the vertical distance between the spillway crest and the bridge to achieve a larger freeboard for driftwood during extreme floods.

As a consequence of the raised full supply level, the main water adduction tunnel needs to be adapted and the intermediate **intake** in the Laggital needs to be rebuilt at a higher level. The upper chamber of the **surge tank** needs to be enlarged. The cantonal **road** along the reservoir, the **substation** and the **inlet** to the **sediment bypass tunnel** need to be adapted and relocated (Fig. 4).

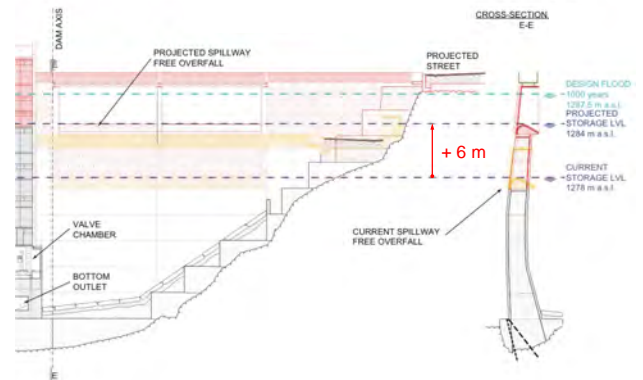


Fig. 3: Downstream view of the proposed dam heightening (left) and cross-section (right) (drawings modified from Lombardi SA)

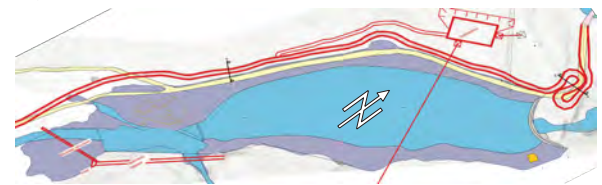


Fig. 4: Schematic plan view of Sera reservoir with full supply level raised by 6 m and corresponding adaptations (modified from SPI Schmidhalter Partner Ingenieure AG)

Due to the higher reservoir water levels, the annual production would increase by **1.6 GWh**, while **0.2 GWh** can be additionally transferred from the summer to the winter semester.

The project costs were estimated as 18.8 Mio CHF. With an interest rate of 2 % and an amortization duration of 80 years, the specific costs of the additional production are 0.3 CHF/kWh, which is above average market conditions. The specific additional cost to shift the 0.2 GWh from summer to winter would even be 2.1 CHF/kWh.

Conclusions and Outlook

The heightening of the Sera dam cannot be economically justified by the increased electricity production in winter. However, the project increases the operational flexibility in the winter months. The adaptation of existing structures such as roads, intakes and surge tanks strongly affect the economic viability of dam heightening projects.

Acknowledgements

The collaboration with Alpiq Group SA is greatly appreciated.



Storage hydropower potential from dam heightening in the cantons of BE, TI and SZ

Cecilia Parravicini, Damiano Vicari, Raphael Werlen, D. Felix, M. Müller-Hagmann, R. Boes - VAW, ETH Zürich

Introduction

Since 2003 the Swiss electricity production in winter is not sufficient to cover the demand. With the planned phase-out from nuclear power according to the *Swiss Energy Strategy 2050*, this deficit will increase. Extending the storage capacity of hydropower plants (HPPs) by heightening of existing dams could contribute to reduce this deficit.

This work aimed firstly at exploring the potential of dam heightening for three Cantons in southern and central Switzerland and secondly at investigating examples of site-specific challenges in a case study at Sambuco dam in the canton of Ticino (Fig. 1).



Fig. 1: Downstream view of Sambuco arch gravity dam.

Part I: Potential study

For 25 reservoirs with a volume of >1 Mio. m³ in the cantons of BE, TI and SZ, dam heightening options by 5%, 10% and 20% of the original dam heights were assessed based on eight criteria. These involved technical, social, ecological and economical aspects. The investigated HPPs contribute currently to 21% of the production from Swiss storage hydropower. In Scenario 1 the most promising options were considered, in Scenario 2 also options with a lower probability of realization.

Results

Figure 2 shows the electricity production which could be additionally shifted from summer to winter in both scenarios. Currently, the investigated HPPs generate annually 4.6 TWh, of which 2.2 TWh in winter. In Scenario 2, the electricity production in winter could hence be increased by 36%.

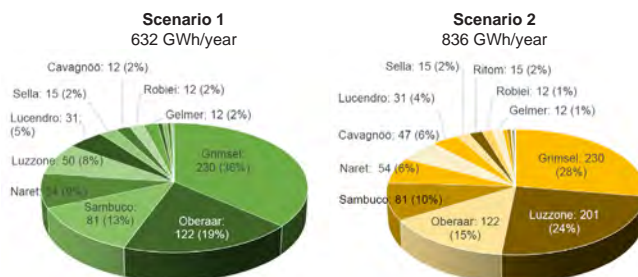


Fig. 2: Estimated electricity production transferred from summer to winter in the cantons of TI, BE and SZ for both scenarios. The absolute numbers are GWh per year, the percentages indicate the contribution to the total of the respective scenario.

The major contribution of 230 GWh per year from Grimsel reservoir results from an assumed 20%-heightening of the Spitalamm arch dam. This correspond to a heightening of 23 m, as studied earlier by the HPP operator (Kraftwerke Oberhasli AG).

Conclusion

If the estimates from the investigated cantons are extrapolated to whole Switzerland, the results are similar to those of previous studies (e.g. Schleiss 2012). Dam heightening has the potential to significantly increase the Swiss electricity production in winter.

Part II: Case Study Sambuco Dam

The Sambuco dam is located upstream of the Peggia HPP and is part of the Maggia cascade. The 130 m high arch gravity dam built in 1956 has a storage capacity of 63 Mio. m³. The elevation difference between its full supply level (1461 m a.s.l.) and the Lago Maggiore at the end of the cascade is 1268 m. The current electricity production at Peggia is about 85 GWh per year, of which 60 GWh (71%) in winter.

Dam heightening option

A dam heightening of 10 m, i.e. 7 % of the current dam height, was chosen considering mainly the estimated reserves in the dam's load-bearing capacity and the average natural inflows (93 Mio. m³/a). The cross section of the proposed concrete structure on the existing dam crest is shown in Figure 3. The active storage volume would increase by 15%. The additional electricity production in winter is estimated as 26 GWh taking into account the whole HPP cascade (of which 9 GWh in Peccia HPP).

The dam's spillway and the upper chamber of the surge tank in connection with a water adduction tunnel have to be adapted according to the higher full supply level. The existing local road along the lake (3.3 km) has to be rebuilt at a higher elevation or replaced by a tunnel (less natural hazards and landscape impact). The estimated total costs of the project are either 72 or 195 Mio. CHF for the open road or tunnel alternative, respectively. The costs of the road adaptation make up 37% or even 58% (without or with tunnel) of the total project costs. With the first road adaptation option, the specific costs per meter dam heightening and per m³ of dam concrete are slightly higher than those of reference projects.

The specific costs to shift the 26 GWh from summer to winter are estimated as 0.068 CHF/kWh. This means that the price of this winter electricity would be considerably higher than average market prices.



Fig. 3: Visualization of heightening the Sambuco dam by 10 m (during construction).

Conclusions

Extending the reservoirs of existing storage HPPs in Switzerland by moderate dam heightening has the potential to considerably increase the electricity generation in winter. However, the economic viability of such projects depends on the regulatory and market conditions in the future. The case study Sambuco shows that local peculiarities such as existing roads might strongly affect the feasibility of such projects, requiring more in-depth studies.

Acknowledgements

We thank OFIMA for having provided information and drawings on the existing Sambuco dam and the HPP scheme.

References

- Schleiss, A. (2012): Talsperrenhöhen in der Schweiz: energiewirtschaftliche Bedeutung und Randbedingungen. *Wasser Energie Luft* 104(3).
- BFE (2016): Schweizerische Elektrizitätsstatistik, Bundesamt für Energie.
- BFE (2017): Schweizerische Wasserkraftstatistik, Bundesamt für Energie.

Storage hydropower potential from dam heightening in the cantons of GL, GR and SG

Marco Baumann, Alain Emmenegger, Andrin Kasper, D. Felix, M. Müller-Hagmann, R. Boes - VAW, ETH Zürich

Motivation

In the last 10 years, on average 3.5 TWh of electric energy were net imported to Switzerland in every winter (BFE 2016). With the planned phase-out from nuclear power according to the Swiss Energy Strategy 2050, the need for electricity imports is estimated to increase to about 10 TWh per winter (Piot 2014).

One possibility to cover this seasonal deficit in domestic production is to enlarge the storage reservoirs of hydropower plants (HPPs). Because the construction of new reservoirs is rather difficult, the heightening of already existing dams is an attractive option. According to previous studies (BFE 2004, Schleiss 2012) an additional electricity production between 0.7 TWh and 2.5 TWh per winter could be reached by this way.

Part I: Potential study in eastern Switzerland

Dam heightening options by 5%, 10% and 20% of the original dam heights were assessed for 24 dams in the cantons of GL, GR and SG based on eight criteria involving technical, social, ecological and economical aspects. In Scenario 1 the most promising options were considered, in Scenario 2 also options with a lower probability of realization.

Results

Figure 1 shows the locations of the reservoirs at which a dam heightening is proposed in the two scenarios. Figure 2 shows the additional storage volumes and the electricity production which could be additionally shifted from summer to winter in Scenario 2. Heightening of 15 dams would increase the electricity production in winter by 600 GWh, of which 500 GWh would come from the largest six reservoirs. In Scenario 1, heightening of six dams would lead to additional 220 GWh in winter.

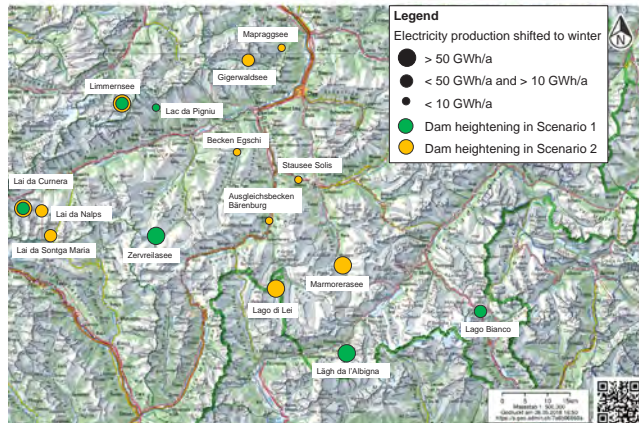


Fig. 1: Location of analysed reservoirs in the two scenarios.

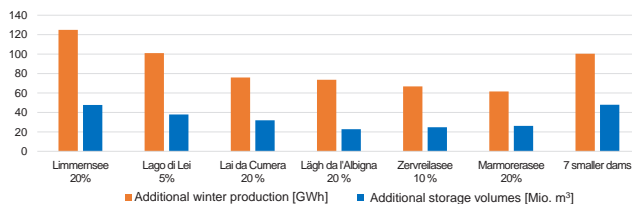


Fig. 2: Additional electricity production in winter and storage volumes in Scenario 2. The percentages indicate the dam heightenings relative to the original dam heights.

Conclusion

If the estimates from the investigated cantons are extrapolated to whole Switzerland, the results are similar to those of previous studies (e.g. Schleiss 2012 and BFE 2004). Dam heightening has the potential to significantly increase the Swiss electricity production in winter.

Part II: Case Study Marmorera Dam

For the 91 m high Marmorera earthfill dam in the Canton of Grisons, Switzerland, various heightening alternatives were considered. The required adaptation works were identified as a function of the extent of dam heightening and the corresponding raise of the full supply level. The considered elements include the dam, its spillway, the water adduction Flix, the surroundings of the lake and the Julier pass road, as well as the surge tank of the HPP Tinizong. The dam heightening alternatives and their key figures are summarized in Table 1.

Tab. 1: Investigated dam heightening alternatives with key figures.

	Project Costs	Annual payment	Additional winter production	Specific costs
	[Mio.CHF]	[kCHF/a]	[GWh/a]	[Rp./kWh]
Alternative +3 m	7.9	198	10.5	1.9
Alternative +8 m	58.6	1'473	28.8	5.1
+8 m (excl. tunnel)	19.6	492	28.8	1.7
Alternative +11m	87.5	2'201	40.4	5.4
+11 m (excl. tunnel)	24.5	615	40.4	1.5

For the alternative “+3 m” the additional cost per kWh transferred from summer to winter are the lowest. This alternative was hence preferred for economical reasons, although a higher electricity production in winter would be favourable from a national energy-policy point of view. For the alternatives “+8 m” and “+11 m”, major adaptations on the Julier pass road are required mainly in the region of the dam. A new road tunnel is proposed leading to relatively high costs but also to better protection against natural hazards. If the tunnel would be paid partly by public means, dam heightening by 8 or 11 m would become more economic.

Alternative +3 m

Tab. 2: Key figures of alternative +3 m

	Existing	Project
	Dam height	91
Hydraulic head	1061	1064 [m]
Lake surface area	1.4	1.43 [km ²]
Storage capacity	61.4	65.7 [Mio. m ³]
Energy equivalent	146	157 [GWh]

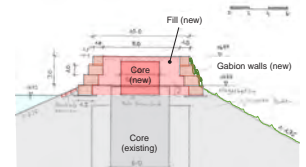


Fig. 3: Cross section of the dam

The following elements would need to be modified: The dam crest (Fig. 3 and item 1 on Fig. 4), the Julier pass road in the region of the dam (item 2 on Fig. 4), the spillway (item 3 on Fig. 4), the water adduction Flix (outlet is item 4 on Fig. 4), the bridge south of the lake (item 5) and finally the surge tank (downstream in the North of Fig. 4).



Fig. 4: Map of the Marmorera lake with modifications for dam heightening by 3 m

References

Schleiss, A. (2012): Talsperrenhöhungen in der Schweiz: energiewirtschaftliche Bedeutung und Randbedingungen. *Wasser Energie Luft* 104(3).
 BFE (2004): Ausbaupotenzial der Wasserkraft. *Studie der Electrowatt-Ekono*.
 BFE (2016): Schweizerische Elektrizitätsstatistik, Bundesamt für Energie.
 Piot, M. (2014): Bedeutung der Speicher- und Pumpspeicherkraftwerke für die Energiestrategie 2050 der Schweiz, *Wasser Energie Luft* 106 (4), 259-265.



Nucleation of laboratory earthquakes: Implications for EGS induced seismicity



M. Acosta^{*1}, F. Passelègue¹, A. Schubnel², B. Gibert³, M. Violay¹

¹EPFL, LEMR, Lausanne, Switzerland; ²Laboratoire de Géologie, CNRS, UMR, ENS, Paris, FR.; ³Géosciences Montpellier, Université de Montpellier, Montpellier, FR.

*Author for correspondence: mateo.acosta@epfl.ch.

1- Abstract

Recent seismological observations highlighted that both aseismic silent slip or foreshock sequences can precede large earthquake ruptures (Tohoku-Oki, 2011, Mw 9.0; Iquique, 2014, Mw 8.1; Illapel, 2015, Mw 8.3). However, the influence of pore fluid pressure level on the earthquake nucleation behaviour remains poorly understood. Here, we report for the first time, experimental results regarding the nucleation of stick-slip instabilities (laboratory proxies for earthquakes) conducted on Westerly Granite saw-cut samples. Experiments were conducted under stress conditions representative of the upper continental crust, i.e. confining pressures from 50 to 125 MPa; fluid pressures (water and argon) ranging from 0 to 45 MPa; and temperatures ranging from 25 to 500 °C. In dry conditions, we observe that slip evolves exponentially up to the main instabilities and is escorted by an exponential increase of acoustic emissions. With pressurized fluids, precursory slip evolves first exponentially then switches to a power law of time. There, precursory slip remains silent, independently of the fluid pressure level. The amount of precursory slip (u_{prec}) depends on both fluid pressure and initial shear stress. While increasing the initial shear stress leads to larger precursory slip, increasing the fluid pressure seems to reduce the amount of precursory slip leading to instabilities. Independently of the fluid pressure level, we demonstrate that the amount of precursory energy density (E_{prec}^*) released prior to the mainshock (the energy dissipated during the precursory stage) scales linearly with the energy density dissipated during the co-seismic stage ($(\tau_1 + \Delta\tau_2) \cdot u_{cos}$). These results suggest that the intensity of the precursory stage is a function of the strength of the asperity which is eventually going to rupture. Our experimental observations imply that the initial background stress and the pore fluid pressure level control the intensity and the nucleation behaviour of the fault. Such observation indicates that (i) that the presence of foreshock sequences is not systematic during earthquake nucleation and seems attenuated in presence of water, (ii) large ambient pore fluid pressure could reduce the intensity and the duration of the precursory stage.

2- Experimental set-ups

2.1 – Oil loading triaxial apparatus

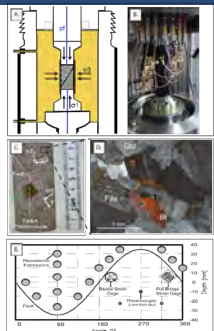
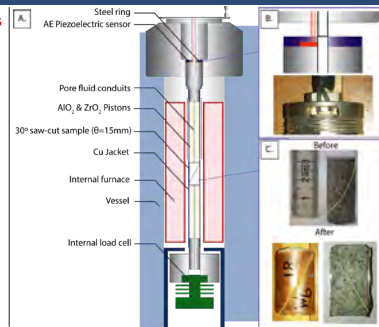


Fig.1 Experimental set-up at ENS Paris.
A. Oil loading triaxial apparatus.
B. Picture of the experimental sample in the machine.
C. Intact Westerly Granite sample (80 mm length and 40 mm diameter) showing the fault orientation, stresses in the sample and instruments used.
D. Map of the instruments used.

- HIGHLIGHTS**
- Upper crustal stress conditions (down-to ~7km depth).
 - Allows for wide instrumentation (15 Piezo-electric sensors, 4 near-fault strain gages, 1 type-K thermocouple).
 - High frequency AE and strain (up to 10 MHz sampling frequency).



2.2 – High Pressure-High Temperature Paterson rig.

Fig.2 Experimental set-up at Géosciences Montpellier.

- A.** High Pressure – High temperature Paterson rig. Confining pressure is argon gas.
B. Detail on the installation of the Acoustic emission sensor located on the top piston 18 cm away from the sample.
C. Intact Westerly Granite sample (32 mm length and 15 mm diameter) showing the fault orientation.
D. Samples after deformation.

- HIGHLIGHTS**
- Upper crustal stress and temperature conditions (down-to ~10km depth).
 - Acoustic Emission monitoring.

3- Experimental results

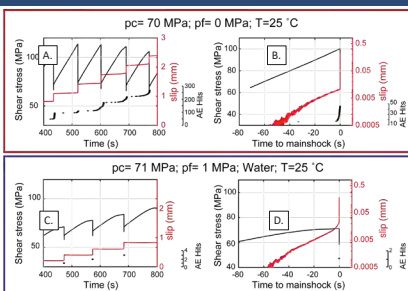


Fig.3. Experimental results from room temperature experiments.

- A.** Shear stress, fault slip and AE arrivals evolution on time for a DRY Experiment (pc=70 MPa). **B.** Fluid pressurized Experiment (pc=71 MPa, pf=1 MPa). **C.** Precursory evolution of shear stress (black), corrected slip (red in log scale), and AE arrivals (black dots) on time prior to the mainshock for one event of the DRY experiment (pc=70 MPa). **D.** same as C. for Fluid pressurized experiment at pf=1 MPa.

- HIGHLIGHTS**
- Water fluid pressure promotes "silent" aseismic slip.
 - Precursory slip behavior can be very different depending on fault conditions

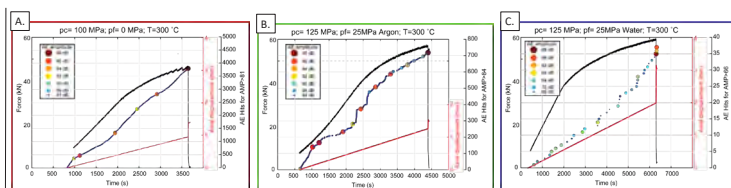


Fig.4 Experimental results from HP-HT experiments.
A. Axial force, axial displacement and AE arrivals evolution on time for a DRY experiment (pc=100 MPa).
B. Argon fluid pressurized Experiment (pc=125 MPa, pf=25 MPa).
C. Water fluid pressurized Experiment (pc=125 MPa, pf=25 MPa).

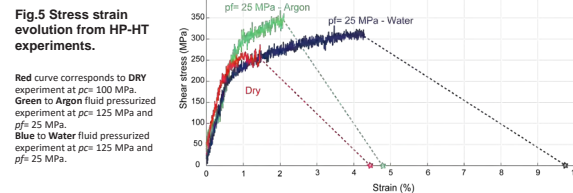


Fig.5 Stress strain evolution from HP-HT experiments.

Red curve corresponds to DRY experiment at pc=100 MPa. Green to Argon fluid pressurized experiment at pc=125 MPa and pf=25 MPa. Blue to Water fluid pressurized experiment at pc=125 MPa and pf=25 MPa.

- HIGHLIGHTS**
- Precursory and co-seismic strain are longer in presence of water than with argon gas and dry conditions

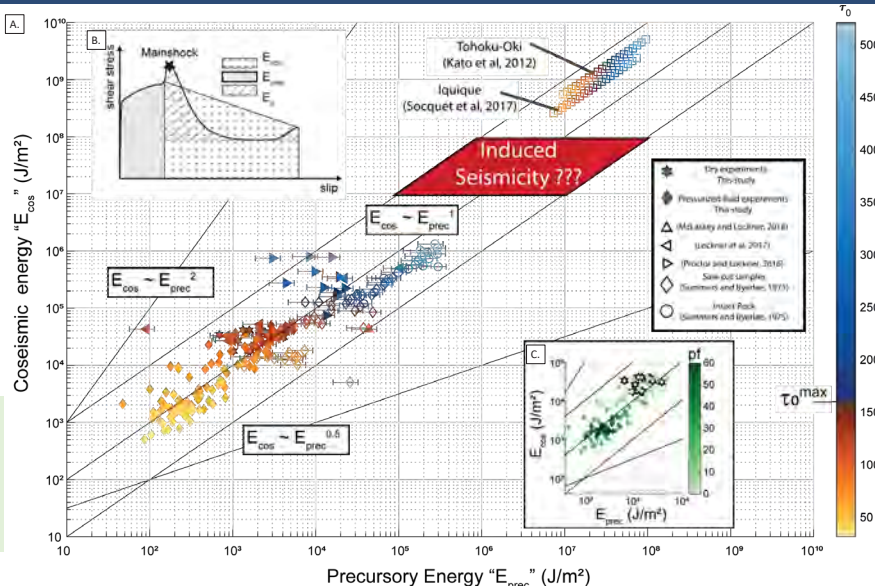
4.2 – Energy dissipation during laboratory earthquakes.

Fig.7. Energy spent during laboratory earthquakes.

A. Schematic of shear stress as function of slip during the seismic cycle. The shaded areas correspond to what we define as "Precursory Energy" and "Co-seismic Energy". The latest corresponds to the Fracture Energy in the case of a linear slip-weakening case.

B. Co-seismic Energy versus Precursory energy for all stick-slip events at room temperature with additional data from other studies on sawcut and intact rock. Colorbar shows static fault shear strength.

C. Co-seismic Energy versus Precursory energy for OUR stick-slip events at room temperature. Colorbar accounts for pf.



- HIGHLIGHTS**
- Co-seismic Energy scales linearly with precursory energy.

5- Conclusions

- Water fluid pressure promotes "silent" aseismic slip and low fault coupling prior to the main instability. The dependence on fluid pressure remains to be determined.
- Slip behavior and foreshock sequences depend on fault conditions.
- The energy dissipated prior to the earthquake seems to scale with the co-seismic energy associated to the event.
- Study of energy dissipation during induced seismicity can bring major insights to earthquake physics

6- References

- Passelègue, F. X., et al., Influence of Fault Strength on Precursory Processes During Laboratory Earthquakes. *Geophys. Mon.* (2017)
 - Summers, R., Byerlee, J.D., Summary of results of frictional sliding studies at confining pressures up to 6.98 kb. in selected rock materials, U.S. Geol. Surv. Open File Rep (1977)
 - Proctor, B., Lockner, D.A., Pseudotachylite increases the post-slip strength of faults. *Geology* (2016)
 - Lockner, D.A., et al. The transition from frictional sliding to shear melting in laboratory stick-slip experiments. *Geophys. Mon.* (2017)
 - Socquet, A., et al., An 8-month slow slip event triggers progressive nucleation of the 2014 Chile megathrust. *Geophys. Res. Lett.* (2017)
 - Kato, A., et al., Propagation of Slow Slip Leading Up to the 2011 Mw 9.0 Tohoku-Oki Earthquake. *Science* (2012)

Blocking probability at spillway inlets under driftwood impact

Paloma Furlan*, M. Pfister, J. Matos and A.J. Schleiss
*corresponding author: paloma.furlan@epfl.ch



Introduction

Dam safety is strongly linked to the probability of occurrence of large floods. **Floods can transport large wood (LW)** into reservoirs and towards water release structures as spillways (Fig. 1 and 2).

For a better assessment of the related risk, the behaviour of LW in contact with hydraulic structures has to be quantified. Thus, the understanding of **LW blockage** process at spillways is important for **safety evaluations of dams**.



Figure 1: Picture of Oroville Dam, USA. (www.sacbee.com)



Figure 2: Picture of Yazagyo Dam, Myanmar. (www.thutatuam.net)

The present research project aims to describe and quantify systematically the **influence of LW characteristics** on the blocking process and the **effects a blockage** can have on the rating curve of an ogee crested spillway with piers.

Methodology and experiments

A physical model was designed and constructed in the facilities of LCH (Fig 3). An ogee crested spillway with round nose piers was chosen as it is a widely used structure and has a great ability to pass floods.

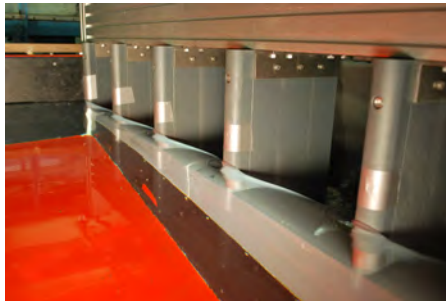


Figure 3: Upstream picture of the experimental facility at LCH

Experiments include different configurations tested, always having a reservoir approach.

Outcomes:

- Furlan P, Pfister M, Matos J, Amado C, and Schleiss A.J (2018) "Experimental repetitions and blockage of large stems at ogee crested spillways with piers", *Journal of Hydraulic Research*, doi: 10.1080/00221686.2018.1478897
- Furlan P, Pfister M, Matos J, and Schleiss A.J (2018) "Influence of density of large stems on the blocking probability at spillways". Daniel Bung, Blake Tullis, *7th IAHR International Symposium on Hydraulic Structures*, Aachen, Germany, 15-18 May. doi: 10.15142/T3664S
- Furlan P, Pfister M, Matos J, and Schleiss A.J (2017) "Entrainement de bois flottant dans un déversoir à crête standard avec piliers: Influence des caractéristiques de bois flottant en probabilités de blocage" *Colloque CFBR-SHF*, Chambéry, France, 29-30 novembre 2017. p. 42-49. DOI : 10.24346/cfbr_shf_colloque2017_a04.

Parameters

Blockage probabilities are estimated by varying the following parameters:

- **Diameter and length** of stems;
- **Stem density**;
- **Spillway bay width**;
- **Hydraulic head** at the spillway crest.

Different scenarios include **individual** stems or **groups**.

Additionally, **head increase** due to large wood blocked at the spillway inlet is investigated to understand the effect of a LW blockage.

Preliminary results

How can interactions between stems influence the blockage process at a spillway inlet? Does the amount of stems reaching a structure affect the blockage process? These questions were approached by systematically increasing the number of supplied stems and estimating blockage. Experiments have been concluded and the analysis is ongoing.

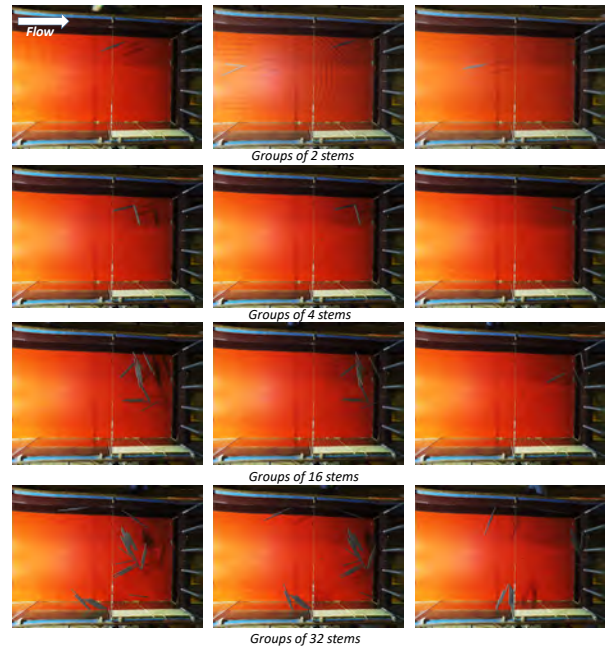


Figure 4: Pictures of blocking probability experiments for varied group sizes

Conclusions

Blocking probabilities were linked to the number of stems travelling towards the structure as a function of the hydraulic head and the length of stems.

For groups up to 4 stems, blocking probabilities increase as the size of the group increases. In some experiments, blockage probability of 4 stems is twice the value than for a single stem.

Acknowledgments

This research project is developed in the scope of the Ph.D. thesis by Paloma Furlan under the joint IST-EPFL doctoral program H2Doc. It is funded by the Portuguese Foundation for Science and Technology, LCH-EPFL and EDF.

Spatial Impulse Wave Generation and Propagation

Eva Sauter, Frederic Evers, Helge Fuchs, Robert Boes

Introduction

Gravity-driven mass movements may generate massive water waves, so-called impulse waves. As part of this thesis, further research is done on the spatial wave generation and propagation by conducting experiments. Besides landslides of small impacts and their underwater depositions, also the effect of slide density as well as of water body geometries are examined.

Background

Computation of wave characteristics usually considers two extreme cases: 2D or 3D. For calculation the impulse product parameter P (Heller & Hager, 2010) is of high significance. Wave characteristics increase with increasing P.

$$P = F M^{0.5} S^{0.25} \cos^{0.5} \alpha / 7 \alpha$$

Evers (2017) developed equations to compute the wave characteristics a_{c1} , a_{t1} , a_{c2} , H_1 and T_1 for varying propagation angles γ and radial distances r (s. Fig. 1). The equations are based on 74 3D tests with material of the same density ($\rho_s > \rho_w$) and for different experimental set-ups.

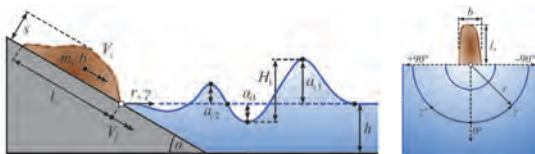


Fig. 1: Visualization of governing parameters and wave features for spatial impulse wave generation (Evers, 2017)

The wave decay is strongly dependent on the water body geometry. Heller and Spinneken (2015) showed that 3D waves decay faster and propagate slower than 2D waves. Furthermore, Heller et al. (2016) determined numerically for geometries with diverging angles θ , that wave amplitudes along the slide propagation angle lie approximately halfway between 2D and 3D for $\theta = 7.5^\circ$ and are practically the same for $\theta = 45^\circ$.

Methodology

Experiments were conducted in a test basin of 8.0 m x 4.5 m and 0.75 m height (s. Fig. 2). Slide velocities were determined by dry tests, using laser distance sensors for measuring. Wave amplitudes were measured with ultrasonic devices (USD). 12 USD were placed in radial distances between 1.6 and 2.8 m on three axes: 0° , 35° and 70° . Overall, 18 different experimental set-ups were tested and evaluated. The considered parameter range can be seen in Table 1. Underwater depositions were measured with a grid on the basin bottom of 5 cm x 5 cm and registered by underwater camera (GoPro).

Tab. 1: Applied parameter range for conducted experiments

Parameter	h [m]	α [°]	Δz_{sc} [m]	b [m]	s_0 [m]	$\frac{W_s}{H}$ [l]
Landslides	0.20 - 0.65	30 - 90	0.65 - 1.20	0.25 - 0.50	0.047 - 0.05	7.5 - 15
Avalanches	0.20 - 0.65	30 - 60	0.65 - 1.20	0.25 - 0.50	0.05	7.5 - 15

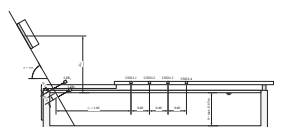


Fig. 2: Test basin, cut along the slide propagation axis ($\gamma = 0^\circ$)

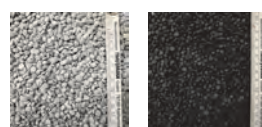


Fig. 3: Replacement materials, 87% BaSO₄, 3% PP, $\rho_s = 1338 \text{ kg/m}^3$ (right), 100% PP, $\rho_s = 573 \text{ kg/m}^3$ (left)

Results and Discussion

Landslides and avalanches of small impact

Measured amplitudes were compared with predicted values according to Evers (2017) and show a relatively poor agreement (s. Fig. 4). Thus, wave amplitudes for small impulses are overestimated by approximately a factor of 2. Largest deviations occur for small amplitudes. It must be noted that for small amplitudes the applied measurement technology meets its limits due to accuracy.

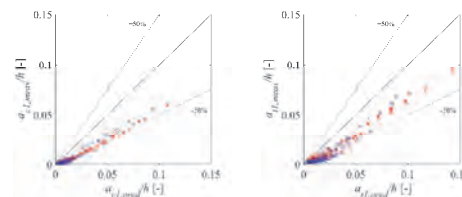


Fig. 4: Comparison of measured amplitudes (first wave crest a_{c1} and trough a_{t1}) with predicted values according to Evers (2017) [red: landslides, blue: avalanches]

Effect of water body geometry

Experiments from earlier work (Evers, 2017) were additionally analyzed. Different geometries with diverging angles were under estimation ($\theta = 10^\circ, 20^\circ$ and 30°) and compared to a 3D test ($\theta = 90^\circ$). All tests are within similar parameter range ($0.67 \leq P \leq 0.82$). The wave shows similar behavior in decay as Heller et al. (2016) determined by numerical modelling. For $\theta = 30^\circ$ the wave amplitudes are already close to those for 3D test (s. Fig. 5).

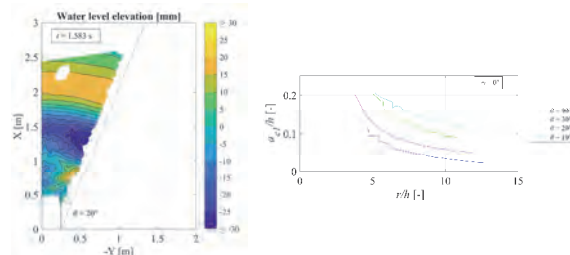


Fig. 5: Spatial wave propagation for $t = 1.583 \text{ s}$ and $\theta = 20^\circ$ (left) and wave decay of the first wave crest along the slide propagation angle for $\theta = 90^\circ, 30^\circ, 20^\circ$ and 10° (right)

Conclusion

The applied parameter range of the experiments lies mainly out of the range of Evers (2017). Further research and more experiments will be needed on spatial propagation of impulse waves to approve the 3D computation for small impacts. The estimated effect of the water body geometry shows the expected behavior. As it was analyzed only for slide impact angles of 30° , further analysis of experiments needs to be done to confirm.

References

Evers, F. M., 2017. Spatial Propagation of Landslides Generated Impulse Waves. Zurich: ETH Zurich.

Heller, V., Bruggemann, M., Spinneken, J. & Rogers, B. D., 2016. Composite modelling of subaerial landslide-tsunamis in different water body geometries and novel insight into slide and wave kinematic. *Coastal Engineering*, 109

Heller, V. & Hager, W. H., 2010. Impulse Product Parameter in Landslide Generated Impulse Waves. *Journal of Waterway, Port, Coastal, and Ocean Engineering*, 136(3).

Heller, V. & Spinneken, J., 2015. On the effect of the water body geometry on landslide-tsunamis: Physical insight from laboratory tests and 2D to 3D wave parameter transformation. *Coastal Engineering*, 104.

Impulse waves: run-up behavior and overtopping at dam structures

Fabian Küttel, Frederic Evers, David Vetsch, Robert Boes

Introduction

Waves generated by impulse of a rockfall, landslide, avalanches or earthquakes will lead to water waves in reservoirs, which run-up at the coast or at dam structures up to several meters. In this Master's thesis a numerical model is implemented in OpenFOAM for the run-up and overtopping at dam structures and compared to given experimental results.

Background

The behavior of an impulse is divided in three stages (Fig. 1, top). For the given topic, the relevant ones are, the wave propagation (stage 2) and the run-up behavior (stage 3). In the propagation stage the solitary wave with its typical profile, a single peak and no wave trough (Fig. 1, bottom), builds up and propagates towards the dam by holding the same shape. Solitary waves illustrate the extreme case for overtopping. Therefore it is used to analyze the structural safety (especially the erosion) of the dam (Heller and Hager 2011).

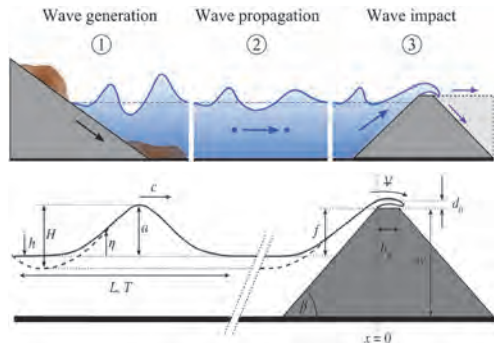


Fig. 1: Top: Impulse wave stages in a reservoir (Evers 2017). Bottom: Parameter definition for solitary wave (solid line) and overtopping at dam structure (Kobel et al. 2017).

In a previous, study experimental results were generated in a rectangular channel at the VAW at ETH Zurich (Kobel et al. 2017). The channel had a length of 11 m, a width of 0.5 m and a the end a dam with a height of 0.3 m. The waves are generated by a piston-type wave generator with a relative wave amplitude of $\epsilon = a / h$.

Methodology

The numerical model is building up by using the open source program OpenFOAM. First the solitary wave behavior has to be proved in a simple numerical channel model, researched by the behavior of the wave amplitude a and the internal velocity field (Munk 1949). To find the final model, the boundary conditions were varied and different wave generator methods were used. Finally the wave generator method by Grimshaw and a rough wall at the bottom is implemented. The prior model, used for stage 2, was modified for the overtopping part (wave stage 3) by implementing the dam and using seven single blocks (Fig. 2) within a particular cell size of 0.5 mm in all directions.



Fig. 2: Numerical model for overtopping with seven blocks (dotted line).

The recorded parameters are the overtopping flux $Q(t)$, the volume Ψ and the maximum overtopping depth $d_o(t)$. The used input parameter range is shown in Table 1.

Results

Before the solitary wave spills over, the internal velocity field is checked at 1.5 m before the dam structure in the non influenced area (Fig. 3). During the overtopping a comparison of the water surface shape is done (Fig. 4).

Tab. 1: Parameter range

Parameter		min	max
Still water depth	h [m]	0.20	0.30
relative wave amplitude	ϵ [-]	0.20	0.70
dam height	w [m]	0.30	
crest width	b_c [m]	0.02	0.16
front face angle	δ [°]	18.4	90

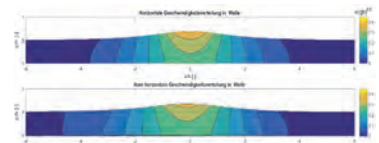


Fig. 3: Internal velocity field distribution at 1.5 m before dam.



Fig. 4: Qualitative comparison of water surface between the experimental and the numerical data. Initial parameters are: $h = 0.25$ m; $a = 0.075$ m; $b_c = 0.02$ m; $w = 0.30$ m.

All simulations are normalized for the overtopping volume Ψ and for the maximum overtopping depth d_o according to Kobel et al. (2017) (Fig. 1 and 5).

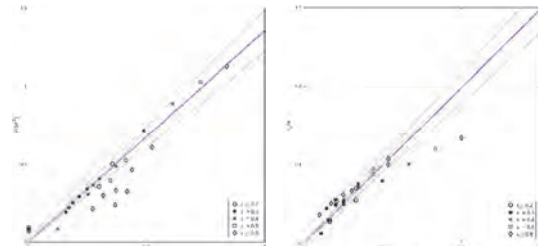


Fig. 5: Left: Relative overtopping volume Ψ and right the relative maximum overtopping depth d_o . The grey - dotted line shows the +/- 10% deviation.

Conclusions

In general, a relative wave amplitude higher than 0.5 results in an internal velocity profile difference >10% of the solitary wave and the wave amplitude is to small. For relative amplitudes between $0.2 \leq \epsilon \leq 0.4$ the received data produce reasonable results. For $\epsilon \geq 0.5$ the overtopping volume is significantly to low. In case the initial water table has the same level as the dam crest ($h = w$), for every relative amplitude, the overtopping depth is too low. Relating to the reality, the most expected wave amplitudes in reservoirs are $0.2 \leq \epsilon \leq 0.4$ and can be calculated by the model.

References

Evers, F. M. (2017). Spatial Propagation of Landslide Generated Impulse Waves. *Dissertation* 24650, ETH Zurich, Zurich.

Heller, V. and Hager, W.H. (2011). Wave types of landslide generated impulse waves. *Ocean Eng.*, 38(4), 630-640.

Kobel, J.; Evers, F. M. and Hager, W.H. (2017). Impulse wave overtopping at rigid dam structures. *Journal of Hydraulic Engineering*.

Munk, W.H. (1949). The solitary wave theory and its applications to surf problems. *Ann. N.Y. Acad. Sci.*, 51:376-424.

Wave generation by submarine mass failures

Nina Landolt, Frederic Evers, Helge Fuchs, Robert Boes

Introduction

Historic events have shown a danger potential in Switzerland regarding tsunamis caused by landslides [1]. Popular examples are Lake Geneva in 563 AD [2] and Lake Lucerne 1601 [3], when subaqueous landslides induced waves of several meters. In this Master's thesis, physical 2D experiments of underwater landslides were performed. The aim is to improve the understanding of the underlying processes of wave generation due to submarine mass failures, as well as the generation of a dataset for the calibration of numerical models.

Background

Fig. 1 shows a wave with its principle parameters. The parameters are required to mathematically classify a wave [4].

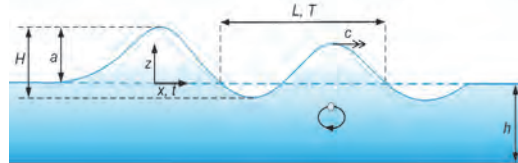


Fig. 1: Definition sketch of principal wave parameters

- c [m/s] = Wave celerity
- h [m] = Still water depth
- L [m] = Wave length
- T [s] = Wave period
- H [m] = Wave height
- a [m] = Wave amplitude

Methodology

Experimental Setup

Fig. 2 shows the setup of the physical 2D model of a channel with a width of 0.5 m, a depth of 1 m and a length of 11 m. Seven ultrasonic device sensors (UDS) are fixed at a distance of $\Delta x = 0.8$ m, to capture the water level change.

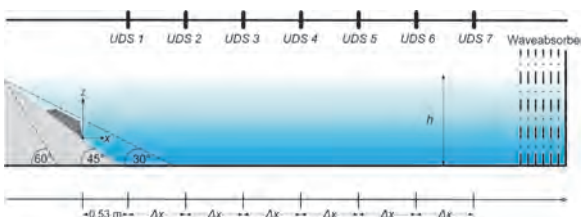


Fig. 2: Definition sketch of experimental setup

Experiments

Two series of experiments were conducted:

- 1) Comparison of granular and rigid slides with slide plane angles $\alpha = 30^\circ, 45^\circ$ and 60° and still water depths $h = 0.7, 0.8$ m and 0.87 m
- 2) Velocity field examinations with Particle Image Velocimetry (PIV).

Velocity vectors were identified by cross-correlating images acquired between two laser pulses. With the measurements of the UDS, the wave amplitudes as well as the time periods were evaluated. The rigid and granular slides were compared visually as well as quantitatively on the basis of maximal amplitudes and time periods.

Results and Discussion

Fig. 3 shows an experiment conducted in the channel at VAW. Below, important experiment parameters are listed.

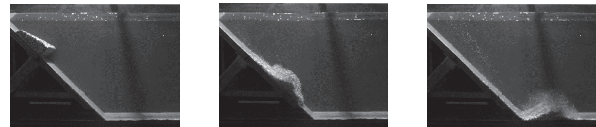


Fig. 3: Image series of experiment in channel $d_g = 8$ mm, $\alpha = 45^\circ$, $h = 0.8$ m, $m_s = 12.3$ kg

- α [°] = Slide plane angle
- d_g [mm] = Particle size
- m_s [kg] = Slide mass
- ρ_s [$\frac{kg}{m^3}$] = Slide density
- $\frac{\Delta h}{h}$ [-] = Water level displacement
- t [s] = Time
- g [$\frac{m}{s^2}$] = Gravit. acceleration, $9.81 \frac{m}{s^2}$

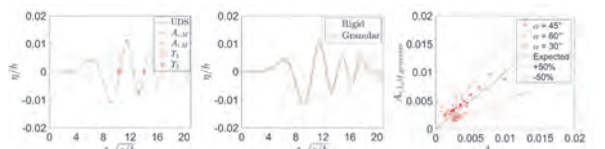


Fig. 4: Exp. with $d_g = 8$ mm, $\alpha = 45^\circ$, $h = 0.8$ m, $m_s = 12.3$ kg, UDS # 3. First wave crest and trough ($A_{c,M}$, $A_{t,M}$) and time periods (T_1 , T_2) of granular slide.

Fig. 5: Comparison between granular ($d_g = 8$ mm) and rigid slides, $\alpha = 45^\circ$, $h = 0.8$ m, $m_s = 12.3$ kg, UDS # 3

Fig. 6: Comparison of first crests between rigid and granular slides. 14 experiments are shown (7 comparison), with 7 UDS each.

The comparison of the conducted experiments (fig. 6) shows differences in max. amplitudes up to 50% for slide plane angles of 45° and 30° and over 100% for an angle of 60° . Fig. 7 and 8 show the velocity fields of slides with $\alpha = 60^\circ$ at $t = 0.8$ s. The quality of the vector field increases with higher water velocities. It can be seen that for an angle of 60° , the granular slide generates higher velocities.

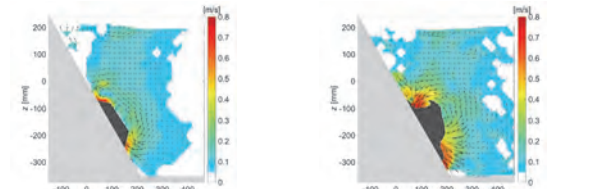


Fig. 7: Rigid slide with $\alpha = 60^\circ$, $h = 0.8$ m, $m_s = 12.3$ kg, $t = 0.8$ s

Fig. 8: Granular ($d_g = 8$ mm) slide with $\alpha = 60^\circ$, $h = 0.8$ m, $m_s = 12.3$ kg, $t = 0.8$ s

Conclusion

Amplitudes of granular slides are generally higher compared to rigid slides when α exceeds 45° and lower for smaller angles. A direct conversion between granular and rigid slides proves to be difficult. Additionally, lower bank inclinations ($\alpha < 30^\circ$) should be considered in further experiments. Particle Image Velocimetry can be used to compare velocity fields and visually examine the wave generation process. However, air trapped in the slide bodies often leads to incorrect velocity vector detection. Therefore, the experiment approach and evaluation processes can still be improved.

References

[1] Strupler, M., Danciu, L., Hilbe, M., Kremer, K., Anselmetti, F. S., Strasser and M., Wiemer, S. (2018): A subaqueous hazard map for earthquake-triggered landslides in Lake Zurich, Switzerland, *Natural Hazards* 90: 51 – 78.

[2] Schnellmann, M., Anselmetti, F.S., Giardini, D., McKenzie, J.A. and Ward, S.N. (2002): Prehistoric earthquake history revealed by lacustrine slump deposits, *Geology* 30, 1131 – 1134.

[3] Kremer, K., Simpson, G. and Girardclos, S. (2012): Giant Lake Geneva tsunamis in AD 563, *Nature Geoscience* 5.

[4] Heller, V., Hager, W.H. and Minor, H.-E. (2009): Landslide generated impulse waves in reservoirs: Basics and computation. *VAW-Mitteilung* 211, Versuchsanstalt für Wasserbau, Hydrologie und Glaziologie (VAW), R. Boes, Ed., ETH Zürich.

Influence of tunnel slope on air demand and flow conditions of bottom outlets

Alexander Williams, Benjamin Hohermuth, Lukas Schmocker, Robert Boes

Introduction and Motivation

Due to the high velocities in bottom outlets, significant negative pressures may occur. To better understand these processes, the different flow conditions as well as the air demand in horizontal and inclined tunnels were analyzed. The overall goal was ensure controlled flow conditions and to minimize negative pressures thereby reduce the danger of cavitation.

Experimental setup and measurements

The experimental analysis has been carried out on a 20 meter long channel (Fig. 1). It consisted of all relevant elements of a bottom outlet. The energy head at the gate and the gate opening were varied to investigate different Froude numbers at the vena contracta. Orifice plates of different size were used to vary the loss coefficient of the air vent.

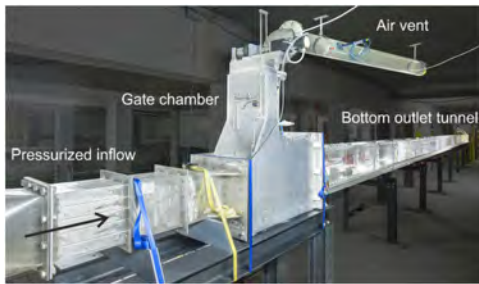


Fig. 1: Hydraulic scale model at Laboratory of Hydraulics, Hydrology and Glaciology (VAW).

To investigate the influence of the tunnel slope, the tunnel was changed from horizontal (0%) to a 4% inclination. Although several flow conditions were observed, the focus of the work was placed on the transition from free surface to slugflow. This transition is the most violent and poses the largest risk of cavitation. Hence, it has to be avoided in bottom outlets.

Results of the flow conditions

With the experimental setup the formation slugflow could be analyzed (Fig. 2). The observations showed that a strong counter-current air flow is responsible for the formation of slugs. Such a counter-current air flow is induced by large water flow velocities and large loss coefficients of the air vent.



Fig. 2: A slug photographed in the hydraulic scale model. Flow direction from left to right.

To analyse slug formation, β_{total} was defined as the total air inflow (through the air vent and from the downstream tunnel end) divided by the water inflow into the system. Furthermore, slugflow depends on the water pressure upstream of the gate P_o and the minimal air pressure $P_{a,min}$ downstream of the gate chamber. These findings resulted in the design diagram shown in Fig. 3.

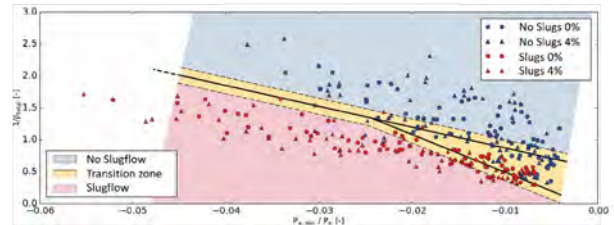


Fig. 3: The resulting correlation of the research results for the identification of slugflow in bottom outlets

Figure 3 allows to delineate slugflow from free surface flow. The total air discharge and the minimal air pressure have a decisive influence on the formation of slugs while the tunnel slope has no significant effect.

Results on air demand

Air demand

Information on the air demand in a bottom outlet are essential for dimensioning the air vent and for calculating the mixed water depth. Measurements have shown, that the influence of the tunnel slope is small. However, it still has some influence on the water depth, especially further downstream of the gate as can be seen in Fig. 4. Due to the higher velocity in the inclined channel, the mixed water depth lies below the one of the horizontal channel.

Backwater curve

In order to understand how the mixed flow depth propagates in bottom outlets, the classic backwater curve was calculated. Knowledge on the water level is needed to avoid the transition to pressurized flow, i.e., flow choking. Considering Fig. 5 it becomes apparent that this approach returns values only for clear-water depth as it does not account for the entrained air. Accordingly, the influence of the air, i.e., flow bulking, has to be taken into account. Therefore, an empirical approach by Speerli and Hager (2000)¹ has been adopted. This returns a calculated mixture flow depth also shown in Fig. 5.

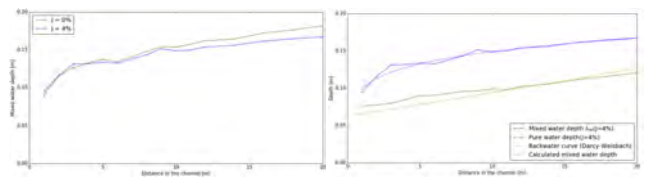


Fig. 4: Measured mixture flow depth h_{30} for the horizontal (0%) and the inclined (4%) channel.

Fig. 5: Backwater curve calculation for the clear-water and mixture flow depth.

Conclusions

Bottom outlets are vital elements for the security of high-head dams. The measurements have shown that the inclination of a bottom outlet tunnel has slight, but not essential influence on the flow conditions and the air demand.

To prevent slugflow or cavitation in bottom outlets, the air vent must be dimensioned large enough.

¹ J. Speerli and W. H. Hager (2000). Air-water flow in bottom outlets. Canadian Journal of Civil Engineering.

Numerical Simulations of Two-Phase Flow in Bottom Outlets

Matthias Bürgler, Benjamin Hohermuth, David Vetsch, Robert Boes

1 Introduction

Bottom outlets are key safety features of high-head reservoirs. Air vents are installed downstream of the gate (Fig. 1) to limit negative pressures and potential problems with cavitation. So far the air discharge $Q_{a,o}$ is calculated based on empirical equations which scatter over one order of magnitude, thus prohibiting a coherent design of air vents. The use of numerical models for air discharge simulations requires accurate modelling of two-phase flow in bottom outlets, currently posing the main limitation.

2 Background

The review of literature, e.g. [1], and previous studies at the Laboratory of Hydraulics, Hydrology and Glaciology (VAW) indicate that Eulerian one-fluid models overestimate $Q_{a,o}$ in bottom outlets. So far, the overestimation was blamed on the description of two-phase flow with one Reynolds averaged Navier-Stokes equation and volume-weighted fluid properties. The more complex Eulerian two-fluid model solves the velocity field of each phase separately [2]. Thus, it results in a less diffusive momentum transfer at the air-water interface and is expected to improve predictions of $Q_{a,o}$.

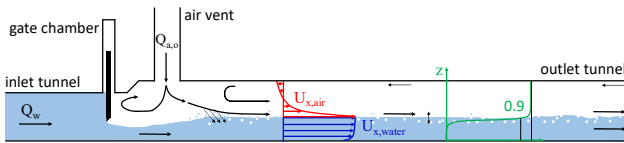


Fig. 1: The high-speed water jet drags a significant amount of air towards the tunnel outlet. Additionally, air is entrained into the water phase resulting an air concentration profile.

However, recent findings in literature suggest that $k-\epsilon$ turbulence models overestimate air-side turbulence near the interface [3], affecting the simulation of air velocities in both one- and two-fluid models. In [3], dampening of air-side turbulence at the air-water interface is proposed. This is achieved by introducing an additional source term in the transport equation of the dissipation rate ϵ_a . In this study, a two-fluid model in combination with an improved turbulence model was implemented in OpenFOAM and was applied for air discharge simulations for the first time.

3 Methodology

Numerical simulations of two-phase flow in a bottom outlet model at VAW were performed using a one- and two-fluid model in OpenFOAM. The one-fluid model is implemented with a realizable $k-\epsilon$ turbulence model. The two-fluid model is combined with an improved standard $k-\epsilon$ model, whereby the air-side turbulence is dampened in proximity of the interface, following the approach of [3]. The idea is to force the dissipation rate ϵ_a at the interface to a "wall-like" value by adding the source term \mathcal{R}_a^{int} in (1) to the r.h.s. of the transport equation of ϵ_a .

$$\mathcal{R}_a^{int} = A C_2 \alpha_a \rho_a \frac{v_a^2 k_a}{\delta^4} \quad (1)$$

The formulation of interface indicator field A given in (2) was developed in this thesis and confines the dampening of turbulence to the region of the air-water interface at 90% air concentration ($\alpha_a \approx 0.9$).

$$A = \max \left[\exp \left(\frac{(0.92 - \alpha_a)^2}{2 \cdot 0.02^2} \right) 0.001, 0 \right] \quad (2)$$

4 Results

The results of the one- and two-fluid model are compared to data from hydraulic model tests.

Velocity profiles & air discharge

The velocity profiles of both models are displayed in Fig. 2. The experimental data serves as rough reference ($\pm 15\%$) for the velocity in the water-air mixture.

The two-fluid model results in smaller velocities than the one-fluid model for $z > 0.1$ m, i.e., in the air-phase. Consequently, the two-fluid model with the improved turbulence model predicts the measured $Q_{a,o}$ with an error of +6%, while the one-fluid model results in an overestimation of +44%.

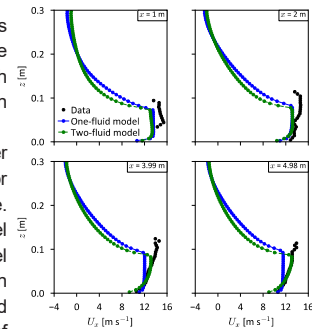


Fig. 2: Comparison of simulated velocities U_x and experimental data.

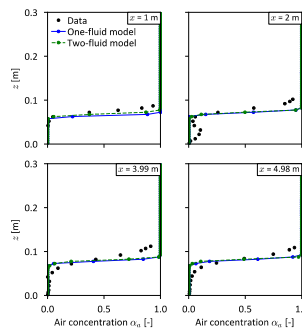


Fig. 3: Comparison of simulated and experimental air concentration profiles

Air concentrations

Both models result in a sharp air-water (Fig. 3) interface because air entrainment is not implemented in the numerical models. For the two-fluid model, predictions of air concentrations were improved by including turbulent dispersion on a sub-grid scale. However, this had a counter-active effect on turbulence dampening and $Q_{a,o}$ predictions.

5 Conclusions

Numerical simulations with one-fluid models and conventional $k-\epsilon$ turbulence models result in a significant overestimation of the air discharge $Q_{a,o}$ by 44%. With a two-fluid model in combination with an improved $k-\epsilon$ turbulence model that dampens turbulence at the air-water interface, the model performance was enhanced and the error in air discharge simulation was reduced to 6%. The measured air concentration profiles were not reproduced accurately by either model. Modelling air entrainment by means of turbulent dispersion in a two-fluid model had counter-active effects on the air discharge simulation and thus requires further research.

6 References

- [1] Shamsai, A., & Soleymanzadeh, R. (2006). Numerical simulation of Air-Water flow in bottom outlet. *International Journal of Civil Engineering*, 4(1), 14.
- [2] Ishii, M., & Hibiki, T. (2011). Drift-flux model. In *Thermo-Fluid Dynamics of Two-Phase Flow* (pp. 361-395). Springer, New York, NY.
- [3] Frederix, E. M. A., Mathur, A., Dovizio, D., Geurts, B. J., & Komen, E. M. J. (2018). Reynolds-averaged modeling of turbulence damping near a large-scale interface in two-phase flow. *Nuclear Engineering and Design*, 333, 122-130.

Les principaux vecteurs d'adaptation d'installations hydroélectriques de montagne en Suisse

Vincent Gaertner, Sabine Chamoun, Pedro Manso

Plateforme en Constructions Hydrauliques (PL-LCH), Ecole Polytechnique Fédérale de Lausanne (EPFL)
Corresponding author: vincent.gaertner@epfl.ch

Introduction

L'adaptation des installations hydroélectriques de montagne en Suisse représente un potentiel non-négligeable d'augmentation de la capacité de production d'énergie renouvelable. L'arrivée à échéance des concessions doit être l'occasion pour les exploitants de prévoir le renouvellement progressif des infrastructures et des équipements existants. En Suisse, ces démarches ont pour objectifs principaux d'augmenter la capacité de stockage pour l'**approvisionnement énergétique hivernal**, de créer de la **flexibilité** (pointe, services réseau) et d'assurer la conformité avec la **LEaux 2013** (Loi fédérale sur la protection des eaux).

Des réflexions peuvent également être menées sur les possibilités de densifier le parc hydroélectrique tout en garantissant une synergie entre les aménagements et une disponibilité accrue des installations (**redundance** systémique). Une vision intégrée du bassin versant est utilisée ici, indépendamment des concessions actuelles, des exploitants actuels ou de la structure d'actionnariat (vision SCCER, soit d'intérêt national).



Figure 1. Le barrage de la retenue de Ze Binnen, Canton du Valais (crédit image: Vincent Gaertner)

Démarche et vecteurs d'adaptation

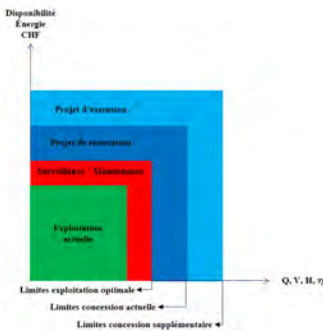


Figure 2. Potentiels d'adaptation d'un aménagement à différentes échelles

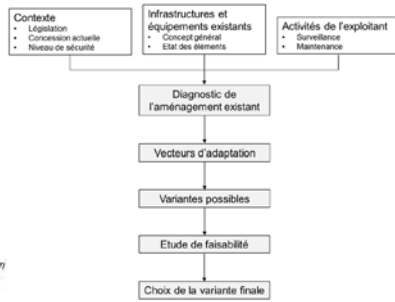


Figure 3. Démarche générale d'analyse pour la génération de variantes d'adaptation d'un aménagement existant

Génération de variantes

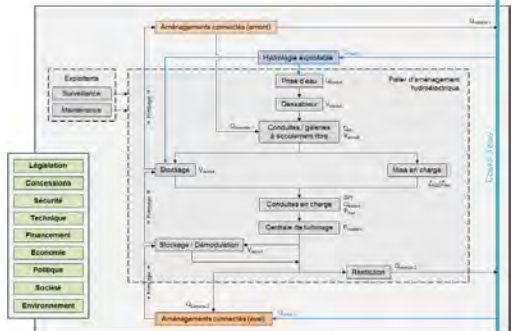


Figure 4. Schéma conceptuel pour la génération de variantes d'adaptation d'aménagements hydroélectriques de montagne

Cas d'étude et variantes d'adaptation

Le travail est effectué sur les aménagements GKW 1 et GKW 2 dans la Vallée des Conches en Valais. Il correspond actuellement à deux palier distincts, le premier reliant la retenue de Kummembord à la centrale de Heiligkreuz et le second reliant plusieurs sources et le bassin de Frid à la centrale de Neubrigg. La retenue de Ze Binnen (exploitée par FMV) pourrait, grâce à sa situation géographique, jouer un rôle central entre les systèmes actuellement déconnectés de cette vallée. Les variantes d'adaptation proposées ci-contre, qui visent à augmenter la flexibilité des aménagements, peuvent être caractérisées par l'échelle des interventions.

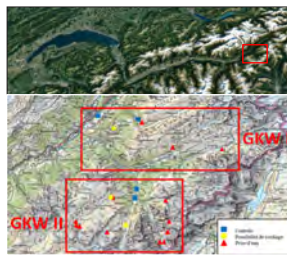


Figure 5. Situation et éléments principaux des aménagements GKW 1 et GKW 2

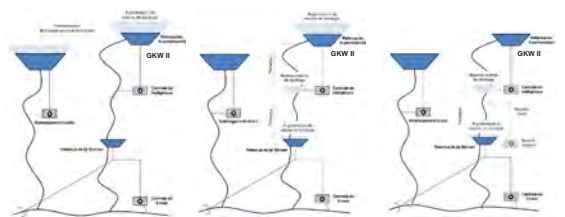


Figure 6. Echelle régionale à internationale. Connexion avec la retenue d'un aménagement voisin.
Figure 7. Echelle locale. Augmentation de volumes de stockage et implantation de systèmes de pompage.
Figure 8. Echelle locale. Création d'un nouveau palier reliant les aménagements GKW 1 et GKW 2.

Discussion – Choix de l'échelle

En considérant que le choix de l'échelle d'analyse dépend principalement de la longueur du système d'adduction, de la topographie relative entre les retenues (canal d'amenée ou besoin de pompage) et des possibilités de stockage, l'estimation du prix de revient doit permettre d'évaluer la faisabilité économique des variantes d'augmentation de production hivernale générées et de déterminer l'échelle d'analyse optimale.

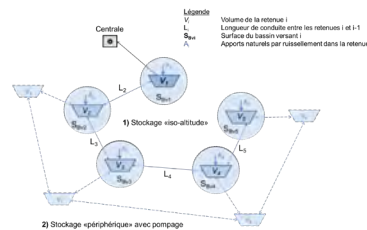


Figure 9. Schéma d'un réseau de stockage d'eau typique en montagne et ses paramètres

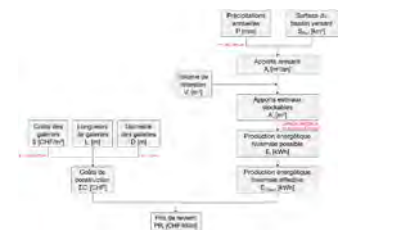


Figure 10. Démarche pour l'estimation des prix de revient en fonction des paramètres du réseau

Perspectives

Le travail en cours envisage l'établissement d'un cadre de réflexion permettant de générer de nouveaux plans d'affaires pour des interventions structurales sur des aménagements existants. L'interconnexion de systèmes ou l'élargissement des réseaux d'adduction pour profiter de nouveaux sites de stockage ("off-stream") seront difficilement justifiés par de simples augmentations d'énergie produite et requièrent des analyses plus fines des modes d'exploitation et des services rendus au réseau.

Valorisation des mesures de mitigation des éclusées en systèmes complexes : quelle échelle spatiale privilégier ?

Mathieu Barnoud, Sabine Chamoun, Pedro Manso

Plateforme en constructions hydrauliques (PL-LCH), Ecole polytechnique fédérale de Lausanne (EPFL), Lausanne.
 contact : mathieu.barnoud@epfl.ch

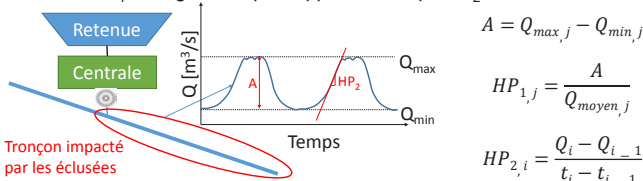


Motivation

Les détenteurs de centrales hydroélectriques existantes ont pour obligation de prendre, jusqu'à fin 2030, des mesures en matière de mitigation des éclusées d'après l'art. 83 de la loi fédérale sur la protection des eaux (LEaux). Cependant, selon la loi sur l'énergie (art. 15), la Société nationale pour l'exploitation du réseau à très haute tension (Swissgrid), en accord avec l'office fédéral de l'environnement (OFEV) et le canton concerné, rembourse les coûts des mesures prises en vertu de la LEaux. Il serait alors intéressant d'essayer de profiter de cette subvention pour proposer des mesures qui répondront aux exigences de la loi tout en améliorant les aménagements concernés.

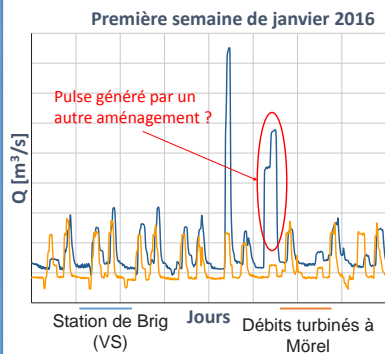
Définition et méthodes d'évaluation des éclusées

Les éclusées désignent des variations quotidiennes du débit d'un cours d'eau, occasionnées par des centrales hydroélectriques fonctionnant par intermittence. En effet, lorsque la demande en courant est élevée, la centrale turbine un débit d'eau important et la restitution de cette eau accroît le débit en aval. Le phénomène inverse se produit lorsque la demande est faible. Meile (2011) propose deux paramètres pour caractériser les éclusées : l'amplitude de la fluctuation journalière du débit relative HP_1 et le gradient par rapport au temps HP_2 .

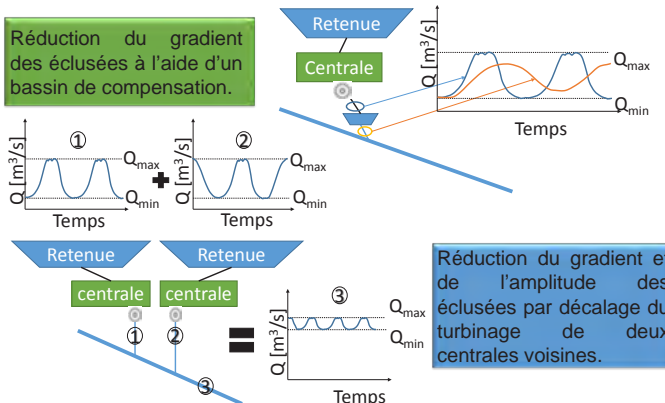


Le calcul de ces indicateurs peut se faire avec les données publiques des stations hydrométriques de l'OFEV ou bien avec les données d'exploitation fournies par les exploitants.

En comparant ces deux types de données, il est possible de déterminer si un aménagement a un impact sur les éclusées telles que mesurées à l'aval par une station publique. Ici par exemple, l'aménagement de Mörel (VS) semble jouer un rôle dans les variations de débit mesurées à Brig. La distance à laquelle les mesures sont faites ne donne pas toujours une estimation directe, due aux multiples apports intermédiaires



Exemples de méthode de mitigation des éclusées



Une autre méthode possible est le changement du programme de turbinage pour réduire l'amplitude et les gradients des éclusées. Cependant cette méthode entraîne souvent des pertes de revenus.

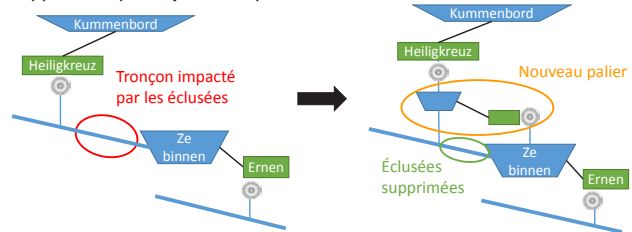
Exemples de valorisation des mesures de mitigation à plusieurs échelles

A l'échelle d'un aménagement :

le bassin de compensation peut être utilisé à des fins de stockage ou de pompage sans modification de la concession.

A l'échelle de plusieurs aménagements :

Cas de la liaison Heiligkreuz-Ze binnen (VS). Les éclusées seraient supprimées par l'ajout d'un palier d'environ 100m de chute.

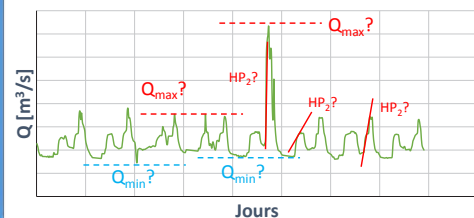


Travailler à l'échelle de plusieurs aménagements ouvre des possibilités intéressantes économiquement et énergétiquement.

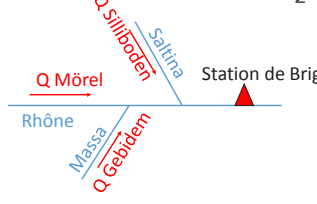
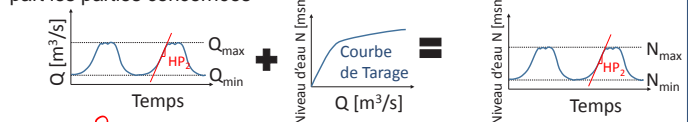
Discussion

Analyser des données réelles pose plusieurs problèmes: quelles valeurs minimales et maximales du débit choisir? Quel gradient considérer ?

Première semaine de janvier 2015 de la station de Brig (VS)



Le gradient est en général exprimé en m³/s/min car les exploitants peuvent fournir facilement les débits turbinés. Cependant, des valeurs en cm/min correspondent aux mesures réelles, permettent de prendre en compte la morphologie du cours d'eau et sont directement perceptibles par les parties concernées



L'aménagement de Mörel n'est pas le seul à l'amont de la station de Brig. Des solutions de mitigation peuvent être trouvées avec les aménagements alimentant Mörel ou avec ceux des autres affluents du Rhône comme Gebidem ou Silliboden.

Perspective

Il ne reste que quelques années aux détenteurs de centrales hydroélectriques existantes pour prendre des mesures de mitigation des éclusées. Au lieu d'une obligation, ces mesures peuvent être perçues comme une opportunité d'amélioration en partie financée, et donc une chance. Pour cela, il sera sans doute nécessaire d'étudier les possibilités au-delà de l'échelle de l'aménagement et d'envisager des projets concernant plusieurs exploitants. A ce stade de réflexion sur le cas d'étude, nous estimons que la création d'un palier d'interconnexion de deux systèmes dans une seule cascade pourrait être éligible pour co-financement par Swissgrid dans le cadres des mesures de mitigation des éclusées.

Références

OFEV, « Assainissement des éclusées – Planification stratégique », 2012
 OFEV, « Eclusées – mesures d'assainissement », 2017
 OFEV, « Assainissement écologique des centrales hydrauliques existantes : Financement des mesures requises », 2016
 Meile, T, Boillat, J-L, Schleiss, A. J, Aquat sci (2011) 73:171-182 DOI 10.1007/s00027-010-0154-7

Task 2.3

Title

Environmental impacts of future operating conditions

Projects (presented on the following pages)

Hydropower and water temperature: modelling the effects of management scenarios on river thermal heterogeneity

[Davide Vanzo](#), [Martin Schmid](#), [Christine Weber](#) and [Michael Döring](#)

Impact assessment of hydropower generation on the acoustics and visual appearance of waterfalls

[Gabriel Zehnder](#)

Coupled effect of pumped-storage operation and climate change on temperature and water quality

[Ulrike Gabriele Kobler](#), [Alfred Wüest](#), [Martin Schmid](#)

How are hydropower thermal alterations affecting trout populations?

[Kunio Takatsu](#), [Martin Schmid](#), [Davide Vanzo](#), [Jakob Brodersen](#)

Künstliches Hochwasser und Geschiebeschüttungen in der Saane

[Severin Stähly](#), [Anthony Maître](#), [Christopher T. Robinson](#), [Anton J. Schleiss](#)

Hydropower and water temperature: modelling the effects of management scenarios on river thermal heterogeneity

Davide Vanzo¹, Martin Schmid¹, Christine Weber¹ and Michael Döring²

1. Eawag, Swiss Federal Institute of Aquatic Science and Technology, Surface Waters - Research and Management, Kastanienbaum, Switzerland
 2. ZHAW, Zurich University of Applied Sciences, Wädenswil, Switzerland

Introduction

- River water temperature is a fundamental physical property of flowing waters
- It is the results of **multiple energy exchanges** involving air, flow, streambed, river morphology and vegetation (Fig. 1, Dugdale et al. 2017)
- **Alterations** of the natural thermal regime at any scale can adversely affect the river biota (e.g. Caissie 2006)
- Artificial **reservoirs** and **hydropower plants** cause thermal alterations on a broad spectrum of temporal scales, and affect longitudinal thermal gradients (e.g. Vanzo et al. 2016)
- The quantification of **lateral** thermal gradient alterations is still a challenge

Motivation

Swiss Energy Strategy 2050: changes in hydropower production patterns

- increase in storage capacity
- alternative production scheme (e.g. pump-storage)
- more frequent fluctuations of water flow (hydropeaking)

Goals

- develop a two-dimensional numerical tool for river thermo-hydrodynamics simulation
- model and quantify the interaction between hydro-thermal alterations and local river morphology
- better understand how thermal heterogeneity changes over time in hydropeaking rivers

Study sites

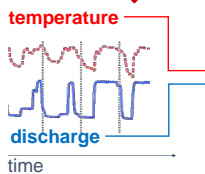


3 reaches with morphological variability and subjected to hydropower production

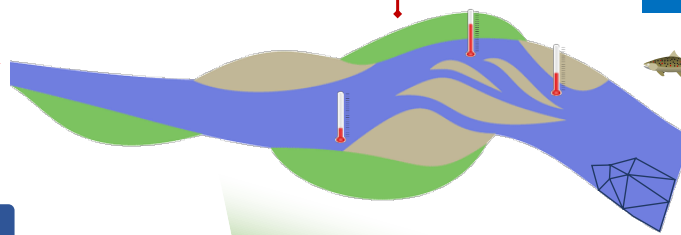
- Moesa River at Lostallo
- Rhein River (Hinterrhein) at Rhäzüns
- Rhein River (Vorderrhein) at Ilanz

Research questions

How is river **thermal regime** affected by **hydropower production**?




Does river **morphology** play a relevant role in the **thermal heterogeneity** of hydropeaking rivers?




How does river temperature affect **early life stages** of fish?

Poster: *How are hydropower thermal alterations affecting trout populations?*
 Kunio Takatsu et al.

Methods

 local continuous measurements of **surface** and **sub-surface** water temperature
 → to evaluate the contribution of **hyporheic fluxes** to thermal heterogeneity

 **remote sensing (UAV)** of reach-scale surface water temperature

→ to understand thermal heterogeneity at **different flow stages** and **seasons**

 **development of a 2D depth-averaged numerical model**

→ to simulate **thermo-hydrodynamics** for current and future production **scenarios**

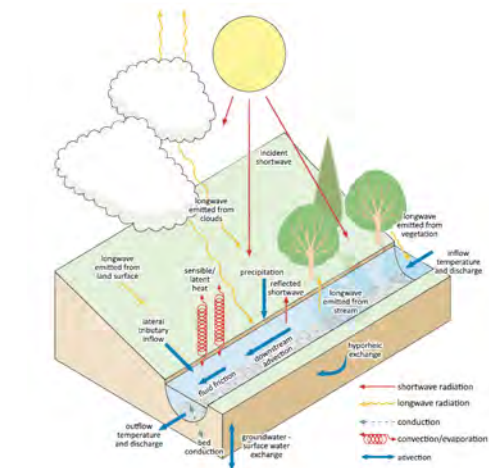


Fig. 1 - Factors influencing the thermal regime in a river reach (Dugdale et al. 2017).

References

- Caissie, D. (2006) 'The thermal regime of rivers: A review', *Freshwater Biology*, 51(8)
 Dugdale, S. et al. (2017) 'River temperature modelling: A review of process-based approaches and future directions', *Earth-Science Reviews*
 Vanzo, D. et al. (2016) 'Characterization of sub-daily thermal regime in alpine rivers: Quantification of alterations induced by hydropeaking', *Hydrological Processes*, 30(7)

Contacts:
 Dr. Davide Vanzo
davide.vanzo@eawag.ch

Impact assessment of hydropower generation on the acoustics and visual appearance of waterfalls

Gabriel Zehnder, VAW (Laboratory of Hydraulics, Hydrology and Glaciology), ETH Zürich, Switzerland

Objectives

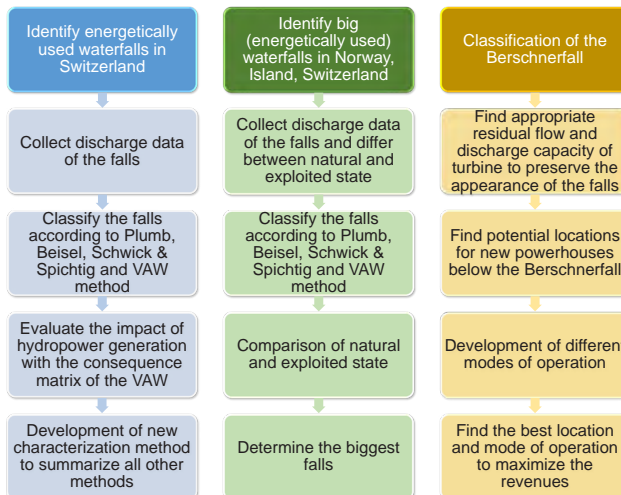
Waterfalls are some of the most impressive nature spectacles on earth. People are and have been fascinated by their appearance regardless of height or shape. Numerous historical narratives and urban histories mention waterfalls and the question of which is the highest and biggest waterfall is still ongoing. However, due to steadily rising energy demand waterfalls are becoming more and more affected by anthropogenic interventions and their impressive appearances are in danger. These facts lead to the first two key questions:

- 1) How big are the impacts of hydropower generation on waterfalls in Switzerland?
- 2) Are the Rhine falls really the biggest falls in Europe?

In the second part of this project a case study on the energetic use of the Berschnerfall (canton of St. Gallen, CH) is performed, with the help of the power plants Walenstadt, to answer the third key question:

- 3) What is the most economic exploitation alternative considering the conservation of the appearance of the Berschnerfall.

Handbook for assessing the key questions



Energetically used waterfalls

22 energetically used waterfalls in Switzerland are identified (see Fig. 1). For these, only little discharge data is available. Therefore, data comparison between measured data from hydrological yearbooks and modelled data from the Federal Office for the Environment FOEN [1] is conducted for 6 reference sites with existing hydrological yearbook data (see Fig. 2). By applying an equation developed by HZP [2], the modelled data can be recalculated, achieving a sufficient accuracy with a deviation of less than 20% (red line in Fig. 2) from the measured data.

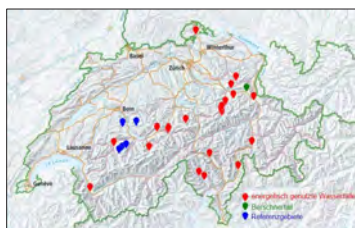


Fig. 1: Map of energetically used waterfalls in Switzerland (red), of the reference sites (blue) and the Berschnerfall (green) [1].

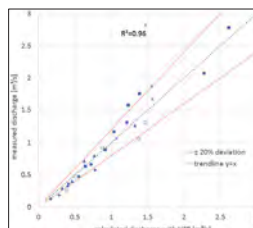


Fig. 2: Data comparison of measured and calculated discharge data.

Based on the recalculated discharge data, the classification and VAW consequence matrix (Fig. 3) is then calculated. The data of the European waterfalls can be found on the federal sites of the corresponding countries [1],[3],[4].

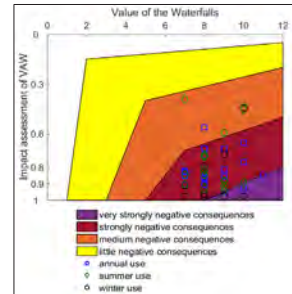


Fig. 3: VAW consequence matrix of the Swiss falls based on annual and seasonal discharge data.

	Rhine falls (CH)	Fiskumfoss (NO)	Detifoss (IS)	Sarpsfossen (NO)
Height [m]	23	34.5	44	23
Width [m]	150	186	100	80
Q_m [m ³ /s] natural	340	302.4	193	662
Q_m [m ³ /s] used	310	185.6	0	308.7
Q_{max} [m ³ /s]	1250	1482	508	3000
Plumb	61.2	66.2	103.2	114.6
Beisel natural	8	7	6	7
Beisel exploited	8	7	0	6
Schwick & Spichtig	10	10	11	10
VAW consequence	0.22	0.43	0	0.67

Table 1: Overview of the biggest waterfalls in Europe.

Case study - Berschnerfall

Two new locations below the Berschnerfall are proposed (Fig. 4). For every location three different residual flows are compared within four different modes of operations (daily use, only night use, day/night different use and seasonal different use). The lowest residual flow is defined by law as 53.1/l/s. The remaining two options are chosen based on a minimized impact on the appearance of the fall: 120/l/s ($= 0.36 \cdot Q_{182d}$) and 162/l/s ($= 0.5 \cdot Q_{182d}$).

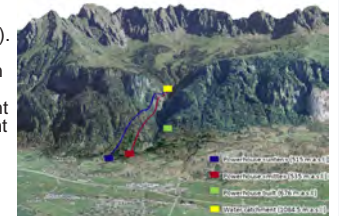


Fig. 4: New proposed locations of the powerhouses [1].

	Powerhouse built	Powerhouse «unten»	Powerhouse «mitte»
Drainage tunnel length	1315 m	1751 m	1624 m
Net drop height	407.6 m	569.5 m	549.5 m
Discharge capacity	1000 l/s ($= Q_{00d}$)	1000 l/s ($= Q_{00d}$)	1000 l/s ($= Q_{00d}$)
Residual flow of best mode of operation	53.1 l/s	winter 53.1 l/s, summer 162 l/s	winter 53.1 l/s, summer 162 l/s
Annual electricity production	11.20 GWh	14.35 GWh	13.45 GWh
Construction costs	21.5 million CHF	24.7 million CHF	23.8 million CHF
Production costs (internal rate 3%)	5.10 Rp/kWh	4.70 Rp/kWh	4.74 Rp/kWh
Profit after concession (80 years) (with electricity price of 5.81 Rp/kWh and internal rate of 3%)	15.3 million CHF	19.8 million CHF	18.1 million CHF

Table 2: Overview of the three powerhouse options for the bestcase scenario.

Conclusions and Perspectives

- 1) Waterfalls in Switzerland experience mostly strongly to very strongly negative consequences from anthropogenic interventions linked to hydropower generation.
- 2) The selection of the biggest waterfall depends on the perspective of the comparison:
 - Plumb = mainly dependent on geometric parameters → Sarpsfossen is the biggest
 - Beisel = focuses on water volume in the falls → Rhine falls are the biggest
 - Water discharge → Sarpsfossen is the biggest in natural conditions, whereas in exploited conditions, the Sarpsfossen and Rhine falls are leading
- 3) The economic and ecological best case is the case with seasonal different residual flow (53.1 l/s and 162 l/s) and with the powerhouse located in the middle.

References

[1] FOEN (2012). Geoinformationplatform of Switzerland. <https://map.geo.admin.ch>. Visited: 22.05.2018.
 [2] Niedermayr, A. (2012). Ermittlung von Abflussdauerlinien in Einzugsgebieten ohne Abflussmessungen. Hunziker, Zarn & Partner AG, Aarau.
 [3] NVE (2018). NVE Atlas. Norwegian Water Resources and Energy Directorate. <https://atlas.nve.no>. Visited: 22.05.2018
 [4] NVE (2018). Xgeo.no – expert tool for notification and emergency. Norwegian Water Resources and Energy Directorate. <http://www.xgeo.no/>. Visited: 22.05.2018

Coupled effect of pumped-storage operation and climate change on temperature and water quality

RESEARCH QUESTIONS

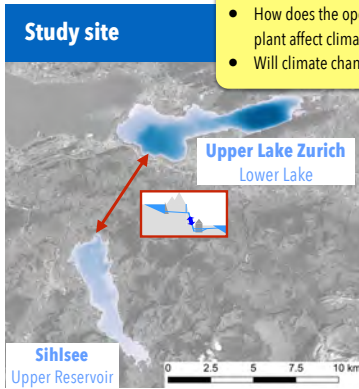
- How does the operation of a pumped-storage (PS) hydropower plant affect climate change impacts on lakes and reservoirs?
- Will climate change impacts be reduced by PS operation?

Ulrike Gabriele Kobler^{1,*}, Alfred Wüest^{1,2}, Martin Schmid¹

¹ Eawag, Swiss Federal Institute of Aquatic Science and Technology, Surface Waters - Research and Management, Kastanienbaum

² EPFL, Physics of Aquatic Systems Laboratory - Margaretha Kamprad Chair

* ulrike.kobler@eawag.ch



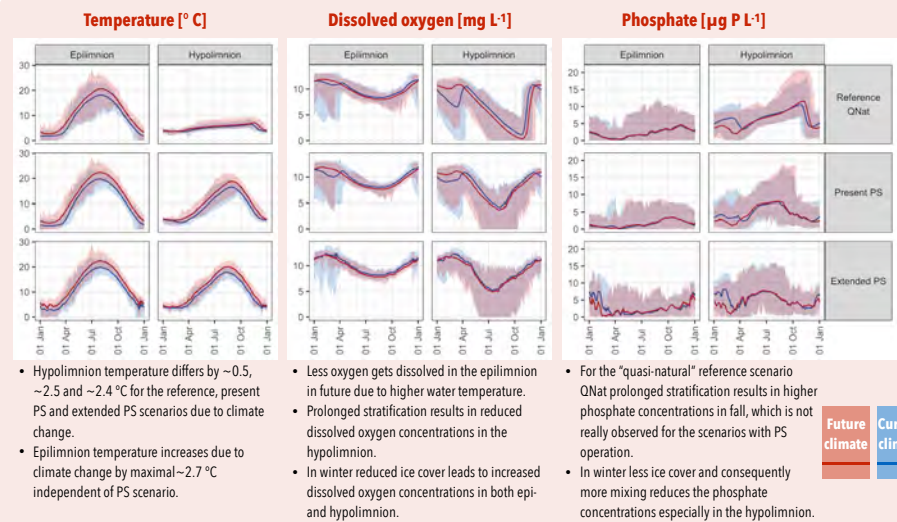
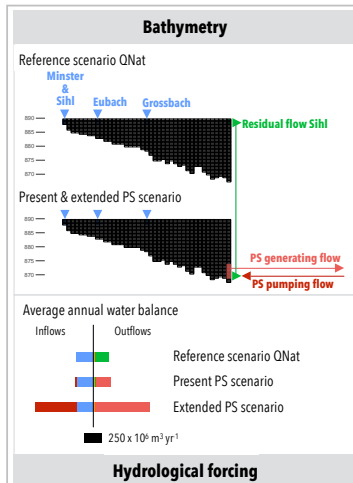
Introduction

Effects of climate change on lakes and reservoirs include increasing surface water temperature, prolonged summer stratification [1, 2], decreasing duration and extent of ice cover [3, 4] as well as decreasing oxygen and increasing nutrient concentrations [5]. Additionally, climate reduction goals enhance the implementation of "new renewable" electricity production, which relies on appropriate storage capacity, that can be provided by PS hydropower plants. However, these PS operations additionally affect physical, biogeochemical and ecological properties of the connected water bodies [6].

As to our knowledge there are no studies on these coupled effects, we combine three different PS operation scenarios with two different climate scenarios to assess the impacts on temperature, stratification and dissolved oxygen at the Etzelwerk PS hydropower plant, which connects Sihlsee and Upper Lake Zurich. The climate scenarios include meteorological and inflow temperature forcing and consist of an ensemble of ten scenarios for both the current (1998-2012) and the future conditions (2078-2092). All climate scenarios were generated with a vector autoregressive weather generator [7]. The climate signal for future conditions was taken from CH2011 [8] for the A2 scenario in northeastern Switzerland in 2085.

Results are aggregated to mean and minima as well as maxima from all realisations of the weather generator and all realised 15 years.

Materials and Methods

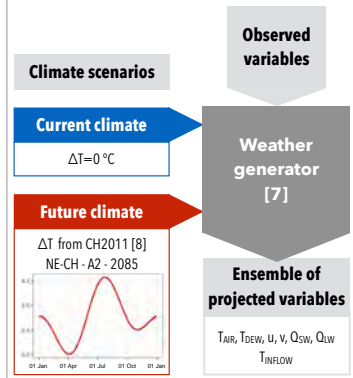


PS scenario dependent forcing [6]

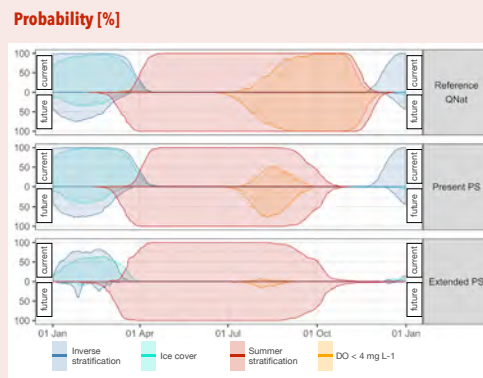
PS scenario independent forcing [9]

MODEL [10]

RESULTS



References



- Inverse stratification is reduced and ice cover could even diminish due to the combination of extended PS operation and climate change.
- Although the duration of summer stratification remains unchanged for the reference scenario QNat under current climate conditions and the extended PS scenario under future climate conditions, the timing changes, which could accordingly affect lake ecology.

CONCLUSIONS

- Temperature of the hypolimnion is strongly increased due to the pumped-storage operations. This effect is further enhanced by climate change.
- In the natural state, hypolimnetic temperatures are only slightly affected by climate change, as long as a lake remains cold enough to mix completely in winter.
- The warming of the epilimnion by climate change increases the stability and prolongs the duration of stratification.
- As a consequence of longer stratification, dissolved oxygen concentrations are lower and phosphate concentrations higher in fall. This effect is stronger in the natural state than in the PS scenarios.
- In winter, the shorter ice cover duration causes increased dissolved oxygen and decreased phosphate concentrations.
- Since concessions for hydropower are often issued for durations of 50 to 80 years, the environmental impact assessment should also consider possible effects from expected climate change.

How are hydropower thermal alterations affecting trout populations?



SWISS COMPETENCE CENTER for ENERGY RESEARCH
SUPPLY of ELECTRICITY

Kunio Takatsu, Martin Schmid, Davide Vanzo, Jakob Brodersen (Eawag)

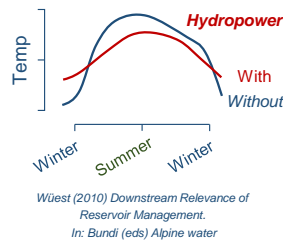
Supported by:
 Schweizerische Eidgenossenschaft
 Confédération suisse
 Confederazione Svizzera
 Confederaziun svizra
 Swiss Confederation
 Innosuisse – Swiss Innovation Agency

Background

Hydropower induced temperature changes

- Reduction in summer temp.
- Increase in winter temp.

The effects can differ depending on hydropower location and local channel heterogeneity

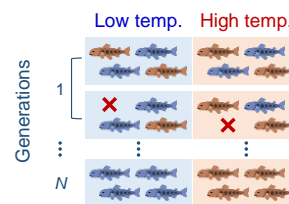


Energy strategy 2050 of Swiss government: Increase hydropower production

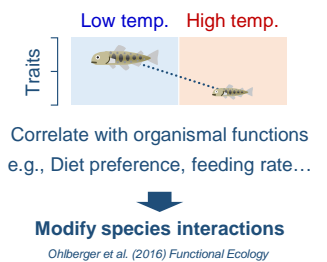
Importance of temperature in evolution & ecology

Temperature can affect...

Selective pressure



Plasticity



Questions

To predict hydropower effects on aquatic organisms, we will address following questions...

How are hydropower effects on temperature affected by location & local channel heterogeneity?

How does temperature affect organismal traits, and consequently, modify species interactions?

Hydropower and water temperature: modelling the effects of management scenario on river thermal heterogeneity
Vanzo et al., (2018)

Develop prediction model

Question we will address

Research plan

Study organism: Brown trout

- Ecologically & commercially important species

Huryň (1998) Oecologia



- Wide altitudinal distribution range: 300 – 2000 m
= Each local trout population may have experienced different temperature regime through many generations

What we will examine

1. How temperature affects

a) Embryonic development

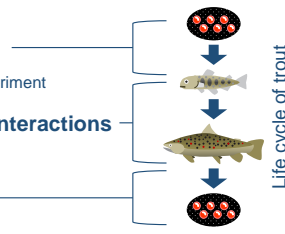
- Laboratory common garden experiment

b) Larval growth & trophic interactions

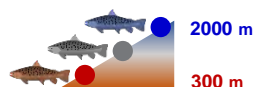
- Field transplant experiment

c) Reproduction

- Field observation



2. How temperature effects differ among altitudinal populations

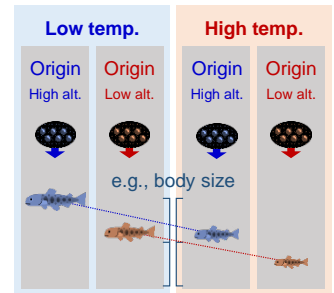


Experiments

< 1-a & 2 >

Laboratory common garden experiment

- Temperature treatments: High & Low
- Altitudinal populations: 18 populations (300-2000 m)
- Focal traits: Size, yolk volume, timing... at hatching & emergence

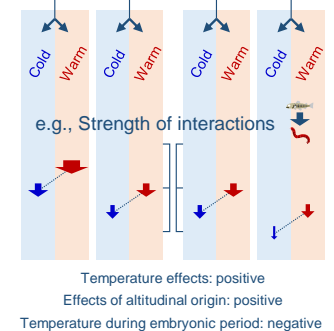


By using hatchlings of common garden experiment...

< 1-b & 2 >

Field transplant experiment

- Experimental streams: Cold & warm streams
- Focal traits: Size, morphology, mortality...
- Focal interactions: Trout - their prey interactions



Künstliches Hochwasser und Geschiebeschüttungen in der Saane

Severin STÄHLY*, Anthony MAÎTRE, Christopher T. ROBINSON, Anton J. SCHLEISS
severin.staehly@epfl.ch

Hintergrund und Motivation

Im Rahmen der Energiestrategie 2050 soll die Wasserkraft in der Schweiz ausgebaut werden. Erneuerungen in Gewässerschutzgesetz und -verordnung (GSchG, GSchV) verpflichten Kraftwerksbetreiber Massnahmen gegen Probleme betreffend Schwall & Sunk, Restwasser, Fischwanderung und Geschiebedurchgängigkeit zu ergreifen. Zudem sollen verbaute Fließgewässer so weit wie möglich revitalisiert werden.

In Zusammenarbeit mit dem Energieversorger Groupe e und des Kanton Fribourgs, wurde im September 2016 eine Reaktivierung der Auen mittels eines künstlichen Hochwassers und Geschiebeschüttungen in der Saane unterhalb der Staumauer Rossens getestet.

Übersicht

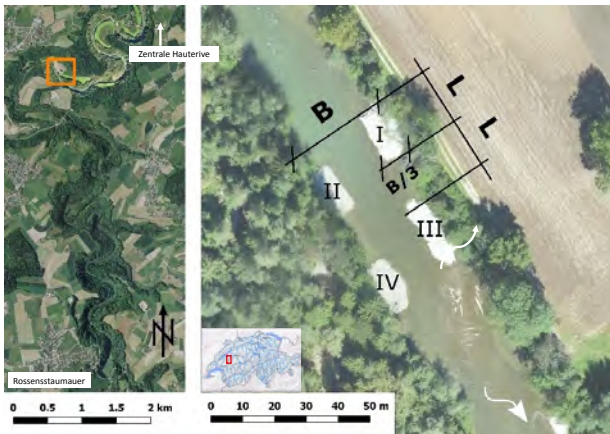


Abb. 1: (LINKS) Saane zwischen der Staumauer Rossens und der Kraftwerkszentrale Hautrive. Der Projektperimeter der Schüttungen ist gelb markiert. (RECHTS) Die Schüttungen erfolgten in vier Depots, welche als mäandrierende Bänke angeordnet wurden. Diese Konfiguration wurde vorgängig in Laborexperimenten optimiert. Mittels gewählter Konstellation wird das Material bereits bei geringeren Abflüssen erodiert (Abflusskonzentration in der Flussmitte). Das eingebrachte Geschiebe soll zur strukturellen Habitatsvielfalt beitragen.

Methode

- 250 m³ Geschiebe pro Depot (total 1000 m³)
- Schüttmaterial durch Aushub aus angrenzendem Auenwald (unsortiert)
- $d_m = 57 \text{ mm}$, $d_{90} = 113 \text{ mm}$
- 489 RFID PIT tags (passive Sensoren, gleichmässig in d_m und d_{90} verteilt)
- Tags in drei verschiedenen Schichten gleichmässig in Depots verteilt
- Nach Hochwasser, RFID PIT tags wieder finden mit Antenne
- Anschliessend: Vergleich mit Laborexperimenten
- Abflussganglinie mit Maximalem Abfluss 195 m³/s (Wiederkehrperiode: 1 Jahr)

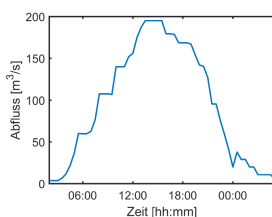


Abb. 2: Abflussganglinie des künstlichen Hochwassers. Der Spitzenabfluss von 195 m³/s entspricht einem jährlichen

Geschiebetransport & Erosion

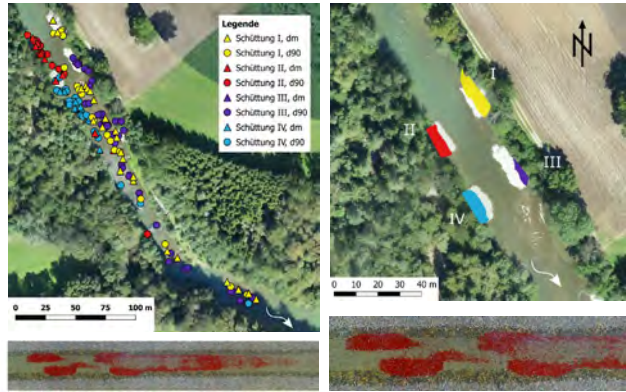


Abb. 3: Verteilung der RFID Pit tags nach dem Hochwasser. Abb. 4: Erosion der Depots nach dem Hochwasser.

Als Vergleich der Laborversuch nach 60 min. Mehr Informationen zu den Laborversuchen in der Doktorarbeit von Elena Battisacco (LCH-EPFL Communication 67)

Analysen

- 277 RFID PIT tags wiedergefunden (166 transportiert, 111 auf den Depots)
- Resultate bestätigen Laborversuche
- Kein Transport quer zur Fliessrichtung
- Depot III praktisch vollständig erodiert
- Linksufrige Depots stärker erodiert und weiter transportiert

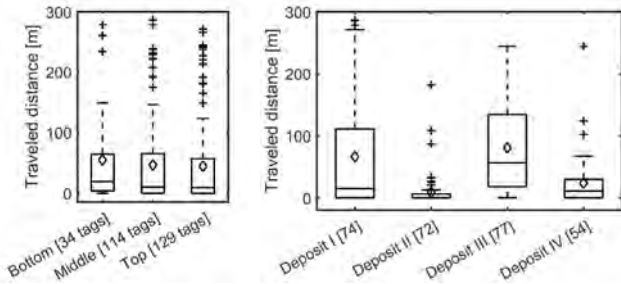


Abb. 5: Distanzen, welche die markierten Steine zurückgelegt haben nach Position in den Depots (links): unten (bottom), mitte (middle) und Oberfläche (top) und nach Herkunftsdepot (rechts).

Erkenntnisse

Trotz unterschiedlichen Randbedingungen, bestätigen die **Resultate des Feldversuches die Laboruntersuchungen**. Das Hochwasser war nicht stark genug, um alle Schüttungen zu erodieren. Die Depots am linken Ufer wurden stärker erodiert und das Material weiter transportiert, was auf die Anordnung der Depots unterhalb einer starken Rechtskurve im Fluss zurückzuführen ist.

Danksagung

Dieses Forschungsprojekt wird im Rahmen des Nationalen Forschungsprogramms „Energiewende“ (NFP 70) des Schweizerischen Nationalfonds (SNF) durchgeführt. Weitere Informationen zum Nationalen Forschungsprogramm sind auf www.nfp70.ch zu finden. Die Laborversuche wurden von Dr. Elena Battisacco durchgeführt. Dr. Diego Tonolla und Dr. Michael Döring sowie an die kantonalen Behörden Fribourg und den Kraftwerksbetreiber Groupe e wird für ihre Zusammenarbeit im Zusammenhang mit dem künstlichen Hochwasser gedankt.

Task 2.4

Title

Integrated simulation of systems operation

Projects (presented on the following pages)

Improved alpine hydropower operation by forecast based optimization

[Daniela Anghileri](#), [Samuel Monhart](#), [Andrea Castelletti](#), [Massimiliano Zappa](#), [Paolo Burlando](#)

Multiobjective optimal operation of the Maggia hydropower systems: tradeoffs between environment conservation and hydropower

[Daniela Anghileri](#), [Andrea Castelletti](#), [Enrico Weber](#), [Nadav Peleg](#), [Paolo Burlando](#)

Improved alpine hydropower operation by forecast based optimization

D. Anghileri¹, S. Monhart², Z. Chuanyun¹, K. Bogner², A. Castelletti¹, P. Burlando¹, and M. Zappa²

1) Institute of Environmental Engineering ETH Zurich; 2) Mountain Hydrology and Mass Movements, Swiss Federal Research Institute WSL

Motivation and objectives

Accurate and reliable forecasts are key to anticipate hydro-meteorological events which may inform hydropower operation over different time horizons from hourly operation, to weekly management, to monthly production planning.

The objectives of this work are:

- to analyze the quality of a set of streamflow forecasts on a retrospective dataset;
- to improve the real-time operations of hydropower system when informed by streamflow forecasts;
- to assess the advantage of pre-processing meteorological forcings when producing streamflow forecasts both in terms of forecasts reliability and improved hydropower performance.

Method and tools

We develop a real-time hydropower operation system (Figure 1), composed of:

Meteorological forecasting model

- ECMWF Integrated Forecasting System extended-range forecasts (CY40r1)
- Temporal resolution: daily
- Spatial resolution: 50 km x 50 km
- 32 days lead time and weekly frequency

Bias correction (pre-processing)

- Gridded observed data of precipitation, temperature
- Quantile Mapping approach: daily and lead-time dependent correction [1]

Hydrological forecasting model

- Hydrological model PREVAH Temporal resolution: daily
- Spatial resolution: 500 m x 500 m

Hydropower system optimization and simulation

- Model Predictive Control (MPC) scheme (rolling horizon: 32 days)
- Objective function: revenue computed using mean historical electricity wholesale price [2]
- Median of streamflow forecast ensemble members
- Temporal resolution: daily

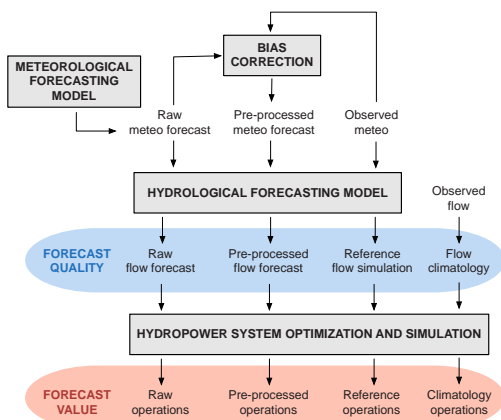


Figure 1: Forecast-based adaptive management scheme. The experimental setting consists of two benchmark (reference and climatology) which are compared with raw and pre-processed forecasts to determine forecast quality and value (see [3] for more details).

Experimental setting

The experimental setting consists of two benchmarks, i.e., climatology and perfect forecasts, which are used to assess the improvement of the forecasts we analyze, i.e., raw forecast and pre-processed forecast (Figure 1).

The **quality of the forecasts** is assessed in terms of Continuous Ranked Probability Score (CRPS) to assess the forecast reliability and sharpness; Mean Error (ME) to assess the forecast systematic bias.

The **value of the forecasts** is assessed in terms of avoided spill and gained revenue.

Study site

The forecast-based adaptive management scheme is applied to the Verzasca hydropower system (Figure 2):



- rain and snow dominated
- reservoir storage: 85-10⁶ m³
- installed power: 105 MW

Figure 2: Study area in white and Verzasca hydropower system.

Results

Forecast quality

- Pre-processing allows for downscaling and systematic bias correction (Figure 3a).
- The pre-processing effect varies with lead time and season: spring and autumn shows the largest improvement, in contrast to summer and winter (Figure 3b, c).

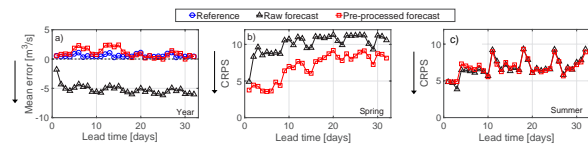


Figure 4: a) Mean annual error of streamflow reference, raw, and pre-processed forecasts, b-c) CRPS computed over spring and summer.

Forecast value

- Increase of 3% when using raw forecasts with respect to climatology (Fig. 5a).
- Increase of 12.5% when considering pre-processed forecasts with respect to climatology (Fig. 5a).
- The improvement is mostly given by the reduction of spill events which are a consequence of the systematic underestimation of reservoir inflows (Fig. 5b).

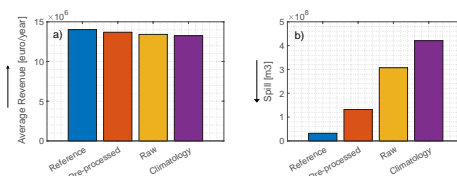


Figure 5: a) Mean annual revenue and b) total spilled volume of the raw and pre-processed forecasts and the two benchmarks.

References

- [1] Monhart et al., submitted to JGR Atmospheres
- [2] EPEX SPOT (<http://www.epexspot.com/en/>)
- [3] Anghileri et al. (2016), WRR, 52, doi:10.1002/2015WR017864.

Multiobjective optimal operation of the Maggia hydropower systems: tradeoffs between environment conservation and hydropower

D. Anghileri¹, E. Weber¹, N. Peleg¹, A. Castelletti¹, and P. Burlando¹.

^{1) Institute of Environmental Engineering ETH Zurich;}

Motivation and objectives

Volatile electricity prices and hydrological conditions might call for more flexible hydropower operations, which may expose downstream riverine ecosystems to increased threats.

The objectives of this work are:

- to analyze the well known conflict between hydropower generation and environment conservation;
- to balance the profitability of hydropower companies and environment conservation.

Research questions

- How much do environmental flows limit hydropower operating interests?
- How much will more flexible operations of hydropower reservoirs harm the environment?
- Do the trade-offs between hydropower interests and environment conservation change with increased energy price and water availability uncertainty?

Method and tools

To analyze the tradeoffs between hydropower interests and environment conservation, we use:

i) an hydrological model (Topkapi-ETH) [1]

- to simulate water availability to hydropower facilities;
- to simulate the effects of different hydropower operations on the downstream riverine ecosystem;

ii) a multi-objective optimization technique (evolutionary multi-objective direct policy search) [2]

- to simulate the effects of different environmental conditions on hydropower performance;
- to explore different trade-off operations that aim at balancing hydropower performance and ecosystem conditions.

[1] Fatichi et al. (2015), *Joh* 525, 362–382.

[2] Giuliani et al. (2016), *ERL* 11, 035009

Study site

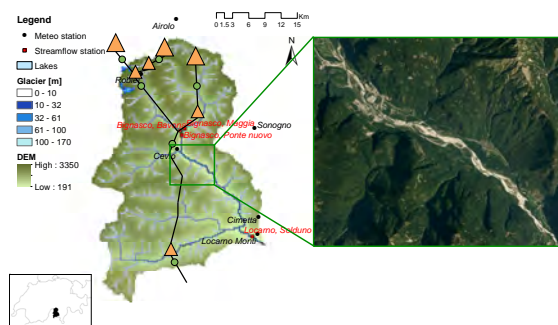


Figure 1: Left: Map of the Maggia river catchment and schematic of the hydropower system (reservoirs and plants are represented with triangles and circles respectively). The system is composed of 7 reservoirs with a total capacity of 600 MW, which produce annually 1265 GWh. Right: satellite image of the natural alluvial river which is regarded a floodplain of national interest.

Preliminary results

Hydrological modeling

We consider two different setups for simulating the pristine ecosystem during the pre-dam condition and the current situation during the post-dam condition.

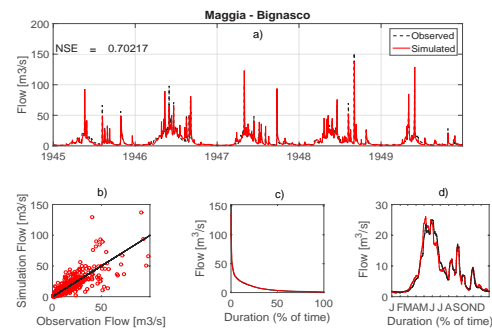


Figure 2: Performances of the Topkapi-ETH hydrological model during the pre-dam condition measured in terms of: a) time series, b) scatter plot, c) duration curve, and d) annual daily mean comparison between observed and simulated flow at Maggia-Bignasco.

Hydropower optimization model

We use multi-objective optimization to balance the following 3 interests:

- maximization of the **net electricity production** (production – pumping);
- maximization of the **net revenue** (production income – pumping cost);
- maximization of the **ecosystem quality** (we consider the pre-dam simulation as the reference target for the optimization).

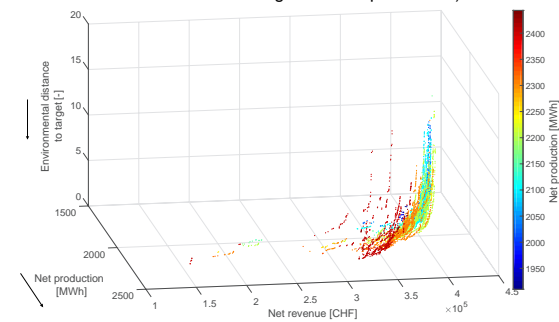


Figure 3: Performances of alternative hydropower systems operations designed using evolutionary multi-objective direct policy search. The different points represent Pareto optimal trade-offs between the above mentioned 3 objective functions.

Outlook

- Compare the optimized trade-offs with different strategies aiming at environment conservation, such as fixed and proportional environmental flows.
- Analyze the evolution of the Pareto optimal trade-offs under climate change and electricity price projections.
- Use a more sophisticated model of the alluvial floodplain to simulate the interaction between surface water and groundwater (in connection to the SNF NFP70 HydroEnv Project).

Work Package 3: Innovation Agenda

WP3 provides technical and computational innovation for hydropower and geo-energies.

Technical Highlights 2018

Refurbishment of large hydropower plants

The objective of the RENOVHydro project is to assist the decision making for hydropower projects and refurbishments, by automating the analysis of civil and electro-mechanical engineering scenarios and their performance in terms of energy generation, installed capacity and ancillary services to the grid. First case studies have been investigated.

Improved residual lifetime assessment of pipelines and penstocks

A new hydraulic test rig inducing water hammers and pressure fluctuations has been designed. Its construction started in December 2017, first tests will be done in September 2018, and in 2019 an eddy current sensor will be added to monitor crack growth. This setup will help to predict the speed of crack growth and to convince plant manager to apply this monitoring solution.

Small hydropower plants

At the beginning of 2018, the Pilot and Demo project Smallflex project was launched. It aims at demonstrating the capacity of small hydropower plants to provide clean, sustainable and renewable energy while delivering ancillary services (see also WP5). In addition, two smaller hydropower plants in Valais (Icogne, Pissevache) consider new plant management systems in the framework of the direct-marketing remunerations to increase profit / minimize loss expected due to the modifications of the feed-in tariff.

Development of new turbines for existing infrastructure

The first product of the new axial turbine DUO TURBO for drinking water networks was delivered in July 2018. The turbine features a robust mechanical design and a global efficiency of 60%. Two pilot sites will be equipped for fatigue investigations before wider deployment of the technology. A first prototype of a kinetic turbine that harvests energy from rivers or artificial channels was successfully tested for hundreds of operating hours in Lavey. The possibility to set up a farm of such turbines on the same site is currently being investigated. Another potential site is also under consideration on the Rhone river.

Improvements in borehole drilling

The work on borehole stability continued with further testing and improvement of the workflow to optimise drilling directions. A statistical approach has been integrated to better assess the reliability of prediction and risk associated with drilling in a given direction. The decision has to be taken rapidly in order to minimize cost associated with rig downtime. A triaxial system was successfully installed and proven under high temperature and pressure. Therefore, it is now possible to test the rock samples under real deep borehole conditions and obtain reliable constitutive rock properties.

Computational Highlights 2018

Prediction of silt-erosion in Pelton turbines

Silt-erosion in Pelton turbines is a crucial question for most of the high head hydropower plants in the Swiss alps. A novel multiscale model has been developed to handle the wide range of length and time scales involved in the sediment erosion phenomena. Additional physical models such as surface tension, turbulence and cavitation have been developed and implemented. Moreover, all the SPHEROS software data-structure and algorithms has been revised to fit with the GPU architecture. As a consequence, the project has been qualified scientifically and technically by Swiss National Supercomputing Centre in order to use the Piz Daint machine, the 3-rd biggest computer in the world.

Advanced anisotropic turbulence models

Advanced anisotropic turbulence models have been developed and implemented to capture flow instabilities at deep part-load in hydraulic turbines. These will allow to better understand the flow behaviour at these operating conditions and, in a later step, support the design process of new turbines with less severe instabilities.

Fluid Structure Interaction

A new simulation method for fluid-structure interaction has been developed, which is based on overlapping domain decomposition. Arbitrary simulation codes can be coupled in parallel using the new mesh coupling tool MoonoLith. Fluid-Structure interaction in turbines or flow through fractured media in reservoir stimulation can now be simulated much easier, especially since existing codes can be re-used, thereby extending the currently available software landscape in geo- and hydro power.

Contact between rough surfaces

A new non-smooth monotone multigrid method in combination with a variational surface transfer allows to efficiently simulate the contact between rough surfaces, e.g. rocks in fracture networks. Numerical studies based on real rock-geometries have served as a first step in the validation and show good simulation/data match.

Fracture networks and phase field models

The simulation of fracture propagation is challenging, as the mesh has to follow the newly developing fractures. We use a so called damage-field for describing the state of the material: 0 for the undamaged state, and 1 for completely broken. Numbers in between stand for increasing damage. The evolution of the damage field follows a phase-field equation, which allows to predict the growth of fracture networks in an elegant way. The computational price are large non-linear coupled systems. A new non-linear multigrid method has been developed, which allow for fast and efficient simulations of fracture growth.

Adaptive mesh refinement for fracture networks in porous rocks

At the mesoscale, i.e. in the order of centimetres, fractures in porous rocks can be modelled as heterogeneities in an embedding background. The creation of computational meshes which explicitly resolve complicated networks of heterogeneities is particularly time-consuming and requires a lot of human interaction. In order to make this process automatic, a novel method was developed based on adaptive mesh refinement. After having defined analytically a set of embedded heterogeneities, the key concept of the method is to start from an initially uniform mesh and then to hierarchically refine elements which have non-empty overlaps with the heterogeneities. This results in a sequence of non-uniform meshes with a large number of elements at the interfaces between the embedding background and the heterogeneities. This strategy allows to represent any distribution of heterogeneities with arbitrary accuracy and allowed for the realization of first stochastic simulations of fractures networks.

Task 3.1

Title

Innovative technologies

Projects (presented on the following pages)

Two-phase flow phenomena in turbines and pump-turbines operating in synchronous condenser mode
Elena Vagnoni, Loïc Andolfatto, Renaud Guillaume, Pierre Leroy, François Avellan

DuoTurbo: First Product and Pilote Test Sites

Daniel Biner, Laurent Rapillard, Loïc Andolfatto, Vlad Hasmatuchi, Shadya Martignoni, François Avellan, Cécile Münch-Alligné

GPU-SPHEROS: A GPU-Accelerated 3-D Finite Volume Particle Method solver

Siamak Alimirzazadeh, Ebrahim Jahanbakhsh, Audrey Maertens, Sebastian Leguizamón, François Avellan

RENOVHydro: Development of a Decision Making Assistant for Hydropower Project Potential Evaluation and Optimization

Christian Landry, Christophe Nicolet, João Gomes Pereira Junior, Loic Andolfatto, Carlo Todde, Julien Derivaz, François Avellan

Pressure oscillation test rig

Anthony Gaspoz, Manuel Almeida, Christophe Nicolet, Samuel Rey-Mermet

Direct-marketing remuneration and flexibility of small hydro

Jérémy Schmid, Shadya Martignoni, Cécile Münch-Alligné

Recent Advances in Numerical Predictions for Off-Design Conditions in Hydraulic Turbomachines

Ernesto Casartelli, Luca Mangani, David Roos Launchbury, Armando Del Rio

Hydrokinetic turbine farm: challenges & expectations

Olivier Pacot, Jérémy Schmid, Shadya Martignoni, Jean Decaix, Nino Brunner, Cécile Münch-Alligné

Configuring a hydrokinetic turbine farm by CFD

Olivier Pacot, Jérémy Schmid, Shadya Martignoni, Jean Decaix, Nino Brunner, Cécile Münch-Alligné

Calibration of borehole failure models using inverse problem methods

Asmae dahrabou, Benoit Valley, Andres Alcolea, Peter Meier, Florentin Ladner, Frederic Guinot

Boreholes stability issues in ultra-deep geothermal production

Antonio Salazar, Leonid Germanovic, Carlo Rabaiotti & Paul Hardegger

Empirical model for the estimation of a Francis turbine complete characteristics curve

Joao Gomes, Loic Andolfatto, François Avellan

Cavitation modelling in GPU-Spheros

Audrey Maertens, Ebrahim Jahanbakhsh, François Avellan

Two-phase flow phenomena in turbines and pump-turbines operating in synchronous condenser mode

E. Vagnoni, L. Andolfatto, R. Guillaume, P. Leroy, F. Avellan

Energy context

Importance of the reactive power in the grid:

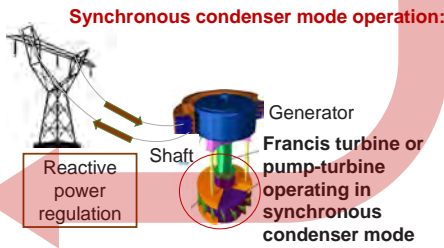
US northeast and Canada blackout, August 2003



Reactive power shortage
Lack in balancing the voltage instability in the grid

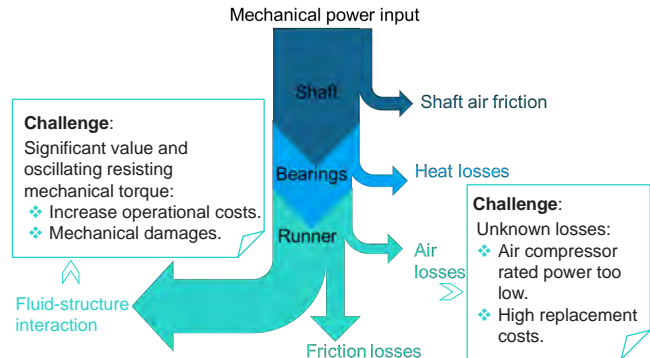
Increasing demand of reactive power supply/absorption:

- ❖ Environmental and policy changes
- ❖ Changes in the generation mix
- ❖ International transit trade of electricity



Objective

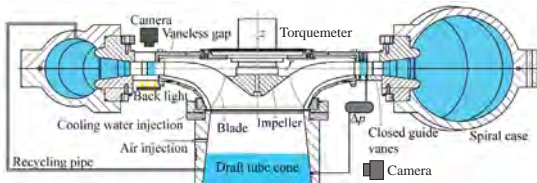
Prediction of the **mechanical power consumption** of a pump-turbine during the operation in **synchronous condenser mode**.



Experimental tests

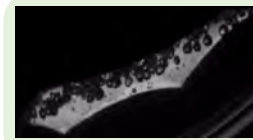
Configuration of a pump-turbine in synchronous condenser mode:

- ❖ Guide vanes are closed.
- ❖ Compressed air injected in the draft tube to keep the water level below the runner.
- ❖ Cooling water discharge.
- ❖ Recycling pipe to reduce the pressure in the spiral case.

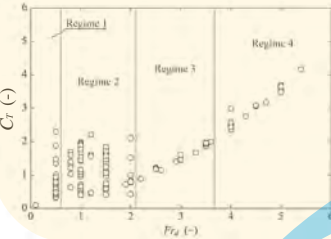


Results

- ❖ Study of torque stability correlated to the air-water ring dynamics.
- ❖ Flow phenomenology and torque can be classified in 4 regimes depending on the densimetric Froude number.
- ❖ Regime 1 is stable and influenced by the pressure.
- ❖ Regime 2 is strongly unstable: operation in this regime should be avoided.
- ❖ Regime 3 and 4 are stable. The torque can be predicted as a function of the densimetric Froude number.

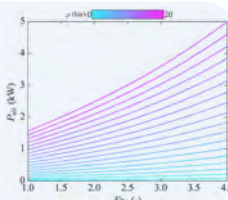


- ❖ Study of the two-phase flow phenomenology.
- ❖ Flow dynamics as a function of the densimetric Froude number.
- ❖ Strong influence on the pressure and torque fluctuations.



Challenges in synchronous condenser mode operation

- ❖ Study of the air diffusion into the water volume.
- ❖ Theoretical model validated on oxygen concentration measurements.
- ❖ The mass flow rate of lost air can be predicted as a function of the pressure, the cooling discharge and the densimetric Froude number.



Prediction of the power consumption



- ❖ Study of the free surface dynamics.
- ❖ Rotating gravity wave at the first azimuthal wave number $m = 1$.
- ❖ Wave breaking is observed by increasing the densimetric Froude number.
- ❖ Torque fluctuation are not correlated with this flow oscillation.

References

1. E. Vagnoni et al., (2018), "Rotating air-water ring in the vaneless gap of a pump-turbine operating in condenser mode," Int. Journal of Multiphase Flow 105, 112-121. doi: 10.1016/j.ijmultiphaseflow.2018.03.022.
2. E. Vagnoni et al., (2018), "Experimental investigation of the sloshing motion of the water free-surface in the draft tube of a Francis turbine operating in synchronous condenser mode," Experiments in Fluids, 59(6):95. doi: 10.1007/s00348-018-2552-x.
3. E. Vagnoni et al., (2018), "Interaction of a rotating two-phase flows with the torque stability of a reversible pump-turbine operating in condenser mode," Int. Journal of Multiphase Flow.

DuoTurbo : First Product and Pilot Test Sites

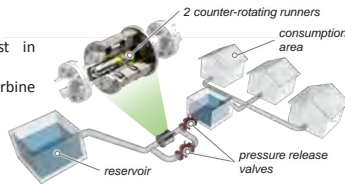
D. Biner¹, L. Rapillard¹, L. Andolfatto², V. Hasmatuchi¹, S. Martignoni, F. Avellan², C. Münch-Alligné¹

¹HES-SO Valais/Wallis, School of Engineering, Hydroelectricity Group, Sion, daniel.biner@hevs.ch

²EPFL, Laboratory for Hydraulic Machines, Lausanne

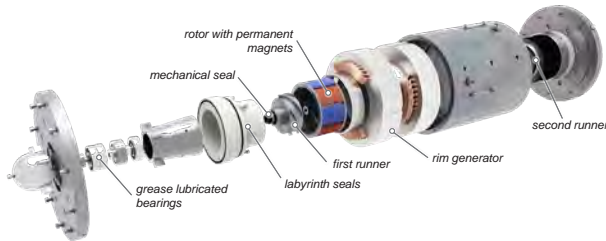
Context

- Recovering hydraulic energy lost in drinking water networks
- Modular in-line "plug and play" turbine from 5 to 25 kW
- No environmental impact
- Low investment costs



Mechanical concept

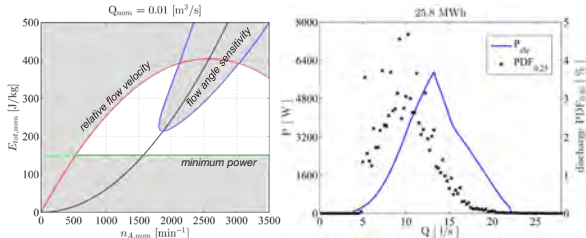
Based on the experience gathered during the prototype phase, a new mechanical concept was established. The achieved mechanical robustness enables the possibility of long term operation at the pilot sites. The mechanical complexity was significantly reduced and a modularity to target a wide discharge range is provided.



Hydraulic design

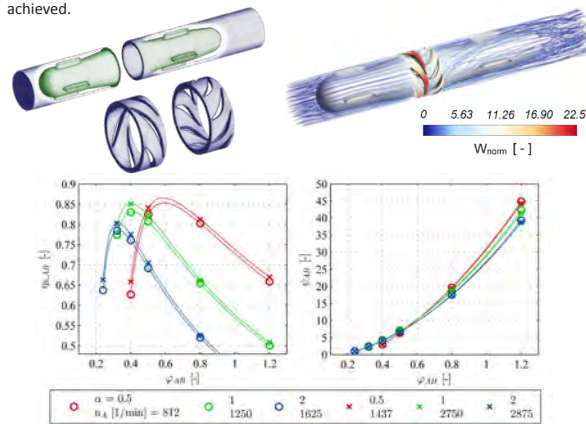
Hydraulic characteristics

The runners of the first product were designed for the pilot site of Savièse. According to different design limitations, a reasonable design point was chosen.

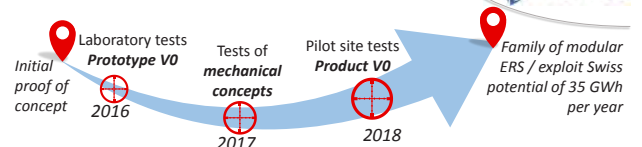


Numerical simulations

The runner design was iteratively established by means of CFD simulations in order to maximize the turbine's performance. A hydraulic efficiency of more than 85 % is achieved.

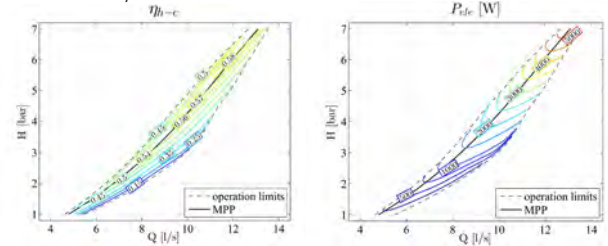


Project



Laboratory tests

Detailed experimental investigations have been carried out on the hydraulic test rig of the HES-SO Valais/Wallis. A maximum regenerated electrical power of 6.5 kW was measured, reaching a global efficiency of nearly 60 % that corresponds to an enhancement of 14 % compared to the prototype V0. Additionally, the automation of the entire system, including the maximum power point tracking algorithm (MPPT), was successfully tested.



Pilot test sites

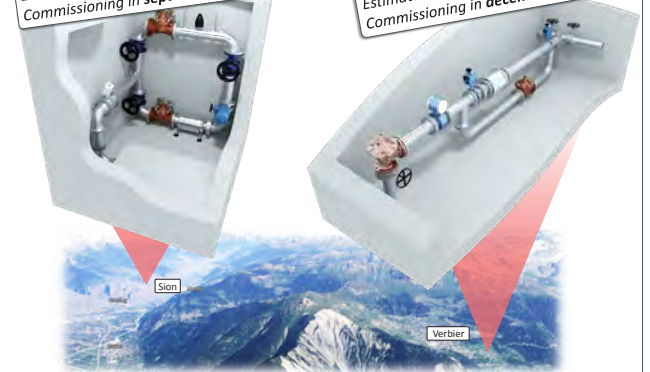
In 2018 two pilot sites are targeted for long term tests of the first DuoTurbo products. On both sites, detailed data of hydraulic, electrical and mechanical measurands will be collected.

Savièse

Net head = 125 m
Average discharge = 10 l/s
Estimated production = 26 MWh/a
Commissioning in september 2018

Médières

Net head = 175 m
Average discharge = 4 l/s
Estimated production = 18 MWh/a
Commissioning in december 2018



Conclusion

To sum up the main achievements of the DuoTurbo project, ending in June 2018, a successful development of a new energy recovery system for future installations on many potential drinking water facilities can be mentioned. Passing from the prototype phase to the first operational product, significant enhancements concerning the turbine's lifecycle and performance were achieved. At the two pilot sites equipped this year, the robustness, expected efficiency and system stability under long-term operating conditions will be assessed.

References

- D. Biner, V. Hasmatuchi, D. Violante, S. Richard, S. Chevailler, L. Andolfatto, F. Avellan, C. Münch, "Engineering and Performance of DuoTurbo: Microturbine with Counter-Rotating Runners", 28th IAHR Symposium - Grenoble, July 2016.

Development team of Duo Turbo (CTI Nr. 17197.1 PFEN-IW)

HES-SO Valais/Wallis:

D. Biner, S. Luisier, S. Martignoni, D. Violante, V. Hasmatuchi, S. Richard, C. Cachélin, L. Rapillard, S. Chevailler, C. Münch-Alligné

EPFL LMH:

L. Andolfatto, V. Berruex, F. Avellan

Industrial partners:

Telsa SA, Jacquier-Luisier SA, Valelectric Farner SA

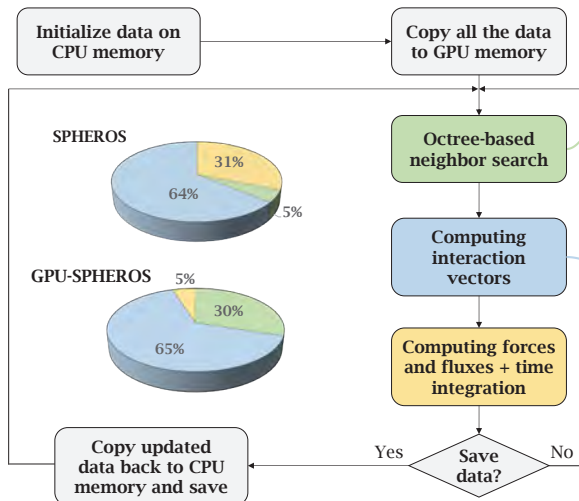
GPU-SPHEROS: A GPU-Accelerated 3-D Finite Volume Particle Method solver

S Alimirzazadeh, E Jahanbakhsh, A Maertens, S Leguizamón, F Avellan

Introduction

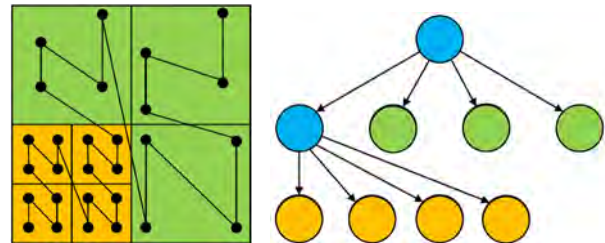
GPU-SPHEROS is a GPU-accelerated particle-based solver based on Finite Volume Particle Method (FVPM) which inherits desirable features of both Smoothed Particle Hydrodynamics (SPH) and mesh-based Finite Volume Method (FVM) and is able to simulate the interaction between fluid, solid and silt [1]. With GPU-SPHEROS, the goal is to perform a industrial size setup simulations of hydraulic machines.

Software flowchart



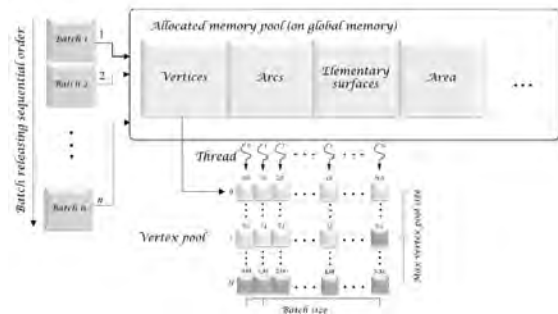
Octree-based neighbor search

- **Memory access efficiency** is a key point for GPU applications to be able to get a good performance.
- The data has been reordered using **space filling curves (SFCs)** to improve memory access.
- An octree-based neighbor search algorithm has been implemented to find the neighbor particles.
- A highly optimized kernel has been implemented for parallel distance check between the particles.



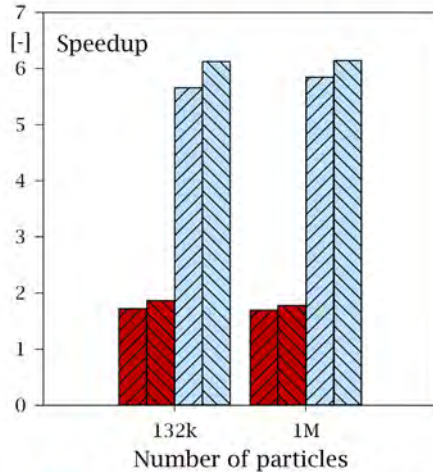
Computing interaction vectors

- GPU-SPHEROS has been developed based on spherical-supported kernels.
- A fixed-size pre-allocated memory is used for computing interaction vectors procedure and the access order considered to have a coalesced memory access to minimize memory transactions.
- The particles are grouped into smaller batches and the computations are divided into different batches in which they are performed in parallel for each batch and the batches themselves are released sequentially.



Speedup

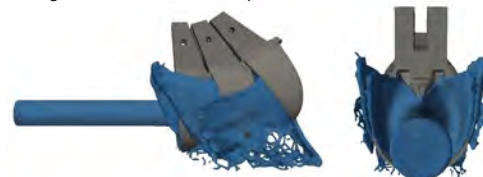
- On NVIDIA Tesla P100, GPU-SPHEROS is almost **5.5x faster** than the CPU version running on a dual CPU node with two Intel® Xeon® E5-2690 v4 Broadwell CPUs and also more than 6x faster compared to a machine with two Intel® Xeon® E5-2660 v2 Ivy-Bridge CPUs.
- Overall throughput reaches higher than **3x10⁵** particles per second on **NVLink-based Tesla P100 SXM-2 16 GB**.



■ Tesla K40 vs. Intel Xeon E5-2690v4
 ■ Tesla K40 vs. Intel Xeon E5-2660v2
 ■ Tesla P100 vs. Intel Xeon E5-2690v4
 ■ Tesla P100 vs. Intel Xeon E5-2660v2

Case study

- **Turbulent** free jet deviated by rotating Pelton buckets has been simulated by GPU-SPHEROS to verify the solver validity. There is a good agreement between the predicted and measured torque.



References

[1] E. Jahanbakhsh, A. Maertens, N. J. Quinlan, C. Vessaz, F. Avellan, Exact finite volume particle method with spherical-support kernels, *Comput. Methods Appl. Mech. Engrg.* 317 (2017) 102–127

[2] S. Alimirzazadeh, E. Jahanbakhsh, A. Maertens, S. Leguizamón, F. Avellan, GPU-Accelerated 3-D finite volume particle method, *Computers & Fluids*. 171 (2018) 79–93

RENOVHydro: Development of a Decision Making Assistant for Hydropower Project Potential Evaluation and Optimization

Christian Landry, Christophe Nicolet, João Gomes Pereira Junior, Loïc Andolfatto, Carlo Todde, Julien Derivaz, François Avellan

Motivation

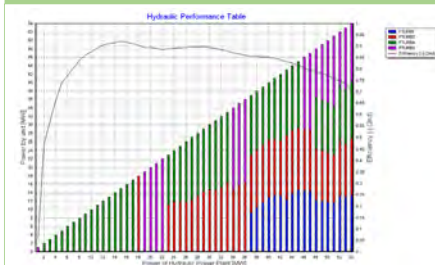
The RENOVHydro project is dedicated to the **renovation** of an existing hydroelectric power plant with a systematic assessment of a **high number of civil and electromechanical potential modifications**. **Energy and economic indicators** such as annual energy generation, annual amount of turbined/pumped water, investment cost, profitability and ancillary services for each renovation option can be analyzed to identify technical trends according to **political, economic and environmental contexts**.

2. Selection of renovation options

Many civil engineering and hydroelectric options are available (add new penstock, increase reservoir storage, upgrade the turbine, add variable speed, ...). For each renovation option, a **pre-dimensioning** and a **cost estimation** are computed.

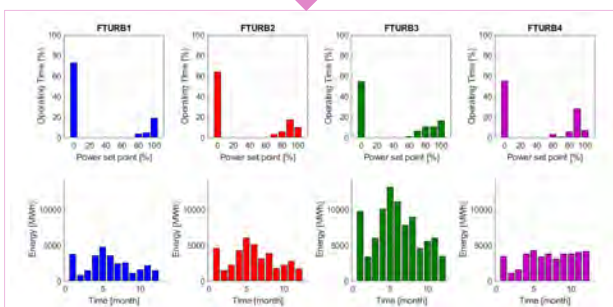
3. Hydraulic performance table

A hydraulic performance table defines the **most efficient distribution of units for all power set points** and all upstream water levels. To evaluate the hydraulic power plant performances over the entire operating range, each unit combination and each guide vane opening combination are evaluated for a given upstream water level.



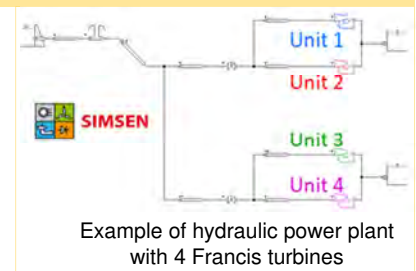
Input data for simulation of an operating year

- The electricity market price and hydrology time history for a reference year.
- Power and level limitations during a year.
- Maintenance periods and possible outage over the whole concession duration.

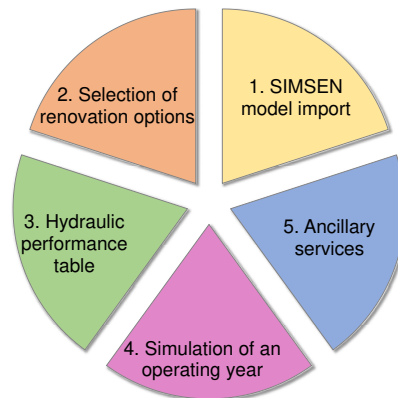


1. SIMSEN model import

The SIMSEN simulation software enables to model an entire power plant including **hydraulic, mechanical and electrical system** and their related control systems. **Realistic performance hill charts** of the turbine were generated with a polynomial bi-variate functions base on Hermite polynomials and can be selected in a database for **Francis, Pelton, Kaplan turbines and pump-turbines**.



Methodology

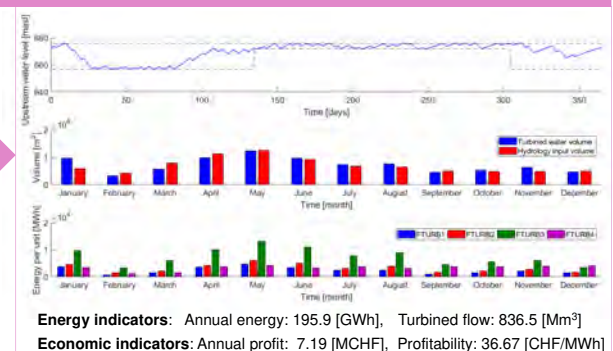


5. Ancillary services

The performance offered by the renovation options regarding **interaction with the electrical power networks**, such as primary and secondary control capabilities, is evaluated to determine the **maximum load step response compatible** with Transmission System Operator requirements.

4. Simulation of an operating year

The best performance of each renovation option is computed with a mathematical optimization approach (**Mixed-Integer Linear Programming algorithm**). **Energy and economic indicators** for each renovation option are quantified to identify technical trends according to political, economic and environmental contexts.



Acknowledgments

The RENOVHydro project is granted by CTI, Commission for Technology and Innovation (Grant funding 19343.1 PFEN-IW) and by SFOE, Swiss Federal Office of Energy (Grant funding SI/501436-01).

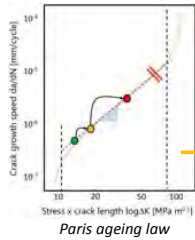


Pressure oscillation test rig

Anthony Gaspoz, Samuel Rey-Mermet HESSO Valais-Wallis

Motivation

As the prices on the electrical market are still low, the hydropower asset managers want to reduce their maintenance costs. With the help of risk management and materials ageing laws, they can make better decision to lower their global costs in the long term. The Swiss Federal Council has evaluated that the investment necessary to maintain the hydropower capacity of Switzerland till 2050 amounts to 30 billions of CHF.

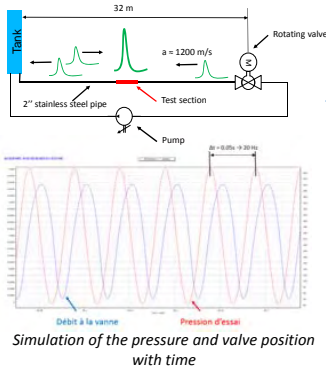


30 billions of CHF
 2010-2050*

*Swiss Federal Council estimation
<https://www.parlament.ch/fr/ratsbetrieb/suche-curia-vista/geschaefter?AffairID=20143501>

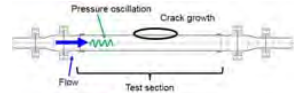
Pipeline

The pipeline length is calculated to obtain the mechanical resonance in the middle of it according to the speed of the valve.

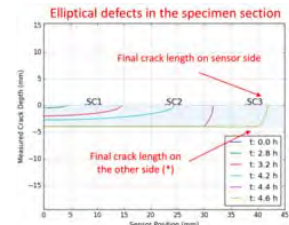


Crack growth in specimen pipe

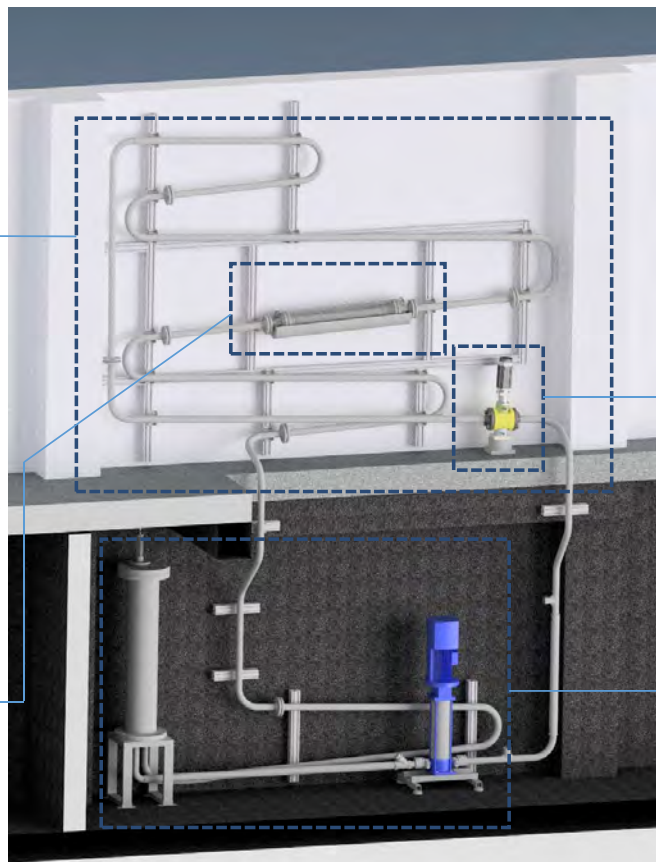
The specimen pipe is located in the middle of the pipeline where the mechanical resonance occurs.



The pipe contains machined cracks that will grow under the pressure oscillations according to the Paris law or a thin section where the fatigue will occur.



A specific Eddy current sensor (Sensima) will monitor the the crack growing speed. In the thin section, the stress variations will be measured by a dedicated gauge and the fatigue will be calculated based on the Wöhler law.



Rotating valve

The rotating valve has a diameter of 2", a nominal pressure of 100 bars and a rotating speed of 1500 rpm. It will create pressure oscillations in the specimen pipe. With its speed it will be possible to simulate 50 years of operations pressure fluctuations in less than 2 days.



Water recirculating system

As the test rig is a close loop system, it is necessary to recirculate water into it. Thus the test rig comprises a variable speed pump (up to 15m³/s, PN12) and a tank (70 l, PN40) in the basement of the building.

Results and benefits

The test rig will be operating in December.

Benefits of the in lab test rig

- Proof of concept of the fatigue monitoring (accumulation of damage due to pressure oscillations)
- Proof of concept of the crack growth monitoring (in water, in real time, with real cracks)
- Study of the ageing laws

Benefits for assets management

Better ageing law → better risk prediction

Partners



Direct-marketing remuneration and flexibility of small hydro

Jérémy Schmid, Shadya Martignoni, Cécile Münch-Alligné

HES-SO Valais, School of Engineering, Hydroelectricity Group, CH-1950 Sion, Switzerland, jeremy.schmid@hevs.ch

Context

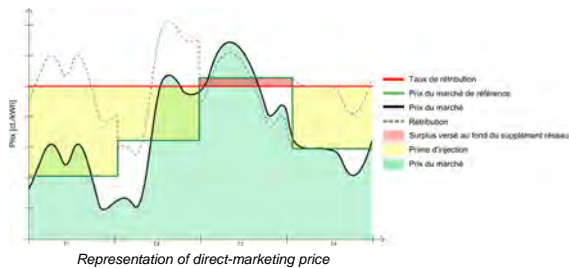
Following the acceptance of the energy strategy 2050, the energy law changes came into force on 1 January 2018, such as the Ordinance on the encouragement of renewable electricity generation (OEnER).

As part of this revision, the system of compensation at cost price of the injected current (RPC) is adapted into a system of compensation of injection (SRI1) based on two models of remuneration including direct marketing. This incentive model implies that the operators of installations must henceforth sell their electricity on the energy market.

This revision will therefore push some distributors with small hydropower plants to better predict their production and to stall at the best market price. The case study is carried out of a 2MW hydropower plant located in Icoigne (VS).

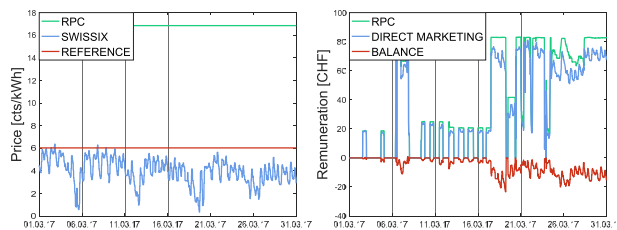
Direct-marketing remuneration

- Have to sell the electricity themselves on the market.
- The quantity of energy produced is traded on the market by the operator itself or through a direct distributor.
- The goal is to encourage to produce and operate renewable installations according to the market.

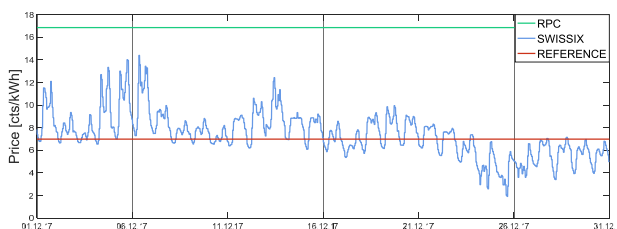


Impacts of the direct-marketing

1) If the market price < the reference price => the distributor lose



2) If the market price > the reference price => the distributor can win

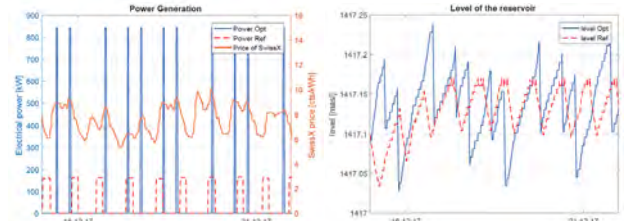


Flexibility of the hydropower plant management

Low peak water flow period

- Simple optimisation with ON/OFF programme
- Low cost management with daily schedule
- Based on historical market price analysis
- Flexibility with turbine flow and reservoir variation level

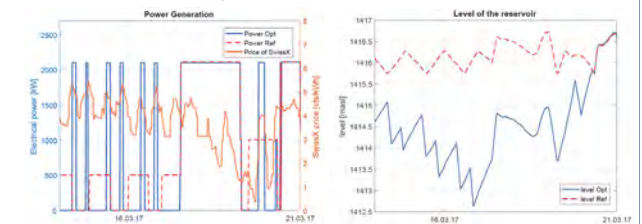
=> Increase average cost-price by 10-15%



High peak water flow period

- Flexible production when the constraints are not reached
- Forced to produce continuously when input flow is high
- Based on historical market price analysis
- Flexibility with turbine flow and reservoir variation level

=> Increase average cost-price by 1%



Conclusion

- Goal of direct-marketing is to encourage small hydropower plants to comply with the electricity market and to provide their injection.
- The flexibility can reduce the impact of the direct-marketing on the hydropower plant remuneration with an increase of the remuneration price by 10-15 % in winter and can absorb all the losses of all year.
- The winter period is more predictable and flexible. It's also easier to make some gains although the production represent a small part of the whole year production.

Acknowledgements



References

[1] Office Fédéral de l'énergie OEFN : Loi du 30 septembre 2016 sur l'énergie (LEne) (Etat le 1er janvier 2018). RO 2017 6839. 2017. Bern.
 [2] Office Fédéral de l'énergie OFEN : Ordonnance du 1er novembre 2017 sur l'encouragement de la production d'électricité issue d'énergies renouvelables (OEnER) (Etat le 1er janvier 2018). RO 2017 7783. 2017. Bern.
 [3] Office fédéral de l'énergie OFEN : Commercialisation directe – Fiche technique. 22 novembre 2017. Bern.

Recent Advances in Numerical Predictions for Off-Design Conditions in Hydraulic Turbomachines

E. Casartelli, L. Mangani, D. Roos Launchbury, A. Del Rio

Introduction

Simulations of off-design conditions in hydraulic machines, especially in unstable operating points, are difficult to perform because the conditions are dominated by unguided, highly turbulent flow in the vaneless spaces which often cannot be accurately predicted using conventional turbulence models. This is due to the fact that the most commonly used models, such as k-Epsilon and the Shear Stress Transport (SST) model assume isotropic turbulence. This assumption is not valid for many flow problems but seems to have an especially large influence in pump turbine instability simulations. Figure 1 shows a close-up of such a typical S-shaped operating curve. The quantity k_{cm1} is a normalised flow rate and k_{u1} is a normalised machine speed.

The goal of the current efforts is to implement advanced turbulence models in a coupled solver and improve their efficiency and robustness for pump turbine instability simulations. This work will be of direct importance in upcoming large-scale simulations as part of the SCCER-FURIES project.

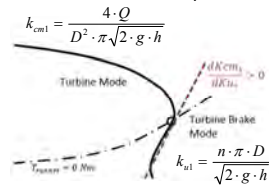


Figure 1: Unstable Operating Range

Second-Moment Closure Turbulence Models

Explicit Algebraic Reynolds Stress Models (EARSM)

EARSMs do not solve additional transport equations but try to reconstruct the unknown stress tensor through an algebraic equation based on the velocity gradients. Two different formulations were implemented, one by Menter [4] and one by Hellsten [2].

Full Reynolds Stress Models

The full Reynolds stress model solves an equation for each component of the Reynolds stress tensor along with an equation for the turbulence length scale, leading to a total of 7 equation in addition to the momentum and pressure equations. Wilcox' Stress Omega model [5] was implemented using the Baseline modifications by Menter [3].

Convergence Improvements for Reynolds Stress Models

The Reynolds stress transport equations are usually solved sequentially. In order to improve convergence and stability, in this work the Reynolds stress equations are solved in a coupled fashion, leading to a 6x6 block matrix structure. This procedure was applied to a simple backward facing step test case and it could be shown that convergence of all solution variables is reached using fewer iterations compared to the segregated version. The segregated version also suffered from oscillations at the reattachment point of the flow that inhibited convergence. Figures 2a and 2b show the improved convergence of the momentum, pressure and Reynolds stress variables respectively.

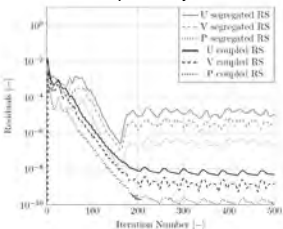


Figure 2a: Pressure/Momentum Convergence

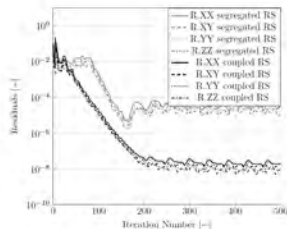


Figure 2b: Reynolds Stress Convergence

Simulation Results

NACA0012 with Full Reynolds Stress Model

To validate the implementation of the full Reynolds stress model the solution of the wing tip vortex around a NACA0012 profile was compared to measurements by Chow et al. [1]. The crossflow velocity $\sqrt{v^2 + w^2}/U_\infty$ along a span-wise line through the vortex core is evaluated at different positions downstream of the wing. Figure 4a shows the comparison between SST, RSM and measurements. The agreement between simulation and measurement is very good and a large improvement over the SST model can be observed. Figure 4b shows a position very far downstream (582%). The vortex has essentially disappeared for the SST model, while RSM is able to sustain the vortex strength. This model will be applied to a full pump turbine simulation in the near future.

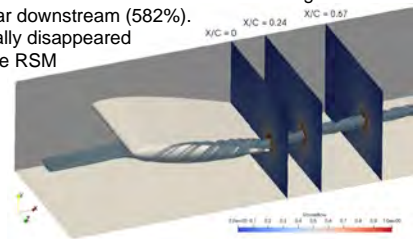


Figure 3: NACA0012 Tip Vortex

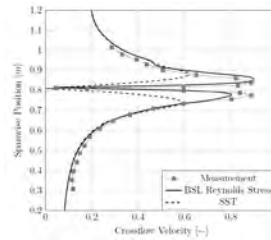


Figure 4a: Crossflow Velocity at X/C = 0.67

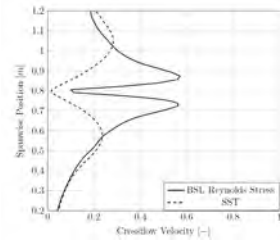


Figure 4b: Crossflow Velocity at X/C = 5.82

Unstable Pump Turbine with EARSM

A validated EARSM model was applied to a 360° unsteady pump turbine simulation in an unstable operating range and compared to our own measurements. It can clearly be seen that while the SST model misses the instability entirely, the more advanced EARSM model is able to accurately reproduce the entire S-shaped instability region.

This finding underlines the importance of turbulence modelling for the simulation of off-design and unstable operating points and shows the validity of the implemented model.

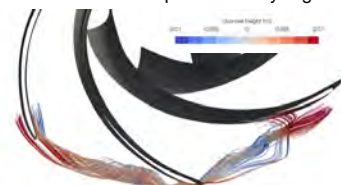


Figure 5: Vortex Formation in Vaneless Space of Pump Turbine

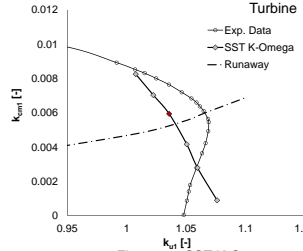


Figure 6a: SST K-Omega

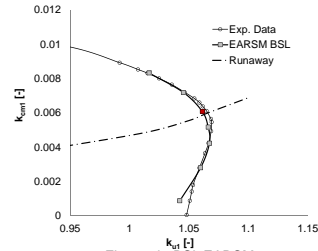


Figure 6b: BSL EARSM

References

- [1] Chow, J. S., Zilliac, G. G., and Bradshaw, P., "Mean and Turbulence Measurements in the Near Field of a Wingtip Vortex," AIAA Journal, Vol. 35, No. 10, pp. 1561-1567.
- [2] Hellsten, A., "New Advanced k-omega Turbulence Model for High-Lift Aerodynamics", AIAA Journal, Vol. 43, No. 9, 2005, pp. 1857-1869.
- [3] Menter, F. R., "Two-Equation Eddy-Viscosity Turbulence Models for Engineering Applications," AIAA Journal, Vol. 32, No. 8, 1994, pp. 1598-1605.
- [4] Menter, F. R., Garbaruk, A.V. and Egorov, Y., "Explicit Algebraic Reynolds Stress Models for Anisotropic Wall-Bounded Flows", Progress in Flight Physics, Vol. 3, 2012, pp. 89-104
- [5] Wilcox, D. C., "Turbulence Modeling for CFD", 3rd edition, DCW Industries, Inc., La Canada CA, 2006.

Hydrokinetic turbine farm: challenges & expectations

O. Pacot¹, J. Schmid¹, S. Martignoni¹, J. Decaix¹, N. Brunner², C. Münch-Alligné¹

¹HES-SO Valais, School of Engineering, Hydroelectricity Group, CH-1950 Sion, Switzerland, olivier.pacot@hevs.ch

²Stahleimbau GmbH, Talstrasse 30, CH-3922 Stalden, Switzerland

Context

- The performance of the first hydrokinetic (Hkt) turbine prototype [1] with a power of 1 kW has been tested and validated for real conditions in Lavey [2].
- To increase the power output, several hydrokinetic turbines will be assembled.
- The small size of the hydrokinetic turbine make it possible to implant it in shallow river: 4-5 meters water height.

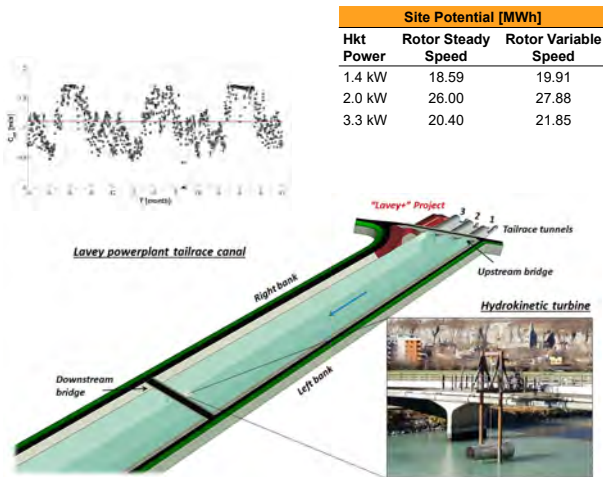
Objective:

- Develop and install a cost-effective hydrokinetic farm with a power output of 10 kW in the tailrace channel in Lavey.

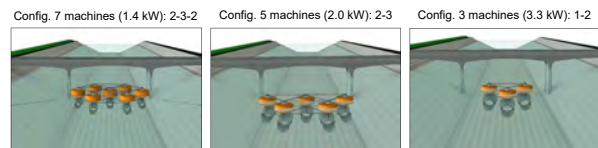
Lavey Pilot Site & Potential

This pilot site of Lavey was selected because of the following characteristics [2-3]:

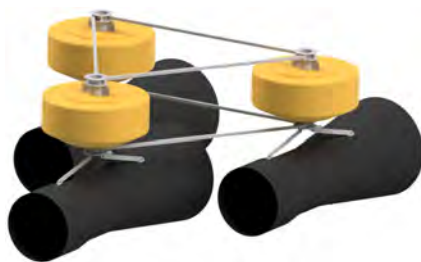
- Artificial channel with a filtered water thanks to the upstream hydropower plant
- Available flow speed between 0.5 and 1.7 m/s
- Averaged flow speed of 1.4 m/s



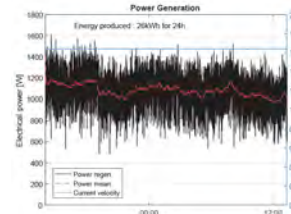
Farm Configuration Options



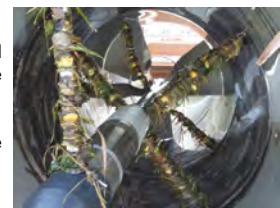
Zoom on the modular structure



Single Hkt Performance & Long Operation Challenge



- Good overall performance of the Hkt in real conditions.
- The power generated during one full day test reached 26 kWh.
- Presently, the rotation frequency is maintained constant. However, variable rotation speed will be implemented.



- Future challenge: how the natural algae, grass and leaves will alter the global performance of the Hkt?
- And how can we design the machine to minimize this sticking problem?

Cost Estimation

- To estimate the cost of the farm, the latter is decomposed in 3 parts: the cost to build the machine, the structure cost and the cost of all electronic and electric equipment.
- The table below shows the estimated prices of a single Hkt and the farm. The prices are normalized by the price of a single 1.4 kW Hkt.

Hkt Max Power	7 x 1.4 kW	5 x 2.0 kW	3 x 3.3 kW
Machine	0.73	0.89	1.00
Farm Structure	0.16	0.18	0.23
Electric & Electronics	0.11	0.11	0.14
Cost of a single Hkt	1.00	1.18	1.36
Cost of a farm	7.00	5.91	4.09

- The increase of the Hkt power increases the price of the machine. However, it is shown that with the reduced number of Hkt required, the configuration using 3 Hkt is the most financially advantageous.

Conclusions

- The performance of a single hydrokinetic turbine in real conditions during several days showed that the expected power output is reached.
- The modular and stable structure allow to implant and adapt the farm configuration to any kind of environment.
- With this assembly of turbines, it is expected to reach a power output of 10 kW and produce 25 MWh.
- The cost estimation showed that a single 3.3 kW Hkt is 36% more expensive than a 1.4 kW Hkt. However, the farm using only three 3.3 kW Hkt is the most advantageous.

References

[1] C. Münch, S. Richard, A. Gaspoz, V. Hasmatuchi, N. Brunner, "New Prototype of a Kinetic Turbine of Artificial Channels" Advances in Hydroinformatics, Springer, Singapore, 2018, pp. 981-996.
 [2] C. Münch, J. Schmid, S. Richard, A. Gaspoz, N. Brunner, V. Hasmatuchi, "Experimental Assessment of a New Kinetic Turbine Performance for Artificial Channels" Water 2018, Volume 10, Issue 3, 311.
 [3] V. Hasmatuchi, A. Gaspoz, L. Rapillard, N. Brunner, S. Richard, S. Chevailler, C. Münch-Alligné, 2016, "Open-air laboratory for a new isokinetic turbine prototype", Annual conference, SCCER SoE, Sion.

Configuring a hydrokinetic turbine farm by CFD

O. Pacot¹, J. Schmid¹, S. Martignoni¹, J. Decaix¹, N. Brunner², C. Münch-Alligné¹

¹HES-SO Valais, School of Engineering, Hydroelectricity Group, CH-1950 Sion, Switzerland, olivier.pacot@hevs.ch
²Stahleinbau GmbH, Talstrasse 30, CH-3922 Stalden, Switzerland

Context

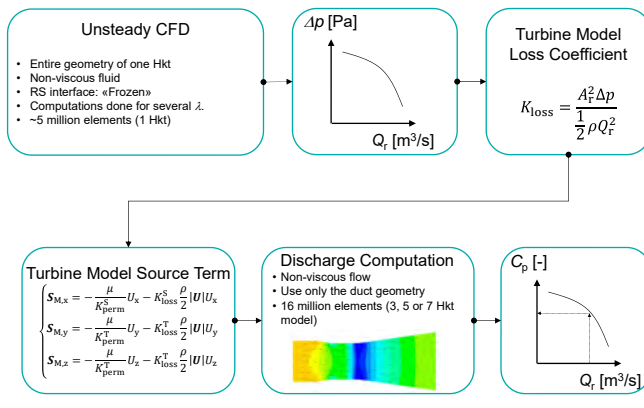
- The performance of the first hydrokinetic (Hkt) turbine prototype [1] with a power of 1 kW has been tested and validated for real conditions in Lavey [2].
- To increase the power output, the idea is to assemble several hydrokinetic turbines as a farm, which requires to investigate the influence of the machines between each other.

Objective:

- Configure a hydrokinetic farm to reach an output power of 10 kW by a cost-effective CFD approach.

Hydrokinetic Turbine Model

To minimise the amount of computational resources and to speed up the computations, a model of the Hkt is used [3]. This model mimics the pressure drops experienced by the fluid from the runner. This approach has the advantage to avoid to compute the unsteady flow between the stationary and rotating domains.

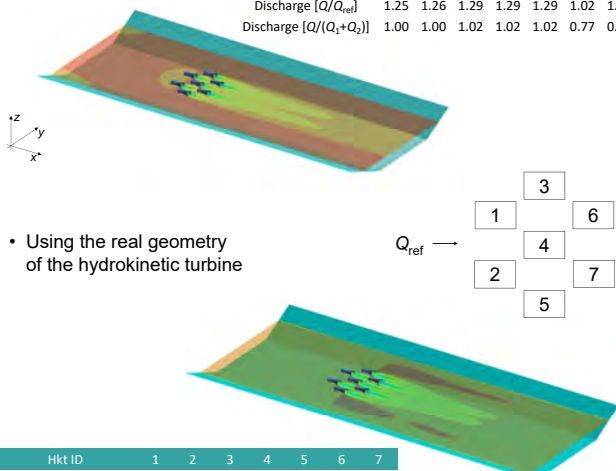


Turbine Discharge Computations

- Using the hydrokinetic turbine model

The simulation using the model overpredict the discharge by 5-10%.

Hkt ID	1	2	3	4	5	6	7
Discharge [Q/Q _{ref}]	1.25	1.26	1.29	1.29	1.29	1.02	1.03
Discharge [Q/(Q ₁ +Q ₂)]	1.00	1.00	1.02	1.02	1.02	0.77	0.78

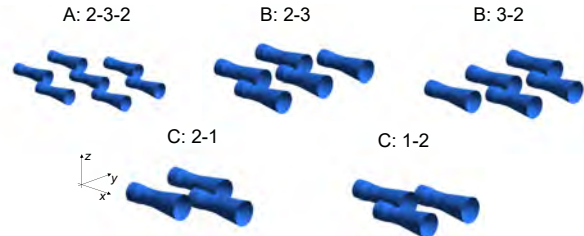


- Using the real geometry of the hydrokinetic turbine

Hkt ID	1	2	3	4	5	6	7
Discharge [Q/Q _{ref}]	1.12	1.12	1.14	1.14	1.14	0.97	0.97
Discharge [Q/(Q ₁ +Q ₂)]	1.00	1.00	1.01	1.01	1.01	0.87	0.87

Similar discharge trend between both simulation.

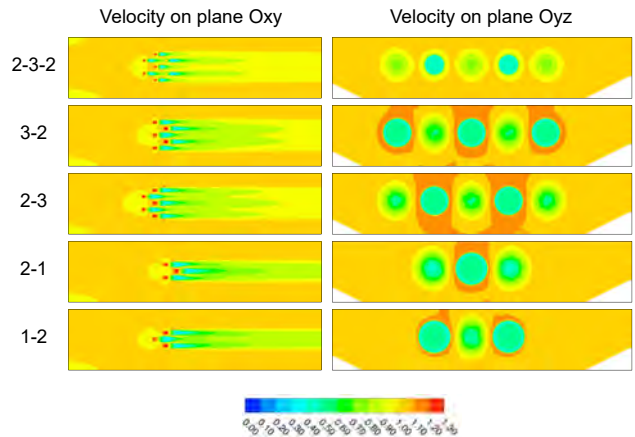
Farm Configurations



Configuration	Power Max [kW]	Diameter [m]	Length [m]
A	1.4	1.0	4.1
B	2.0	1.4	5.8
C	3.3	1.6	6.5

Configuration	2-3-2	3-2	2-3	2-1	1-2
Estimated Power Max [kW]	9.51	10.24	10.21	10.07	10.04

Results



Conclusions

- The use of CFD analysis with a hydrokinetic turbine model allowed us to estimate cost-effectively the performance of a farm.
- 5 different configurations were analysed. The suitable ones are a configuration with 5 hydrokinetic turbines.
- For a final assessment, a full unsteady simulation will be required.

References

[1] C. Münch, A. Gaspoz, S. Richard, V. Hasmatuchi, N. Brunner, 2017, "New prototype of a kinetic turbine for artificial channels". Simhydro Conference, Nice, 14-16 June.
 [2] V. Hasmatuchi, A. Gaspoz, L. Rapillard, N. Brunner, S. Richard, S. Chevallier, C. Münch-Alligné, 2016, "Open-air laboratory for a new isokinetic turbine prototype". Annual conference, SCCER SoE, Sion.
 [3] W. M. J. Batten, M. E. Harrison, A. S. Bahaj, 2013, "Accuracy of the actuator disc-RANS approach for predicting the performance and wake of tidal turbines". Phil Trans R Soc A 371: 20120293.

Calibration of borehole failure models using inverse problem methods

Asmae Dahrabou⁽¹⁾, Benoît Valley⁽¹⁾, Andres Alcolea⁽²⁾, Florentin Ladner⁽²⁾, Frédéric Guinot⁽²⁾, Peter Meier⁽²⁾

(1) Centre for Hydrogeology and Geothermics, University of Neuchâtel, Emile-Argand 11, 2000-Neuchâtel, Switzerland.

(2) Geo-Energie Suisse AG, Reitergasse 11, 8004 Zürich, Switzerland.

I- Project context and objectives

In the frame of a CTI-project, the CHYN and Geo-Energie Suisse AG are developing a workflow and associated software tools that allow a fast decision-making process for selecting an optimal well trajectory while drilling deep inclined wells for EGS-projects. The goal is to minimize borehole instabilities as it enhances drilling performance and maximize the intersection with natural fractures because it increases overall productivity or injectivity of the well. The specificity of the workflow is that it applies to crystalline rocks and includes an uncertainty and risk assessment framework.

II- Calibration study by using inverse problem method

The main challenge in these analyses is that the strength and stress profiles are unknown independently. Calibration of a geomechanical model on the observed borehole failure has been performed using data from the Basel Geothermal well BS-1 and inverse problem method (PEST: Parameter ESTimation software).

2.1- Model sensitivity to individual measurements

A sensitivity study performed on data from the well BS-1 (DHM project Basel) by using PEST showed that the most influential parameters on borehole stability are the magnitude of the maximum and minimum horizontal stresses, S_{Hmax} , S_{Hmin} , the uniaxial compressive strength, UCS, and the internal borehole pressure P_{mud} .

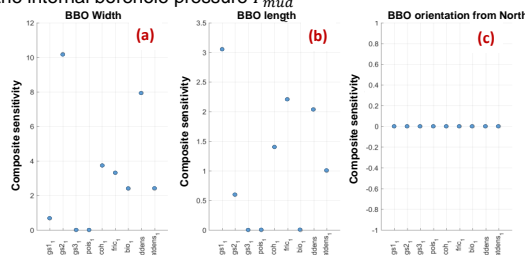


Figure 1. Calculated sensitivity of (a) borehole breakout width, (b) breakout length and (c) breakout orientation with respect to the geographical North by using PEST. The studied inputs are the gradient of the maximum, intermediate and minimum principal effective stresses respectively g_{s1} , g_{s2} , g_{s3} , Poisson ratio, the cohesion, the internal frictional angle, the Biot coefficient, mud and water densities.

2.2- The geomechanical model to calibrate

In a first approximation, a purely elasto-brittle analytical solution in combination with Mohr-Coulomb failure criterion were used. Three borehole failure indicators were used so far: the breakout width, the breakout penetration and the cross-sectional area.

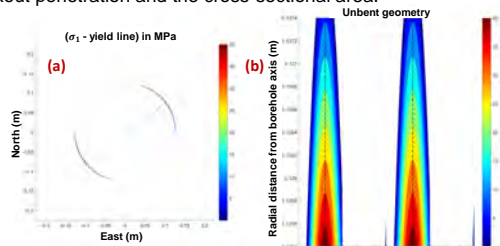


Figure 2. (a) Calculated failure in BS-1 hole at z=3500m. The blue arrow corresponds to the borehole breakout orientation (54° from the geographical North) that aligns with the orientation of S_{Hmin} , the minimum horizontal principal stress. (b) Unbent spalled zone, computed in (a). The plotted geometry corresponds to the failed zone based on Mohr-Coulomb failure criterion (σ_1 - yield line) in MPa.

2.3- First results from PEST

Marquardt algorithm aims at minimizing an objective function F that relates measurements, model parameters, prior information and their weights.

$$F = \underbrace{\sum_{i=1}^{n_w} (\gamma_w (w_i - w_i^*))^2}_{\text{Contribution of breakout width measurements}} + \underbrace{\sum_{i=1}^{n_l} (\gamma_l (l_i - l_i^*))^2}_{\text{Contribution of breakout length measurements}} + \underbrace{\sum_{i=1}^{n_\theta} (\gamma_\theta (\theta_i - \theta_i^*))^2}_{\text{Contribution of breakout width orientation}} + \underbrace{\sum_{i=1}^{n_p} (\gamma_p (p_i - p_i^*))^2}_{\text{Contribution of prior information}}$$

2.3.1- Objective function computation

The total objective function F as well as the contribution made to this latter by measurements and prior information were computed for several iterations. If the plotted objective function is fluctuating, this means that we have an instability problem of our model parameters.

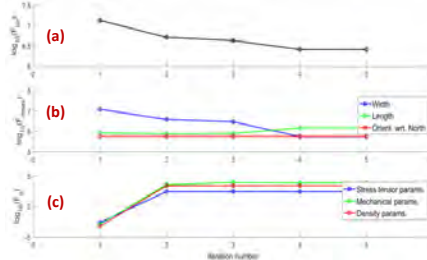


Figure 3. (a) Computed total objective function F and (b) the contribution of measurements (breakout width, breakout penetration and their orientation with respect to the geographical North) and (b) prior information (stress tensor, mechanical and density parameters) to F.

2.3.2- Residuals of measurements after calibration

In order to check if our model leads to a good match with observations, residuals were calculated.

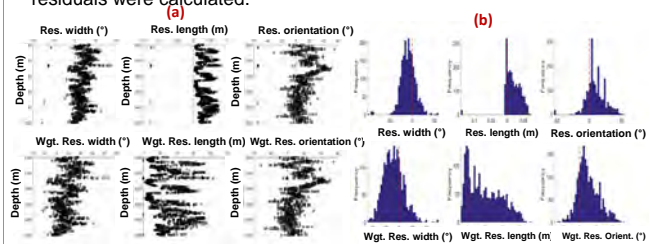


Figure 4. (a) Residuals of borehole breakout width [°], penetration [mm] and orientation with respect to the North [°] are plotted Vs. the depth [m]. (b) Histograms corresponding to each residual computed in (a).

2.3.3- Posterior covariance and correlation of parameters

If two parameters we want to estimate are highly correlated, this dependence causes the confidence intervals of the parameters to be larger than they would have been if they were independent.

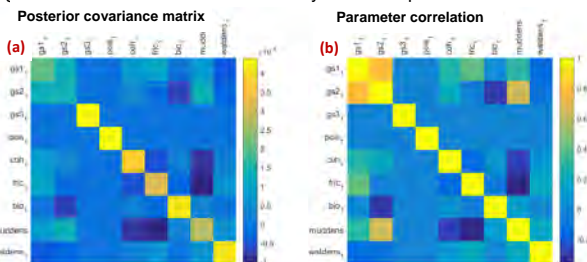


Figure 5. (a) Computed posterior covariance of parameters after calibration, (b) Computed correlation between model parameters.

III- Conclusions

- UCS and S_{Hmax} (maximum horizontal principal stresses) are the parameters the most influential on failure computation.
- High computed residuals means that we are either overestimating or underestimating our model parameters.
- If two parameters we want to estimate are highly correlated, this dependence causes the confidence intervals of the parameters to be larger than they would have been if they were independent.
- The diagonal elements of the covariance matrix are eventually high, which means that the confidence interval of the estimated parameters are very large. This means that our model is not well calibrated yet.

Boreholes Stability Issues in Ultra-Deep Geothermal Production

Antonio Salazar V., Leonid Germanovich, Carlo Rabaiotti, Paul Hardegger & Hansruedi Schneider

Introduction

Ultra-deep geothermal energy production is a promising source of clean energy. It is available everywhere and has the potential to supply the world's energetic needs.

The natural geothermal gradient is approximately 30°C per km. Economically feasible geothermal energy production needs rock temperatures in the range of 200° - 300° C. Therefore drilling of deep to ultra-deep boreholes (6 - 10km) is a prerequisite to successfully harvest geothermal energy in the geologic setting of Switzerland.

The objective is to physically and numerically analyze the wellbore short- and long-term stability, improving existing constitutive models to be able to realistically simulate the rock mass behavior under high pressure and high temperature conditions.

PT Triaxial device

The University of Applied Sciences in Rapperswil (HSR) has developed (with Wille AG) a unique testing device, which allows to apply a confining pressure of up to 200 MPa (2'000 bar) and a maximum axial load of 20'000 KN (Fig. 2). The tests can be performed either stress or strain controlled. An outside heating jacket allows to increase the sample's temperature up to 250° C. The apparatus can accommodate samples up to 7 cm in diameter with a corresponding length of 14 cm (Fig. 1a and 1b).

These unique features allow to impose in situ stress and temperature conditions on rock specimen corresponding to depths down to 8 km.



Figure 1a: Granite intact samples from Wassen.



Figure 1b: Tested sample under 200 MPa and 200°C.



Figure 2: High PT triaxial device with heating jacket.

Distributed Fibre Optic measurement

The radial and vertical strains of the rock samples, as well as temperature, are obtained by means of distributed fibre optic measurements. The readings are carry out adopting SWI technology with the commercial device OBR 4600 [1]. The cable is glued to the sample's surface in different geometric shapes (lines, circles and spirals), as shown in Fig. 3. The deformation can be measured over the entire length at 5 mm intervals (resolution) with a precision of 1 micro strain.



Figure 3: Fiber optic instrumented samples.

Assessment of material strength

Drucker-Prager (D-P) and Mogi-Coulomb (M-C) failure criteria are presented in the following equations and depicted in Fig. 4. The M-C surface was calibrated for the Westery Granite ([2]) and the two D-P criteria were fitted for comparison.

As can be seen, the difference is that M-C doesn't depend in the intermediate stress.

$$\tau_{oct} \leq \sigma_{oct}$$

$$\tau_{oct}^{MC} = \tau_{oct}^{DP} = \sqrt{\frac{(\sigma_1 - \sigma_2)^2 + (\sigma_2 - \sigma_3)^2 + (\sigma_1 - \sigma_3)^2}{6}}$$

$$\sigma_{oct}^{MC} = A + B(\sigma_1 + \sigma_3)$$

$$\sigma_{oct}^{DP} = A' + B'(\sigma_1 + \sigma_2 + \sigma_3)$$

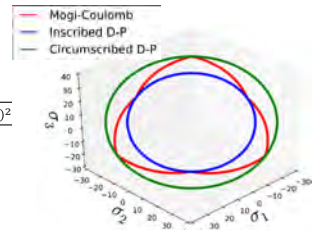


Figure 4: Octahedral-plane comparison.

Fig. 5 shows the difference between τ_{oct} and σ_{oct} ("safety factor"), when considering the criteria depicted in Fig. 4 and the stress from the analytical solution of a borehole in a homogeneous semi-infinite space. As can be seen, the circumscribed D-P can't predict the failure (Fig 5a), instead the safety factor increases with depth. On the other hand M-C apparently predicts a more realistic failure (Fig. 5c) than the inscribed D-P (Fig. 5b).

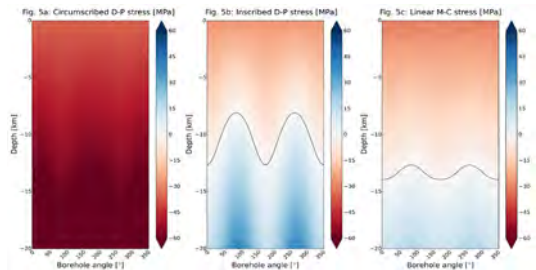


Figure 5a, 5b and 5c: $\sigma_{oct} - \tau_{oct}$ ("safety factor") for D-P and M-C criteria. Black line represent failure.

Radius of influence

Figure 6 and the following equation represent the analytical solution for the temperature of an infinite plane while extracting constant heat at a point, based on real granite properties [3]. As can be seen the temperature gradient will cause additional stresses in the rock mass, therefore it is important to evaluate the borehole stability not only due stress redistribution as a result of the drilling operation but also because of heat flow.

$$T = \frac{q}{4\pi k} \int_{r^2/4Dt}^{\infty} \frac{e^{-u}}{u} du$$

$t = \text{time}$
 $r = \text{distance from the point}$
 $k = \text{thermal conductivity}$
 $D = \text{thermal diffusivity}$

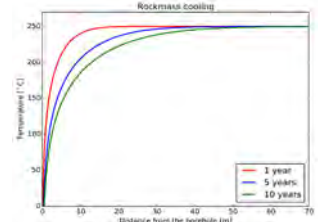


Figure 6: Rock mass temperature evolution.

References

[1] Hauswirth, D. (2015). A Study of the Novel Approaches to Soil Displacement Monitoring Using Distributed Fiber Optic Strain Sensing (Doctoral dissertation, ETH Zurich).
 [2] Al-Ajmi, A. M., & Zimmerman, R. W. (2005). Relation between the Mogi and the Coulomb failure criteria. *International Journal of Rock Mechanics and Mining Sciences*, 42(3), 431-439.
 [3] Kant, M. A. et al. (2017). Thermal properties of Central Aare granite for temperatures up to 500° C: Irreversible changes due to thermal crack formation. *Geophysical Research Letters*, 44(2), 771-776.

Empirical model for the estimation of a Francis turbine complete characteristic curves

J. Gomes, L. Andolfatto, F. Avellan

Motivation

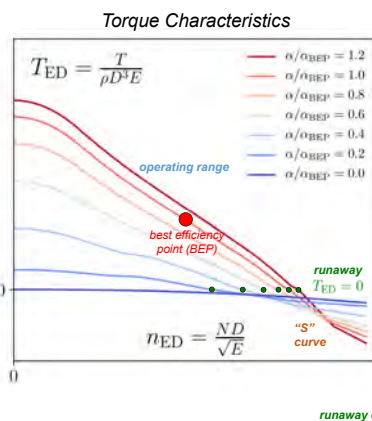
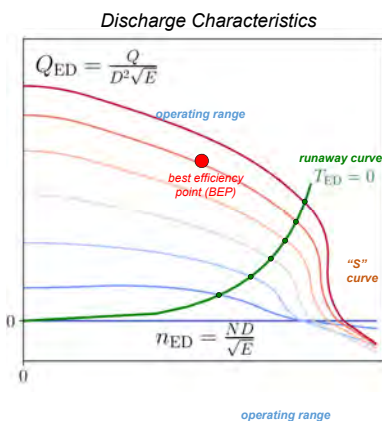
- The **Energy Strategy 2050**: more energy generation from renewable sources;
- In Switzerland, **many hydropower plants can be upgraded or rehabilitated** therefore generating more power with the same amount of water [1];
- Feasibility studies, such as those for upgrading or rehabilitating the power plants, require estimated performance data for turbines that do not exist yet.
- Being able to properly estimate the turbine characteristics and optimize the project from the very beginning is the added-value of this research work

The RenovHydro CTI project no. 19343.1 PFIW-IW will create a **decision making assistant for hydropower project potential evaluation and optimization**.

- 3 years project, started in Dec. 2016;
- Empirical models for the turbine characteristics estimation inside the Work Package 1 (Francis, Pelton and Kaplan turbine types);
- Partners:



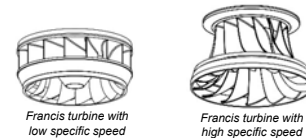
Typical Francis Turbine Characteristics



Methodology

- Data available at the **Laboratory for Hydraulic Machines** is used to defined the parameters of the empirical model.
- The turbine specific speed v and the position of the best efficiency point are used to estimate the complete characteristics.

$$v = n_{ED,BEP} \sqrt{Q_{ED,BEP}}$$



➢ Empirical model to estimate the **normalized guide vanes angle**. Available data is used to define the 10 required parameters through squared error minimization.

➢ The **peak efficiency** value is estimated according to the turbine year of commissioning, specific speed and runner diameter (see ref. [2]).

➢ The empirical model to predict the **runaway curve** where torque is zero contains 6 parameters, also defined through error minimization.

➢ After the runaway curve, 3 possible types of "S" curves are assumed: **stable, critical and unstable**.

➢ Another empirical model estimates the loss in efficiency as the turbine operates away from the **best efficiency point (BEP)**. This empirical model that calculates the **normalized efficiency** is based on the combination of Hermite polynomials and a standardization function.

Legend for ρ : 0.10, 0.15, 0.20, 0.25, 0.30, 0.35, 0.40

Discharge Characteristics are defined

Torque Characteristics are defined

$$T_{ED} = \frac{1}{2\pi n_{ED}} \times Q_{ED} \times \eta_{BEP} \times \frac{\eta}{\eta_{BEP}}$$

Conclusion

By means of a combination of empirical models trained with measurements from a large number of different Francis turbines, a procedure for the estimation of any Francis turbine discharge and torque characteristics has been developed.

This empirical model created inside the RenovHydro Project will be used in an optimization loop that searches for the best combination of electro-mechanical equipment, civil engineering components and ancillary services to be applied to future generating units.

References

- [1] – Association Suisse pour l'Aménagement des eaux, 2012 - *Droit de retour et renouvellement de concession des centrales hydroélectriques*
[2] – Gordon, J. L., 2001. - *Hydraulic Turbine Efficiency*, Canadian Journal of Civil Engineering, 28(2), pp. 238-253

Cavitation modelling in GPU-SPHEROS

Audrey Maertens, Ebrahim Jahanbakhsh, François Avellan

Cavitation in hydraulic machines

- High velocities encountered in hydraulic machines can lead to cavitation.
- Cavitation causes decreased efficiency, vibrations and erosion.
- Cavitation often takes the form of clouds or ropes.
- The collapse of cavitation bubbles locally causes very high pressures that can damage the turbine.

Cavitation vortex ropes in the draft tube of a Francis turbine at part load operation

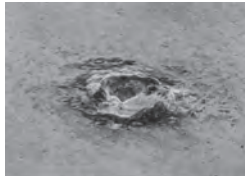


(a) $Q_{ED}/Q_{ED}^* = 0.80$

A. Favrel et al., *Journal of Hydraulic Research*, 2018.



Crater produced by the collapse of a single cavitation bubble in a Francis turbine

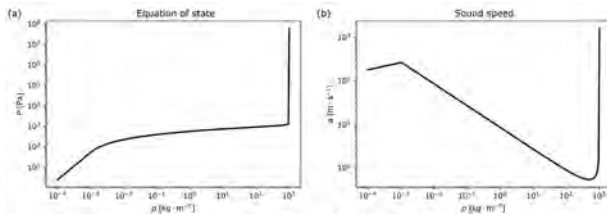


A. Karimi and F. Avellan, *Wear*, 1986.

Barotropic equation of state

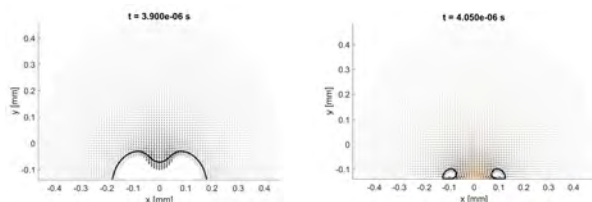
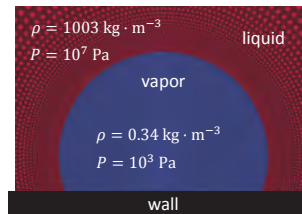
- The influence of thermal effects are omitted.
- A barotropic equation of state (EOS) is constructed as a piecewise function.
- The Murnaghan-Tait equation of state is used for the liquid phase.
- The isentropic gas equation of state is used for the vapor phase.
- The Wallis sound speed for a two-phase mixture is used to define the EOS in the mixture.

$$p(\rho) = \begin{cases} B_v \left(\frac{\rho}{\rho_v} \right)^{\gamma_v} & \text{if } \rho \leq \rho_v, \\ p_l - B_v \gamma_v \ln \left[1 + \frac{B_l \gamma_l}{B_v \gamma_v} \left(\frac{\rho_l}{\rho} - 1 \right) \right] & \text{if } \rho_v < \rho < \rho_l, \\ p_l + B_l \left[\left(\frac{\rho}{\rho_l} \right)^{\gamma_l} - 1 \right] & \text{if } \rho_l < \rho. \end{cases}$$



Bubble collapse near a wall

- Low pressure vapor bubble inside a high pressure fluid attached to a wall.
- Density ratio greater than 1000 is easily handled and sharpness is maintained.
- After initial shrinking of the bubble, a re-entrant micro-jet forms toward the wall and the bubble becomes a ring.
- The collapse of the ring generates a very large pressure with pressure waves that meet in the center.



Riemann formulation for flows with discontinuities

- Cavitating flows are characterized by discontinuities, large density ratios, and shock waves.
- The conservation laws are recast into a Riemann problem:

$$\frac{\partial U}{\partial t} + \nabla \cdot F(U) = \nabla \cdot D(U, \nabla U)$$

- Kurganov's central-upwind scheme is revisited and adapted to FVPM: $\frac{d}{dt} (\bar{U}_i(t) V_i(t)) = - \sum_{j \neq i} H_{ij}(t)$

- Fluxes are computed as: $H_{ij} = G_{ij} \cdot \Gamma_{ij} - G_{ji} \cdot \Gamma_{ji}$

- Where $G_{ij} = \tilde{F}_{ij} - \hat{x}_j \tilde{U}_{ij} - R_{ij} - D_{ij}$ includes:

➤ Conservative flux $\tilde{F}_{ij} = \frac{a_{ij}^+ - \hat{x}_j \cdot n_{ij}}{a_{ij}^+ - a_{ij}^-} F(U_{ij}^+) - \frac{a_{ij}^- - \hat{x}_j \cdot n_{ij}}{a_{ij}^+ - a_{ij}^-} F(U_{ij}^-)$

➤ Conserved variables $\tilde{U}_{ij} = \frac{a_{ij}^+}{a_{ij}^+ - a_{ij}^-} U_{ij}^+ - \frac{a_{ij}^-}{a_{ij}^+ - a_{ij}^-} U_{ij}^-$

➤ Smoothing flux $R_{ij} = \frac{a_{ij}^+ a_{ij}^-}{a_{ij}^+ - a_{ij}^-} (U_{ij}^+ - U_{ij}^-) \otimes n_{ij}$

➤ Dissipative flux D_{ij}

Cavitation cloud through a Venturi tube

- Simulation of a Venturi tube with pressure boundary conditions.
- $P_{in} = 0.6 \text{ MPa}$ and $P_{out} = 0.12 \text{ MPa}$.
- Tube length is 40 mm, diameter gradually decreases from 3.6 mm to 1.19 mm and increases again.
- The constriction causes a flow acceleration and pressure drop, creating a cavitation cloud.
- The cloud detaches and bubble collapses cause pressure spikes.



Task 3.2

Title

Computational energy innovation

Projects (presented on the following pages)

Contact Simulations in Rough Fractures

Cyrill von Planta, Daniel Vogler, Patrick Zulian, Martin O. Saar, Rolf Krause

GPU-accelerated simulation of free jet deviation by rotating Pelton buckets for SmallFlex project

Siamak Alimirzazadeh, Ebrahim Jahanbakhsh, Audrey Maertens, Sebastian Leguizamón, T. Kumashiro, K. Tani, Francois Avellan

Simulations of hydro-mechanical processes based on the Immersed Boundary Method

Cyrill von Planta, Daniel Vogler, Xiaoqing Che, Maria Nestola, Martin O. Saar, Rolf Krause

Toward a Multifidelity method for estimating the influence of overpressure on induced seismicity

Alessio Quaglino, Marco Favino, Dimitrios Karvounis, Stefan Wiemer, Thomas Driesner, Rolf Krause

High-performance C++ code for forecasting induced seismicity

Dimitrios Karvounis, Marco Favino, Patrick Zulian, Andreas Fink, Nur A. Fadel, Stefan Wiemer, Rolf Krause, Thomas Driesner

Adaptive Simulation Methods for Attenuation and Dispersion of Seismic Waves in fractured Media

Marco Favino, Jürg Hunger, Klaus Holliger, Rolf Krause

Towards Multiscale Numerical Simulations of Pelton Turbine Erosion

Sebastián Leguizamón, Ebrahim Jahanbakhsh, Audrey Maertens, Siamak Alimirzazadeh, François Avellan

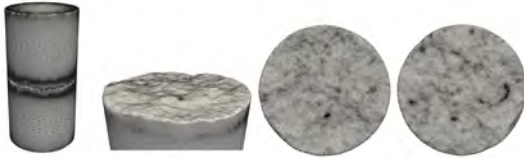
Contact Simulations in Rough Fractures

Cyrril von Planta¹, Patrick Zulian¹, Daniel Vogler², Martin Saar², Rolf Krause¹

¹Institute of Computational Science, Università della Svizzera italiana

²Institute of Geophysics ETH Zurich

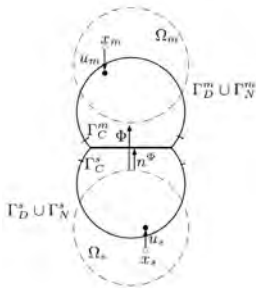
Introduction



The mechanical behavior of fractures in solids, such as rocks, has strong implications for reservoir engineering applications. Deformations, and the corresponding change in solid contact area and aperture field, impact rock fracture stiffness and permeability thus altering the reservoir properties significantly.

Simulation of contact between fractures is numerically difficult. The non-penetration constraints lead to a nonlinear problem and the surface meshes of the solid bodies on the opposing fracture sides may be non-matching. We use a parallel mortar method to resolve the contact conditions between the non-matching surfaces, a three dimensional finite element formulation of linear elasticity and linearized contact conditions.

Linear elasticity and contact



$$\begin{aligned}
 u &:= [u^m, u^s] \\
 -\operatorname{div} \sigma(u) &= f \text{ in } \Omega^s \cup \Omega^m \\
 u_i &= 0 \text{ on } \Gamma_D^s \\
 \sigma_{ij}(u) \cdot n_j &= p_i \text{ on } \Gamma_N^s \\
 \sigma_n &\leq 0 \text{ on } \Gamma_C \\
 \sigma_n(u^m \circ \Phi) &= \sigma_n(u^s) \text{ on } \Gamma_C \\
 [u] &\leq g \text{ on } \Gamma_C \\
 ([u] - g)\sigma_n(u^s) &= 0 \text{ on } \Gamma_C \\
 \sigma_T &= 0 \text{ on } \Gamma_C.
 \end{aligned}$$

Figure: Left: Two-body contact problem. Right: Formulation of linear elasticity and frictionless contact with boundary conditions.

Mortar approach

We use a Mortar approach, in which the test space is dual to the trace space of the finite element space. The non-penetration condition is enforced in a weak sense. The resulting discretization error is local and can be reduced with local refinements.

$$\int_{\Gamma_C^s} ([u] - g)\lambda^t d\gamma \leq 0 \quad \forall \lambda^t \in L,$$

Eq: Weak non-penetration condition over the slave side of the boundary. The condition ensures that the overall jump $[u]$ of the displacements across the fracture is smaller than g , tested against a dual space L of the trace space at the slave boundary.

Enforcing the weak penetration is hard in practice. The nodes of the finite element discretization are non-matching and apart, and must be related to each other using a mortar projection. The parallel assembly of this operator has only become feasible recently with the introduction of the MOONolith library.

Implementation

We implemented the contact simulation using MOONolith, libMesh, PETSc and MOOSE. All components are open source and designed for parallel computing.

Numerical experiments

The simulations ran on 4 nodes (2 x Intel Xeon E5-2650 v3 @ 2.30GHz) with 10 CPU's each, on the cluster of the Institute of Computational Science in Lugano, Switzerland.

Validation

We first validated our method with a Hertzian contact experiment, after Hertz who derived analytical solutions for this problem class in 1881.

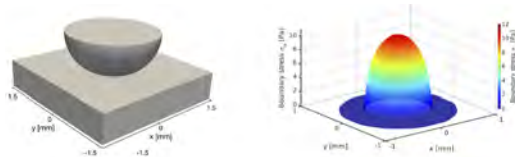


Figure: Hertzian contact; correct methods must replicate the parabolic shape of the boundary stresses σ_n as shown on the right.

Fracture closure

We meshed two rock bodies from granite specimens of the Grimsel test site in Switzerland and applied an increasing load on top of it up to 20MPa in direction of the z-axis. The aim here is to replicate the nonlinear closing behaviour of fractures and to see how our formulation gives insight to interior stresses and the change in aperture distributions.

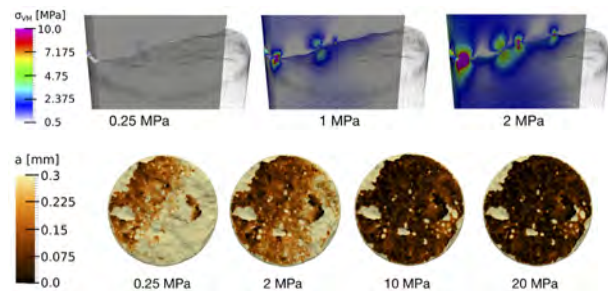


Figure: Top: Von Mises stresses developing inside the rock under increasing confining pressure. Bottom: Aperture fields under increasing normal stresses.

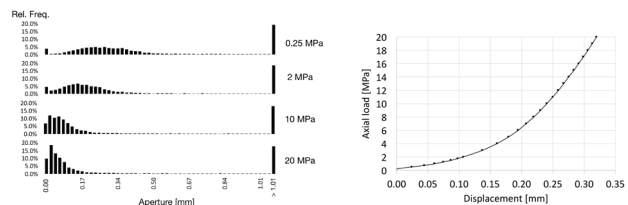


Figure: Left: distribution of aperture fields under increasing pressure. Right: nonlinear closing behavior of the fracture under increasing load.

Outlook

We have developed a parallel contact method using a mortar approach. We now have a tool to simulate contact in rough fractures, the results of which we can further use in Fluid simulations within fractures.

References

Planta, Vogler, Zulian, Saar, Krause, Solution of contact problems between rough body surfaces with non matching meshes using a parallel mortar method, 2018, submitted.

GPU-accelerated simulation of free jet deviation by rotating Pelton buckets for SmallFlex project

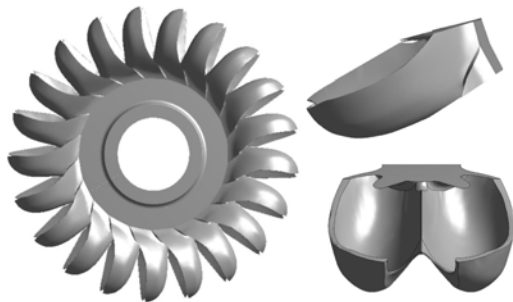
S Alimirzazadeh, E Jahanbakhsh, A Maertens, S Leguizamón, T Kumashiro, K Tani, F Avellan

GPU-SPHEROS

GPU-SPHEROS is a GPU-accelerated particle-based versatile solver based on Arbitrary Lagrangian Eulerian (ALE) Finite Volume Particle Method (FVPM) which inherits desirable features of both Smoothed Particle Hydrodynamics (SPH) and mesh-based Finite Volume Method (FVM) and is able to simulate the interaction between fluid, solid and silt [1]. With GPU-SPHEROS, the goal is to perform industrial size setup simulations of hydraulic machines.

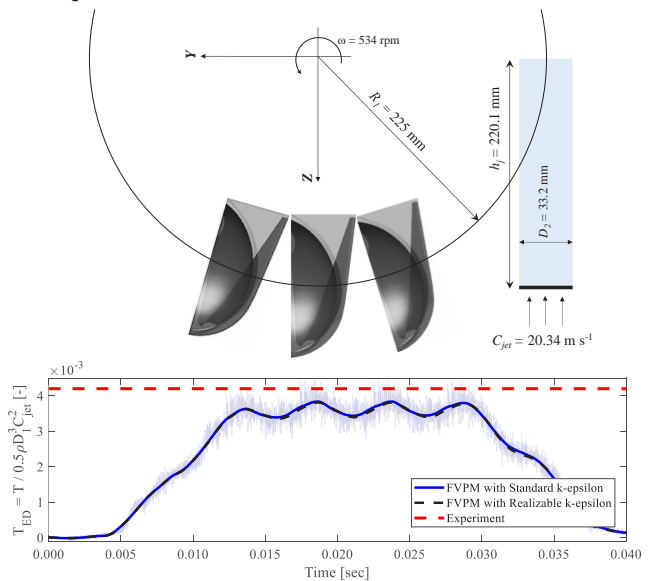
SmallFlex Project

Small hydropower plants are expected to produce a large share energy by 2050. The SmallFlex project is **demonstrator for flexible Small Hydropower Plants** (SHPs) and aimed to investigate the eco-compatible winter peak energy production by them. SmallFlex has been integrated in the activities of the SCCER-SoE [2]. A Pelton turbine is being simulated in different operating points with our in-house GPU-accelerated software, GPU-SPHEROS to predict the Pelton efficiency, torque and powerplant flexibility. Here is the geometry:



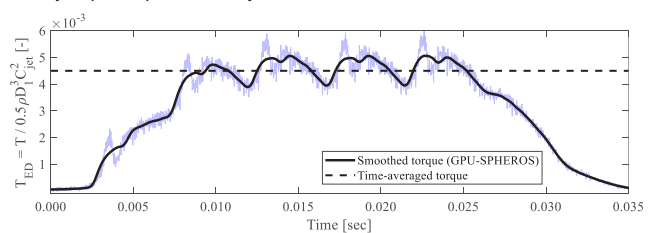
Validation for rotating Pelton turbine

- The torque generated by rotating Pelton turbine bucket has been validated by the torque measurements for a Pelton geometry with available experimental data.
- Two-equation Boussinesq-based RANS turbulence models have been integrated with FVPM as an ALE method.



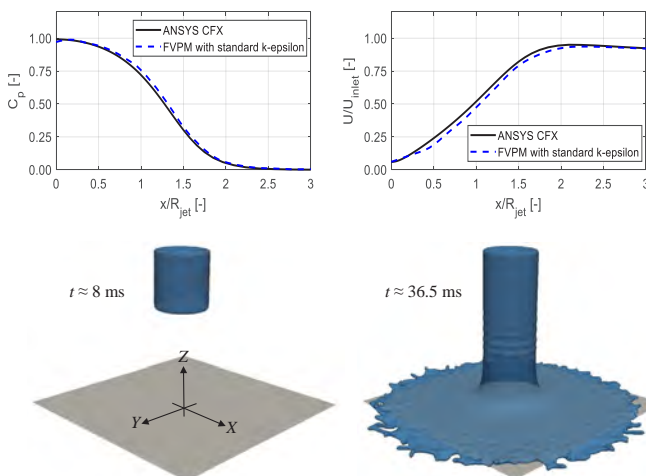
SmallFlex Pelton turbine

- A Pelton turbine has been simulated for its best efficiency point (BEP) with GPU-SPHEROS and the torque has been predicted.
- Off-design conditions are being simulated to evaluate turbine efficiency and hydropower plant flexibility.



Validation for turbulent impinging jet on a flat plate

- Turbulent fluid jet impinging on a flat plate (a similar case to a jet deviation by rotating Pelton turbine buckets) has been simulated as a validation test case ($C_{jet} = 19 \text{ m}\cdot\text{s}^{-1}$ and jet inlet is located at $Z_{jet} = 4x_{D_{jet}}$ while plate is located at $X-Y$ plan).
- Both the pressure and velocity are in a good agreement with ANSYS-CFX finite volume/element solver results.
- The software has been then used to simulate of free jet deviation by SmallFlex rotating Pelton buckets.



References

S Alimirzazadeh, E Jahanbakhsh, A Maertens, S Leguizamón, F Avellan, GPU-Accelerated 3-D finite volume particle method, *Computers & Fluids*. 171 (2018) 79–93
C Münch, P Manso, C Weber, M Staehli, M Schmid, C Nicolet, F Avellan, A Schleiss, J Derivaz, SmallFlex: Demonstrator for flexible Small Hydropower Plant, SCCER-SoE Annual Conference 2017

Simulations of hydro-mechanical processes based on the Immersed Boundary Method

Cyrrill von Planta(1), Daniel Vogler(2), Xiaoqing Chen(2), Maria GC Nestola(1), Martin O. Saar(2), Rolf Krause(1)

1)Institute of Computational Science, Università della Svizzera italiana, Lugano, 6900, Switzerland
2)ETH Zurich, Institute of Geophysics, 8092 Zurich, Switzerland

Motivation

Hydro-mechanical (HM) processes in rough fractures are highly **nonlinear** and govern productivity or associated risks in a wide range of reservoir engineering problems.

To enable high-resolution simulations of HM processes in fractures, we present an **immersed boundary method** to compute the fluid flow between rough fracture surfaces and adopt a **variational parallel transfer operator** to couple the fluid and the solid subproblem.

We simulate both the incompressible **fluid flow** and the **solid structure** in a Finite Element framework. The structural fractures are modelled as a **linear elastic material** by using **unstructured meshes** embedded into **structured fluid grids**.

The **fluid and the solid solvers are coupled by transferring fluid velocities, pressure field and surface forces** between the structured and the unstructured meshes by means of variational transfer operators.

Fictitious Domain Method

- The **solid phase** is embedded in the **Fluid phase**
- **Eulerian Formulation** (Fixed Grid) for the fluid flow
- **Lagrangian Formulation** for the solid structure

Find $(u_f, p_f; \eta_s, p_s; \lambda) \in (V_f \times Q_f \times V_s \times Q_s \times L)$ such that

$$\int_{\Omega_f} \rho_f \frac{\partial u_f}{\partial t} \cdot v_f dV + \int_{\Omega_f} \rho_f [(u_f \cdot \nabla) u_f] \cdot v_f dV + \int_{\Omega_f} \sigma_f \cdot v_f dV - \int_{\mathcal{I}} \lambda \cdot v_f dV = 0$$

$$\int_{\Omega_s} q_f \nabla \cdot u_f dV = 0$$

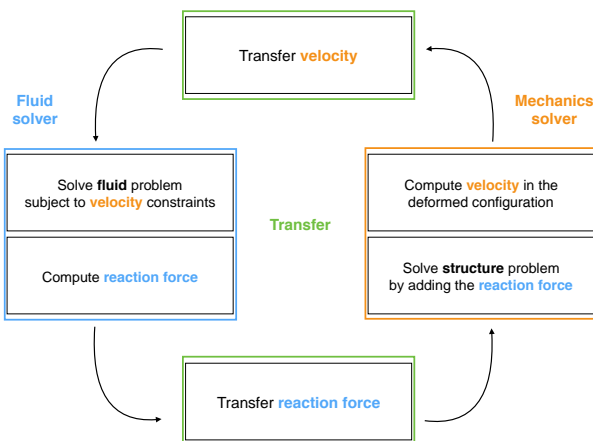
Transfer $\rightarrow \int_{\mathcal{I}} \mu \cdot \left(\frac{\partial \eta_s}{\partial t} - u_f \right) dV = 0$

$$\int_{\Omega_s} \hat{\rho}_s \frac{\partial^2 \eta_s}{\partial t^2} \cdot \hat{v}_s + \int_{\Omega_s} \hat{P}(\hat{F}) : \nabla \hat{v}_s dV - \int_{\Omega_s} \hat{\rho}_s \hat{J} \hat{F}^{-T} : \nabla \hat{v}_s dV + \int_{\mathcal{I}} \lambda \cdot \hat{v}_s dV = 0$$

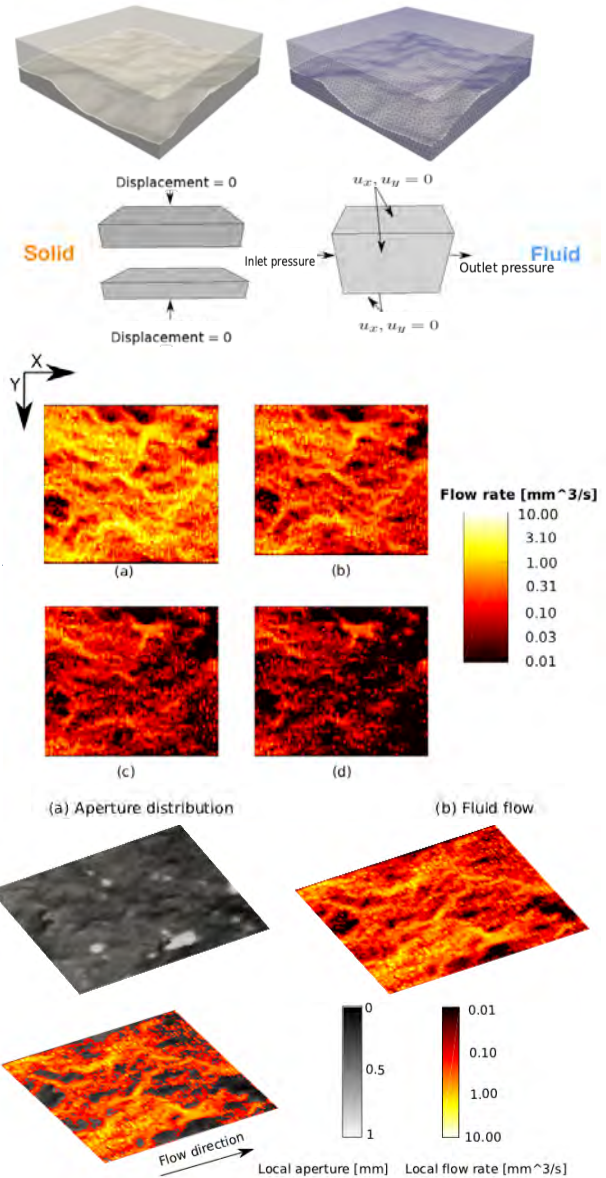
$$\int_{\Omega_s} (\hat{J} - 1) q_s dV = 0$$

for all $(v_f, q_f; v_s, q_s; \mu) \in (V_f \times Q_f \times V_s \times Q_s \times L)$, where $\mathcal{I} = \Omega_s \cap \Omega_f$

Fixed point iteration



Results



Discussion

The numerical experiments with real fracture geometries show that the approach is able to resolve the boundary of the rough fracture surface into the fluid and also to simulate the change of the fluid flow paths within the fractures under increasing normal loads.

References

An immersed boundary method based on the L2-projection approach. Maria Giuseppina Chiara Nestola, Barna Becsek, Hadi Zolfaghari, Patrick Zulfian, Dominik Obrist, and Rolf Krause. Proceedings of the 24th International Conference on Domain Decomposition Methods, 2018.

A Parallel Approach to the Variational Transfer of Discrete Fields between Arbitrarily Distributed Unstructured Finite Element Meshes. Rolf Krause and Patrick Zulfian. SIAM Journal on Scientific Computing, 2016.

Toward a Multifidelity Method for Estimating the Influence of Overpressure on Induced Seismicity

Alessio Quaglini, Marco Favino, Dimitrios Karvounis, Claudio Tomasi, Stefan Wiemer, Thomas Driesner, Rolf Krause

Motivation: the FASTER project

Induced seismicity hazard from Enhanced Geothermal Systems (EGS) needs to be reliably forecasted. The Swiss Seismological Service (SED) has developed a hybrid 3D-2D model that forecasts induced seismicity in EGS. The fracture distribution in the subsurface is only known in a stochastic sense, hence to evaluate the seismic hazard, in terms of the seismic events number and magnitude, several fracture distributions have to be simulated with a Monte Carlo approach. While fast solution methods are necessary to solve each single sample, Multifidelity and Multilevel Monte Carlo methods are necessary for accelerating the convergence of the expectation of the number of seismic events. The idea behind these methods is to employ surrogate models which are computationally cheaper but also well-correlated with the detailed one. The project FASTER arises from a strong collaboration between SED, ETH Zurich, USI-Lugano, and the Swiss National Supercomputing Center (CSCS), in order to improve the simulated model, the solution algorithms, and their software implementation.

Models and Methods

Balance of mass leads to a set of diffusion equations

$$c \frac{\partial p}{\partial t} = \nabla \cdot K \nabla p + q \quad \text{background}$$

$$c \frac{\partial p_i}{\partial t} = \nabla \cdot K_i \nabla p_i + q_i, \quad i \in A \quad \text{Triggered fractures}$$

$$q = \sum q_i$$

Diffusion equation in a fracture is solved only when the fracture has been triggered: pressure in its hypocenter exceeds a "sliding condition".

- Discretization is based on
- finite volume method;
 - semi-implicit Euler schemes.

UQ problem

Interested in number of seismic events and maximum magnitude

Example 3D:

- Monte Carlo with 250 samples
- In particular, magnitude > 3.5
- 75 simulations out of 250 (30%)
- With ~250 samples, RMSE is 1% of the mean

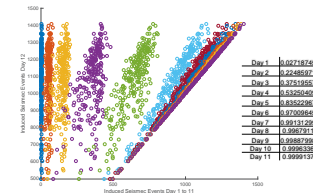
Can we reach the same accuracy with less effort?

Multifidelity Monte Carlo

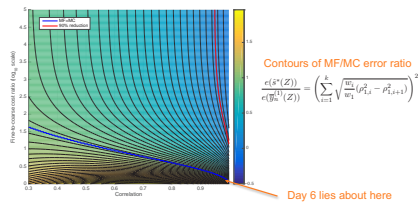
	Single-fidelity	Multi-fidelity [Peherstorfer15]
(Co)Variance	$\sigma_z^2 = \text{Var}[f^{(1)}(Z)]$	$\rho_{i,j} = \frac{\text{Cov}[f^{(i)}(Z), f^{(j)}(Z)]}{\sigma_i \sigma_j}$
Estimator	$\bar{y}_m^{(1)} = \frac{1}{m} \sum_{j=1}^m f^{(1)}(z_j)$	$\hat{s} = \frac{1}{m_1} + \sum_{i=2}^k \alpha_i \left(\bar{y}_{m_i}^{(i)} - \bar{y}_{m_{i-1}}^{(i-1)} \right)$
Cost	$c(\bar{y}_m^{(1)}(Z)) = w_1 m$	$c(\hat{s}(Z)) = \sum_{i=1}^k w_i m_i = w^T m$
MSE	$e(\bar{y}_m^{(1)}(Z)) = \frac{\sigma_z^2}{m}$	$\frac{\sigma_z^2}{m_1} + \sum_{i=2}^k \left(\frac{1}{m_{i-1}} - \frac{1}{m_i} \right) (\alpha_i^2 \sigma_i^2 - 2\alpha_i \rho_{i,i-1} \sigma_i \sigma_{i-1})$
Optimal allocation of budget p	$m = p/w_1$	Minimize MSE w.r.t. m and α at fixed cost p

Surrogate models

1) Shorter final time



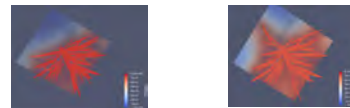
Despite the good correlation, the error is higher than standard MC



2) Space-time coarsening

Correlation between high- and all low-fidelity models

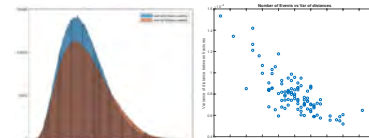
- $\rho_{12} = 0.8654$ (1 level of coarsening) – cost 1/4
- $\rho_{13} = 0.8433$ (2 levels of coarsening) – cost 1/16
- $\rho_{14} = 0.7496$ (3 levels of coarsening) – cost 1/64



3) 0D model

correlation between distances of hypocenters and seismic events

- $\rho_{15} = 0.7574$ (0D model) – cost negligible



Best combination of 2 models

- High-fidelity + 0D = error reduced to 43%

Best combination of 3 models

- High-fidelity + 2 levels of coarsening + 0D = error to 40%

Conclusions

- more statistical analysis on the fracture networks may lead to better surrogates
- extension to 3d is under development
- better solver to achieved desired mesh resolution

References

Dimitrios C. Karvounis, Valentin S. Gischig, Stefan Wiemer, Towards a Real-Time Forecast of Induced Seismicity for Enhanced Geothermal Systems, Shale Energy Engineering 2014
 Karvounis, D. C., & Jenny, P. (2016). Adaptive Hierarchical Fracture Model for Enhanced Geothermal Systems. Multiscale Modeling & Simulation,
 Karvounis, D. C., & Wiemer, S. (2015). Decision making software for forecasting induced seismicity and thermal energy revenues in enhanced geothermal systems. Proceedings World Geothermal Congress 2015
 B. Peherstorfer, K. Wilcox, M. Gunzburger, Optimal model management for multifidelity Monte Carlo estimation, SIAM J. Sci Comp, 2015

High-performance C++ code for forecasting induced seismicity

Dimitrios Karvounis, Marco Favino, Patrick Zulian, Andreas Fink, Nur A. Fadel, Stefan Wiemer, Rolf Krause, Thomas Driesner

FASTER project

For the safe implementation of the Energy Strategy 2050, induced seismicity hazard from Enhanced Geothermal Systems (EGS) needs to be reliably forecasted and the electricity produced needs to be maximized for the affordable hazard. To this end, the Swiss Seismological Service (SED) has developed a 3D hybrid model, which consists of a stochastic and a deterministic part, and forecasts both induced seismicity and produced electricity in EGS. Main aim of the FASTER project is these forecasts to be concluded in almost real time. The project started approximately one year ago, it will last three years, it is funded by the Platform for Scientific Computing (PASC), and it brings together researchers from ETH Zurich, SED, USI university, and the Swiss National Supercomputing Center (CSCS). A speedup of approximately 670 times has been achieved up to now from optimizing the coding and employing more efficient algorithms.

Forecasting induced seismicity with the 3D hybrid model

The hybrid model consists of HFR-Sim and of the so-called "Seed model". HFR-Sim is the in-house EGS simulator of ETH Zurich that can deterministically model flow and heat transport in a fractured reservoir. The "Seed model" is a stochastic modelling approach for seismicity, where a large number of fractures and of potential seismic events along these fractures is sampled for each simulation of the MC integration, and the pore-pressure value that triggers each of the events is computed ("Seed setup"). At each time step of the hybrid simulation are called:

1. The Solver: HFR-Sim approximates the solution of pore-pressure diffusion inside the fractures, the well and the matrix surrounding the fractures. Necessary input the considered injection strategy.
2. Seed Update: The stochastic model locates the seeds triggered with the current deterministic solution and updates the HFR-Sim model accordingly.

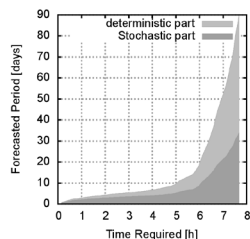
Final outputs of the hybrid model are a synthetic catalogue of induced seismicity, as well as a network of discrete fractures. With the latter as necessary input, the expected power generated due to the considered injection strategy can be estimated and the stimulation of an EGS can be optimized.

Accelerating the stochastic part

Significant speedup, which reaches up to two orders of magnitude, is achieved by pre-processing the sampled Seeds during their setup and not repeating time-costly searches over the set of all seeds for each new time step. During setup, the sampled seeds are divided into subsets according to their location. The subsets, where induced seismicity is possible, are located at each time step, and only the seeds of these subsets are updated. Triggered seeds are collected and are sorted by the order with which they were sampled, before the HFR-Sim model is updated. The latter sorting is necessary only for comparing the new optimized code with its initial version; i.e. the sorting ensures identical outputs between the two codes.

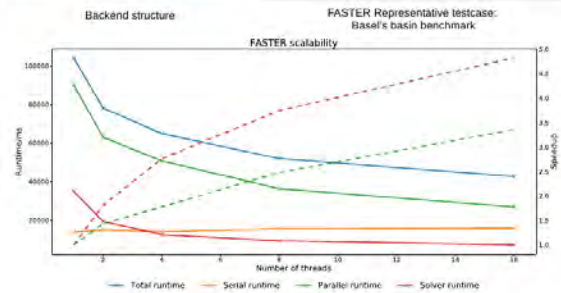
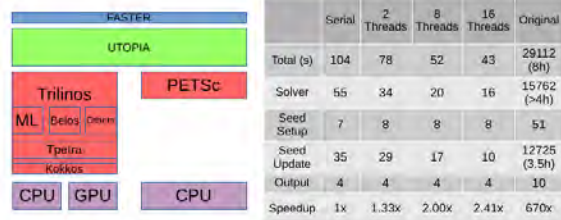
Further acceleration has been achieved by:

1. coupling the code with the Eigen library.
2. Employing features introduced with c++11 (e.g. enumerators)
3. Resolving computational bottlenecks during the updating of the HFR-Sim mesh.
4. Employing the Counter-Based Random123 Number Generators, instead of the sprng library.



preFASTER representative testcase: Basel's basin benchmark

Accelerating the deterministic part



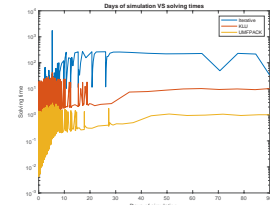
Comparison of performance of solution methods

Due to the structure of the stiffness matrices, naïve application of efficient solution methods, such as algebraic multigrid (AMG), is not trivial. While good convergence rates of AMG have been obtained in the early times of simulation, performances degraded when fractures were added, resulting in a total solution time of more than 4 hours.

Given the relative small size of the linear system, direct solution methods have also been tested, in particular:

- KLU (direct solver of Trilinos) and
- UMFPACK, which implements an Unsymmetric MultiFrontal method.

The first one allowed to reduce the solution time to approx. 2 hours, while the latter to 8.8 minutes.



	ML	KLU	UMFPACK
Mean solving time per time step	24.44 s	7.84 s	0.71 s
Total time for numerical solving	4.3 h	1.63 h	8.84 m (530.6 s)
Mean residual per time step	5.4207e-05	1.7455e-10	6.2338e-10

Discussion

FASTER is about to complete its first year and almost three orders of magnitude speedup is achieved in forecasting induced seismicity. Current run times allow the integration of the software in the Adaptive Traffic Light System (ATLS) of SED, where ATLS plans to assist in real time the operators of EGS to safely achieve the targets of Energy 2050. Due to the improved runtime, finer scenarios can be studied and fundamental research on induced seismicity can be performed at length scales that were previously prohibitive.

Possible next steps in this agile project include accelerating the convergence of the non-symmetric linear system solvers, improving accuracy with adaptive mesh refinement approaches, employing Multi Level Monte Carlo approaches for uncertainty quantification, the Phase Field Method for modeling microseismicity, and validating the analytical model of the code with real experimental data.

Adaptive Simulation Methods for Attenuation and Dispersion of Seismic Waves in fractured Media

Marco Favino^{1,2}, Jürg Hunziker², Klaus Holliger², Rolf Krause¹

¹Institute of Computational Science, Università della Svizzera italiana
²Institute of Earth Sciences, University of Lausanne

Motivation

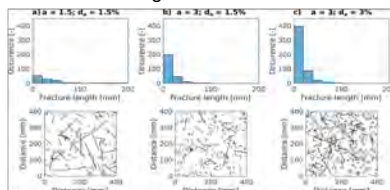
Numerical simulations of seismic waves in fractured rocks can result in significant advances for the indirect characterization of such environments. In fact, attenuation and modulus dispersion are due to fluid flow induced by pressure differences between regions of different compressibilities. Understanding these mechanisms in fractured rocks may provide information not only on fracture density but also on fracture connectivity. The main bottlenecks for these kinds of simulations are:

- mesh generation: the creation of computational grids which resolve numerous and complex interfaces still remains a tedious and time-consuming task, which requires a highly degree of human interaction.
- solution of the Finite Element (FE) system due to its complicated structure, the large jumps in the material parameters, the complex nature of the variables in the frequency domain.

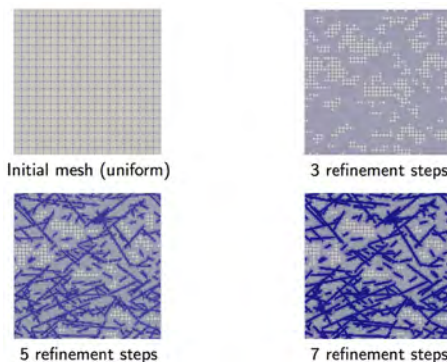
Methods

To enable a fast and easy meshing procedure of complex fracture networks, we developed a novel strategy based on adaptive mesh refinement (AMR) (Favino et al., 2018). The strategy has been implemented in MOOSE. In particular, the new app Parrot has been developed to simulate Biot's equations (Biot, 1941) in the time-frequency domain and to study attenuation and modulus dispersion of seismic waves caused by fluid pressure diffusion in heterogenous materials. MOOSE has also been extended in order to work with complex variables and hence to speed-up the solution process when parallel direct solvers are employed. The strategy comprises the following steps:

1. Generation of a natural fracture networks, e.g. using a power-law distribution for fractures lengths



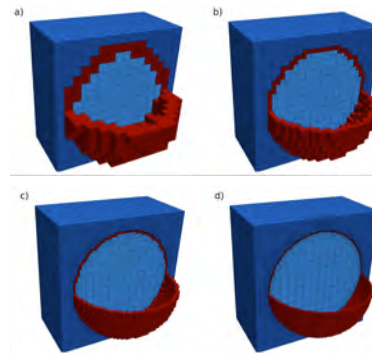
2. Adaptive mesh refinement (AMR) starting from a uniform coarse mesh



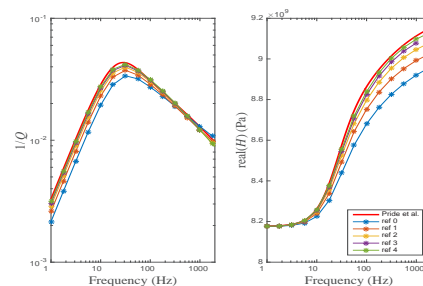
3. Solution of the linear system: the generated mesh is used to solve Biot's equations. The different levels can be employed in a multigrid solution process. The library MOONLith allows for the parallel transfer between arbitrarily distributed meshes.

Validation

To show the effectiveness of our approach, we consider the problem of a spherically shaped inclusion. For this problem, an analytical solution has been provided by Pride et al. (2004). Starting from a coarse mesh 16x16x16, we applied 6 AMR steps.



Convergence



Discussion

The AMR approach allowed to reproduce the predicted attenuation and dispersion curves with a moderate number of unknowns compared to a uniform refinement strategy (3M vs 135M). In particular, it confirmed the importance of refining meshes at the interfaces where numerical inaccuracies are concentrated. The discretization of Biot's equations with complex FE allowed to reduce the computational cost by a factor of 4 with respect to a real FE implementation, employing a parallel direct solver (MUMPS). The simulation time is about 3-4 minutes per simulated frequency.

References

Biot, M. A., General theory for three-dimensional consolidation, Journal of Applied Physics, (1941), 12, 155–164.
Hunziker, J., Favino, M., Caspari, E., Quintal, B., Rubino, J. G., Krause, R., and Holliger, K., Seismic attenuation and modulus dispersion in porous rocks containing stochastic fracture networks, Journal of Geophysical Research (2017).
Marco Favino, Jürg Hunziker, Eva Caspari, Beatriz Quintal, Klaus Holliger, Rolf Krause, Fully-Automated Adaptive Mesh Refinement for the Simulation of Fluid Pressure Diffusion in Strongly Heterogeneous Poroelastic Media, Journal of Computational Physics (2018, under review).
Pride, Berriman, Harris, Seismic attenuation due to wave-induced flow, Journal of Geophysical Research, (2004), vol. 109.

Towards Multiscale Numerical Simulations of Pelton Turbine Erosion

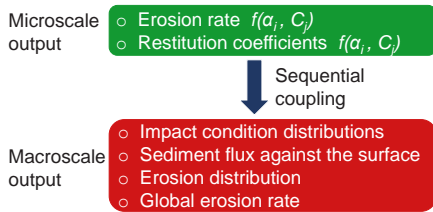
Sebastián Leguizamón, Ebrahim Jahanbakhsh, Audrey Maertens, Siamak Alimirzazadeh, François Avellan

Motivation and Problem Description

The hydro-abrasive erosion of turbomachines is a **significant problem** worldwide. In the context of the Energy Strategy 2050, it is a problem which will become **more severe in the future** due to the retreat of glaciers and permafrost caused by **climate change**. Our objective is to provide the **capability of simulating** the erosion process using the Finite Volume Particle Method [1]. Such simulations will become **advantageous** for the **design** and the **operation** of the machines. The erosion of hydraulic turbomachines is an **inherently multiscale process**, so its simulation is complicated. It demands a multiscale modeling approach.

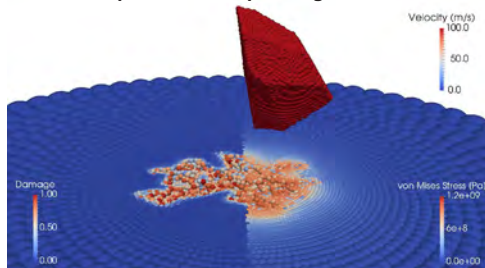
Multiscale Coupling and Validation

A multiscale model has been formulated and then validated [1]. It encompasses two submodels to tackle the multiscale character of the problem.



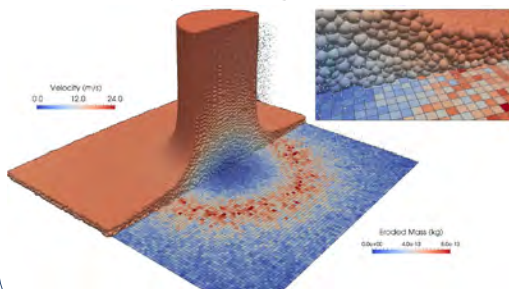
In the **Microscale Model** we perform detailed impact simulations that take into consideration all the important physical effects. This results in the **erosion rate** for each impact condition.

Sharp Sediment Impacts against Solid



In the **Macroscale Model** the turbulent sediment transport is computed. Each time a sediment impact is detected, the results of the microscale model are used, resulting in the macroscopic **erosion accumulation**.

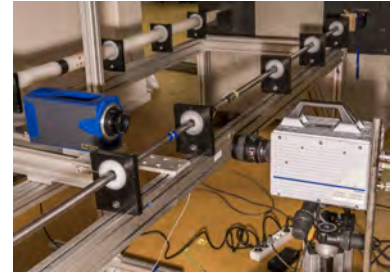
Slurry Jet Eroding a Flat Plate



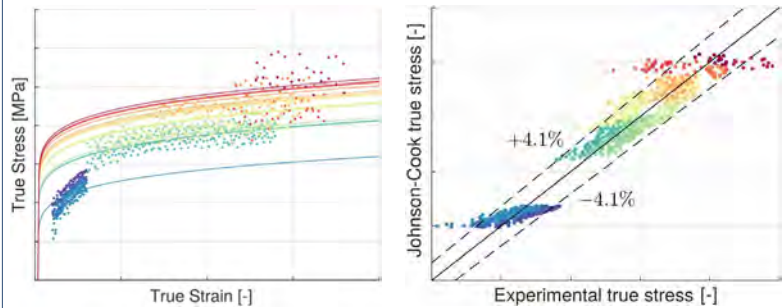
Material Characterization

To perform realistic multiscale simulations of the erosion of turbines it is necessary to perform a characterization of the material: **stainless steel 13Cr-4Ni**. A combination of quasi-static tension tests and split-Hopkinson tension bar tests is used to find the parameters of the **Johnson-Cook Model** that best describe the material behavior. A **genetic algorithm** was programmed to find the optimum set of model parameters that fit the experimental data obtained.

Split-Hopkinson Bar Experiment

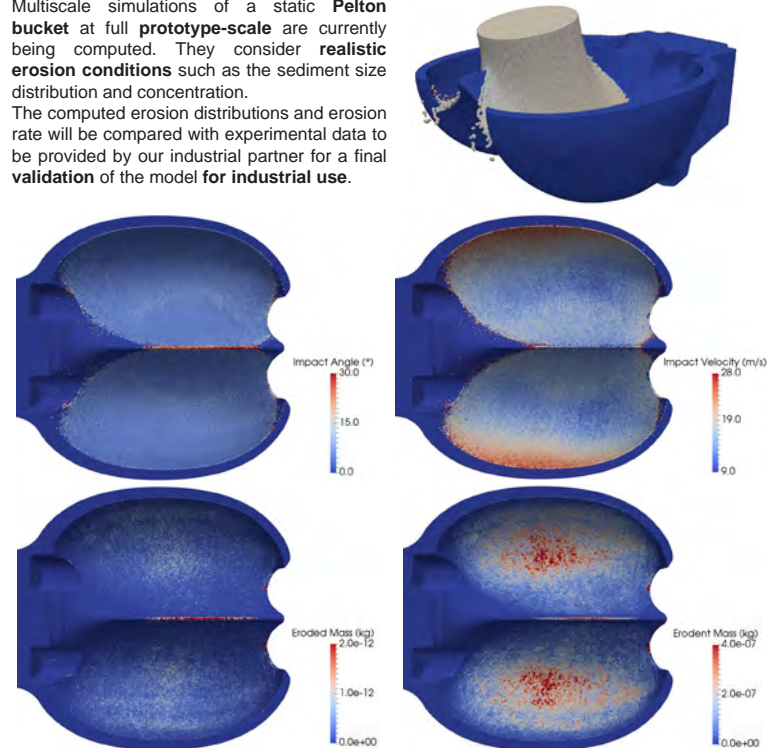


High Strain-Rate Material Response and Johnson-Cook Model Fit



Multiscale Erosion Simulation of a Pelton Bucket

Multiscale simulations of a static **Pelton bucket** at full **prototype-scale** are currently being computed. They consider **realistic erosion conditions** such as the sediment size distribution and concentration. The computed erosion distributions and erosion rate will be compared with experimental data to be provided by our industrial partner for a final **validation** of the model for **industrial use**.



References

[1] S. Leguizamón, E. Jahanbakhsh, A. Maertens, S. Alimirzazadeh and F. Avellan, A multiscale model for sediment impact erosion simulation using the finite volume particle method, *Wear* 392-393 (2017).

Work Package 4: Future Supply of Electricity

The transformation of the Swiss energy system as envisaged within the Energy Strategy 2050 is far more than just a technological challenge for hydropower and geothermal energy. WP4 addresses therefore a variety of related aspects such as:

- risks, safety and societal concerns,
- new emerging energy technologies, and
- the integration within the overall energy system.

Within this broader perspective sustainability and security of supply aspects need to be addressed, conflicting objectives and potential trade-offs analyzed and resolved by means of risk-cost benefit analysis, Multi-Criteria Decision Aiding processes, long-term energy economic modeling, and consideration of socio-economic and political drivers.

Technical Highlights 2018

Risk, safety and societal acceptance for geoenergy and hydropower

The induced seismicity risk governance framework has been further developed by quantifying the trade-off between seismic safety and security of supply. This was done by developing a meta-model that includes analytical models for energy production, pricing (levelized cost of electricity), seismic risk and stakeholder behaviour (using Cumulative Prospect Theory to assess both loss and risk aversions). The risk analysis in the hydropower domain focused on the probabilistic analysis of historical dam accidents and the systematic uncertainty quantification (UQ) in the modelling of dam-break consequences.

Global observatory of electricity resources

The final report on “Potential, costs, and environmental effects of electricity generation technologies” has been released. The report provides a comprehensive evaluation of technology-specific potentials, costs and environmental effects of domestic and import electricity generation options for Switzerland up to 2050. A Multi Criteria Decision Analysis (MCDA) tool was developed to assess the sustainability of potential areas for deep geothermal energy (DGE) systems in Switzerland. Preliminary results show that (1) a higher sustainability index is mainly found in the northeastern part of Switzerland, and (2) different weighting profiles can influence performance of both plant type and area.

Energy-economic modelling and socio-political drivers

Various approaches were developed and applied to specific problems related to the Swiss energy transition: An electricity market model (BEM, cross-border electricity market model) to understand price-formation and investments is now fully operational. It can run in different modes: (i) with endogenous investment and production decision or with fixed investments, (ii) single scenario or stochastic mode, and (iii) social welfare maximization or profit maximization. New EU decarbonisation scenarios were analysed using the updated EU electricity investment and dispatch model EUSTEM. A further modelling approach studied the possibility of a fully renewable Switzerland. This goal appears achievable without having to increase electricity import significantly, and the current grid infrastructure is sufficient under the assumption of a reasonable mix of wind and photovoltaic generation.

Joint activities

Work within the Joint Activity IDEA (Integrated Development Processes for Hydropower and Deep Geothermal Projects: Regulatory, Political and Participatory Perspectives) focusses on the “less-technical” aspects of the energy transition such as the challenges experienced by the various actors in the energy arena. Media analysis and stakeholder interviews revealed that despite the current difficulties of hydropower, the economic situation is not seen as a long-term threat. Within the Joint Activity Scenarios & Modelling (JASM) the modelling teams of the eight SCCER work together to generate scenarios for a Swiss energy system in 2050 that cuts CO₂ emissions from today's 38 MTCO₂/a to 10 MTCO₂/a. First results are available and confirm the importance of sector coupling for achieving the Swiss climate targets.

Task 4.1

Title

Risk, safety and societal acceptance

Projects (presented on the following pages)

Reservoir stimulation's effect on depletion-induced seismicity

Barnaby Fryer, Gunter Siddiqi, Lyesse Laloui

Increase of the EGS levelized cost of electricity, or the financial cost of public safety

Arnaud Mignan, Dimitrios Karnouvis, Marco Brocardo

JA IDEA-HG: Initial version of recommendations for regulating & governing DGE seismic risk

Arnaud Mignan, Goran Seferovic

Probabilistic Fatigue Model for predicting plaster cracks on unreinforced masonry walls caused by induced seismic hazard

Giuseppe Abbiati, Marco Brocardo, Adrian Gabbi, Nebojsa Mojsilović, Milos Petrović, Max Didier, Bozidar Stojadinović

From a "steam monster" to energy projects: moving forward to geothermal social acceptance in Chile

Sofía Vargas Payera

Optimal PV and Wind Locations for an Efficient & Renewable Swiss Power System

Bert Kruyt, Annelen Kahl, Stuart Bartlett, Jérôme Dujardin, Michael Lehning

Comprehensive Historical Accident Data for Comparative Risk Assessment of Energy Technologies

Peter Burgherr, Wansub Kim, Matteo Spada, Anna Kalinina, Stefan Hirschberg

Mapping the landscape of participation in Geneva

Franziska Ruef, Michael Stauffacher, Olivier Ejderyan

Semiotic analysis of technoscientific promises in geothermal energy

Olivier Ejderyan

Framing geothermal energy in the UK: a media analysis

Xue Xu, Olivier Ejderyan, Michael Stauffacher

Application of the Polynomial Chaos Expansion for uncertainty quantification of the flood wave propagation resulting from a concrete dam break

Anna Kalinina, Matteo Spada, Peter Burgherr, Christopher T. Robinson

Quantitative assessment of uncertainties and sensitivities in life loss estimates due to an instantaneous dam-break

Anna Kalinina, Matteo Spada, Peter Burgherr, Christopher T. Robinson

Toward a new framework for chemical risk assessment in the context of accidental events in deep geothermal energy (DGE) systems

Matteo Spada, Peter Burgherr

Understanding social perception of geothermal energy in Chile
Amanda Martinez Reyes, Sofia Vargas Payera, Olivier Ejderyan

Application to the Swiss Alps of the Landslide Generic Cellular Automaton (LSgCA)
Ahoura Jafarimanesh and Arnaud Mignan

Reservoir stimulation's effect on depletion-induced seismicity

Barnaby Fryer, Gunter Siddiqi, Lyesse Laloui

barnaby.fryer@epfl.ch

Motivation

Fluid production can induce earthquakes by inducing total stress changes [1]. In the conservation of momentum equation, it is the gradient of pore pressure which induces these stresses. A smaller pore pressure gradient leads to smaller induced stresses. Darcy's Law tells us that higher permeabilities will require smaller pore pressure gradients to produce an amount of fluid. Therefore, can we manipulate permeability to reduce the pore pressure gradient required to produce fluid and thereby reduce the induced stresses and seismicity associated with fluid production?

In this work, we will be using a hydraulic fracture near the well to reduce the seismicity rate far from the well.

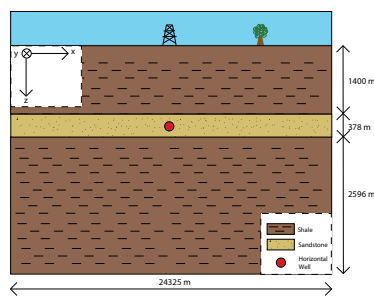
Methods

Poroelastic reservoir simulator

Seismicity rate predicted based on [2,3] using:

$$\frac{dR}{dt} = \frac{R}{t_a} \left(\frac{\dot{\tau}}{\dot{\tau}_0} - R \right)$$

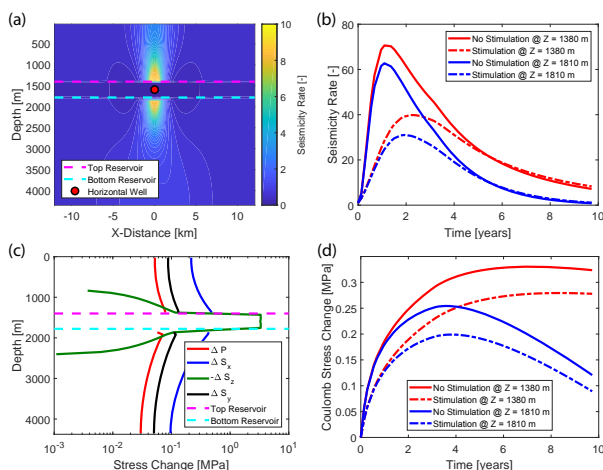
Hydraulic fracture simulated using standard field results from literature. Results in high permeability region near well



Stimulation's effect on seismicity

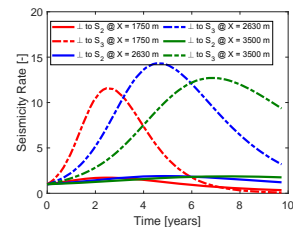
Reverse faulting stress regime example ($S_{Hmax} > S_{Hmin} > S_V$):

- a) Seismicity rate with no hydraulic fracturing
- b) Seismicity rate comparison above and below reservoir for the case with and without hydraulic fracture
- c) Stress changes in-line with well when no fracture
- d) Difference in Coulomb stress when fractured

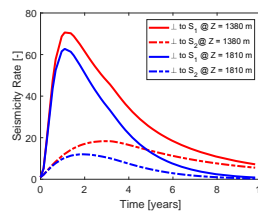


Wellbore orientation

Because stress changes are not independent of direction, there are implications for horizontal well orientation. On the right it is clear that drilling a well parallel to S_{Hmax} in a normal faulting stress regime would result in a higher seismicity rate. This is because the stress changes are larger perpendicular to the well. If S_3 is perpendicular to the well, a larger amount of tension in this direction increases differential stress, worsening seismicity rate.



The same reasoning applies to reverse faulting stress regimes. Drilling parallel to S_{Hmax} in this case would reduce the seismicity rate. This is because the largest compression above and below the reservoir is happening in the direction perpendicular to the well. S_1 is horizontal in this case, and so it is not ideal to large amount of induced compression in the direction of S_{Hmax} .



Discussion & Conclusion

The reduction of the pore pressure gradient required to produce fluid has been shown here to reduce the induced stresses and seismicity associated with production. This effect is significant for reverse and strike-slip faulting stress regimes and moderate for normal faulting stress regimes.

Care should be taken, however, as hydraulic fracturing is generally not well accepted publicly and there have been instances of the process itself inducing seismicity.

Additionally, hydraulic fracturing is not the only way to reduce required pore pressure gradients and it may be that there are other, less controversial, ways of achieving similar results.

The optimal orientation of a horizontal well was also found (in the case fracturing was not considered). In terms of induced seismicity, it was found that the optimal orientation of a horizontal well is:

- Parallel to S_{Hmin} in a normal faulting stress regime
- Parallel to S_{Hmax} in a reverse faulting stress regime
- In a strike-slip faulting stress regime well direction changes the likely location of seismicity from above and below the reservoir (parallel to S_{Hmin}) to the outskirts of the reservoir (parallel to S_{Hmax})

References & Funding

[1] Segall, P. (1989), Earthquakes triggered by fluid extraction, *Geology*, 17, 942-946.
 [2] Dieterich, J. (1994), A constitutive law for rate of earthquake production and its application to earthquake clustering, *Journal of Geophysical Research*, 99, 2601-2618.
 [3] Segall, P., S. Lu (2015), Injection-induced seismicity: Poroelastic and earthquake nucleation effects, *Journal of Geophysical Research: Solid Earth*, 120, 5082-5103.

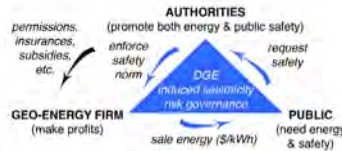
This work has been funded by a research grant (SI/500963-01) of the Swiss Federal Office of Energy.

Increase of the EGS levelized cost of electricity, or the financial cost of public safety

Arnaud Mignan, Dimitrios Karnouvis, Marco Broccardo

Rationale

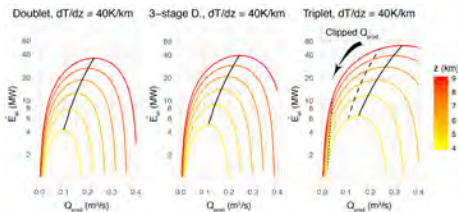
A multitude of models exist that compute the levelized cost of electricity (LCOE) for Enhanced Geothermal Systems but none take into account the costs associated with induced seismicity, although seismic risk remains the main problem facing the EGS industry today.



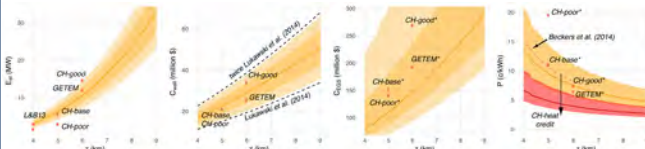
We present a meta-model that quantifies the LCOE taking into account the “cost of public safety”, i.e., the cost of mitigation measures against induced seismicity. This is implemented within a Deep Geothermal Energy (DGE) seismic risk governance framework where a trade-off must be decided between public safety & energy safety.

A meta-model for EGS LCOE computation

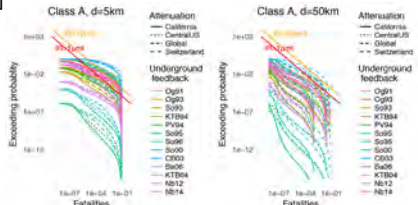
(1) **Energy model:** Composed of EGS, conversion cycle & district heating | Fully analytical | Optimizes injection production rate Q_{prod} to maximize electricity produced | Heat loss based on exponential decline along supply pipe



(2) **Economic model:** LCOE = tot. energy produced / tot. costs | Function of distance d to EGS plant because of heat loss | In agreement with existing models (MIT GETEM, TA-Swiss CH-*, etc.)



(3) **Seismic risk model:** Computes induced seismicity risk [1] to be compared to safety norm (individual risk IR in micromort μm) | Tectonic maximum magnitude assumed | Same method for traffic light system (TLS) [2,3]



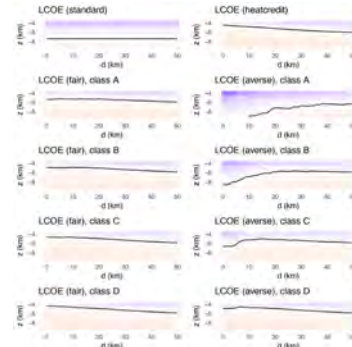
(4) **Behavioural model:** probability p of safety norm failure = probability reservoir stimulation would be stopped by TLS = probability of losing the injection well for foreseeing future | LCOE translated into null expectation following Bernoulli trial (P : price, E : energy, C : costs) | Cumulative Prospect Theory (CPT) risk aversion & loss aversion included (π : distorted probability, v : utility function) [4]

$$(1 - p)(P_{fair}E - C) + p(-C_{TLS}) = 0 = \mathbb{E}[X] = (1 - p)x_1 + px_2$$

$$\pi^+ v^+(P_{averse}E - C) + \pi^- v^-(-C_{TLS}) = 0 = \mathbb{E}[v(x)]$$

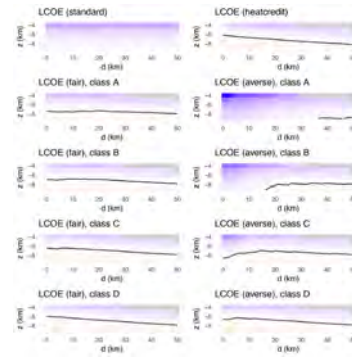
Results

(1) Mitigating seismic risk during reservoir stimulation (via TLS):

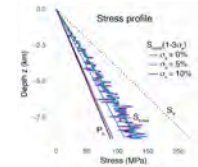


- Black curve: break-even price, red: competitive price, for building classes A to D
- Impact of safety norm limited on the fair price
- However the small probability p of losing a well leads to risk aversion, which amplifies the price
- Benefit of heat credit at small distances d from EGS plant lost by cost of seismic risk mitigation
- Best EGS plant siting = $d(\text{min LCOE})$

(2) Mitigating seismic risk during production phase (via Q_{prod} clipping):



- Strong impact of Q_{prod} clipping (to avoid any induced seismicity) on LCOE
- Depends on local stress field, which is very uncertain
- The safety-norm-based TLS could also be used during the production phase



Discussion

(1) Meta-model as regulatory sandbox to improve DGE risk governance & regulation (see poster by Mignan & Seferovic, SCCER SoE-CREST joint activity)

(2) Seismic risk better controlled, via the use of a safety norm. However the seismic risk being stochastic in nature, the safety norm can only be respected on average

(3) Public acceptance could be improved via such a transparent approach & their understanding of the trade-off between public safety & energy safety

- (4) How to decide from the public-safety/energy-safety trade-off?
- Public-safety prone (zero-risk policy): LCOE becomes too high & EGS industrial potential collapses
 - Energy-safety prone (high risk tolerance): EGS projects prosper
 - Must find right balance putting it into the perspective of the climate change existential risk & the need to quickly find energy solutions

References

[1] Mignan et al. (2015), Induced seismicity risk analysis of the 2006 Basel, Switzerland, EGS project: Influence of uncertainties on risk mitigation, *Geothermics*, 53, 133-146
 [2] Mignan et al. (2017), Induced seismicity closed-form TLS for actuarial decision-making during deep fluid injections, *Sci. Rep.*, 7, 13607
 [3] Broccardo et al. (2017), Hierarchical Bayesian Modeling of Fluid-Induced Seismicity, *Geophys. Res. Lett.*, 44, 11,357-11,367
 [4] Mignan et al. (2019), Autonomous Decision-Making Against Induced Seismicity in Deep Fluid Injections, *Energy Geotechnics*, SEG, 369-376



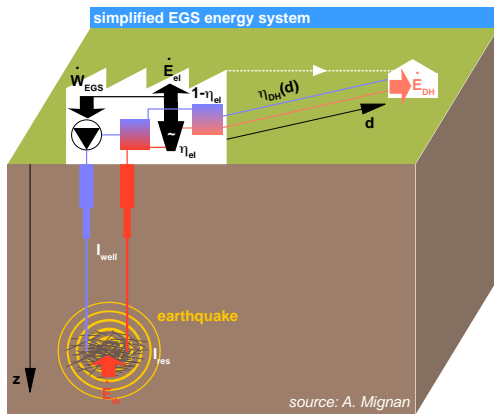
JA IDEA-HG: Initial version of recommendations for regulating & governing DGE seismic risk

With Deep Geothermal Energy (DGE) remaining at the demonstration level in Switzerland, we provide an initial set of recommendations on how the legislative framework and the governance structure related to DGE's main risk, induced seismicity, could be enhanced to facilitate the resolution of conflicts among stakeholders and thus increase investments in DGE via a reduction of project risk. Our approach is twofold: (1) We develop a regulatory sandbox for induced seismicity risk governance based on a transparent meta-model with DGE electricity price (or levelized cost of electricity; LCOE) as main metric. (2) We do a Q&A, assessing the existing problems and envisioning possible legislative solutions, considering existing laws, risk transfer, etc., hence merging SCCER-SoE and SCCER-CREST knowledge towards one comprehensive governance framework.

DGE seismic risk regulatory sandbox

Based on a quantitative & transparent meta-model

- *Energy model:* both electricity & heat
- *Economic model:* Levelized Cost of Electricity (LCOE)
- *Seismic risk model:* Safety-norm-based mitigation
- *Behavioral model:* Risk-averse & loss-averse decision



Trade-off between public safety & energy safety

- *Traffic light system:* safety norm verified on average
- *Cost of public safety:* LCOE increases due to possible loss of wells & investor's fear of uncertainty

Initial recommendations

In the short-term

- *Existing safety norms must be adapted:* (i) Vibration norms (construction industry) & risk-based norms (chemical industry) to be combined for full risk spectrum; (ii) Maximum earthquake magnitude ambiguity to be considered, by assuming the worst-case scenario (tectonic M_{max}) based on minimax, or mean risk to be used instead of median risk if an M_{max} logic tree is still preferred.

In the medium-to-long-term

- *Creation of a DGE catastrophe fund:* in the case of a large earthquake occurrence, losses would be beyond the DGE insurance cover. Would allow risk transfer from firm (possibly bankrupted) and canton/state to dedicated fund.
- *Proposal of a legislative framework:* to allow the federal legislator to set a nationwide DGE safety norm to best deal with the public-safety/energy-safety trade-off, finding a balance between 2 extremes: public-safety prone (very conservative safety norm that hampers all DGE projects) and geo-energy industry-prone (loose or no safety norm, likely leading to public opposition).

Research Partners



University of Basel

ETH zürich



UNIVERSITÄT LUZERN

Contact

Arnaud Mignan, Swiss Federal Institute of Technology Zurich (ETH Zurich)
arnaud.mignan@sed.ethz.ch

Goran Seferovic, Zurich University of Applied Sciences (ZHAW)
sefe@zhaw.ch

www.sccer-crest.ch

Probabilistic Fatigue Model for Predicting Plaster Cracks on Unreinforced Masonry Walls Caused by Induced Seismic Hazard

ETH zürich Abbiati, G., Broccardo, M., Gabbi, A., Mojsilovic, N., Petrovic, M., Didier, M., and Stojadinovic, B.

Abstract

In Basel and St. Gallen, CH, two pilot enhanced geothermal systems projects caused sequences of induced earthquakes with magnitudes up to 3.5. In Basel, non-structural damage that arose from the events stooped the project. Thus, prediction and quantification of non-structural damage due to long sequences of repeated induced ground motions is central for estimating the related financial risk.

Test Protocol

To investigate plaster cracking on plastered URM walls caused by induced ground motions, a fatigue test campaign was recently conducted at ETH Zurich (Figure 1). Ten URM walls were constructed using modern techniques. The first nine URM walls were subjected to constant amplitude horizontal displacement sequences of 3, 5 or 7 mm (Table 1). An additional wall was tested considering a combination of cycles with different amplitudes. Digital Image Correlation (DIC) was used to measure the strains and displacements on the plaster surface. Further image processing was used to detect and quantify the induced cracks in the plaster.

Table 1. Summary of fatigue tests.

Wall IDs	Displacement amplitude (A) [mm]	Applied number of cycles [-]
1,4,8	3	200, 200, 200
2,5,7	5	100, 100, 70
3,6,9	7	50, 80, 42
10	2.4, 3.6, 4.8	70, 15, 13

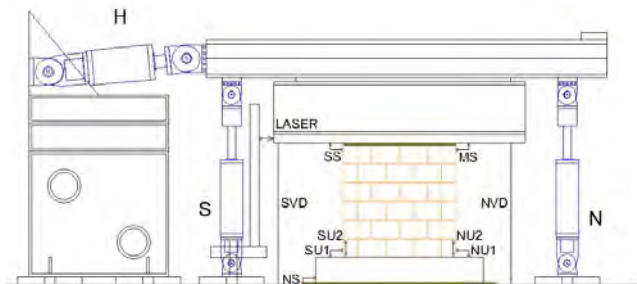


Figure 1. Experimental setup.

Damage Quantification

The Normalized Cumulate Cracked Area (NCCA) was calculated to quantify the area of cracked plaster. The NCCA corresponds to the percentage of the total plaster area A_w affected by cracks:

$$NCCA [\%] = \frac{A_c}{A_w} \cdot 100$$

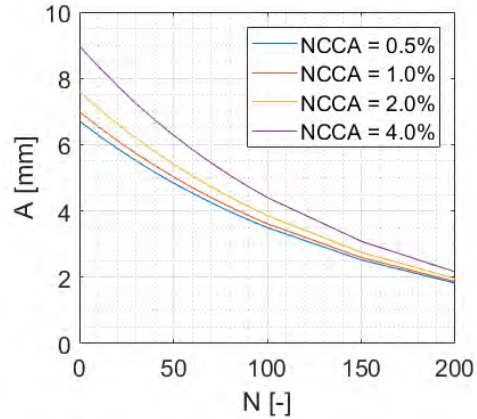


Figure 2. Evaluation of the probabilistic fatigue model for different values of NCCA.

Plaster Fatigue Model

Recorded NCCA histories were sampled at predetermined NCCA values and corresponding numbers of cycles were used to calibrate a logarithmic fatigue model:

$$\ln(A|NCCA) = a + bN + \varepsilon|NCCA$$

- A: displacement amplitude of the cyclic test [mm]
- N: number of cycles corresponding to the specific NCCA value [-]
- $\varepsilon \sim N(0, \sigma|NCCA)$: regression error, assumed Gaussian with zero mean and standard deviation $\sigma|NCCA$.
- a, b: regression parameters

The regression parameter a and b are:

$$a = NCCA m_a + q_a; b = NCCA m_b + q_b$$

Figure 2 shows the mean value of the displacement amplitude for different NCCA values: for a given NCCA level and displacement amplitude A_i (i represents the index of a cycle bin) the curve provides the average number of cycles $N_{max,i}^{ave}$ that are needed to reach a target NCCA value associated with the plaster failure limit state.

Validation and Conclusion

Wall #10 was subjected to a displacement sequence with non-homogeneous amplitude to test the fatigue model. A NCCA threshold value of 1.00 % was selected to denote the plaster failure. According to the fatigue model, Wall #10 fails as the NCCA measured is equal to 1.57% > 1.00%.

This suggests that the proposed URM wall plaster fatigue model is suitable for predicting the damage caused by long sequences of induced earthquakes.

From a “steam monster” to energy projects: moving forward to geothermal social acceptance in Chile

Sofía Vargas-Payera – Andean Geothermal Center of Excellence

Context:

In Chile there is an urgency to adopt the use of renewable energy sources due to the high level of air pollution, the country's high dependency on oil imports and severe droughts that have affected the country, and there has been an increase in social resistance movements.

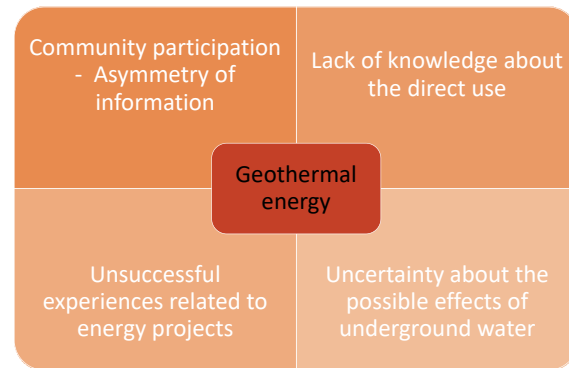
After 100 years of geothermal explorations, in 2017, the first geothermal power plant was inaugurated in Chile and South America along with the world's first large-scale facility of this kind to be built at 4,500 meters above sea level.

In 2018, the exploitable potential of the explored areas goes from approximately between 1,300 MW to 3,800 MW.

The direct use of the energy by geothermal heat pump is represented by 8.6MWth (83% of which goes to the services, industries and public buildings sector, and only 17% in residential use).



Social aspects that affect the resource acceptance* :



* According to indigenous consultation reports.

Methodology:

To illustrate the state of art of geothermal energy after 100 years of explorations, this work includes the analysis of secondary sources of information, including:

- Ministry of Energy reports (4)
- Indigenous consultation reports (5)
- Geothermal research center annual report (1)
- Chilean scientific publications (3)

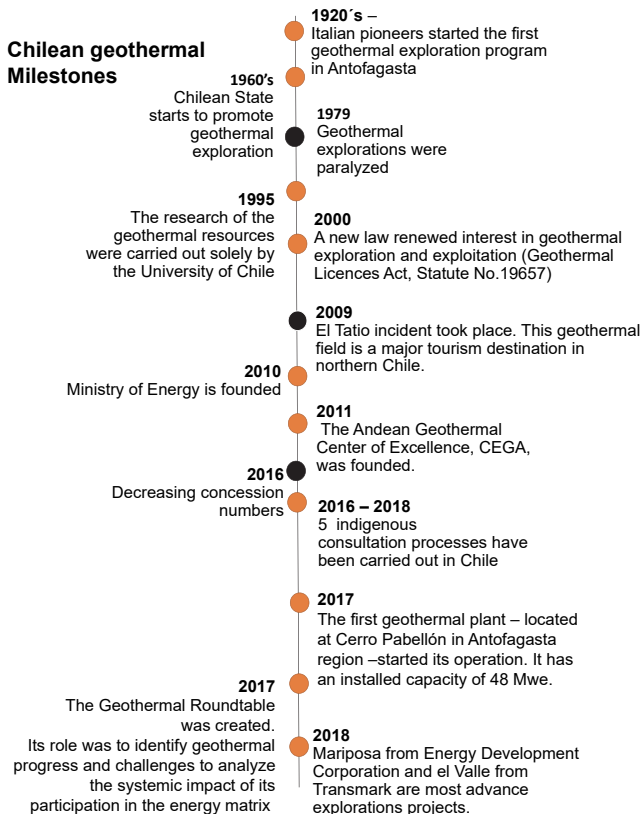


The main goal is to describe the big picture of the Chilean geothermal development, paying attention to public engagement strategies and social aspects.

Main conclusions:

- There is no mechanism to promote geothermal heat pump systems beyond general renewable energy measures.
- The most common communication material among all organizations involved in geothermal energy development is the brochure with general information describing this energy source.
- The energy policy 2018-2022 promotes the direct use of geothermal energy, but the mechanisms are not clear.
- The current geothermal law did not include the social worries, such as underwater owner and environmental impact (the law is under revision).
- The lack of citizen engagement in early stages of energy projects affects the social perceptions. Currently, the social demands of participation in exploratory stage is not reflected in the geothermal law.
- Environmental impact assessment is developed in the exploitation phase. The late relationship between energy companies and community promotes distrust among them.
- The mechanism to promote geothermal energy for the Andean Geothermal Center of Excellence since 2015 has been to interact with communities through workshops in territories with high geothermal potential.
- Although Chile is a territory with a great geothermal potential, this energy development is still emerging, characterized by up and down moments.
- Geothermal developments are still located at a technical level. The discussions and efforts have been made to overtake economic barriers, but the discussion about social strategies to increase public acceptance is still underdeveloped.
- High enthalpy projects have been the most important focus to the Ministry of Energy and companies in Chile. The direct use of the energy is still emergent.

Chilean geothermal Milestones



References

- Chilean Geothermal Roundtable final report, 2018.
- Indigenous consultation reports: Tacora, Licancura, Pampa Lirima, 1, 2, Puchuldiza Sur 2. 2016 -2017. Ministry of Energy.
- Andean Geothermal Center of Excellence annual report, 2017.
- Annual progress report, *Andean Geothermal Center of Excellence* 2017.
- Energy Route 2018-2022, Ministry of Energy.



Optimal PV and Wind Locations for an Efficient & Renewable Swiss Power System

Bert Kruyt, Annelen Kahl, Stuart Bartlett, Jérôme Dujardin, Michael Lehning

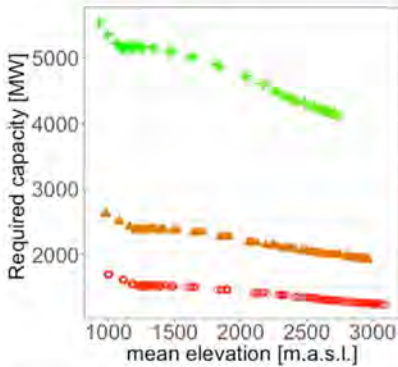
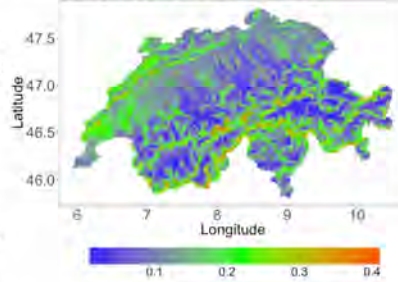
Highlights

- We demonstrate that it is possible to **shift PV production to winter** without compromising total annual production by making use of:
 - higher albedo due to snow cover
 - low cloud cover in winter at high elevations
 - increased panel tilt to account for lower sun angles in winter
- We calculate the **wind turbine capacity required to reach the ES2050 target (4TWh)**, and show that this target can be reached with minimal capacity if we allow for high elevations to be used:
 - 1230 MW when selecting optimal locations
 - 1596 MW when limited to the locations in 'Konzept Windenergie Schweiz'.
- Line use is investigated in scenarios with varying degrees of renewables, and it is found **the current transmission network is capable of supporting a fully renewable power system**. (Line use is actually lower for a fully renewable Swiss power system than for the current system).

Wind turbine capacity required to produce 4, 6, or 12 TWh

We used 100m wind speeds from the COSMO-1 model and the Enercon E82 power curve to calculate power time series and capacity factors for each 0.01° pixel in Switzerland. Using locations with the highest capacity factors, capacity was located until annual production reached 4, 6, or 12 TWh.

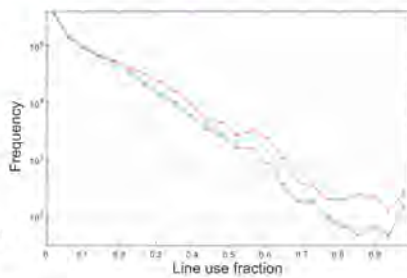
Capacity Factors for Wind Power in Switzerland



This was repeated while varying the maximum elevation at which turbines are allowed to be located, resulting in the graph on the left.

Line use

Line use under 3 scenarios (Current, Intermediate, Renewable) with varying shares of renewables. The frequency of high line use fractions is actually lower under high renewable scenarios.



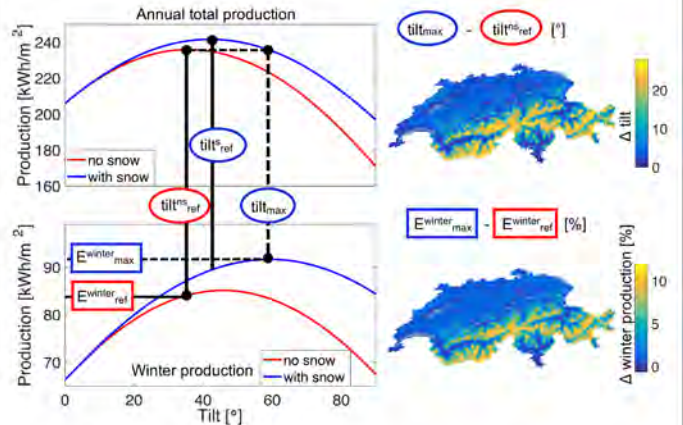
Acknowledgements

Thanks to MeteoSwiss, CSCS and

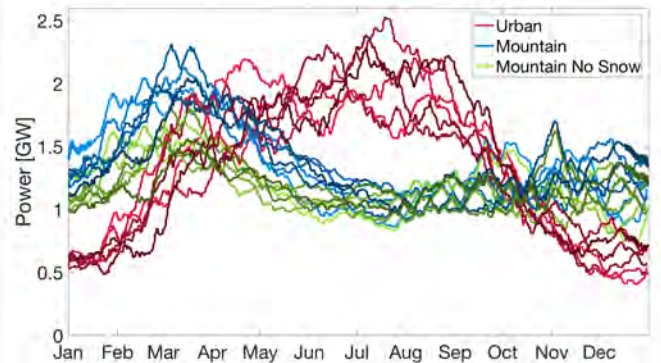
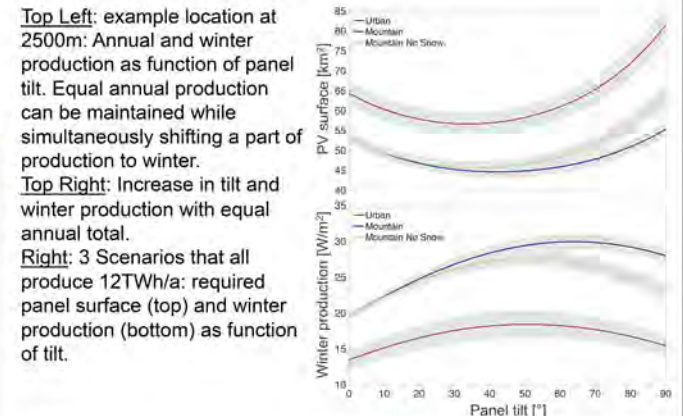


Energy Turnaround
 National Research Programme

Increase Winter PV Production



Top Left: example location at 2500m: Annual and winter production as function of panel tilt. Equal annual production can be maintained while simultaneously shifting a part of production to winter.
Top Right: Increase in tilt and winter production with equal annual total.
Right: 3 Scenarios that all produce 12TWh/a: required panel surface (top) and winter production (bottom) as function of tilt.



Above: 5 years (increasing darkness) of PV production for the 3 scenarios. A clear **shift to winter** production is observed when moving from **Urban** to **Mountain** PV allocation.

References

- B. Kruyt, J. Dujardin, M. Lehning (2018) Improvement of wind power assessment in complex terrain: The case of COSMO-1 in the Swiss Alps. *Frontiers in Energy Research* (in press)
- A. Kahl, J. Dujardin, M. Lehning (2018) The bright side of PV production in snow covered mountains. *PNAS* (in press)
- S. Bartlett, J. Dujardin, A. Kahl, B. Kruyt, P. Manso, M. Lehning (2018) Charting the Course: A Possible Route to a Fully Renewable Swiss Power System. *Energy*

Comprehensive Historical Accident Data for Comparative Risk Assessment of Energy Technologies

P. Burgherr¹, W. Kim², M. Spada¹, A. Kalinina¹, S. Hirschberg¹

¹Laboratory for Energy Systems Analysis (LEA), Paul Scherrer Institut, Villigen PSI, Switzerland
²Future Resilient Systems (FRS), Singapore-ETH Centre, Singapore

Supported by:

Schweizerische Eidgenossenschaft
Confédération suisse
Confederazione Svizzera
Confederaziun svizra
Swiss Confederation
Innosuisse – Swiss Innovation Agency

(FRS) FUTURE RESILIENT SYSTEMS 未来韧性系统

Introduction

The **systematic and consistent, comparative risk assessment of energy technologies** is a central element both in the comprehensive evaluation of the performance of energy technologies, as well as in the broader context of **sustainability, energy security and critical infrastructure protection**, ultimately contributing to a more **resilient energy system** (Burgherr et al., 2017; Burgherr & Hirschberg, 2014). PSI's Energy-related Severe Accident Database (ENSAD) provides the most complete and authoritative source for historical accidents in the energy sector worldwide. With the development of ENSAD v2.0 an updated and significantly extended, web-based version is available that builds upon cutting-edge, open source technologies.

Structure and Implementation of ENSAD v2.0

The newly established **ENSAD v2.0** is a **spatial database** with fully integrated **GIS capabilities**. Its design and implementation was driven by simplifying the database structure compared to ENSAD v1.0, and to ensure full **scalability and flexibility** in view of potential future extensions. The overall structure of the database is shown in Figure 1. The core table, i.e. the **general accident information**, is linked through a 1:n relationship to the **consequences information** ensuring that information from different primary information sources is stored individually in the consequence table. **Infrastructure-dependent information** is stored in separate tables for each infrastructure type (e.g. dam, pipeline, power plant) and linked through a 1:1 relationship to the core table. Furthermore, reference **background data** and additional infrastructure information (e.g. third party databases) can be directly linked through the infra-dependent tables. Finally, the **user and data history information** tables provide important information about a user's role and activities, and what changes have been made to accident records and fields over time.

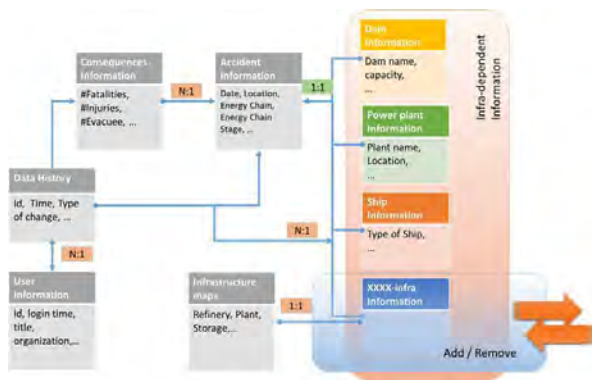


Figure 1: Overall structure of an accident record in ENSAD v2.0. (Kim et al., 2018).

ENSAD v2.0 has been developed as a **responsive web application**, based on a **cloud server** and **open-source technologies**. Depending on a user's role (e.g. Basic, Editor, Admin, Public) and the device used (e.g. PC, smartphone, tablet) the corresponding version is selected on the client side and displayed in the web browser. Figure 2 shows the three dedicated ENSAD versions that are available.

The main interface of the **desktop viewer** has a **similar layout to a typical GIS software** (Figure 2a). The layer panel is located on the left, and the preview panel for information sources is on the right of the map. The main menus and buttons are placed on the top, whereas the query form and the attributes table are on the bottom.

The **mobile viewer** has three main functions (Figure 2b): (1) **“Search”** for a location, (2) **“Locate”** accidents around the current user, and (3) select **“Layers”** to display (2b, left). The layer panel manages accident and base maps (2b, middle). When the user selects an accident on the map by touching its symbol, the corresponding attribute information for this accident is displayed as a popup window (2b, right).

The **ENSAD Visual Explorer (EVE)** (Figure 2c) has a **filtering panel** that allows choosing energy chains, chain stages and damage types. If at a location more than one accident occurred, they are displayed on the map as a pie chart with one slice per energy chain, and the total number of accidents is also indicated. The user can also select from several **predefined chart options to generate summary graphs**.

Numerous case study applications with ENSAD v2.0 data highlight its usefulness and versatility, including: (1) Bayesian hierarchical modeling to assess the **risk of dam accidents** (Kalinina et al., 2018), (2) risk assessment of energy **accidents in the natural gas sector** (Cinelli et al., 2017), and (3) **network analysis of the European natural gas infrastructure** (Lustenberger et al., 2018), among others.



Figure 2: (a) Desktop viewer layout with full database access and functionality. (b) Mobile viewer with reduced features: main interface, layer selection and attribute table. (c) ENSAD Visual Explorer (EVE) for public users focuses on visualization with less detailed information (Kim et al., 2018).

Acknowledgements

This work has been carried out within the **Swiss Competence Center on Energy Research – Supply of Electricity** (concept, data management and preparation of data migration), the **Energy Turnaround National Research Programme (NR70)** of the Swiss National Science Foundation (dam accident prototype), and the **Future Resilient Systems (FRS) program** of the Singapore-ETH Centre (SEC) (tool development and implementation, data migration).

References

Burgherr, P., Spada, M., Kalinina, A., Hirschberg, S., Kim, W., Gasser, P., Lustenberger, P. (2017) The Energy-related Severe Accident Database (ENSAD) for comparative risk assessment of accidents in the energy sector. IN: Capin, M., Bris, R. (Eds.) Safety and Reliability - Theory and Applications. London, UK, CRC Press, Taylor & Francis Group.
Burgherr, P., Hirschberg, S. (2014) Comparative risk assessment of severe accidents in the energy sector. Energy Policy, 74, S45-S56.
Cinelli, M., Spada, M., Miebs, G., Kadziński, M., Burgherr, P. (2017) Classification models for the risk assessment of energy accidents in the natural gas sector. The 2nd International workshop on Modelling of Physical, Economic and Social Systems for Resilience Assessment. Brussels, Belgium.
Kalinina, A., Spada, M., Burgherr, P. (2018) Application of a Bayesian hierarchical modeling for risk assessment of accidents at hydropower dams. Safety Science, 110, 164-177.
Kim, W., Burgherr, P., Spada, M., Lustenberger P. (2018) Energy-related Severe Accident Database (ENSAD): a cloud-based geo-spatial platform. In submission.
Lustenberger, P., Kim, W., Schumacher, F., Spada, M., Burgherr, P., Hirschberg, S., Stojadinović, B. (2018) Network analysis of the European natural gas infrastructure to identify potential bottle-necks. IN: Haugen, S., Barros, A., van Gulijk, C., Kongsvik, T., Vinnem, J.E. (Eds.) Safety and Reliability – Safe Societies in a Changing World. London, UK, CRC Press, Taylor & Francis Group.

Mapping the landscape of participation in Geneva

Franziska Ruef, Michael Stauffacher, Olivier Ejderyan – D-USYS TdLab, ETH Zürich

Research Context and Objectives

This study takes place in the context of the Geneva program for geothermal energy, **GEothermie 2020**, which is funded by the public utilities SIG and the canton of Geneva. We accompany the program in its work on participation and the public.

This study maps participatory experiences of GEothermie 2020 program managers and inhabitants, and confronts those to their expectations and ideal types of participation.

The goal is to analyze the interplay between the different formats of participation used in GEothermie 2020 and identify potential misalignments between what is expected by participation and what specific formats can deliver.

Research Questions

How can the landscape of participation be drawn for geothermal in the Geneva context?

Does this landscape differ for program managers of the geothermal program and for local inhabitants? And if so, in what way?

Methods – two different perspectives on participation

We conduct a qualitative analysis in order to identify preferences about participation in the actors' own words.

Participant observation in strategic management meetings:

- Attendance to weekly sessions during 18 months
- Internal meetings with their project partners and public events
- *Data: observation notes, Memos and documentation.*

Focus groups with inhabitants:

- 6 focus groups in different municipalities and neighborhoods
- 5-10 participants in each group
- Same structure for all groups
- *Data: focus group transcripts and Memos.*

Framework for Analysis

We analyze the data using a framework that focuses on 3 aspects of the participatory process:

- **Formats of participation:** the ideal format for participation that leads to the implementation of a specific participatory process
- **Subjects:** the actors that participate in the given format
- **Objects:** the issues that are addressed in the given format

Each of these aspects is related to a wider space that influences the content of a specific participatory format and is simultaneously affected by what happens during participation. These relationships constitute a landscape of participation.



Fig. 1 Relational co-productionist framework adapted from Chilvers, Pallett, & Hargreaves, 2018

Preliminary Results

Below are first results from an analysis on the formats of participation

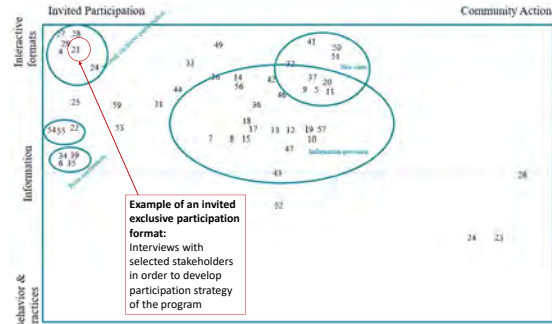


Fig. 2: Wider spaces of participation formats – program managers' perspective

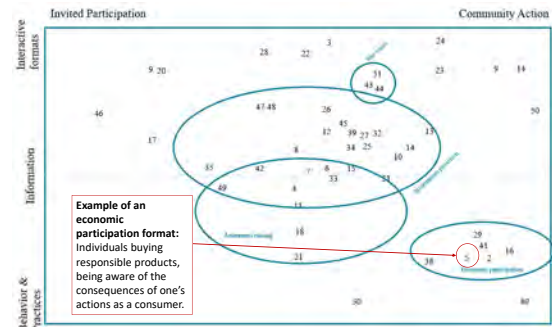


Fig. 3: Wider spaces of participation formats – local inhabitants' perspective

- Numbers represent references to participation formats made by the program managers (Fig. 2) and local inhabitants (Fig. 3).
- Blue circles: *wider spaces of participation*, thus a grouping of similar formats of participation.

Discussion

- Program managers see participation formats mostly as classical formats of information provision and site visits; only very few references to participation through behaviour and practices.
- Invited/internal participation that is exclusive in terms of who may participate is important in the program managers' view.
- Focus group participants also see information provision as one important format of participation;
- Focus group participants also often referred to other formats going more into individual actions and awareness on an individual level.

The diversity of participation collectives that could be identified for the Geneva context shows that there are many ways in which participation may be considered for a program like the geothermal one. However, depending on the perspective, these collectives may or may not be part of daily decision making of program managers or local inhabitants.

References & Acknowledgement

Chilvers, J., Pallett, H., & Hargreaves, T. (2018). Ecologies of participation in socio-technical change: The case of energy system transitions. *Energy Research & Social Science*, 42(March), 199–210. <https://doi.org/10.1016/j.erss.2018.03.020>

This research is co-funded by SCCER-SoE, the Canton of Geneva and SIG



Semiotic analysis of technoscientific promises in geothermal energy

Olivier Ejderyan (ETH Zürich, D-USYS TdLab)

Background

Future oriented statements and discourses projecting potential uses and benefits of a new technology are a common feature of innovation paths. Such statements and discourse can take various forms such as imaginaries, visions, scenarios or promises (Borup et al. 2006).

Promises are a specific form of future oriented statements: they formulate an engagement to deliver in a given time frame. They seek to secure research funds and investments and mobilize supporting actors (Audétat 2015; July 2010). They are characteristic of *performative statements* aimed to enact what they enounce.

This study analyses the structure of promises related to geothermal energy development in Switzerland and evaluates their performative features. The goal is to focus how these promises might influence social siting and public engagement.

Methods

We conducted a semiotic analysis on promises about geothermal energy development in a corpus composes of:

- Newspaper articles
- Public relations material from energy operators and public authorities (flyers, pamphlets, websites...)
- Project presentation materials from developers

“By promises we mean optimistic expectations sketching the potential and assumed benefits which may be achieved by a technology, but nevertheless require work to be done.” (te Kulve et al. 2013)



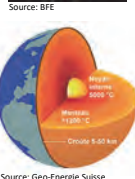
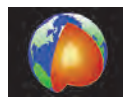
Source: Energiea, n°1, 2005

“Promises are not just a matter of discourses and representations. They also involve practices of exploration and experimentation; they are related to investment, and to mobilization, circulation, and accumulation of resources.” (July 2010)

We analysed the explicit content of the promises (what is to be delivered, when and how) and their audience (direct and indirect).

Insights

A common feature of promises about deep geothermal energy is to start from statements about the abundance of heat available in the earth. Images of a earths section depicting the mantle in a glowing orange are a popular visual trope.



Such pictures are instrumental in backing up one of the main arguments in favour of the development of EGS, that is the possibility to be deployed “anywhere”.

Exemplary features of promissory statements:



Source: Hot Dry Rock, Geo-Energie Suisse

“Thanks to this we will have unlimited access to geothermal resources. This announces, already today, a guaranteed and serene energetic future”

«[HDR] These three letters, initials of « Hot Dry Rock », name a technique that enables to use geothermal energy independently from the availability of hot springs or hot aquifers.» (Tribune de Genève 29.12.2003)

L'énergie géothermique est



Source: www.geothermie2020.ch

«In a near future, geothermal energy will enable us to heat whole neighborhoods, and possibly produce electricity. Well hidden in the underground, this promising renewable energy must first be ferreted out in places where it can be exploited. (...) Since traditional water-divining rods are not of a big use in this case, the SIG are betting on techniques elaborated to dig up oil» (Tribune de Genève 23.08.2010)

Table: Performative features of promises of Swiss geothermal energy

	Petrothermal/ EGS	Hydrothermal / conventionnal
Development formulated as...	Necessity	Opportunity
Reference to science	«top» science Pushing back frontiers Connexion au désir scientifique	Exploration Adding knowledge Reference to luck and vernacular knowledge
Source of funding	National states Research agencies International organisation Investors	Public bodies Local utilities End users Local universities
Future	Far but already here and clearly defined	Close but uncertain
Space	Delocalised Top down site selection Power for the network	Anchored Locally identified potential Resource justifies site Local direct use of heat
Vision of the public	Abstract Challenge to overcome Needs to be educated	Local Needs to be mobilised

Discussion

- Differentiated structure of promises for EGS and hydrothermal
- Performative effects of promises relate to specific features of the siting process (principles for site selection) or and public engagement (framing potential participants to involve)
- Project managers must take into account these effects when developing communication and public engagement strategies.

References

- Audétat, M. 2015. "Why so Many Promises ? The Economy of Scientific Promises and Its Ambivalences." In *Knowing New Biotechnologies: Social Aspects of Technological Convergence*, M. Wienroth and E. Rodrigues (eds), London, New York: Routledge: 29–43.

- Borup, M., N. Brown, K. Konrad, and H. Van Lente. 2006. "The Sociology of Expectations in Science and Technology." *Technology Analysis & Strategic Management* 18 (3–4): 285–98. doi:10.1080/09537320600777002.

- July, P.-B. 2010. "On the Economics of Techno-Scientific Promises." In *Débordements. Mélanges Offerts à Michel Callon*, M. Akrich, Y. Barthe, F. Muniesa, and P. Mustar (eds.), Presse des Mines: 203–22.

- te Kulve, H., K. Konrad, C. Alviaj Palavicino, and B. Walhout. 2013. "Context Matters: Promises and Concerns Regarding Nanotechnologies for Water and Food Applications." *NanoEthics* 7 (1): 17–27. doi:10.1007/s11569-013-0168-4.

Framing geothermal energy in the UK: A media analysis

Xue Xu, Michael Stauffacher, Olivier Ejderyan (ETH Zürich, D-USYS TdLab)

Goals of the study

- Identifying how UK's mass media frames geothermal energy
- Providing a foundation for analysing the social acceptance and for public communication of geothermal energy in the UK

Background

- No mature development of geothermal energy and no sufficient social analysis on geothermal energy in the UK
- Media frames impact public perception and social acceptance
- Sound social analysis including media analysis on geothermal energy in other countries (e.g. Switzerland, Australia)
- Social analysis on other energy technologies in the UK (e.g. shale gas, wind power)

Method: Media framing analysis

We conducted a qualitative content analysis to identify the framing on geothermal energy of two British newspapers with national audience

- Corpus: *The Independent* (1989-2017, n = 97 articles) & *The Guardian* (1975 - 2017, n = 192 articles)
- Statements about geothermal energy were coded using NVivo by combining deductive codes (predefined by literature and theoretical framework) and inductive codes (interpretation of salient statements)
- Exploring the relations between categories of codes, for example, actors and their attitudes, actors and the topics they relate to

Results

Frequency

- The number of articles per year increases over time, especially after 2000
- Peaks in reporting are not attributed to specific events related to geothermal energy but to an increase of reporting about energy related issues



Number of articles mentioning geothermal energy published per year (*The Guardian* and *The Independent*)

Identified frames

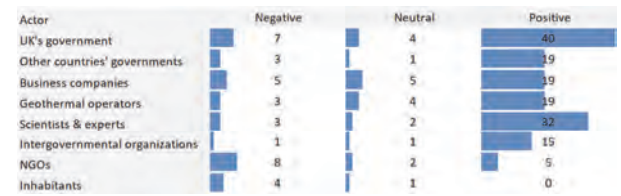
- Ordering the codes into categories of related topics enabled to identify following frames
- These frames are the main angles through which geothermal is discussed in the UK press

Name	Sources	References
Environment	168	260
Technology	105	199
Energy	113	153
Finance	73	101
Politics	52	74
Risk	17	30

Main frames of geothermal energy identified in *The Independent* and *The Guardian*

Actors, their frames, and attitudes

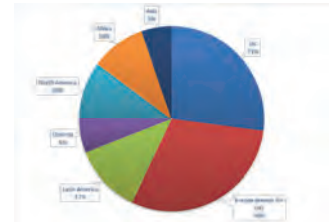
- Some actors appear more strongly associated to specific frames:
 - Scientists and experts with technology
 - UK's government with environment and energy
 - Geothermal operators with finance
- Actors' arguments were evaluated through interpretation. Arguments were classified as:
 - Positive: potential benefits of geothermal, financial and political support, successes
 - Neutral: facts without evaluative statement
 - Negative: drawbacks or nonsupport for geothermal
- Most quoted actors with more positive arguments
- NGOs and inhabitants are quoted with more negative ones



Attitudes towards geothermal energy of the actors mentioned in *The Independent* and *The Guardian*

Area of reporting

- Only a quarter of the articles report about geothermal in the UK as a source of energy discussed or under development



Countries mentioned in relationship to geothermal energy in *The Guardian* and *The Independent*.

Discussion

- The general tone of reporting on geothermal energy in the UK is positive (this does not mean that social acceptance is high!)
- Geothermal is described as a promising energy, but with still lacking governmental funding and political support
- Geothermal mainly appears as an energy source in foreign countries, outside of the UK
- Geothermal is most often treated aside other energy related topics, mainly solar and wind power, shale gas and fracking
- Polarized quotes of actors might make discussions about geothermal energy appear as more controversial than they are: governments and operators are mostly quoted in favor while NGOs and inhabitants are more often quoted to convey negative views of geothermal energy.
- Little discussion of risks. This is a challenge to project developers who will need to develop proactive communication schemes here

References

- Stauffacher, M., Muggli, N., Scolobig, A., & Moser, C. (2015). Framing deep geothermal energy in mass media: the case of Switzerland. *Technological Forecasting and Social Change*, 98, 60-70.
- Trutnevyte, E., & Ejderyan, O. (2017). Managing geoenergy-induced seismicity with society. *Journal of Risk Research*, 1-8.

Application of the Polynomial Chaos Expansion for uncertainty quantification of the flood wave propagation resulting from a concrete dam break

Anna Kalinina¹, Matteo Spada¹, Peter Burgherr¹ & Christopher T. Robinson²

¹Laboratory for Energy Systems Analysis (LEA), Paul Scherrer Institut, Villigen PSI, Switzerland; ² Department of Aquatic Ecology, Eawag, Dübendorf, Switzerland

Research Objectives

1. Quantification of flow quantities downstream of a large concrete hydropower dam in case of its failure;
2. Application of Polynomial Chaos Expansion for Uncertainty Quantification (UQ) and Sensitivity Analysis (SA) of the modeled flow quantities;
3. Development of a generic model for Swiss conditions (i.e. >= 100 meters, arch concrete dams located in the Alpine area).

Framework for uncertainty quantification & sensitivity analysis

Modeled input uncertainty is propagated through the surrogate model created using Polynomial Chaos Expansion (PCE) (Fig. 1):

$$M_i^{PCE} \stackrel{\text{def}}{=} \sum_{\alpha \in N^M} y_\alpha \Psi_\alpha(X_j)$$

M_i^{PCE} - PCE response, X_i - input vector, y_α - coefficient, Ψ_α - polynomials.

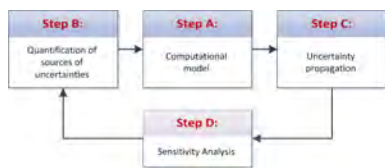


Fig. 1. Global framework for uncertainty quantification (Sudret, 2007)

Sensitivity Analysis is performed by calculating 1st order Sobol' indices of individual contributions of each model input to the total variance D ; Sobol' indices are calculated from the coefficients of the PCE-metamodel (Sudret, 2008), such that:

$$S_i = \sum_{\alpha \in A_i} y_\alpha^2 / D, A_i = \{\alpha \in N^M: \alpha_i > 0, \alpha_{j \neq i} = 0\}$$

The metamodel was built using UQLab (Marelli and Sudret, 2014).

Step A: Computational model of the flood wave propagation

Complete and instantaneous failure of the dam is assumed; thus, the dam-break is treated as a Riemann problem (Fig. 2(a)); The amount of water released from the dam is characterized using 3 parameters: H, V, L_{cr} , (Table1), whereas, flood propagation is simulated for a generic model of the downstream valley characterized by 6 parameters: $L_{ch-rel}, W, S_b, S_s, M_b$ & M_s (Table 1).

The model output is given by 6 parameters (Fig. 2(b)): $Q_{peak}, t_{peak}, t_{ar}, k$, maximal velocity v_{max} , and maximal depth h_{max} . A 1D model is built in the BASEMENT software (ETHZ).

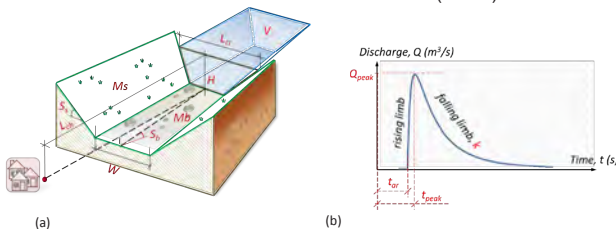


Fig. 2. (a) Parametrization of the input parameters of the dam, reservoir, and valley topography downstream of the dam; (b) Parametrization of the model output

Step B: Marginal distributions for uncertain model inputs

Table 1. The marginal distributions specified for the input of the metamodel

Parameter	Name	Unit	Distribution	Information sources
Physical characteristics of the dam and reservoir				
H	Dam height	[m]	$H \sim \text{Beta}(1.3, 3.117, 250)$	data on large hydropower dams (SwissCO, 2016)
V	Reservoir volume	[m ³]	$V \sim \text{Beta}(1.3, 3.9200, 2E5)$	
Lcr	Length of the dam crest	[m]	$L_{cr} \sim U(256.610)$	
Physical characteristics of the channel				
Lch_rel	Relative channel length	[m/m]	$L_{ch_rel} \sim U(5.9, 123.6)$	data on slopes from GeoVITE & Rosgen, et al. (2013)
W	Channel width	[m]	$W \sim U(1.163, 7)$	
Sb	Slope of the channel bed	[-]	$S_b \sim U(28.3, 45.9)$	
Ss	Slope of the channel embankments	[-]	$S_s \sim \text{Beta}(3.2, 3.2, 5)$	
Characteristics of the environment				
Mb	Roughness coefficient of the channel bed	[s/m ^{1/2}]	$M_b \sim \text{Beta}(0.33, 2.1)$	Land cover data from GeoVITE
Ms	Roughness coefficient of the channel embankments	[s/m ^{1/2}]	$M_s \sim \text{Beta}(0.4, 1.9)$	

Step C: Results for uncertainty propagation

PCE of different degrees are built on the experimental design of 2,000 samples for the 6 parameters of the model output (Fig.3):

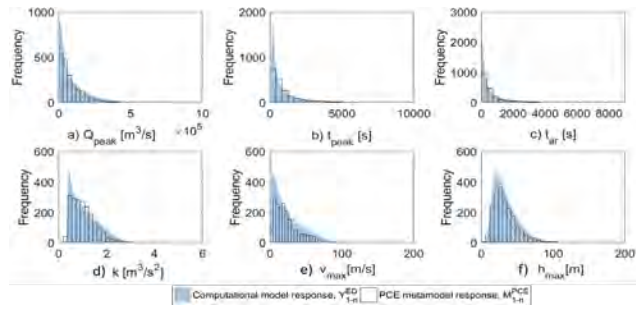


Fig. 3. Model response ($Y_{t=1}^{ED}$) and PCE response ($M_{t=1}^{PCE}$) for a) Q_{peak} ; b) t_{peak} ; c) t_{ar} ; d) k ; e) v_{max} ; f) h_{max}

Step D: Results for sensitivity analysis

Sobol' indices indicate that the reservoir volume, length of the valley, and surface roughness contributed most to the variability of the model output (Fig. 4)

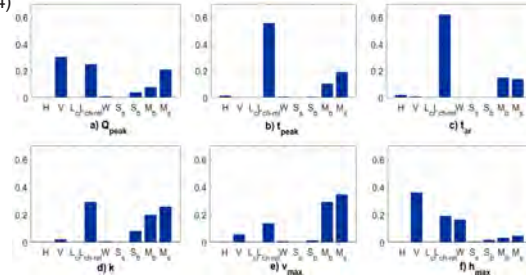


Fig. 4. Results for sensitivity of a) Q_{peak} ; b) t_{peak} ; c) t_{ar} ; d) k ; e) v_{max} ; and f) h_{max}

Conclusions

- The applied metamodeling approach is in good agreement with the physical model;
- Application of the constructed metamodel enables reducing computational effort with respect to, for example, Monte Carlo approaches;
- Sensitivity analysis can help to understand how the variability of each model input affected variability of the model output;
- The constructed metamodel can support informed risk management and reliability-based design for typical Swiss hydropower dams.

Acknowledgement: This research project is part of the National Research Programme "Energy Turnaround" (NRP 70) of the Swiss National Science Foundation (SNSF). Further information on the National Research Programme can be found at www.nrp70.ch. It is also integrated with the activities of the Swiss Competence Center on Energy Research – Supply of Electricity (SCCER SoE). The authors express their sincere thanks to Prof. Dr. Bruno Sudret and Dr. Stefano Marelli, ETHZ, Dr. David Vetsch, ETHZ, and to Dr. Calvin Wheaton, PSI, for valuable comments and assistance.

References

- Sudret, B. 2007. Uncertainty propagation and sensitivity analysis in mechanical models: Contributions to structural reliability and stochastic spectral methods., Report: Habilitation "a diriger des Recherches, Universit'e Blaise Pascal.
- Sudret, B. 2008. Global sensitivity analysis using polynomial chaos expansions. Reliability Engineering & System Safety, 93: 964-979.
- Rosgen, et al., 2013. Waldo Canyon Fire Watershed Assessment: The WARSSS Results. W. Hydrology
- Marelli, S. & Sudret, B., 2014. UQLab: A framework for uncertainty quantification in Matlab 257 Vulnerability, Uncertainty, and Risk. 2nd ICVRAM2014, UK.
- ETH Zurich, 2016. BASEMENT, Accessed in: <http://www.basement.ethz.ch/>.
- SwissCOD, 2016. Dams in Switzerland, Accessed in: <http://www.swissdams.ch/index.php/en/swiss-dams/dams-in-switzerland>.

Quantitative assessment of uncertainties and sensitivities in life loss estimates due to an instantaneous dam-break

Anna Kalinina¹, Matteo Spada¹, Peter Burgherr¹ & Christopher T. Robinson²

¹Laboratory for Energy Systems Analysis (LEA), Paul Scherrer Institut, Villigen PSI, Switzerland; ² Department of Aquatic Ecology, Eawag, Dübendorf, Switzerland

Research scope

This work focuses on the model that estimates the life loss resulting from the impact of the dam-break flood in the locality downstream of the dam (Block 2 in Fig. 1). The model of the corresponding flood (Block 1 in Fig.1) is presented by the authors in the poster “Application of the Polynomial Chaos Expansion for uncertainty quantification of the flood wave propagation resulting from a concrete dam break”.

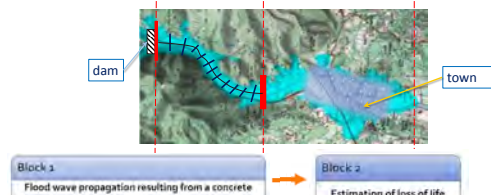


Fig. 1. Essential computational blocks for the modeling of the dam-break event

Research objectives

1. Application of the HEC-LIFESim life-loss (LL) modeling software to a case study with conditions relevant for Switzerland;
2. Application of metamodeling for quantification of uncertainties in the estimation of life loss provided by HEC-LIFESim;
3. Global analysis of the model sensitivities.

Framework for uncertainty quantification (UQ) & global sensitivity analysis (GSA)

The framework for uncertainty quantification (UQ) and global sensitivity analysis (GSA) in Fig.2 is developed specifically for the model estimating LL due to an instantaneous dam break. The physical model is run with the HEC-LIFESim software and reflects conditions relevant for Switzerland. The framework aims at demonstrating benefits of the use of metamodeling for quantification of uncertainties in comparison with the sampling-based Uncertainty Mode implemented in HEC-LIFESim. The framework also includes calculation of global sensitivity indices for different model inputs in order to understand their contribution to the overall variability of LL estimates.

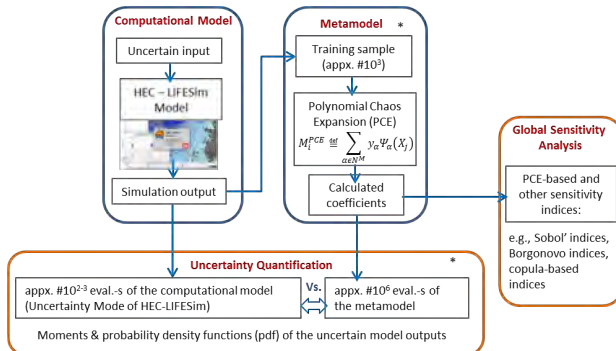


Fig. 2. Main computational steps of the framework for UQ and GSA

* The module is explained by the authors in the poster “Application of the Polynomial Chaos Expansion for uncertainty quantification of the flood wave propagation resulting from a concrete dam break”.

The modules on the computational model and GSA are further elaborated in detail in this poster.

Computational HEC-LIFESim model

The HEC-LIFESim software (USACE 2017) is a spatial dynamic system for modeling LL of a flood event. It is a modular system consisting of four modules, namely flood routing module, warning and evacuation module, loss of shelter module, and life loss module. These modules are built around databases and exchange data through geo-layers.

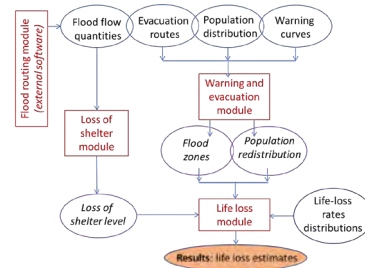


Fig. 3 HEC-LIFESim approach for LL estimation (modified from Bowles, 2007)

HEC-LIFESim estimates the number of LL by redistributing the initial Population At Risk (PAR), i.e., the amount of people living in the inundated area, based on the information about evacuation, warning, flood severity and other factors. Combining further the recalculated PAR in different zones with the historical LL-rates, the total LL caused by a specific dam-break event can be estimated.

Global Sensitivity Analysis (GSA)

A number of different techniques are applied for the purpose of the GSA in this study. They include Sobol' indices, Borgonovo indices, copula-based indices, etc.

For example, Sobol' indices, S_i , define individual contributions of each model input to the total variance D . They can be determined using the PCE coefficients calculated in the previous step (so-called PCE-based Sobol' indices); in this case, GSA requires no additional sampling (Sudret, 2008):

$$S_i = \frac{\sum_{\alpha \in A_i} y_{\alpha}^2}{D}, A_i = \{\alpha \in N^M : \alpha_i > 0, \alpha_{j \neq i} = 0\}$$

The Borgonovo index, δ_i , (Borgonovo, 2007) of a random input variable X_i is a measure of the expected shift in the probability distribution of the model output when X_i is set to a fixed value. If the expected shift is close to zero, then the variable is not important, otherwise for more important variables it takes a larger value:

$$\delta_i = \frac{1}{2} E_{X_i} \left[\int |f_Y - f_{Y|X_i}| dy \right]$$

Where f_Y is the probability distribution of the model output and $f_{Y|X_i}$ is the conditional distribution of X_i . Other sensitivity indices used in this study are elaborated in Kalinina et al. (2018).

Status and Outlook

- The dynamic spatial LL-model built in HEC-LIFESim can fully address the risk to which people are exposed in a dam-break flood event.
- Furthermore, it is important to adjust LL-rates to reflect study-specific characteristics of the dam type and failure mode. For Swiss dams, alternative LL-rates had different shapes and frequency ranges than the generic ones used by HEC-LIFESim.
- PCE-metamodeling and GSA allowed for rigorous and computationally efficient assessment of uncertainties in LL estimates.

Acknowledgement: This research project is part of the National Research Programme “Energy Turnaround” (NRP 70) of the Swiss National Science Foundation (SNSF). Further information on the National Research Programme can be found at www.nrp70.ch. It is also integrated with the activities of the Swiss Competence Center on Energy Research – Supply of Electricity (SCCER SoE).

References

- Borgonovo, E. 2007. A new uncertainty importance measure. Reliability Engineering and System Safety 92, 771-784. 14, 15.
- Bowles, D. S. 2007. Life Loss Estimation for RAMCAP, Appendix D, Conventional Dams and Navigation Locks, Sector-Specific Guidance (SSG), Risk Analysis and Management for Critical Asset Protection (RAMCAP)
- Kalinina A., Spada M., Burgherr P., 2018. Quantitative assessment of uncertainties and sensitivities in the life loss due to the instantaneous break of a hypothetical dam in Switzerland (in preparation).
- Sudret, B. 2008. Global sensitivity analysis using polynomial chaos expansions. Reliability Engineering & System Safety, 93: 964-979.
- USACE 2017. HEC-LifeSim 1.0. U. S. Army Corps of Engineers, Hydrologic Engineering Center.

Toward a new framework for chemical risk assessment in the context of accidental events in deep geothermal energy (DGE) systems

Matteo Spada, Peter Burgherr

Technology Assessment Group, Laboratory for Energy Systems Analysis, Paul Scherrer Institut (PSI)

Supported by:



Schweizerische Eidgenossenschaft
Confédération suisse
Confederazione Svizzera
Confederaziun svizra
Swiss Confederation

Innosuisse – Swiss Innovation Agency

Motivation & Objectives

The aim of this study is to move toward a framework for chemical risk assessment of accidental events in Deep Geothermal Energy (DGE) systems. In particular, the scope of this work is to develop a framework for a hypothetical accidental chemical release in the air compartment that considers both uncertainty and variability in the inputs to account for uncertainty and variability in the outputs. Furthermore, a global sensitivity analysis of the model outputs with respect to the inputs will be performed. The focus of this preliminary study is on the presentation of the framework and on a preliminary analysis on the chemical concentration (mg/m³) in air at different distances from the source of the accident.

A Framework for Chemical Risk Assessment

Chemical Risk Assessment (CRA) is estimated as the product between the exposure duration and concentration to a chemical under interest (Exposure Assessment (EA)) and the maximum level of acceptable concentration (i.e. without consequences) within a period of time by the receptor under interest (e.g. humans and/or the environment) (Hazard Assessment (HA)) [1], see Figure 1.

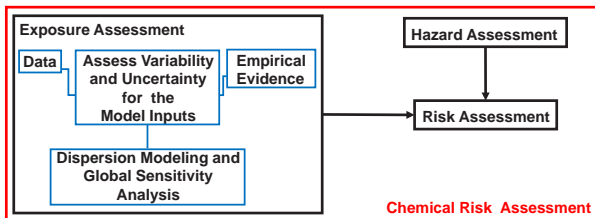


Figure 1: Scheme of the proposed framework for Chemical Risk Assessment with uncertainties

The HA is given by laboratory experiment results, which can be found in the literature for the most common chemicals [2]. Therefore, the focus of this study is on the EA. As shown in Figure 1, the proposed framework for the EA could be subdivided into four major steps. First, empirical evidence from historical accidental releases of the chemical under interest needs to be collected along with other crucial information (data) for different parameters that could affect the chemical dispersion (e.g., wind speed, wind directions, etc.). Second, variability and uncertainty of the abovementioned information are assessed to be used as inputs for the model. Third, a dispersion model (e.g. Gaussian Plume model [3]) for chemicals is used in a stochastic environment (e.g. Monte-Carlo sampling, etc.) to assess the chemical concentration in air including its uncertainty at different distances and times from the source. Furthermore, a Global Sensitivity Analysis (GSA) of the model outputs is performed to assess the effect of the inputs of the model to the outputs. Finally, the results of the concentrations under uncertainty at different distances and times are used as exposure values for the estimation of the risk on human health and/or the environment.

Case Study

Hazardous substances are used in different phases of the life cycle of a deep geothermal power plant [4]. In here, the focus is on the most common chemicals used for the matrix acidizing treatment during the stimulation phase (e.g. Hydrogen Chloride (HCl) and Hydrogen Fluoride (HF)), see Figure 2.

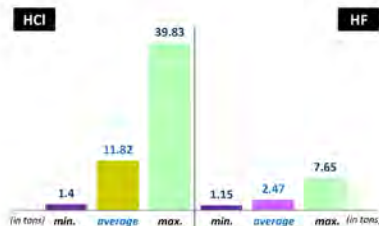


Figure 2: Average, minimum and maximum quantities of the most common hazardous chemicals used in the stimulation phase for deep geothermal energy systems [5].

The analyzed accident scenario is defined as a leak from a circular hole (of variable size: 0.5, 1, 2.5, 4, 8, 15 cm) located at 25 cm from the tank bottom, in a 100% full horizontal cylindrical storage tank (length = 7 m; diameter = 0.95 m; volume = 5 m³) located at the plant.

Weather data (temperature, dew point, humidity, wind speed, wind direction, etc.) have been collected for a hypothetical location in the Molasse Basin in Switzerland from 2010 to 2018 (Figure 3).

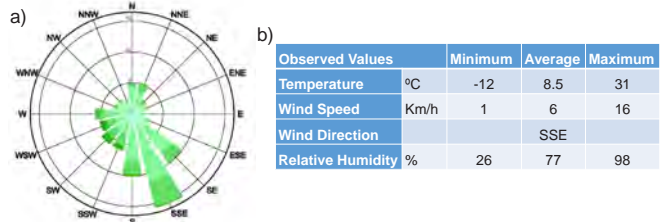


Figure 3: a) Average distribution of Wind Speed and Direction at a hypothetical location in Switzerland; b) Selected weather data used as inputs in the chemical dispersion model (www.wunderground.com).

Weather information and hole size in the storage tank have been sampled 10'000 times with a Monte-Carlo algorithm and input in ALOHA® (<https://www.epa.gov/cameo/aloha-software>), the chemical dispersion model used in this study, to assess the EA with uncertainty (Figure 4).

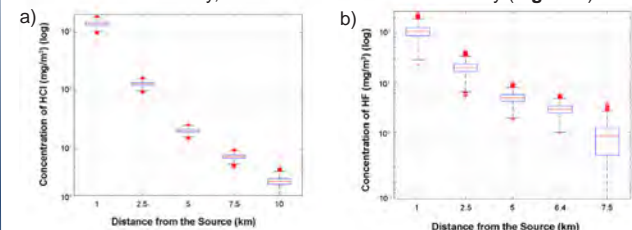


Figure 4: Chemical concentration including uncertainty at different distances along the axis of the main wind direction from the source. a) HCl; b) HF.

A preliminary sensitivity analysis has been carried out by allowing only one parameter to vary per ALOHA® run, keeping all the other parameters fixed (Figure 5).

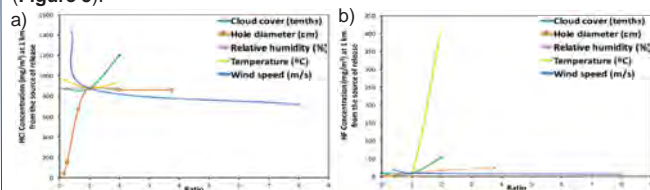


Figure 5: Sensitivity analysis for different model parameters. a) HCl; b) HF

Summary & Outlook

- A new framework for Chemical Risk Assessment including uncertainty quantification and sensitivity analysis has been proposed.
- Along the axis of the main wind direction, uncertainties for the emitted chemical concentrations appear relatively small in general, except for the most distant sample in the HF case.
- The preferential role of some parameters, e.g. wind speed and hole diameter (and also cloud cover for HF), on the atmospheric dispersion of the selected hazardous chemicals is evidenced.
- Further developments of the model framework are needed. On the one hand, by including reactions of the chemicals with the ambient humidity, the deposition process of the chemicals, etc. in the EA model. On the other hand, to optimize and automatize the process along with including the GSA.

References

[1] European Chemicals Agency (ECHA) (2012). Risk Characterization. Guidance on information requirements and chemical safety assessment. Helsinki, Finland: European Chemicals Agency (ECHA).
 [2] Weidrum M. (1999). Toxicology of Hydrogen Fluoride in Relation to Major Accident Hazards. Regulatory Toxicology and Pharmacology, 30(2), 110-6
 [3] Stockie JM. (2011). The Mathematics of Atmospheric Dispersion Modeling. SIAM Review, 53(2), 349-72.
 [4] Spada M, Burgherr P. (2015). Accident Risk. In: Hirschberg S, Wiener S, Burgherr P, editors. Energy from the Earth: Deep Geothermal as a Resource for the Future? Zurich, Switzerland: vdf Hochschulverlag AG; 2015. p. 229-62
 [5] Sutra E, Spada M, Burgherr P. (2017). Chemicals usage in stimulation processes for shale gas and deep geothermal systems: A comprehensive review and comparison. Renewable and Sustainable Energy Reviews, 77, 1-11

Understanding social perception of geothermal energy in Chile

Amanda Martínez Reyes[†], Sofía Vargas Payera[‡], Olivier Ejderyan[†] and Michael Stauffacher[†]
[†]Swiss Federal Institute of Technology Zurich, [‡]Andean Geothermal Center of Excellence.

Motivation

Caring for a positive social perception of geothermal energy is necessary to foster this technology in Chile. By 2030, the Chilean portfolio is planning to add up to 5.2 GW, from a 16 GW total capacity, to the current 48 MW installed capacity [1,2,3]. However, there are social and political barriers that have prevented projects to succeed [4]. One can learn from these cases to identify firms' practices on stakeholders engagement and understand how such strategies may trigger a positive and negative social perception. Few studies have addressed this problem worldwide.

Focus and objectives

This study was focused on a geothermal exploration project in southern Chile, in which community stakeholders were approached to inform and create trust. The goal of this study was to disentangle such approach and explain the resulting social perception. Three objectives were addressed:

- To evaluate actors perception of the project in the past.
- To disentangle the company's stakeholder engagement strategy and understand how it influenced perception.
- To identify external variables that influenced perception and explore how.

Method for data collection

The testimonies of 27 stakeholders were collected from: tourism companies (TR), local authorities (LA), indigenous communities (IN), neighbor associations (DC/NC), landowner (LO), and NGOs.



Review of written documents:



Method for analysis

The software NVivo 12 Plus was employed to arrange data. The next steps were followed:

1. Transcription of collected data.
2. Timeline of project's milestones.
3. Coding into nodes of variables, topics and categories. One node for perception.
4. Allocation of nodes in timeline.
5. Matrix crossing of nodes from point 3 with perception.
6. Explanation of perception by reading the references of overlaps of point 5.

Results

The stakeholders' perception along the geothermal project's lifetime varied due to the influence of different variables. These variables were arranged in 3 categories: Stakeholder Engagement Strategy, Project Activities, and Context. Such influence is explained and shown in Figure 1 and 2, respectively. Overall, 5 stakeholders had a negative perception, 2 a positive and 2 a neutral.

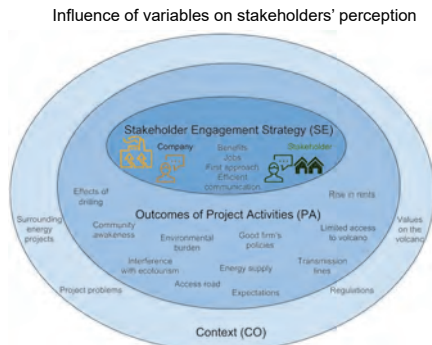


Figure 1. Variables that influenced perception. The engagement process cannot be isolated from the project activities and context.

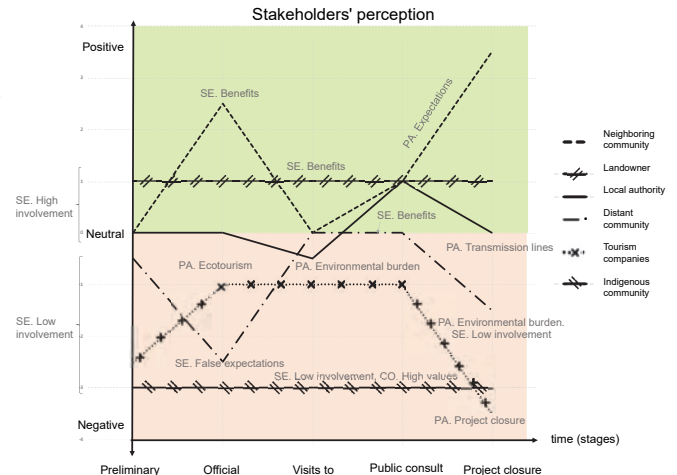


Figure 2. Stakeholders' perception over time. The variables that influenced perception are shown.

Conclusions

- Not only the company's engagement strategy, but also the project activities and context influenced social perception. It varied for each stakeholder.
- Both, Chilean regulations and the company did not promote the realization of an environmental impact assessment from the beginning (exploration). Thus, distrust was built.
- Stakeholders were involved differently, so that different attitudes toward the project were developed.
- The novelty of this study was the description of different stakeholders' views on geothermal energy in the Chilean context, and the development of a methodology that allowed to study the perception of a project that occurred 9 years before.

References & Acknowledgements

Financially supported by own resources from ETHZ USYS Transdisciplinarity Lab. Special acknowledgements to the Andean Geothermal Center of Excellence (CEGA) for their enthusiastic support

1. Lahsen, A.; Rojas, J.; Morata, D.; Aravena, D. Geothermal exploration in Chile: country update. Paper presented to the World Geothermal Congress, Melbourne, Australia. 2015. Viewed 07.2018. www.researchgate.net/publication/280720382_Geothermal_Exploration_in_Chile_Country_Update
2. Almaraz, D. Geothermal Development in Chile. Paper presented to the Short Course VI on Utilization of Low- and Medium-Enthalpy Geothermal Resources and Financial Aspects of Utilization. Santa Tecla, El Salvador. 2014. Viewed 07.2018. www.scribd.com/document/257185420/Geothermal-Development-Chile
3. "Enel and ENAP inaugurate South America's first geothermal power plant Cerro Pabellón" Enel Green Power. September 12. 2017. www.enelgreenpower.com/media/press/d/2017/09/enel-and-enap-inaugurate-south-americas-first-geothermal-power-plant-cerro-pabellon
4. Saldívar Olave, Miguel. 2013. *Barreras a la entrada de la geotermia en Chile*. Santiago, Chile: Universidad de Chile - Facultad de Derecho. <http://repositorio.uchile.cl/handle/2250/114500>



Application to the Swiss Alps of the Landslide Generic Cellular Automaton (LSgCA)

Abstract:

The scaling exponent α of the power-law in the frequency-size distribution of landslides is a critical parameter in landslide hazard assessment. A recent study by Jafarimanesh et al. (NHES, 10.5194/nhess-2018-167) proposed a generic cellular automaton approach (LSgCA) to retrieve the range of α values observed in the literature. While LSgCA was applied to simulated topographies with a wide range of possible soil characteristics, this study is the first to apply the method to a real case study with site-specific parameters.

Our site is located in the Illgraben catchment of the Swiss Valais Alps, a very active catchment which potentially produces large sediment discharge that surpasses the average alpine rate. A multi-temporal record of the landslide process in the study slope has been previously quantified by Bennett et al. (2012) with α values observed in the range of $\alpha = 1.7-2$, in the low range compared to the $\alpha = 2.21 \pm 0.53$ of the literature. We verify that a similar α distribution is retrieved when using the site-specific characteristics of the Illgraben catchment to validate the application of LSgCA in real case conditions and demonstrate the importance of rheology for a refined landslide hazard assessment.

Method: Landslide Generic Cellular Automaton (LSgCA):

A. Initiation phase: Landslide initiate when the factor of safety (Fs) is ≤ 1 .

$$FS = \frac{c+h(\gamma_t-\gamma_w)\cos\theta \tan(\phi)}{\gamma_t \sin\theta}$$

c stands for the cohesion of soil, ϕ is the angle of friction angle, θ is the slope gradient, γ_t is the total material unit weight, γ_w is the water unit weight, and h stands for the slope normal thickness of the failure slab.

B. Propagation phase: Input parameters are the initial topography (z, h) and soil properties ($c, \gamma_t, \theta, \phi$). The maximum slope θ_{max} is calculated based on the Moore neighbourhood nomenclature (Tofoli and Margolus 1988) and defines the direction of the landslide flow. The mass movement is defined by:

$$\Delta h = [z(x, y) - z(dir_{Moore}[\theta_{max}(x, y)]) - \Delta s \tan(\theta_{stable})]/2$$

Case study: Illhorn peak, Illgraben catchment, Swiss Valais Alps

- ~ 1 km² surface area.
- The Illhorn peak is 2716 meters above the sea levels.
- Quarzitic dominated slope with the layer of dolomite and schist intersecting.
- The size of the past slope failures are measured with the photogrammetric analysis of historical aerial photographs from 1986 to 2005 by Bennett et al. (2012).

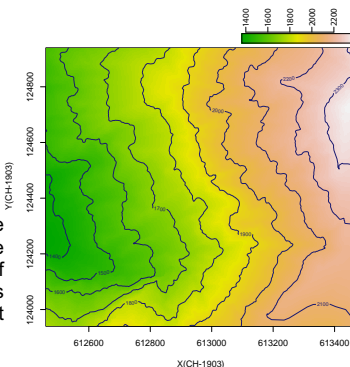


Fig.1: The topography of the case study in the Swiss coordinate system.

	Min	Max
Cohesion (kPa)	5	20
Soil unit weight (kN/m³)	11	18
Water unit weight (kN/m³)	9.8	-
Internal friction angle (deg)	11	30
Soil thickness (meters)	1	10
Slope gradient (deg)	15	85

Table 1: The range of the typical soil characteristics involved in this study (Swiss standards).

The application of LSgCA to the case study: The FS contour and the propagated landslide map:

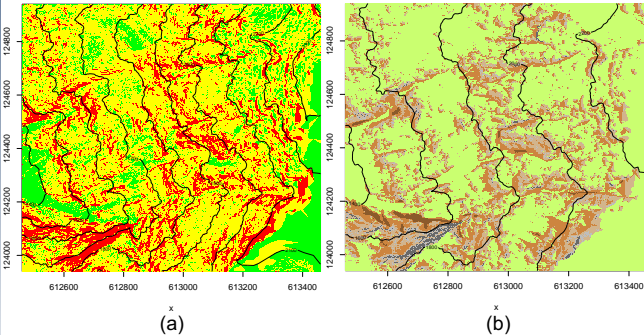


Fig. 2 : (a) The factor of safety (FS) contour map before the application of LSgCA, red patches indicating the unstable cells (FS ≤ 1). (b) Propagated landslide after the application of LSgCA; brown patches represent the landslide thickness; Scarps are shown in dark grey color.

Results :

- Comparison of the frequency size distributions (FSD), observed and simulated:

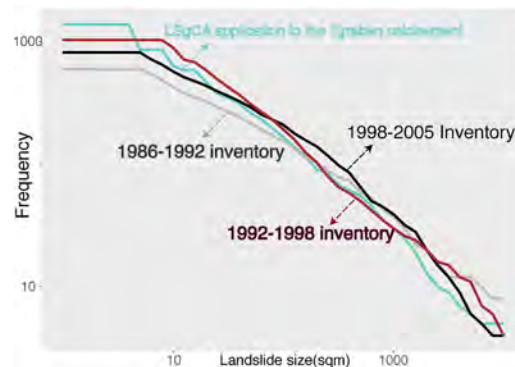
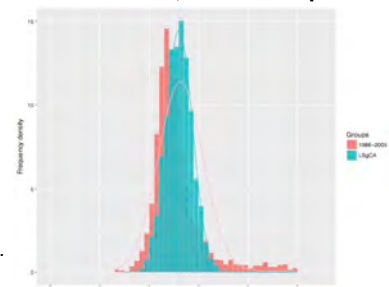


Fig. 3: The comparative FSD of the application of LSgCA in the study slope versus the FSD of the landslide inventories in the periods of 1986-1992 (A), 1992-1998 (B), 1998-2005 (C). We obtained the average non-cumulative scaling exponent α of the power-law equal to $\alpha=1.8$ for $n=50$ simulations similar to $\alpha_A=1.7, \alpha_B=2, \alpha_C=1.9$ for the three time periods.

- Uncertainty analysis on the power-law α range for the resampled landslide size datasets with 10,000 bootstraps.

Fig. 4: The distribution of the power law exponent α on the resampled landslide size data ($n=10,000$). The green fit demonstrates the distribution of LSgCA with the $\alpha_{avg}=1.76$, whereas the red fit shows the α range in 1986-2005 landslide inventory with the $\alpha_{avg}=1.77$.



Reference

- Bennett, G. L., Molnar, P., Eisenbeiss, H., & Mcardell, B. W. (2012). Erosional power in the Swiss Alps: Characterization of slope failure in the Illgraben. Earth Surface Processes and Landforms, 37(15), 1627–1640. doi:10.1002/esp.3263.
- Jafarimanesh, A., Mignan, A., and Danciu, L.: Origin of the power-law exponent in the landslide frequency-size distribution, Nat. Hazards Earth Syst. Sci. Discuss., <https://doi.org/10.5194/nhess-2018-167>, in review, 2018.

Task 4.2

Title

Global observatory of electricity resources

Projects (presented on the following pages)

Long term EU electricity supply scenarios: Impact of EU electricity policies on Switzerland
Antriksh Singh, Ramachandran Kannan, Tom Kober

Marginal electricity supply – a country-specific analysis on the global level
Laurent Vandepar, Christian Bauer, Karin Treyer, Chris Mutel

Potentials, costs and environmental assessment of electricity generation technologies
Christian Bauer

A preliminary sustainability analysis of potential areas for deep geothermal energy (DGE) systems:
Application to Switzerland
Matteo Spada, Marco Cinelli, Peter Burgherr

Spatial hot spots and cold spots of new renewable electricity projects that received federal feed-in
tariff in Switzerland
Christoph Thormeyer, Jan-Philipp Sasse, Evelina Trutnevyte

Long term EU electricity supply scenarios: Impact of EU electricity policies on Switzerland

Ramachandran Kannan, Tom Kober, Antriksh Singh
Energy Economics Group, Laboratory for Energy Systems Analysis,
Paul Scherrer Institut, 5232 Villigen PSI, Switzerland



The development of the Swiss electricity system will be highly influenced by technical, economic, and energy policy developments in the neighboring countries. To assess the impacts of key EU policies on the Swiss electricity system, the European Swiss TIMES Electricity Model (EUSTEM) developed at PSI is recalibrated to 2015 electricity data. Near-term EU energy policies are implemented along with new electricity storage options. Preliminary scenario analysis results show that gas power plants serves as transition technologies in the short-/mid-term. In our baseline, the

committed EU polices for the electricity sector would reduce the sector's CO₂ emission in 2050 by 60% from 2010 level. To further decarbonize the electricity sector requires high share of renewable (>40% of the generation) and gas-based CCS technology. In order to integrate large shares of variable renewable energy production, 250-450 TWh of electricity would need to be shifted by storage systems in 2050. For the power sector alone, the marginal cost of CO₂ emissions reduction in 2050 varies between 300-445 CHF/t-CO₂ depending on the market conditions.

European Swiss TIMES model (EUSTEM)

The EUSTEM is a multi region, cost-optimization model of the EU electricity system. It has a long time horizon (2050+) and an hourly time resolution. The model covers 96% of EU-28 electricity supply (Fig. 1) with a detailed representation of the Swiss electricity system. The model is calibrated to 2015 electricity statistics [1] and technology characterisation and resource potentials are updated. Now, new storage technologies and key EU polices are implemented. With the newly refined model, we conducted a scenario analysis of which we present preliminary results.

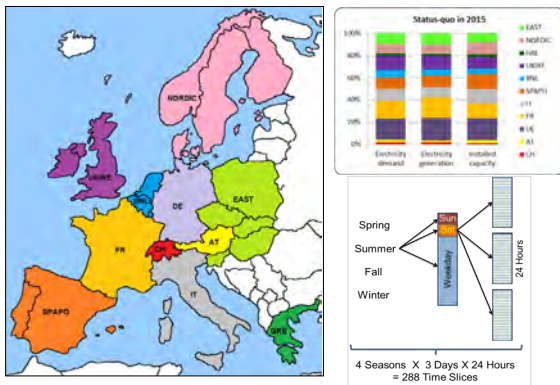


Fig 1. Regions in EUSTEM and intra-annual resolution

Electricity supply scenarios

Two core scenarios on future electricity supply, viz. *Base* and *Climate* scenarios.

- Base** scenario: least cost electricity supply for the electricity demands from the EU reference scenario while fulfilling existing policy targets of EU member states, incl. nuclear phase-out, renewable targets and CO₂ emission, etc.
- Climate (LC95)** scenario: reduction of the CO₂ emissions from the EU electricity sector by 95% until 2050 (from 2010 levels) without any national targets.

Variants: While curtailment of renewables is allowed in the core scenarios, we looked at a scenario without curtailment (*LC95_NoCurtail*). As a variant, self-sufficiency in electricity supply is considered in each region (*LC95_SS*).

Preliminary results in the *Base* scenario show a shift towards gas-based generation in the mid-term due to planned nuclear/coal phase-outs in some countries. In the long run, there is a growth in renewable based generation and coal based electricity with carbon capture and storage (CCS) which become cost-effective.

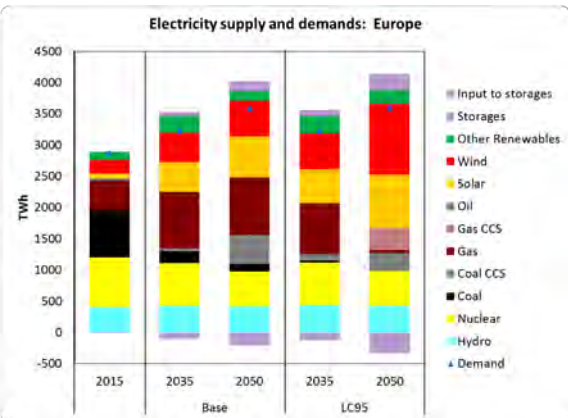


Fig 2. Electricity supply in the *Base* and *Climate* scenarios

In the *Base* scenario, EU electricity sector's CO₂ emissions reduce by 60% in 2050 relative to 2010 level. However, reducing the remaining CO₂ emission is challenging and incurs high cost. By 2050, over 700 GW of solar PV and 550 GW of wind turbines supply 40% of the electricity demand (Fig. 2) in the *LC95* scenario. This high share of RES requires large electricity storage (and curtailment) to cope with the diurnal and seasonal variabilities. At increasing climate change mitigation ambition, a shift from coal-CCS to gas-CCS can be observed to unlock further CO₂ emission reductions. This comes at high operational costs due to the increasing gas price. The marginal cost of CO₂ grows from 73 CHF/t CO₂ in 2030 to 300 CHF/t CO₂ in 2050. Additional renewables would need to be deployed together with additional storage capacity, in case CCS is excluded as a mitigation technology (*LC95_NoCCS* scenario in Fig. 3).

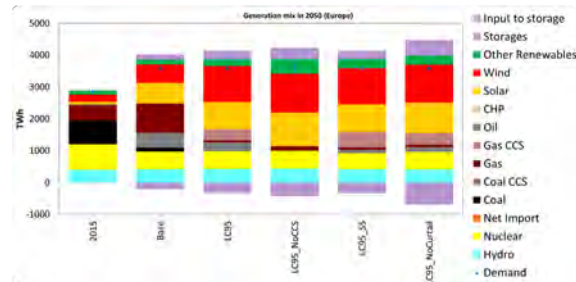


Fig 3: European electricity supply in 2050

The results indicate that some level of curtailment is cost-effective. In the non-curtailment scenario (*LC95_NoCurtail*), storage increases despite reduced investment in variable renewable technology.

If the regions would aim at maintaining autarky in their overall annual electricity supply while still using the flexibility from the EU network, the investments of renewable technologies are shifted to regions where their generation is less competitive compared to other regions while additional investments are needed for gas power plants and storages (Fig. 3).

Across the scenarios, the average cost of Swiss cross border electricity supply varies between 70 and 127 CHF/MWh in 2050 whereas the hourly spread of marginal cost is very significant (Fig. 4). When curtailment of solar PV and wind is restricted, the average cost in 2050 increase by about 11-20 CHF/MWh (from *LC95* levels). However, the hourly cost spread increases substantially with the occurrence of negative prices for few hours.

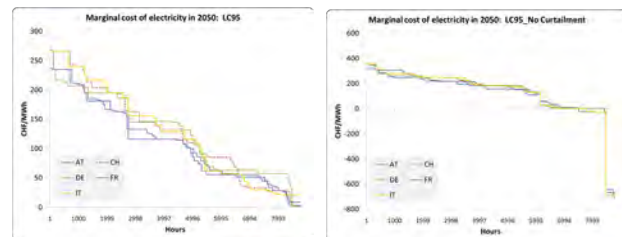


Fig 4: Cross border marginal cost of electricity in 2050 with and without curtailment

Summary

- Gas power plants serve as transition technologies in the short-/mid-term.
- The current EU polices and the least cost based electricity supply would reduce CO₂ emission of the power sector in 2050 by 60% (vs. 2010). To meet a 95% CO₂ reduction target requires shares of intermittent renewable above 40% and large storage capacity with diurnal and seasonal storages.
- Depending on the market conditions, 125-355 GW of installed storage capacity store about 250-450 TWh electricity (or ~ 5-10% of the demands) in 2050.
- CCS-based technologies contribute cost-effectively to climate change mitigation.
- In the climate scenarios, marginal cost of CO₂ emissions reduction vary between 300-445 CHF/t-CO₂ in 2050 depending on the availability of CCS, curtailment of production from renewable energy, and storage availability.

Marginal electricity supply – a country-specific analysis on the global level

Laurent Vandepaer^{1,2}, Karin Treyer², Chris Muter¹, Christian Bauer² and Ben Amor¹

1. Interdisciplinary Research Laboratory on Sustainable Engineering and Ecodesign (LIRIDE), Civil Engineering Department, Université de Sherbrooke, 2500 boul. de l'Université, Sherbrooke J1K 2R1, Québec, Canada;
2. Laboratory for Energy Systems Analysis, Paul Scherrer Institute, CH-5232 Villigen PSI, Switzerland

Introduction

The long-term marginal electricity supply mixes of 40 countries were calculated and integrated into the consequential system model of version 3.4 of the ecoinvent Life Cycle Assessment (LCA) database.

In LCA, marginal electricity supply mixes are used to model the origin of the electricity consumed when one additional unit of a product is produced; this approach represents so-called "consequential LCA".

As such, the marginal mixes are composed only of electricity generation capacity able to react to a change in demand by a corresponding change in supply. In the case of long-term mixes, they reflect the accumulated effect of changes in demand for electricity on the installation and operation of new generation capacities.

In this study an overview of the methodology used to calculate the long term marginal mixes is provided. The influence of key parameters and methodological choices on the results is also evaluated.

Methods

The marginal electricity supply mixes were calculated using equation (1) from (Schmidt 2012; Muñoz et al. 2015):

$$Share_{i,TH} = 100 \cdot \frac{P_{i,TH} - P_{i,ref}}{\sum_i (P_{i,TH} - P_{i,ref})}$$

Where:

- i: electricity-producing technology
- TH: the year chosen as time horizon
- ref: the year chosen as a reference for the time of the decision
- P: the quantity of electricity generated at time "TH" or "Ref" by technology i
- n: includes all unconstrained electricity producing technologies with a growing production at TH with respect to ref
- Share i: the percentage that supplier i contributes to the marginal mix

The reference year is 2015 and time horizon is 2030. The formula is fed by data source from public projections from national and international authorities (e.g., European Commission, International Energy Agency, Swiss energy perspectives).

Results

In total, consistent electricity production scenarios were available for 40 countries. These were implemented, as displayed in Fig.1. The total electricity production originating from these countries accounts for 77% of the current global electricity generation.

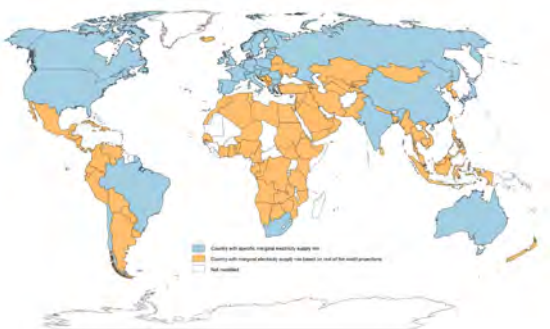


Fig. 1 Geographical coverage of the marginal electricity supply mixes in the consequential system model of ecoinvent v3.4, differentiated between countries where specific energy projections were used as a source of data and countries where rest of world shares were assumed.

The marginal electricity supply mixes are comprised, on global average, of 59% from renewable energy sources (RES), 27% from fossil-based sources and 14% from nuclear power.

Among the RES, onshore wind turbines dominate with an average share of 21% of the total mix and is followed by solar power with 17%.

In terms of fossil-based energy, natural gas combined cycle power plants are the largest marginal electricity source contributing 23%.

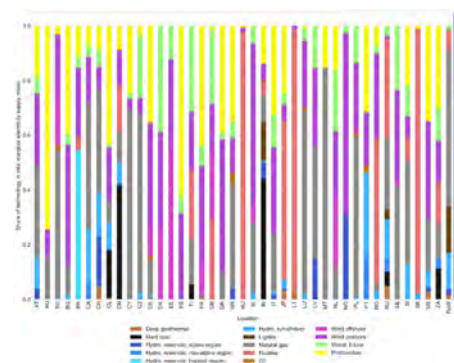


Fig. 2 Composition of marginal electricity supply mixes, as implemented in ecoinvent v3.4, consequential, at the low voltage level per country.

Impact assessment and local sensitivity analysis

Figure 3 shows the comparison of life-cycle emissions of CO₂ equivalents per kWh (CO₂-eq/kWh) between the mixes obtained in this study and other approaches to calculate the electricity mixes.

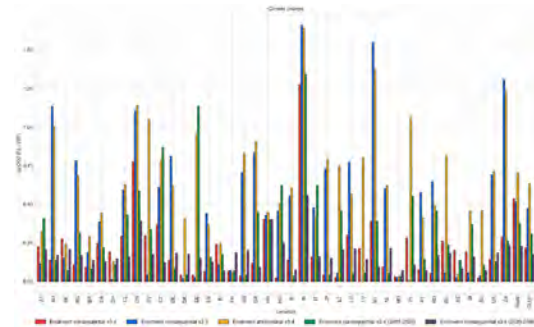


Fig. 3 Comparison of results for the climate change impact category (IPCC 2013, GWP 100a) of marginal electricity supply mixes in ecoinvent consequential v3.4, ecoinvent consequential v3.3, ecoinvent attributional v3.4 ("cut-off by classification"), ecoinvent consequential v3.4 (2015-2020) and ecoinvent consequential v3.4 (2030-2040).

The average life-cycle emission factor of the marginal mixes is 0.216 kg CO₂-eq/kWh and the median value amounts to 0.158 kg CO₂-eq/kWh. India has the highest emission factor with 1.275 kg CO₂-eq/kWh.

Conclusion

The marginal mixes integrated into the consequential system model of ecoinvent version 3.4 eliminate important limitations from the previous version of the database.

The use of energy scenarios allows for the accounting of the future evolution of the electricity system in line with the definition of electricity markets.

Reference

- (1) Muñoz I, Schmidt J, De Saxcé M, et al (2015) Inventory of country specific electricity in LCA - consequential scenarios version3.0. Aalborg
- (2) Schmidt JH (2012) Modelling of electricity in life cycle inventory and comparisons and recommended approach. In: SETAC Europe 18th LCA Case Study Symposium, 2012.

Potentials, costs & environmental assessment of electricity generation technologies

Christian Bauer, S. Hirschberg, Y. Bäuerle, S. Biollaz, A. Calbry-Muzyka, B. Cox, T. Heck, M. Lehnert, A. Meier, H.-M. Prasser, W. Schenler, K. Treyer, F. Vogel, H.C. Wieckert, X. Zhang, M. Zimmermann (alle PSI), V. Burg, G. Bowman, M. Erni (WSL), M. Saar (ETHZ), M.Q. Tran (EPFL)

Background

This analysis represents an input to the next update of the Swiss Energy perspectives and serves as basis of the Energy Strategy 2050. Furthermore, it is part of the technology monitoring of SFOE. Consistent and up-to-date potentials and costs up to year 2050 are also important for the SCCER joint activity scenarios and modelling.

The work was commissioned by SFOE and supported by SCCER biosweet.

Scope

The following power generation technologies were evaluated:

Generation in Switzerland

- Hydropower
- Photovoltaics
- Wind turbines
- Electricity from biomass
- Deep geothermal power
- Fuel Cells
- Natural gas CC & CHP
- Nuclear

Electricity imports

- Offshore wind turbines
- Solar thermal power
- Wave and tidal power
- Coal

Potentials for electricity generation and supply

Exploitable electricity generation potentials were estimated until 2050: these potentials represent technical potentials reduced by environmental and economic constraints; social constraints are only partially taken into account.

Photovoltaic electricity generation represents the largest potentially far among the renewable energy carriers. Deep geothermal power generation is associated with the highest uncertainties due to lack of technology readiness.

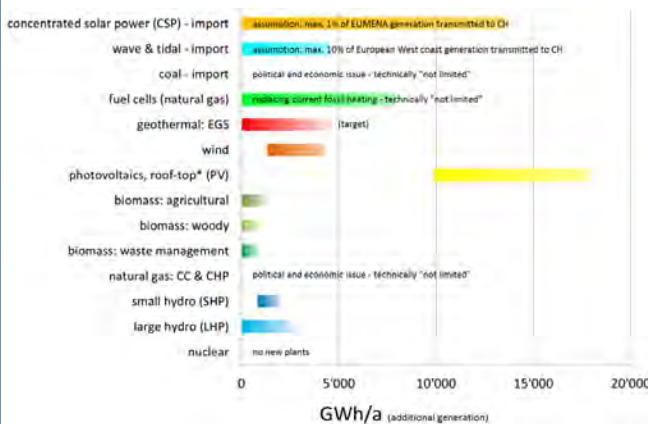


Figure 1: Estimated “exploitable potentials” for additional electricity generation (compared to 2015) with different fuels and technologies in Switzerland and for electricity imports from generation abroad, respectively, in 2050. NG: natural gas; CC: combined cycle; CHP: combined heat and power; LHP: large hydropower; SHP: small hydropower; CSP: concentrated solar power; PV: photovoltaics; EGS: enhanced geothermal systems; EUMENA: Europe, Middle East, North Africa; “coal” includes hard coal and lignite. * PV potential does not include generation by modules installed on building facades – the sustainable potential of such facade PV installations is in the range of 3-5.6 TWh/a.

Electricity generation costs

Levelised costs of electricity (LCOE) were estimated up to year 2050, taking into account expected developments of technology-specific investment, O&M and fuel costs. Compared to current generation costs, most substantial reductions can be expected for photovoltaics.

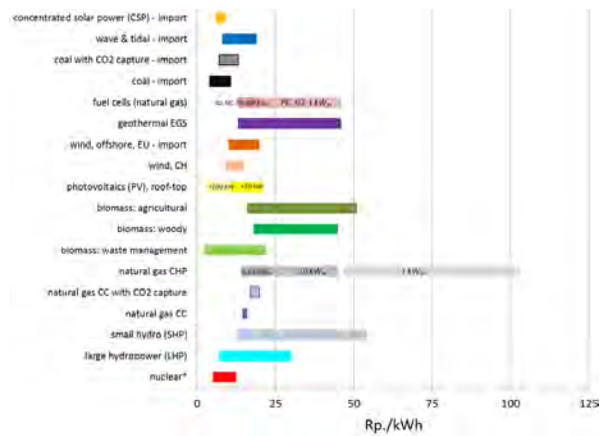


Figure 2: Costs of electricity generation (LCOE) with different technologies and fuels in year 2050.

Impact on climate change

Life-cycle greenhouse gas emissions were quantified, representing impacts on climate change. Life-cycle emissions include emissions due to construction, operation and end-of-life of power plants as well as fuel and material supply chains.

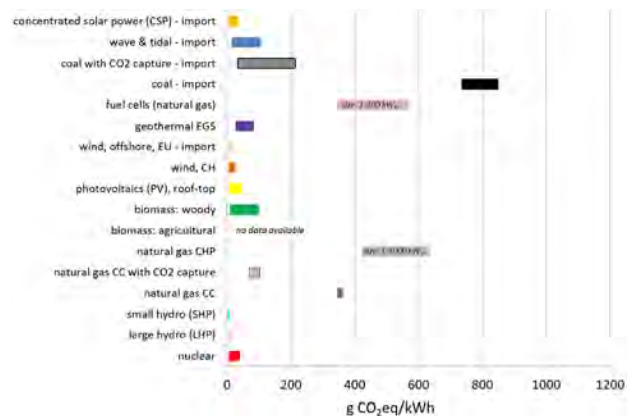


Figure 3: Life cycle GHG emissions of electricity generation technologies in year 2050.

Current limitations and further work

- Swiss-specific cost-potential curves – important for renewables – are currently not available and need to be established.
- Systemic issues such as short- and long-term electricity storage and the interconnection of the Swiss electricity market with the European electricity grid need to be investigated.
- External costs of power generation – important factor for technology assessment – should be quantified.



A Preliminary Sustainability Analysis of Potential Areas for Deep Geothermal Energy (DGE) Systems: Application to Switzerland

Matteo Spada¹, Marco Cinelli², Peter Burgherr¹

¹Technology Assessment Group, Laboratory for Energy Systems Analysis, Paul Scherrer Institut (PSI)

²Future Resilient Systems (FRS), Swiss Federal Institute of Technology (ETH) Zürich, Singapore-ETH Centre (SEC), Singapore

Supported by:



Schweizerische Eidgenossenschaft
Confédération suisse
Confederazione Svizzera
Confederaziun svizra
Swiss Confederation
Innosuisse – Swiss Innovation Agency

Motivation

The aim of this study is to move toward a Multi-Criteria Decision Analysis (MCDA) Tool for Deep Geothermal Energy (DGE) systems in Switzerland. In particular, the scope of this work is to identify the most sustainable area for hypothetical DGE plants in Switzerland using spatial MCDA, which combines Geographical Information Systems (GIS) capabilities with MCDA frameworks. The focus is on the Molasse basin, Rhine Graben, and Jura mountains regions (i.e., not the Alpine region) where most of the Swiss DGE projects are planned. The proposed approach combines spatial information from both explicit data (e.g., heat flow) and calculated ones (e.g., risk indicators, environmental impact indicators, etc.) for specific *a priori* defined plant characteristics (e.g., capacities, number of drilled wells over lifetime). Results are then presented for different hypothetical power plants.

Method

The sMCDA framework consists of different steps. First, the characteristics of the technology to be used in the sustainability assessment have been selected. In this study, since no running DGE plants exist in Switzerland, two hypothetical power plants based on SCCER-SoE Phase 1 activities are considered (Table 1).

Table 1: Key physical parameters of DGE plant capacity cases considered in this study

Model Assumption	Unit	Doublet Plant	Triplet Plant
Net Plant Capacity	MWe	1.47	2.81
Annual Generation	MWh/year	11849	22703
Life Time	years	20	20
Number of Wells		2	3
Well Depth	km	5	5
Well Life Time	year	20	20

Next, criteria are established to cover all 3 pillars of sustainability (environment, economy and society). Furthermore, indicators are chosen for each criterion based on availability and potential spatial variability (Table 2).

Table 2: Selected criteria and indicators used in this study.

Criteria	Indicators	Unit
Environment	Climate Change	kg CO2 eq to air
	Human Toxicity	kg 1,4-DCB eq to urban air
	Particulate Matter Formation	kg PM10 eq to air
	Water Depletion	m3 (water)
	Metal Depletion	kg Fe eq
Economy	Average Generation Cost	Rp/kWhe
Society	Non-seismic Accident Risk	Fatalities/kWh
	Natural Seismic Risk	Ordinal Scale [1-3]
	Induced Seismicity	Flow Rate [l/sec]

Indicators are then quantified for the hypothetical plants in Table 1 and for a set of 32 potential areas defined using Heat Flux (HF) and Natural Seismic Risk maps (<https://map.geo.admin.ch>). Environmental and economic indicator values have been estimated based on the temperature gradient (ΔT) in the area of interest, since ΔT is the ratio between the HF and the thermal conductivity of rocks (on average 3 W/m²°C in Switzerland [1]). On the other hand, the non-seismic accident risk indicator considers blow out risk and release of selected hazardous chemicals, which are related to the number of drilled wells [2]. The natural seismic risk indicator is considered in this study as a proxy of social acceptance, meaning that high risk is associated with lower social acceptance of a DGE system. The induced seismicity indicator is estimated based on the flow rate expected for the stimulation (i.e. higher the flow rate, the higher the risk of induced seismicity) for each of the plant capacities considered in this study.

Once the indicators are estimated for the 32 areas in the study, a Stochastic Multi-criteria Acceptability Analysis (SMAA-TRI) [3] has been applied and adapted to the spatial case. The SMAA-TRI algorithm is a classification method, which does not allow compensation between criteria and the weights are considered independent from the measurement scales.

The SMAA-TRI assigns a class of sustainability (e.g., high, medium-high, medium, medium-low, low) to an area in probabilistic terms (Figure 1). It estimates the Class Acceptability Index (CAI), which measures the stability of the assignment to a class in terms of probability for membership in the class. The CAI is driven by the weights of the indicators and according to the cutting level (λ), which gives a measure on how demanding the decision maker is (i.e., lower λ implies that a better class is easier to be reached). In this study, λ are arbitrarily distributed parameters analyzed using 10000 Monte Carlo simulations.

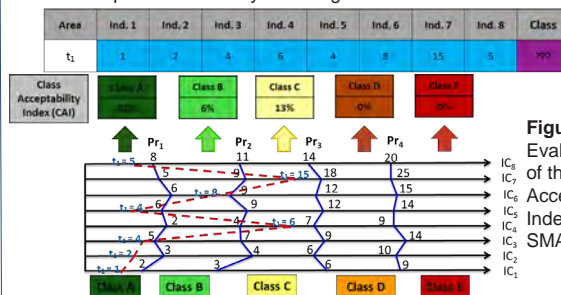


Figure 1: Evaluation steps of the Class Acceptability Index (CAI) in SMAA-TRI

Results

No stakeholder interaction, e.g., through elicitation has been performed in this study to assess weighting profiles of “real world” stakeholders. Instead, four artificial preference profiles have been defined:

- equal weights at all levels (both criteria and indicators in Table 2), which corresponds to the spirit of sustainability, where all pillars have the same weight.
- three weighting profiles that strongly favor one of the sustainability pillars (weight 80%), whereas the two other are both weighted 10%, and all indicators are equally weighted.

As an example, the results of the profile focusing on the Environment (weight 80%) are shown in Figure 2. For both Doublet and Triplet Plants, the most sustainable areas are the ones in North-East Switzerland. Furthermore, Triplet Plant, in Figure 2b, performs generally better than Doublet Plant, in Figure 2a.

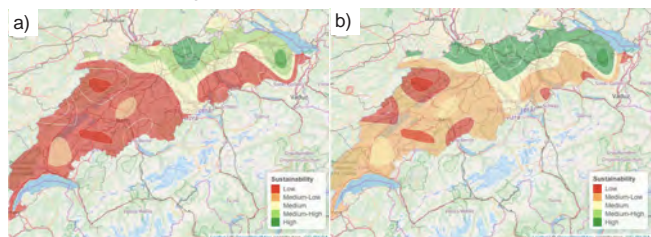


Figure 2: Environment-focused profile. a) Doublet Plant. b) Triplet Plant.

Conclusions

- First application of a spatial MCDA based on SMAA-TRI & GIS, demonstrating its suitability as decision-making tool for deep geothermal energy in Switzerland.
- Rankings of profiles representing equal weighting and focusing on economy are practically the same, for both capacity plants. Generally, areas in NE Switzerland perform best.
- Environment-focused results strongly differ from equal weighting and economic-focused profiles, i.e. Triplet Plant performs generally better than Doublet Plant.
- When focusing on social indicators, results differ from all other profiles with most areas falling into the medium sustainability category, and Triplet Plant performs generally worse than Doublet Plant.

References

[1] Bodmer Philippe H., (1982): Beiträge zur Geothermie der Schweiz. Diss. Naturwiss. ETH Zürich, Nr. 7034, 210 p.
 [2] Spada, M., Burgherr, P. (2015). Chapter 6.1: Accident Risk. In Hirschberg S., Wiemer S. and Burgherr P.: Energy from the Earth. Deep Geothermal as a Resource for the Future? TA-SWISS Study TA/CD 62/2015, vdf Hochschulverlag AG, Zurich, Switzerland, pp. 229-262. <http://dx.doi.org/10.3218/3655-5>.
 [3] Tervonen T., Lahdelma R., Almeida Dias J., Figueira J., Salminen P. (2007) SMAA-TRI. In: Linkov I., Kiker G.A., Wenning R.J. (eds) Environmental Security in Harbors and Coastal Areas. NATO Security through Science Series (Series C: Environmental Security). Springer, Dordrecht.

Spatial hot spots and cold spots of new renewable electricity projects that received federal feed-in tariff in Switzerland

Christoph Thormeyer¹, Jan-Philipp Sasse^{1,2}, Evelina Trutnevyte^{1,2}

¹ Renewable Energy Systems, Institute for Environmental Sciences (ISE), Section of Earth and Environmental Sciences, University of Geneva
² Institute for Environmental Decisions (IED), Department of Environmental Systems Science, ETH Zurich

Introduction

Spatially-resolved energy models with detailed renewable energy representation are widespread tools for informing renewable energy expansion, infrastructure planning and policy design [1]. A significant amount of evidence has shown that such models have represented the actual deployment of renewable energy very poorly [2]. An often-voiced argument is that existing models may not capture the real-world drivers and constraints of renewable energy diffusion comprehensively enough. In order to inform such models, we investigate the real-world spatial diffusion patterns of solar PV, small hydropower, biomass, and wind power projects in 2'222 Swiss municipalities. Using a dataset of feed-in tariff recipients in 2016 [3], we analyse to what extent the differences in renewable resource potential, electricity demand, environmental and socio-demographic characteristics determine the spatial heterogeneity in the deployment of new renewable electricity projects.

Methods

Two methods [4] are applied for investigating the spatial diffusion of renewable electricity projects in Switzerland: spatial analysis of hot spots and cold spots [5] and step-wise regression. These methods are applied on a spatially-explicit dataset of 11'545 solar PV, 270 biomass, 27 wind, and 527 small hydropower projects, using the number of projects as the primary variable of interest. The number of projects was chosen as the primary variable because it is a proxy for general level of activity in each municipality in terms of renewable projects and it is independent from the annual variations in electricity generation, for instance, due to weather. The analysis, first of all, is applied for Switzerland as a whole and then regional differences for transferability of insights are investigated.

Results

Fig. 1 shows the identified hot spots and cold spots of all types of new renewable electricity projects (Solar PV, biomass, small hydro, wind) in Switzerland in 2016. Additional graphs per technology were analysed as well. The main findings are:

- Spatial clustering of high vs. low density of new renewable projects can be distinguished from other areas, which supports the findings in previous literature [6] about the regional spillover effects
- Swiss hot spots, i.e. spatial aggregation of municipalities with above-average number of renewable projects, can be observed in the cantons of Glarus, St. Gallen, Luzern, and parts of Bern and Zurich
- Swiss cold spots with spatial aggregation of municipalities with below-average number of projects are located in the cantons of Vaud, Fribourg, Jura, and parts of Ticino
- Solar PV and small hydropower projects are more densely clustered, while wind and biomass projects diffuse more randomly dispersed

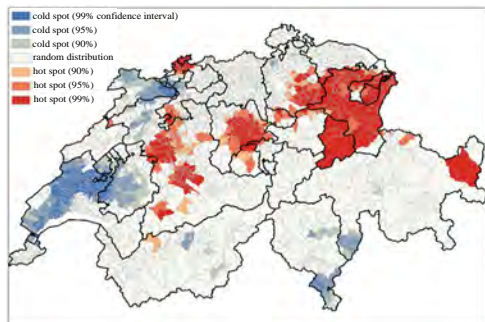


Fig. 1. Spatial hot spots and cold spots of new renewable electricity projects that received federal feed-in tariff in 2016

Table 1 summarizes additional findings:

- 359 Swiss municipalities (16% of all Swiss municipalities) fall in the category of hot spot and 478 municipalities (22%) are cold spots
- These 16% of municipalities that are hot spots include 35% of all new renewable electricity projects (4'380 projects) and cover 24% of electricity generation in 2016 in our dataset (455 GWh/year)
- 22% of municipalities that are cold spots include only 9% of all projects (1'145) and 8% of electricity generation (150 GWh/year)

- Hot spots generally have statistically significantly higher renewable electricity generation resource potential than cold spots
- Hot spots tend to be located in urbanized areas with high density of inhabitants, buildings and economic activity in the third sector
- Remote, rural and forested areas with a stronger forestry and agricultural activity tend to be cold spots
- Cold spots also have lower shares of conservative voters, higher shares of liberal voters and, interestingly, have supported stronger the Swiss Energy Strategy 2050
- The German-speaking region has the highest shares of hot spots (25%) while the French-speaking region has the highest share of cold spots (55%)

Table 1. Comparison of the municipal characteristics in the Swiss hot spots and cold spots of new renewable electricity projects and the other areas

Parameter	Units	Mean		
		Hot spots (99%, 95%, and 90% confidence)	Other municipalities	Cold spots (99%, 95%, and 90% confidence)
Overall characteristics				
Number of municipalities	municipalities	359	1385	478
Number of projects	projects	4'380	6'855	1'145
Number of projects per municipality	projects/municipality	12.2	4.9	2.4
Electricity generation in all renewable projects in 2016	GWh/year	455	1'262	150
Electricity demand and potential for renewable electricity generation				
Total electricity demand	GWh/(year-municipality)	50.6***	24.5	12.5*
Total renewable electricity potential	GWh/(year-municipality)	186***	151	95
Socio-demographic and other municipal characteristics				
Population	inhabitants	6920***	3639	1872**
Population density	inhabitants/km ²	603***	411	326*
German-speaking region	%	25	71	4
French-speaking region	%	1	44	55
Local economy				
Total number of employees	employees/municipality	4379*	2187	999
Share of employees in the first sector (raw material extraction)	%	12.8***	16.5	20.8***
Share of employees in the second sector (manufacturing)	%	27.3	26.4	24.5*
Share of employees in the third sector (services)	%	59.8**	56.7	54.1*
Political orientation and Energy Strategy 2050 vote				
Liberal left	%	22.4	22.5	27.4***
Liberal right	%	36.5	37.2	39.5**
Conservative	%	38.3	38.2	31.3***
Share of 'yes' vote for the Energy Strategy 2050	%	51.1	52.4	61.7***

Statistical significance for comparing hot spot and cold spots with the other municipalities: * p<0.05, ** p<0.01, *** p<0.001

Conclusions and discussion

- There is a substantial spatial heterogeneity across the Swiss regions and the types of renewable technologies, which originates to a large extent from the heterogeneity in renewable resource potential, especially for solar PV and small hydropower
- Densely populated and built-up areas with many available rooftops for solar PV or areas in the proximity of rivers for small hydropower plants are also the areas, where such projects primarily emerge
- Biomass power projects do not depend on biomass potential but rather on the presence of economic activity in the first sector
- The spatial diffusion of wind power in Switzerland is even less determined by the wind resource potential
- Some Swiss regions are still faster in deploying renewable projects with federal feed-in tariff than others, especially the German-speaking region. This finding is thus in line with previous literature [4] on regional spillover effects

References

[1] M. Welsch, et al. Supporting security and adequacy in future energy systems: The need to enhance long-term energy system models to better treat issues related to variability, *International Journal of Energy Research* 39(3) (2015) 377-396.
 [2] A. Q. Gilbert, et al. Looking the wrong way: Bias, renewable electricity, and energy modelling in the United States, *Energy* 94 (2016) 533-541.
 [3] Bundesamt für Energie, Liste aller KEV-Bezüger im Jahr 2016, 2017. http://www.bfe.admin.ch/php/modules/publikationen/stream.php?extlang=de&name=de_620208649.xlsx&endung=Liste%20aller%20KEV-Bez%FCger%20im%20Jahr%202016. (Accessed 15.05.2017)
 [4] C. Thormeyer, et al. Spatial dimension of renewable energy diffusion: empirical evidence on solar PV, biomass, wind, and small hydropower in Switzerland, *Renewable Energy* (under review).
 [5] ArcMap Hot Spot Analysis (Getis-Ord Gi*), 2018. <http://desktop.arcgis.com/en/arcmap/latest/tools/spatial-statistics-toolbox/hot-spot-analysis.htm>. (Accessed 25.05.2018).
 [6] G. J. Allan, et al. Green in the heart or greens in the wallet? The spatial uptake of small-scale renewable technologies, *Energy Policy* 102 (2017).

This project was supported by the SNSF Ambizione Energy (Grant No. 160563).

Task 4.3

Title

Socio-economic-political drivers

Projects (presented on the following pages)

Downstream fish guidance systems with horizontal bars

[Julian Meister](#), [Helge Fuchs](#), [Robert Boes](#)

Fishfriendly Innovative Technologies for hydropower (FIThydro) Swiss case studies HPP Bannwil & HPP Schiffmühle

[Julian Meister](#), [Claudia Beck](#), [Helge Fuchs](#), [Ismail Albayrak](#), [Robert Boes](#)

Downstream fish guidance systems for large run-of-river hydropower plants

[Claudia Beck](#), [Ismail Albayrak](#), [Robert Boes](#)

Media Analysis on Hydropower: First Results

[Corinne Moser](#), [Selma L'Orange Seigo](#), [Fabienne Sierro](#), [Olivier Ejderyan](#)

Challenges to Swiss hydropower. Perspective from cantonal authorities

[Olivier Ejderyan](#), [Fintan Oeri](#), [Fabienne Sierro](#), [Aya Kachi](#)

JA IDEA-HG: Highlights from a first year of joint research

[Joint Activity CREST-SoE](#)

Financial Flows from Water Fees and Fiscal Equalization on National and Cantonal Level

[Werner Hediger](#), [Marc Herter](#), [Christoph Schuler](#)

Distributional effects of the revision of Swiss water fees

[Regina Betz](#), [Thomas Geissmann](#), [Mirjam Kosch](#), [Moritz Schillinger](#), [Hannes Weigt](#)

Profitability of Swiss Hydro Power with and without Water Fees

[Regina Betz](#), [Thomas Geissmann](#), [Mirjam Kosch](#), [Moritz Schillinger](#), [Hannes Weigt](#)

Downstream fish guidance systems with horizontal bars

Julian Meister, Helge Fuchs, Robert Boes – VAW, ETHZ

1. Motivation and Objectives

The natural behavior of many fish species involves the migration of up to hundreds of kilometers within river systems. This migration is impeded since the construction of hydropower plants (HPPs). Therefore, the European Water Framework Directive (WFD) and the Swiss Water Protection Act (WPA) demand to restore the free up- and downstream migration. While many HPPs were already successfully equipped with upstream passage facilities, downstream fish passage facilities are still under development.

The “Fishfriendly Innovative Technologies for hydropower” project (FITHydro) was launched as part of the Horizon 2020 EU Research and Innovation program to promote the development of innovative technologies for sustainable and fish-friendly operation of hydropower plants in Europe. As one part of FITHydro, the current research project focuses on the hydraulics and fish guiding efficiency of horizontal bar rack bypass systems (HBR-BSS). Operational aspects like clogging with organic fines will be investigated and live fish experiments will be conducted to quantify the fish guiding efficiency.

2. Introduction to HBR-BSS

HBR-BSS are considered state-of-the-art of fish downstream migration in Europe (Ebel, 2016). They consist of two main elements: (1) the bar rack itself to prevent fish from entering the turbines and (2) the bypass to safely guide the fish to the downstream reach (Fig. 1). To keep the hydraulic losses low, automated rack cleaning systems are used to minimize clogging. Although a number of HPPs were equipped with HBR-BSS in the last decade at small- to medium-sized HPPs ($Q_d < 88 \text{ m}^3/\text{s}$), there is still a lack of systematic studies on the optimization and verification of these state-of-the-art downstream fish passage facilities.

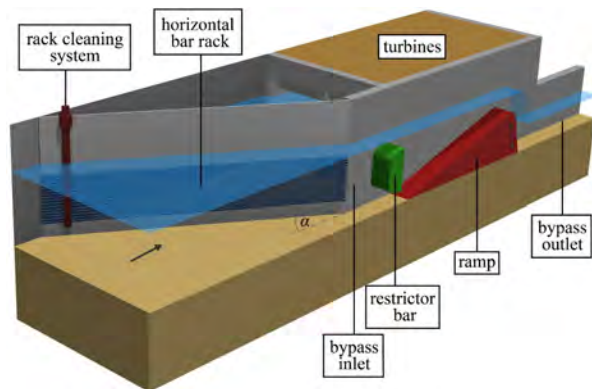


Fig. 1: Principle sketch of a HBR-BSS, adapted from Ebel (2016)

3. Experimental setup

To fill the described research gaps, hydraulic experiments with horizontal bar racks (HBRs) are conducted in a laboratory flume (Fig. 2a). The flow depths upstream h_o and downstream h_{ds} of the rack are measured using Ultrasonic Distance Sensors (UDSs) and the velocity field is measured using an Acoustic Doppler Velocimeter (ADV). The governing parameters are the horizontal approach flow angle to the rack α , the clear bar spacing s_b , the bar depth d_b and the cross-sectional bar shape (Fig. 2b). Additional bottom and top overlays can be used to enhance the guiding efficiency for bottom and surface orientated migrating fish.

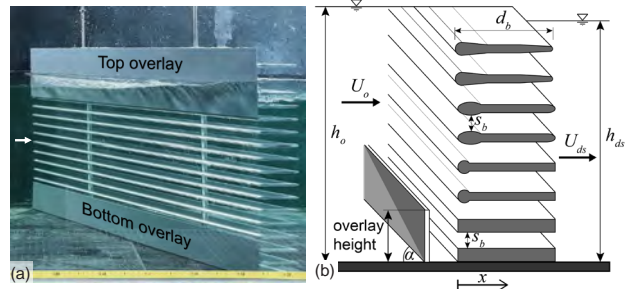


Fig. 2: (a) Laboratory experiment on a HBR with bottom and top overlays (b) Definition sketch for governing HBR parameters

4. First results

Fig. 3 shows the velocity fields of HBRs (a) without overlays and (b) with a 40% overlay blocking (20% bottom and top overlay each) at mid water depth for an approach flow velocity $U_o = 0.5 \text{ m/s}$.

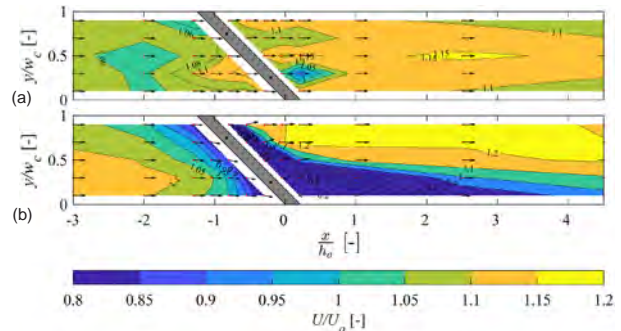


Fig. 3: Velocity fields of HBR with foil-shaped bars, $\alpha = 45^\circ$, $s_b = 20 \text{ mm}$ (a) without and (b) with 20% overlay blocking by bottom and top overlays each

The flow field at the rack without overlays is almost unaffected with a homogeneous velocity distribution (Fig. 3a). In contrast, for a configuration with overlays the approach flow is decelerated and a rack-parallel velocity component establishes (Fig. 3b), thereby increasing the guiding efficiency for fish, bed load material and floating debris. Disadvantages of overlays include the larger hydraulic losses and the asymmetrical downstream velocity field, leading to uneven turbine admission and therefore reduced turbine efficiency.

5. Conclusion and Outlook

HBR-BSS are considered as state-of-the-art fish downstream passage facilities in Europe. Despite the successful operation at prototype HPPs, several research questions remain. First laboratory experiments demonstrate small hydraulic losses and minor effects on the velocity field of configurations without overlays, indicating a great potential for further applications. Future experiments will focus on operational aspects of HBR-BSS and the fish guiding efficiency.

6. References

Ebel, G. (2016). Fish Protection and Downstream Passage at Hydro Power Stations — Handbook of Bar Rack and Bypass Systems. Bioengineering Principles, Modelling and Prediction, Dimensioning and Design. ISBN 9783540437130. 2nd edn. Büro für Gewässerökologie und Fischereibiologie Dr. Ebel, Halle (Saale), Germany [in German].

Fishfriendly Innovative Technologies for hydropower (FIThydro) Swiss case studies HPP Bannwil & HPP Schiffmühle

J. Meister, C. Beck, H. Fuchs, I. Albayrak, R. Boes

Laboratory of Hydraulics, Hydrology and Glaciology (VAW), ETH Zürich, Switzerland

Introduction

Two case studies at run-of-river hydropower plants (HPPs) in Switzerland are conducted within the scope of the interdisciplinary “Fishfriendly Innovative Technologies for Hydropower (FIThydro)” project which is funded by the Horizon 2020 framework program (grant agreement No 727830) of the European Union for research and innovation. The investigations focus on the velocity field (ADCP measurements and numerical modeling), the monitoring of fish downstream migration, and the sediment connectivity.

Run-of-river hydropower plant Bannwil

The run-of-river HPP Bannwil is a block-unit power plant at the River Aare in Switzerland (Fig. 1) with a design discharge of 450 m³/s. The gross head amounts to 5.5 – 8.5 m depending on up- and downstream water levels. The three 4.35 m diameter bulb turbines have an installed capacity of 28.5 MW, resulting in an average annual production of 150 GWh. The downstream Aare reach features nine run-of-river HPPs and two nuclear power plants with water abstractions for cooling.



Fig. 1: Head water of block-unit HPP Bannwil with the turbine intakes in the background (Photo: VAW)

Restoration targets

The target fish species in that Aare reach are salmon and barbel. For upstream migration, a fish pass is installed which has to be renewed until 2020. Downstream migrating fish are routed through the turbines or over the weir in case of flood events. Fish protection and bypass systems have to be installed until 2025.

Field measurements within FIThydro

Within the FIThydro project, 250 fish will be equipped with radio-telemetric tags. Their migration routes in the vicinity of the HPP will be observed for 2 years. The fish behaviour will be further observed with DIDSON sonar systems at specific locations (e.g. in front of the intake rack).

VAW will conduct ADCP measurements of the velocity field (Fig. 2) and will set up a 3D numerical model. Hydraulics and fish data will be evaluated to assess the current situation and the effectiveness of operational measures (e.g. spill flow). Furthermore, the installation of a fish guidance structure with vertical bars and an adjacent bypass system will be considered in the numerical study.



Fig. 2: ADCP measurements downstream of HPP Bannwil (Photo: VAW)

Residual flow hydropower plant Schiffmühle

The HPP Schiffmühle is located at the River Limmat some 30 km downstream of Zurich. The 400 m long Schiffmühle side weir divides the river into the headrace channel of the main HPP and the residual flow reach. The residual flow HPP is located at the upstream end of the side weir and is equipped with a 1.45 m diameter bulb turbine to use the residual flow for electricity production. With a gross head of 2.97 m and a design discharge of 14 m³/s the installed capacity is 285 kW. The annual electricity production is 1.9 GWh corresponding to the electricity consumption of approx. 430 households. Aiming at a natural sediment continuum, a vortex tube was installed on the headrace channel invert at about half the channel length to divert bed load material into the residual flow reach (Fig. 3a). The residual flow HPP Schiffmühle is equipped with a natural fishway and a vertical slot fish pass for upstream migration. In 2013 it was equipped with a horizontal bar rack bypass system for fish downstream passage (Fig. 3b). Resulting from the lateral HPP intake, the horizontal bar rack is arranged parallel to the main flow. The bars with rectangular profiles have a clear spacing of 20 mm. The approach flow velocity at design discharge is 0.5 m/s. At the downstream rack end 3 bypass openings are located at different water depths (near-bottom, mid-depth, and near-surface) leading into a vertical shaft. The subsequent downstream passage into the residual flow reach is provided via a 0.25 m diameter bypass pipe.

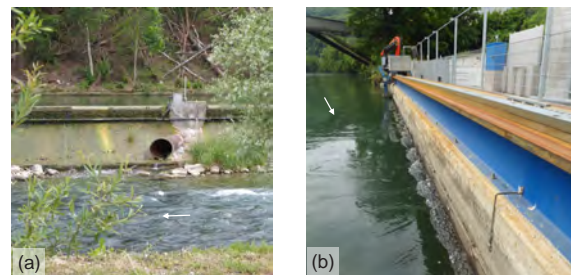


Fig. 3: (a) Vortex tube connecting the headrace channel with the residual flow reach (Photo: VAW)
(b) Horizontal bar rack for fish protection (Photo: VAW)

Field measurements and numerical modeling

The velocity field around the residual flow HPP Schiffmühle will be measured with an ADCP. More than 1000 individual fish will be marked with PIT-tags to monitor their migration. To track their swimming paths, all upstream and downstream migration corridors are equipped with RFID antennas. To quantify the sediment balance, the bed load transport in the vortex tube and sediment deposition and erosion will be monitored. For the residual flow reach the investigations include sediment sampling, habitat and shelter mapping and the quantification and numerical modeling of flow conditions.

Partners:



Partners:



Downstream fish guidance systems for large run-of-river hydropower plants

C. Beck, I. Albayrak, R. Boes – VAW, ETHZ

1. Motivation and objectives

Run-of-river hydropower plants (HPPs) disrupt fish migration routes decimating fish populations worldwide. While various technologies for the fish upstream migration technologies are well developed, there is still a lack of knowledge on downstream fish passage technologies with regard to fish species, hydraulic conditions and operational issues at HPPs.

The main goal of this research study is to develop a fish protection and guidance technology for downstream migrating fish with minimum impact on power plant production or operation. The focus lies on fish guidance systems with vertical bars (i.e. louvers and angled bar racks) for large HPPs with design discharges above 100 m³/s (Fig. 1). The present study contributes to a fish-friendly and sustainable usage of hydropower.



Fig. 1: Fish guidance structure with bypass at a run-of-river HPP

2. Fish guidance structures with innovative bar design

Although modified bar racks (MBR) developed based on louver design provide high fish guidance efficiency (Kriewitz, 2015), they still negatively impact HPP production due to high head losses and poor admission flow quality. To mitigate these negative effects an innovative curved bar design was developed (Fig. 2). In the present study, these so-called *modified curved-bar racks* (MCR) are studied with regard to hydraulic conditions and fish guidance.

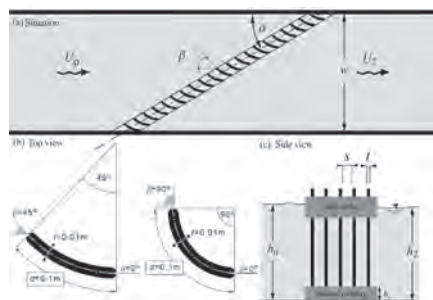


Fig. 2: Geometric and hydraulic rack parameters of modified curved-bar racks (a) rack top view, (b) bar shape top view, (c) side view

3. Research plan

To meet the objectives, different models are set up (Fig. 3). The effects of main rack angle, bar angle, bar spacing, bar depth and top or/and bottom overlays on the hydraulic head losses and flow fields at MCRs are studied in a 1:2 scaled detailed model (cf. Fig. 2). Different bypass systems are developed and optimized with 1:1 scaled experiments. Fish guidance efficiencies (FGE) of the optimized MCR-bypass system are assessed with life-fish tests. Finally, operational issues such as large wood accumulation and sediment transport are investigated.



Fig. 3: Different model setups to optimize the design of FGS and bypass and maximize the FGE

4. First results

With the new bar shape, head losses are significantly reduced. The head losses of MCRs are up to 5.5 times lower than those for MBRs and are in the same range of $0 \leq \xi_{R'} \leq 3$ as for most trash racks used at Swiss hydropower plants (Meusburger, 2002). The bar angle β has the largest effect on head losses and the flow field as shown in Fig. 4. Upstream of the rack, flow velocities steadily increase up to $1.25 U_0$ and $1.85 U_0$ for $\beta = 45^\circ$ and $\beta = 90^\circ$, respectively. The mild acceleration for $\beta = 45^\circ$ is a good indication for a high FGE (Boes & Albayrak, 2017). Fig. 4a also shows the flow straightening effect of curved bars with $\beta = 45^\circ$ resulting in a quasi-symmetrical velocity distribution downstream of the rack as compared to the low admission flow quality for $\beta = 90^\circ$ (Fig. 4b). In the next step, the recommended MCR configuration with $\alpha = 30^\circ$, $\beta = 45^\circ$ and $s = 50$ mm (Fig. 4a) will be tested in the 1:1 model and with live-fish experiments.

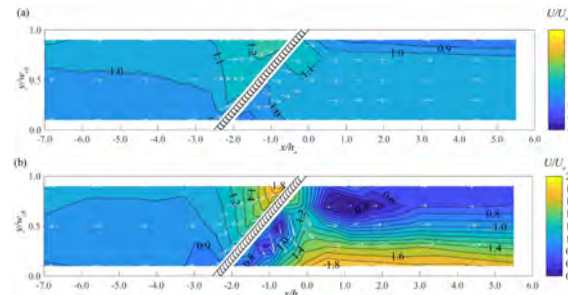


Fig. 4: Measured flow field of U/U_0 at MCR configuration $\alpha = 30^\circ$, $s = 50$ mm (a) $\beta = 45^\circ$ and (b) $\beta = 90^\circ$.

Given the highly reduced head losses and improved flow field, MCRs present a promising potential over louvers and MBRs for fish protection and guidance facilities at HPPs.

5. References

Kriewitz, C. R. (2015). Leitrechen an Fischabstiegsanlagen – Hydraulik und fischbiologische Effizienz (Guidance racks at fish passage facilities – Hydraulics and fish-biological efficiency). VAW-Mitteilung 230, R. M. Boes, ed., Laboratory of Hydraulics, Hydrology and Glaciology (VAW), ETH Zurich, Zürich, Switzerland [in German]

Meusburger, H. (2002). Energieverluste an Einlaufrechen von Flusskraftwerken (Head losses of trash racks at run-of-river hydropower plants). VAW-Mitteilung 179, H.-E. Minor, ed., Laboratory of Hydraulics, Hydrology and Glaciology (VAW), ETH Zurich, Zürich, Switzerland [in German]

Boes R. M., Albayrak I. (2017). Fish guidance structures: New head loss formula and fish guidance efficiencies, Proceedings of the 37th IAHR World Congress, Kuala Lumpur, Malaysia



Media Analysis on Hydropower: First Results

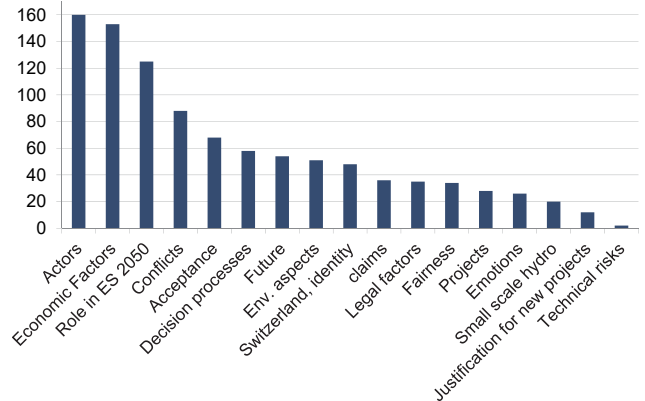
Dr. Corinne Moser (ZHAW), Dr. Selma L'Orange Seigo (ETHZ),
 Fabienne Sierro (ETHZ) & Dr. Olivier Ejderyan (ETHZ)

Goals of the project

- Identification of most important media frames on hydropower (HP) in Switzerland
- Complementing media analysis on deep geothermal energy DGE (already completed; Stauffacher et al. 2015, Ejderyan et al., 2019)
- Providing a basis to test impacts of media frames on public acceptance of hydropower
- Exemplary headlines (Source: tagi.ch, nzz.ch):

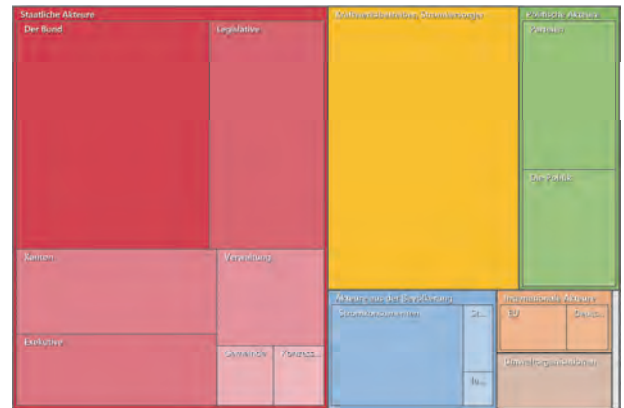


Results: Frequencies of superior codes



- HP is mainly framed as an economic issue with important themes being the level of subsidies received by the industry, falling market prices, remittances and current investment levels
- HP is presented as having an important role in the Energy Strategy 2050 because of its energy storage capacity and complementary role to other renewables
- HP is framed as a conflictual issue. Environmental conflicts are reported but most often conflicts about economic factors

Results: Most frequently mentioned actors



- Operators and the federal state are the main actors appearing in media reports
- The public appears mostly as consumers

Method

- Coding of newspaper articles (NZZ, Tages-Anzeiger, Le Temps)
- Timeframe: 1.01.2011-31.12.2017
- Key words: hydropower, energy strategy (DE: Wasserkraft + Energiestrategie / F: «stratégie énergétique» + barrage, «énergie hydraulique»)
- N = 170 articles
- Coding tree has been developed iteratively
- Coding was done with the software N'Vivo (illustration below)



Preliminary conclusions

- HP in the ES 2050 is mostly discussed as an economic issue and from the perspective of the operators and the (federal) state
- Other actors appear as marginal.
- Technical risks and periglacial hydropower are non-issues

References

Ejderyan, O., Ruef, F., & Stauffacher, M. (2019). Geothermal energy in Switzerland: Highlighting the role of context. In Geothermal Energy and Society, A. Manzella et al. (eds), 239–57. Cham: Springer. doi:10.1007/978-3-319-78286-7.

Stauffacher, M., Muggli, N., Scolobig, A., & Moser, C. (2015). Framing deep geothermal energy in mass media: The case of Switzerland. Technological Forecasting and Social Change, 98, 60–70. http://doi.org/10.1016/j.techfore.2015.05.018.

Challenges to Swiss hydropower. Perspective from cantonal authorities

Olivier Ejderyan ^a, Fintan Oeri ^b, Fabienne Sierro ^a, Aya Kachi ^b (^a ETH Zürich, ^b University of Basel)

Background and goal of the study

Cantons are the authority delivering the authorisation for the building of new hydropower (HP) infrastructure or improvement of existing ones. They are often shareholders in utilities operating HP plants. In some cases they might also own water rights and as such grant concession to operators. More generally, cantons are responsible for land use and energy planning, which makes them crucial actors for the development of Swiss HP capacity.

Yet public debates about the governance of Swiss HP focuses mainly on the Federal state and operators as the driving actors of HP. The role of mountain municipalities as concession givers is often discussed with regard to the amount of remittances they receive. The role of cantons is overlooked despite their key role.

In order to make relevant and realistic recommendations for the development of Swiss HP it is therefore necessary to examine the role of cantons. The goal of this study is to provide base knowledge to make relevant recommendations for decision-making in HP.

Methods

The study takes a practice based approach to identify the main challenges encountered by cantonal officers responsible for HP in their daily work.

- 9 Interviews with cantonal officers in charge of supervising authorisation processes for HP infrastructure
- Interviewed cantons cover 83% of Swiss HP production
- Theoretical sampling: Maximum variation in cantonal structure + wide coverage of production.
- Semi-structured narrative interviews to produce thick description of daily activities about HP
- Interviews covered five topics:
 - Challenges in daily work
 - Interaction with stakeholders
 - Public involvement
 - Description of projects
 - Vision for HP.



Map of interviewed cantonal authorities in charge of hydropower.

- Interviews are analysed through qualitative content analysis
Explicit and implicit content of the interview is coded and statement categorised according to thematic closeness

Analysis of the interviews is ongoing.

First insights

The following first insights can be made from the analysis of the explicit content of the interviews:

Finances

In contrast to the main framing of HP in news media, financial questions are not considered as a pressing issue. Most cantonal officers believe that current discussions about profitability or remittances are conjunctural and will evolve.

"If we look into the future, when coal prices will rise again, when Germany will phase-out nuclear plants in 22, then things will look clearer."

"Some nuclear power plants were turned off in France in 2017 and immediately the price per KW/h went up. Just a few cents more and hydropower was again profitable."

Exemplary quotes on financial situation of HP

Conflicts with environmental goals

Dealing with environmental goals and regulations appears as the main challenge for cantonal HP practitioners. Primary cause in their perception are not environmental NGOs but the lack of coordination on priority goals between BFE and BAFU.

"Currently, things are floating. And we don't know exactly how courts will rule in the end. That does not make sense, does it? I would say that BFE and BAFU don't really agree with each other."

"In principle, we try to be constructive [in negotiations], and I believe that to a large extent, we are constructive. But in the end, it is clear that environmental NGOs also have their own policy"

Exemplary quotes on conflicts with environmental goals

Public engagement

Cantons do not play an active role in public engagement for HP projects. Negotiations with stakeholders are organised by operators. Cantonal officers see themselves as representatives of the public. They do not consider that the wider public should be more involved in discussions about HP projects.

"We have a water use strategy, in which we, the Canton, have formulated relatively clear goals. And it's validated by the parliaments. This means that there was a form of participation [of the wider public]. I mean they represent the public."

"The project applicant negotiates with NGOs. If an opposition is reached in, we inform the applicant."

Exemplary quotes on public engagement

Outlook

First results indicate that:

- Cantonal officers do not see Swiss HP as being in a deep crisis situation
- However they are rather skeptical about a strong expansion of Swiss HP capacities
- Cantons do not seem to hold an initiating role for HP development.
- A first result from the analysis of the implicit content of the interview indicates that Cantons have very little capacity to plan HP development.



Supported by:



Schweizerische Eidgenossenschaft
Confédération suisse
Confederazione Svizzera
Confederaziun svizra

Swiss Confederation

Innosuisse – Swiss Innovation Agency

JA IDEA-HG: Highlights from a first year of joint research

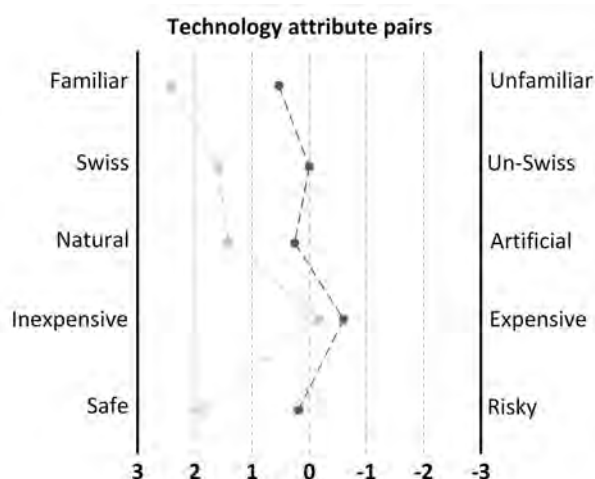
The JA IDEA-HG aims to provide recommendations on how to address conflict related to the legislative framework, governance structures and project development processes for hydropower (HP) and deep geothermal energy (DGE). During the first year, researchers worked on integrating methods and concepts developed in SCCER CREST and SCCER SoE. They conducted following tasks:

- Review of legal conditions for HP and DGE at cantonal level;
- Survey on how HP and DGE are perceived in relationship to the federal energy strategy;
- Media analysis on the discourse on HP;
- Interviews on challenges encountered by the authorizing offices in charge of HP

A stakeholder workshop gathering federal and cantonal officers, operators and NGOs from both discussed first insights and narrowed the main challenges to be addressed.

Exploring the role of beliefs in opinions about the energy strategy

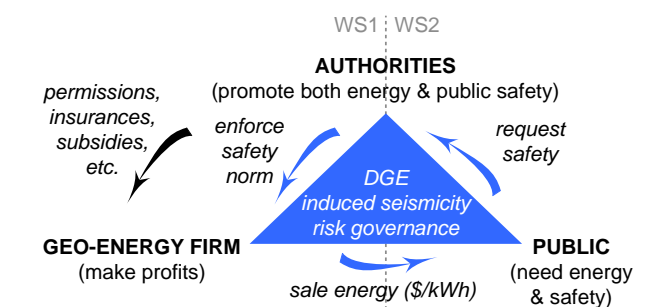
In Work Stream 2, research conducted at pilot study to investigate support for HP and DGE within the energy strategy. The study found that while support for the energy strategy depends significantly on their beliefs, support for a specific technology does less so. The figure below illustrates the attributes associated to each technology by the respondents.



Blumer, Y., Braunreiter, L., Kachi, A., Lordan-Perret R. and Oeri, F. 2018. "A Two-Level Analysis of Public Support: Exploring the Role of Beliefs in Opinions about the Swiss Energy Strategy." In Energy Research & Social Science (in press).

Regulating and governing risks to local communities by DGE projects

Researchers at ETHZ and ZHAW from Work Stream 1 developed an approach to make recommendations for regulating and governing DGE related seismic risk. They developed a regulatory sandbox with DGE electricity prices as main metric. It integrates a governance scheme with the goals and priorities of actors (see figure). The regulatory sandbox enables to assess problems and envision possible legislative solutions.



Authors: A. Mignan & G. Seferovic

Research Partners



Contact

Sebastian Heselhaus, University of Lucerne
Coordinator Joint Activity

Olivier Ejderyan, ETH Zurich
Coordinator of Work Stream 2

Andrea Ottolini, University of Basel
Managing Director SCCER CREST

www.sccer-crest.ch

The Future of Swiss Hydropower:
Distributional Effects of Water Fee Reform Options

Financial Flows from Water Fees and Fiscal Equalization on National and Cantonal Level

Background

- a) Water fees are the remuneration to be paid by the hydropower operators to the owners of the water resource right (i.e. the cantons, etc.).
- b) Fiscal equalization systems aim to mitigate differences between cantons/municipalities in their financial capacity and cost burden.

Research objectives

1. Analyze financial flows from water fees payments between cantons based on ownership through direct and indirect shareholdings:
→ Overview of ownership structure and attribution of water fee flows to shareholdings (Fig. 1)
2. Analyze the distributional effects within cantons:
→ Impact of water fees on municipal and cantonal finance in the canton of Grisons (Tab. 1)

First results (objective 1)

The analysis of the shareholdings and attribution of financial flows from hydropower between ZH & GR shows (for 2016):

- The canton and municipalities of GR themselves account for approx. 11.5% of their water fee revenues.
- The canton and municipalities of ZH account for over 33% of Grisons' water fee revenues.
- More than 55% of water fee flows to GR are attributable to other cantons.

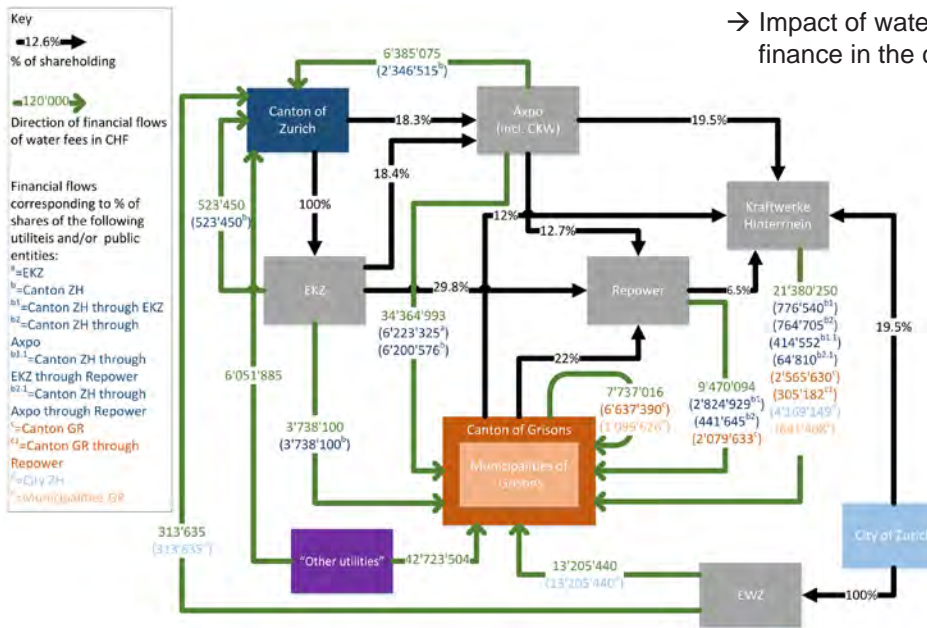


Figure 1: Hydropower in the cantons ZH & GR: shareholdings and financial flows (2016)

First results (objective 2)

- In GR, a reduction in water fees would
- directly affect the resource potential of "hydropower municipalities",
 - alter resource equalization in GR,
 - indirectly effect the financial situation of other municipalities,
 - progressively reduce the number of resource-strong and thus paying municipalities,

All municipalities and the canton would lose fiscal revenues.

Impact of alternative water fees (CHF/KW) on municipal finance in Grisons

Hypothetical case: fiscal year 2012, with 146 municipalities as of 01/01/2014	Reference	Water fee scenarios			
	110	100	80	50	none
Change in Mio CHF/year:					
- Municipal water fee receipts :	0	-4.87	-14.61	-29.21	-53.56
- Net resource equalization :	0	-0.14	-0.34	-0.40	-0.63
- Total change:	0	-4.96	-14.78	-29.27	-54.19
No. of municipalities ...					
- paying into ...	54	54	51	42	30
- receiving transfers from ...	90	90	93	102	124
- excluded from ... the cantonal resource equalization.	2	2	2	2	2

Table 1: Relevance of water fees in municipal finance in GR

Source and further information: Betz et al.: The Future of Swiss Hydropower: Distributional Effects of Water Fee Reform Options. Interim Project Report, 2018.



SCCER CREST



Energy Turnaround
National Research Programme

Supported by:



Schweizerische Eidgenossenschaft
Confédération suisse
Confederazione Svizzera
Confederaziun svizra

Swiss Confederation

Innosuisse – Swiss Innovation Agency

Work Package 3

DISTRIBUTIONAL EFFECTS OF THE REVISION OF SWISS WATER FEES

Hydro power is most important electricity source of Switzerland (around 60% of production)

Situation 2009: Large profits due to high electricity prices, low variable costs, and large price spread. Profits mainly made by cantons who owned large utilities (valley).

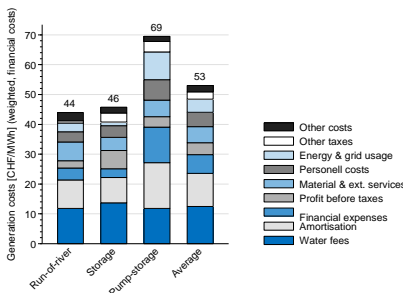
Situation Today: Lower returns because of lower prices and spread due to low fossil fuel and CO₂ allowance prices, larger shares of renewables. Utilities have problems to cover fixed costs.

Water fee reform: Water fees are under reconsideration since the Swiss Water law will be revised. Government has decided that up to 2024 there will be no changes, but different options need to be considered for the time after 2024.

Open questions

- What is was the situation of hydro power in Switzerland in 2015/16?
- How will different future water fee options change profitability of hydro power?

Production Cost 2015/15

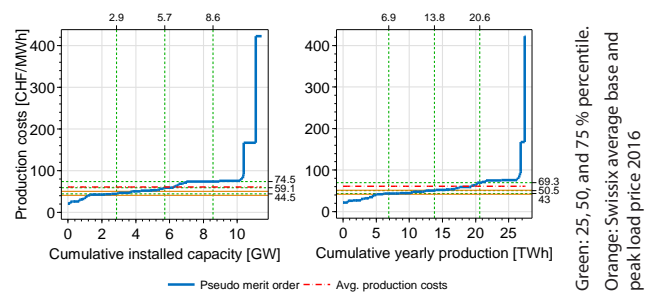


Sources:

Data based on annual reports, income statements, balance sheets of 62 hydropower companies and statistics of hydropower plants in Switzerland (WASTA) provided by Swiss Federal Office of Energy (SFOE)

- Share of water fee of total production costs varies with type of plant (average share: 23% or 12.4 CHF/MWh)

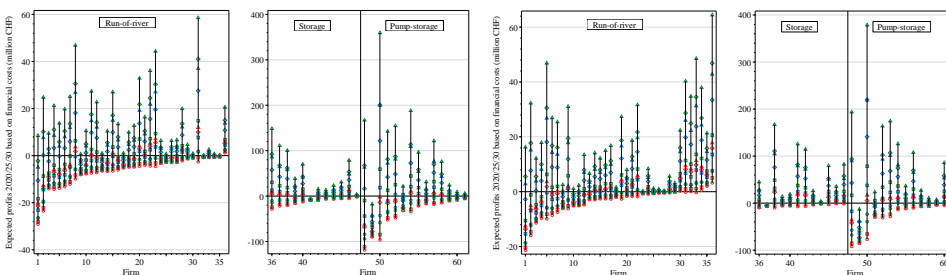
Pseudo Merit Order 2015/16



Green: 25, 50, and 75 % percentile.
Orange: Swiss average base and peak load price 2016

- Average production costs of all 62 hydropower companies for the years 2015 and 2016 (adjusted for inflation)

Profits with (left) and without (right) water fees



Fuel and Carbon Price Scenarios

- Base 2015 :Fuel and carbon prices as in 2015
- EU Trend: Prices EU reference scenario
- C++F++: Fast linear increase in carbon (50€/t) and fuel prices (+100%) until 2030
- C--F--: Linear decrease in carbon (4€/t) and fuel prices (-50%) until 2030



- Profit situation depends on electricity price pathway (Swissmod: Schlecht & Weigt, 2014)
- Without water fees:
 - Improved situation for companies close to break-even
 - Little impact under favorable market conditions
 - Not sufficient for high-cost companies

Contact

SCCER CREST - Work Package 3
Prof. Dr. Regina Betz - regina.betz@zhaw.ch
ZHAW Zurich University of Applied Sciences

www.sccer-crest.ch





SCCER CREST



Energy Turnaround
National Research Programme

Supported by:



Schweizerische Eidgenossenschaft
Confédération suisse
Confederazione Svizzera
Confederaziun svizra

Swiss Confederation

Innosuisse – Swiss Innovation Agency

Work Package 3

Profitability of Swiss Hydro Power with and without Water fees

Hydro power is most important electricity source of Switzerland (around 60% of production)

Situation 2009: Large profits due to high electricity prices, low variable costs, and large price spread. Profits mainly made by cantons who owned large utilities (valley).

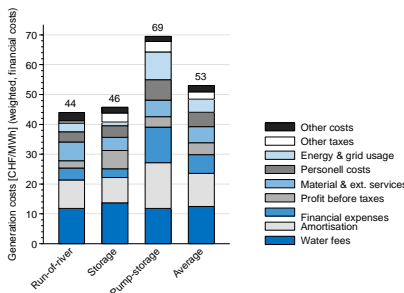
Situation Today: Lower returns because of lower prices and spread due to low fossil fuel and CO₂ allowance prices, larger shares of renewables. Utilities have problems to cover fixed costs.

Water fee reform: Water fees are under reconsideration since the Swiss Water law will be revised. Government has decided that up to 2024 there will be no changes, but different options need to be considered for the time after 2024.

Open questions

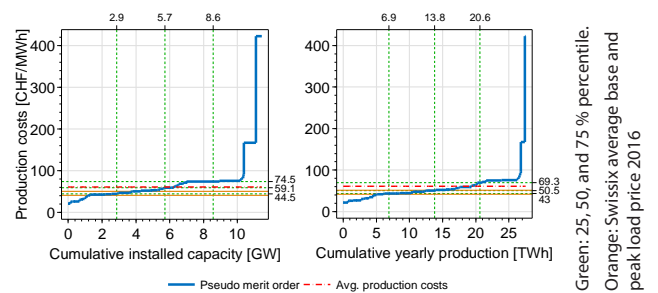
- What is was the situation of hydro power in Switzerland in 2015/16?
- How will different future water fee options change profitability of hydro power?

Production Cost 2015/16



Sources:
Data based on annual reports, income statements, balance sheets of 62 hydropower companies and statistics of hydropower plants in Switzerland (WASTA) provided by Swiss Federal Office of Energy (SFOE)

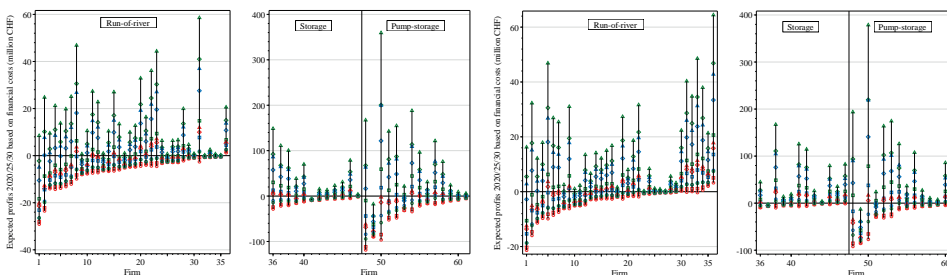
Pseudo Merit Order 2015/16



- Share of water fee of total production costs varies with type of plant (average share: 23% or 12.4 CHF/MWh)

- Average production costs of all 62 hydropower companies for the years 2015 and 2016 (adjusted for inflation)

Profits with (left) and without (right) water fees



Fuel and Carbon Price Scenarios

- Base 2015 :Fuel and carbon prices as in 2015
- EU Trend: Prices EU reference scenario
- C++F++: Fast linear increase in carbon (50€/t) and fuel prices (+100%) until 2030
- C--F--: Linear decrease in carbon (4€/t) and fuel prices (-50%) until 2030



- Profit situation depends on electricity price pathway (Swissmod: Schlecht & Weigt, 2014)
- Without water fees:
 - Improved situation for companies close to break-even
 - Little impact under favorable market conditions
 - Not sufficient for high-cost companies

Contact

SCCER CREST - Work Package 3
Prof. Dr. Regina Betz - regina.betz@zhaw.ch
ZHAW Zurich University of Applied Sciences

www.sccer-crest.ch



Task 4.4

Title

Joint Activity Scenarios & Modeling (JA-S&M)

Project (presented on the following page)

Joint Activity Scenario & Modelling (JASM)

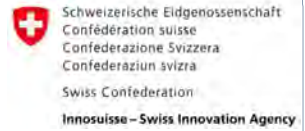
[The JASM team](#)

Are Interactive Web-Tools for Public Engagement Worth the Effort? An Experimental Study on the Swiss Electricity Supply Scenarios

[Georgios Xexakis, Evelina Trutnevyte](#)

Investment and generation cost trade-offs between cost-efficient vs. regionally equitable distribution of renewable electricity

[Jan-Philipp Sasse, Evelina Trutnevyte](#)



Joint Activity Scenarios & Modelling

The JASM team representing all 8 SCCER
(Contact: gianfranco.guidati@sccer-soe.ethz.ch)



Our mission

The Swiss energy system supplies electricity, heat and mobility services to the domestic, commercial, industrial and transport sectors. The combustion of fossil fuels – mostly for heating and transportation – emits approx. **38 MT_{CO2/a}**. Following the objectives of the Energy Strategy 2050 and the Swiss INDC, we will create scenarios how to reduce emissions in 2050 down to **10 MT_{CO2/a}**.

Three questions shall be answered:

1. What technical means are most effective to reach the 2050 goals?
2. Which political instruments are needed to push this development?
3. What is the economical and social impact of this transition?

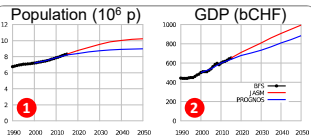
Our principle: Open team / Open data

Modelling teams from seven institutions – representing the eight SCCER – work together towards the objectives of JASM. Every other school, institute or company is invited to contribute with data and to profit from the combined knowledge of the JASM framework.

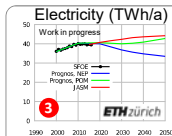
The idea is to agree on input data such as the future evolution of demand, supply potential and technology characteristics but to maintain the diversity of modelling approaches. All data is shared on the project website www.sccer-jasm.ch.

Elements of scenarios

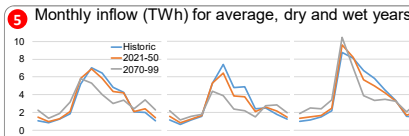
Major driver	Yearly aggregate	Hourly time series	Generation technologies	Technology characteristics
Population 1	Electricity 3	Electricity 4	Solar PV	Thermal power
GDP 2	Space heating 6	Space heating 4	Solar thermal	Renewable power
Sectoral GVA	Warm water	Warm water	Hydro river	Heat generation
Energy ref. area	Process heat	Process heat	Hydro storage 5	Efficiency measures 7
Climate change	Person-kilometer	Person-kilometer	Wind	Storage
Energy intensity	Ton-kilometer	Ton-kilometer	Geothermal	Fuels



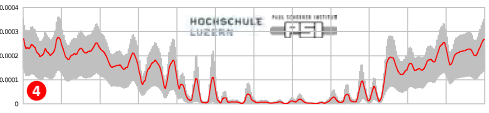
Higher expected population growth impacts extrapolation of future energy demand



Updated future demand higher than Prognos



Swissmod estimates impact of climate change on hydro power production



Synthetic heating demand time series using population-weighted daily temperature distribution and intra-day shape functions

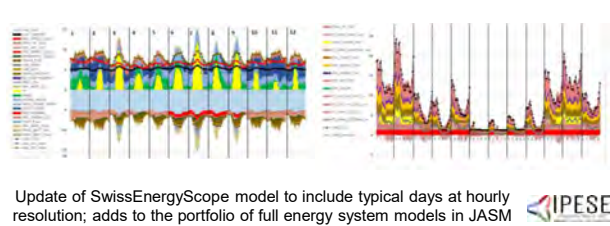


EECC tool ranks cost-effective renovation measures to reduce future heating demand

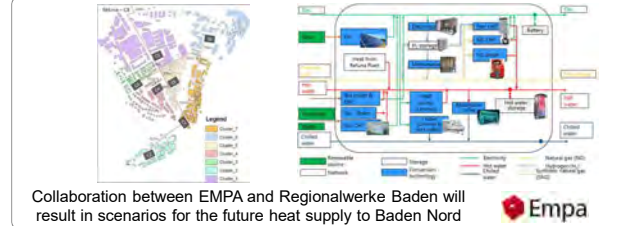
Technology	Invest. costs	O&M costs	Efficiency	CO2 intensity
Thermal power				
Renewable power				
Heat generation				
Efficiency measures				
Storage				
Fuels				

Technology characteristics structured and published on www.sccer-jasm.ch

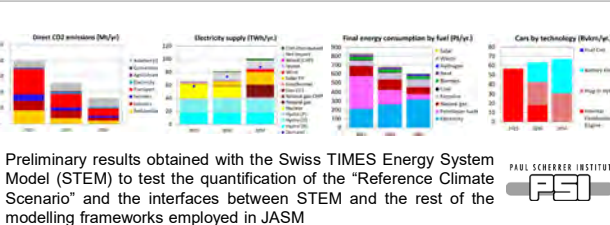
Selected results



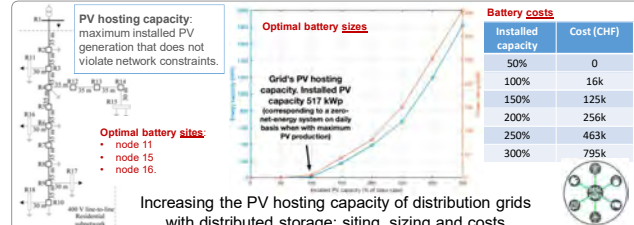
Update of SwissEnergyScope model to include typical days at hourly resolution; adds to the portfolio of full energy system models in JASM



Collaboration between EMPA and Regionalwerke Baden will result in scenarios for the future heat supply to Baden Nord



Preliminary results obtained with the Swiss TIMES Energy System Model (STEM) to test the quantification of the "Reference Climate Scenario" and the interfaces between STEM and the rest of the modelling frameworks employed in JASM



Increasing the PV hosting capacity of distribution grids with distributed storage: siting, sizing and costs

References

Panos, E., Kannan, R. (2018). Challenges and Opportunities for the Swiss Energy System in Meeting Stringent Climate Mitigation Targets. In Giannakidis G., K. Karlsson, M. Labriet, B. Ö Gallachóir (eds.) Limiting Global Warming to Well Below 2°C: Energy System Modelling and Policy Development, p. 155-172

Gupta, R., Sossan, F., Scolari, E., Namor, E., Fabietti, L., Jones, C., and Paolone, M. (2018). An ADMM-based coordination and control strategy for PV and storage to dispatch stochastic prosumers: Theory and experimental validation. 20th Power Systems Computation Conference, PSCC, 2018.

Are Interactive Web-Tools for Public Engagement Worth the Effort? An Experimental Study on the Swiss Electricity Supply Scenarios

Georgios Xexakis^{1,2}, Evelina Trutnevyte^{1,2}

ETH zürich

¹Renewable Energy Systems group, Faculty of Science, Department F-A, Forel for Environmental and Aquatic Sciences, Institute for Environmental Sciences, University of Geneva, Switzerland

²Institute for Environmental Decisions, Department of Environmental Systems Science, ETH Zurich, Switzerland

Introduction and research questions

Interactive web-tools are often regarded as powerful methods to familiarize and engage the public with complex problems, such as those related with a national energy transition [1]. Nevertheless, including interactivity is much more resource-consuming than traditional methods and, in some cases, may even complicate communication [2]. Although studies exist on how to design and assess interactive web-tools [3], there is little empirical evidence whether they can be more effective in comparison with static methods [4]. We studied this in an experimental design survey with non-experts in the German-speaking part of Switzerland. As a case study, we used the Swiss electricity supply scenarios for 2035 and their environmental, health, and economic impacts.

Our study [5] aimed to address the following questions:

- How do interactive and static web formats of scientific information perform in terms of making this information understandable, trustworthy and engaging for non-expert users?
- How do the demographics, prior experience with the topic, numeracy, and website navigation skills of the non-expert users, influence this performance for each format type?

Methodology

We conducted a between-groups experiment online (N=313 total), where the two experimental groups differed in the format of scenario information they received: (a) an interactive web-tool that we have developed in a previous study [6] as an interface for exploring a large database of electricity supply scenarios and impacts (Figure 1), and (b) a static website presenting only four distinct electricity supply scenarios with their impacts (Figure 2). The selection of electricity supply technologies and impacts was informed by a series of non-expert interviews we did in a past study [7]. We compared the two groups in terms of (a) self-reported and tested understanding, (b) self-reported and tested engagement and (c) self-reported trust of information. The two groups of respondents were representative of the population in gender, age, and highest education level and with comparable previous experience with the energy subject, website-navigation skills, and numeracy.



Figure 1. The interactive web-tool for exploring Swiss electricity supply scenarios for 2035 and related impacts.



Figure 2. The static equivalent webpage, presenting four electricity supply scenarios along with short introductory storylines. The arrows show the order of the graphics and text in the website.

Results

We found that the interactive condition did not lead to a perceived advantage over the static one, as there were no statistically significant differences between the two groups in self-reported understanding, engagement and trust of the information (Table 1). In fact, it seems that the interactive web-tool may even complicate the usability because we observed that the interactive web-tool's users scored statistically significantly worse than the users in the static condition, when they had to answer a quiz that required to extract information from the scenarios ("Understanding – tested" in Table 1).

In both conditions, we found a low to moderate correlation of website-navigation skills and numeracy with tested understanding, suggesting that these skills are important but not imperative. Participants with higher prior experience with the energy subject were also more engaged in both conditions, while demographics did not have any effect. Although the effects of the control variables varied between the conditions, only one statistically significant difference was found: high website navigation skills increased self-reported understanding in the static condition but not in the interactive one. This suggests that another factor might have moderated the effects of these skills in the interactive condition, such as a possible overload of information from the interactive web-tool.

Dependent variables	Experimental conditions		Statistic
	Static (n = 157)	Interactive (n = 156)	
Understanding – tested (quiz with 7 items, max. score: 7)	4.03 ± 1.99	3.54 ± 1.66	t(311) = 2.318*
Understanding – self-reported (6 items, 7-point Likert scale, max. score: 42)	26.64 ± 5.50	25.88 ± 5.82	t(311) = 1.195
Trust – self-reported (7 items, 7-point Likert scale, max. score: 49)	32.56 ± 5.95	32.62 ± 6.04	t(311) = -.090
Engagement – self-reported (7 items, 7-point Likert scale, max. score: 49)	31.55 ± 8.36	31.76 ± 8.60	t(311) = -.218
Engagement – tested			
Time spent in website (seconds)	339 ± 273	366 ± 334	t(311) = -.806
Drop-out rates in website (count)	7	10	χ ² (1) = .504

Table 1. Dependent variables by experimental condition. *p < .05.

Conclusions

These results indicate that the interactive web-tools do not come automatically with the benefits of understanding and engagement claimed in the literature or believed by experts. In fact, they might lead to a discrepancy between the actual and perceived understanding in non-experts, making users believe they comprehend more than they actually do. As the trends of using such interactive web-tools for digital participation continue, more empirical research is needed to evaluate which formats meet the needs and abilities of the intended users.

References

- Pidgeon, N., Demski, C., Butler, C., Parkhill, K., Spence, A., 2014. Creating a national citizen engagement process for energy policy. Proc. Natl. Acad. Sci. U. S. A. 111, 13606–13613.
- Zikmund-Fisher, B.J., 2012. The Right Tool Is What They Need, Not What We Have: A Taxonomy of Appropriate Levels of Precision in Patient Risk Communication. Med. Care Res. Rev. 70, 1–23.
- Wong-Parodi, G., Fischhoff, B., Strauss, B., 2014. A method to evaluate the usability of interactive climate change impact decision aids. Clim. Change 126, 485–493.
- Moss, R.H., 2016. Assessing decision support systems and levels of confidence to narrow the climate information "usability gap." Clim. Change 135, 143–155.
- Xexakis, G., Trutnevyte, E., 2018. Are Interactive Web-Tools for Public Engagement Worth the Effort? An Experimental Study on Energy Transition. Under preparation.
- Volken, S., Xexakis, G., Trutnevyte, E., 2018. Perspectives of informed citizen panel on low-carbon electricity portfolios in Switzerland and the empirical evaluation of informational materials. Environ. Sci. Technol. To be resubmitted after minor revisions.
- Volken, S., Wong-Parodi, G., Trutnevyte, E., 2017. Public awareness and perception of environmental, health and safety risks to electricity generation: an explorative interview study in Switzerland. J. Risk Res. 9877, 1–16.

Investment and generation cost trade-offs between cost-efficient vs. regionally equitable distribution of renewable electricity

Jan-Philipp Sasse^{1,2}, Evelina Trutnevte^{1,2}

¹ Renewable Energy Systems, Institute for Environmental Sciences (ISE), Section of Earth and Environmental Sciences, University of Geneva
² Institute for Environmental Decisions (IED), Department of Environmental Systems Science, ETH Zurich

Introduction

The Swiss Energy Strategy 2050 aims at drastically increasing electricity from renewable sources until the year 2035 [1]. Decentralised renewable electricity (solar PV, wind, biomass, small hydro power and enhanced-geothermal systems) is growing fast, especially solar PV, which grew by more than 500% in the last 5 years in Switzerland [2]. The appropriate spatial allocation of decentralised renewable electricity generators is highly controversial, because there is a trade-off between the most economically efficient distribution and a more regionally equitable distribution [3]. Investors prefer sites with good harvesting conditions (i.e. strong winds, high solar radiation) which leads to a concentration of renewable power plants to locations with the best conditions. Previous studies [4,5] have however shown the importance of a regionally even distribution in siting decentralised renewables. An uneven distribution of both negative consequences (i.e. noise, visual disturbance) and positive consequences (i.e. regional investments) can highly affect the public acceptance and therefore the successful diffusion of renewables.

This study is the first of its kind to study the economic and electricity generation trade-offs between the equitable and the cost-efficient spatial distribution of renewable generators in Switzerland. We use a bottom-up electricity generation model EXPANSE [6] with Modeling to Generate Alternatives (MGA) to assess the cost-optimal and 1'200 near cost-optimal spatial allocation scenarios of renewables in 2'258 Swiss municipalities.

Objectives

1. Develop a spatially-explicit electricity demand and supply database for 2'258 Swiss municipalities for the years 2016 and 2035.
2. Simulate the Swiss electricity generation at a municipal level with a spatially-explicit EXPANSE model to systematically explore cost-optimal and 1'200 near cost-optimal scenarios.
3. Assess trade-offs of cost-efficient vs. regionally equitable distribution of investments in renewables and the electricity generation cost.

Methodology

We simulate the Swiss electricity system with a spatially-explicit EXPANSE model [6] in order to assess the diversity of possible spatial allocation scenarios for decentralised renewables on a municipal level. The model integrates the electricity generation potentials for hydro power, gas, solar PV, wind, biomass and enhanced geothermal systems (EGS) as well as electricity savings and imports on a municipal level.

In order to assess the economic potential of each potential power generator, we incorporate the predicted future capital investment and O&M costs [7] to determine the levelized cost of electricity (LCOE) for each potential site. The additional economic potential of decentralised renewables until the year 2035 is shown in Figure 1.

With MGA methodology, the cost-optimal and 1'200 near cost-optimal scenarios of renewables were simulated for the year 2035, which provided the yearly electricity generation, installed capacity and cumulative investments per technology in each Swiss municipality. The simulation was conducted with yearly temporal resolution and municipal spatial resolution.

In order to assess the most equitable spatial allocation of decentralised renewables, we introduced a measure for regional equity which reflects the burden from decentralised renewable electricity generation across the Swiss population. Equity is defined as the even distribution of decentralised renewable electricity generated across the population and is measured using the Gini (G) coefficient [8]. The Gini coefficient measures the inequality of values of a frequency distribution, where the value of 1 stands for maximum inequality and the value 0 for maximum equality.

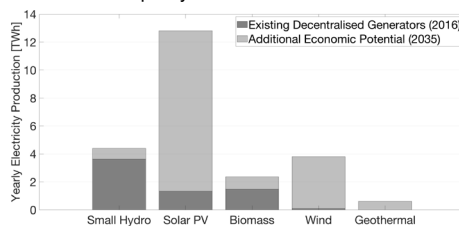


Figure 1. Current electricity generation (2016) and assumed additional economic potential (2035) of decentralised renewable electricity generation in Switzerland

Results

We find a moderate trade-off between efficiency and regional equity (Fig. 2). The difference in electricity generation cost between the most equitable and the cost-optimal scenario amounts to 1 Rp./kWh (8% above the generation costs in the cost-optimal case), while the regional equity (Equity = 100 - Gini coefficient [%]) applied on electricity generation more than doubles from 18% to 38%. An additional observation is that the share of electricity supplied from solar PV increases with increasing regional equity (Fig. 3), as the solar PV electricity generation potentials are proportional to the available rooftops and therefore also to the population size. In the cost-optimal scenario, up to 500MW in installed wind turbine capacity is concentrated in Vaud, Fribourg and Berne (Fig. 4a), where there are relatively strong winds and relatively low legislative land constraints for wind farm installations.

The cost-optimal scenario leads to distorted regional investments in the above mentioned three cantons, where 67% of all renewable investments are accumulated (Fig. 5a). With increasing equity, solar PV systems instead of wind turbines are installed evenly across all cantons (Fig. 4b), which in return leads to more spatially even investments (Fig. 5b). The cantons Zurich, Vaud and Berne together receive the highest share of investments of 38% even in the scenario of maximum equity.

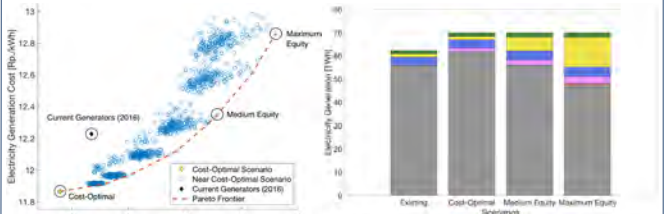


Fig. 2: Trade-off between equity and cost efficiency in spatial allocation of renewable generators

Fig. 3: Electricity generated from decentralized generators for various scenarios

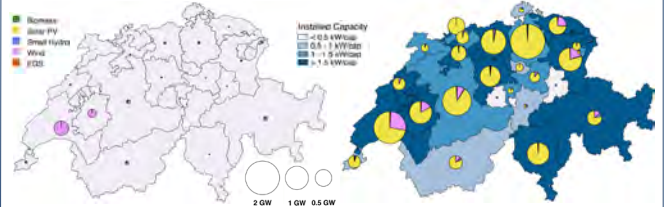


Fig. 4a: Cost-optimal scenario (11.85Rp./kWh, G=82%) Fig. 4b: Maximum Equity Scenario (12.85Rp./kWh, G=62%)

Figure 4: Cantonal distribution of additionally installed capacity from decentralized renewables (2016-2035)

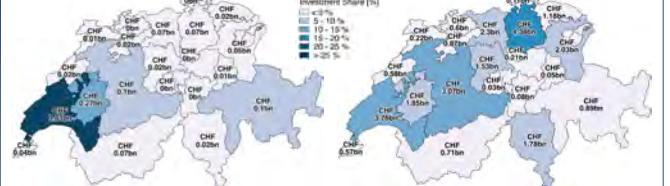


Fig. 5a: Cost-Optimal Scenario (CHF 1.76bn in total) Fig. 5b: Maximum Equity Scenario (CHF 28.62bn in total)

Figure 5: Cantonal distribution of additional cumulative investment in renewables (2016-2035)

Conclusions

We find a moderate trade-off between the cost-optimal and regionally equitable scenarios. Regional equity can be doubled with a moderate increase of 1 Rp./kWh in electricity generation costs, which is only 8% percent higher than the generation costs in the cost-optimal case. A cost-optimal spatial allocation leads to a concentration of 67% of renewable investments in Vaud, Fribourg and Berne (mostly wind), while equitable scenarios allow for more even renewable investments in all cantons (mostly in solar PV).

References

- [1] Bundesamt für Energie (BFE), Energiestrategie 2050 nach dem Inkrafttreten des neuen Energiegesetzes (2018). http://www.bfe.admin.ch/energiestrategie2050/index.html?lang=de&dossier_id=07008, Accessed 29.8.2018.
- [2] Schweizerischer Fachverband für Sonnenenergie, Markterhebung Sonnenenergie (2012-2017), <https://www.swissolar.ch/uebersichtenergiefakten-und-zahlen/markterhebung/>, Accessed 29.8.2018
- [3] Drechsler, M., Egerer, J., Lange, M., Masurowski, F., Meyerhoff, J., & Oehlmann, M. (2017). Efficient and equitable spatial allocation of renewable power plants at the country scale. *Nature Energy*, 2(9).
- [4] Langer, K., Decker, T., Roosen, J. & Menrad, K. A qualitative analysis to understand the acceptance of wind energy in Bavaria. *Renew. Sustain. Energy Rev.* 64, 248–259 (2016).
- [5] Wüstenhagen, R., Woloski, M. & Bürer, M. J. Social acceptance of renewable energy innovation: an introduction to the concept. *Energy Policy* 35, 2683–2691 (2007).
- [6] Trutnevte, E., Stauffacher, M., Schlegel, M., & Scholz, R. W. (2012). Context-specific energy strategies: Coupling energy system visions with feasible implementation scenarios. *Environmental Science and Technology*, 46(17), 9240–9248
- [7] Bauer, C. et al. Potentials, costs and environmental assessment of electricity generation technologies. *Paul Scherrer Institut, Villigen* (2017)
- [8] Gini, C. (1912) Variabilità e mutabilità. In: Pizetti, E. and Salvemini, T., Eds., Rome: Libreria Eredi Virgilio Veschi, *Memorie di metodologica statistica*.

Work Package 5: Pilot & Demonstration Projects

The key objective of the SCCER-SoE in Phase II is the initiation and in some case completion of pilot & demonstration (P&D) projects, which will be executed in close collaboration with industrial partners. The new WP5 combines the integrated approaches developed for geo-energies (WP1), hydropower (WP2), and the innovative technologies of WP3 in a series of seven P&D projects. The successful completion of these projects is a key milestone to deliver a portfolio of tested solutions, which shall enable Switzerland to reach the targets of the Energy Strategy 2050. Status and highlights are summarized below.

The seven demonstrator projects are:

Demo-1: Flagship stimulation experiment in the Deep UnderGround Laboratory

Demo-2: Reservoir engineering for heat exchange in Haute Sorne

Demo-3: Geneva basin-scale hydrothermal play for heat extraction and storage

Demo-4: CO₂ geological storage pilot

Demo-5: Small Hydro-Power Plant

Demo-6: Controlled fine sediment release from a reservoir by a hydrodynamic mixing device

Demo-7: Complex large hydropower scheme

Demo-1: Flagship stimulation experiment in the Deep UnderGround Laboratory

The project aims at a better understanding of the hydro-seismo-mechanical coupled processes that are associated with high pressure fluid injections in a crystalline rock mass. Experiments are carried out at various scales ranging from centimeters to hundreds of meters. Intermediate experiments at ten-meter scale were successfully performed in 2017 and early 2018 at the Grimsel Test Site, Switzerland. Subsequently, all personnel and funding has moved to the new Bedretto Deep Underground Laboratory for Geosciences (BULG), where hydraulic stimulation will be demonstrated at hundred-meter scale. The BULG lab is currently under construction, experiments will start early 2019.

Demo-2: Reservoir engineering for heat exchange in Haute Sorne

GeoEnergie Suisse AG is developing a pilot and demonstration project for deep petrothermal electricity generation in the village of Haute-Sorne (Jura). The system aims at depths of 4000 – 5000 m and is projected to deliver up to 5 MW electricity and/or heat for industrial processes as well as district heating. The project will implement the so-called multi-fracture system in a granitic environment. Many activities within the SCCER are targeted towards enabling the technology but also using the data for calibration, upscaling and validation of methods and results, such as strategies for adaptive traffic light seismic monitoring systems, underground heat exchanger design, construction, and optimization, as well as research on optimal fluid circulation and associated heat extraction strategies.

Demo-3: Geneva basin-scale hydrothermal play for heat exchange and storage

This demonstration project is being implemented as part of the “Geothermie 2020” program of the Canton of Geneva. A step-wise approach including drilling wells (production and storage) at progressively increasing depths (1500-2500 m) is being performed by SIG during Phase II (Q4 2016 – 2019). The encouraging preliminary results obtained and those ones which will be obtained with future drilling campaigns will provide the opportunity to test and validate the effectiveness of exploration concepts and models developed within WP1 as well as proof the feasibility of direct heat production and subsurface storage potential in sedimentary basins at relatively shallow depths. The project, approved in 2016, is in the early stage of realization with the drilling of the first Geo-01 well that successfully reached fractured carbonate reservoirs.

Demo-4: CO₂ Geological Storage Pilot

According to IEA, IPCC and COP21, (Carbon Capture & Storage) CCS has to be implemented to keep global warming within 2°C. ELEGANCY, an SFOE funded P&D project, embedded in a larger European framework, has the mission to provide clean hydrogen for heat and mobility based on steam-methane-reforming. CCS is an essential part of this concept. Underground experiments at the Mt Terri Lab study the potential CO₂ migration through a fault in the caprock and the effects of fault activation. Drilling has started in Sep 2018. The underground experiments are complemented by lab experiments on rock samples, modelling of injection and CO₂ migration, and the identification of regions in the Swiss sedimentary basin that are suitable for a future CO₂-storage pilot site.

Demo-5: Small Hydro-Power Plant

The SFOE P&D project Smallflex was launched in January 2018. The project is led by HES SO Valais, partners are EPFL, EAWAG, WSL and the two companies FMV and PVE. The Gletsch-Oberwald small hydropower plant commissioned in spring 2018 is the heart of the project. The aim of this project is to demonstrate the capacity of small hydropower to provide clean, sustainable and renewable energy while delivering ancillary service. A first campaign to investigate the flexibility of this run-off-river power plant is planned in Fall 2018.

Demo-6: Controlled fine sediment release from a reservoir by a hydrodynamic mixing device

Following physical tests in the laboratory of hydraulic constructions (PI-LCH) at EPFL and numerical simulations of the future Trift reservoir, we will implement a project in collaboration with HP industry. The project aims to demonstrate the effectiveness of technologies to artificially stir the water stored in a dam reservoir to prevent fine sediment from settling and allow for the sediment to be conveyed downstream at acceptable rates through the turbines during their normal operation. The mobile mixing device will be tested at a few dams to show its efficiency in different conditions. The expected outcome is (i) to validate the flushing efficiency as compared to laboratory development conditions; (ii) to characterize the dependence from local conditions; (iii) to identify practical difficulties and shortcomings of field implementation; (iv) to control the modifications to the sediment regime in the river downstream of the powerhouse as well as in the residual flow strength, and the resulting environmental impacts. We will seek funding for industry and SFOE to initiate the demonstrator in 2019.

Demo-7: Complex large hydropower scheme

FLEXSTOR comprises testing a set of innovative tools for flexible operation of storage hydropower plants in changing environment and market conditions. This demonstrator is motivated by the need to allow for flexible operation targeting premium remuneration hours, for which comprehensive methodologies for hydropower upgrading projects are still missing. It started at the end of Q3'2016; it is composed of six complementary research projects. Two projects are now completed, one related with hydropeaking, another with the optimization of storage use. The first project provides tools for validation of discharge demodulation basins, such as that of KWO at Innertkirchen. The second provided tools to assess the operation of complex hydropower systems with cascading reservoirs and multiple plants over several decades, in a way to support operational management and strategic planning. The other four project are up and running, as illustrated by preliminary results and conclusions. They concern (i) management of reservoir sedimentation across a cascade of alpine reservoirs, (ii) address mountain slope instability risks in glacier-liberated zones, avoiding non-optimal "preventive reservoir lowering", (iii) mitigation of turbine abrasion; (iv) extend the operating range of hydraulic machinery, whilst avoiding instabilities. These issues are being addressed in the complex system of KWO Oberhasli, for later replication in other hydropower schemes in Switzerland.

WP 5 Projects

Title

Pilot & Demonstration projects

Projects (presented on the following pages)

L'influence de la disposition relative des ouvrages d'entrée/sortie sur la déposition de sédiments fins dans les retenues profondes

Samuel Vorlet, Sebastian Guillen Ludena, Pedro Manso, Anton Schleiss

CFD and FEM investigations of a Francis turbine at speed no-load

Jean Decaix, Vlad Hasmatuchi, Maximilian Titzschkau, Laurent Rapillard, Pedro Manso, François Avellan, Cécile Münch-Alligné

Preliminary discussion on the use of raw monthly hydrological forecasts during the summer 2018 drought in Switzerland

Massimiliano Zappa, Luzi Bernhard, Konrad Bogner, Samuel Monhart, Käthi Liechti, Norina Andres, Christoph Spirig, Manfred Stähli

Implementation of an operational seamless nowcast to short range forecast system for the small hydropower plant at Gletsch

Konrad Bogner, Matteo Buzzi, Michael Schirmer, Massimiliano Zappa

Investigation of transient mixed flow at hydropower plant intake

Anthony Gaspoz, Vlad Hasmatuchi, Christophe Nicolet, Cécile Münch-Alligné

Assessment of a pressurized flushing event in a deep alpine reservoir

Maria Ponce, Samuel Vorlet, Azin Amini, Pedro Manso

Scaling up and specifying a stirring device (SEDMIX) from laboratory to prototype

Anass Chraibi, Azin Amini, Pedro Manso, Anton Schleiss

Detection of harsh operating conditions on a Francis prototype based on in-situ onboard and non-intrusive measurements

Vlad Hasmatuchi, Jean Decaix, Maximilian Titzschkau, Laurent Rapillard, Pedro Manso, François Avellan, Cécile Münch-Alligné

Mise à profit hivernale d'un dessableur souterrain en milieu alpin pour l'exploitation hydroélectrique flexible

Jessica Zordan, Pedro Manso, Cécile Münch

Subsurface Fluid Pressure and Rock Deformation Monitoring using Seismic Velocity Observations

Joseph Doetsch, V. Gischig, L. Villiger, H. Krietsch, M. Nejati, F. Amann, M. Jalali, C. Madonna, H. Maurer, S. Wiemer, T. Driesner, D. Giardini

GEo-01 : The first GEothermie 2020 P&D well in the Canton of Geneva - Preliminary results.

SIG Services Industriels de Genève - Canton of Geneva, Service de géologie, sols et déchets, Hydro-geo Environment Sarl - Geneva Geo-Energy Sarl - University of Geneva, Department of Earth Sciences

CO₂ sequestration: progress in the ELEGANCY-ACT project

Alba Zappone, Melchior Grab, Antonio Rinaldi, Claudio Madonna, Anne Obermann, Stefan Wiemer

Computational Modelling of an Innovative Water Stirring Device for Fine Sediment Release: The test case of the Future Trift Reservoir.

Anass Chraibi, Samuel Luke Vorlet, Azin Amini, Pedro Manso.

L'influence de la disposition relative des ouvrages d'entrée/sortie sur la déposition de sédiments fins dans les retenues profondes

Samuel L. Vorlet^{1*}, Sebastián Guillén Ludeña², Pedro Manso¹, Anton J. Schleiss¹

1) Platform of Hydraulic Construction (PL-LCH), École Polytechnique Fédérale de Lausanne (EPFL), Switzerland
 2) Hidram Group, Universidad Politécnica de Cartagena, Spain
 *Corresponding author: samuel.vorlet@epfl.ch



Contexte

Les ouvrages hydroélectriques alpins sont sujets à la sédimentation, un des problèmes principaux pour la durabilité de ces ouvrages. Cette sédimentation se traduit par le remplissage des réservoirs par déposition de sédiments fins, ce qui a un impact négatif sur la production hydroélectrique. Cela pose de nombreux problèmes, notamment la réduction du volume de stockage ou le blocage des ouvrages annexes.

Il y a donc une nécessité de mieux connaître les mécanismes de la sédimentation qui a lieu dans les retenues profondes, afin d'avoir à terme un management adéquat des sédiments.



Figure 1: Ouvrages annexes et sédimentation observés lors de l'abaissement du niveau de l'eau

Méthodes

Des simulations numériques sur un logiciel de mécanique des fluides computationnelle ont été réalisées sur quatre configurations de retenues profondes rectangulaires ($B = 250m, L = 500m, H = 85m$) avec entrée et sortie modélisées par des tubes $D = 4m, v = 1m/s$, situés à mi-profondeur. Des simulations avec de l'eau claire uniquement et des simulations incluant des sédiments fins ($d = 4\mu m, C_0 = 88mg/L$) ont été effectuées. Le modèle de turbulence $k-\epsilon$ et un modèle inhomogène multiphase Eulerien pour modéliser l'interphase eau-sédiment ont été utilisés.

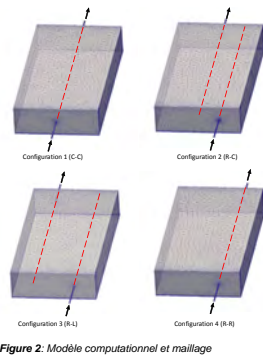


Figure 2: Modèle computationnel et maillage

Champs d'écoulement dans les retenues profondes

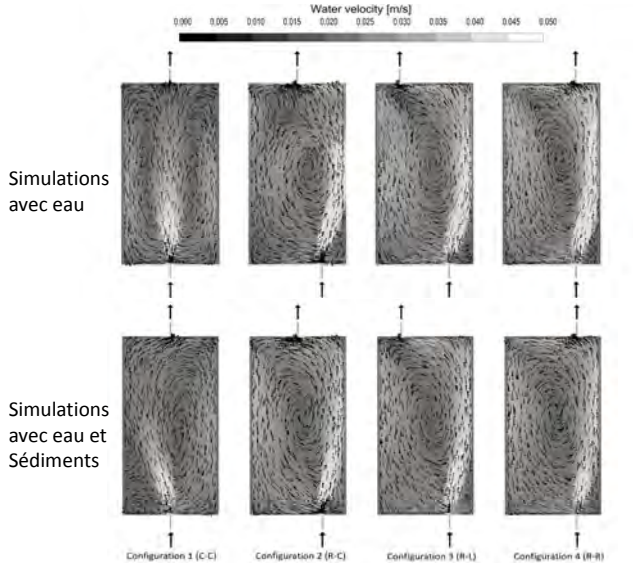


Figure 3: Vitesses d'écoulement de l'eau à mi-profondeur [m/s] pour simulations avec eau claire (en haut) et avec sédiments (en bas) à l'état stationnaire; vitesses d'écoulement (contours) et projection 2D de la direction de l'écoulement (flèches)

Références

Camnasio, et al. (2014). Prediction of Mean and Turbulent Kinetic Energy In Rectangular Shallow Reservoirs. Engineering Applications of Computational Fluid Mechanics, DOI:10.1080/19942060.2014.1
 Muller, M., De Cesare, G. and Schleiss, A. J. (2014). Continuous long-term observation of suspended sediment transport between two pumped-storage reservoirs. Journal of Hydraulic Engineering, 140(5), 05014003. doi: 10.1061/(ASCE)HY.1943-7900.0000866
 Vorlet, et al. (2018). Parametric study on the influence of Jet-like Inflows and Outflows on fine Sediment Settling. Trento, 5th IAHR Europe Congress, 12-14 June 2018, doi: 10.3850/978-981-11-2731-1_197-cd

Déposition des sédiments fins et champs de turbulence

Parmi d'autres paramètres turbulents analysés, le taux de variation spatiale de ϵ est celui qui présente la meilleure corrélation avec les dépôts.

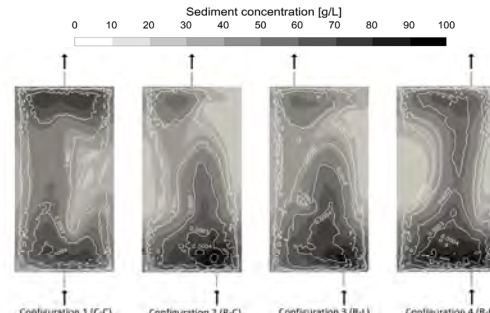


Figure 4: Déposition de sédiments fins au fond de la retenue [g/L] et taux de dissipation d'énergie cinétique turbulente ϵ [m^2/s^3] au fond de la retenue; simulations avec sédiments à l'état stationnaire

Evolution temporelle des niveaux de turbulence

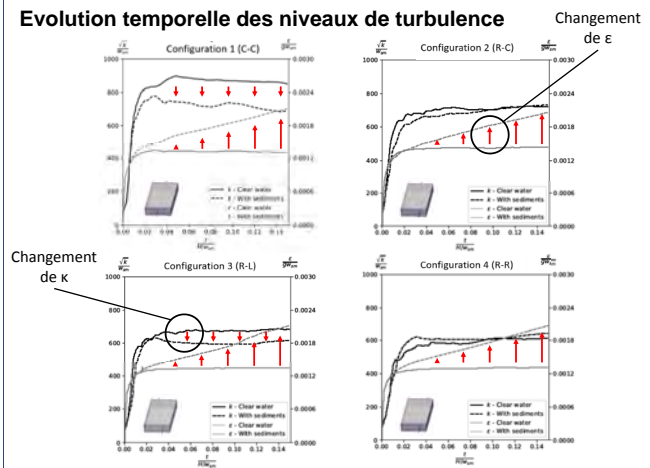


Figure 6: Evolution de l'énergie cinétique de turbulence k et taux de dissipation d'énergie cinétique de turbulence ϵ moyennés sur le volume

Discussion

Les champs d'écoulement dépendent de la configuration entrée/sortie, de la profondeur, de la présence de sédiments, et semblent avant tout conditionnées par les débits entrants. La déposition de sédiments fin est plus importante proche des entres/sorties et dépend du taux de dissipation d'énergie cinétique de turbulence ϵ . Plus le taux de dissipation d'énergie est important, plus la déposition de sédiments est importante, et inversement. La présence de sédiments fins modifie l'hydrodynamique et les niveaux de turbulence des retenues. On observe un changement au niveau des valeurs pour l'énergie cinétique de turbulence k , avec des valeurs plus faibles de sédiments, et un changement de comportement pour le taux de dissipation d'énergie cinétique de turbulence ϵ .

Conclusions

La déposition des sédiments dépend des champs d'écoulement et des niveaux de turbulence dans les retenues. Contrairement aux réservoirs peu profonds, les champs d'écoulement des réservoirs profonds varient en fonction de la hauteur. Pour anticiper le champ de déposition des sédiments, les champs d'écoulement et les niveaux de turbulence doivent être considérés au fond du réservoir.

CFD and FEM investigations of a Francis turbine at speed no-load

J. Decaix¹, V. Hasmatuchi¹, M. Titzschkau², L. Rappillard¹, P. Manso³, F. Avellan⁴, C. Münch-Alligné¹

¹HES SO Valais, Haute École d'Ingénierie, Hydroelectricity Group, Sion

²Kraftwerke Oberhasli AG, Grimsel Hydro, Innertkirchen

³EPFL, PL-LCH, Lausanne

⁴EPFL, LMH, Lausanne

Motivation

Due to the development and the integration of renewable energies, the electrical grid undergoes instabilities [1]. Hydraulic turbines and pump-turbines are a key technology to stabilize the grid. However to reach this objective, the hydraulic machines have to extend their operating range. Such an extension requires to deal with start-up and stand-by operations, which often leads to a reduction of the lifespan of the machines [2].

Nowadays, CFD and FEM simulations allow dealing with fluid-structure interactions, which help better understanding of the life time of hydraulic machines [3].

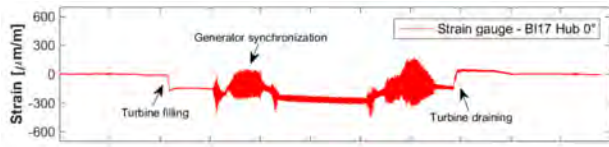
Context

The Grimsel 2 hydropower plant is equipped with horizontal ternary units with a complete motor-generator coupled with a Francis turbine on one hand and a single stage radial pump on another hand.

The Francis turbine undergoes cracks at the junction between the trailing edge of the blades and the hub. The cracks appeared after the operating conditions of the turbine changed from a few to a large daily number of start and stops.

The origin of the cracks is however not yet fully understood despite the fact that the case has been already studied [4].

A recent measurement campaign put in evidence the large fluctuations of the strain rate at the trailing edge of the runner blades close to the junction with the hub during the operation of the turbine at speed no-load (*i.e* during synchronization procedure) [5].

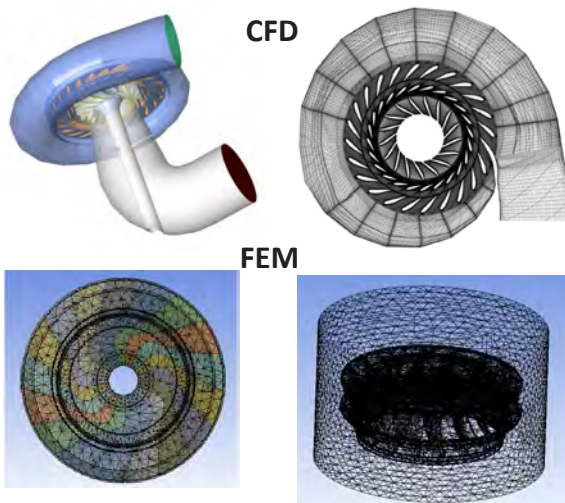


CFD and FEM set up

For the CFD analysis, the SST-SAS turbulence model is used to compute the flow. The inlet flow discharge is set at the inlet of the spiral according to the measured value at speed no-load.

For the stress analysis, the pressure field provided by the CFD simulation is applied on the runner blade, whereas no displacement is imposed at the junction between the runner and the shaft.

For the modal analysis of the runner, the surrounding water is taken into account in order to capture the damping of the natural runner frequency due to the added mass effect.

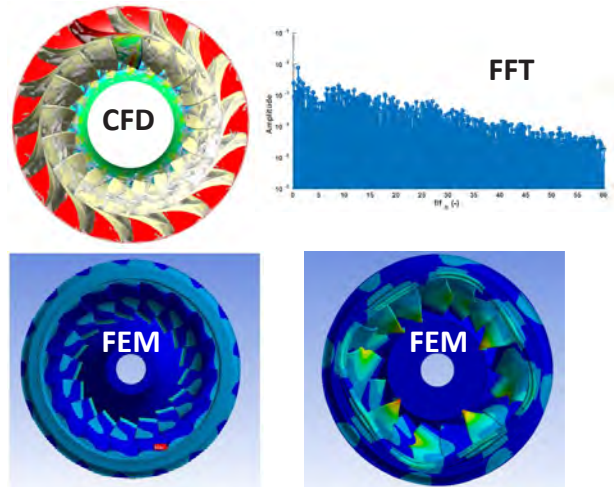


Results

The CFD simulation shows the presence of several vortices close to the trailing edge of the blade. The vortices lead to local pressure fluctuations. However, no specific frequency is observed on the pressure spectra of a probe located at the junction between the runner blade and the hub.

The stress analysis confirms that the maximum stresses are located at the junction between the runner blade and the hub.

The modal analysis put in evidence the existence of a natural mode of the runner around 600 Hz close to the dominant frequency deduced from the signal provided by the strain gauges.




Conclusions & Perspectives

The CFD simulation does not show any evident excitation at the frequency observed on the strain gauges. The FEM analysis confirms the weakness region at junction between the runner blade and the hub. The modal analysis suggests the existence of a natural mode of the runner close to the frequency observed on the strain gauges. Therefore, this mode could be excited by a source, which does not seem for instance clearly related to the fluid.

References

[1] Vu, T. L., & Turitsyn, K. 2016, 'Robust transient stability assessment of renewable power grids'. In IEEE International Conference on Sustainable Energy Technologies (ICSET) (pp. 7–12).
 [2] M Gagnon et al, 2010, 'Impact of startup scheme on Francis runner life expectancy', IOP Conf. Ser.: Earth Environ. Sci. 12 012107
 [3] B. Hübnér, W. Weber, and U. Seidel, 2016 'The role of fluid-structure interaction for safety and life time prediction in hydraulic machinery,' IOP Conf. Ser. Earth Environ. Sci., vol. 49, 072007.
 [4] C. Müller, T. Staubli, R. Baumann, and E. Casartelli, 2014 "A case study of the fluid structure interaction of a Francis turbine," IOP Conf. Ser. Earth Environ. Sci., vol. 22, 032053.
 [5] J. Decaix, V. Hasmatuchi, M. Titzschkau, L. Rappillard, P. Manso, F. Avellan, C. Münch-Alligné, 2018, 'Experimental and numerical investigations of a high-head pumped-storage power plant at speed no-load', IAHR Symposium, 2018, Kyoto, Japan .

Acknowledgements

Supported by:
 Schweizerische Eidgenossenschaft
 Confédération suisse
 Confederazione Svizzera
 Confederaziun svizra
 Swiss Confederation
 Innosuisse – Swiss Innovation Agency

FlexSTOR

Partners of the FLEXSTOR - WP6 project (17902.3 PFEN-IW-FLEXTOR)

Hes-so VALAIS WALLIS
 School of Engineering

EPFL
 ÉCOLE POLYTECHNIQUE
 FÉDÉRALE DE LAUSANNE

KWO
 GRIMSELSTROM

Preliminary discussion on the use of raw monthly hydrological forecasts during the summer 2018 drought in Switzerland

Massimiliano Zappa¹, Luzi Bernhard¹, Konrad Bogner¹, Samuel Monhart^{1,2,3}, Käthi Liechti¹, Norina Andres¹, Christoph Spirig², Manfred Stähli¹

¹ Swiss Federal Research Institute, WSL
² Federal Office of Meteorology and Climatology, MeteoSwiss
³ ETH Zurich, Institute for Atmospheric and Climate Science

MONTHLY FORECASTS UP AND RUNNING IN REALTIME !

The summer of 2018 in Switzerland has been characterized by a severe DROUGHT.

In the framework of the NRP70 project "HEPS4POWER" (separate poster) and NRP61 "drought.ch", tools for elaborating monthly predictions of water resources for hydropower and early prediction of hydrological droughts have been elaborated.

Starting from August 9th 2018, WSL and MeteoSwiss agreed to run a pilot operation period of such forecasts, with the goal of obtaining users feedback on such new forecasts tool going far beyond the lead time of hydrological predictions currently available in Switzerland.

The 2018 drought recorded lowest precipitation amounts from April until mid-August. It has been accompanied by an heatwave during the second half of July. The public interest on predictions concerning the drought situation and its possible end has been huge (Figure 1).

Motivation and feedback in the news

«Es müsste über Wochen stark regnen»

Das Ende der Trockenheit könnte voraussagbar sein

Die üblichen Prognosen in der Schweiz scheitern nur fünf Tage in der Zukunft – technisch möglich wären bis zu dreissig Tage

30-Tage-Prognose

BIRMENSDORF | Hydrologen der Forschungsanstalt WSL testen derzeit eine 30-Tage-Trockenheitsvorhersage. Demnach könnten sich die ausgetrockneten Böden zumindest in manchen Gebieten der Schweiz bis Ende August erholen. Bisher konnten Hydrologen der Forschungsanstalt für Wald, Schnee und Landschaft (WSL) auf der Webplattform trockenheit.ch eine 5-Tage-Prognose anbieten. Für diesen Zeitraum liefern Wettermodelle ausreichend sichere Daten über Niederschläge. Angesichts der angespannten Lage testen die WSL-Forschenden nun aber in Zusammenarbeit mit MeteoSchweiz eine 30-Tage-Trockenheitsvorhersage, wie die Forschungsanstalt am Donnerstag mitteilte. Ab sofort sei die Monatsvorhersage online abrufbar. **sda**

MATTHIAS SANDER

Wann endet die Trockenheit? Diese Frage stellen sich derzeit in der Schweiz Landwirte, Schiffskapitäne, Fischer, Hobbygärtner und viele mehr. Die Antwort: Keiner weiss es. Aber Experten wären womöglich in der Lage, das Ende der Trockenheit zu prognostizieren – wenn sie genügend Ressourcen hätten. Das sagt der Hydrologe Massimiliano Zappa.

Vor Trockenheit könnte man warnen

TROCKENHEIT: Erstmals ist eine Langzeitprognose verfügbar Leichte Entspannung in Sicht



Die Tiere bei Saland am 4. August 2018: Das Flussbett ist vollständig trocken. (Bild: Gottardo Pestalozzi)

ge-Modelleurechnungen des Europäischen Zentrums für mittelfristige – Wettervorhersage EZMW geführt. Diesen Pilotbetrieb werden sie während der nächsten drei Wochen weiterführen. «Wir möchten zeigen, wie weit unsere Methoden sind, und der Öffentlichkeit die Möglichkeit geben, den Nutzen der Monatsvorhersage zu prüfen», sagt Zappa.
Mit Unsicherheiten
Und hier nun die – vorsichtige – Vorhersage für die nächsten drei Wochen: Abgehend von der Situation am 2. August

Figure 1

Sources: NZZ, sda, WSL, Landbote, 20Minuten
17. July to 11. August 2018



Figure 4

Feedback and Discussion

- Monthly hydrological forecasts well received by media and users
- Visitors on www.drought.ch from 8000 in June to 20000 in July and August
- Very timely demonstration of possibilities of hydrological forecasts using raw meteorological input. HEPS4POWER by NRP70 showed the potential of further improvement by bias correcting such forecasts (Monhart et al., 2018)
- Forecasts issued since the end of July (Fig. 3c and 3d) were well able to confirm that drought in soil moisture would slightly recover within 30 days, while drought in runoff and baseflow would hold-on

- Recalculations of forecasts in early July (Fig. 3a and 3b) indicate, that only few scenarios would have hinted to such a severe drought.
- Previous analyses on the potential of monthly forecasts for water resources management during drought situations is confirmed
- The use of this information for management of hydropower in Switzerland has been explored in the HEPS4POWER project in case of the reservoir of the Verzasca river. A study for runoff river plants along the major rivers would be an interesting outlook

References

Bogner K, Liechti K, Bernhard L, Monhart S, Zappa M. 2018. Skill of hydrological extended range forecasts for water resources management in Switzerland. Water Resources Management, 32(3), 969-984. <http://doi.org/10.1007/s11269-017-1849-5>

Fundel F, Joerg-Hess S, Zappa M. 2013. Monthly hydrometeorological ensemble prediction of streamflow droughts and corresponding drought indices. Hydrol. Earth Syst. Sci., 395-407, [doi:10.5194/hess-17-395-2013](http://doi.org/10.5194/hess-17-395-2013)

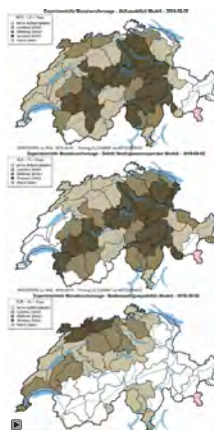
Monhart, S., Spirig, C., Bhend, J., Bogner, K., Schär, C., & Liniger, M. A. (2018). Skill of subseasonal forecasts in Europe: Effect of bias correction and downscaling using surface observations. Journal of Geophysical Research: Atmospheres, 123. <https://doi.org/10.1029/2017JD027923>

Zappa, M., Bernhard, L., Spirig, C., Pfändler, M., Stahl, K., Kruse, S., Seidl, I., and Stähli, M. 2014. A prototype platform for water resources monitoring and early recognition of critical droughts in Switzerland, Proc. IAHS, 364, 492-498. <https://doi.org/10.5194/iahs-364-492-2014>

Methods

- 51 numerical weather forecasts by ECMWF for the next month every Tuesday and Friday
- Hydrological model PREVAH forced by weather forecasts and by MeteoSwiss observations
- Applications for the Thur basin as in Fundel et al. (2012) and for Switzerland as in Bogner et al. (2018)
- Realtime since August 9th 2018. Reruns for July 2018 completed
- Publication of the forecasts (as deviation from climatology, Figure 2) for precipitation (P), runoff (R), soil moisture (SM), and baseflow storage (B) on WWW.DROUGHT.CH (Zappa et al., 2014)
- Communication on social media (Figure 4)

Figure 2: Forecast 2.8.18



Results (Thur basin) BOXPLOTS: Forecast LINE: Actual values

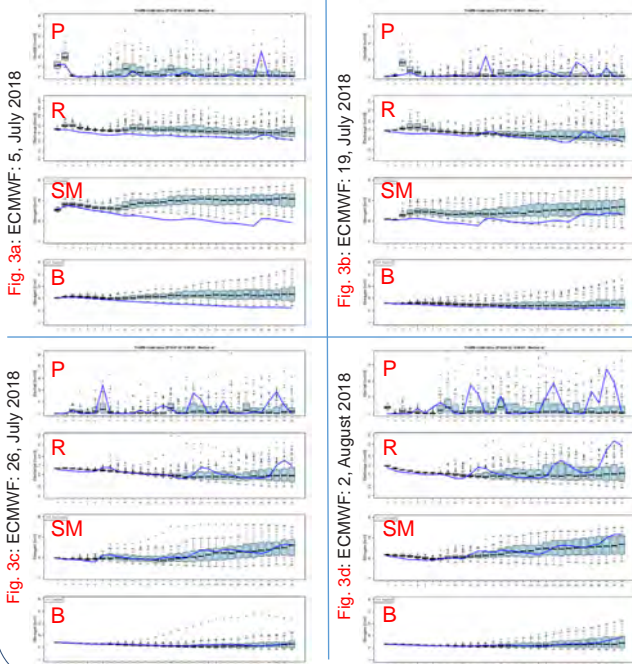


Fig. 3a: ECMWF: 5, July 2018

Fig. 3b: ECMWF: 19, July 2018

Fig. 3c: ECMWF: 26, July 2018

Fig. 3d: ECMWF: 2, August 2018

Implementation of an operational seamless nowcast to short range forecast system for the small hydropower plant at Gletsch

K. Bogner, M. Buzzi, M. Schirmer, M. Zappa

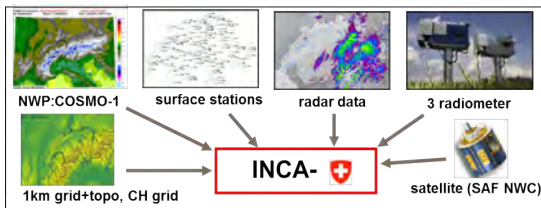
Motivation

In order to highlight the possibilities of increasing the flexibility in managing Small Hydropower Plants (SHP) with very limited storage capacities high resolution forecasts have been adapted to the small alpine catchment at Gletsch (VS) within the Demonstrator Project **SmallFlex**. Therefore the meteorological nowcast system INCA – CH has been combined with the short range weather forecast system COSMO-1. These two forecast are taken as input for the hydrological model PREVAH in order to produce stream-flow forecasts. Because of the differences in the initialization the forecasts need to be integrated into one seamless forecast system.

Methods

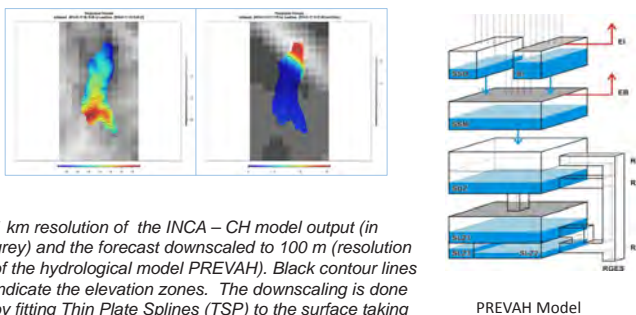
The forecast chain consists of :

- Meteorological forecasts:
INCA – CH system + COSMO 1 (+ COSMO-E)



INCA – CH: Spatial resolution ~ 1km
Temporal resolution: Precipitation: 10 min
Temperature: 1h

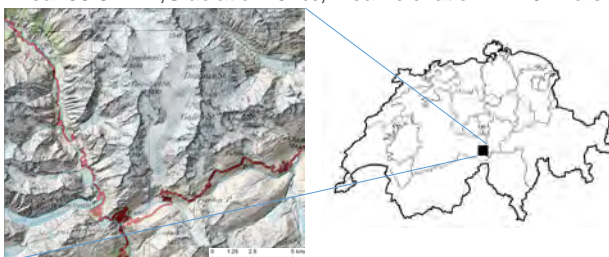
- Hydrological model PREVAH (+ Post-Processing of the inflow forecasts)



1 km resolution of the INCA – CH model output (in grey) and the forecast downscaled to 100 m (resolution of the hydrological model PREVAH). Black contour lines indicate the elevation zones. The downscaling is done by fitting Thin Plate Splines (TSP) to the surface taking the elevation as co-variate.

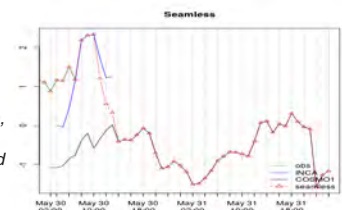
Study Area

Gletsch catchment:
Area: 39.8 km² ;Glaciation: 52%; Mean elevation: 2719 m a.s.l.



Seamless stream-flow forecast

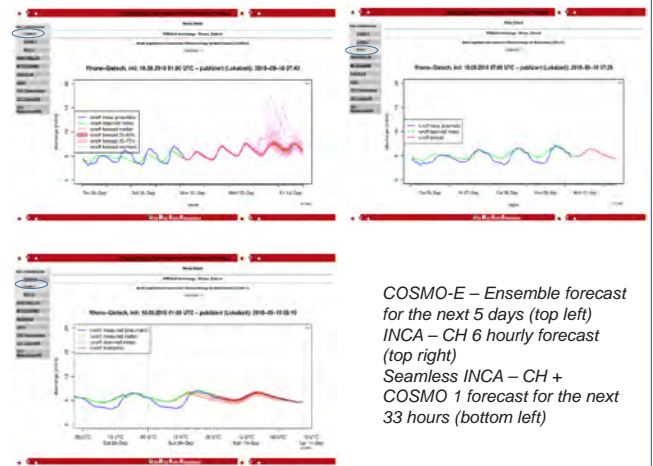
The INCA – CH system is a forecast bridging the information gap between the latest available observations in real-time (e.g. CombiPrecip) and COSMO 1 forecasts. However, because of different times of initialization and data, resp. forecast availability at WSL, the resulting stream-flow forecasts show jumps between the different data sets. Therefore a simple weighting schema is applied to create seamless stream-flow forecasts without abrupt junctions.



Example of a temperature forecast showing the latest available observations (green), INCA –CH forecast (blue), the COSMO 1 forecast (black) and the seamless forecast (red)

Operational implementation

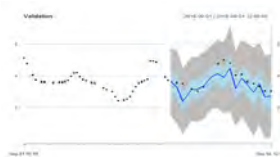
The results of these different forecast systems are available now operationally for Gletsch on the web showing the 5 days forecasts driven by COSMO-E, the INCA forecast for the first 6 hours and the seamless forecast combining the INCA and COSMO-1 for the next 33 hours



COSMO-E – Ensemble forecast for the next 5 days (top left)
INCA – CH 6 hourly forecast (top right)
Seamless INCA – CH + COSMO 1 forecast for the next 33 hours (bottom left)

Outlook

- Collection of longer forecast data sets in order to train Machine Learning techniques for post-processing the stream-flow forecasts.
- Implementing a Nowcast Ensemble Prediction System*
- Deriving the predictive uncertainty



Example of a post-processing test applying MARS (Multivariate Adaptive Regression Splines)

* Ongoing research at MeteoSwiss
D. Nerini, et al, 2017: A non-stationary stochastic ensemble generator for radar rainfall fields based on the short-space Fourier transform, Hydrology and Earth System Sciences 21(6), <http://doi.org/10.5194/hess-21-2777-2017>

Investigation of transient mixed flow at hydropower plant intake

A. Gaspoz¹, V. Hasmatuchi¹, C. Nicolet², C. Munch-Alligné¹

¹HES-So Valais, School of Engineering, Hydroelectricity Group, CH-1950 Sion, Switzerland, anthony.gaspoz@hevs.ch
²Power Vision engineering Sàrl, Chemin des Champs Courbes 1, CH-1024 Ecublens, Switzerland

This study is performed in the framework of the **SmallFlex** project which aims to show that small-hydropower plants can provide winter peak energy and ancillary services, whilst remaining eco-compatible.

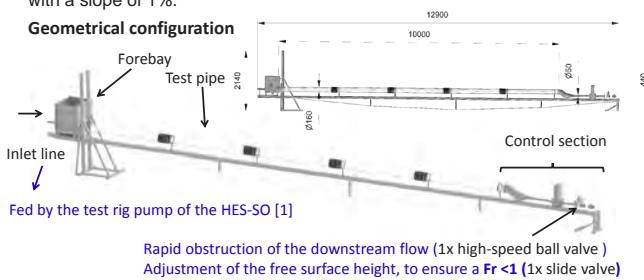
Objectives of this study

- Development, design and building of a reduced-scale test bench as well as its control to reproduce transient behaviour developing at hydropower plant intake and its penstock.
- Numerical modelling and simulations of those phenomena with Simsen.
- Analysis and comparison of numerical and experimental results for two test cases.

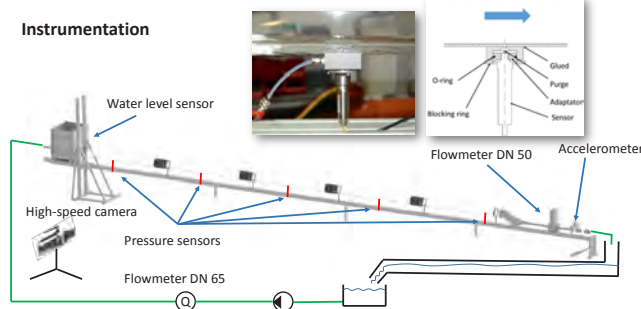
Laboratory reduced-scale test bench

The test bench is mainly manufactured with transparent parts to allow flow visualisation and contains a forebay, a test pipe and a control section. The whole test section is mounted on an inclinable support allowing slope setting. A return pipe, a free-surface tank and a pump completes the closed-loop hydraulic circuit. A high speed closing ball valve has been specially developed to obstruct the flow in less than 10 milliseconds. This obstruction speed generates a direct water hammer in case of a full filled pipe. The principal test case is a fast valve closure at the downstream of a mixed flow with a slope of 1%.

Geometrical configuration

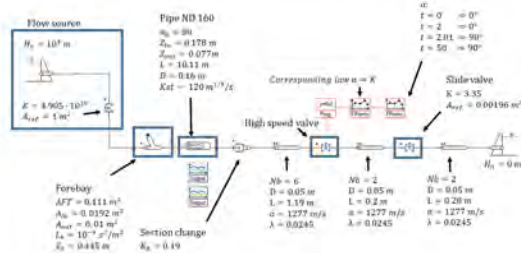


Instrumentation



Numerical approach

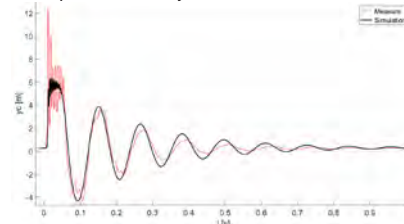
A compressible numerical approach was considered using a 1D software called Simsen [2]. This software allows to compute both transient electrical and hydraulic schemes. The Preissmann model [3], specially developed for the computation of transient compressible mixed flow, was used. The considered Simsen model is the following:



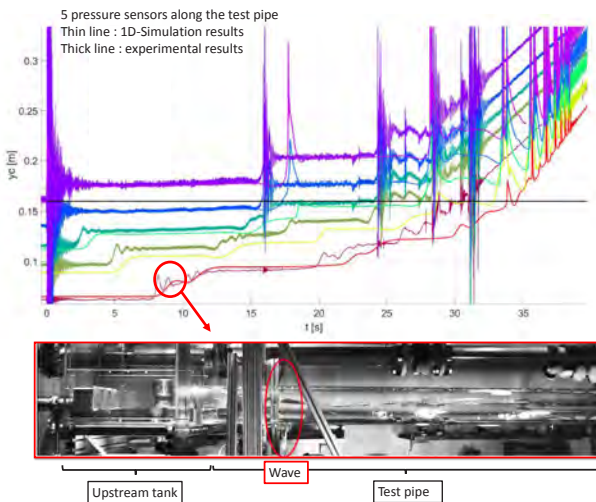
Results

Experimental and the numerical results have been compared in the case of a fast closure using the high speed valve. A good agreement is observed for both considered flow initial conditions, the fluid structure interactions being discarded.

1) Full pipe with a quasi-stationary flow:



2) Mixed flow in the test pipe, free surface mainly parallel to the pipe bottom, the end of the test pipe being completely filled. The flow was quasi-stationary and the Froude number was everywhere below 1.



Conclusions and perspectives

These investigations have shown that:

- The developed test bench allows to reproduce transient flow observed at the intake of hydropower plant.
- The transient behaviour of the flow, either monophasic or mixed, is globally well predict with Simsen 1D-Simulation with a correct calibration of some parameters.
- Ongoing work: development and implementation of a model able to simulate flows with a Froude number > 1 and its validation on this test bench.

Acknowledgements



References

- [1] Hasmatuchi V., Botero F., Gabathuler S., Münch C., "Design and control of a new hydraulic test rig for small hydro turbines" The International Journal on Hydropower & Dams, Volume 22, Issue 4, pp. 51-60.
- [2] Nicolet, C., Greiveldinger, B., Hérou, J.-J., Kawkabani, B., Allenbach, P., Simond, J.-J., Avellan, F., High Order Modeling of Hydraulic Power Plant in Islanded Power Network, IEEE Transactions on Power Systems, Vol. 22, Number 4, November 2007, pp.: 1870-1881.
- [3] Jean A Cunge and M Wegner. Intégration numérique des équations d'écoulement de barré de saint-venant par un schéma implicite de différences finies. La Houille Blanche, (1) :33-39, 1964.

Assessment of a pressurized flushing event in a deep alpine reservoir

Maria Ponce*, Samuel L. Vorlet, Azin Amini, Pedro Manso

Platform of Hydraulic Construction (PL-LCH), École Polytechnique Fédérale de Lausanne (EPFL), Switzerland
*Corresponding author: maria.ponceguzman@epfl.ch



Framework

Mountainous reservoirs face a serious problem with sediment management. The retention of sediments through time reduces the water storage capacity and can lead to the blockage of bottom outlets and power intakes. In case of blockage, drastic emergency maneuvers at the dam maybe will be required to control the harmful impacts on the downstream river system. Therefore, regulating or removal of the deposited sediments must be anticipated, planned and properly implemented.

Grimsel reservoir in the Swiss Alps is affected by high glacier erosion and periodically uses the pressurized flushing to evacuate fine sediment.

The objective of this study is simulate a pressurized flushing event in order to estimate the amount of sediment removed and identify the morphologic evolution of the flushing channel bed with reasonable computational resources.

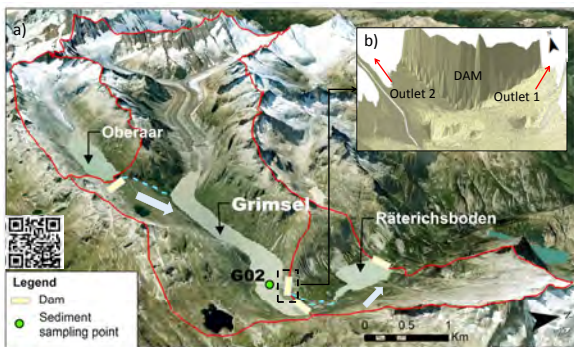


Figure 1: a) Upper view to west of the Grimsel Lake as a part of the cascade hydropower scheme, and b) Sketch of the generated mesh close to the outlets (galleries).

Methods

- The numerical model was built in Basement 2.8, using a 2D depth-averaged formulation.
- The scenario modeled is a future planned event based on the second stage of the 2000 flushing event during the winter season characterized by a partial reservoir drawdown lasting 5 hours.

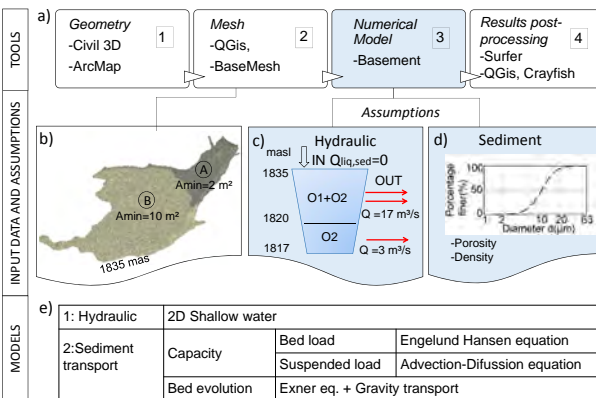


Figure 2: Model construction framework: a) Tools, b) Mesh was done with the bathymetry of 2016 (triangular elements with two areas of refinement), c) Boundary conditions, d) Granulometry curve (G02 sample, ETH-VAW, 2017), and e) Mathematical models for water and sediment transport.

Preliminary results and discussion

The computational time for a full simulation has been for 10 hours, with a CPU with 28 cores, which is considered a reasonable duration for a scenario assessment.

The volume of the bed load removed through the outlets is 3200 m³ which corresponds to the volume of the flushing cone estimated by EPFL in 2009. This low volume can also be validated with the bathymetries of 2000 and 2016 that show a loss of 90% of storage capacity below the elevation 1834 masl.

The suspended concentration at outlet 2 was only taken into account during the first 15 min during which it reached 960 mg/l after 10 min then reduced to 260 mg/l.

It can be noticed small bed changes on the border of the contours, some re-deposition areas close to the dam and significant erosion close to the outlets due to the higher velocities (figure 3d).

The channels formed by flushing did not show any significant bed change during the simulation. However, the bed width of the existed incised channel agreed with the results of the empirical equation derived by Tsinghua University reported in White (2001) showing that the flushing discharge is the key factor for the channel formation in this reservoir, and therefore highlight the necessity to improve the normal flushing operation to change the depositional areas.

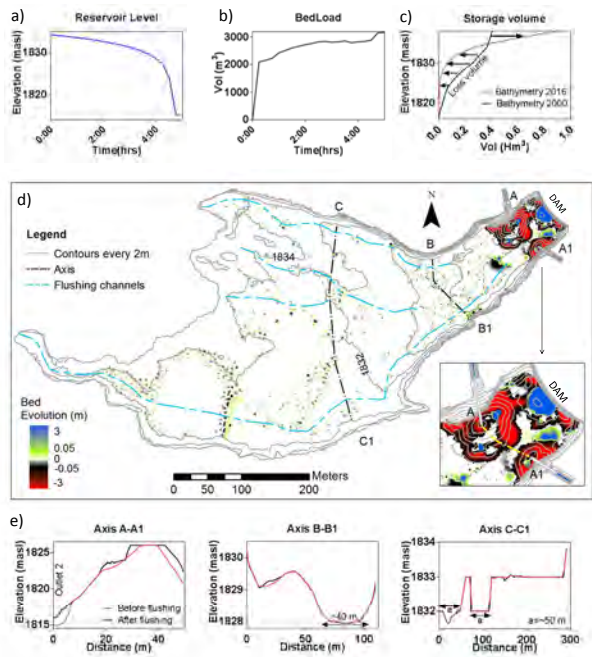


Figure 3: Main results of 5-hour flushing event from partial drawdown level of El. 1835: a) Reservoir level and b) Removed bedload volume reached during the simulation, c) Storage water lost between 2000 and 2016, d) Bed evolution after the flushing event, and e) Bed change at the respective cross section at the beginning and at the end of the modeled event.

Conclusion and Perspectives

The preliminary results provide only limited deposit close to the outlets, and show that the flushing event is ineffective to remove the deposited sediment away from the dam, and is ineffective to form new flushing channels across the reservoir.

To optimize the flushing operation (remove sediments at an adequate rate and minimize downstream impacts), two possible scenarios will be considered:

- Adding a constant input discharge from Oberaar (coordinated operation) and changing the duration and the discharge of the outlets.
- Modifying the bed topography of the reservoir, enlarging the section and increasing the longitudinal slope of the flushing channel immediately upstream of the dam in order to increase the movement of the sediment in the subsequent flushing operation.

References

- Castillo, L. G., Carrillo, J. M., & Álvarez, M. A. (2015). Complementary methods for determining the sedimentation and flushing in a reservoir. *Journal of Hydraulic Engineering*, 141(11), doi:10.1061/(ASCE)HY.1943-7900.0001050
- Chaudhary, H. P., Isaac, N., Tayade, S. B., & Bhosekar, V. V. (2018). Integrated 1D and 2D numerical model simulations for flushing of sediment from reservoirs. *ISH Journal of Hydraulic Engineering*, 1-9. doi:10.1080/09715010.2018.1423580
- Kantoush, S. A., & Schleiss, A. J. (2009). Channel formation during flushing of large shallow reservoirs with different geometries. *Environmental Technology*, 30(8), 855-863. doi:10.1080/09593330902990162
- White, W. R. (2001). *Evacuation of sediments from reservoirs*. London: Thomas Telford.

Scaling up and specifying a stirring device (SEDMIX) from laboratory to prototype

Chraibi, A.* , Amini, A., Manso, P., Schleiss, A.J.
 Platform of Hydraulic Constructions (PL-LCH), EPFL; *corresponding author: anass.chraibi@epfl.ch



Introduction

Sedimentation is a key challenge in reservoir management. A recent PhD study at EPFL (Jenzer-Althaus, 2011) proposed an innovative system (called SEDMIX, Figure 1) allowing to keep in suspension or re-suspend the fine particles near the dam. The current project's aim is to develop a real-sized prototype of SEDMIX device. It is equipped with 4-nozzle pressurized water jets inducing sufficient upwind turbulence to maintain fine sediments in suspension.

The work encompasses the following aspects:

- Hydraulic and structural design as well as technical specification of the device.
- Installation procedure.

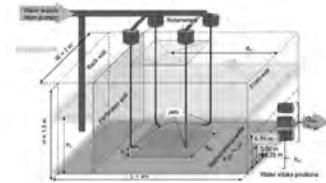


Figure 1: SEDMIX experimental model (Jenzer-Althaus, 2011)

Up-Scaling

- To guaranty a similar efficiency as in the hydraulic model, the scaling factor (λ_L) used to design a real-sized SEDMIX should satisfy two conditions:
 - Froude similarity, expressed by a relationship between the jet discharges used in the test and those of the real case.
 - the circulation velocity compared to the settling velocity should at least be the same as in test conditions.
- SEDMIX would be supplied either with a pump or directly connected to a water conveying tunnel which transfers water from a neighbouring catchment.
- For the presented prototype, a total jet discharge of $5 \text{ m}^3/\text{s}$ is considered. This leads to a scaling factor of $\lambda_L = 38$

Design

- The design of SEDMIX prototype has been performed to fulfil the following objectives:
 - Minimise head losses and consequently the required power during operation.
 - Minimize fabrication and installation costs, specially for the manifold pipe diameter (Figure 2).
 - Optimal structural stability and strength according to the relevant design standards (ANSI/ASME ...) (Figure 3).
 - Figure 4 illustrates the manifold specifications

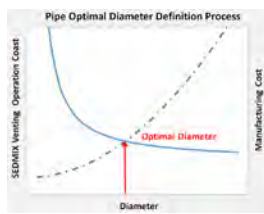


Figure 2: Pipe diameter optimization

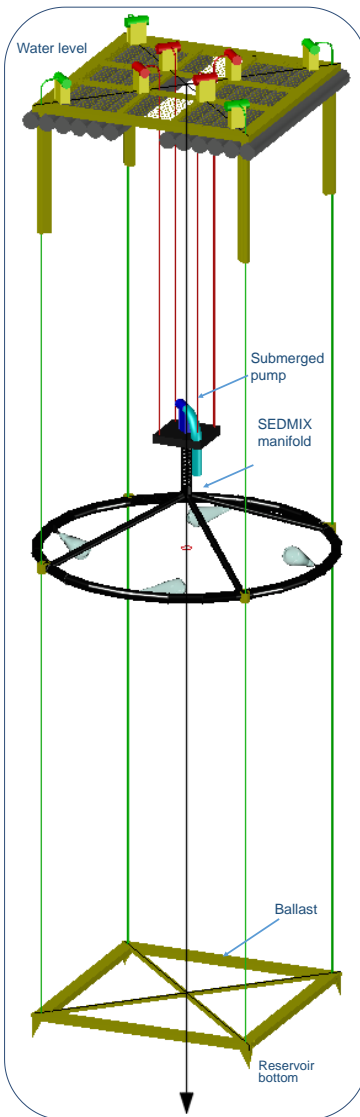


Figure 5: SEDMIX device

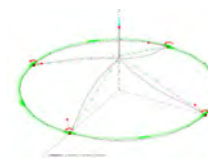


Figure 3: Typical SEDMIX structural analysis.

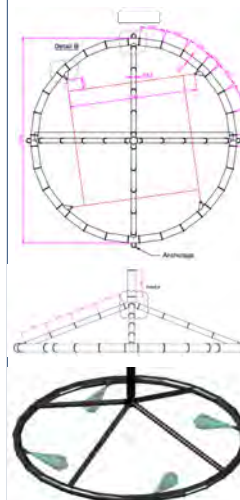
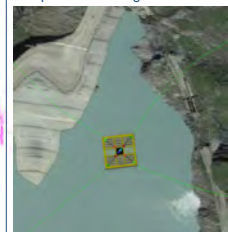


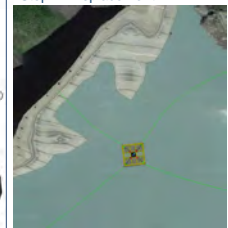
Figure 4: SEDMIX manifold specification



Step 1: assembling



Step 2: Displacement



Step 3: Anchoring

Figure 7: SEDMIX installation steps

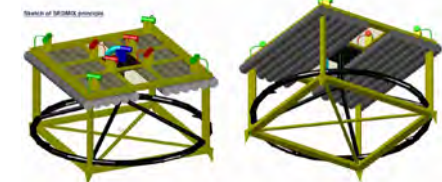


Figure 6: Floating platform details

Installation method

- The multi-nozzle manifold frame is kept in place using a floating platform at water surface elevation and a ballast at the reservoirs' bottom (Figure 5 & Figure 6).
- The manifold is mobile along the vertical chains which allows to locate it at its optimal position, derived from numerical simulations, and even change the position during the same operation (Figure 5).
- The device can be assembled and installed in a given dam reservoir then disassembled and moved to another.
- All the system components can be displaced by moving the floating platform which is anchored onshore (Figure 7).

Reference

- Jenzer Althaus, J., 2011, Sediment evacuation from reservoirs through by jet induced flow, LCH EPFL, DOI : 10.5075/epfl-thesis-4927.

Detection of harsh operating conditions on a Francis prototype based on in-situ onboard and non-intrusive measurements

V. Hasmatuchi, J. Decaix, M. Titzschkau, L. Rapillard, P. Manso, F. Avellan, C. Münch-Alligné

Motivation

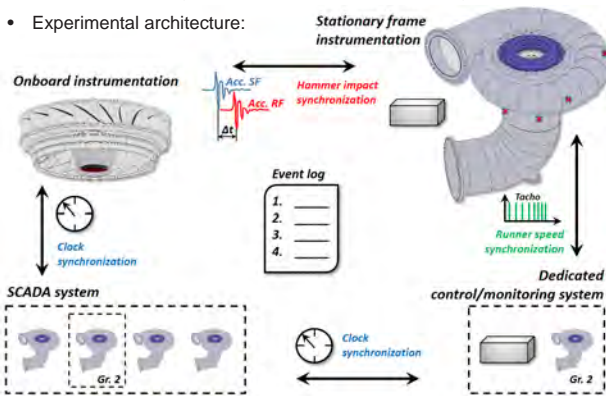
- Pumped-storage power plants: key components of a successful integration of renewable energy sources into electrical grid.
- Hydraulic turbines and pump-turbines:
 - operation in a wide range to offer power regulation flexibility;
 - subject to frequent start-up and/or stand-by operating regimes;
 - facing harsh structural loadings with impact on their lifetime.

Objectives:

- Establishment of a hydrodynamic instability level hill-chart of the machine based on several experimental monitoring parameters;
- Proposal of an alternative less-harmful start-up path and stand-by position with direct effect on the long-term maintenance costs;
- Elaboration of a diagnosis protocol to redraw hydrodynamic instability level hill-charts on different hydropower units, using only a simplified instrumentation set.

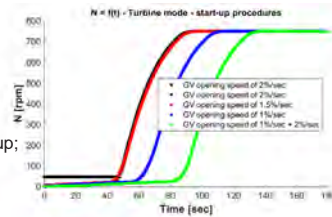
Experimental instrumentation architecture

- Case study: a 100 MW Francis turbine prototype, part of one of the four horizontal ternary groups of Grimsel 2 pumped-storage power plant.
- Experimental architecture:



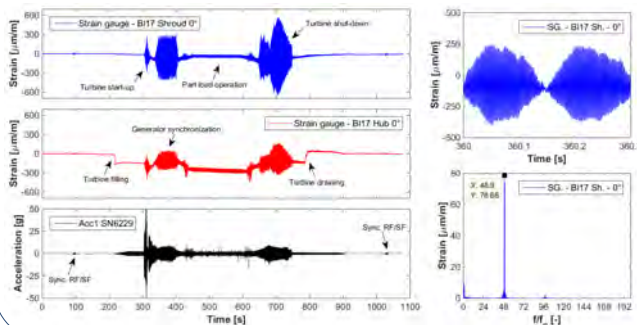
Experimental results

- Conducted tests focused on:
 - Turbine full operating range;
 - Turbine deep part-load;
 - Turbine normal start-up;
 - Modified slower turbine start-up;
 - Pump start-up.



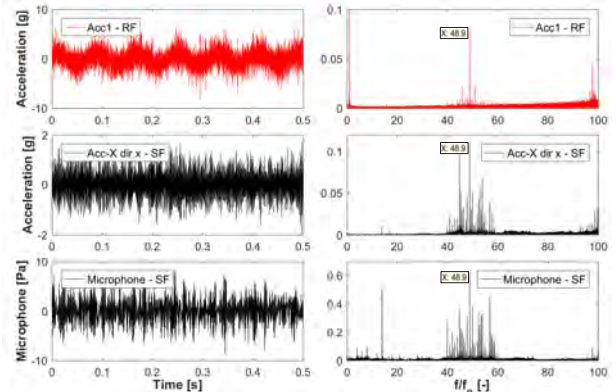
Evidence of harsh turbine start-up and shut down procedures

- Evidence of harmful structural loading of the turbine runner blades during the normal start-up and shut down procedures – signals recorded with the onboard instrumentation.



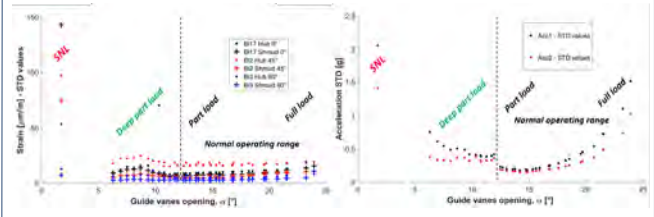
Non-intrusive instrumentation detection capabilities

- Identification of the harmful structural loading fluctuation of the runner blades at SNL condition using the non-intrusive instruments.



Strain and vibration fluctuations charts

- Fluctuations STD of the runner blades strain and the runner vibrations at SNL, deep part load, and the full normal operating range.



Conclusions & Perspectives

- Two successful experimental measurements campaigns conducted on a 100 MW high-head Francis turbine prototype;
- A 3rd experimental campaign based only on non-instrumentation successfully driven in 2018 on a different machine.
- Still seeking for a feasible simple technical solution to avoid harsh turbine runner blades loading during start-up and shut down;
- Final analysis of results ongoing;
- Diagnosis protocol based on a simplified instrumentation set to identify harsh operating conditions on a different hydropower unit ongoing.

References

[1] Hasmatuchi V., Titzschkau M., Decaix J., Avellan F., Münch-Alligné C., 2017, "Challenging onboard measurements in a 100 MW high-head Francis Turbine prototype", SCCER-SoE Annual Conf., Birmensdorf (ZH), Switzerland.
 [2] Decaix J., Hasmatuchi V., Titzschkau M., Rapillard L., Manso P., Avellan F., Münch-Alligné C., 2018, "Experimental and numerical investigations of a high-head pumped-storage power plant at speed no-load", Proceedings of the 29th IAHR Symposium on Hydraulic Machinery and Systems, Kyoto, Japan, 2018
 [3] Hasmatuchi V., Decaix J., Titzschkau M., Münch-Alligné C., 2018, "A challenging puzzle to extend the runner lifetime of a 100 MW Francis turbine", Hydro 2018, Gdansk, Poland.

Acknowledgements

Partners of the FLEXSTOR - WP6 project

Mise à profit hivernale d'un dessableur souterrain en milieu alpin pour l'exploitation hydroélectrique flexible

Jessica Zordan¹, Pedro Manso¹, Cécile Münch-Alligné²

¹ Plateforme en Constructions Hydrauliques (PL-LCH), École Polytechnique Fédérale de Lausanne (EPFL),

² HES-So Valais/Wallis, School of Engineering Hydroelectricity Group, Sion

corresponding authors: jessica.zordan@epfl.ch; pedro.manso@epfl.ch



1. Introduction

Le projet de recherche SmallFlex a pour objectif de démontrer la capacité des petites centrales hydroélectriques à fournir de l'énergie de pointe et des services systèmes malgré l'absence d'un lac d'accumulation d'eau en amont, tout en mesurant l'impact de ce nouveau fonctionnement sur l'environnement, le productible et les revenus. L'aménagement hydroélectrique de **Gletsch-Oberwald** a été sélectionné par les partenaires comme site pilote pour une telle démonstration d'exploitation flexible en milieu alpin. Il a été mis en service début 2018.

Parmi les méthodes visant à augmenter les possibilités d'exploitation, nous pouvons citer l'ajout de stockage intra-journalier, les prévisions à court terme des apports en eau et en sédiments ou encore l'exploitation adaptée des turbines Pelton à jets multiples.

La présente étude se concentre sur l'utilisation «intelligente» du **dessableur souterrain** pour le **stockage d'eau**, en particulier dans la période hivernale de faibles débits. Ceci, à turbiner dans les moments de pointe de demande et à débit le plus possible proche au débit équipé des turbines pour en augmenter leur rendement.

2. Disponibilités hydrologiques

Le régime hydrologique du bassin versant du site pilote est fortement influencé par la **fonte glaciaire**, avec des débits très importants en été, et de débits très faibles en fin d'automne, hiver et début du printemps.

Pour le cas d'étude, le débits horaires d'apports, turbinés, résiduels, module et débit équipé basé sur les données horaires de 1974 à 2016 à la ont été analysés (Figure 1).

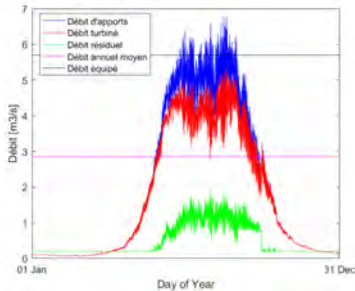


Figure 1. Débits horaires d'apports, turbinés, résiduels, module et débit équipé basé sur les données horaires de 1974 à 2016 à la station hydrométrique de Gletsch N°2268 (OFEV).

On remarque que souvent pendant l'hiver l'eau, même si elle pouvait est captée parce que le débit est supérieur au débit de dotation, elle n'est pas turbinée vu que le débit est inférieur au débit plancher de la turbine (Figure 2).

Afin de **réduire les volumes d'eau perdus** (zone jaune dans la Figure 2) une solution est de ajouter un moyen de stocker ces volumes captés, pour le turbiner plus tard dans la journée. Les cavernes existantes ou des excroissances à réaliser peuvent être mises à profit moyennant des modifications d'usage et des adaptations du système de pilotage de l'aménagement.

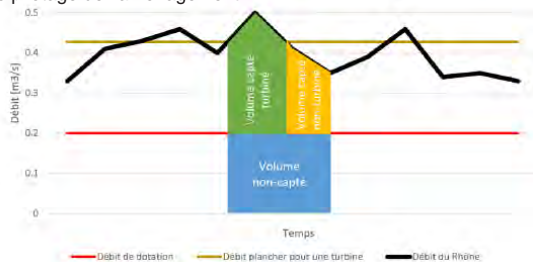


Figure 2. Illustration des volumes d'eau captés et turbinés dans l'aménagement au fil de l'eau en hiver.

Références

- Morand G. (2017) Augmentation de la flexibilité d'exploitation d'aménagements hydroélectriques de haute-chute au fil de l'eau en Valais, Projet de diplôme Master, LCH, EPFL.

3. Concept d'un volume de stockage «flexible»

A Gletsch le dessableur (Figure 3) a un volume de stockage disponible pour être utilisés en mode flexible, qui est défini entre les niveau de submergence minimal et du seuil trop-plein:

- Volume utile pour mode flexible (V_{flex}) 2050 m³
- Niveau d'eau maximal (N_{MAX}) 1747.45 masl
- Niveau d'eau minimal (N_{MIN}) 1742.70 masl

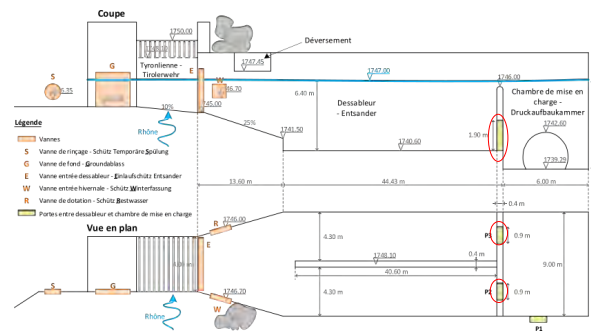


Figure 3. Prise d'eau et dessableur (schème opérationnel de l'exploitant, à l'état printemps 2018).

Suite à l'étude préliminaire (Morand et al., 2017), la géométrie du **dessableur a été adapté sur chantier** afin de créer deux ouvertures de fond (cercles rouges en Figure 3) qui permettent une connexion avec la chambre de mise en charge et donc d'utiliser le volume d'eau stocké. Ces ouvertures sont obturés pendant le fonctionnement en mode dessableur. Le fonctionnement s'articule dans les phases suivantes:

1. Le dessableur se remplit jusqu'au niveau du trop plein N_{MAX} .
2. Quand N_{MAX} est atteint :
 - Soit le trop plein du dessableur évacue l'excès d'eau (V_{OUT});
 - Soit l'eau est utilisé pour alimenter une des turbines, vidant progressivement le dessableur jusqu'au niveau d'eau minimal qui déclenche la fermeture des vannes-injecteurs.
3. Un nouveau cycle de remplissage s'initie.

3. Campagne d'essais sur prototype

Un campagne de tests sur site est prévue pour **novembre 2018**. Différents modes d'exploitation flexible de l'aménagement hydroélectrique de Gletsch-Oberwald seront testés. Tous les partenaires seront actifs pour la campagne des tests sur le terrain. L'EPFL-LCH se concentrera particulièrement sur le fonctionnement de la prise d'eau, du dessableur et de la chambre de mise en charge, à l'aide du système de mesures actuel et de nouveaux instruments à installer dans le but de mesurer:

- Les débits prélevés, déversés et retournés;
- Les niveaux d'eau dans les différents ouvrages;
- Les apports en sédiments (quantité, granulométrie, densité);
- Les temps de passage entre modes d'exploitation;
- La fréquence d'utilisation du dessableur et des vannes de purge. La présence de neige ou glace.

4. Conclusions

Des solutions innovatrices simples ont déjà été implémentés dans le site pilot permettant de nouveaux modes d'exploitation flexibles, notamment **en période hivernale**. Des essais sur site sont la prochaine étape pour valider le concept des points de vue énergétique, environnemental et économique, et mesurer son réel potentiel. Ce projet s'inscrit parfaitement dans la stratégie énergétique suisse et dans le marché d'un futur proche sans RPC où l'**énergie de pointe** sera fortement valorisée.

Subsurface Fluid Pressure and Rock Deformation Monitoring using Seismic Velocity Observations

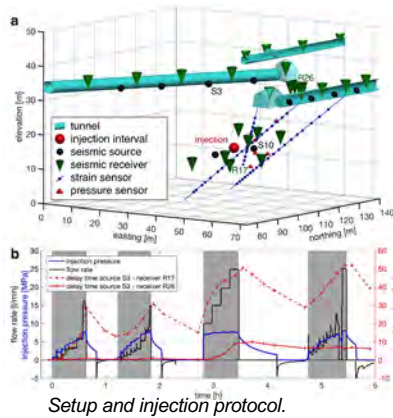
Joseph Doetsch, V. Gischig, L. Villiger, H. Krietsch, M. Nejati, F. Amann, M. Jalali, C. Madonna, H. Maurer, S. Wiemer, T. Driesner, D. Giardini

Abstract

The pressure of fluids in the subsurface is generally a function of depth as well as the regional geological history. Changes to the subsurface fluid pressure – be it natural or human-induced – disturb the stress field and are known to drive volcanic eruptions, as well as to trigger earthquakes. For example, pressure increase by fluid injection for hydraulic stimulation and wastewater disposal has been linked to earthquake activity. Unfortunately, pressure measurements need direct access through boreholes, so that pressure data is only available for few locations. A method for estimating the spatial distribution of fluid pressure remotely would thus be highly beneficial. From measurements in a 20-m-scale experiment in granite, we find that fluid pressure propagation can be predicted from observed seismic velocity variations, based on a strong correlation between observed changes in seismic velocities and fluid pressure measured within the rock.

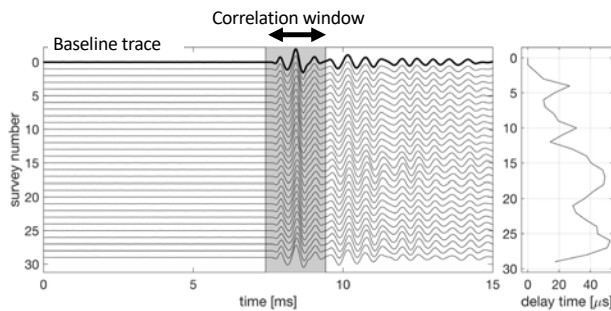
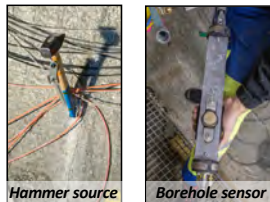
Setup and data acquisition

- Hydraulic stimulation with injection volume of 1.25 m³
- Deformation monitoring using 60 fibre-bragg grating strain sensors
- In-situ pressure monitoring using 10 pressure sensors
- Active seismic monitoring using 8 hammers, 2 piezo-sources, 26 piezo-receivers



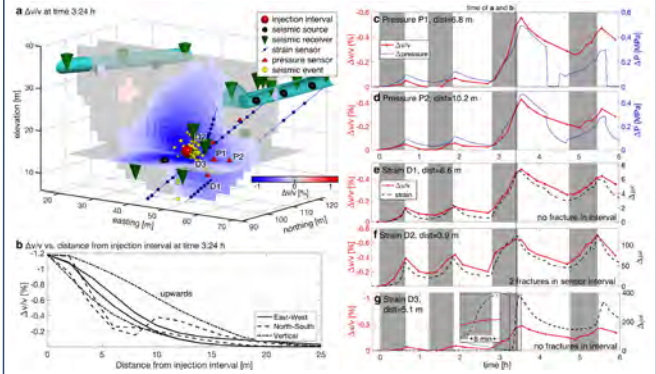
Active seismic monitoring

- Repeated surveys (every ~10 min) using 10 sources
- Highly repeatable signals
- Correlation analysis to extract variation in first arrivals



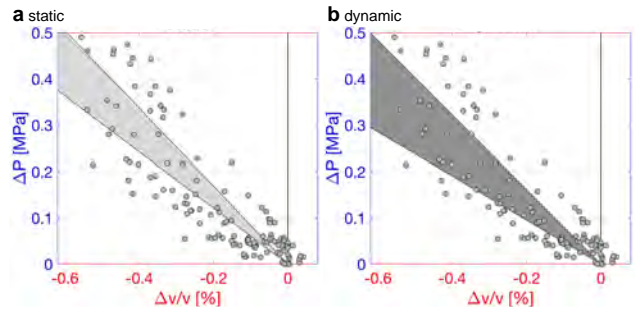
Inversion results

- Transient 3D travelttime inversion in order to determine seismic velocity variation over time
- Comparison with in-situ pressure and strain measurements shows strong correlation



Discussion and validation

Comparison with laboratory measurements shows the same linear relationship between seismic velocities and stress changes. This implies that seismic monitoring can be used to remotely measure the in-situ pressure evolution.



Field measurements (dots) and laboratory predictions show the same relationship between pressure change (ΔP) and relative velocity variation ($\Delta v/v$).

Conclusions

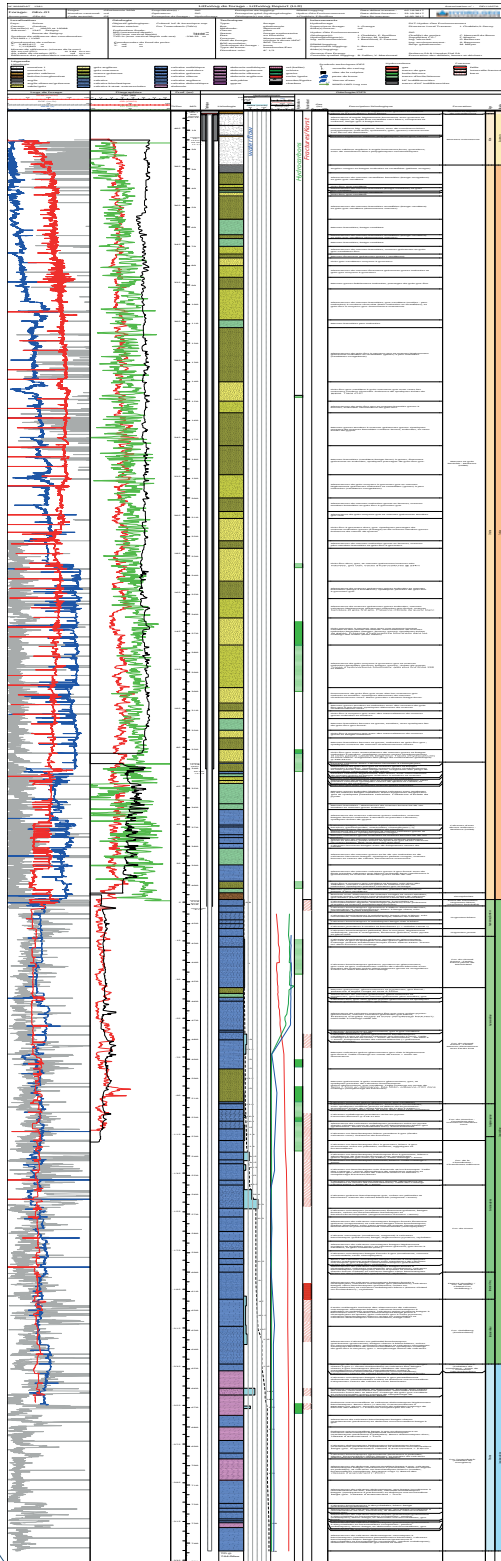
Active seismic transmission data recorded during a 1.25 m³ water injection experiment show a direct response to the high-pressure fluid injection cycles. Inversion of these data yield a transient 3D seismic velocity model of the injection volume. Comparison with fluid pressure measured within the rock volume reveals a strong correlation, which enables prediction of subsurface fluid pressure based on the seismic velocity variations. The link between seismic velocity variations and rock deformation is more complex, with a clear link existing for reversible deformation driven by the fluid-pressure related stress change. We conclude that seismic velocity changes measure volumetric strain resulting from effective stress changes, while shear dislocation does not affect seismic velocity.

This study has been published with the same title and authors as: Doetsch et al. (2018), *Geophysical Research Letters*. <https://doi.org/10.1002/2018GL079009>

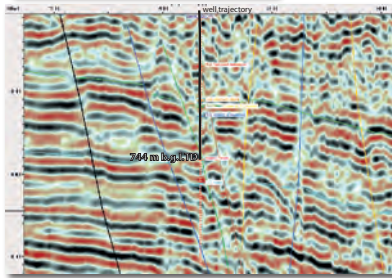


GEO-01 : The first GEOthermie 2020 P&D well in the Canton of Geneva - Preliminary results.

SIG Services Industriels de Genève - Canton of Geneva, Service de géologie, sols et déchets,
Hydro-geo Environment Sarl - Geneva Geo-Energy Sarl - University of Geneva, Department of Earth Sciences
Project coordinator: Dr. Carole Nawratil De Bono, SIG



The GEOthermie 2020 program, consisting of three main phases i.e. prospection, exploration and exploitation, has recently entered into the exploration phase with the drilling of a series of shallow boreholes i.e. ca 600 -1000 m deep below ground level (b.g.l.). The first exploration well GEO-01 has been successfully drilled in 2018 in Satigny, North-West of the city of Geneva, finding artesian water flowing at 50 l/s and 34°C from faulted lower Cretaceous carbonate units at various depth intervals ranging between 460 and 670 m b.g.l.



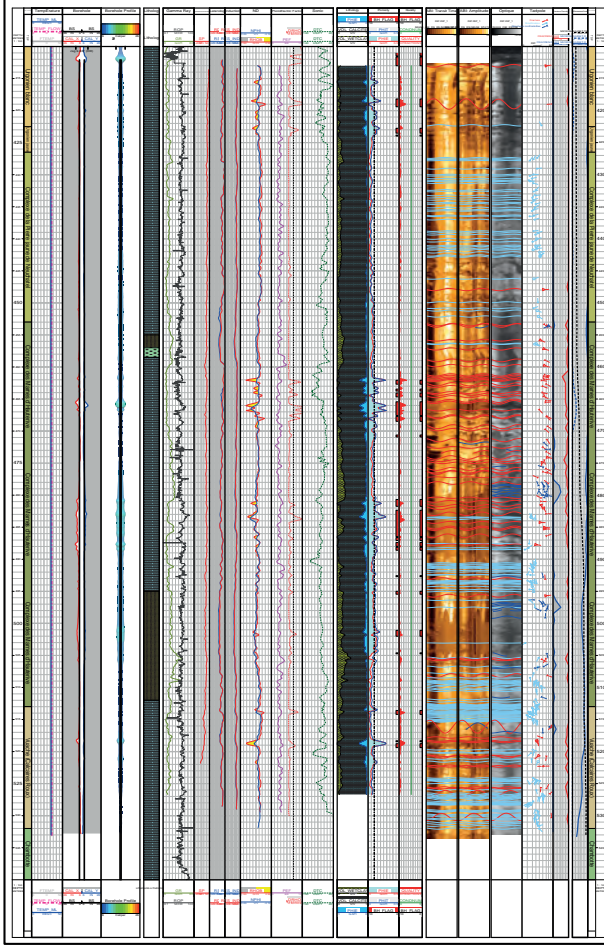
2D seismic line passing near the GEO-01 well location

Aerial view of the GEO-01 Drilling site



Well GEO-01	
Well ID	GEO-01
Well Name	GEOthermie 2020
Well Type	Exploration
Well Status	Completed
Well Depth (m)	1130
Well Diameter (mm)	150
Well Completion	Open
Well Production	50 l/s
Well Temperature (°C)	34
Well Location	Satigny, Geneva
Well Coordinates	45.760000, 4.830000
Well Date	2018
Well Operator	SIG
Well Contractor	Hydro-geo Environment Sarl
Well Designer	Hydro-geo Environment Sarl
Well Driller	Hydro-geo Environment Sarl
Well Tester	Hydro-geo Environment Sarl
Well Recorder	Hydro-geo Environment Sarl
Well Logger	Hydro-geo Environment Sarl
Well Corer	Hydro-geo Environment Sarl
Well Cementer	Hydro-geo Environment Sarl
Well Cement	Hydro-geo Environment Sarl
Well Cement Volume (m³)	Hydro-geo Environment Sarl
Well Cement Pressure (bar)	Hydro-geo Environment Sarl
Well Cement Temperature (°C)	Hydro-geo Environment Sarl
Well Cement Time (min)	Hydro-geo Environment Sarl
Well Cement Quality	Hydro-geo Environment Sarl
Well Cement Test	Hydro-geo Environment Sarl
Well Cement Results	Hydro-geo Environment Sarl
Well Cement Comments	Hydro-geo Environment Sarl

Long-duration hydraulic tests on the artesian flow will be conducted for the next 6 months. During this phase, continuous measurements of temperature, pressure, flow rate, turbidity and hydro-chemical and isotopic analysis will be performed.



The second exploration well GEO-02 will be spud in January 2019. The overall goals of this well are similar to the GEO-01 well: test the faulted lower Cretaceous and Upper Jurassic limestones, reach the Kimmeridgian reef complex at 950m as well as improve our knowledge of performing successful geothermal drilling projects. The expected total depth of the well GEO-02 is 1130 m b.g.l.



CO₂ sequestration: progress in the ELEGANCY-ACT project

Alba Zappone^{a,b}, Melchior Grab^d, Antonio Rinaldi^c, Claudio Madonna^c, Anne Obermann^b, Stefan Wiemer^b

^aInstitute of Process Engineering, ^bSwiss Seismological Survey, ^cGeology Institute, ^dInstitute of Geophysics, ETH Zurich, Switzerland
*alba.zappone@sed.ethz.ch

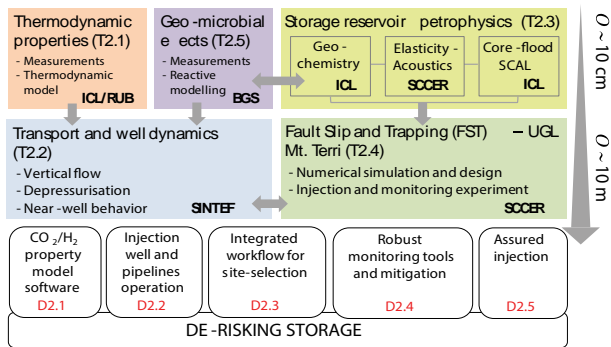
The European project

ELEGANCY (Enabling a Low-Carbon Economy via Hydrogen and CCS) is an European project within the ACT (Accelerating CCS Technologies) initiative, aiming at fast-track the decarbonization of Europe's energy system by exploiting the synergies between two key low-carbon technologies: CCS and H₂.

Main objectives of ELEGANCY are:

- Develop and demonstrate CCS technologies with high industrial relevance
- Validate key elements of the CCS chain by frontier pilot and laboratory scale experiments
- Optimize combined systems for H₂ production and H₂-CO₂ separation
- De-risk storage of CO₂ from H₂ production by providing experimental data and validated models
- Develop simulators enabling safe, cost-efficient design and operation of key elements of the CCS chain
- Assess societal support of key elements of CCS

The Work package on CO₂ injection and storage (WP2)



The geological storage of CO₂ is an essential component for enabling the efficient generation of H₂ as a transport fuel. The large volumes of CO₂ produced in the natural gas reforming H₂ manufacture require a coupling with direct CO₂ separation techniques, and safe geological storage. The contribution of SCCER-SoE is at centimeter and decameter lab scales: Laboratory and pilot scale.

The laboratory scale



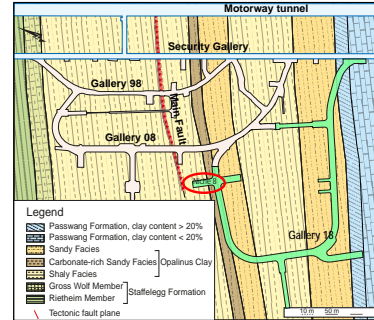
First joint experimental campaign at ICL on March 20-28 2018 in collaboration with colleagues from ETH/SCCER to investigate and image fluid transport in a fractured rock using the new core-holder and X-ray tomography. The first experiment was conducted on fracture aperture characterization on Westerly Granite and Carrara Marble with and without shearing

Laboratory experiments are performed by ETH Zurich, EPF Lausanne, Imperial College London and McGill University. The focus of the experiments is the characterization of the elastic, mechanical and transport properties of intact and fractured rock samples. The majority of the experiments will be done on samples extracted from the borehole campaign in the underground laboratory at the Mt. Terri, which has started at the end of August 2018.

The following activities have been completed:

- First samples selection for petrophysical studies (elastic mechanic and transport properties).
- Characterization of the pore and gas sorption properties of Opalinus Clay
- First experimental campaign on the observation of tracer transport through fractured cores by X-ray Computed Tomography .

The field scale: Mont Terri CS-D experiment



Partners in CS-D:



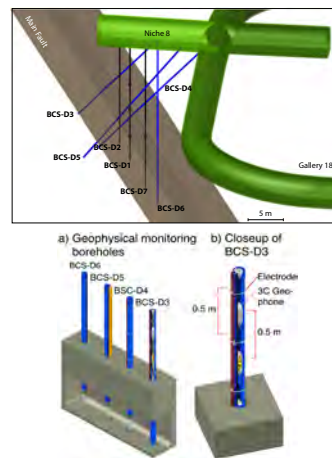
A new niche has been drilled and equipped by Swisstopo to host the CS-D experiment.

The CS-D experiment aims to investigate the sealing capability and caprock integrity by determining CO₂-rich brine mobility in a fault zone hosted in a clay rich formation (Opalinus Clay).

In Particular we investigate:

- the migration of CO₂-rich brine through the core of the Main Fault (MF, scaly clay fabric),
- the interaction of the CO₂ with the neighboring intact rocks, and damaged zone
- the impact of long time exposure to CO₂ on the rocks permeability in the

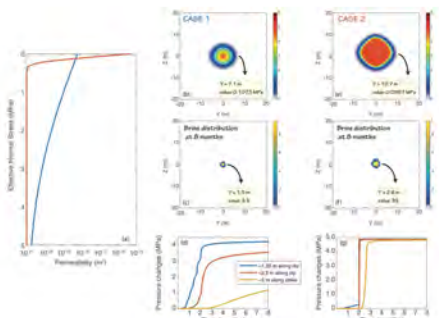
The experimental layout



The borehole setup of the CS-D experiment comprises three vertical boreholes for fluid injection, pressure monitoring, displacement monitoring, and fluid sampling. For geophysical monitoring, boreholes BCS-D3 and D4 will be drilled inclined in order to enable the tomographic planes being parallel to the symmetry axis of the anisotropy (normal to the bedding). The boreholes BCS-D5 and -D6 will be equipped with sensors to locate microseismic events in 3-D. All boreholes will be equipped with fiber optics for deformation and temperature measurements.

Modeling for CS-D experiment

We investigate the possible distribution of pressure and brine in the Mont Terri fault with the continuum hydro-mechanical code TOUGH-FLAC. We limited the injection pressure to be below the reactivation threshold observed previously. The fault plane is simulated with a finite width (1 m) and we model it as a fracture zone accounting for possible elastic opening. We analysed two cases: (i) a constant increase of permeability with decreasing normal effective stress (elastic behavior) and (ii) assuming that the fracture jack opens after reaching small value in effective normal stress (opening). For both cases both pressure and brine should reach a distance at which the monitoring should be possible (i.e. around 2 m).



Computational Modelling of an Innovative Water Stirring Device for Fine Sediment Release: The test case of the Future Trift Reservoir

Chraibi, A.¹, Vorlet, S.L., Amini, A.², Manso, P.

Platform of Hydraulic Constructions (PL-LCH), EPFL; ¹corresponding author: anass.chraibi@epfl.ch, ² azin.amini@epfl.ch



Introduction

- This work is part of a development project which aims to carry out an innovative system (SEDMIX) allowing to keep in suspension or re-suspend fine particles near the dam. With its 4-nozzle pressurized water jets, SEDMIX is expected to induce sufficient upwind vortex flow to maintain fine sediments in suspension.
- The aim of this part is to analyse the performance of a real-sized SEDMIX operating in the future Trift reservoir (Figure 1) via numerical analyses. This study allows to validate or to improve SEDMIX optimal configuration experimentally determined in a recent PhD study at EPFL (Jenzer-Althaus, 2011).



Figure 1: Trift Glacier over time

Methodology

The numerical simulations were performed with ANSYS-CFX v.18 on five different positions for the SEDMIX device (Figure 4). Steady state simulations as well as transient simulations were computed for the same boundary conditions, namely, the mass flow rate for the inlet ($M_{in} = 21002.7 \text{ kg/s}$), the relative pressure for the outlet ($P_{outlet} = 0 \text{ Pa}$) and 4 Source points (SEDMIX jets) with specific discharge and directions + 1 source point with negative discharge (submerged SEDMIX supplier pump) (Figure 3). All the simulations are multiphase since they include sediment ($D_s = 0.1 \text{ mm}$, $\rho_s = 2600 \text{ kg/m}^3$, $C_s = 0.7 \text{ g/L}$). The chosen turbulence model was the $k - \epsilon$ model combined with inhomogeneous Eulerian model. The performance of SEDMIX in each position has been evaluated and tested for different jet discharges.

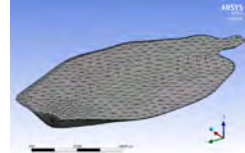


Figure 2: Computational model and mesh

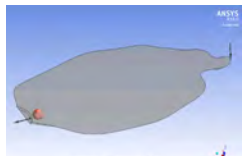


Figure 3: Numerical model geometry with the boundary conditions



Figure 4: SEDMIX tested positions

Results

Analysis of the numerical simulation results has shown:

- the presence of SEDMIX does create a vortex flow pattern and sediment movement upward (Figure 5).
- The sediment volume fraction in the higher layouts of the reservoir increases with time (Figure 5)
- The transient simulation with SEDMIX does reach a Steady State S_i (at a $t \approx 3\tau_j$ with $\tau_j = V/\Sigma Q_j$) (Figure 6 & 7). 43% increase in sediment release.
- the supplementary sediment evacuation ratio, defined as follow (reference case: without SEDMIX), has confirmed the increase of the sediment release with SEDMIX (Figure 8):
- The performance of SEDMIX in each position (Ps1, Ps2...) has been compared and evaluated according to the evacuated sediment ratio γ_s (Figure 9):

$$\gamma_s = \lim_{t \rightarrow \infty} \frac{M_{s,out}(t)}{M_{s,in}(t)} = \lim_{t \rightarrow \infty} \frac{\dot{M}_{s,out}(t)}{\dot{M}_{s,in}(t)} \quad (\text{L'Hôpital rule})$$

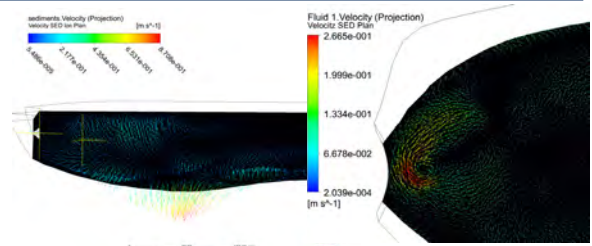


Figure 5: (a) appearance of a vortex flow generated by SEDMIX (b) Sediment velocity showing movement upward

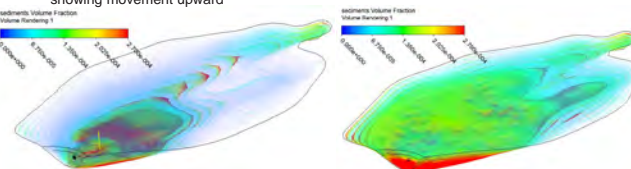


Figure 6: Sediment volume fraction (a) at $t = 8 \times 10^6 \text{ s}$ (b) at $t = 5 \times 10^6 \text{ s}$

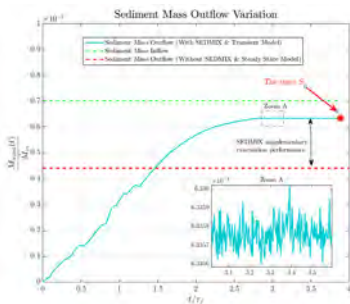


Figure 7: Sediment Mass Outflow: Steady and transient models, with and without SEDMIX

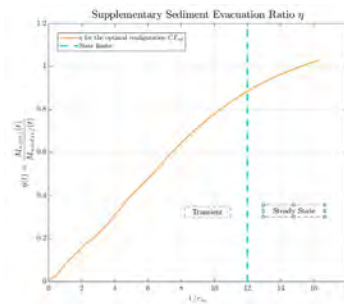


Figure 8: SEDMIX supplementary sediment evacuation compared to the reference case

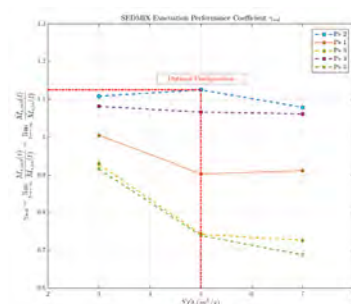


Figure 9: SEDMIX performance in each position

Conclusions

- The optimal discharge corresponds, as expected, to the SEDMIX geometric up-scaling discharge ($5 \text{ m}^3/\text{s}$) (Jenzer Althaus, 2011).
- The optimum position is P2, where the SEDMIX device is located in front of the water intake.

References

Jenzer Althaus, J., 2011, Sediment evacuation from reservoirs through by jet induced flow, LCH EPFL, DOI : 10.5075/epfl-thesis-4927
Amini, P.A, Manso, S, Venuleo, N, Lindsay, C, Leupi, A.J, Schleiss "Computational hydraulic modelling of fine sediment stirring and evacuation through the power waterways at the Trift reservoir" Hydro 2017, Seville, Spain.
De Cesare G., Manso P., Chamoun S., Guillén-Ludeña S., Amini A., Schleiss A. J. "Innovative methods to release fine sediments from seasonal reservoirs". ICOLD Congress Vienna 2018 July 2-8., Question 100. (book in print).

Academic Research Partners

ETH zürich



Hes·SO VALAIS WALLIS



Lucerne University of Applied Sciences and Arts
HOCHSCHULE LUZERN

eawag
aquatic research



Cooperation Partners

